PETROLOGY OF THE COMPOSITE MAFIC-FELSIC PLUTONIC ROCKS OF THE FOGO ISLAND BATHOLITH: A WINDOW TO MAFIC MAGMA CHAMBER PROCESSES AND THE ROLE OF MANTLE IN THE PETROGENESIS OF THE GRANITOID ROCKS

NURDAN SEBILE AYDIN

ISBN 0-612-17568-5

PETROLOGY OF THE COMPOSITE MAFIC-FELSIC PLUTONIC ROCKS OF THE FOGO ISLAND BATHOLITH: A WINDOW TO MAFIC MAGMA CHAMBER PROCESSES AND THE ROLE OF MANTLE IN THE PETROGENESIS OF THE GRANITOID ROCKS

by

©Nurdan Sebile Aydın, B.Sc., M.Sc.

A thesis submitted to the School of Graduate Studies

in partial fulfilment of the requirements for the degree of

Doctor of Philosophy

Department of Earth Sciences

Memorial University of Newfoundland

May 1995

St John's Newfoundland

ABSTRACT

Field, petrographic, geochemical, geochronologic (U/Pb) and Nd isotopic studies of the diverse plutonic rocks in the Tilting area, Fogo Island, NE Newfoundland, were carried out to elucidate the relative roles of crust and mantle in the petrogenesis of this example of Siluro-Devonian magmatism in the Appalachian-Caledonide orogen.

The plutonic rocks of the study area are part of the Fogo Island Batholith (FIB) and display a wide range of fabrics, textures, mineralogies and compositions. Based primarily on field and petrographic characteristics they have been divided into three main suites, these are: the **Tilting Layered Suite** (TLS) composed of layered ultramafic, mafic and intermediate rocks; the **Fogo Suite** (FS) dominated by monzogranite with minor amounts of granodiorite; and the **Wild-Sandy Cove Suite** (W-SCS) containing mainly quartz diorite and diorite with minor amounts of leucogabbronorite, hornblendite and granodiorite.

The TLS is a composite intrusion and contains four main zones (Zones I- IV). Layering features (physical and chemical) of the suite reflect the complex interaction of several magma chamber processes including magma replenishment with or without subsequent mixing of newly introduced and residual magmas, in situ crystallization, current deposition and postcumulus/subsolidus modifications. Effects and consequences of these processes vary from place to place within the suite.

Two distinct magma compositions have been recognized in the TLS (quartz-tholeiitic, Zones I-III and olivine-tholeiitic, Zone IV). The interrelationship between silica-saturated and silica-oversaturated magma types is attributed to differences in pressure of partial melting of the same or similar source material(s). Variation in water pressure and silica activity are significant parameters controlling the sequence of

crystallization within the suite.

The TLS shows slight to strong LREE enrichment relative to HREE and significant negative Nb-anomalies. There is significant ϵ_{Nd} variation within the suite from -0.1 to +5.1 (at 420 Ma) and much of the range of this heterogeneity appears to have existed before emplacement of magma batches into the chamber which suggests crustal contamination prior to intrusion.

The FS and W-SCS are geochemically and isotopically distinct, temporally unrelated, high-level granitoid intrusions. The FS has been dated at 420 $\pm$2 Ma and is a C-type, metaluminous granitoid body. It typically displays: i) LREE enrichment relative to HREE with flat $HREE_N$ patterns; ii) negative Eu- and Nb- anomalies; and iv) relatively positive ϵ_{Nd} values (-1.0 to +1.3). The FS is interpreted to have been mainly derived from lower crustal material.

The W-SCS has been dated at 408 $\pm$2 Ma and is an H-type, metaluminous, composite intrusion. It contains three distinct units: the **Pigeon Island Unit**-hornblendite; the **Sandy Unit**-leucocratic gabbronorite; and the **Wild Unit** - quartz diorite, tonalite and minor granodiorite. The suite is characterized by i) LREE enrichment relative to HREE with steeply sloping REE_N patterns; ii) no notable Eu-anomalies; iii) significant negative Nb- anomalies; and iv) a wide range of Nd isotopic compositions (+0.3 to +3.2).

The Wild Unit dominates the W-SCS and typically contains various types of mafic-intermediate dykes, microgranular enclaves and country-rock xenoliths. Magma mixing and mingling processes between mantle-derived mafic and lower crust-derived felsic magmas played important roles in the evolution of the Wild Unit.

The proposed petrogenetic model envisages that the TLS, the FS and the W-SCS are the products of the same mechanism, *i.e.* mafic magma underplating the lower crust.

Each suite represents a significantly different mode of interaction between mafic magmas and the lower crust. The mode of such interactions varies from mass transfer (*i.e.* crustal contamination- the TLS) → heat transfer ± minor mass transfer (crustal anatexis with or without a minor contribution from mantle-derived mafic magma- the FS)→ to both mass and heat transfer (magma mixing and mingling- the W-SCS).

ACKNOWLEDGEMENTS

I am most grateful to my primary supervisor, Dr. J. Malpas, for his supervision and continuous encouragement. Without his support, this thesis would not have been possible. I am thankful to Dr. G. Jenner, my other supervisor, who provided productive criticism and discussion during the preparation of the manuscript.

I am indebted to Dr. G. Dunning whose enthusiasm for the project and generosity with the use of his laboratory facility made U-Pb dating possible. I would like to extend my thanks to Dr. D. Wilton for his encouragement.

I thankfully acknowledge the individuals who have helped during this project in various ways: P. Horan, C. Collins, J. Brydie, J. Buckle, N. Fagan, S. Dunsworth, D. Williams, L. Jurnaliah, S. Awadallah, A. Mahgoub, and the lapidary shop personnel.

I am grateful to my husband, A. Aydın, for his continuous encouragement and support throughout our times as students. I am also thankful to my mother, S. Düzgören, for her patience during my long absence abroad.

Financial support was provided by NSERC operating grants to Drs. J. Malpas and G.Jenner and by Memorial University of Newfoundland (Graduate student fellowship). Dr. D. Wilton provided partial financial support at the beginning of my program.

I dedicate this thesis to my late father, Latif Düzgören.

TABLE OF CONTENTS

LIST OF FIGURES

(Figures appear at the end of each chapter)

LIST OF TABLES

(Some of the following tables are also provided on disk in the map pocket)
(Tables appear at the end of each chapter)

LIST OF PLATES

LIST OF ABBREVIATIONS

A/NK	molar ratio (Al_2O_3/ Na_2O+ K_2O)
A/CNK	molar ratio (Al_2O_3/CaO+ Na_2O+ K_2O)
Ab	albite; molecular % = (Na/ (Ca+Na+K))x 100
adC	adcumulate
AFM	Na_2O + K_2O - FeO_{total} - MgO
amp	amphibole
An	anorthite; molecular % = (Ca/ (Ca+Na+K))x 100
ap	apatite
bt	biotite
°C	degree Celsius
CHUR	Chondritic Uniform Reservoir
cm	centimeter
cum	cumulate
cpx	clinopyroxene
dl	detection limit
En	enstatite; molecular % = (Mg/(Mg+Fe^{+2}+Ca))x 100, all Fe as Fe^{+2}
Enc	microgranular enclave
FIB	Fogo Island Batholith
FS	Fogo Suite
ga	garnet
hbl	hornblende
HREE	heavy rare earth element(s)
Hy	hypersthene
ICP-MS	inductively coupled plasma-mass spectrometer
il	ilmenite
kbar	kilobar
k-fd	K-feldspar
km	kilometer
L	liquid
LREE	light rare earth element(s)
LC	lower crust
mesoC	mesocumulate
metased	hornfelsic volcano-sedimentary rocks
mg	magnetite
Mg# or X_{Mg}	mol (Mg/(Mg+Fe^{+2}))
mm	millimeter
NA	not applicable

NE	North East
Nfld	Newfoundland
NNE	North north-east
orthoC	orthocumulate
ol	olivine
opx	orthopyroxene
url	uralite
P	pressure
pc	postcumulus
pk	poikilitic
plg	plagioclase
P. Loc	point location
PM	Primitive Mantle
pseud	pseudomorphic
PU	Pigeon Island Unit
ppb	parts per billion
ppm	parts per million
px	pyroxene
REE	rare earth element(s)
REE_N	chondrite normalized rare earth element(s)
QAP	Quartz- Alkali feldspar - Plagioclase
qtz	quartz
s	Sulphide minerals (pyrite and chalcopyrite
SCR	Supracrustal rocks
sem	standard error mean
SU	Sandy Unit
src	sericite
srp	serpentine
SSW	South south-west
T	Temperature
TLS	Tilting Layered Suite
trc	trace
UC	upper crust
wo	Wollastonite; molecular % = (Ca/(Mg+Fe^{+2}+Ca))x 100, all Fe as Fe^{+2}
W-SCS	Wild-Sandy Cove Suite
wt %	weight per cent
WU	Wild Unit

CHAPTER 1

INTRODUCTION

1.1 INTRODUCTION

Close spatial and temporal relationships exist between mafic and felsic rocks seen in composite igneous intrusions- *e.g.* the Appin district, western Scotland (Hamidullah and Bowes, 1987); the Coastal Maine magmatic province (Hogan and Sinha, 1989); the Chilliwack batholith, north Cascades (Tepper et al.,1993); the Variscan batholith of Corsica (Cocherie et al., 1994); and the Sierra Nevada batholith, California (Pickett and Saleeby, 1994). A significant problem in igneous petrology is to understand the processes involved in interactions between the mantle-derived mafic melts and crustal-derived (or evolved) silicic melts in these occurrences (Watson and Jurewicz, 1984; Huppert and Sparks, 1985; 1988; Sinigoi et al., 1991; van der Laan and Wyllie, 1993; Wiebe, 1994). To define the numerous aspects of such relationships requires a combination of field, geochemical and isotopic investigations.

The close relationships between mafic and felsic rocks seen in composite plutons suggest three main processes in which:

a) a mantle-derived component, now represented by the mafic rocks, supplies thermal energy to melt pre-existing crust (*e.g.* Pitcher, 1987; Huppert and Sparks, 1988) giving rise to the felsic portion;

b) differentiation of the mafic mantle-derived magma either by crystal fractionation or more complex fluid dynamic controlled processes (*i.e.* convective fractionation, Huppert and Sparks, 1984) produces felsic rocks (*e.g.* Turner et al., 1992); or

c) a mantle-derived component is an integral part of the compositional spectrum observed which itself is produced by either assimilation or magma mixing, or a

combination of both (*e.g.* Frost and Mahood, 1987; Barbarin and Didier, 1992; Wiebe, 1994).

Siluro-Devonian magmatism in the Appalachian-Caledonian orogen is typically characterized by composite mafic-felsic plutonic rocks (*e.g.* Williams et al., 1989; Bevier and Whalen, 1990; Dunning et al., 1990a). In central Newfoundland these composite bodies, including the Mount Peyton, Hodges Hill and Fogo Island batholiths, make up a significant portion of the exposed bedrock, and provide potential target areas to study the evolution of Siluro-Devonian magmatism in central Newfoundland. Among them, the Fogo Island Batholith (FIB), where primitive, layered mafic rocks occur together with granitoid rocks, is perhaps the best example in which to examine various aspects of interactions outlined above. Furthermore, relatively well-exposed mafic layered rocks in the Tilting area of Fogo Island provide a window into mafic magma chamber processes. Thus, in Fogo we have two independent perspectives on Siluro-Devonian magmatism in the Appalachian-Caledonian orogen.

The principal goal of this study is to develop petrogenetic constraints on the origin and evolution of the FIB. This involves:

a) characterization of the mafic and felsic components of the FIB within the study area in terms of their field relationships, age, petrography, geochemistry and isotopic composition; and

b) elucidation of the constraints on the chemical evolution of mafic and felsic magma-chamber systems.

Specific attention will be paid to the identification and description of:

a) the diversity of plutonic rocks;

b) the layering characteristics of the mafic rocks; and

c) the relationships between dykes, enclaves and the granitoid rocks.

1.2 THESIS OUTLINE

This thesis reports the results of a combined field, petrographic, geochemical and isotopic study of the mafic and felsic rocks of the FIB and contains four parts.

a) Following 1.1 and 1.2, section 1.3 of this chapter establishes the general geological background which involves a brief review of: a) the regional geology and tectonic setting of the Newfoundland Appalachians; b) the geology of Fogo Island; and c) previous studies. It also introduces new magmatic/stratigraphic sections and a revised nomenclature for rocks of the area.

b) Chapters 2 and 3 examine the mafic rocks of the study area - the Tilting Layered Suite (TLS). Chapter 2 presents field and petrographic characteristics of the TLS and constructs a fundamental framework into which geochemical, isotopic and petrogenetic arguments can be fitted. Chapter 3 introduces whole-rock major, trace, REE and Nd isotopic characteristics and mineral chemistry of the TLS, and discusses geochemical constraints on magma chamber processes.

c) Chapters 4 and 5 focus on the granitoid rocks- the Fogo Suite (FS) and the Wild-Sandy Cove Suite (W-SCS), and associated rocks including dykes, microgranular enclaves and country-rock xenoliths. Chapter 4 presents field and petrographic features of the granitoid suites and associated rocks and provides a framework for geochemical studies. Chapter 5 introduces the absolute chronology of the FS and the W-SCS and discusses the significance of U-Pb results on both the local and regional scales. This chapter also outlines whole-rock geochemical and Nd isotopic characteristics of the granitoid and associated rocks and discusses the geochemical evolution of the granitoid suites.

d) Chapter 6 integrates the physical, geochemical and isotopic data for the

plutonic rocks of the study area (the TLS, the FS and the W-SCS) and proposes an internally consistent petrogenetic model. Chapter 7 summarizes the thesis.

Appendices 1-9 contain modal analyses, geochemical data, sample preparation procedure, analytical techniques, sample location map and trace element normalizing values used in this study. Figures and tables are located at the end of each respective chapters.

1.3 GENERAL GEOLOGICAL BACKGROUND

The following sections: a) briefly review the regional geology and tectonic setting of the Newfoundland Appalachians; b) outline the geology of Fogo Island and summarize previous studies; and c) present the basis for the subdivision of plutonic rocks in the study area.

1.3.1 Regional geological setting

The study area is located on the northeast corner of Fogo Island, NE Newfoundland (Figure 1.1). Newfoundland lies at the centre of the Appalachian-Caledonian orogenic belt which records the Late Precambrian to mid-Palaeozoic formation and destruction of the Proto-Atlantic or Iapetus Ocean (Wilson, 1966; Harland and Gayer, 1972). Rocks of the Newfoundland Appalachians have been divided into four major tectonostratigraphic zones on the basis of contrasting early Palaeozoic and older rocks (Williams, 1979, Figure 1.1). These are from west to east: the Humber Zone - ancient continental margin of North America or Laurentia; the Dunnage Zone - arc and back-arc basin volcano-sedimentary sequences formed within and along the margins of the Iapetus Ocean; the Gander Zone - inferred continental margin sequence to Gondwana; and the Avalon Zone - a Gondwanan terrane of Pan-African affinity (Williams, 1979; O'Brien et al., 1983).

The allochthonous Dunnage Zone (Colman-Sadd and Swinden, 1984) has also been further subdivided into the Notre Dame and Exploits subzones based on a variety of geological contrasts between rock groups including stratigraphy, lithology, structure, fauna, plutonism, and geophysical signature (Williams et al., 1988).

Plutonic rocks, mainly granitoids, which range in age from middle Proterozoic to upper Palaeozoic, make up about 30% of the bedrock of the Newfoundland Appalachians and occur in all tectonostratigraphic zones (Figure 1.1). In central Newfoundland, composite mafic-felsic Siluro-Devonian plutons, including the Mount Peyton, Hodges Hill and Fogo Island batholiths, are particularly common and have been classified as Mt. Peyton type (Williams et al., 1989). These composite plutons may have a correlative in the Scottish Caledonides, *i.e.* the "Appinite Suite" (*e.g.* Dunning et al., 1990a; Rogers and Dunning, 1991).

1.3.2 Geology of Fogo Island and review of previous studies

Fogo Island lies within the confines of the Exploits Subzone (Figure 1.1) and is composed of volcano-sedimentary rock sequences, intruded by plutonic rocks (Williams, 1957; Baird, 1958). A number of possible stratigraphic successions have been proposed for Fogo Island and the surrounding area (Baird, 1958; Eastler, 1969; Williams et al., 1993a; b), but as schematically outlined in Table 1.1, the subdivisions, nomenclature and relationships between rock groups on Fogo Island, as well as NE Newfoundland, are somewhat enigmatic and incomplete. Therefore, a simplified stratigraphic succession for the rocks of the island is introduced here to provide a clear framework for further presentations in this thesis (Table 1.1). The following sections briefly summarize the previous work of other geoscientists on Fogo Island and explain the rationale behind this proposed stratigraphic succession.

Preliminary reconnaissance surveys of Fogo Island were carried out by Jukes (1843), Murray and Howley (1881) and Twenhofel and Shrock (1937). However, the only comprehensive geological map of the island was prepared by Baird (1958) as part of Geological Survey of Canada Memoir 301. In this memoir, the volcano-sedimentary rocks of Fogo Island were defined as the Fogo Harbour and Brimstone Head formations, both part of the Ordovician Fogo Group, whereas the plutonic rocks of the island were defined as the Fogo Island Granite Batholith and Gabbro-Diorite Complex, *i.e.* the granitic and non-granitic rocks, respectively (Baird, 1958). However, since then the terminology and definition of the rock groups have been changed drastically.

During this study, the new stratigraphic succession of Williams (1993a; b) for middle Palaeozoic rocks of the northeast coast of Newfoundland has been utilized (Table 1.1). In this recent review, Williams (1993b) considered all volcano-sedimentary rocks of Fogo Island to be part of the revised Silurian Botwood Group.

Similarly, the terminology and definition of the plutonic rocks of Fogo Island have been subject to significant modification in the past 50 years. The granitic rocks of the island were informally renamed the Fogo Batholith and correlated with the Mount Peyton Batholith by Strong and Dickson (1978). In their recent review of granites and related rocks in Newfoundland, Williams et al. (1989) informally redefined the Fogo Island Batholith (FIB) as a composite mafic-felsic pluton and included the non-granitic plutonic rocks as well as granitic rocks of the island. They also included the FIB within the Siluro-Devonian Mt. Peyton-type category (Figure 1.1). In the present study, the term FIB is used to refer to all plutonic rocks of the island, as defined by Williams et al. (1989), and includes early mafic and late felsic phases.

There are only a few relatively detailed studies of the FIB. Although granites and

granodiorites dominate its geology, the only petrological study on granitoid rocks was carried out by Sandeman (1985) as a B.Sc. thesis. In this study, he proposed a petrogenetic link through fractional crystallization for the various silicic igneous units exposed on the western part of the island. Sandeman and Malpas (1995) documented geochemical characteristics of the granitic rocks of the western part of the island and argued against the direct correlation of the FIB with the Mount Peyton Batholith.

Mafic rocks occur in the southern and northern part of Fogo Island and comprise approximately 30% of the exposure. These two geographically separate mafic bodies are both characterized by locally well-developed igneous layering, but a linkage between them has not been established. The small mafic exposure in and around the community of Tilting, where the most primitive mafic rocks occur together with granites, has been the subject of three previous investigations, carried out by Williams (1957), Cawthorn (1978) and Saunders (1990).

Williams (1957), in his M.Sc. thesis, provided the fundamental geological background, defined the non-granitic rocks of the area as the Tilting Igneous Complex, and first recorded the layered nature of the mafic rocks. In his study, he also recognized three petrographically different granitic rocks including: i) alaskite-type granite; ii) granophyric "normal granite"; and iii) granodiorite and quartz diorite.

Cawthorn (1978) built on the work of Williams (1957), informally changing the name of the same body to the Tilting Harbour Igneous Complex and presenting some petrographic and geochemical data. He recognized two distinct mafic rock associations as "magnetite-free" and "magnetite-bearing" and developed a petrogenetic model proposing the existence of two different magma types to account for them: i) an older magma which gave rise to the "magnetite-free" rocks; and ii) younger magma which produced "magnetite-bearing" rocks. Chemical compositions of the host granitic rocks

led Cawthorn (1978) to suggest that they are not genetically linked to the mafic rocks. In this study, however, he was considering only that the granitic rocks may represent extreme differentiates of the mafic magmas.

Recently Saunders (1990) studied the same area as part of a B.Sc. thesis. His study expanded on Cawthorn's (1978) geochemical and petrological database with additional field and petrographic descriptions and preliminary mineral chemistry.

1.3.3 Introduction to the present study

In the early phase of this study, it became apparent that available field and petrographic descriptions and the existing chemical data set were not comprehensive either in coverage or in consistency. Therefore, this study aimed at providing a sound background on which a petrogenetic model of the area might be built. The area was mapped at 1:12500 scale (Plate 1) and a new magmatic/stratigraphic succession and nomenclature proposed (Figure 1.2).

As spatially and schematically illustrated in Plate 1 and Figure 1.2 the study area contains a diverse collection of plutonic rocks. They display a range of fabrics, textures, mineralogies and compositions, but can be generally divided into three main associations on the basis of field observations, petrography and relative and absolute geochronology (Figure 1.2).

The main rock associations are:

1) **Tilting Layered Suite (TLS)** (new name) composed of layered ultramafic, mafic and intermediate rocks;

2) **Fogo Suite (FS)** (new name) dominated by monzogranite with minor amounts of granodiorite; and

3) **Wild-Sandy Cove Suite (W-SCS)** (new name) containing mainly quartz diorite and diorite with minor amounts of leucogabbronorite, hornblendite and granodiorite.

The W-SCS represents the youngest intrusion recognized within the FIB (Chapters 4 and 5) and cross-cuts the other assemblages. Contact relationships between the TLS and the FS are not clear, but in areas where the contacts are exposed the TLS appears to be older. The oldest lithology in the area consists of siliceous hornfelsic rocks which have been found as xenoliths in all younger lithologies and which are termed as "supracrustal" rocks during this study. The plutonic rocks are cut by numerous dykes which exhibit a wide range of composition from mafic to felsic.

Late faults trending east-west offset most of the plutonic rocks of the area, particularly the layered rocks, and commonly cause observable lateral dislocations (Plate 1). All lithologies typically exhibit primary igneous textures, but low temperature alteration such as sericitization, uralitization and serpentinization are common.

1.3.4 Rock nomenclature

In this study, usage of the term "**suite**" is in conformity with recommendations of the North American Stratigraphic Code (1983). The term is entirely descriptive and does not imply any genetic relationship between rock types. In addition, two systems of nomenclature have been used to describe and classify lithologies in the study area: a) the conventional Streckeisen (1976) classification; and b) that recommended by Irvine (1982) for layered intrusions. Rock names conforming to the Streckeisen classification are based on visual estimation of total modal mineralogy both in the field and from thin sections. Layered rocks with similar total modes may have quite different cumulus assemblages, thus the terminology of Irvine (1982) based on cumulus mode has also been used.

Terminology for Layered Intrusions

The terminology for layered intrusions is still a controversial subject in igneous petrology. The following sections summarize: a) some basic principles of the terminology; and b) differences between original usage and that now recommended. This summary is not meant to provide authoritative definitions, but has been designed to prevent, rather than create, argument.

The original terminology for layered igneous intrusions was proposed by Wager et al. (1960) who considered that rocks of these intrusions were **cumulates** formed by concentration of minerals by crystal settling. This concept of cumulates and cumulus processes was seriously criticised by several authors during the late 1970's (*e.g.* Campbell, 1978; McBirney and Noyes, 1979; Morse, 1979). Wager et al.'s cumulate theory fails to explain several crucial features of layered rocks, such as: why plagioclase crystals, which are less dense than their parental liquid, should settle; the presence of plagioclase-rich cumulates at the base and pyroxene-rich cumulates at the top of layers; and layers with near-vertical primary dips which have exactly the same textural features as those having very gentle dips. Criticism of the nomenclature of cumulate rocks arose because terminology was felt to be tied too firmly to petrogenetic models. Nevertheless, Irvine (1982) partly overcame these problems by redefining "cumulate" so that crystal settling is a possible but not essential process in the origin of the rocks.

In this thesis, **cumulates** are igneous rocks characterized by a framework of cumulus minerals that were somehow accumulated and concentrated through fractional crystallization (Irvine, 1982). The fractionated crystals are named "**cumulus**" crystals, and the term "**postcumulus**" refers to those minerals which have been crystallized from liquid in the interstices of the cumulus framework. Transport of the cumulus mineral to the site of deposition is not required, that is the cumulus mineral(s) can form <u>in situ</u>. The

names of the cumulates are based upon a decreasing order of abundance of cumulus minerals. The interchangeable order of two minerals is expressed by a slash diagonal between them (*e.g.* opx/cpx-plg). **Adcumulates, mesocumulates** and **orthocumulates** are terms that simply describe the present proportions of intercumulus material 0-7, 7-25, and 25-50% respectively (Irvine, 1980; Irvine, 1982).

In this thesis, the terms "**zone**" and "**subzone**" have been applied to subdivisions of layered rocks of the study area and are considered as first- and second-rank stratigraphic divisions of the layered rocks (*i.e.* a subzone is always part of a zone and a zone part of a suite, Irvine, 1982). Additionally, the term "**lamination**" has been used for a subtle planar feature, pervasive throughout a cumulate on the scale of the rock's grain size, but that does not itself define a distinctive layering plane (Irvine, 1987a).

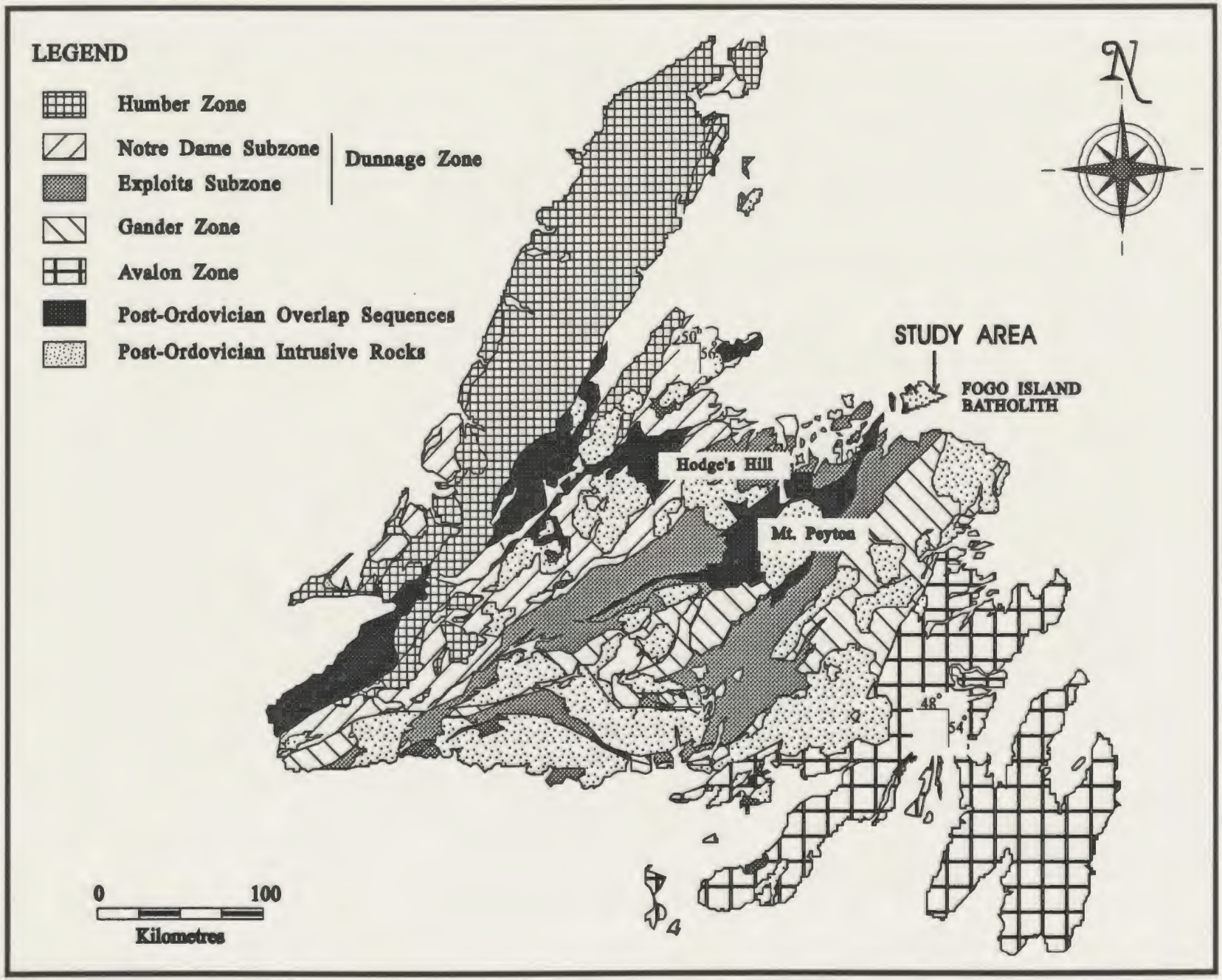

Figure 1.1 Location map and simplified tectonostratigraphic zones of Newfoundland Appalachians (after Williams, 1979).

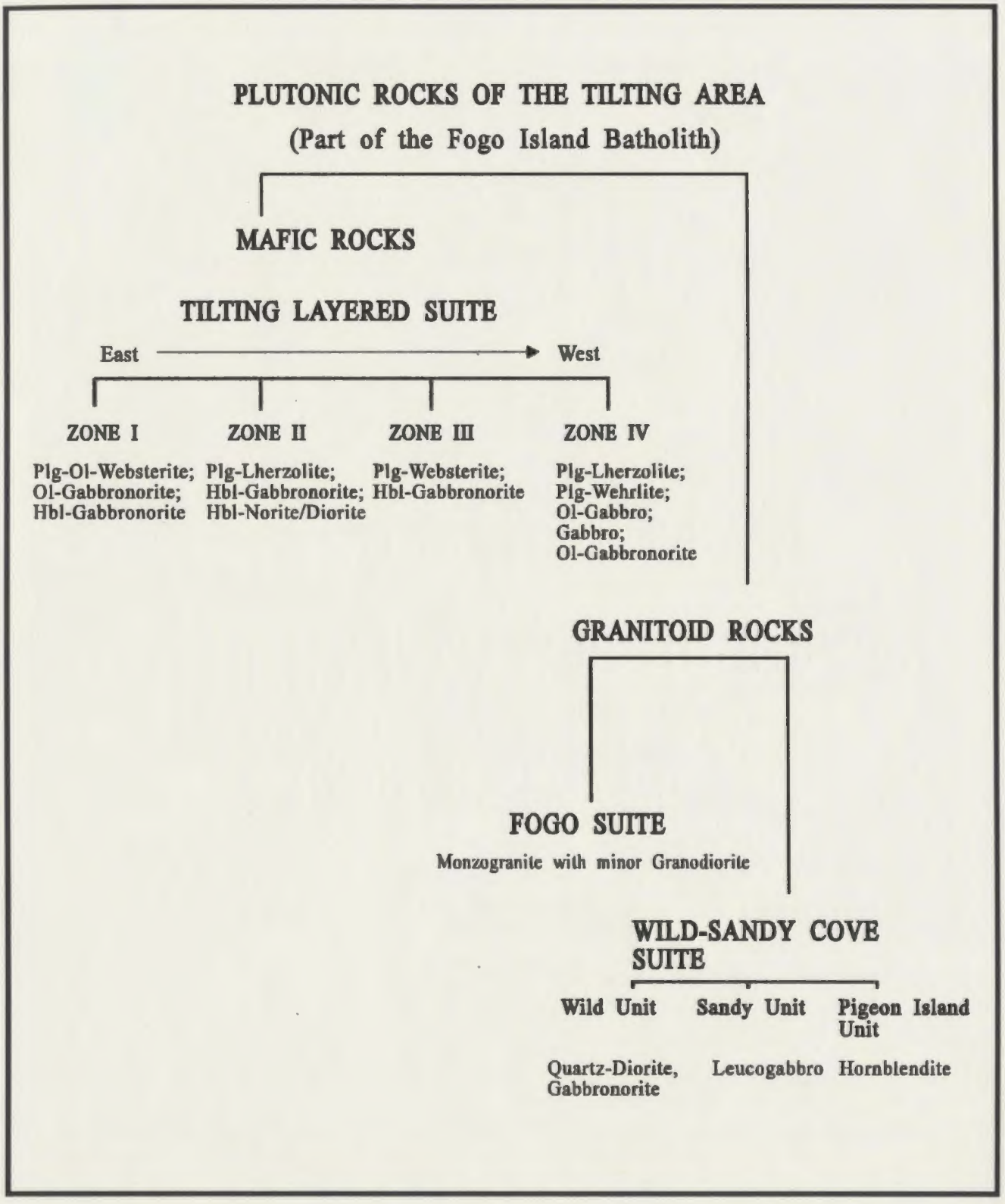

Figure 1.2 Subdivision and nomenclature of the plutonic rocks of the study area.

Table 1.1 Summary of proposed stratigraphic successions for Fogo Island and the surrounding area.

AUTHOR	Baird (1958)	Eastler (1969)	Williams (1993)	This Study
STUDY AREA	Fogo Island, Change Islands& Indian Islands	Change Islands	Northeast coast of Nfld, Change Islands, Indian Islands & western side of Fogo Island	Fogo Island
DEVONIAN	Fogo Island (Granite) Batholith Gabbro-Diorite Complex	Intrusive Rocks	Intrusive Rocks	Fogo Island Batholith
SILURIAN	Indian Islands Group	Botwood Group	Indian Islands Group Botwood Group	Not Represented Botwood Group
ORDOVICIAN	Farewell Group Fogo Group		Badger Group	Not Represented

CHAPTER 2

PHYSICAL CHARACTERISTICS OF THE TILTING LAYERED SUITE

2.1 INTRODUCTION

Most of our present understanding of mafic magma-chamber processes is based on mafic layered intrusions, as remnants of magma chambers in which the chamber processes dominate the chemical evolution of the magma and regulate the layering features of the intrusion. Spectacular and locally well-exposed igneous layering occurs in the Tilting Layered Suite (TLS) which provides a unique window into mafic magma-chamber processes during Siluro-Devonian magmatism in the Appalachian-Caledonian orogen. The TLS represents the most primitive mafic rocks occurring together with Siluro-Devonian granitoid rocks in central Newfoundland.

This chapter describes the field and petrographic features of the TLS in order to provide a fundamental framework upon which geochemical, isotopic and petrogenetic aspects of the suite can be based. In the following sections, emphasis is placed on layering characteristics of the suite. Modal analyses and nomenclature of selected samples from Zone I-IV are given in Appendix 3 (Table A3.1- A3.5).

2.2 FIELD AND PETROGRAPHIC CHARACTERISTICS OF THE TLS

The TLS underlies approximately 4 km^2 and is characterized by a wide range of layered rocks from peridotite and pyroxenite to gabbronorite, gabbro and diorite (Table 2.1). The TLS has been divided on the basis of field relations and petrography into four main zones (I to IV). Zone IV is further divided into two subzones (IVa and IVb) on the sole basis of petrography. In many places the contact relationships between the zones are

not clear due to later intrusion(s) by the Wild-Sandy Cove Suite (W-SCS) and/or Fogo Suite (FS), and poor exposure. Late east-west trending faults have affected most of the layered rocks and commonly cause observable lateral dislocation, which makes it difficult to reconstruct the magmatic stratigraphy of the suite.

The layering, *i.e.* type, mode, scale, orientation and continuity, may differ considerably from zone to zone as well as within any one zone (Table 2.1). The majority of layers throughout the TLS are uniform and planar, and dip at steep angles (about 60-70°) towards NNW (Plate 1). The present attitude of layers is attributed to tilting associated with the intrusion of the W-SCS. The stratigraphic sequence appears to young to the NNW, as originally suggested by Cawthorn (1978). Modal, textural, phase, cryptic and grain-size layering all occur, but only the first two types are common. In this chapter, cryptic layering of the TLS is not described, because of the complexity of compositional variations both within and between the zones, which require detailed explanations. Cryptic layering and whole-rock geochemical features together with Nd isotopic signatures of the TLS are presented in Chapter 3.

After a brief summary of common petrographic characteristics of the TLS, physical features of the each zone will be discussed separately.

Petrographic characteristics of the TLS

Orthopyroxene, clinopyroxene, plagioclase and olivine are the principal cumulus minerals. Orthopyroxene may exhibit very fine exsolution lamellae of clinopyroxene parallel to (100) but there is no trace of pigeonite. The principal cumulus minerals are usually euhedral to subhedral and their average grain sizes, measured from oriented thin sections, exhibit limited variation from 1 to 2 mm. Other cumulus minerals present are minor apatite (0.2-0.4 mm), only in the more differentiated rocks, and euhedral calcic hornblende (3-4 mm), only in Zone I.

The most abundant postcumulus mineral is calcic hornblende which usually exhibits brown cores and pale green rims (associated with varying Ti and Al contents). The hornblende mostly occurs as large oikocrysts (up to 1-2 cm across) or overgrowths on pyroxenes and only rarely as discrete interstitial crystals (1 mm long). The poikilitic hornblendes in places contain roughly aligned, tiny rods of opaque oxides and may engulf several euhedral-subhedral chadacrysts of pyroxene and plagioclase. Locally, chadacrysts, mostly plagioclase, tend to occur in the margins of hornblende oikocrysts (Figure 2.1). Orthopyroxene, clinopyroxene and plagioclase crystals have also been recognized as postcumulus phases. The orthopyroxene and clinopyroxene mainly appear as oikocrysts (up to 1 cm) in olivine-orthocumulates, whereas postcumulus plagioclase is quite common and occurs either as interstitial grains (1 mm long) or oikocrysts (up to 1 cm long). Other postcumulus minerals are biotite, quartz, magnetite, ilmenite, K-feldspar and sulphides, including pyrite and chalcopyrite, all appearing as discrete anhedral forms with an average size of less than 1 mm. The percentages of the postcumulus minerals vary significantly from zone to zone and locally within the same zone. For example, Zone I does not have oxides but includes up to 10% K-feldspar and quartz; while Zone IVb contains 3-10% magnetite and ilmenite, but is free of quartz and K-feldspar (see Table A1.1).

Optical zoning of minerals throughout the TLS is very common and corresponds to significant compositional variation (Chapter 3). Plagioclases are characterized by different types of zoning. Although in detail this zoning varies from one grain to another, common features are as follows: a) euhedral to subhedral cores; b) partly embayed cores; and c) isolated patchy zones consisting of optically discontinuous areas. The cores of the plagioclase grains are usually saussuritized.

Several samples display evidence of postcumulus modification and/or subsolidus

reaction including recrystallization, and reaction coronas such as: a) rims of orthopyroxene around olivine; b) symplectic intergrowths of pyroxenes and magnetite; and c) amphibole rims around pyroxenes.

2.3 ZONE I

Zone I occupies about 15% of the TLS on the eastern side of Tilting Harbour, around the Curless Point area and on the east end of Pigeon Island (Plate 1). This zone is composed of hbl-gabbronorite and plg-websterite and includes cpx-opx±hbl (Figure 2.2) opx-cpx-plg, plg-cpx-opx and minor amounts of opx-cpx-ol cumulates (Table 2.1). Rocks of Zone I are easily recognized in the field by their dark-green colour, medium/coarse-grain size and poikilitic texture.

Layers of Zone I vary in thickness from 3 cm to 3 m and can be traced for up to 20 m laterally. They usually do not exhibit lamination and may occur in tapered and lensoidal form. Typically some layers bifurcate. Layers generally dip at steep angles (about 70°) towards the NNW, *i.e.* conformably with the majority of layers throughout the TLS. However, layers around the Curless Point area, which is geographically separated from other parts of the layered suite, consistently dip 70° NNE (Plate 1). The orientation of layers in Zone I also varies significantly both on the outcrop and map scale. It is evident that the internal structure of Zone I has been severely disturbed by the intrusion(s) of the W-SCS and/or FS, and it has, therefore, proved impossible to reconstruct the magmatic stratigraphy of the zone.

Zone I displays fairly well-developed modal layering reflecting variations in bulk proportions of melanocratic (pyroxene and/or hornblende) and leucocratic (plagioclase, quartz and K-feldspar) minerals. Alternating opx-cpx-plg and plg-cpx-opx layers define modal layering and involve cumulus pyroxenes and plagioclase; whereas, modal layering

developed in opx-cpx cumulates usually contains postcumulus hornblende and plagioclase (Figure 2.3). The layering can be macrorhythmic (1-2 m) (Figure 2.4), mesorhythmic (5-70 cm) or microrhythmic (<5 cm), although the most common form is mesorhythmic. Modal variations seem to have little relation to the grain size of the cumulus phases, whereas the grain size of the poikilitic hornblende varies locally from 1-3 mm to 10-15 mm in alternating layers and therefore defines a textural layering.

Channels and finger structures have also been recognized in this zone. As illustrated in Figure 2.5, a channel structure is well defined by alternating dark and light pairs of gabbronorites and became filled and progressively levelled by younger cumulates. Finger structures apparently cut through overlying layering without any associated disruption of the planar structures (Figure 2.4).

Order of crystallization

Zone I is characterized by the early crystallization of orthopyroxene and clinopyroxene and late crystallization of plagioclase, which indicate crystallization under relatively high water pressure (Irvine, 1970; Green, 1982). Zone I typically does not contain magnetite or ilmenite, a feature which distinguishes it from the other zones of the TLS and led to its classification as "magnetite-free" rocks by Cawthorn (1978). The order of crystallization of Zone I appears to be olivine (rarely present)→ orthopyroxene→ clinopyroxene→ hornblende/plagioclase→ quartz→ K-feldspar/sulphide minerals.

2.4 ZONE II

Approximately 20% of the TLS is classified as Zone II, and is exposed on the northern part of Pigeon Island and around Tilting Harbour (Plate 1). This zone is composed of hornblende norite or diorite (An < 50) and gabbronorite (Table 2.1), and involves plg-opx±cpx and plg-ap±opx cumulates (Figure 2.6). Layers display a variety

of features including: modal lamination due to the segregation of plagioclase and hornblende; and textural lamination (Irvine, 1987a) due to the platy alignment of hornblende oikocrysts (Figure 2.7).

Layers can be traced up to 50 m laterally, and change in thickness from 2 cm to 20 m. The average thickness of melanocratic layers decreases higher in the stratigraphic section. In this zone, the most common type of rhythmic layering is on a cm scale (2-20 cm) (Figure 2.8). It involves both variation in modal proportions of cumulus plagioclase and postcumulus hornblende (modal layering) and alternation of non-poikilitic and poikilitic textures (textural layering) in successive plg-opx$\pm$cpx$\pm$ap layers (Figure 2.9). Locally observed macrorhythmic modal layering (5-20 m) comprises alternations of mesocratic plg-opx$\pm$cpx and leucocratic plg-ap$\pm$opx cumulates (Figure 2.9).

Zone II alone displays locally developed modally-graded layers. These are thin (5-10 cm) and mafic minerals (orthopyroxene and/or clinopyroxene) are concentrated at their bases and plagioclase at their tops. These layers typically show sharp lower contacts and gradational (through 1-2 cm) upper contacts. Some local structural features include folded, deformed, cross-bedded and wispy discontinuous layers, truncated layer contacts and cognate xenoliths (Figure 2.10).

Order of crystallization

Zone II is characterized by relatively early formation of plagioclase and orthopyroxene indicating crystallization under relatively low water pressure compared to Zone I. The crystallization order in Zone II is orthopyroxene/ plagioclase→ clinopyroxene → apatite→ magnetite/ ilmenite → hornblende→ quartz.

2.5 ZONE III

Zone III makes up approximately 10% of the TLS and is restricted to the area around the Light House and the western end of the Pigeon Island (Plate 1). This zone is composed of websterite and gabbronorite and contains opx-cpx, opx-cpx-plg and plg-cpx-opx cumulates (Table 2.1). Rocks in this zone can easily be distinguished in the field by their relatively continuous (up to 200 m) and remarkably well-developed layering (cm to m scale, Figure 2.11). The contact between Zones II and III is sharp, and discordant where layering of Zone III truncates that of Zone II. The contact between Zone III and IV is faulted.

Zone III can be subdivided into at least three macrorhythmic units (Irvine, 1987a), each defined by repeated successions of layers displaying modal layering (Figure 2.12). Appearance of this modal layering varies greatly depending on the bulk proportion of cumulus pyroxene and plagioclase, and presence or absence of igneous lamination. The most complete macrorhythmic unit, in younging direction, begins with a melanocratic opx-cpx cumulate (up to 5 m) which is characterized by poikilitic plagioclase glomerocrysts. This level is followed by several successions of melanocratic opx-cpx-plg and leucocratic plg-cpx-opx cumulate pairs on a 5-20 cm scale. These successions constitute micro-mesorhythmic modal layering. The unit ends with macrorhythmic modal layering which comprises a few alternations of thick (2-5 m) melano-mesocratic opx-cpx/plg and leucocratic plg-cpx-opx cumulates (Figure 2.12).

This zone also exhibits textural and phase layering. Textural layering (cm scale) is defined by the alternation of cumulates with poikilitic and non-poikilitic textures (Figure 2.13), and varies in appearance, especially as the abundance, shape, grain size and type of the poikilitic minerals (including hornblende and/or plagioclase) changes. Phase layering (m scale) is recognized where opx-cpx cumulates alternate with either

opx-cpx-plg or plg-cpx-opx cumulates (Figure 2.12).

Significant locally observed features include finger structures, slump folds and deformed layers. Finger structures are recognized where websterite is overlain by gabbronorite and apparently cuts through layering without any associated disruption of the planar structures (Figure 2.14). In their present aspect, they are gravitationally stable *i.e.* denser websterite is at the bottom. The contact between the websterite and the gabbronorite is sharp. Their geometry is consistent and distance between individual fingers is regular, at approximately 5-10 cm. Additionally, some thin (3-5 cm), coarse-grained, hbl-gabbronorite dykes cross-cut the layered rocks and can be traced up to 3 m vertically. These dykes typically turn to the horizontal and become thin, apparently concordant layers. They possibly represent intercumulus liquid which is concentrated due to compaction of the cumulus pile (filter pressing, Irvine, 1980) and injected into early formed fractures in the cumulates (Butcher et al., 1985). Similar features have been recognized in the Rhum intrusion and cited as direct evidence of localized postcumulus modifications (Butcher et al., 1985). Similarly, slump folds (Figure 2.15) have commonly been interpreted as evidence for the movement of pore liquids (Brown et al., 1987). In places, layers have been deformed as a result of the impact of fallen blocks which are draped and smoothed-over by yet younger layers (Figure 2.16).

Order of crystallization

Zone III, like Zone I, is characterized by the early crystallization of orthopyroxene and clinopyroxene with respect to plagioclase suggesting crystallization under relatively high water pressure. The order of crystallization of Zone III is orthopyroxene→ clinopyroxene→ plagioclase→ magnetite/ilmenite→ hornblende→ quartz.

2.6 ZONE IV

Zone IV occupies more than 50 % of the TLS. It is composed of ol-gabbro, gabbronorite, plg-lherzolite, wehrlite and websterite, and includes plg/cpx-ol± opx and olivine cumulates (Table 2.1). This zone has been divided into two subzones (IVa and IVb) on the sole basis of petrography. Zone IVa, exposed at the eastern side of Sandy Cove (Plate 1), contains orthopyroxene grains (up to 20%) mainly as a postcumulus phase and rarely as a cumulus phase, whereas Zone IVb, on the western side of Sandy Cove, contains little postcumulus orthopyroxene (2-10 %) which is sparsely distributed (Figure 2.17).

Layers in Zone IV are typically discontinuous and can be traced laterally to a maximum of 30 m. They vary in thickness from 5-10 cm to 1-20 m. Some melanocratic layers show a decrease in thickness from 20 cm to 2-3 cm moving up-section. In places, monomineralic domains (plagioclases and/or clinopyroxenes) display textural equilibrium features (Hunter, 1987) including 120° triple junctions and straight grain boundaries (Figure 2.17). This zone displays fairly well-developed modal and phase layering. Modal layering (cm to m scale) involves cumulus plagioclase, clinopyroxene and/or olivine (Figures 2.18; 2.19). The most common modal layering is on a meter scale and is recognized where uniform, leucocratic (5-20 m) plg-cpx±ol cumulates alternate with melanocratic (5-10 m) distinctly layered cpx-plg±ol cumulates (*i.e.* intermittent layering of McBirney and Noyes, 1979).

Micro-mesorhythmic modal layering (5-20 cm) is accompanied rarely by grain-size layering in which cumulus clinopyroxene and/or plagioclase vary from 0.2 mm to 1 mm in size in alternating layers. However, there is no observable grading within the individual grain-size layers.

Alternation of olivine cumulates with either cpx-plg-ol or plg-cpx-ol cumulates

define phase layering in this zone. Phase contacts are typically sharp and discordant.

Locally, Zone IV displays a unique type of glomerocryst which is defined by a very coarse-grained, strongly altered mafic core rimmed by an outer shell of quartz and K-feldspar crystals (Figure 2.20). Rock with this texture, here called "trap texture", are easily recognized due to their mottled differential weathering and are mainly confined to the western side of Sandy Cove (Zone IVb). The shape and size of this textural feature varies from elliptical to circular with a maximum dimension of between 2 and 20 cm. The inner mafic core contains clinopyroxene, but usually replaced by actinolite and/or chlorite crystals. Apparent alignment of the texture may give a pseudo-lineated appearance to the rock (Figure 2.20) and possibly reflects the preferred orientation of fractures which controlled their development. This texture likely results from late stage build up of volatiles in the melt (*e.g.* Tepper, 1991).

Order of crystallization

The order of crystallization of Zone IV is olivine→ clinopyroxene/plagioclase→ orthopyroxene→ hornblende→ biotite. The relatively late crystallization of orthopyroxene distinguishes Zone IV from the other zones of the TLS.

2.7 VARIATION IN ORDER OF CRYSTALLIZATION WITHIN THE TLS

Every layered intrusion has its own distinctive layer sequences involving recognizable orders of crystallization and phase layering. The sequence of crystallization mainly depends on initial magma composition, prevailing pressure and temperature conditions, and periodically-developed closed and open system evolution including fractionation, magma replenishment and/or subsequent magma mixing, assimilation, and postcumulus modifications.

The TLS displays four different orders of crystallization of cumulus minerals;

in Zone I: olivine (rarely present)→ orthopyroxene → clinopyroxene→ hornblende/plagioclase;

in Zone II: orthopyroxene/plagioclase→ clinopyroxene→ apatite

in Zone III: orthopyroxene→ clinopyroxene→ plagioclase; and

in Zone IV: olivine→ clinopyroxene/plagioclase→ orthopyroxene.

Although each zone of the TLS has its own cumulate sequence, two main crystallization sequences have been recognized. The early crystallization of cumulus orthopyroxene occurs in Zones I-III and the late crystallization of cumulus orthopyroxene in Zone IV. This variation in crystallization order may indicate a change in magma composition that can be attributed to: a) the presence of at least two different primitive liquids (*e.g.* Irvine et al., 1983); b) the combined effect of magma replenishment, fractionation and wall-rock assimilation (*e.g.* Irvine, 1970); or c) a chamber occupied by magma with significant chemical and thermal gradients (*e.g.* Robins et al., 1987). However, Irvine (1970) suggested that many different crystallization paths involving olivine, orthopyroxene, clinopyroxene and plagioclase, require only slightly different initial magma compositions, but involve different water and load pressures, and CaO/Al_2O_3 and Na_2O/Al_2O_3 values.

The time of appearance of cumulus plagioclase with respect to pyroxenes and/or hornblende varies and may indicate rapidly changing water pressures. As illustrated in Figure 2.21, increasing water content in the magma not only depresses liquidus temperatures, but also significantly reduces the stability field of plagioclase (Green, 1982). In other words, whereas plagioclase might be an early-crystallizing mineral in dry systems (tholeiitic or andesitic), it crystallizes much later when water is present (Green, 1982; Hess, 1989).

Similarly, the absence of pigeonite inversion suggests that during crystallization the stability curve separating orthorhombic and monoclinic ferromagnesian pyroxenes was depressed relative to Bushveld-type crystallization, likely due to higher water pressure (*e.g.* Best and Mercy, 1967; Strong, 1979). These observations suggest that water pressure is a significant parameter controlling the sequence of crystallization within the TLS.

2.8 POSSIBLE ORIGINS OF LAYERING AND RELATED FEATURES

The origin of igneous layering has been discussed at length by a number of authors (*e.g.* Wager and Brown, 1968; Campbell, 1978; McBirney and Noyes, 1979; Huppert and Sparks, 1984; Irvine, 1987b) and it is clear that there is no single comprehensive model to explain every type observed. Instead, several different mechanisms have been proposed mainly on the basis of type and thickness of layering (*e.g.* Rice, 1981; Brandies et al., 1984; Boudreau, 1987, Maaloe, 1978; Morse, 1986).

The TLS displays modal, textural, phase and grain-size layering. Among these, modal layering is the most common and occurs both on the centimeter and meter scale. The origin of micro-mesorhythmic modal layering can be attributed to: a) deposition by magmatic density currents (Wager and Brown, 1968); b) sedimentation in a convecting magma chamber (Sparks et al., 1993); c) nucleation-controlled in situ crystallization (McBirney and Noyes, 1979, Maaloe, 1978; Brandies et al., 1984); d) microrhythmic differentiation by crystal nucleation, resorption and coarsening (Boudreau, 1987; McBirney et al., 1990); and e) interaction between non-linear mineral growth rates and the segregation of chemical components at crystallization fronts (Wang and Merino, 1993). However, the origin of macrorhythmic modal layering is less clear and might be the result of: a) crystal sorting by gravity controlled processes (Irvine, 1987b); b) a

combination of current transport and in situ crystallization (Irvine, 1987c) or sedimentation in convecting magma chambers (Sparks et al., 1993); and c) variations in crystal supply related to nucleation and growth kinematics (Parson, 1979).

The choice amongst these mechanisms of origin for the layering depends, to a large extent, on whether the crystals of each layer were transported to the site of deposition by settling or current deposition, or whether they crystallized in situ (McBirney and Noyes, 1979; Irvine, 1987c). However, the choice for each of the modal layering types in the TLS is not unique. Some general features, including non-graded layers and sharp layer contacts, may favour a process of in situ crystallization. Supporting this, small-scale textural layering is usually coupled with modal layering and may indicate a nucleation control mechanism. Similarly, locally observed lenticular and tapered layers may be the result of a process which involves in situ growth nodes and subsequent termination of further growth and coalescence into a layer (Cawthorn, 1993). However, several local features involving folded, cross-bedded and deformed layers, and truncated layer contacts, may indicate that current deposition played an important role in the formation of some layers or that these features were developed at those points where vigorous convective overturn was taking place (*e.g.* Upton, 1987). Also, channel structures may be related to localized magmatic erosion due to currents or convective overturn plus layer forming processes (Irvine, 1987b).

Phase layering involving sudden reversals to a more primitive crystallization order is usually attributed to: a) a periodic replenishment of relatively primitive magma into the magma-chamber (Brown, 1956; Wager and Brown, 1968; or b) vigorous convective overturn which brings fresh magma into the region of crystallization (*e.g.* Upton, 1987; Cawthorn, 1993). Cognate xenoliths may result from proximity to the feeder system (*e.g.* Irvine, 1987c). Important postcumulus modifications are evident as finger and slump

structures which provide significant evidence for the movement of pore liquids (*e.g.* Brown et al., 1987).

The field and petrographic studies of the TLS indicate that formation and evolution of the suite involved dynamic and complex magma-chamber processes, and the consequences of these processes varied locally.

2.9 SUMMARY

1) The TLS is a composite mafic layered intrusion and comprises four main zones. Each zone typically displays its own characteristic layering features including type, mode, scale, form, and attitude.

2) In general, layers are planar, uniform and steeply inclined (60-70° NNW). Layer contacts are sharp and concordant, and layers vary in thickness from 1-2 cm to 1-20 m.

3) Features observed locally are: variation in thickness along the strike; slump folds; deformed, wispy and modally graded layers; gradational and truncated layer contacts; finger and channel structures and cognate xenoliths.

4) Modal, textural, phase, grain-size and cryptic variation are present, although only the first two are common.

5) Although, each zone has its own characteristic order of crystallization, there are two main crystallization sequences throughout the TLS; the early crystallization of cumulus orthopyroxene occurs in Zones I to III; the late crystallization of cumulus orthopyroxene occurs in Zone IV. Variation in water pressure is likely a significant parameter controlling the sequence of crystallization within the suite.

6) From field and petrographic data, it appears that the evolution of the TLS involved complex interaction of several processes including magma replenishment, in situ crystallization, current deposition and postcumulus/subsolidus modifications.

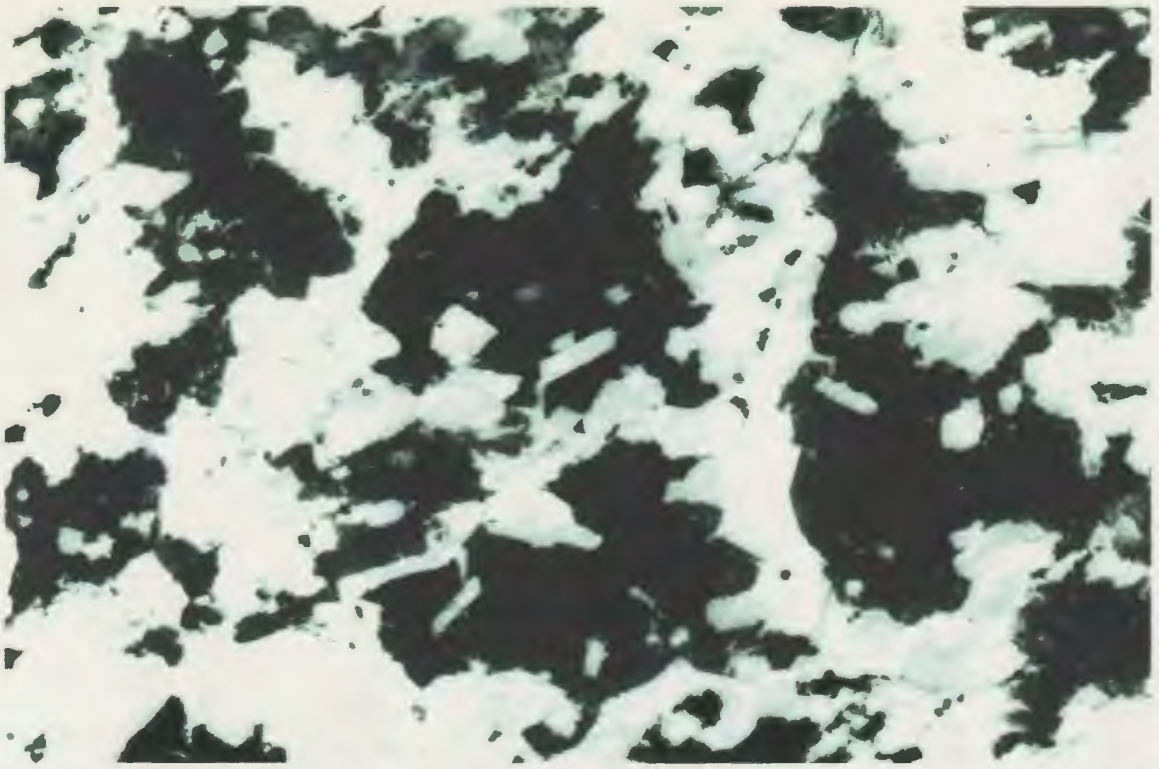

2.1 Euhedral plagioclase chadacrysts tend to occur in the margins of the hornblende oikocrysts, hbl-gabbronorite from Zone II (F-91-532). Plane polarised light; field of view: 3 cm.

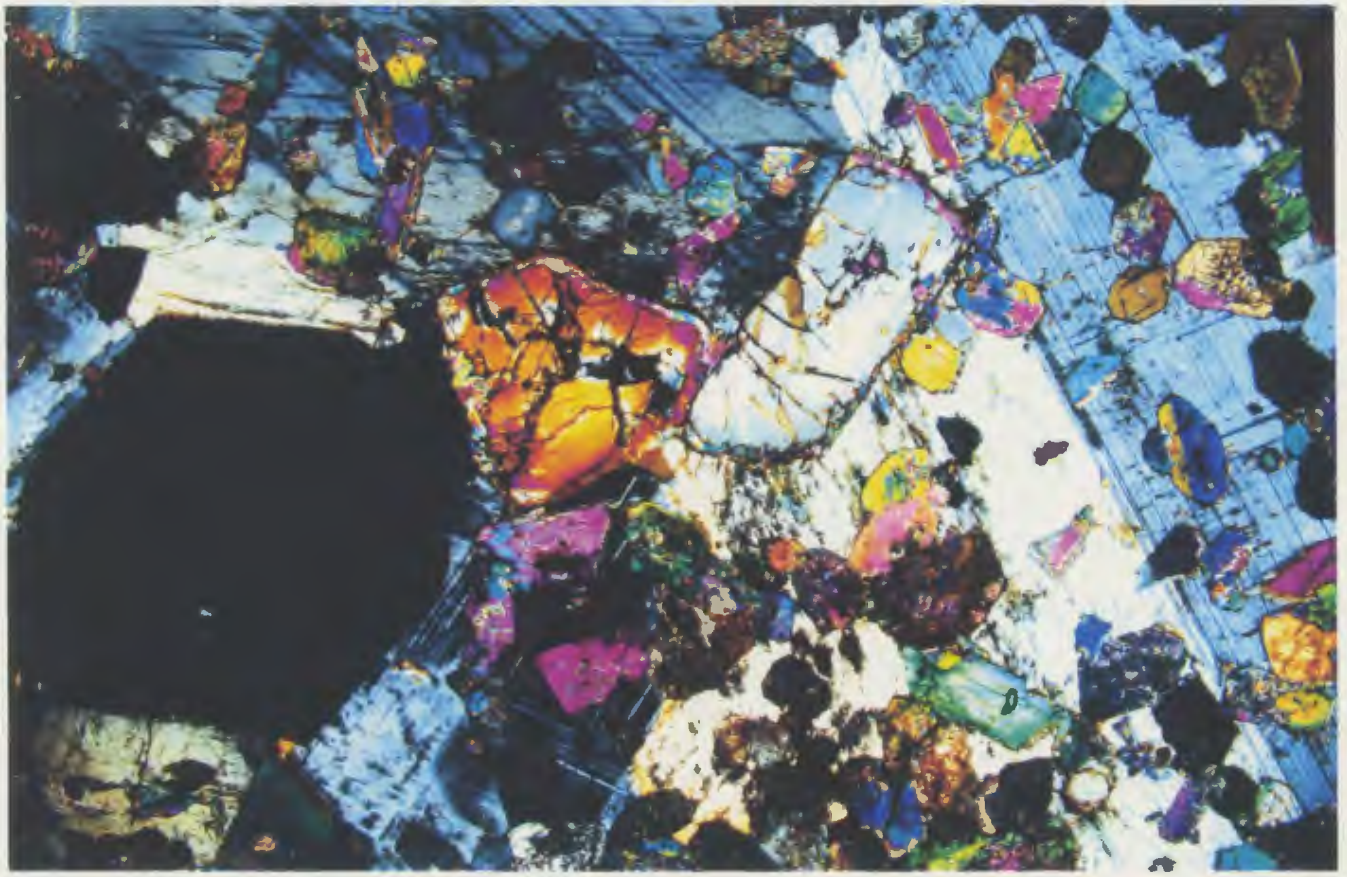

2.2 Photomicrograph of cpx-opx-hbl cumulate from Zone I (F-91-125). The poikilitic plagioclase (light matrix) engulfs euhedral hornblende, subhedral orthopyroxene and several euhedral clinopyroxenes. Note orthopyroxene pseudomorphs after olivine (centre). Crossed nicols; field of view: 14 mm.

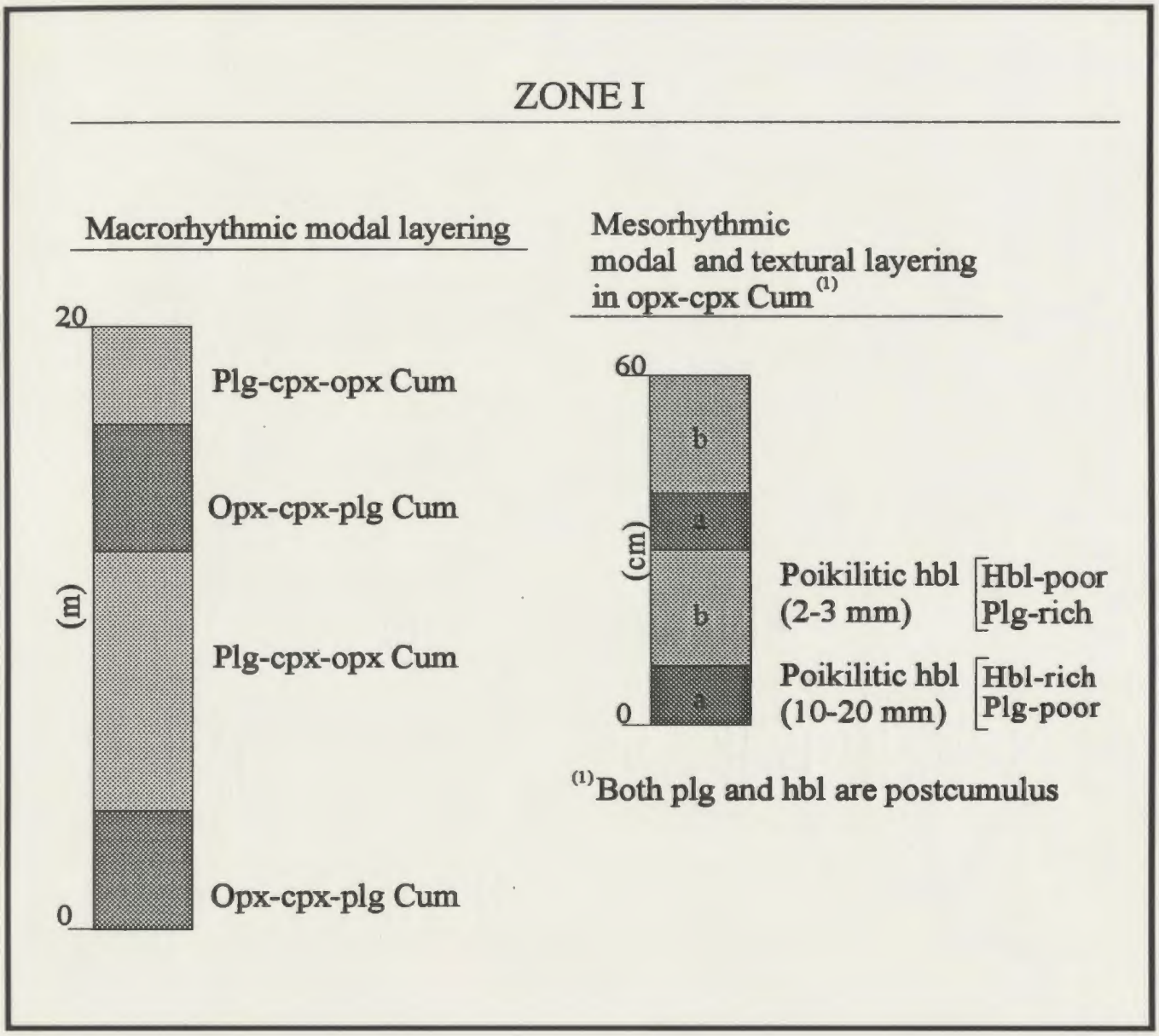

Figure 2.3 Representative layered sequences of Zone I with examples of mineral assemblages and layering types.

2.4 Alternating opx-cpx-plg (dark) and plg-cpx-opx (light) layers (macrorhythmic modal layering), Zone I. Note finger structure. Scale 30 cm.

2.5 Well developed channel structure due to alternation of leuco- and meso-gabbronorites. Note the structure is progressively filled and levelled by younger cumulates. Zone I. Scale: 30 cm.

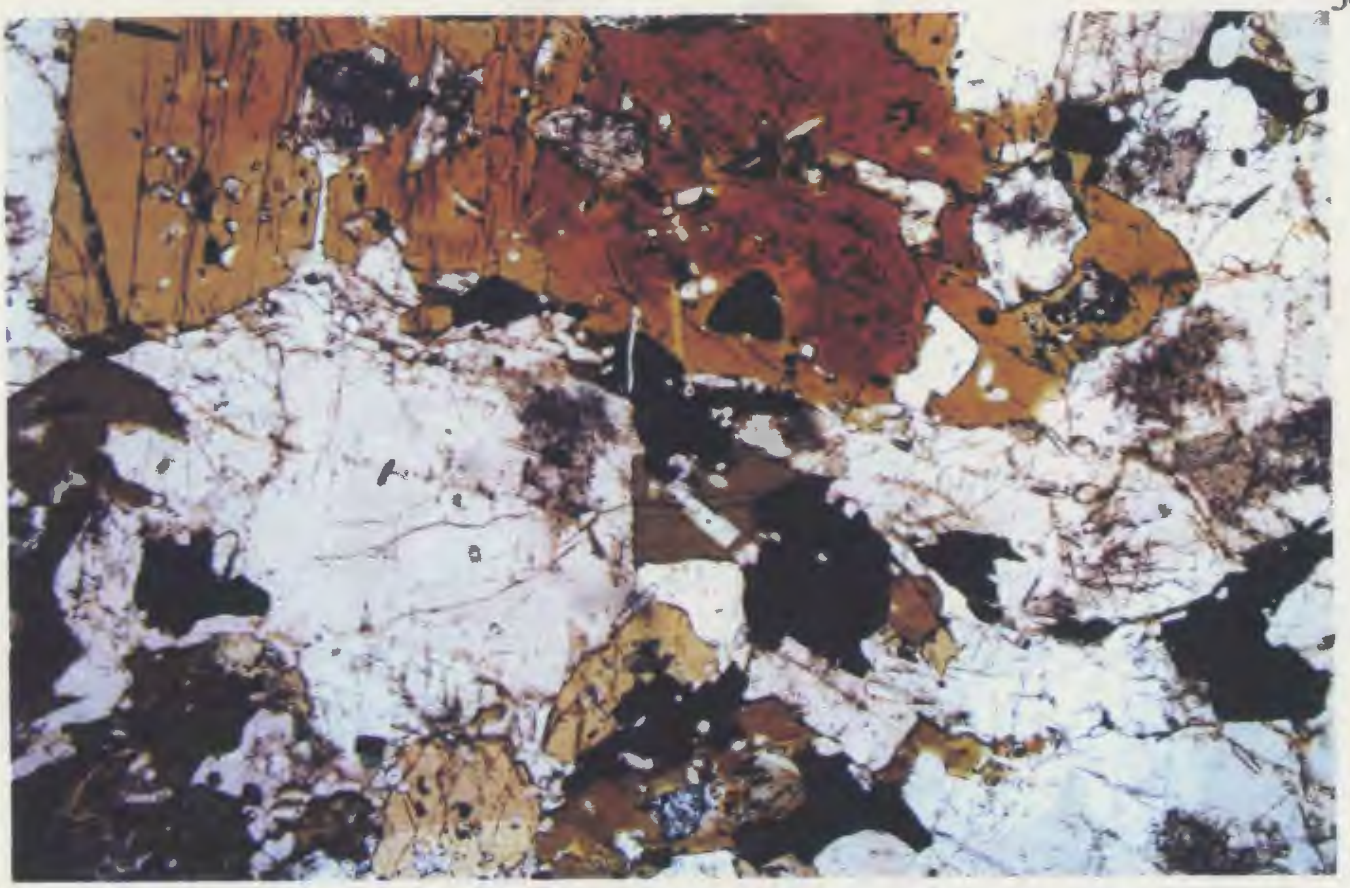

2.6 Photomicrograph of plg-opx-ap cumulate from Zone II (F-91-532). Poikilitic hornblendes include euhedral apatite, subhedral plagioclase and altered orthopyroxene. Hornblende overgrowth on orthopyroxene. Intercumulus magnetite-ilmenite (dark). Crossed nicols; field of view: 26 mm.

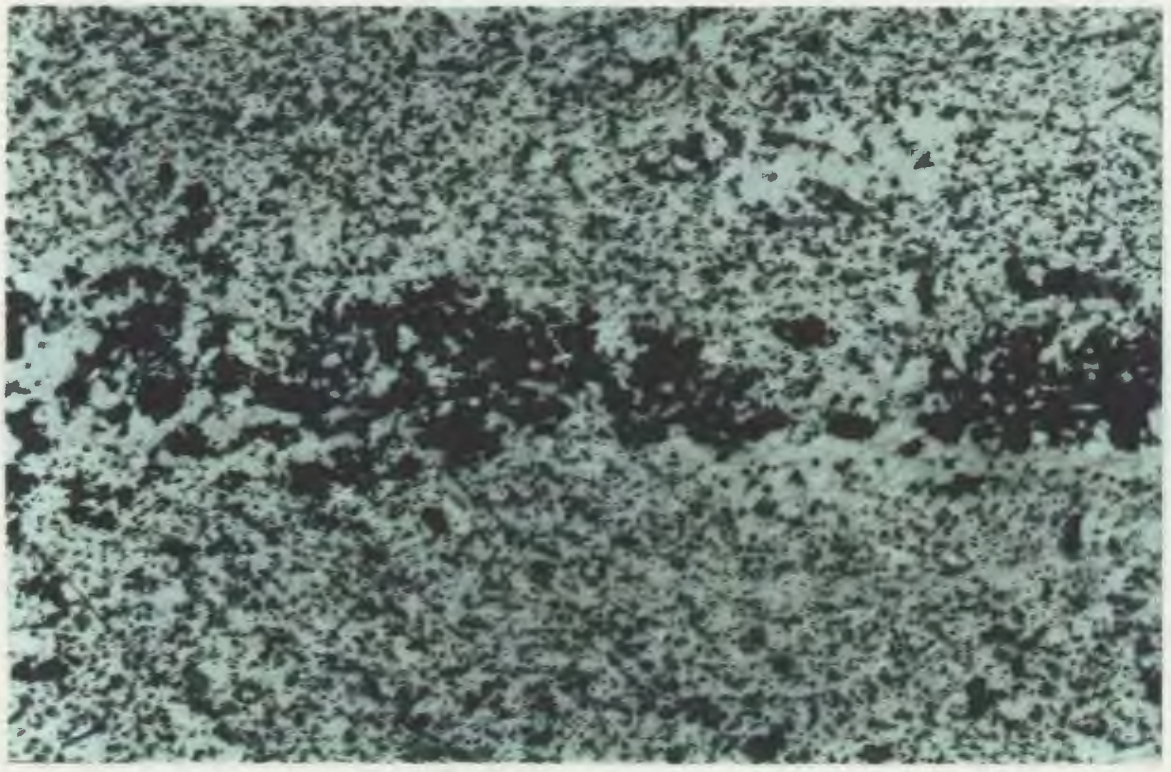

2.7 Textural lamination due to platy alignment of hornblende oikocrysts. Field of view: 3 cm.

2.8 Alternating non-poikilitic, hornblende-poor (light) and poikilitic hornblende-rich (dark) plg-opx-ap layers (left) define microrhythmic combined modal and textural layering. Note folded and truncated layers and discontinuous modal lamination. Scale: 80 cm.

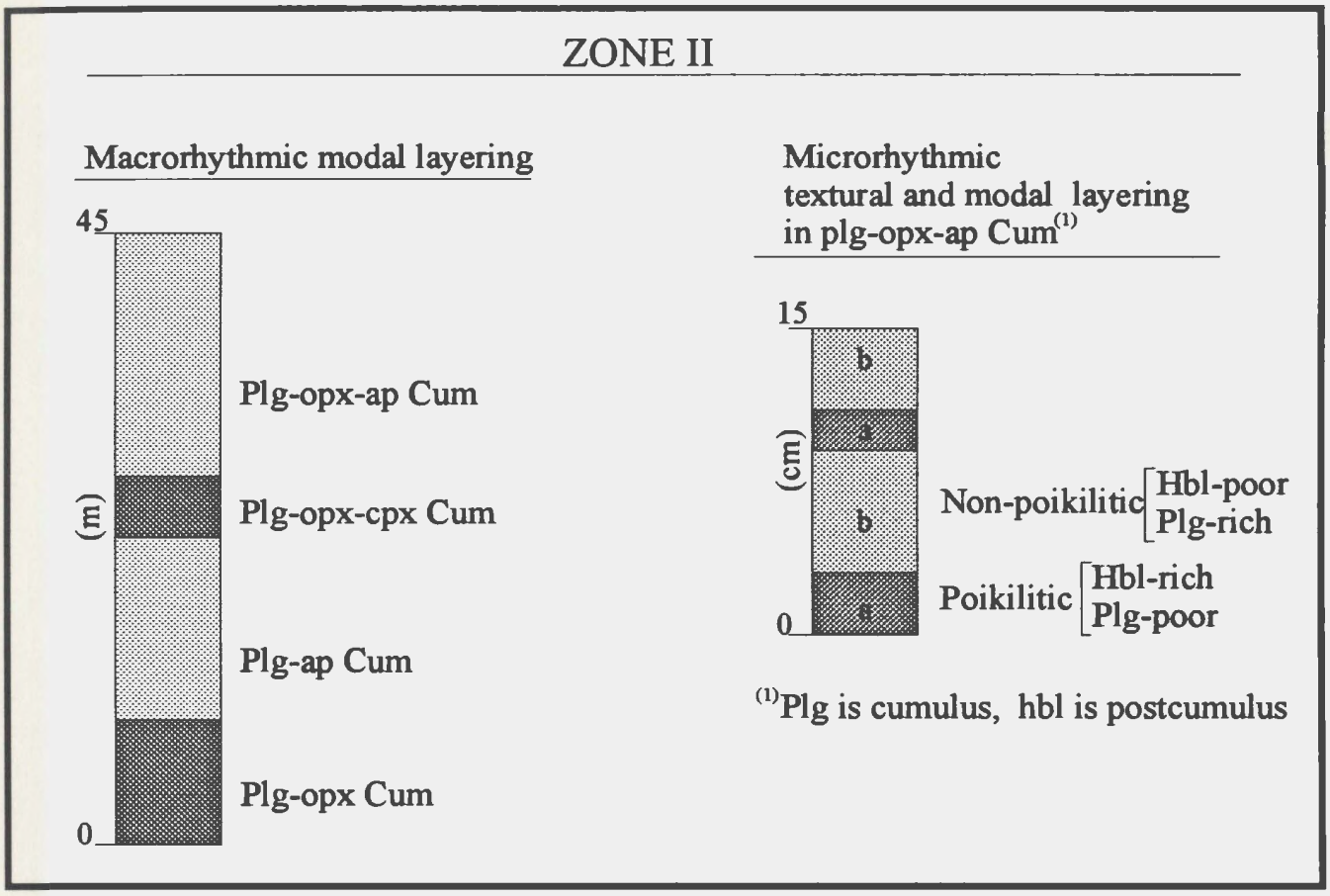

Figure 2.9 Representative layered sequences of Zone II with examples of mineral assemblages and layering types.

2.10 Cognate xenolith (dark) displays visible layering and modal lamination within deformed gabbronorites (light). Scale: 15 cm.

2.11 Well-developed modal layering from Zone III. Layers are uniform, planar and steeply inclined and layering contacts are sharp and concordant. Layering is disrupted by late faulting. (See Figure 2.12 for detailed descriptions of layering). Field of view: 30 m.

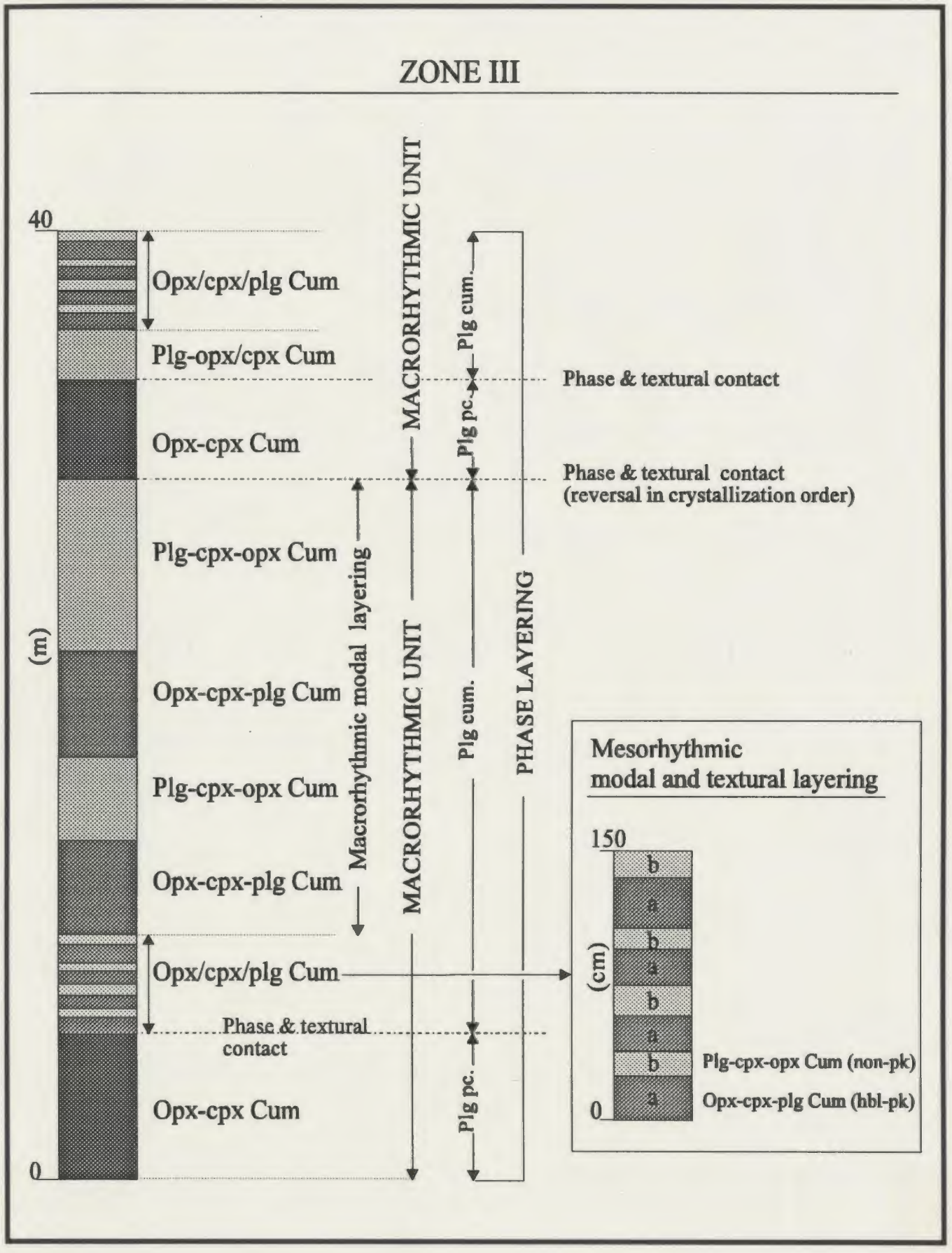

Figure 2.12 Representative layered sequences of Zone III with examples of mineral assemblages and layering types.

(a)

(b)

2.13 Distinct textural features from Zone III; field of view: 14 mm: a) Photomicrograph of opx-cpx cumulate (F-91-15) where poikilitic plagioclase glomerocryst encloses euhedral orthopyroxene and clinopyroxene chadacrysts. Crossed nicols. b) Photomicrograph of laminated plg-opx-cpx cumulate (N-19). Plane polarised light.

2.14 Well developed finger structure where websterite (dark) is overlain by gabbronorite (light). Note lack of disruption of planar features. Zone III. Scale: 15 cm.

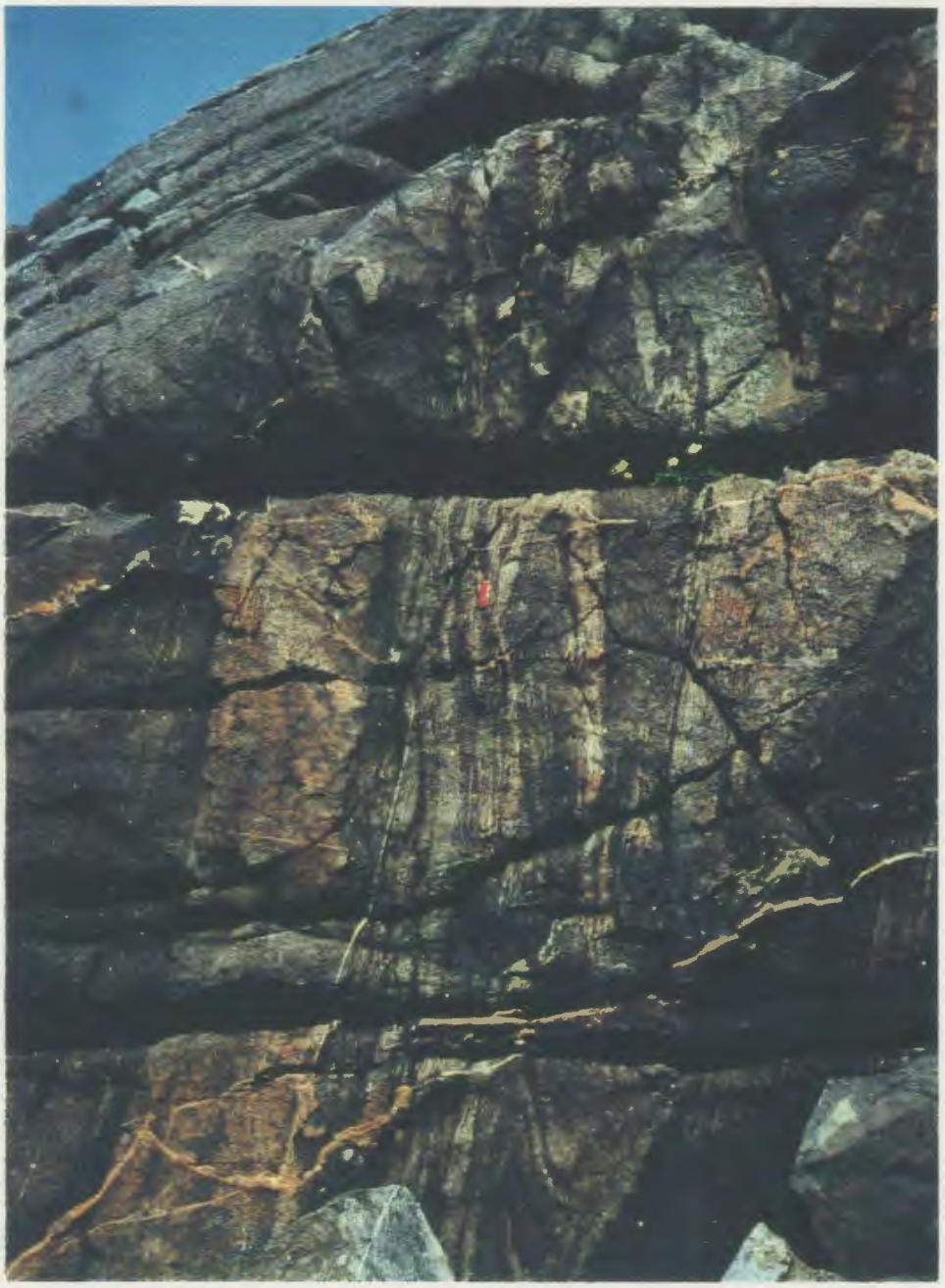

2.15 Slump folding in gabbronorites, Zone III. Field of view: 2 m.

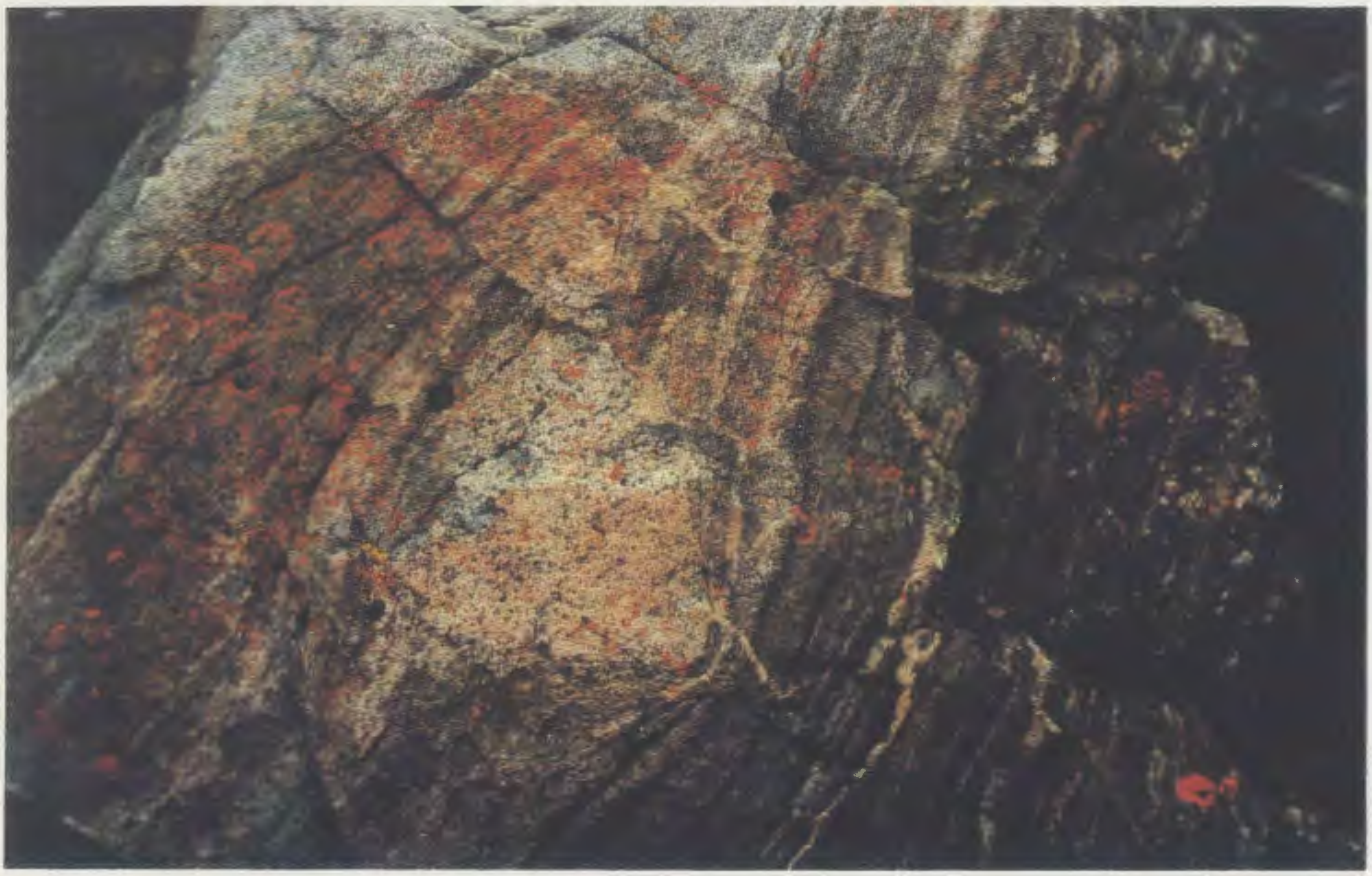

2.16 Deformed layers due to impact of fallen block. Note smoothing and draping of cumulates over the block. Field of view: 2 m.

(a)

(b)

2.17 Photomicrograph of: a) plg-cpx-opx cumulate (F-91-307), from Zone IVa; b) plg-cpx-c cumulate (F-91-50.4), from Zone IVb, note monomineralic domain (plagioclase) displays straigh grain boundaries with 120° triple junctions (centre). Crossed nicols; field of views: 14 mm.

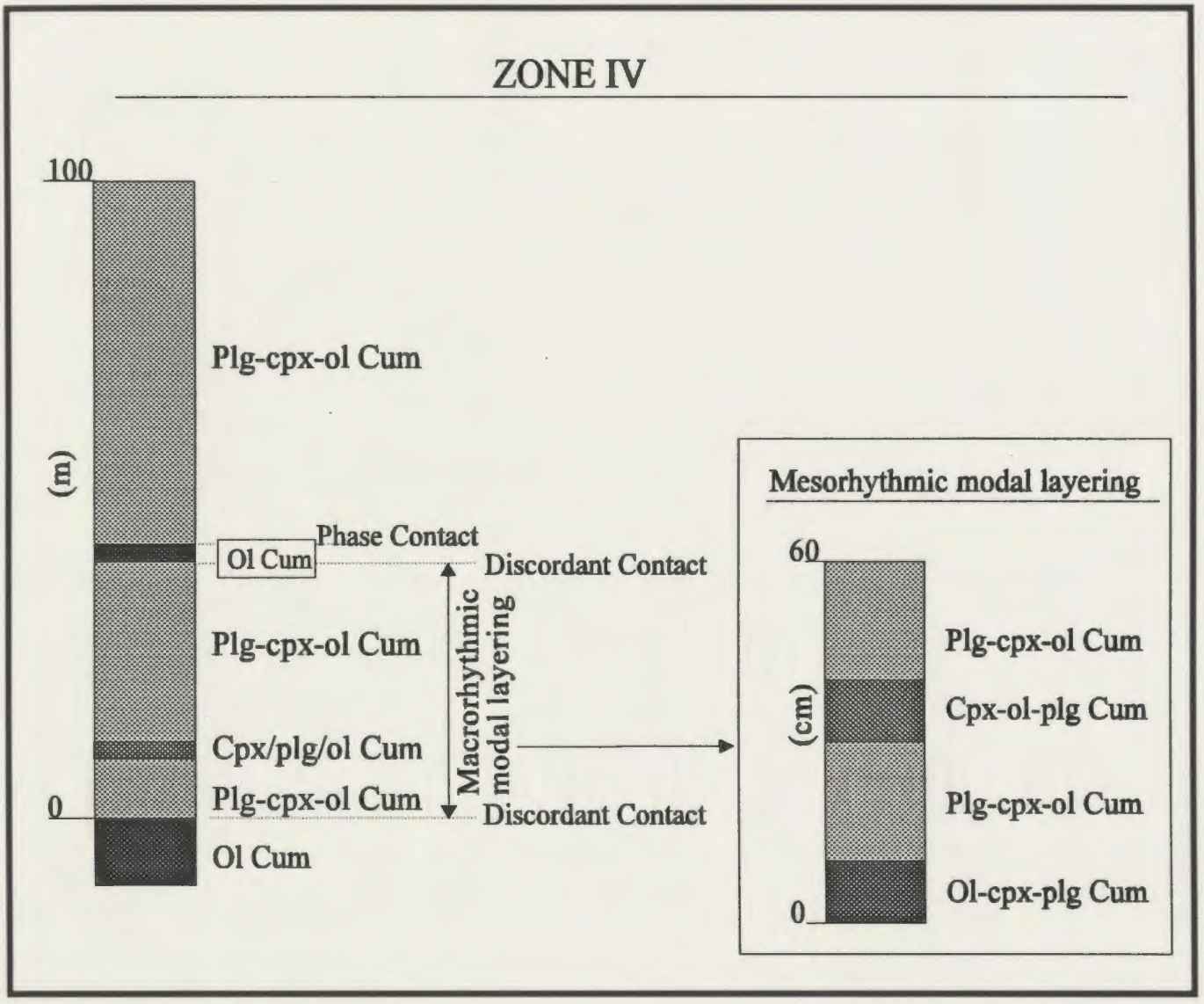

Figure 2.18 Representative layered sequences of Zone IV with examples of mineral assemblages and layering types.

2.19 Alternation of ol-cpx-plg (dark) and plg-cpx-ol (light) layers (mesorhythmic modal layering). Scale: 80 cm.

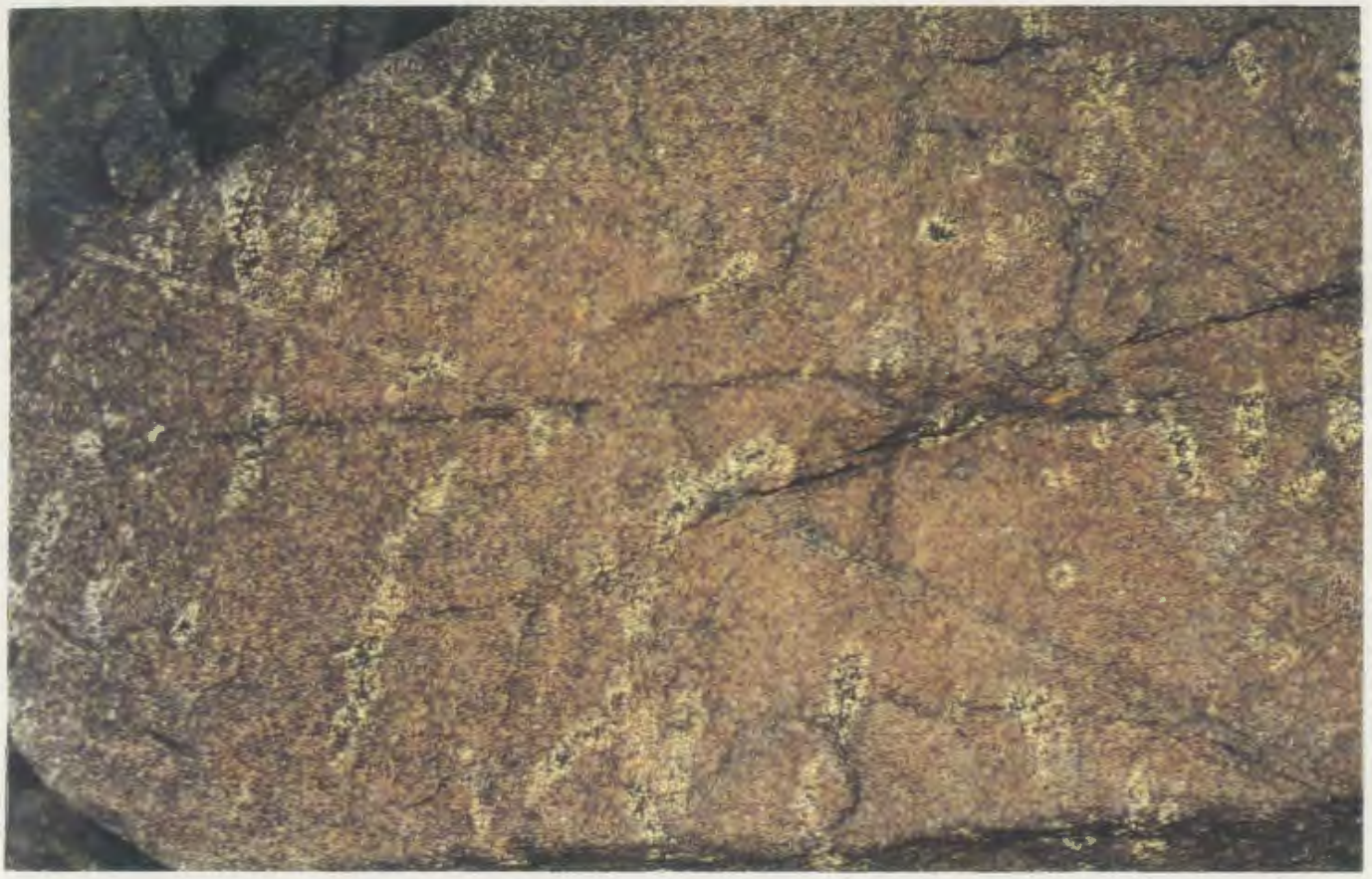

2.20 "Trap texture": coarse-grained amphibole rimmed by quartz and K-feldspar, Zone IVb. Note the apparent alignment of the texture possibly reflects preferred orientation of fractures which controlled their development. Field of view: 1 m.

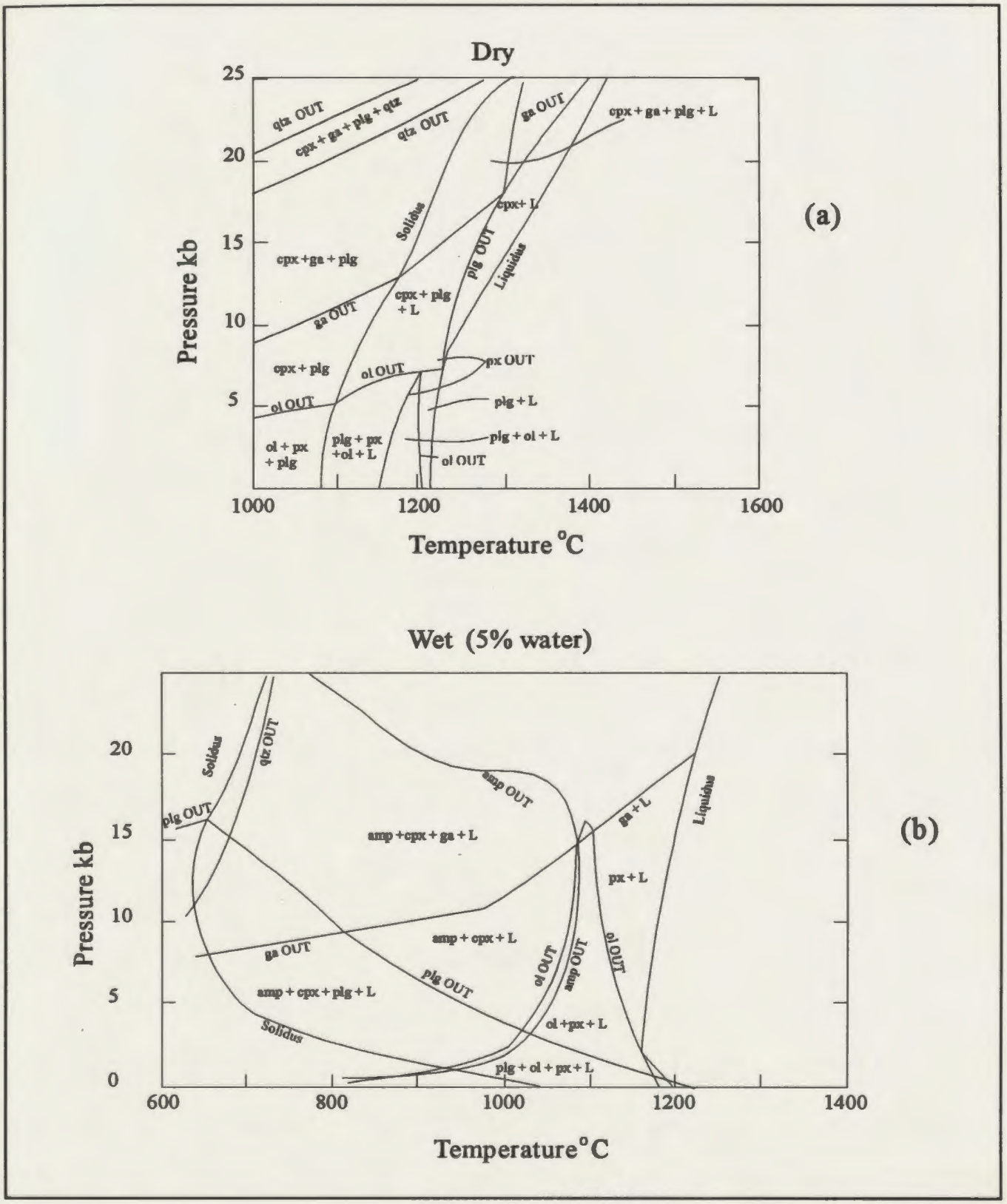

Figure 2.21 Composite P-T diagrams for dry (a) and wet (5 % water; b) tholeiitic compositions, from Green (1982). plg= plagioclase; opx= orthopyroxene; cpx= clinopyroxene; qtz= quartz; amp= amphibole; ga= garnet ;L= liquid; ol= olivine.

Table 2.1 Summary of field and petrographic characteristics of the Tilting Layered Suite.

	Zone I	Zone II	Zone III	Zone IVa	Zone IVb
Type Area	Curless Point	Pigeon Island	East-Tilting Harbour	East-Sandy Cove	West-Sandy Cove
Petrographic characteristics					
Rock Type	Hbl-Gabbronorite Plg-Websterite	Hbl-Norite/Diorite Hbl-Gabbronorite	Plg-Websterite Hbl-Gabbronorite Gabbronorite	Gabbronorite Ol-Gabbronorite Plg-Lherzolite Plg-Websterite	Ol-Gabbro; Gabbro Plg-Wehrlite Plg-Lherzolite
Cumulate Type	Cpx-opx±hbl Opx-cpx-plg Plg-cpx-opx Opx-cpx-ol	Plg-opx±cpx Plg-ap±opx	Opx-cpx Opx-cpx-plg Plg-opx-cpx	Ol; Cpx-ol Plg-cpx-ol Plg-cpx Plg-cpx-opx	Ol; Ol-cpx-plg Plg-cpx-ol Plg-cpx
	Ortho-mesocumulate	Ortho-mesocumulate	Ortho-meso-adcumulate	Ortho-meso-adcumulate	Ortho-meso-adcumulate
Order of crystallization (cumulus minerals)	ol-opx-cpx-hbl/plg	opx/plg-cpx-ap	ol-opx-cpx-plg	ol-cpx-plg-opx	ol-cpx-plg
Postcumulus minerals	hbl>plg>qtz>k-fd>s	hbl>qtz>mg-il	hbl>mg-il>qtz	hbl>mg-il>bt	mg-il>opx>hbl
Layer characteristics					
	Zone I	**Zone II**	**Zone III**	**Zone IV**	
Attitude	110/70 NNE 50/70 NNW	55/60 NNW	50/65 NNW	50-90/45-90 NNW	
Form	planar, lensoidal, tapered	planar ± convoluted wispy	planar±deformed	planar	
Lamination	not observed	±lineate; modal; textural	±lineate; modal; textural; grain size	±lineate	
Mode	uniform	uniform±graded	uniform	uniform	
Thickness (range)	(3cm-3m)	(2cm-20m)	(2cm-5m)	(5cm-20m)	
Contacts	sharp, irregular	sharp, gradational	sharp, irregular	sharp, irregular	
	concordant±discordant	concordant±discordant	concordant	discordant±concordant	
Layering characteristics					
Type	modal, textural	modal, textural	modal, textural, phase	modal , phase & grain size	
Mode	meso>macrorhythmic	micro>meso> macrorhythmic	meso>macro> microrhythmic	macro>meso microrhythmic	
Other structures	bifurcation channelling & finger	cross-bedding, slump folds, cognate xenoliths	Finger, slump folds, replacement	recrystallization	

CHAPTER 3

CHEMICAL AND ISOTOPIC CHARACTERISTICS OF THE TILTING LAYERED SUITE

3.1 INTRODUCTION

This chapter presents mineral chemical data and the whole rock major and trace element and Nd isotopic characteristics of the TLS. These data are important in constraining the nature of possible processes operative during the physical and chemical evolution of the TLS. However, the main focus in this chapter is presentation, description and limited discussion of the data. A more complete discussion of aspects of the data will be found in Chapter 6 (petrogenesis), since isotopic and chemical data presented in Chapter 5 are also required for modelling purposes.

3.2 MINERAL CHEMISTRY

One major disadvantage of studying magma chamber processes using layered intrusions is that the bulk composition of a cumulate does not generally equate to the liquid from which it crystallized. Hence, the mineral chemistry (obtained by microprobe analysis) of cumulus olivine, pyroxene, plagioclase and hornblende from the TLS is here utilized to help evaluate the magma-chamber processes that produced the cumulates. In the following sections, compositional variation of cumulus phases is documented and discussed with regard to:

a) overall range of variation observed within the TLS;

b) inter- and intra-zone ranges;

c) the magmatic stratigraphy; and

d) the chemical range found within different cumulate types.

Analytical techniques and methodology, together with full mineral analyses and respective mineral formulas are given in Appendix IV. It is important to note that the data presented below represent the first comprehensive attempt to determine mineral chemistry and cryptic variation in the TLS, which displays very complex physical characteristics (see Chapter 2). Sampling and time constraints necessitated that some sampled lithological sections were somewhat short and in such cases, where complexities may be oversimplified, the discussion serves as a framework upon which more detailed studies can later be based.

3.2.1 Overall range

Inter- and intra-zone compositional variations of cumulus phases are summarized in Table 3.1 and illustrated in Figure 3.1. Unless stated otherwise, the following remarks are based on average core compositions of cumulus phases. However, note that within a given sample the average core compositions of the same cumulus phase obtained from different grains may differ significantly (*i.e.* show a greater range than that of the analytical uncertainty - estimated at 0.5 mole percent Fo for olivine, 0.5 mole percent En for pyroxene and 1.0 mole percent An for plagioclase). This type of variation is referred to as "grain heterogeneity", the magnitude of which is different from one phase to another (Table 3.2). In general, grain heterogeneity of olivine is fairly small, up to 3 mole percent Fo with an average of less than 1 mole percent Fo. In pyroxene (both ortho- and clino-pyroxene) the grain heterogeneity is moderate, up to 7 mole percent En with an average $\leq$ 5 mole percent. Plagioclase shows a considerable range of grain heterogeneity, up to 22 mole percent An with an average of 10 mole percent.

Olivine

The Fo contents of olivines throughout the suite vary within a narrow range from Fo_{81} to Fo_{72} (Table 3.1). However, it is important to note that:

a) olivine is a primary cumulus phase only in Zone IV. Here the Fo contents of olivine range from Fo_{81} to Fo_{72}, (Figure 3.1);

b) olivine (Fo_{80}) is only rarely present in Zone I and where present is generally replaced by serpentine and/or orthopyroxene-opaque symplectites;

c) one of the most magnesian olivines analyzed in the TLS (Fo_{81}) is from an olivine cumulate found as a cognate xenolith within Zone II; and

d) no olivine has been recognized in Zone III.

Pyroxene

The En contents of orthopyroxene vary from 86 to 59 (bronzite to hypersthene) and display three recognizable clusters in the range En_{80-86}, En_{70-80} and En_{59-70}, which mainly correspond to Zone I, Zone IV and Zones II and III, respectively (Figure 3.1).

Clinopyroxenes range from $Wo_{47}En_{45}Fs_8$ to $Wo_{43}En_{41}Fs_{15}$, *i.e.* from diopside and endiopside to salite and augite (Figure 3.1). However, as illustrated in Figure 3.2, Al_2O_3 and TiO_2 contents of clinopyroxene are quite variable and can be used to help differentiate between clinopyroxenes from different zones. Clinopyroxenes from Zone I form a distinct population, primarily based on their higher Mg numbers (X_{Mg}). Those in Zone IV generally differ from the other zones, particularly in their high Al and Ti contents for a given X_{Mg} (compared to Zones II and III).

The ratio of $(Mg/Fe)_{clinopyroxene}/(Mg/Fe)_{orthopyroxene}$ for coexisting pyroxenes within the TLS is 1.0 to 1.13. This ratio is 1.0 in Zone I; ranges from 1.11 to 1.13 in Zones

II and III; and from 1.0 to 1.10 in Zone IV. These values and the general pattern of the tie lines in Figure 3.3, are consistent with those observed in co-existing, equilibrium Ca-rich and Ca-poor pyroxenes (*cf.* Deer et al., 1966). However, it should also be noted that the crossing tie-lines observed in Zones I and III may indicate some disequilibrium.

Plagioclase

The An contents of plagioclase range from An_{85} to An_{43} (bytownite to andesine) and display three overlapping but relatively distinct clusters in the ranges An_{80-85}, An_{60-80} and An_{43-60}, which correspond to Zone I, Zone IV and Zones II and III, respectively (Figure 3.1).

Optical zoning is accompanied by large variation in An content. Sharp and gradational contacts between cores and rims are both present. Normal zoning is pervasive throughout the TLS, but reverse, complex oscillatory and patchy zoning are also present. In detail, compositional zoning varies from one crystal to the next in the same thin section. A representative selection of plagioclase compositional profiles are shown in Figure 3.4.

Amphibole

Cumulus amphiboles are very rare and are only recognized in Zone I. They belong to the calcic amphibole group and are of magnesio-hastingsite composition, based on variation in Al^{IV} versus (Na+K) (Leake, 1978). In general, optical zoning of individual hornblende grains corresponds to compositional zoning and reflects variation in TiO_2 and Al_2O_3 content.

3.2.2 Cryptic variation

The compositional variation in cumulus olivine, pyroxene and plagioclase with position in the magmatic stratigraphy of Zone I to Zone IV, measured perpendicular to

modal layering, is illustrated in Figure 3.5. In the following sections, the cryptic variation within each zone is presented and discussed separately.

Zone I

As discussed in the previous chapter (Chapter 2), the internal structure and hence the magmatic stratigraphy of Zone I has not been reconstructed because of post-emplacement disruption by later granitoid intrusions. Therefore, only very limited sections of the zone are represented in Figures 3.5 and 3.6, where it can be seen that variations in orthopyroxene (X_{Mg}=75-86), clinopyroxene (X_{Mg}=83-86), and plagioclase (An_{core}=80-85) are relatively large. This zone usually contains the most primitive mineral compositions analyzed in the TLS, in particular note the X_{Mg} for the pyroxenes. The olivine-bearing sample in this zone is an opx-cpx-ol cumulate (d-type in Figure 3.6) and the Fo content (Fo_{80}) of the olivine is slightly lower than the most magnesian olivine composition (Fo_{81}) analyzed in the TLS (Table 3.1).

Mineral compositions of opx-cpx-plg cumulates (b-type in Figure 3.6; *e.g.* $X_{Mg,clinopyroxene} \approx$ 86) are characteristically more primitive than those of the olivine-bearing cumulate (*e.g.* $X_{Mg,clinopyroxene}$= 83; Figure 3.6). Typically, orthopyroxene compositions of plg-cpx-opx cumulates (a-type in Figure 3.6; X_{Mg}=79-82) are slightly less magnesian than those of the alternating opx-cpx-plg cumulates (b-type in Figure 3.6; X_{Mg}=84-86), whereas overall clinopyroxene compositions within these alternating cumulates (a- and b-type in Figure 3.6) show little variation (X_{Mg}= 85-87).

Zone II

Compositions of orthopyroxene (X_{Mg}= 59-73), clinopyroxene (X_{Mg}=72-80) and plagioclase (An_{core}= 43-59) display noticeable variations throughout the zone, but these are not simple, regular variations from bottom to top of the stratigraphy (Figure 3.7).

Low in the stratigraphic section (0-50 m, Figure 3.7), the pattern of cryptic

variation exhibits systematic compositional changes between a few alternating, relatively thick, melanocratic plg/opx ± cpx cumulates and leucocratic plg±opx±cpx-ap cumulates (c- and b-type in Figure 3.7). In general, pyroxene compositions (average orthopyroxene X_{Mg}=70 and clinopyroxene X_{Mg}=79) of melanocratic cumulates are significantly more magnesian than those of leucocratic cumulates (average X_{Mg}= 62 and 73 for orthopyroxene and clinopyroxene, respectively). These compositional discontinuities between alternating cumulates apparently occur at the layer contacts. Plagioclase compositions display a wide range of variation in An content (Figure 3.7).

Plg±opx±cpx-ap cumulates dominate the upper range of the stratigraphic section (100-260 m; Figure 3.7) where they display a fairly limited range of compositional variation (*e.g.* $X_{Mg,\ orthopyroxene}$= 64-66). It is noticeable that the samples from the uppermost section (*e.g.* Z2-13 and Z2-14) have very similar pyroxene and plagioclase compositions to those from the lower section (*e.g.* Z2-2, Z2-3 and Z2-9).

Zone III

In Zone III, compositional variation for each phase is summarized as: orthopyroxene (X_{Mg}= 63-69); clinopyroxene (X_{Mg}= 71-79) and plagioclase An_{core}= 50-55). These overlap the range of compositional variation seen in Zone II (Table 3.1 and Figure 3.5).

The overall cryptic variation of Zone III indicates systematic compositional changes between the cumulate types (Figure 3.8). This is most evident from the compositional profiles of pyroxene (particularly orthopyroxene), whereas those of plagioclase display little variation throughout the zone. In general, pyroxene compositions of the leucocratic plg-cpx-opx cumulates (a-type in Figure 3.8; X_{Mg}= 65 and 74 for orthopyroxene and clinopyroxene, respectively) are less magnesian than those of the

alternating melanocratic opx/plg/cpx (c-type in Figure 3.8; X_{Mg}= 68 and 77 for orthopyroxene and clinopyroxene respectively) and opx-cpx cumulates (b-type in Figure 3.8; X_{Mg}= 67 for orthopyroxene and X_{Mg}= 75 for clinopyroxene). Furthermore, pyroxene (ortho- and clino-pyroxene) compositions of opx-cpx cumulates are slightly lower than those of opx/plg/cpx cumulates. It is important to note that within these alternating individual cumulates, particularly opx-cpx cumulates, mineral compositions appear to be fairly consistent. The result is an overall zig-zag compositional pattern where the noticeable compositional discontinuities occur at the layer contacts.

Zone IV

Zone IV, which contains two geographically separated subzones (Chapter 2), has the second-most primitive mineral compositions analyzed in the TLS. The range of compositional variation is relatively wide (olivine Fo=72-81; orthopyroxene X_{Mg}= 69-78; clinopyroxene X_{Mg}= 73-79; and plagioclase An_{core}= 50-76%) (Table 3.1).

Typically, mineral compositions of Zone IVb are slightly more primitive than those of Zone IVa (Table 3.1). Compositional variations for each phase in Zone IVa and Zone IVb are, respectively, as follows: olivine (Fo= 72-75 and 73-81); orthopyroxene (X_{Mg}= 67-78; no cumulus orthopyroxene in Zone IVb); clinopyroxene (X_{Mg}= 73-78 and 76-79); and plagioclase (An_{core}= 55-65 and 59-76). Note that the petrographic descriptions in Chapter 2 emphasized the absence of cumulus orthopyroxene and the abundance of olivine in Zone IVb (Chapter 2). However, these findings contradict expectations from the relative stratigraphic position of these subzones, *i.e.* Zone IVa below Zone IVb and therefore, supposedly, the more primitive.

The stratigraphic section outlined for Zone IVa (Figure 3.9) is dominated by plg-cpx-opx cumulates (a-type in Figure 3.9) which reveal a fairly limited range of compositional variations disrupted by sudden compositional reversals. The major

compositional reset occurs at about 50 m, within the plg-cpx-opx cumulates, where orthopyroxene, plagioclase ± clinopyroxene compositions are shifted to more primitive values (*e.g.* $X_{Mg,\ opx}$ change from 74 to 78). A second reset occurs at 260 m between plg-cpx-opx and plg-cpx cumulates (b-type in Figure 3.9) and corresponds to a disappearance of orthopyroxene as a cumulate phase. Olivine-bearing cumulates (c- and d-type in Figure 3.9) typically have more primitive cumulus plagioclase (An% = 65 - 70) compositions than those of plg-opx-cpx cumulates (An% = 57 - 63).

Zone IVb shows a weakly developed regular fractionation pattern between Z4b-12 and Z4b-14 (Figure 3.10) where both pyroxene and plagioclase compositions become less magnesian and more sodic, respectively, with increasing stratigraphic height. There are some abrupt changes, particularly in the composition of olivine. One of these changes occurs at about 10 m (Z4b-9) between ol/cpx-plg and plg-cpx-ol cumulates (b- and c-type in Figure 3.10) and another occurs within the plg-cpx-ol cumulates between Z4b-11 and Z4b-12. At the bottom of the stratigraphic section, the transition between the olivine cumulate and ol-cpx-plg cumulate is marked by a substantial change in olivine composition, *i.e.* from Fo= 80 to 75. Note that the olivine cumulate, Z4b-15 (Figure 3.10) has the least magnesian olivine analyzed in this zone and it displays some evidence of postcumulus/subsolidus modifications including recrystallization and reaction coronas (*e.g.* orthopyroxene around olivine).

3.2.3 Summary and discussion of variation in mineral composition

As expected for a layered igneous intrusion, there are changes in the composition of the cumulus phases throughout the suite. However, the correlation of these changes with stratigraphic height is not regular. For a magma(s) evolving in a closed system one

might expected to find the mafic cumulus phases enriched in Fe and the plagioclase more sodic with increasing stratigraphic height; however, in the TLS there are several different trends. For example: a) in Zone IVa there is little overall change in cumulus mineral compositions (Figure 3.5); b) in the upper part of Zone IVb there is some evidence for a correlation with stratigraphic height; c) there are several sudden changes in composition, such as those illustrated in Zone II and Zone IVb (Figures 3.7 and 3.10); d) in Zone IVb at 10 meters height there is "suddenly" a more magnesian orthopyroxene, which is accompanied by significant grain heterogeneity in clinopyroxene and plagioclase; and e) in Zone II at ~ 30 meter height (Figure 3.7), there is a sudden compositional reversal which is accompanied by a reversal in crystallization order.

The complexity in these trends makes it unlikely that there is any one mechanism that accounts for the changes in mineral composition. Reversal in compositional trend might result from introduction of new, relatively primitive magma into the region of crystallization. It is important to note that during this study, this concept of introducing a new magma batch into the region of crystallization can be interpreted either as: a) addition of new magma into the chamber; or b) vigorous convective overturn of existing magma in the chamber which brings "fresh" magma into the region of crystallization (*e.g.* Upton, 1987; Cawthorn, 1993). Apparently, the consequences of these two different processes are very similar. Each zone exhibits its own unique cryptic variation pattern. In the following sections, cryptic variation pattern of each zone is discussed separately in terms of possible magma chamber processes involved in the formation of cumulates.

Zone I

As noted earlier, the data outlined above do not form a significant foundation for a comprehensive study of Zone I, since only a very limited section of the zone is considered and the olivine-bearing cumulate is presented by only one sample. These factors clearly pose some limitations on generalizing the observations and Zone I requires further investigation. However, the compositional changes observed in Zone I, particularly compositions of pyroxene from opx-cpx-ol cumulate which are less primitive than those of opx-cpx-plg cumulates, suggest that different cumulate types (*i.e.* opx-cpx-ol and opx/cpx/plg cumulates) are unlikely to have crystallized from the same batch of magma and thus there must have been addition of new magma batch(es) into the chamber (*e.g.* Cawthorn et al., 1991).

Zone II

Zone II is characterized by: a) overall limited range of compositional variations, particularly higher in the stratigraphic section; and b) apparently systematic compositional variations between alternating cumulates at the bottom of the outlined section. Introduction of a new magma batch into the region of crystallization and subsequent mixing of new and resident magmas can lead to an overall limited range of compositional variations. Compositional discontinuities between alternating cumulates apparently imitate the modal layering (meter scale). This implies that the cryptic variation pattern records the chemical signature of the process producing changes in the mode of layering. Although the reason for this observation is not clearly understood, it might be attributed to introduction of different (less fractionated versus more fractionated) magma batches into the region of crystallization either by means of: a) magma replenishment into the chamber (*e.g.* Bedard et al., 1988); or b) discrete sedimentation events in a convecting magma chamber (Sparks et al., 1993). Although, the chemical consequences of these two

different mechanisms appear to be similar, meter scale, systematic multiple magma replenishment into the magma chamber is unrealistic. "Discrete sedimentation" in a convecting magma chamber is based on fluctuations in sedimentation rate and mineral proportions and requires that crystals formed at the roof can escape by settling. Discrete sedimentation events are expected when the concentration of crystals exceeds the critical value, above which convection is unable to keep the crystals suspended. "*Because minerals of different density and size have different critical concentration and settling velocities, complex fluctuations in sedimentation rate and mineral proportions are predicted in a multi-component systems. This may lead to regular repetitive cycles*" (Sparks et al., 1993). Several field observations including: a) graded modal layering; b) cross-bedded layers; and/or c) cognate xenoliths, are consistent with vigorous magmatic currents (Chapter 2), which favour discrete sedimentation events.

Zone III

Zone III is characterized by systematic compositional changes between the cumulate types, *i.e.* the cryptic variation pattern mimics the modal layering (cm to m scale). Such changes might be attributed to the introduction of different (less fractionated versus more fractionated) magma batches into the region of crystallization. However, considering the scale of modal layering and accompanied cryptic variation, the introduction of new magma batches into the magma chamber cannot be the main process producing changes in the mode of layering. Additionally, several field observations including a lack of graded bedding and sharp layer contacts, are inconsistent with the idea of transportation of crystals to the site of deposition (see Chapter 2)- *i.e.* "discrete sedimentation in a convecting magma chamber". Furthermore, several processes including rhythmic nucleation and in-situ crystallization proposed for micro-mesorhythmic modal layering (Chapter 2), cannot solely explain observed cryptic

variation (*cf.* Quadling and Cawthorn, 1993). It is clear that understanding the processes producing the observed systematic compositional changes between alternating cumulates requires further investigation.

In Zone III, different postcumulus processes appear to be operative at different stratigraphic levels, especially where the amount of intercumulus liquid varies considerably over small vertical intervals. Deviation from the expected mineral composition based on order of crystallization and stratigraphic height might be due to re-equilibration of cumulus phases with trapped liquid (*e.g.* Cawthorn, 1982; Barnes, 1986; Mathison and Booth, 1990; Cawthorn et al., 1992). Certainly several field observations, including slump folds and finger structures, indicate noticeable migration of intercumulus liquid through the cumulus pile (Chapter 2).

Zone IV

The overall cryptic variation pattern of Zone IV records a reversal in magma composition corresponding to the boundary between subzones IVa and IVb. This means that the cumulates of Zone IVa are not the fractionation products of the magma producing Zone IVb and compositional variation between subzones are likely due to the addition of a new magma batch into the chamber.

Zone IVb is the only subzone within the TLS in which mineral chemistry records relatively small scale cryptic layering implying that fractional crystallization is one of the important processes involved in the formation of the some layers of Zone IVb.

3.2.4 Temperature and pressure estimates

Crystallization temperature of the TLS has been estimated utilizing pyroxene compositions, in which the Fe/Mg partitioning is temperature dependent (*e.g.* Wood and Banno, 1973; Wells, 1977). This method provides an approximation of the equilibrium

temperature, where the accuracy of the results is largely based on the quality of analyses and the Fe^{+3} and Fe^{+2} contents of the minerals. Since the oxidation state of iron cannot be determined by electron microprobe analysis, it has been assumed that all of the iron is Fe^{+2}, which is the simplest choice to make. The temperatures were calculated using a computer program written by Mengel (1987), in which the activities of pyroxenes are calculated from measured cation concentrates utilizing the mixing model of Wood and Banno (1973) (see Table 3.3).

For meaningful temperature estimates, two main conditions must be simultaneously satisfied: a) there must have been chemical equilibrium between pyroxene phases; and b) the chemistry of the pyroxenes must not have been modified by postcumulus and/or subsolidus processes. In this study, pyroxenes utilized in temperature calculations display no visual or textural evidence of modification and their chemical equilibrium was visually ascertained using the tie-line relationships between co-existing pyroxenes plotted in Figure 3.3.

Temperature estimates from eleven samples of the TLS are presented in Table 3.3. The temperature range is from 854 to 1036°C, with the average temperature of each zone (increasing from I to IV) being 984, 886, 924 and 962° C, respectively. These temperatures are somewhat low for mafic magmas (*cf.* Philpotts, 1990), but this is not too surprising considering the fractionated mineral compositions and possibly hydrous nature of the parental magmas (Chapter 2).

Prevailing pressure conditions of the zones can be estimated from their mineral assemblages. For Zones I-III, the presence of amphibole, either as postcumulus or cumulus phase, together with early crystallization of orthopyroxene (Chapter 2) suggests crystallization from hydrous magma at less than about 1-2 kbar total pressure (Eggler and Burharn, 1973; Cawthorn, 1978). In Zone IV, which lacks amphibole, a prevailing

pressure is estimated as <5 kbar utilizing tholeiitic dry-magma stability fields (Green, 1982; see Figure 2.21).

3.2.5 Conclusions and Summary of mineral chemistry

a) In general, cumulus olivine, pyroxene and plagioclase compositions display three recognizable clusters (Figure 3.1) which correspond to Zone I, Zone IV and Zones II and III.

b) Olivine and orthopyroxene compositions were apparently more sensitive to changes in magma composition or other fractionation processes than those of clinopyroxene. (Figure 3.6 - 3.11). Certainly the range of overall clinopyroxene compositions within the individual zones is limited. Plagioclase displays a wide range of variation even within a single sample.

c) There is no single comprehensive model to explain every feature observed in the TLS and evolution of the suite appears to involve the complex interaction of several processes including: i) introduction of new magma batches (magma replenishment), with or without subsequent mixing of newly introduced and residual magmas, into the region of crystallization (Zone II); i) fractional crystallization (Zone IVb); iii) sedimentation in convecting magma (Zone II ± Zone III); and iv) postcumulus and/or subsolidus modifications (Zone IV).

d) The effects and consequences of processes involved in the formation of the TLS vary from zone to zone. Furthermore, different processes can be operative at different stratigraphic levels of the same zone.

e) The information presented above is consistent with the field and petrographic observations that the TLS is a composite intrusion (Chapter 2).

f) The crystallization of the TLS took place at ~950°C and low pressures (~1-2 kb).

3.3 GEOCHEMICAL DATA

In the following sections whole rock geochemical results for a wide range of samples from plg-lherzolite (olivine orthocumulate) and gabbronorite (plg-cpx-opx adcumulate) to hbl-diorite (plg-ap mesocumulate) are reported. The analytical techniques and methodology, plus the complete data set for the fifty samples are given in Appendix V.

Most samples illustrated in Figures 3.11 to 3.15 are orthocumulates, and as such their bulk composition probably does not equate to the liquid from which they crystallized. Nevertheless, in the following discussion, whole rock geochemical analyses from the TLS will be utilized to indicate average cumulus compositions (*cf.* Wager and Brown, 1968). This section is organized as follows; presentation of a) whole rock (major and minor element) analyses and CIPW norms calculations; b) whole rock REE; and c) Nd isotope analyses.

3.3.1 Presentation of whole rock major and minor element analyses

Samples from the TLS display: a) a wide range of MgO (4 to 29 wt%); CaO (4 to 14 wt%); FeO (4 to 13 wt%); Al_2O_3 (3 to 34 wt%); Na_2O (0.81 to 4 wt%) and TiO_2 (0.3 to 4 wt%) contents; and b) a relatively narrow range of SiO_2 (42 to 55 wt%) content. In the following sections, compositional variation of cumulates, in terms of selected major/minor oxides/elements, is presented and discussed with regard to intra- and inter-zone ranges.

Zone I

A total of six samples have been analyzed from Zone I. All analyzed samples, except one (Z1-9, opx-cpx-ol cumulate), are opx-cpx-plg and plg-opx/cpx cumulates. As illustrated in Figure 3.11, the olivine-bearing sample (Z1-9) has higher MgO, Cr, P_2O_5, TiO_2 and FeO than those of the other cumulates (opx/plg/cpx cumulates). Additionally, in several diagrams including SiO_2, Al_2O_3, Na_2O and Ni versus MgO, the olivine-bearing sample (Z1-9) plots in a manner inconsistent with the general distribution trend of other cumulates.

Samples with cumulus plagioclase (opx/plg/cpx cumulates) display a relatively wide range of Al_2O_3 (5 to 14 wt%) content, while other oxides including, MgO (14 to 18 wt%), SiO_2 (50 to 54 wt%); CaO (10 to 12 wt%); FeO (4 to 5 wt%); Na_2O (1 to 1.4 wt%) and TiO_2 (0.2 to 0.4 wt%) display little variation. Other significant observations are as follows:

a) Samples rich in cumulus pyroxene phases are rich in Mg, Fe, Cr and Ni, and poor in Al, Na and Ca compared to plagioclase-rich samples. Thus, increasing Al_2O_3, CaO, Na_2O contents with decreasing MgO content is consistent with plagioclase accumulation, while increasing Cr and Ni contents with increasing MgO content is consistent with pyroxene (particularly clinopyroxene) accumulation;

b) The SiO_2 contents apparently increase with increasing MgO content. This can be best explained in terms of significant orthopyroxene accumulation;

c) The positive correlation between FeO and MgO apparently reflects the relative difference in FeO content of plagioclase and pyroxene cumulus phases, *i.e.* the FeO content of plagioclase (≤ 1 wt%) is significantly less than that of pyroxenes

(8-15 wt%) and, thus, samples rich in cumulus plagioclase have low FeO and MgO contents relative to samples rich in cumulus pyroxenes.

d) K_2O, TiO_2 and P_2O_5 contents stay almost constant for MgO ranging from 14 to 18 wt%.

Zone II

A total of eight samples have been analyzed from Zone II, with a strong bias towards the plg±opx±ap cumulates. This bias indeed reflects the true nature of the zone (*i.e.* Zone II is dominated by plagioclase-rich cumulates) and leads to significant discontinuities in the variation diagrams (Figure 3.12). In general, there is a poor correlation between SiO_2 and MgO contents; in particular, SiO_2 contents vary from 48 to 54 wt% at MgO < 6 wt%. Similarly, FeO (6-11 wt%), TiO_2 (1 - 2.5 wt%) and P_2O_5 (0.1-1.8 wt%) are also scattered at MgO < 6 wt %. In contrast, at the same low MgO content, a number of samples have relatively constant Al_2O_3 (16-18 wt%), CaO (8-9 wt%) and Na_2O contents. These observations can be explained in terms of: a) plagioclase accumulation which strongly controls the distribution of Al_2O_3 CaO and Na_2O; b) apatite accumulation in low MgO samples, controlling the P_2O_5 content; and c) minor but variable amounts of cumulus pyroxene phases (ortho- and clino-pyroxene) which effect the distribution of TiO_2, FeO and SiO_2; and/or d) presence of variable amounts of opaque oxide (magnetite/ilmenite) postcumulus phases which can modify the TiO_2 and FeO content of the samples. Additionally, apparent distributions of Cr and Ni versus MgO are consistent with pyroxene accumulation (*i.e.* samples rich in pyroxene phases have higher MgO, Cr and Ni contents than those of plagioclase rich cumulates).

Zone III

For Zone III, a large number of samples from opx-cpx and opx-cpx-plg cumulates to plg-opx/cpx cumulates were analyzed. The samples display a relatively wide range of

MgO (4 to 16 wt%); SiO_2 (44- 54 wt%); Al_2O_3 (4 to 18 wt%); Na_2O (1 to 4 wt%); TiO_2 (0.2 to 5 wt%); FeO (10 to 16 wt%) and CaO (5 to 11 wt%) contents. Selected major/minor oxides versus MgO are given in Figure 3.13. The significant observation is that rocks of Zone III can be subdivided into three clusters on the basis of their MgO contents. These are: a) opx-cpx cumulates with relatively high MgO content (12-16 wt%); b) opx-cpx-plg cumulates with intermediate MgO (9-10 wt%) content; and c) plg-cpx/opx cumulates with low MgO content (4-7 wt%). Similarly Al_2O_3, Na_2O and Cr contents display three noticeable clusters and are marked by compositional discontinuities between alternating cumulates. These observations are consistent with the mineral chemistry reported for this zone, where there are small scale zig-zags in mineral composition associated with the different types of cumulate layers.

Overall, increasing Na_2O and Al_2O_3 and decreasing Cr and Ni versus decreasing MgO are in accord with plagioclase and pyroxene accumulation. The accumulation of plagioclase together with pyroxene phases likely leads to the scattered data in several diagrams including SiO_2, TiO_2, $K_2O \pm$ FeO versus MgO. Additionally, the presence of variable amounts of opaque oxide (magnetite/ilmenite) and/or amphibole postcumulus phases, at least partly, leads to the scattered distribution in TiO_2, FeO and/or K_2O vs MgO diagrams. The P_2O_5 versus MgO diagram reveals two distinct group of samples: a) samples with low MgO ($\sim$ 6 wt%) and P_2O_5 (0.2 to 0.4 wt%); and b) samples with low MgO and high P_2O_5 ($\sim$ 1.3 wt%) contents. This can be explained in terms of apatite accumulation in some of the low MgO cumulates.

Zone IV

A total of thirteen samples (six from Zone IVa and seven from Zone IVb) were analyzed from Zone IV. Selective major/minor oxide versus MgO diagrams are given in Figures 3.14 and 3.15. In Zone IVa, the CaO, Al_2O_3, $Na_2O \pm SiO_2$ contents increase

with decreasing MgO content, while FeO and Ni contents increase with increasing MgO content (Figure 3.15). These observations appear to be consistent with plagioclase and olivine accumulation. The TiO_2 (~0.5 wt%); P_2O_5 (~0.1 wt%) and Cr (~340 ppm) contents do not vary much over a wide range of MgO (4-22 wt%).

Zone IVb, similar to Zone III, typically displays two distinct clusters which correspond to olivine-rich and plagioclase-rich cumulates. Olivine-rich samples have high MgO (20-30 wt%) and low Al_2O_3 (~10 wt%), CaO (6-8 wt%) and Na_2O (~ 1 wt%) contents relative to those of the plagioclase-rich cumulates - MgO (4-12 wt%), Al_2O_3 (16-24 wt%), CaO (12-14 wt%) and Na_2O (1.5- 3 wt%). In Zone IVb, clinopyroxene is one of the major cumulus phases, together with olivine and plagioclase. However, a group of cumulus clinopyroxene-bearing samples have low Cr contents relative to their whole rock MgO contents (Figure 3.14). Although the reason for this observation is not clear, these samples characteristically display both olivine and clinopyroxene as primary cumulus phases and this may provide for the relatively high MgO values relative to Cr contents.

3.3.2 Summary of whole rock major/minor element data

Several major and/or minor element trends are consistent with the petrographic observations. For example, whole rock Al_2O_3 content is sensitive to plagioclase accumulation. Similarly, Cr, Ni $\pm$ FeO contents are somewhat associated with accumulation of ferromagnesian minerals including clinopyroxene, orthopyroxene and olivine. The positive correlation between FeO and MgO reflects the fact that ferromagnesian minerals have higher FeO content than that of plagioclase. Thus, intra-zone variation in FeO content partly reflects the relative abundances of cumulus ferromagnesian minerals and plagioclase.

Several minor/trace element diagrams including TiO_2, P_2O_5 and K_2O vs MgO display scattered and/or limited ranges of variation over a relatively wide range of MgO. These observations can be attributed to: a) variable amounts of postcumulus phases like magnetite/ilmenite and/or amphibole; or most importantly; b) the dominantly orthocumulus nature of the analyzed samples.

3.3.3 Inter-zone whole rock geochemical (major/minor) element variations

As illustrated in Figure 3.16 the zones, excluding Zone II, exhibit independent but sub-parallel linear trends in Al_2O_3, FeO and/or CaO when plotted against MgO. Furthermore, samples with the same or similar MgO from different zones usually have fairly distinct FeO, CaO and Al_2O_3 contents. These observations appear to be consistent with the fact that overall cumulus olivine, pyroxene and/or plagioclase compositions display three recognizable clusters (see Figure 3.1), which correspond to Zone I, Zone IV and Zones II and III. Furthermore, the range of whole rock compositional variation seen in the most differentiated rocks of Zone III overlaps most of the compositional variation seen in Zone II. This is similar to the compositional variation observed in the mineral chemistry.

3.3.4 CIPW norms

CIPW norms of the rocks from the TLS are presented in Appendix 4. There is a remarkable overall consistency within the individual zones and throughout the TLS, despite the fact that only a few analyzed samples have cotectic cumulus contents, and therefore might approximate liquid compositions. All analyzed samples are hypersthene-normative with or without modal orthopyroxene. Most of the samples from Zones I- III are quartz-normative, while the samples belonging to Zone IV are olivine-normative. The

few samples from Zones I-III which are olivine-normative, are either olivine- or pyroxene-rich orthocumulates.

It is important to note that, besides the overall consistency within the individual zones and throughout the TLS, recognition of two distinct magma compositions is consistent with both petrographic observations and mineral chemistry data. In other words, olivine-tholeiitic magma gave rise to Zone IV which: a) is the only zone in which olivine is preserved as a major cumulus phase; b) has lower silica activity than that of other zones; and c) displays an order of crystallization characterized by late crystallization of cumulus orthopyroxene. On the other hand, quartz-tholeiitic magmas gave rise to Zone I- III which are characterized by: a) a lack of olivine cumulus phase; b) relatively higher silica activity than Zone IV; and c) early crystallization of orthopyroxene.

3.3.5 Presentation of whole rock REE analyses

Chondrite normalized (Taylor and McLennan, 1985) rare earth element patterns (REE_N) for fifteen rocks from Zone I-Zone IV are shown in Figures 3.17 and 3.18. All REE_N patterns of the TLS lie in the range of 1-50 times (X) chondrite and show negative slopes, *i.e.* slight to strong light rare earth element (LREE) enrichment relative to heavy rare earth elements (HREE). There is no major discordance between the patterns of the zones in Table 3.6. The following sections describe some details of the REE patterns of each zone from Zone I to Zone IV (Figure 3.17).

Zone I

The REE_N patterns of Zone I lie in the range of 2-20 X chondrite and include hbl-gabbronorites (plg-cpx-opx and opx-cpx-plg cumulates). They are characterized by: a) $(La/Lu)_N = (6.4 - 6.9)$, and $(La/Sm)_N = (2.1 - 2.4)$; and b) no significant Eu anomalies

$(Eu/Eu^*)_N \approx 1.0$, despite the fact that they are cumulus plagioclase-bearing samples (Figure 3.17). They display very similar, parallel patterns.

Zone II

For Zone II, samples representing three distinct cumulate types have been analyzed for their REE including: a) gabbronorite (plg/opx cumulate, Z2-4); b) hbl-diorite (plg-ap cumulate, Z2-3); and c) plg-lherzolite (olivine cumulate, Z2-1) which occurs as a cognate xenolith in F-92-70. They lie in the range of 4-40 X chondrite and exhibit $(La/Lu)_N = (3.5 - 6.0)$ and $(La/Sm)_N = (2.1\text{-}2.5)$. Although the samples display similar, almost parallel REE_N patterns, significant observations are as follows:

a) the REE_N abundances of samples are not fully correlative with the level of differentiation as indicated by either their MgO contents or their mineralogy. Specifically, it was not predictable that Z2-4 would have higher REE_N abundances than those of Z2-3; and

b) all three samples display somewhat unexpected behaviour with regard to Eu, *i.e.* sample, Z2-4 with cumulus plagioclase reveals no noticeable Eu-anomaly $(Eu/Eu^*) = 0.90$; while sample Z2-1 (olivine cumulate) with postcumulus plagioclase shows a minor positive Eu-anomaly $(Eu/Eu^* = 1.2)$. Furthermore, sample Z2-3 with cumulus plagioclase and apatite has a similar Eu-anomaly $(Eu/Eu^* = 1.2)$ with that of the olivine cumulate (Z2-1).

Zone III

Two different rock types, with three different cumulate types, including plg-hbl-websterite (Z3-14, opx-cpx cumulate) and gabbronorites (Z3-15, opx-cpx-plg and Z3-1, plg-cpx-opx cumulates) were analyzed from Zone III. Z3-14 and Z3-15 display parallel trends which are characterized by distinct flat REE_N patterns (7-40 X chondrite) with $(La/Lu)_N = (2.4 - 2.9)$ and $(La/Sm)_N = (1.4 - 1.5)$. Sample, F-92-N-10, which has a

comparable $(La/Sm)_N$ (1.5) with that of other samples, displays somewhat significant LREE enrichment relative to HREE [$(La/Lu)_N$= 5.4]. This leads to discordance (cross-cutting trends) in the REE_N patterns (Figure 3.17). It is important to note that samples with cumulus plagioclase (Z3-15 and Z3-1) do not reveal the expected positive Eu-anomaly [*i.e.*$(Eu/Eu^*) \approx 1.0$]; whereas, a sample with postcumulus plagioclase (Z3-14) shows a negative Eu-anomaly [$(Eu/Eu^*) = 0.7$].

Zone IV

The REE_N patterns of Zone IVa lie in the range of 2-11 X chondrite and include those of plg-lherzolite (ol-plg cumulate, Z4a-7) and gabbro (plg-cpx-ol cumulate, Z4a-9). They display similar REE_N patterns with minor crossing and are characterized by $(La/Lu)_N = (4.2\text{-}5.7)$ and $(La/Sm)_N = (2.2 - 2.7)$. Zone IVb including, olivine-(Z4b-1), ol-cpx-plg (Z4b-2) ol-cpx-plg (Z4b-5), and ol-cpx-plg (Z4b-9) cumulates lie in the range of 1-20 X chondrite. They display minor discordant patterns within a wide range of $(La/Lu)_N = (5.7 - 11.9)$ and $(La/Sm)_N = (1.9 - 3.0)$. The REE_N patterns of samples with primitive olivine compositions, *i.e.* Z4b-1 and Z4b-9, show significant LREE enrichment relative to HREE [$(La/Lu)_N$= (10.5 to 11.9) and $(La/Sm)_N$= (2.9 to 3.0)], and have relatively high total REE abundances with respect to other samples. These observations would not have been predicted on the basis of their order of mineral crystallization or mineral compositions. Samples with cumulus plagioclase typically display positive Eu-anomaly [$(Eu/Eu^*) = (1.1 - 1.9)$]. The magnitude of the Eu-anomaly appears to vary with the proportion of cumulus plagioclase.

Extended REE diagrams

Primitive mantle normalized (Taylor and McLennan, 1985) extended REE_N patterns of selected samples from Zone I - Zone IV are presented in Figure 3.18. Significant observations are as follows:

a) samples with cumulus plagioclase display a positive Sr-anomaly;

b) in general, samples from Zones II, III and IV reveal minor positive Ti-anomalies; whereas, samples from Zone I display negative Ti-anomalies; and

c) all samples show a significant negative Nb-anomaly.

3.4 WHOLE ROCK Sm-Nd ISOTOPIC DATA

Sm-Nd isotopic compositions were determined for nine samples from the TLS. These data, including duplicates and triplicates, are reported in Table 3.4. Petrographic classification, map unit and average ϵ_{Nd} are given in Table 3.5

Samples for Sm-Nd isotopic analysis were dissolved in teflon screw-top bombs and then split and spiked. A mixed spike, made from Oakridge National Labs ^{147}Sm and ^{150}Nd, was used. Sm-Nd separations were carried out using two different techniques. The first technique used standard cation resin for bulk REE separation and HDEHP for Sm-Nd separation. This is the same technique as described in Swinden et al. (1990; see Appendix 7). Blanks for the procedure are better than ~100 pg for Nd and 40 pg for Sm. The second technique used to separate REE and Sm-Nd uses specific Truspec Resin from the Gchrom company. The blanks for this technique are 5 pg Nd and 2.1 pg Sm. These analyses are indicated by an asterix in Table 3.4 and were carried out by Pat Horan at Memorial University.

Early results during this study indicated that it could be difficult to reproduce the results as precisely as was hoped. To ascertain whether this was due to analytical uncertainty (including separation, technique and methodology), a number of samples were re-analyzed as complete duplicates or triplicates, *i.e.* using new sample and complete new dissolutions and separations. The six samples done as duplicates or triplicates indicate that uncertainty was not dependent on either the technician or separation technique (or

blank). Uncertainty in the analyses can be discussed with regard to Sm/Nd error, $^{143}Nd/^{144}Nd$ reproducibility and ϵ_{Nd} values.

Experience in the laboratory indicates that Sm/Nd determinations are usually precise to $\pm$ 0.29 % (one sigma). In this study three of the multi-analyzed samples (Z4b-5, Z4b-9; Z4a-7) reproduce Sm/Nd ratios at or better than this uncertainty. The remaining three samples (Z2-1; Z2-3; Z2-4) produced Sm/Nd ratio with errors of $\pm$0.5 to 1.4 %.

Reproducibility of isotopic compositions is illustrated in Figure 3.19. Samples Z2-1 and Z4a-7 show identical means and overlapping errors. Sample Z4b-5 shows only marginally overlapping error bars and is a good example of the worse-case scenario for reproducing the isotopic compositions (IC) (*i.e.* error bars do not overlap means, just the error). Values for sample Z4b-9, in spite of large uncertainties in the IC, do not overlap. The patterns for Z2-3 and Z2-4 are complex with IC's with error less than $\pm$10 not overlapping, whereas a third value with a large uncertainty overlaps both previous values for Z2-4, but only one value for Z2-3.

The range of ϵ_{Nd} values resulting from this type of reproducibility is 0 (perfect) to 0.8 ϵ units. The range of variability in ϵ unit is 0 to 0.6 for those samples with Sm/Nd $\leq$ 0.2 % and 0.1 to 0.8, for samples with Sm/Nd 0.5 to 1.4 %. It is clear that, as expected, the major contributing factor to error in ϵ_{Nd} is the error in the isotopic composition. Taking Z4b-5 as representing analytical worse-case scenario, a range of 0.3 ϵ_{Nd} unit is the largest expected analytical uncertainty. Therefore, it is suspected that three samples (Z4b-9, Z2-4 and Z2-3) have isotopic heterogeneity. Obviously, the scale of this heterogeneity is not large and near or at the limit of an analytical uncertainty. However, the inability to reproduce the values in Z4b-9 and Z2-3, in particular, appears to be real and not an analytical artifact.

Variation in ϵ_{Nd} values in the TLS

The overall range of average ϵ_{Nd} in the TLS is -0.1 to +5.1 (Tables 3.5). This is a quite significant isotopic heterogeneity. For Zone I and Zone III, there are only limited data and no duplicate samples, so it is difficult to establish the degree of intra-zone heterogeneity in these cases. Zone I has a ϵ_{Nd} value of +0.3, which overlaps only with that from Zone IV (Zone IVb). Zone III is characterized by the highest value which does not overlap those from any other zones. Zone II is characterized by a range of 0.4 ϵ_{Nd} units and is at first glance apparently homogeneous. However, two samples (Z2-3 and Z2-4) show some evidence of intra-sample heterogeneity suggesting a range of about 1 ϵ_{Nd} unit for this zone. Samples Z4b-5 and Z4b-9 are from Zone IVb and ϵ_{Nd} ranges from -0.1 to +1.0, indicating intra-zone heterogeneity. Furthermore Z4b-9 shows some evidence of intra-sample heterogeneity. The value for Zone IVa is +1.0, which is not significantly different from sample Z4b-9 of Zone IVb.

3.5 DISCUSSION: GEOCHEMICAL AND ISOTOPIC CHARACTERISTICS

This section integrates mineral chemistry, whole rock major element and REE chemistry, and Sm-Nd isotopic compositions of the TLS to construct a framework upon which the petrogenesis of the TLS can be based (Chapter 6). Topics to be discussed, here, are:

a) interrelationship between the whole rock REE abundances and patterns and whole rock MgO content;

b) presence or absence of Eu-anomaly within the TLS;

c) extended REE patterns;

d) interrelationship between ϵ_{Nd} values and mineral chemistry and whole rock MgO and SiO_2 contents; and

e) interrelationship between REE_N and ϵ_{Nd}.

3.5.1 Interrelationship between the whole rock REE and MgO content

Figure 3.20 illustrates the variation in total REE abundances, $(La/Sm)_N$, $(La/Lu)_N$ and total REE abundances versus MgO content. The significant observations are as follows:

a) For a given MgO content, there is a significant variation in total REE abundances between zones;

b) Within the zones, total REE abundances show complicated relationships. This is most evident in Zone III, where samples with similar MgO (~ 13 wt%) display different REE abundances (51 ppm - 132 ppm, see Table 3.6);

c) Zone III has its own characteristic $(La/Sm)_N$ (~ 1.4) value over a wide range of MgO content (6 to 13 wt%). Similarly, Zone II displays a somewhat consistent $(La/Sm)_N$ (2.1 to 2.5) over a wide range of MgO content (6 to 23 wt%). Whereas Zone I displays a similar variation in $(La/Sm)_N$ (2.1 to 2.4) to that in Zone II but over a much more restricted MgO content (14 to 16 wt%). Zone IVa shows $(La/Sm)_N$ variation from 2.2 to 2.7, over a wide range of MgO content (9 to 21 wt%). Zone IVb reveals a complex relationship with samples of similar MgO (~22 wt%) having the same $(La/Sm)_N$ (2.4); whereas, other samples show a different, but constant $(La/Sm)_N$ (2.9 to 3.0) for a wide range of MgO content (4 to 29 wt%);

d) All zones, excluding Zone IVb, display subparallel trends- *i.e.* increasing $(La/Lu)_N$ with decreasing MgO content; whereas, Zone IVb shows a complicated relationship. For example - at a given MgO content (~22 wt%), samples have different $(La/Lu)_N$ (4.4 vs 5.6).

To be able to understand the relationship between the whole rock REE and MgO data for the TLS, it is important to realize that: a) samples analyzed from the TLS do not represent liquid compositions; b) MgO contents of samples are sensitive to accumulation of ferromagnesian minerals including pyroxene and olivine (*i.e.* samples dominated by cumulus pyroxene and/or olivine have higher MgO content than samples dominated by cumulus plagioclase); c) K_D's of La, Sm, and Lu are somewhat different for distinct cumulus phases. In other words, depending on the mode and type of cumulus phase, and concentration of La, Sm and Lu within the cumulus phases, their ratios can vary significantly.

Taking these facts together, it is expected that: a) samples dominated by ferromagnesian minerals, particularly clinopyroxene (*i.e.* high MgO content) will have lower $(La/Lu)_N$ and $(La/Sm)_N$ then those of samples dominated by plagioclase; and b) there should be less significant variation in $(La/Sm)_N$ relative to $(La/Lu)_N$ between samples dominated by ferromagnesians and samples rich in cumulus plagioclase. In general, these expectations are consistent with the observations presented above, except for Zone IVb. It is significant to note that major differences between the zones with respect to total REE abundances and overall slope are consistent with the fact that the TLS is a composite intrusion.

Significant differences in total REE abundances and patterns within the individual zones (particularly in Zone IVb and Zone III) are not clearly understood and cannot be solely explained by accumulation of cumulus phases, but might reflect:

a) the complex chemical evolutionary history of individual zones, like magma replenishment in the chamber and subsequent accumulation from slightly different magma batches; and/or

b) a significant contribution from postcumulus minerals to the whole rock REE

data.

Amphibole (hornblende) is the most common and widespread postcumulus phase throughout the suite, excluding Zone IV. Since hornblende has higher K_D's for MREE (Gd-Ho) relative to HREE (Er-Lu), a lack of enrichment of MREE with respect to HREE throughout the TLS may suggest that postcumulus crystallization has no significant effect on overall REE_N patterns. Furthermore, samples with comparable amounts of postcumulus hornblende from Zones II and III have notably different overall REE_N patterns and abundances. Thus, a lack of systematic variation of REE_N abundances within zones cannot be attributed to postcumulus hornblende.

3.5.2 Presence or absence of Eu-anomaly within the TLS

There are discrepancies between Zone IV and Zones I-III in terms of presence or absence of Eu-anomaly. Many samples with cumulus plagioclase from Zone I-III do not display an expected positive Eu-anomaly, while cumulus plagioclase-bearing samples from Zone IV exhibit positive Eu-anomalies the extent of which is proportional to plagioclase abundance. This could be attributed to differences in:

a) oxygen fugacity; and/or temperature of crystallization, because the extent of the Eu-anomaly in plagioclase decreases with increasing oxygen fugacity and temperature (Hanson, 1978; 1980); and/or

b) melt composition and structure (Moller and Muecke, 1984).

However, as discussed above, the temperatures of crystallization are fairly consistent throughout the TLS. Similarly, a lack of cumulus magnetite/ilmenite suggests overall low oxygen fugacity throughout the TLS (Philpotts, 1990). Thus, temperature and/or oxygen fugacity cannot be the main contributing factors. From their experimental studies, Moller and Muecke (1984) suggested preferential stabilization of Eu^{+2} by a

strong aluminosilicate complexes in the melt phase. They also emphasized the pronounced influence of aluminosilicate complexes in melts with a strongly polymerized structure. The addition of water leads to significant depolymerization of silicate structure and decreases concentrations of aluminosilicate complexes (Moller and Muecke, 1984), Thus, addition of water can reduce the extent of the Eu-anomaly. This is consistent with the fact that Zones I-III crystallized from magmas that have somewhat higher water content than that of Zone IV (Chapter 2). To sum up, the differences in Eu-anomaly between Zone IV and other zones are best attributed to crystallization from magmas with different water contents.

3.5.3 Extended REE diagrams

The presence of a minor positive Ti-anomaly within the TLS, except Zone I, is consistent with petrographic observation which indicates: a) a lack of opaque-oxide phases in Zone I; and b) the postcumulus nature of opaque-oxides in Zones II-IV.

The presence of a significant negative Nb-anomaly, particularly with a minor positive Ti-anomaly, is consistent with this signature being indicative of the source materials or mixing of source materials. Certainly the bulk distribution coefficients of the observed phases cannot account for a significant deviation of Nb behaviour away from that of Th and La.

3.5.4 Interrelationship between Nd isotopic and the mineral and whole rock geochemistry

Figure 3.21 illustrates the interrelationship between Nd isotopic and the mineral and whole rock geochemistry. Significant observations are as follows:

a) for a given similar MgO, SiO_2, orthopyroxene and clinopyroxene composition,

Zone II and Zone III have significantly different and higher ϵ_{Nd} values than Zone IV and Zone I.

b) Zone II and Zone III have consistent ϵ_{Nd} values over a wide range of MgO and SiO_2 content ($+2.6 \pm 0.2$ for Zone II and $+5.0 \pm 0.1$ for Zone III).

c) In Zone IVb, ϵ_{Nd} values vary from -0.1 to +1.0, and overlap ϵ_{Nd} values obtained from Zone IVa and Zone I. For Zone I and Zone IVa, only one sample was analyzed, so it is difficult to establish intra-zone heterogeneity in this case. However, it is significant to note that the defined intra-sample and intra-zone isotopic heterogeneities are ≤ 1 ϵ_{Nd}.

Interrelationship between Nd isotopic composition and $(REE)_N$ patterns are illustrated in Figure 3.22. There is an overall consistency within the TLS, *i.e.* the ϵ_{Nd} value decreases with increasing $(La/Sm)_N$ and with decreasing Sm/Nd. In Zone II and Zone III, the ϵ_{Nd} values are consistent over a wide range of $(La/Lu)_N$.

The main conclusion from these observations is that Nd isotopic heterogeneity within the TLS (-0.1 to +5.0) existed before the magma batches giving rise to the zones were emplaced into the chamber. This may suggest that the TLS suites crystallized from isotopically distinct parental magmas either as a result of: a) source heterogeneity (*e.g.* Weaver and Tarney, 1983; Leeman and Hawkesworth, 1986); and/or b) crustal contamination (*e.g.* Dickin , 1981; Carlson et al., 1981; Huppert and Sparks, 1985). These alternatives are discussed in detail in Chapter 6.

3.5.5 Summary

a) The variation in REE_N abundances do not reflect the level of differentiation within the TLS and/or within the indivual zones. In general samples with cumulus pyroxene and/or olivine have notably lower $(La/Lu)_N$ than those of samples

dominated by cumulus plagioclase.

b) There is a significant ϵ_{Nd} variation within the TLS from -0.1 to +5.1 and there are three different levels of isotopic heterogeneity:

i) intra-sample (0.6 to 0.8 ϵ_{Nd} unit);

ii) intra-zone ($\leq$ 1 ϵ_{Nd} unit); and

iii) inter-zone (1 to 5 ϵ_{Nd} unit).

c) Inter-zone isotopic heterogeneity appears to exist before the emplacement of magma batches into the chamber.

d) The presence of a significant Nb-anomaly appears to be source related.

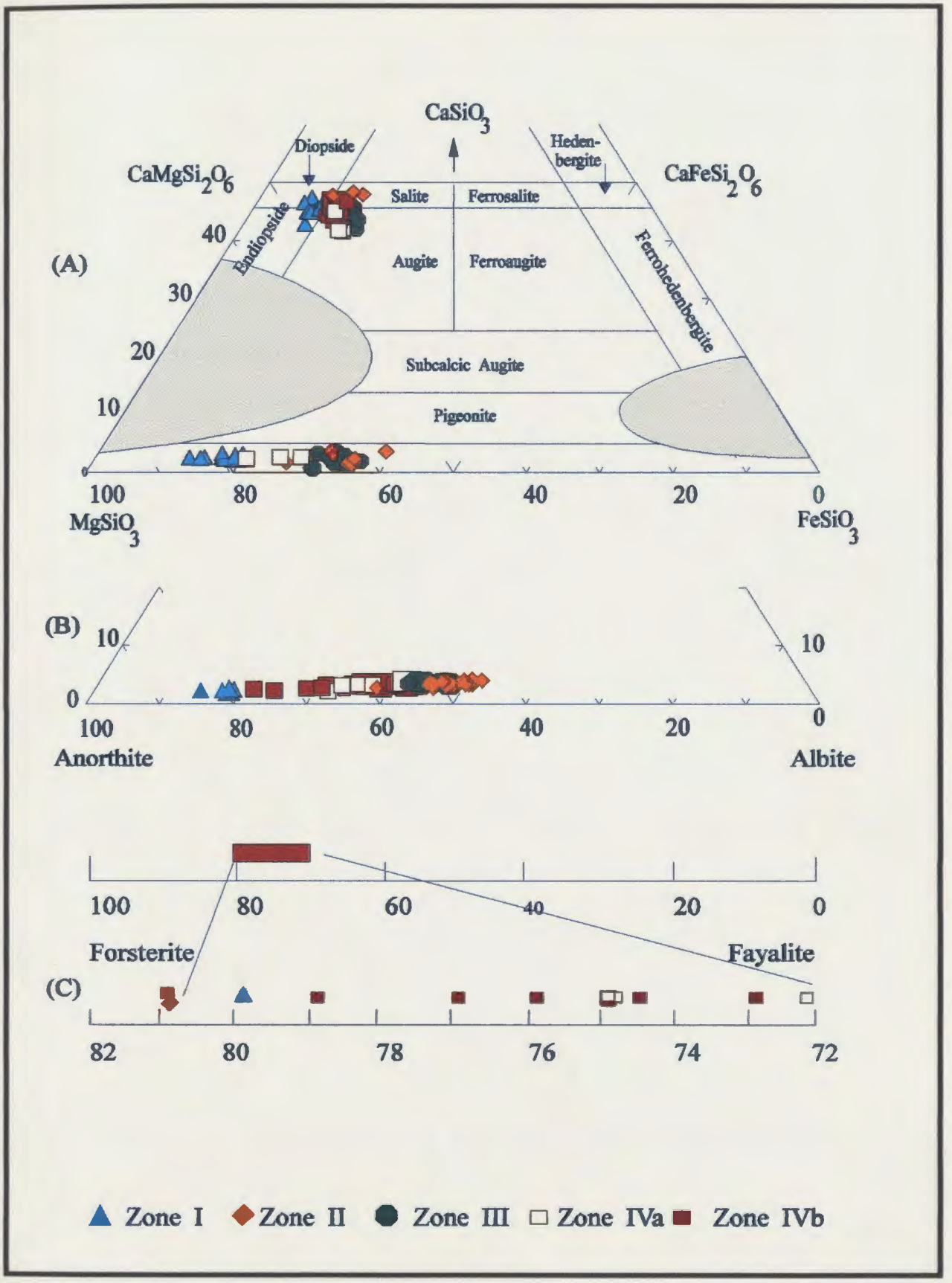

Figure 3.1 Average mineral compositions of pyroxene (A), plagioclase (B), and olivine (C) in the TLS.

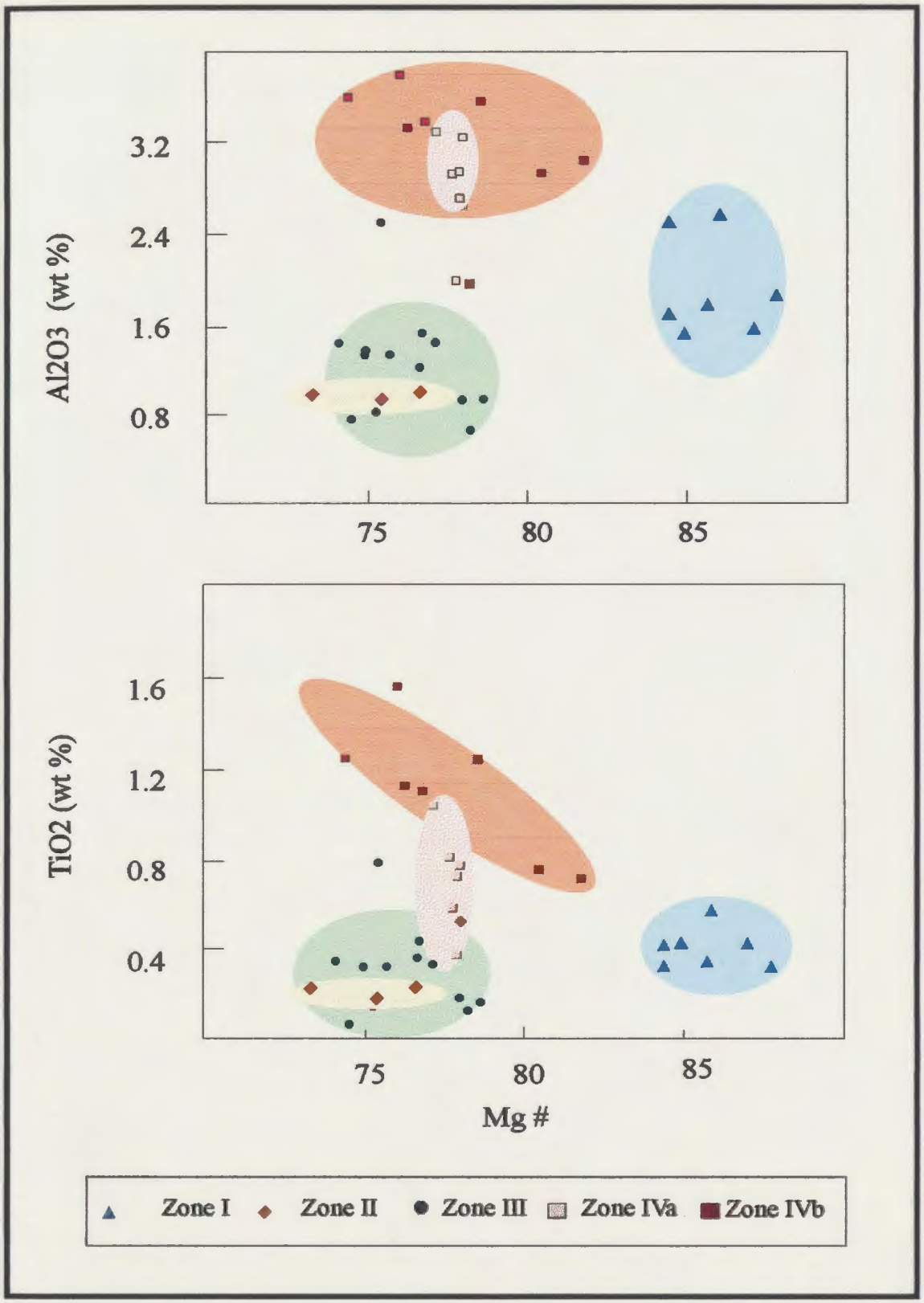

Figure 3.2 Plots of Al2O3 and TiO2 aganist Mg # of clinopyroxenes from the TLS.

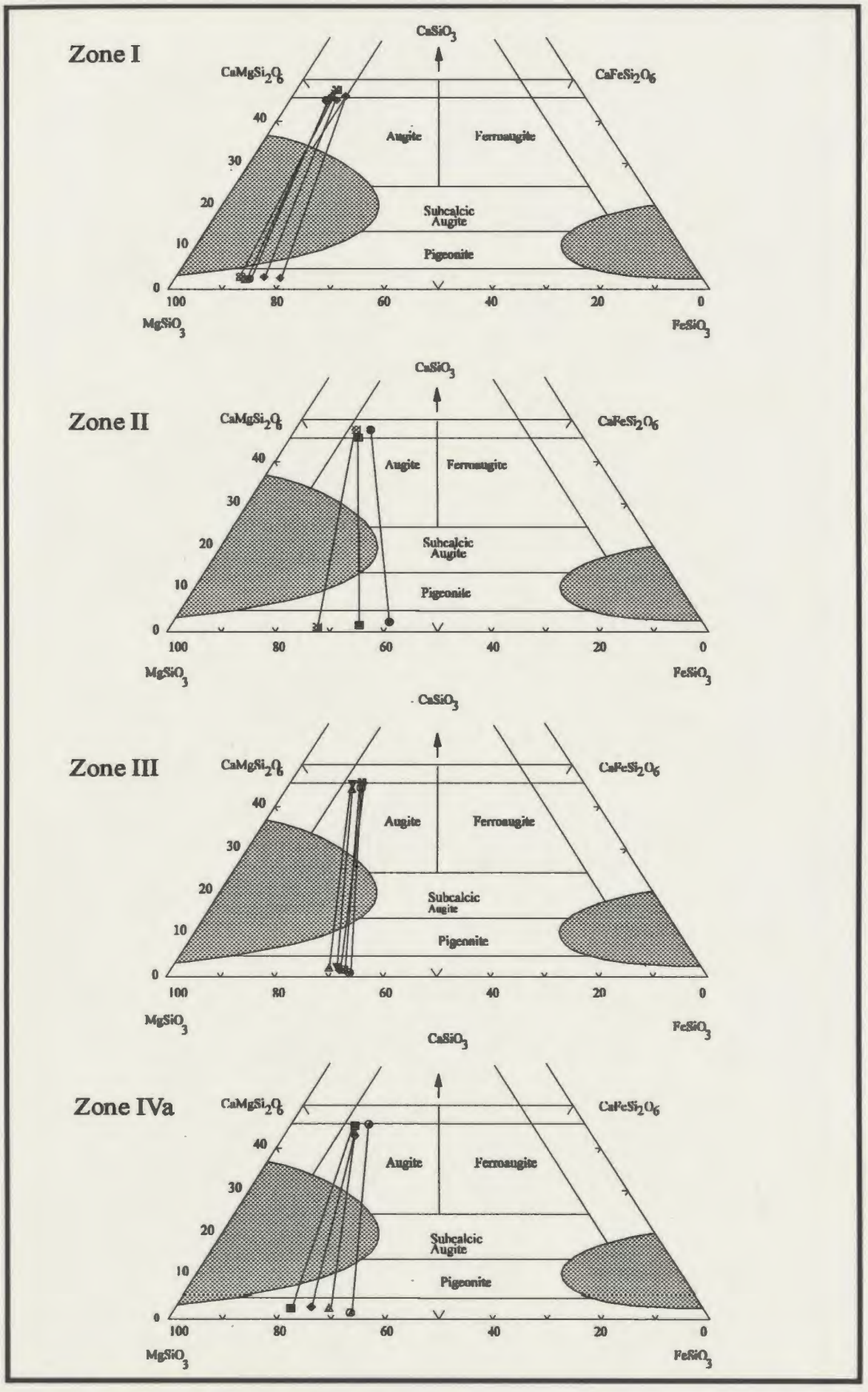

Figure 3.3 Coexisting average pyroxene compositions from the TLS. (after Poldervaart and Hess, 1951 and Deer et al., 1966; same for Figure 3.1).

F-91-582.2 , Zone 1.

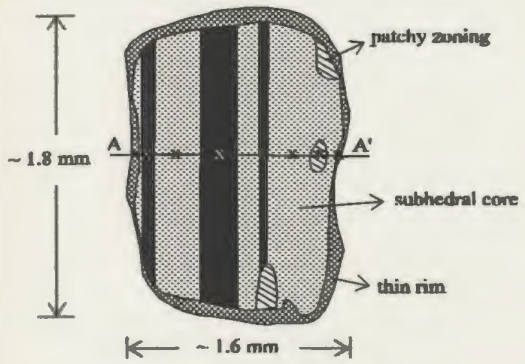

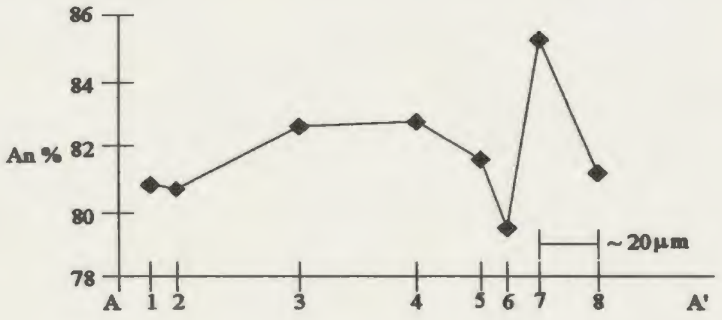

F-92-71, Zone II.

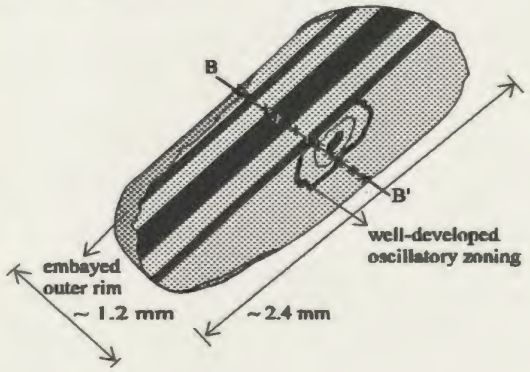

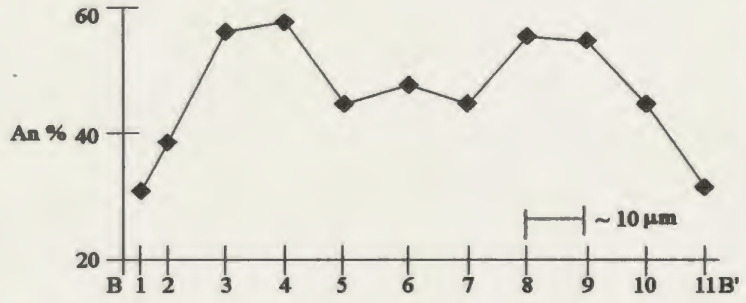

F-91-21, Zone III.

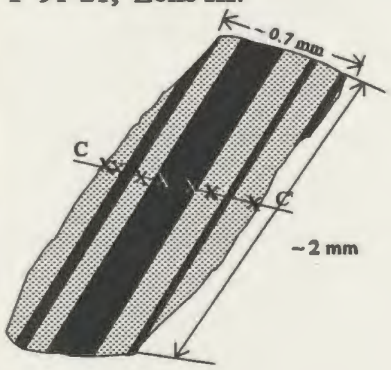

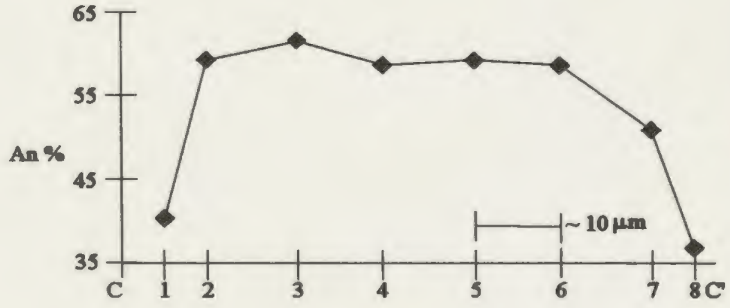

F-91-279.2
post cumulus, Zone IV.

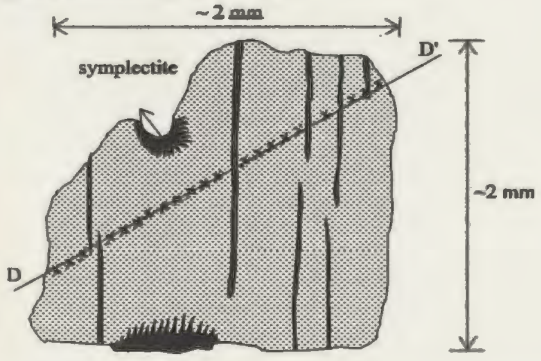

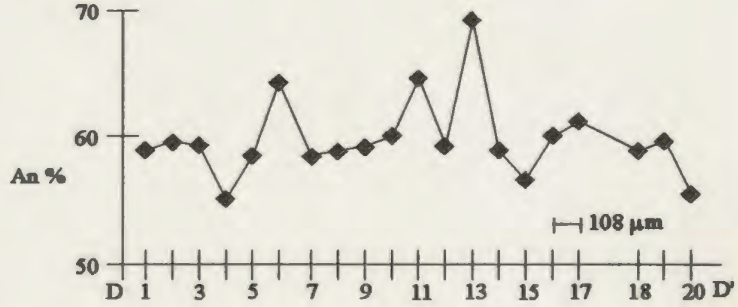

Figure 3.4 Representative plagioclase zoning profiles from the TLS.

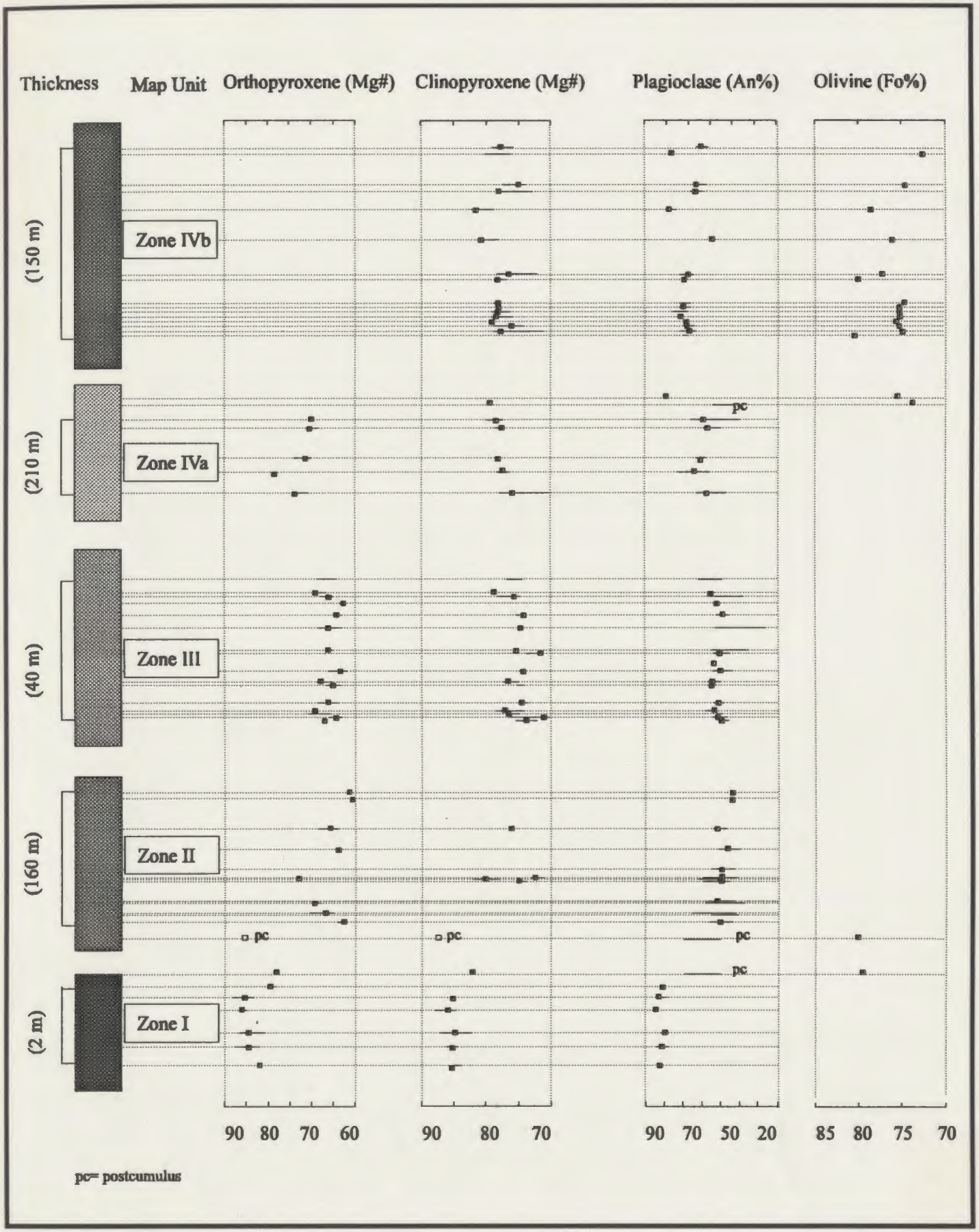

Figure 3.5 Variation in pyroxene (Mg#), plagioclase (An%) and olivine (Fo%) compositions within the TLS. Symbol indicates average composition, bar indicates range of variation.

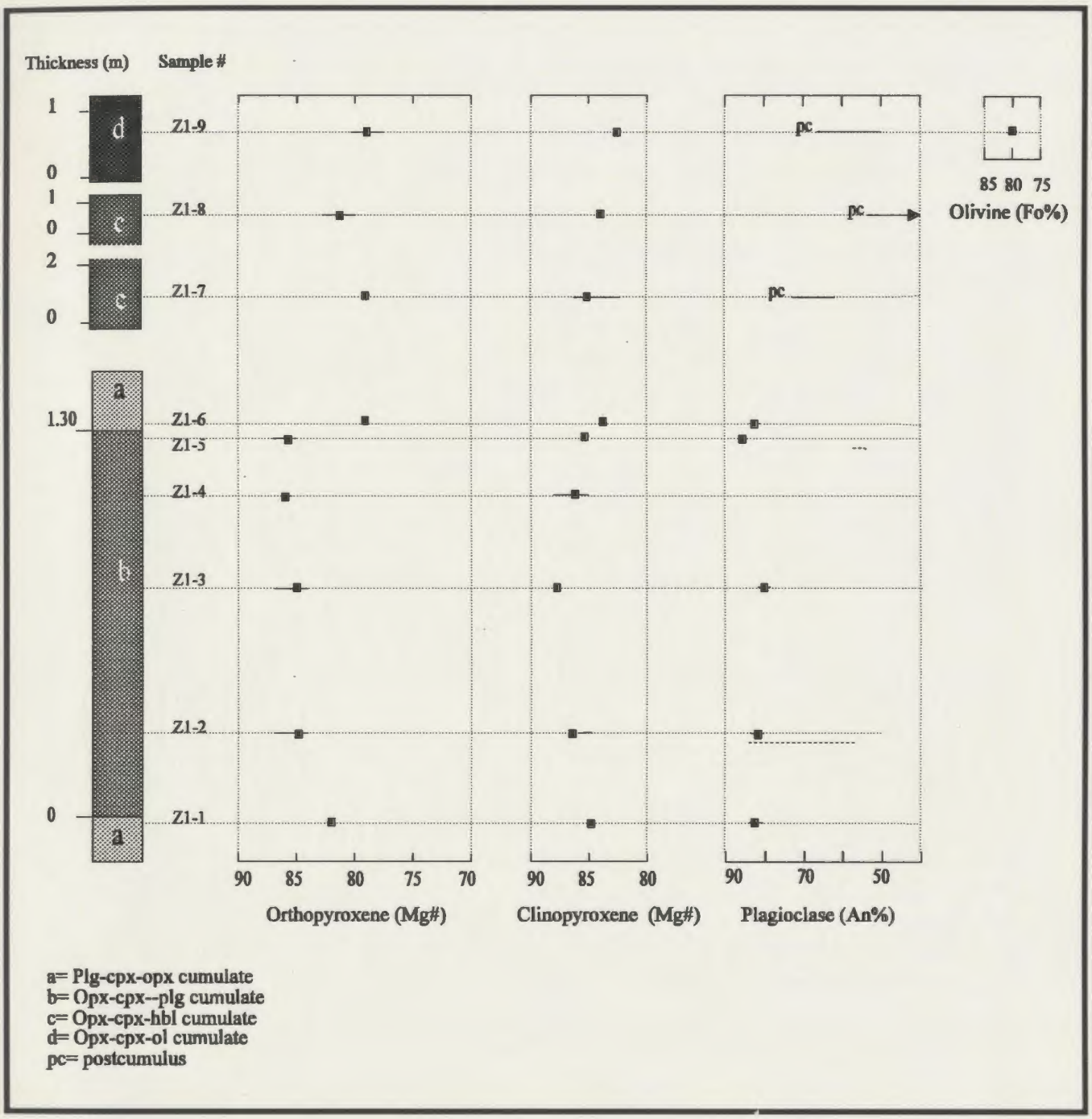

Figure 3.6 Variation of Mg # in pyroxene, An% in plagioclase (core ±rim) and Fo% in olivine in Zone I. Range of rim composition of plagioclase is indicated by lower dashed line in each pair. Symbol indicates average composition, bar indicates range of variation.

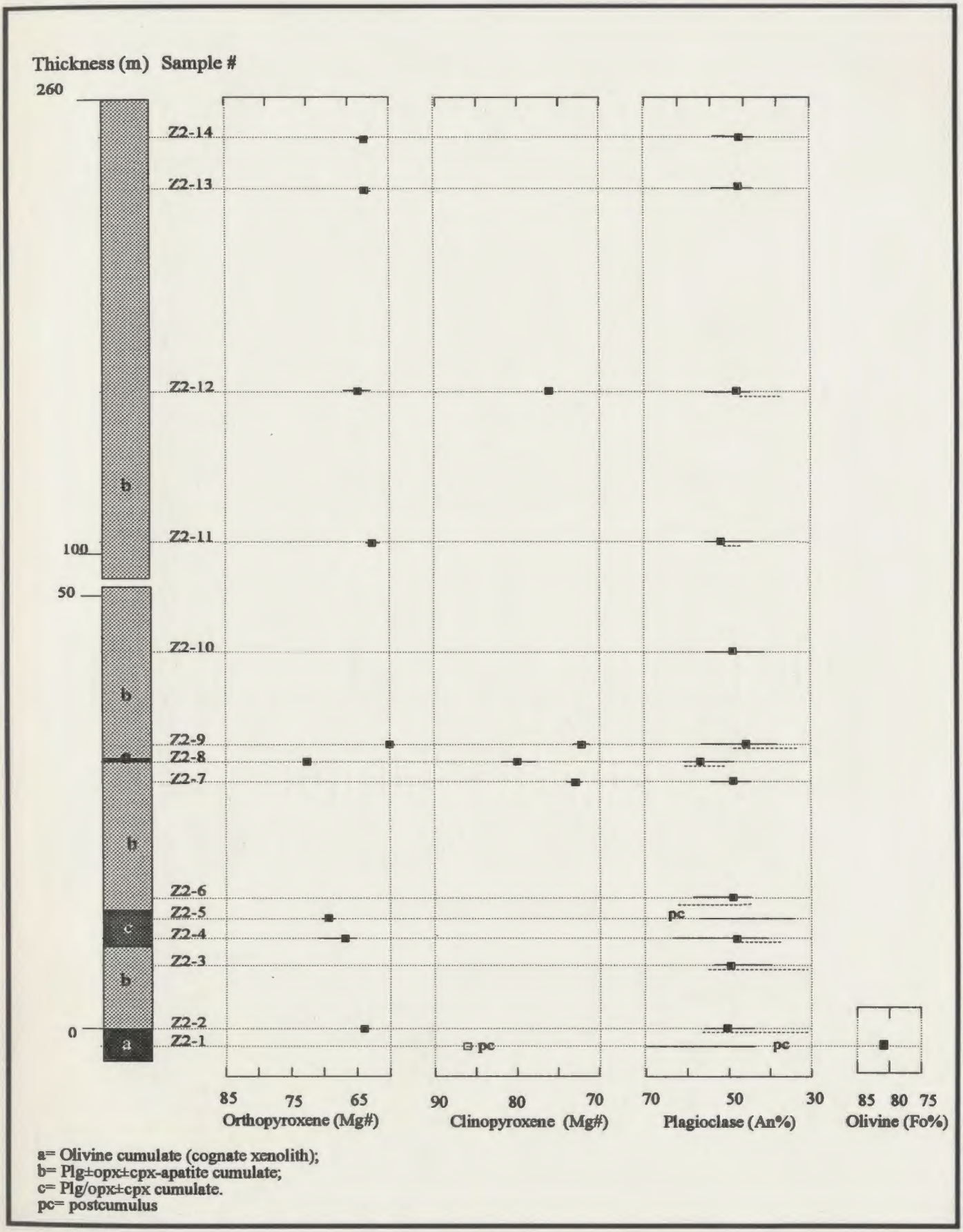

Figure 3.7 Variation of Mg# in pyroxene, An% in plagioclase (core±rim) and Fo% in olivine, in Zone II. Range of rim composition of plagioclase is indicated by lower dashed line in each pair. Symbol indicates average composition, bar indicates range of variation.

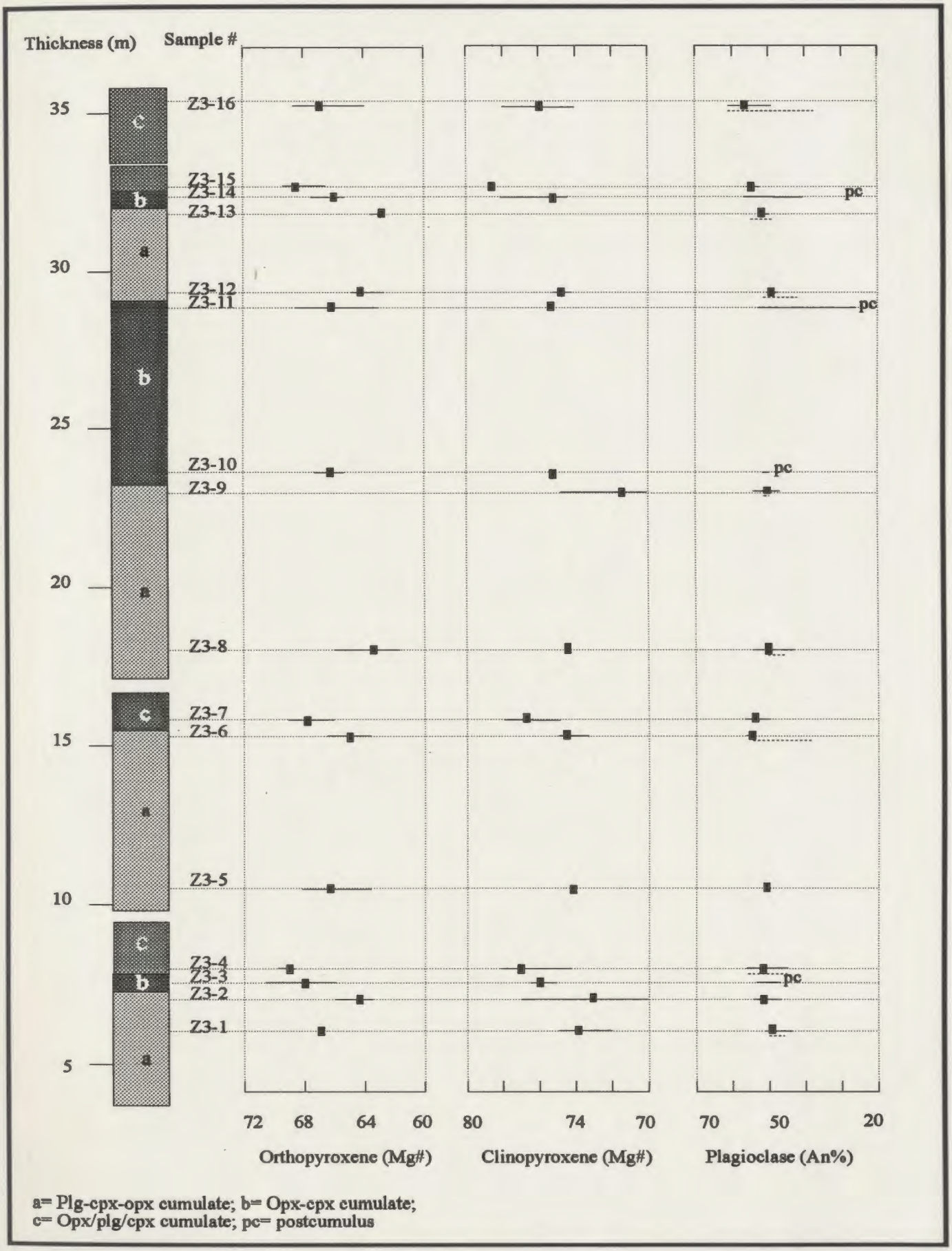

Figure 3.8 Variation of Mg# in pyroxene (core) and An % in plagioclase (core±rim) in Zone III. Range of rim composition of plagioclase is indicated by lower dashed line in each pair. Symbol indicates average composition, bar indicates range of variation.

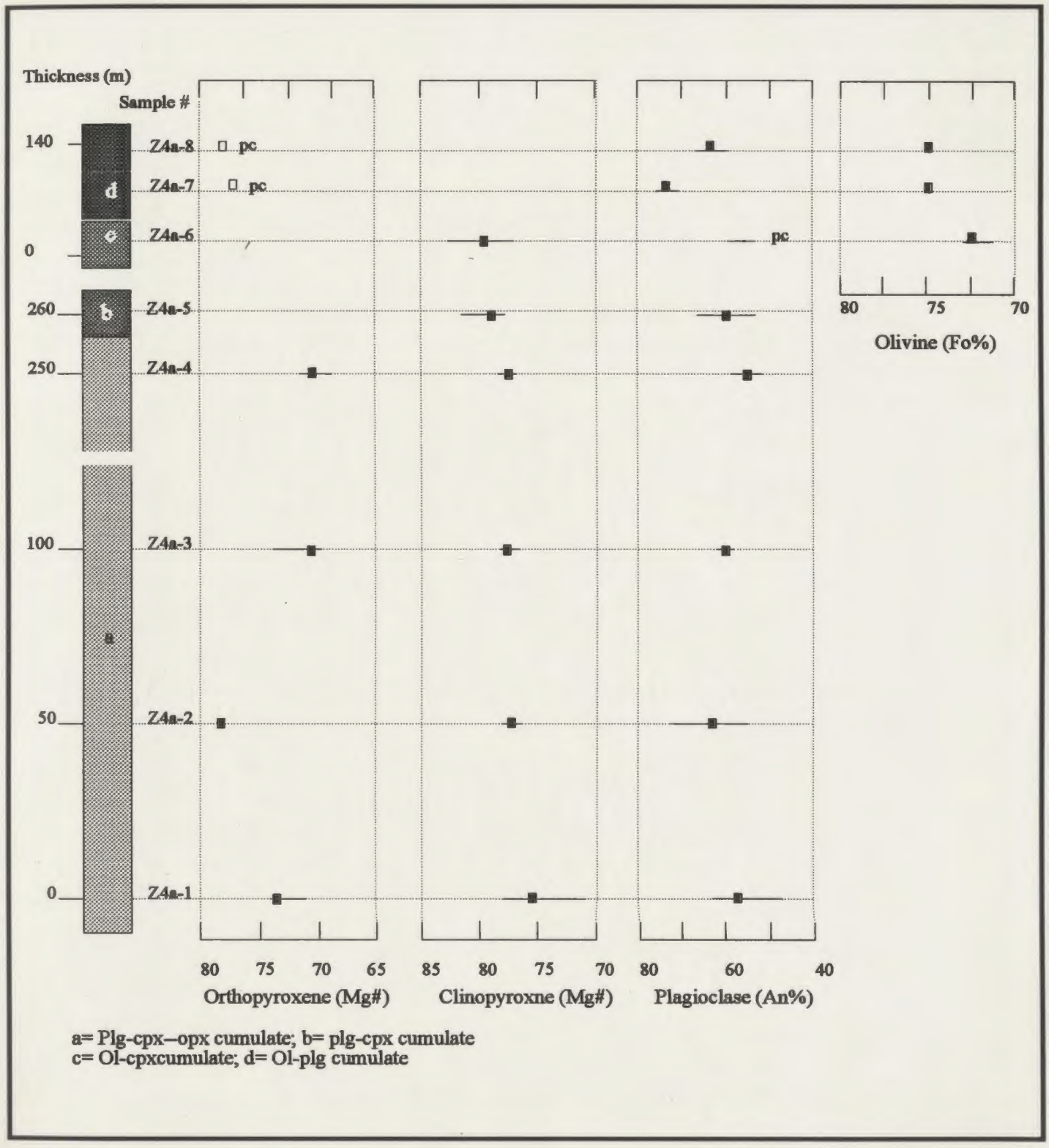

Figure 3.9 Variation of Mg # in pyroxene, An% in plagioclase, Fo% in olivine, in Zone IVa. Symbol indicates average composition, bar indicates range of variation.

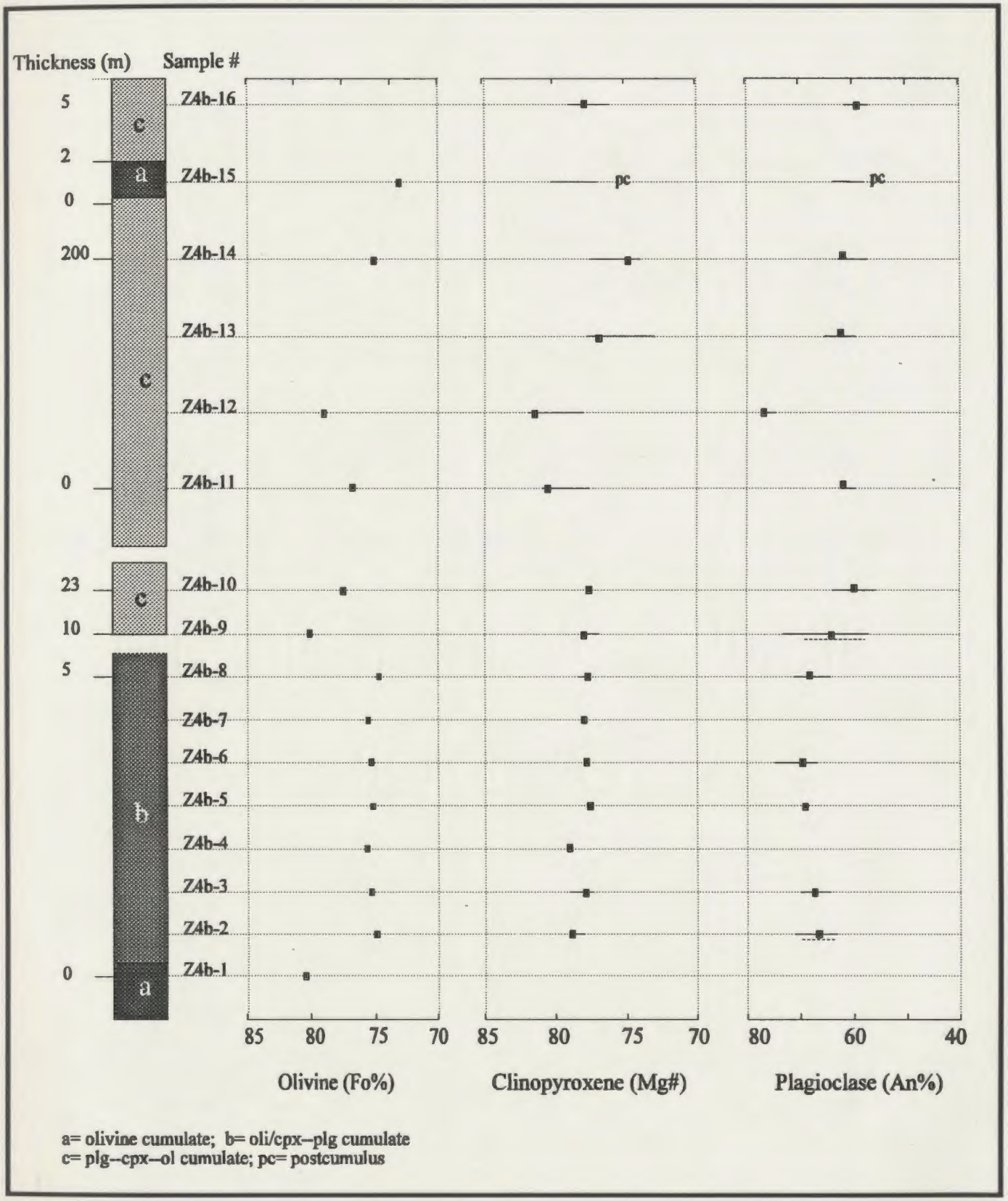

Figure 3.10 Variation in Fo% in olivine, Mg# in clinopyroxene and An% in plagiocalase in Zone IVb. Symbol indicates average composition, bar indicates range of variation.

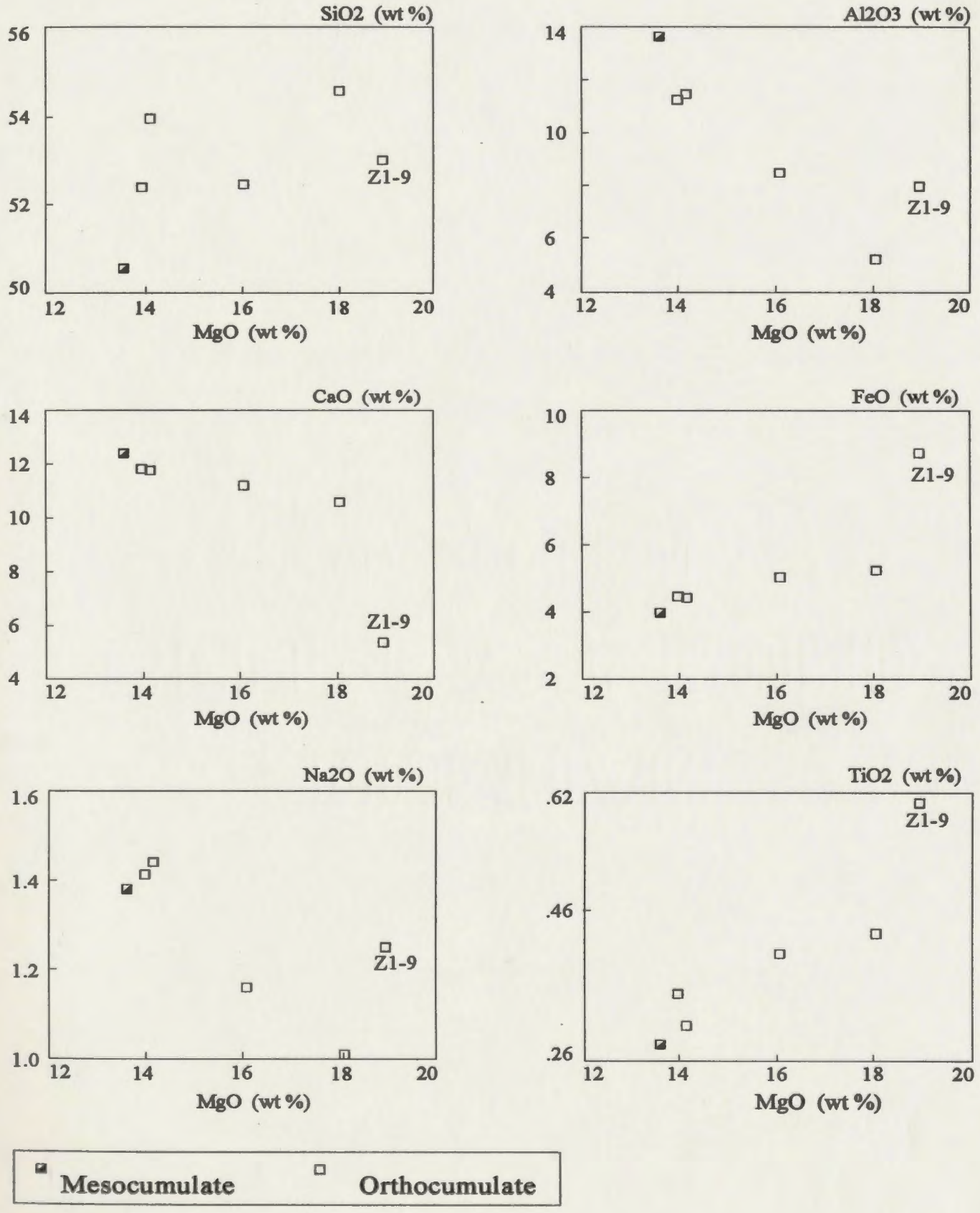

Figure 3.11a Major element variation diagrams, for Zone I.

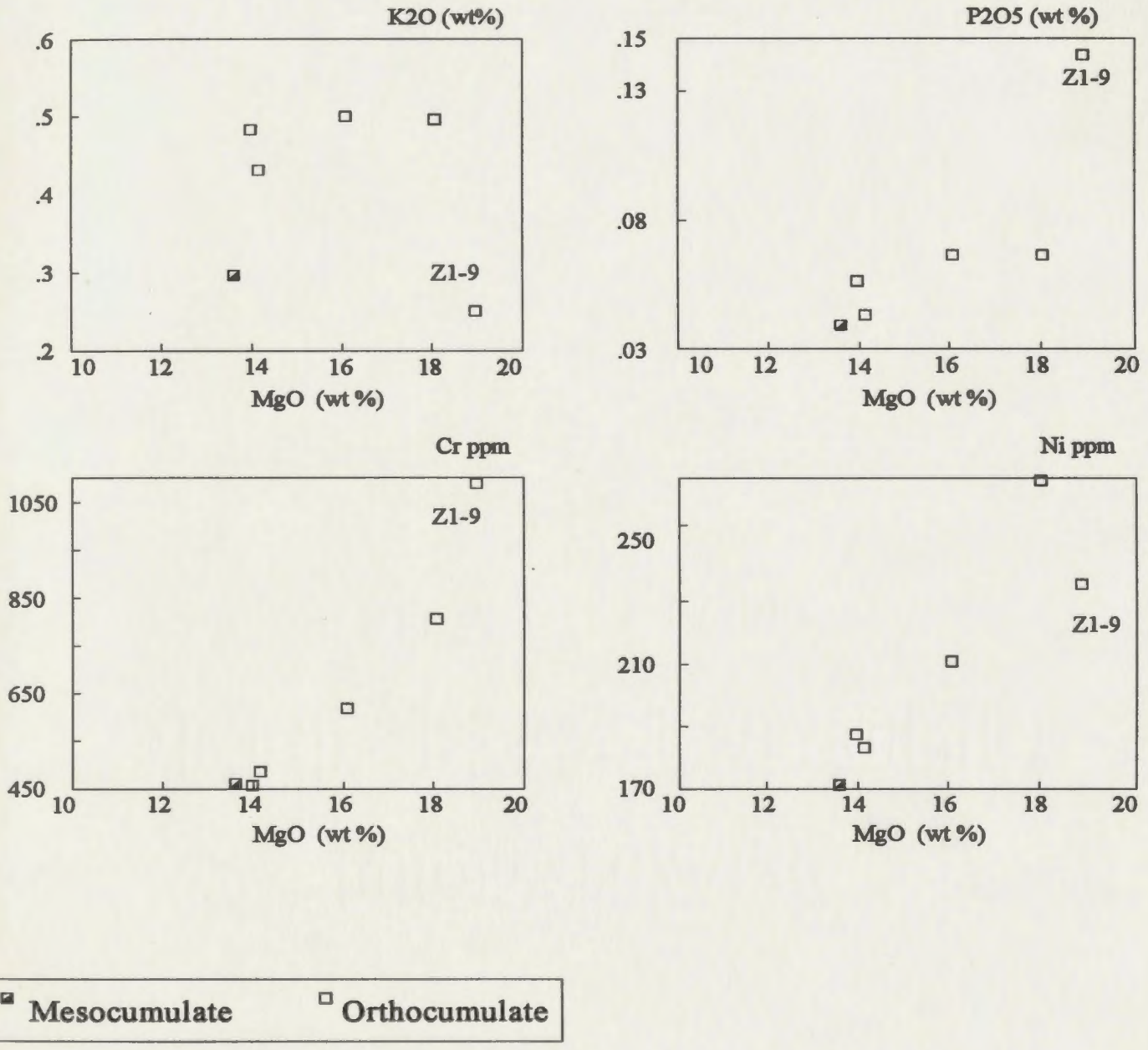

Figure 3.11b Selected minor and trace element variation diagrams, for Zone I.

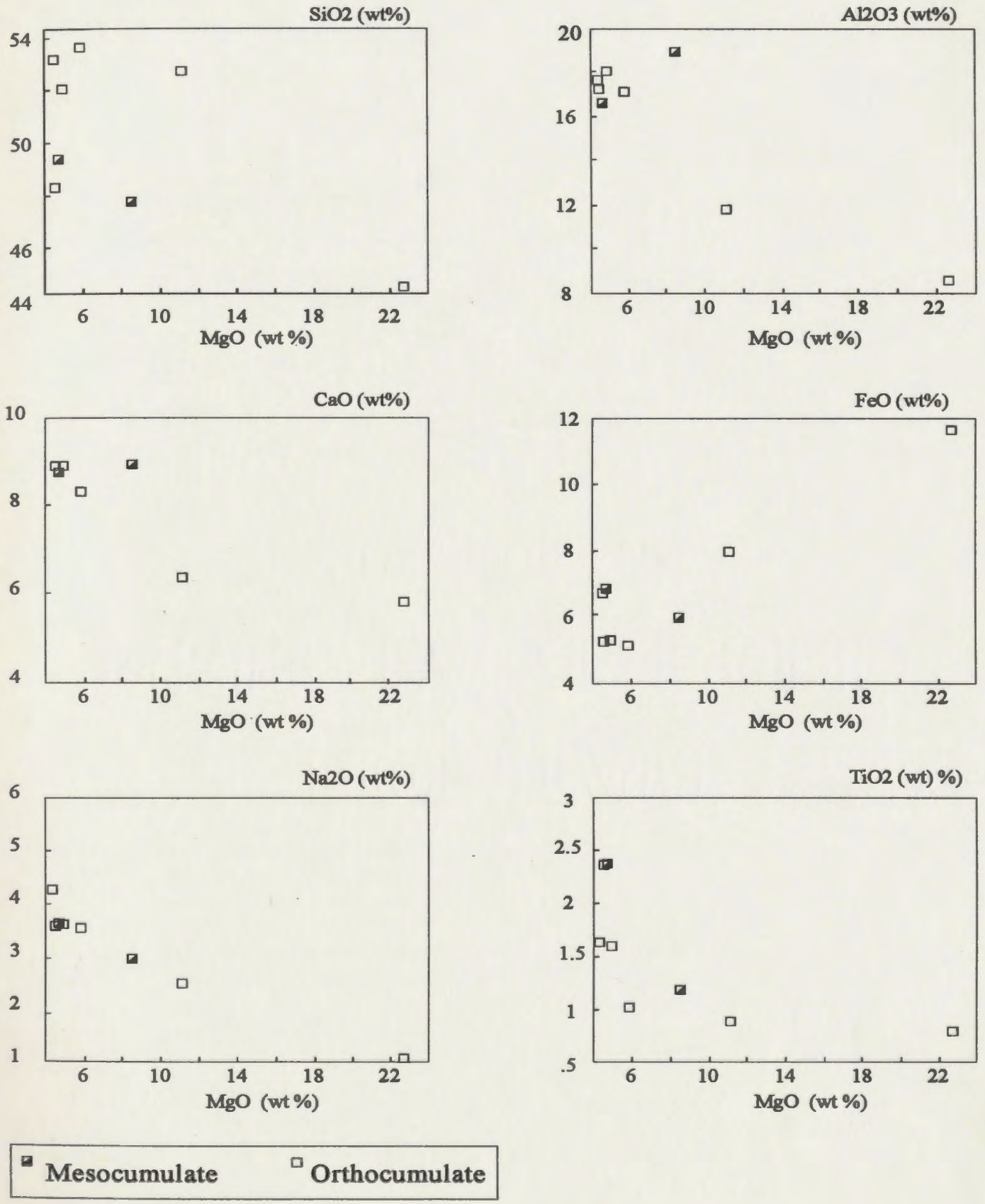

Figure 3.12a Major element variation diagrams, for Zone II.

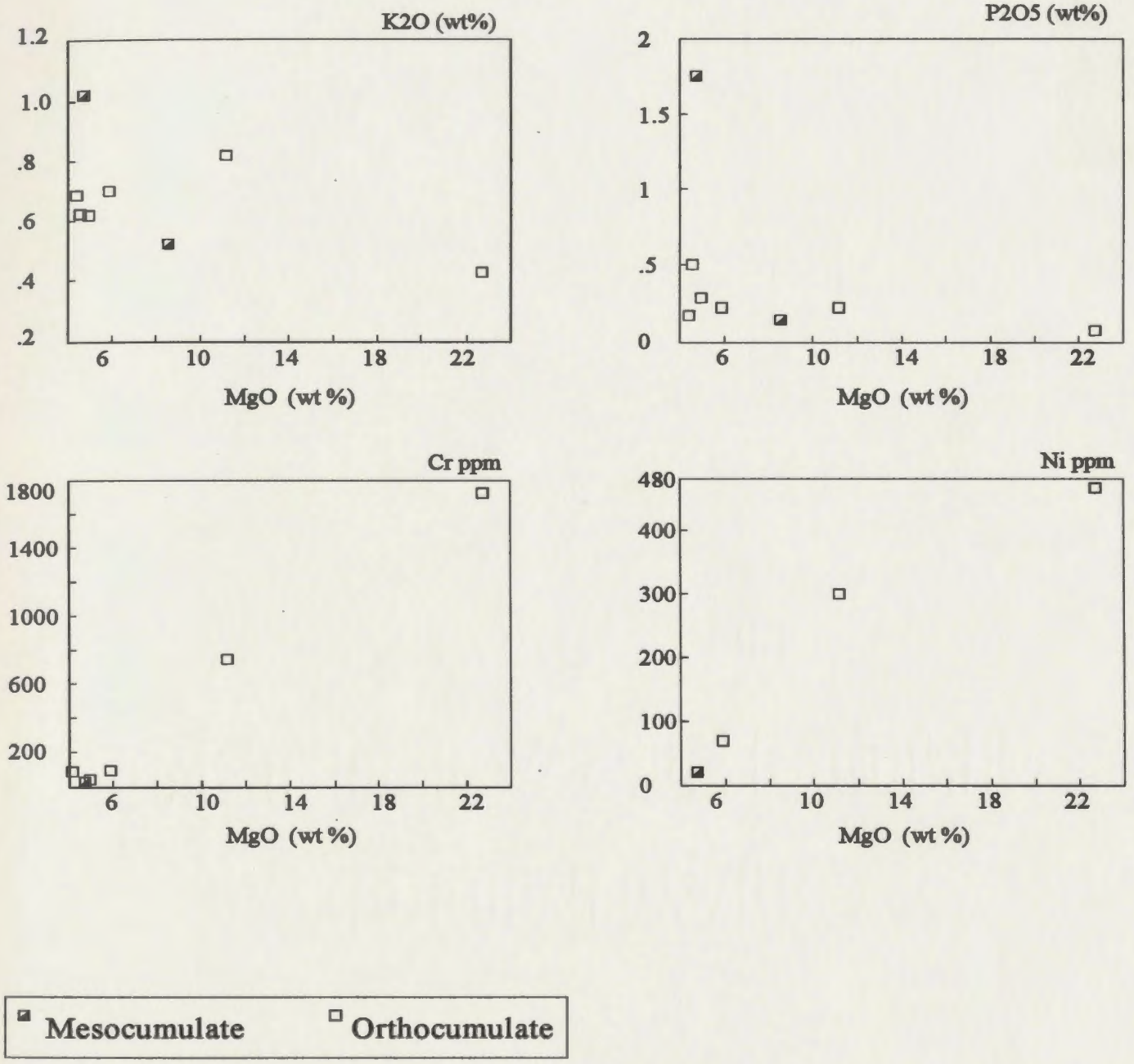

Figure 3.12b Selected minor and trace element variation diagrams, for Zone II.

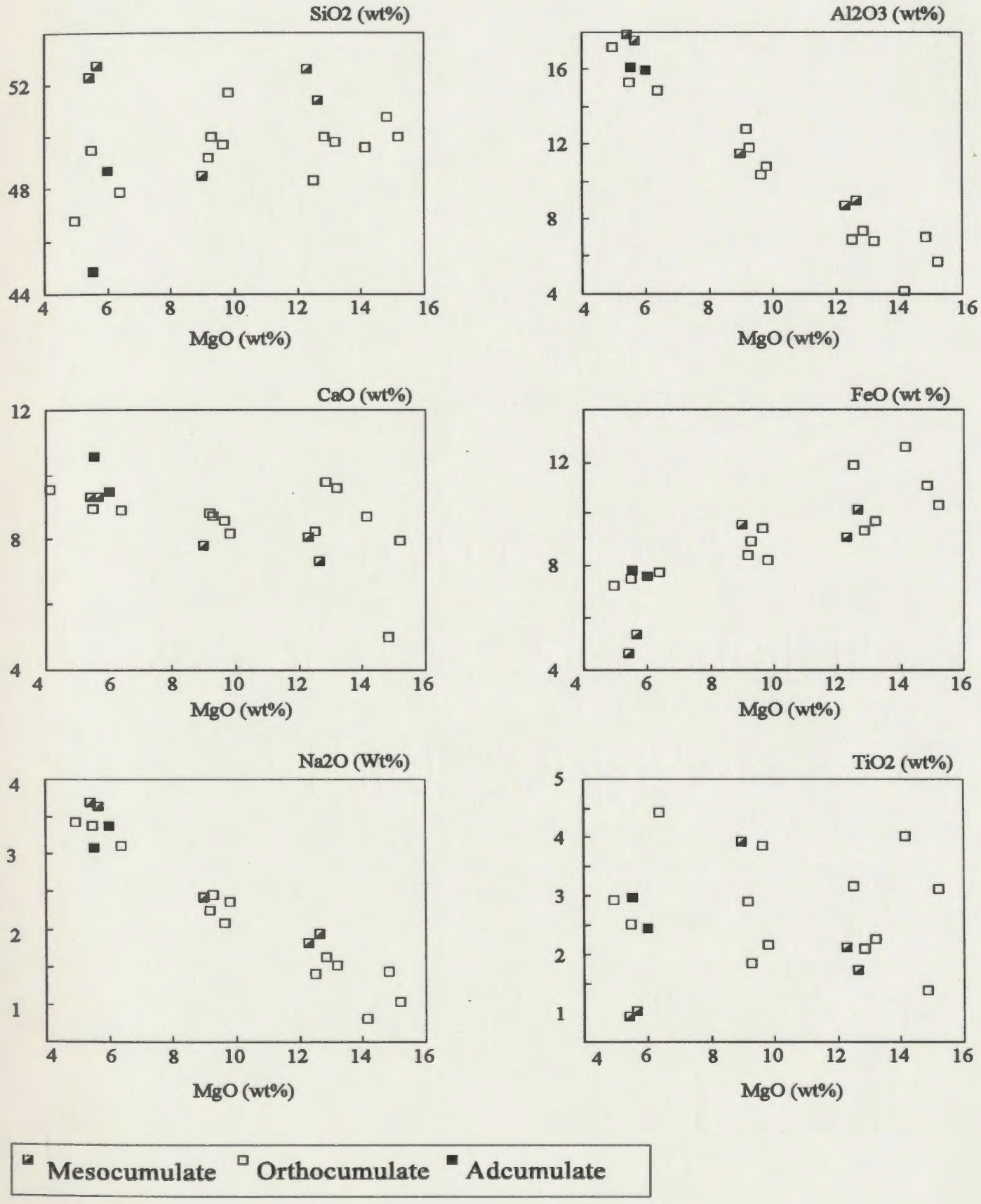

Figure 3.13a Major element variation diagrams, for Zone III.

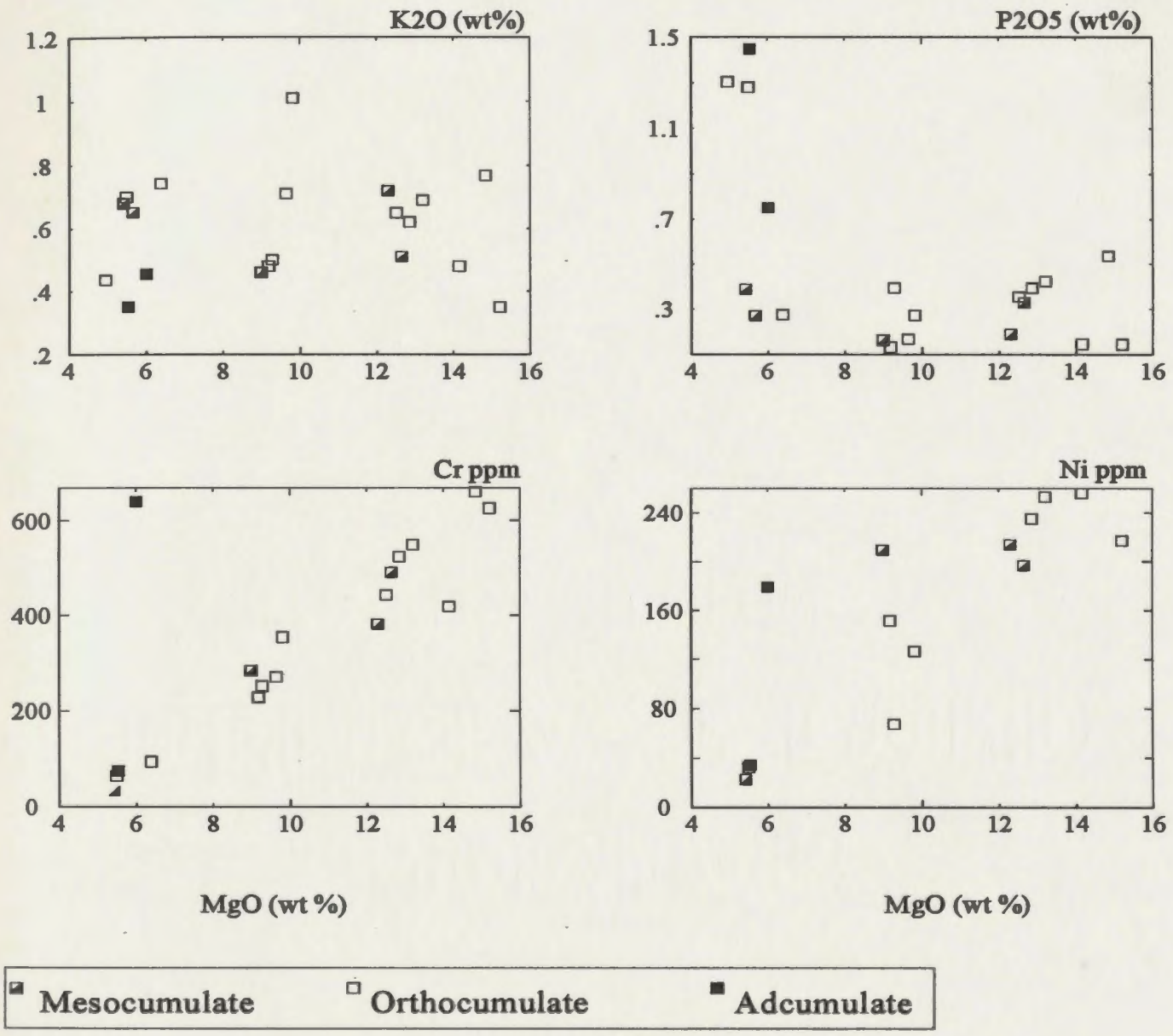

Figure 3.13b Selected minor and trace element variation diagrams, for Zone III.

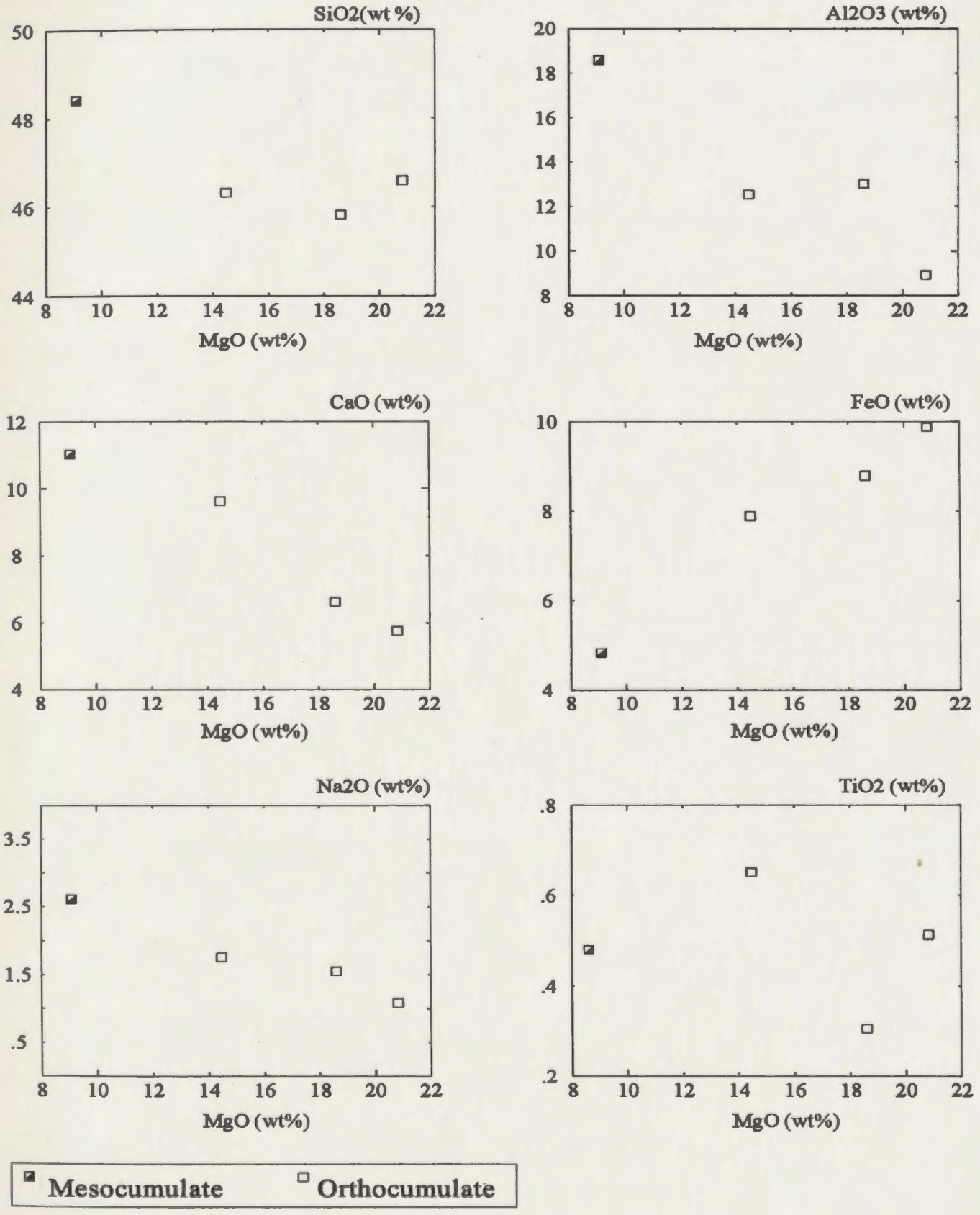

Figure 3.14a Major element variation diagrams, for Zone IVa.

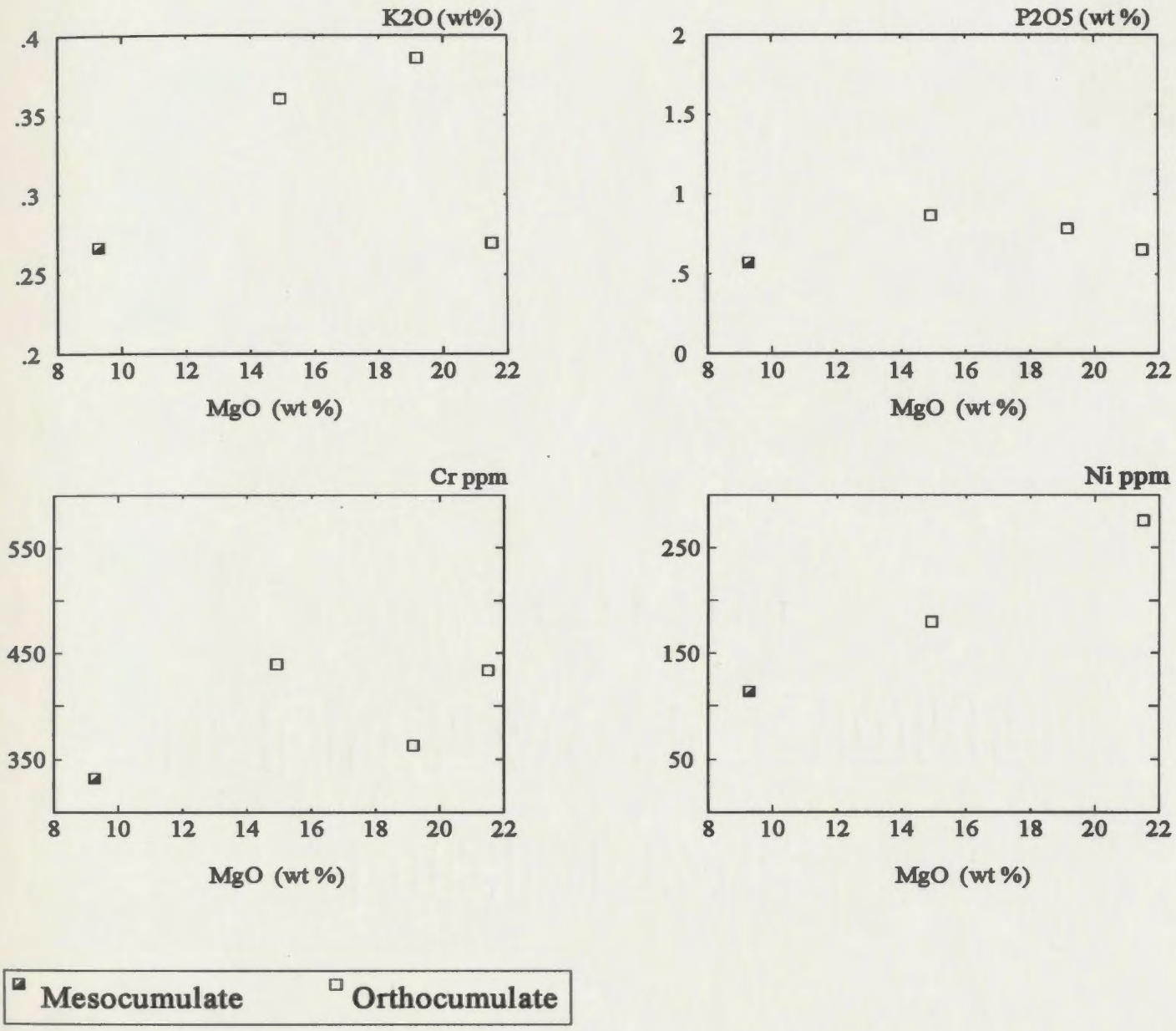

Figure 3.14b Selected minor and trace element variation diagrams, for Zone IVa.

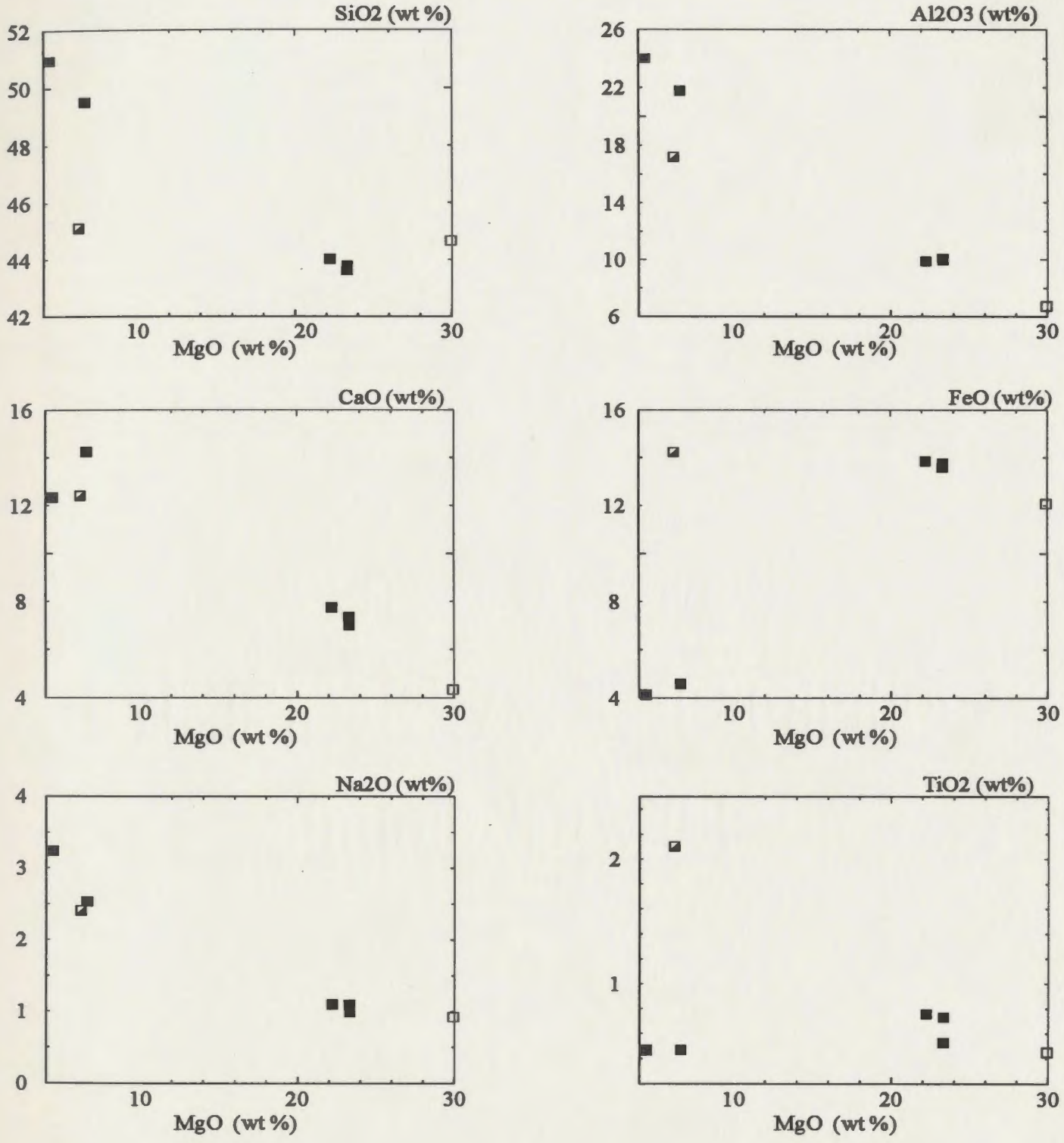

Figure 3.15a Major element variation diagrams, for Zone IVb.

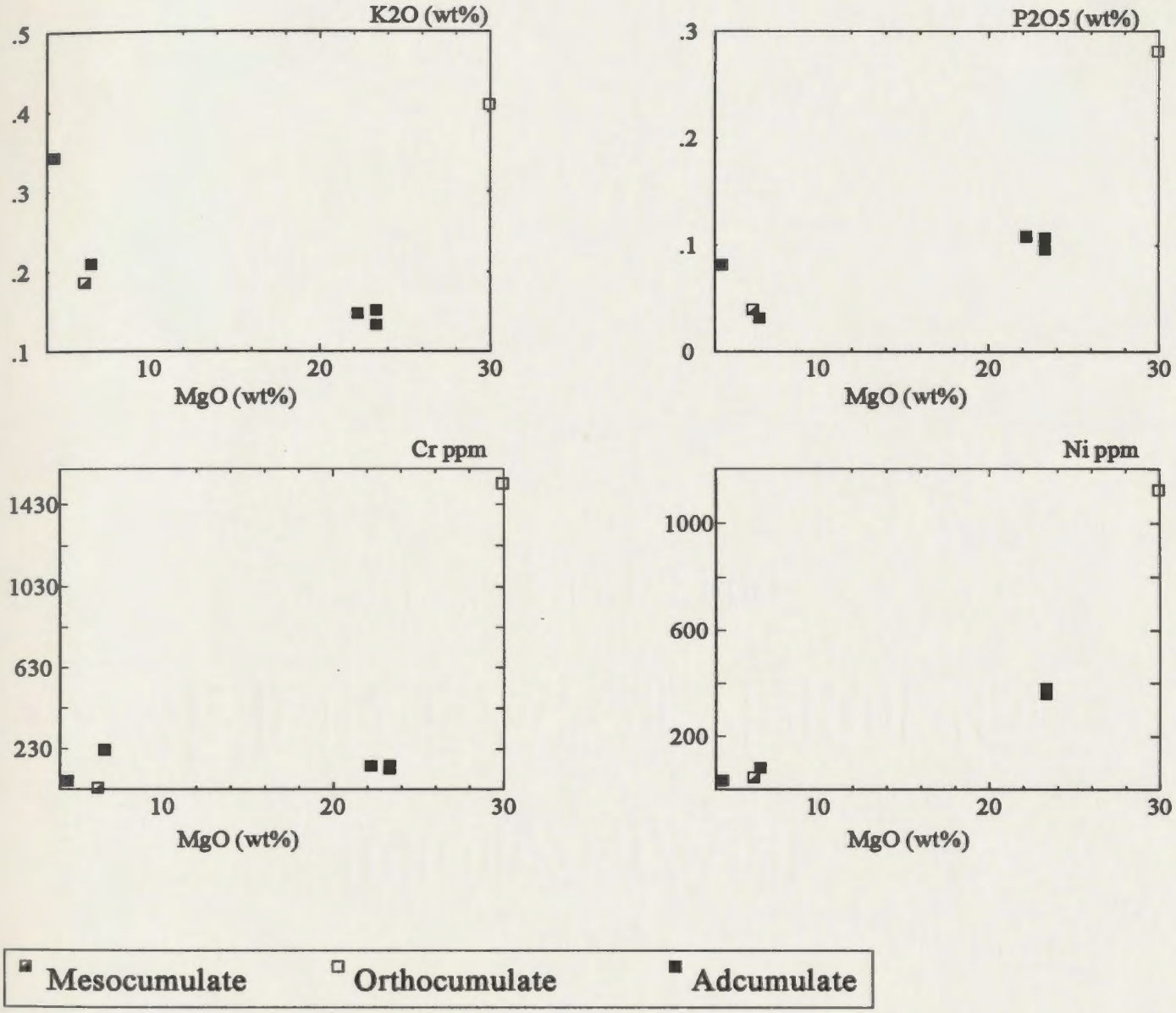

Figure 3.15b Selected minor and trace element variation diagrams, for Zone IVb.

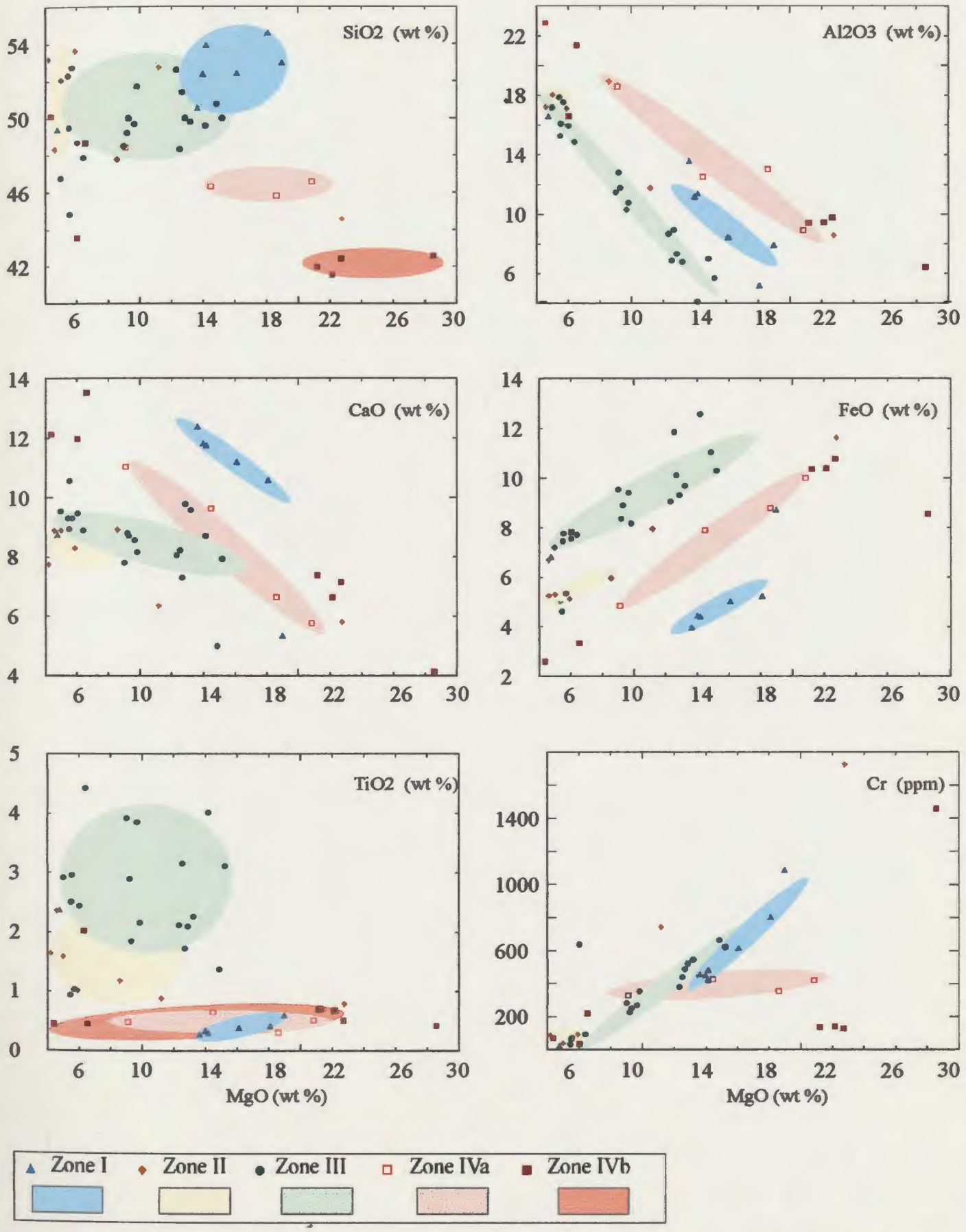

Figure 3.16 Combined, selected major, minor and trace element variation diagrams for the TLS.

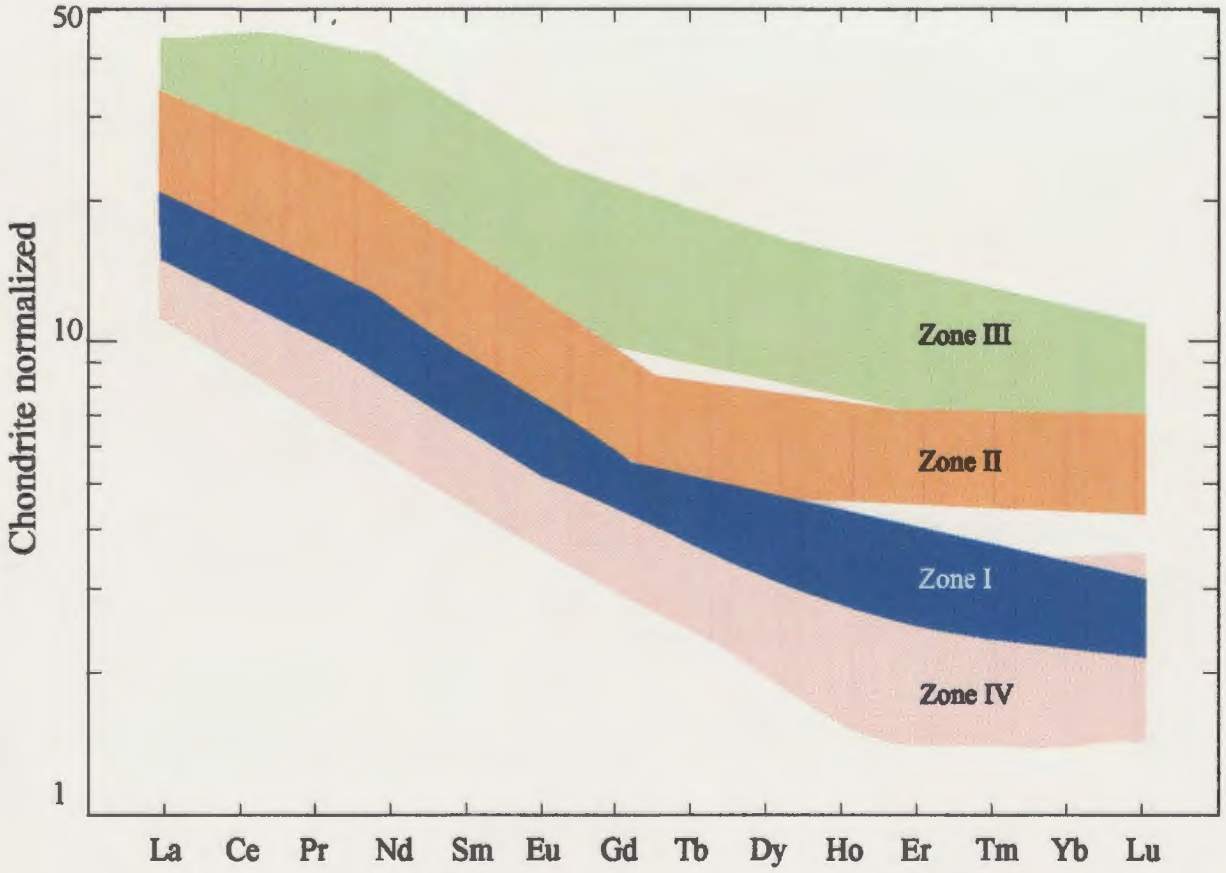

Figure 3.17a Inter-zone chondrite normalized REE patterns, for the TLS.

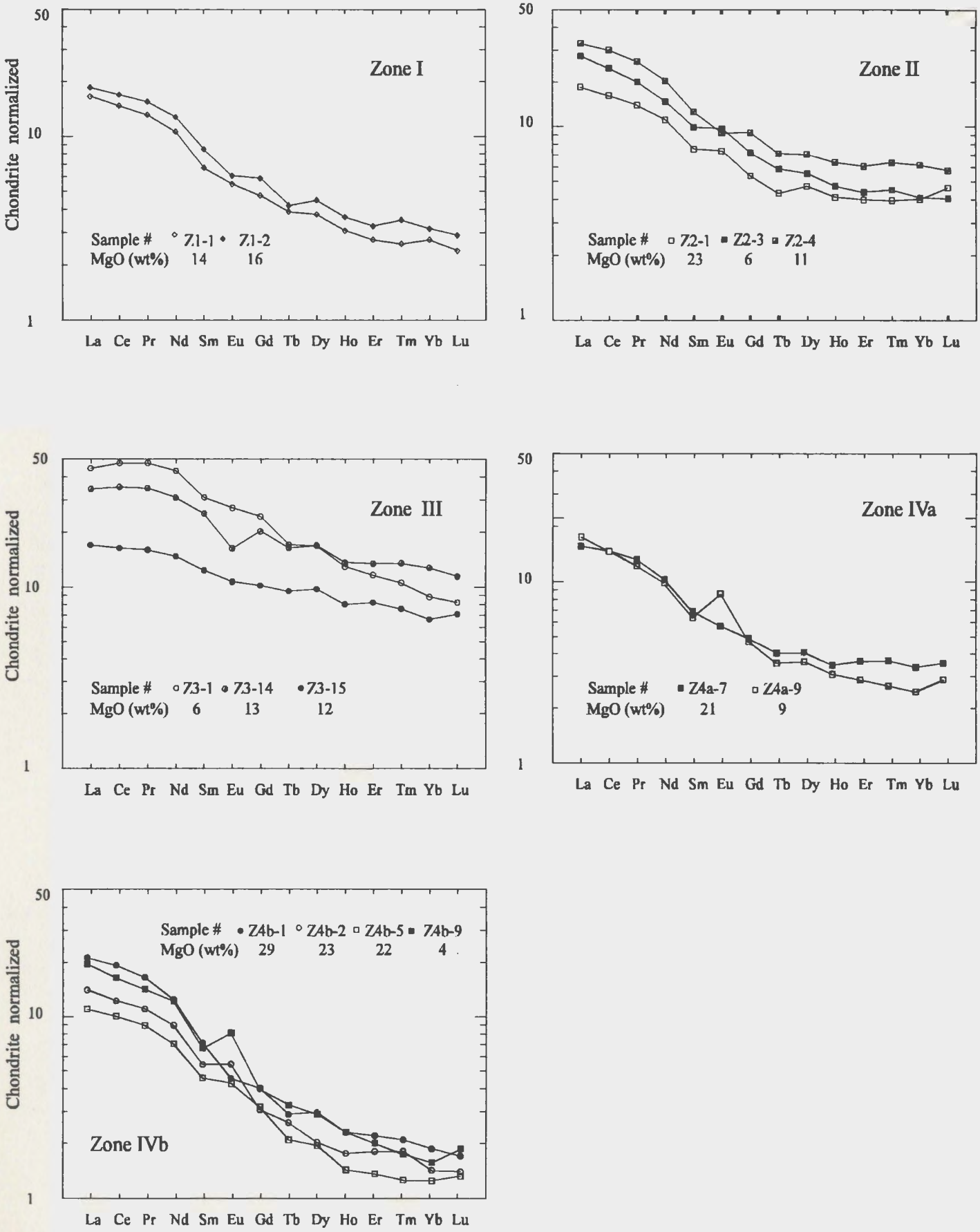

Figure 3.17b Chondrite normalized REE diagrams for Zones I-IV

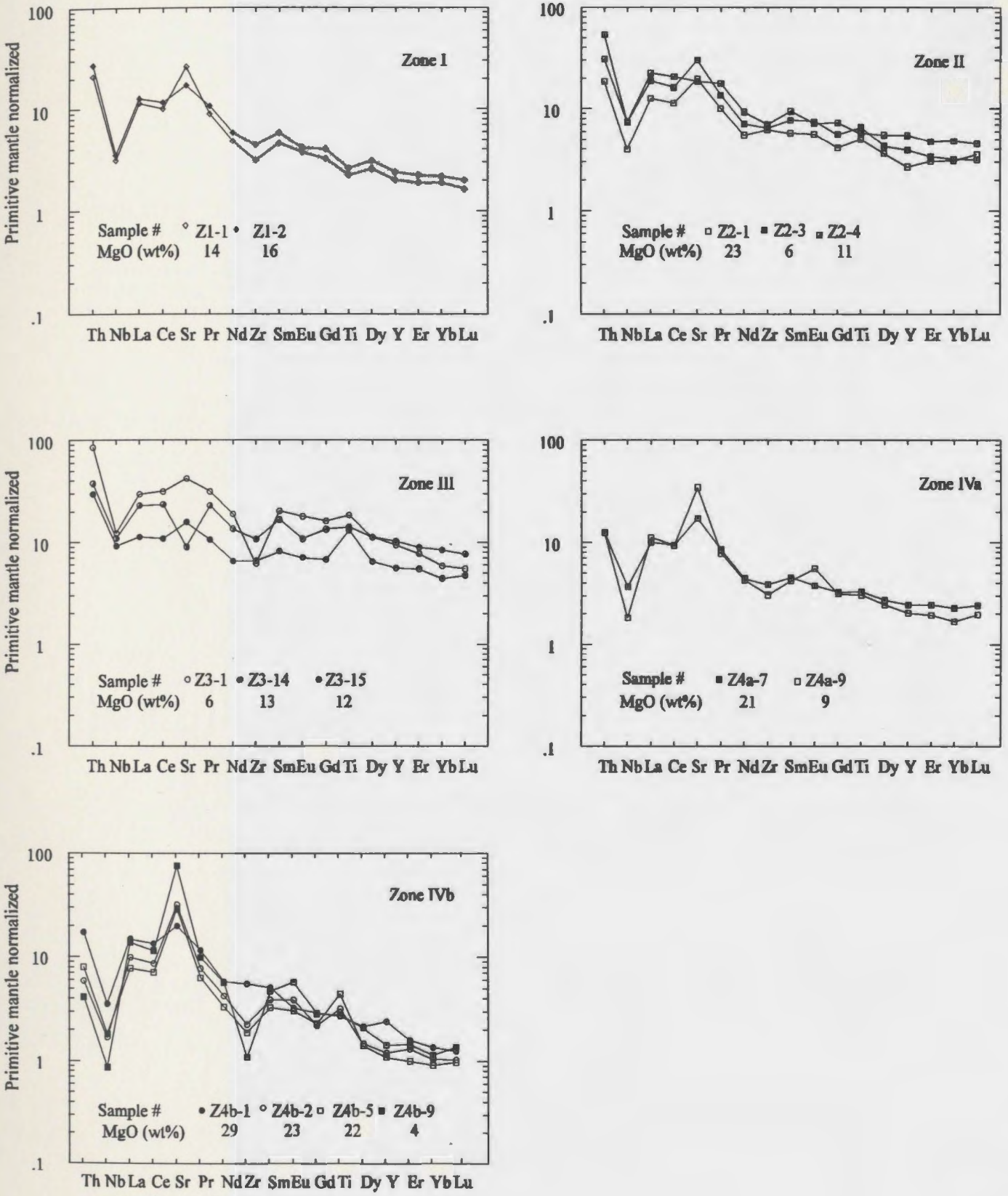

Figure 3.18 Primitive mantle normalized extended REE diagrams for Zones I-IV.

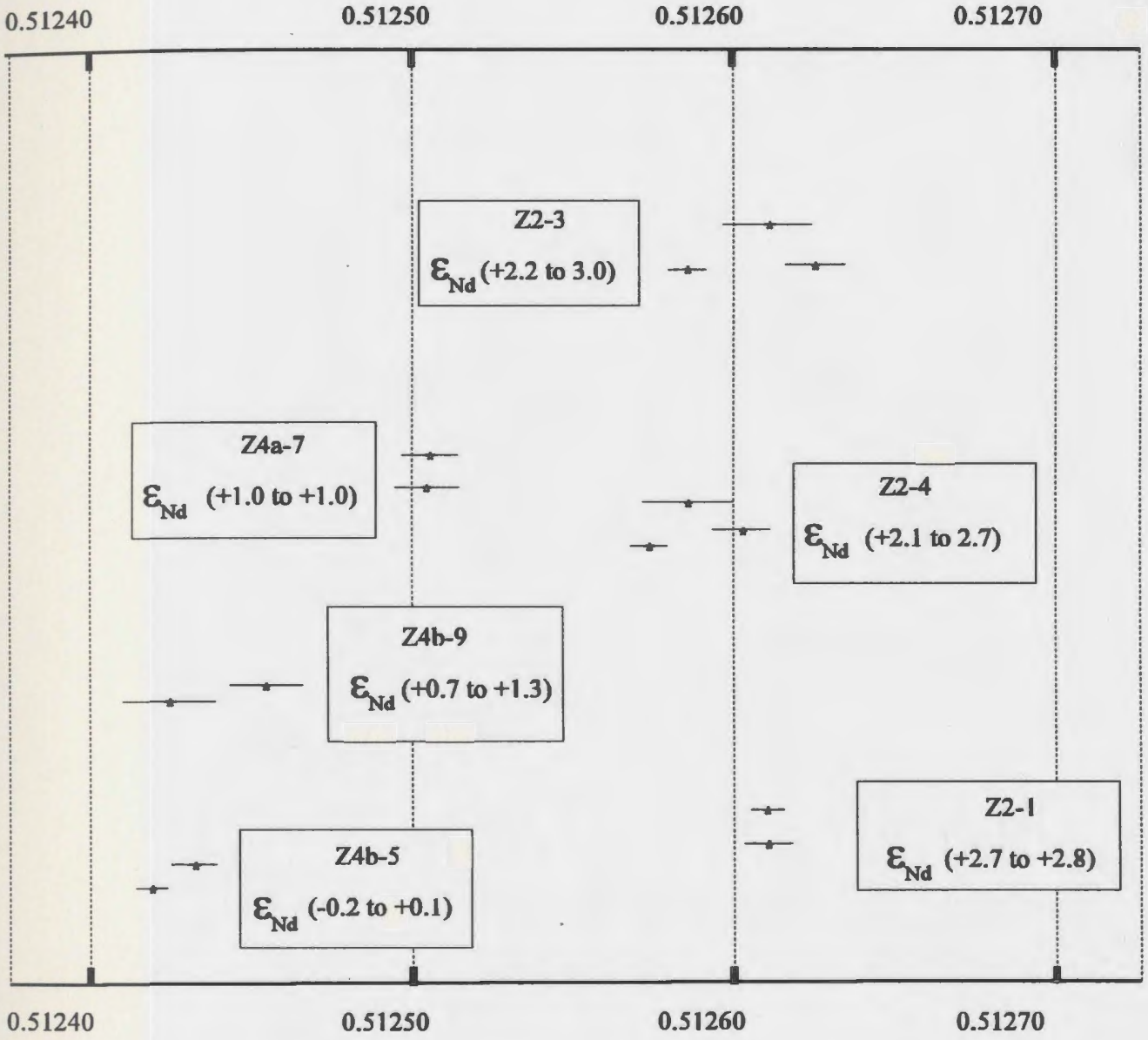

Figure 3.19 Duplicate and triplicate whole rock, initial $^{143}Nd/^{144}Nd$ measurements for the samples from the TLS, • : mean, bar: 2 s.e.m..(Vertical separation is for ease of presentation).

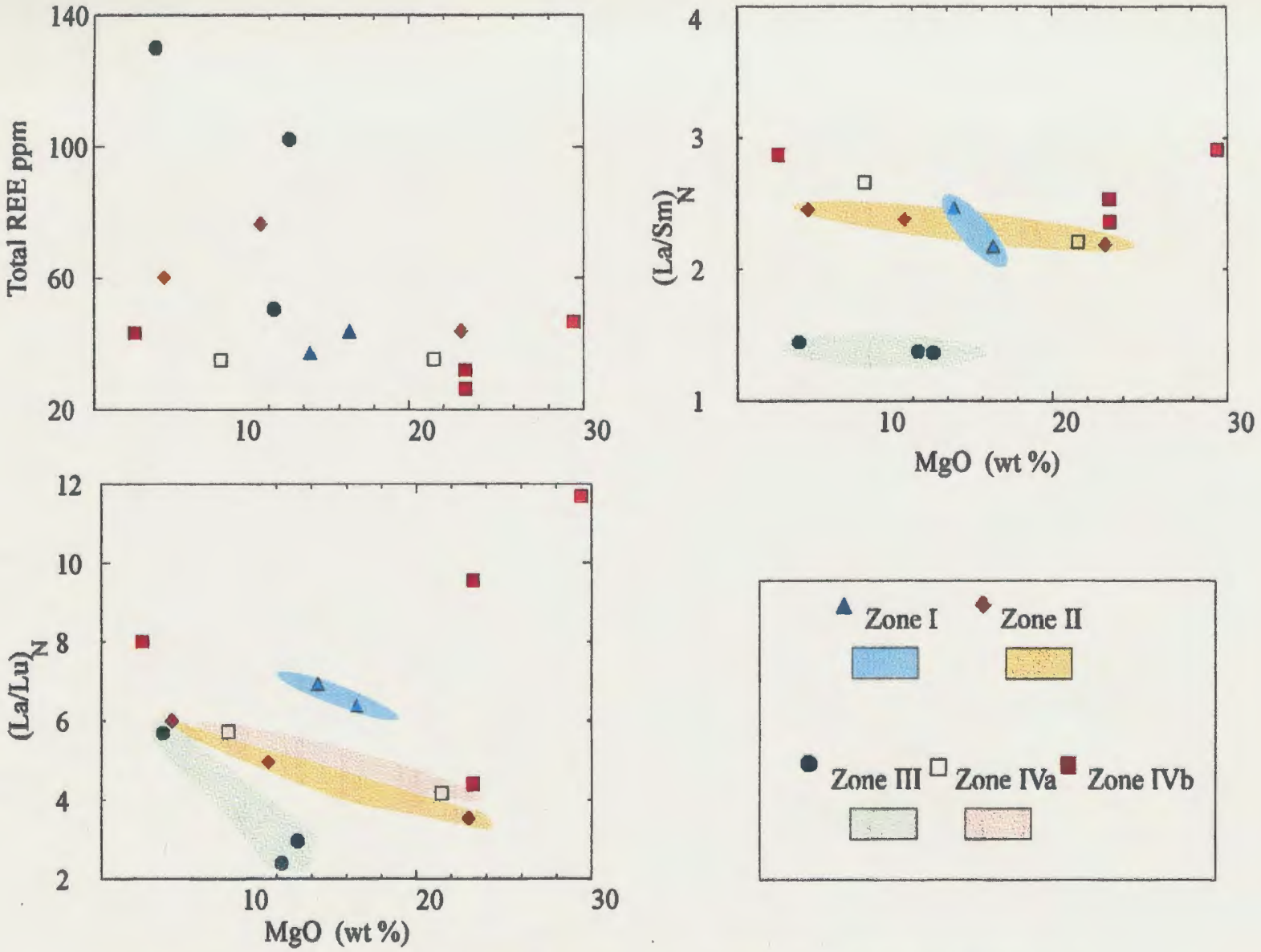

Figure 3.20 Total REE abundances, $(La/Lu)_N$, $(La/Sm)_N$ versus MgO. for the TLS.

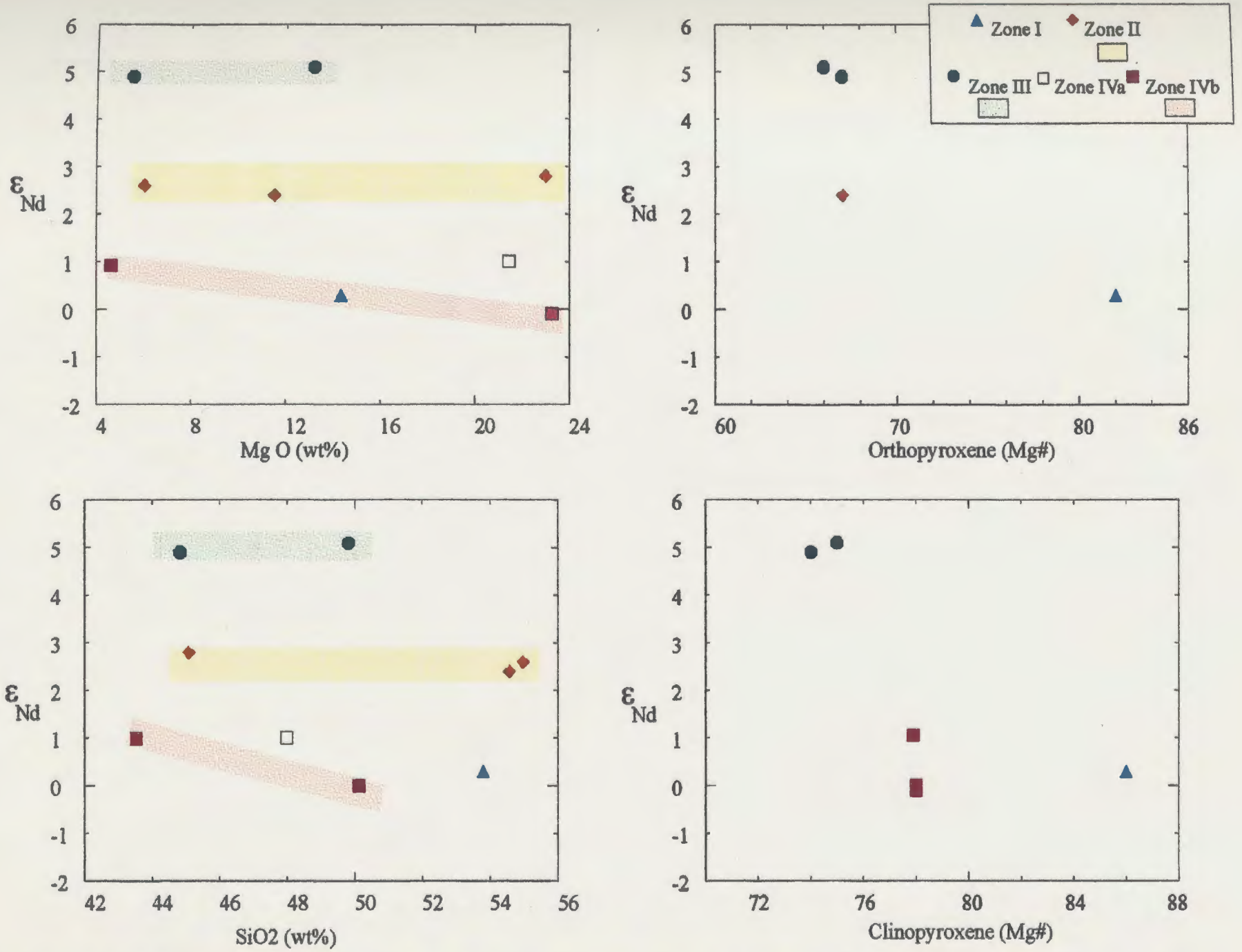

Figure 3.21 Interrelationship between Nd isotopic composition and the mineral and whole rock major element chemistry, for the TLS.

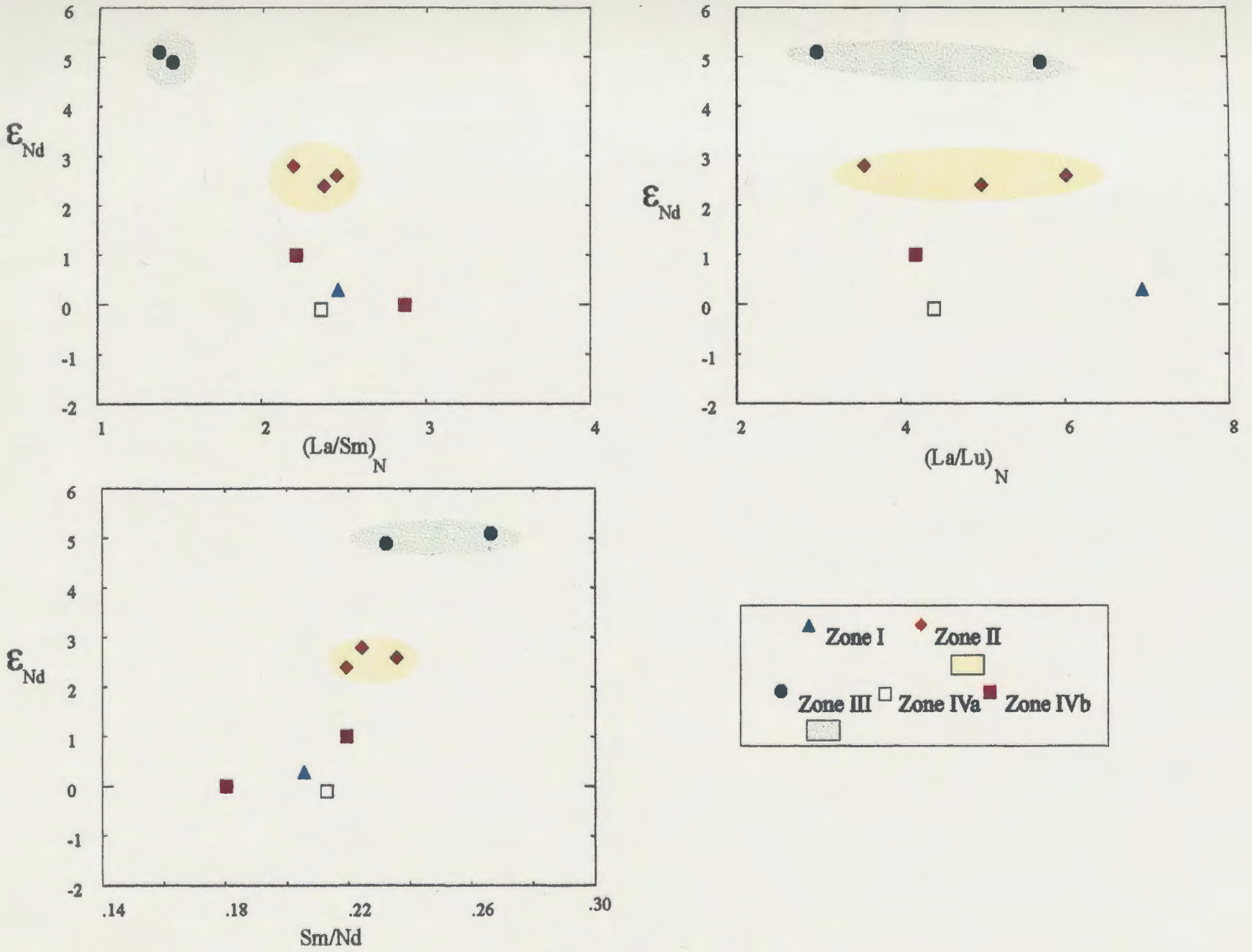

Figure 3.22 Interrelationship between Nd isotopic composition and the $(La/Lu)_N$, $(La/Sm)_N$ and Sm/Nd.

Table 3.1 Inter- and intra- zone compositional variations of common cumulus phases, for the TLS.

Map Unit	Zone I	Zone II	Zone III	Zone IV		Overall range for the TLS
				Zone IVa	Zone IVa	
Olivine Fo%	80	81	-	(72-75)	(73-81)	(72 - 81)
Orthopyroxene (Mg#)	(75 - 86)	(59 - 73)	(63 - 69)	(67 - 78)	-	(59 - 86)
Clinopyroxene (Mg#)	(83 - 86)	(72 - 80)	(71 - 79)	(73 - 78)	(76 - 79)	(71 - 86)
Plagioclase (An% core)	(80 - 85)	(43 - 59)	(50 - 55)	(55 - 65)	(59 - 76)	(43 - 82)

Table 3.2 Compositional varitaions of individual cumulus grains within the same sample.

Map Unit	Orthopyroxene (Mg#)	Clinopyroxene (Mg#)	Plagioclase (An%)
Zone I	(<1 - 4) (av. ~ 3%)	(<1 -3) (av. ~2%)	(1 -3) (av. 2%)
Zone II	(<1 - 6) (av.~ 3%)	(<1 -4) (av. ~3%)	(5 - >20) (av. ~15%)
Zone III	(<1 - 6) (av.~ 3%)	(<1 -7) (av. ~4%)	(7 -14) (av. ~10%)
Zone IVa	(<1 - 5) (av.~ 4%)	(<1 -5) (av. ~3%)	(6 - 17) (av. ~10%)
Zone IVb	not present	(<1 -4) (av. ~2%)	(5 - 16) (av. ~7%)

Table 3.3 Estimated temperature for the TLS.

Sample #	XMg, opx	XMg, cpx	aEn, cpx	aEn, opx	T °C	Average T °C
Zone I						
Z1-1	0.819	0.849	0.099	0.606	1036	(984 ± 47)
Z1-4	0.861	0.878	0.078	0.629	938	
Z1-8	0.834	0.844	0.073	0.622	975	
Z1-9	0.803	0.819	0.056	0.575	925	
Zone II						
Z2-8	0.726	0.782	0.040	0.501	854	(886 ± 45)
Z2-12	0.648	0.766	0.054	0.386	918	
Zone III						
Z3-2	0.635	0.766	0.058	0.365	933	(924 ± 8)
Z3-7	0.693	0.771	0.055	0.429	919	
Z3-10	0.664	0.752	0.058	0.402	928	
Z3-15	0.690	0.786	0.055	0.420	915	
Zone IVa						
Z4a-2	0.771	0.781	0.060	0.529	943	(962 ± 27)
Z4a-3	0.710	0.776	0.071	0.439	981	

Range of variation in the TLS
(854 - 1036) T °C

Average temperature within the TLS
(944 ± 47) T °C

Table 3.4 Reproducibility of whole rock Nd isotopic compositions.

Sample		143Nd/144Nd	2 sem	147Sm/144Nd	Nd ppm	Sm ppm
Single determination						
Z1-1		0.512482	6	0.1330	5.811	1.296
Z3-14		0.512797	7	0.1582	17.38	4.609
Z3-1		0.512745	7	0.1431	17.05	4.092
Duplicate determination						
Z4b-5		0.512438	7	0.1211	4.589	0.932
	*	0.512424	5	0.1217	6.073	1.239
Z4b-9		0.512460	11	0.1074	9.343	1.682
	*	0.512430	14	0.1076	9.426	1.700
Z4a-7		0.512510	10	0.1308	4.805	1.054
	*	0.512511	9	0.1307	7.091	1.554
Z2-1		0.512616	7	0.1356	4.089	0.929
	*	0.512616	5	0.1372	4.286	0.986
Triplicate determination						
Z2-4		0.512579	6	0.1350	11.09	2.510
		0.512608	9	0.1347	8.400	1.897
	*	0.512591	14	0.1338	15.01	3.365
Z2-3		0.512631	9	0.1373	6.137	1.413
		0.512591	6	0.1377	3.646	0.841
	*	0.512616	15	0.1404	12.03	2.831

sem= standard error of the mean.

* technique II (see text for discussion)

Normalized to 146Nd/144Nd= 0.7219

35 LaJolla determination during course of this study gave 143Nd/144Nd= 0.511854± 6

Table 3.5 Average Epsilon Nd value for the samples from the TLS.

MAP UNIT	SAMPLE	CUMULATE TYPE	Av.ε_{Nd}*	(RANGE)
Zone I	Z1-1	Plg-opx-cpx Cum	+ 0.3	-
Zone II	Z2-1	Olivine Cum	+2.8	(+2.7 to +2.8)
	Z2-3	Plg-ap Cum	+2.6	(+2.2 to +3.0)
	Z2-4	Plg-opx Cum	+2.4	(+2.1 to +2.7)
Zone III	Z3-1	Plg-opx-cpx Cum	+4.9	-
	Z3-14	Opx-cpx Cum	+5.1	-
Zone IVa	Z4a-7	Ol-plg Cum	+1.0	(+1.0 to +1.0)
Zone IVb	Z4b-5	Ol-cpx-plg Cum	-0.1	(-0.2 to +0.1)
	Z4b-9	Plg-cpx-ol Cum	+1.0	(+0.7 to +1.3)

* Age = 420 Ma

Table 3.6 Cumulus types, mineral compositions, whole rock MgO contents and REE characteristics of samples from the TLS.

Map Unit	Cumulate Type	opx (Mg#)	cpx (Mg#)	ol (Mg#)	MgO wt%	Total REE	(La/Lu)N	(La/Sm)N	(Eu/Eu*)N
Zone I									
Z1-1	plg-cpx-opx orthCum	82	85	-	14	37	6.3	2.4	1.0
Z1-2	opx-cpx-plg orthCum	85	86	-	16	44	7.0	2.1	0.9
Zone II									
Z2-1	olivine orthCum	pc	pc	80	23	44	3.5	2.1	1.2
Z2-3	plg-sp mesoCum	-	-	-	6	60	5.3	2.5	1.2
Z2-4	plg-opx orthCum	67	-	-	11	77	6.2	2.4	0.9
Zone III									
Z3-1	plg-cpx-opx adCum	67	74	-	6	130	5.7	1.5	1.0
Z3-14	opx-cpx orthCum	66	75	-	13	102	3.0	1.4	1.0
Z3-15	opx-plg-cpx mesoCum	69	77	-	12	51	2.4	1.4	0.7
Zone IVa									
Z4a-7	ol-plg orthCum	pc	pc	75	21	21	5.5	2.2	1.0
Z4a-9	plg-cpx-opx adCum	na	na	-	9	35	6.2	2.7	1.5
Zone IVb									
Z4b-1	olivine orthCum	pc	pc	81	29	47	8.4	3.0	0.8
Z4b-2	ol-cpx-plg adCum	-	78	75	23	23	5.6	2.4	1.9
Z4b-5	ol-cpx-plg adCum	-	78	75	22	26	4.4	2.4	1.1
Z4b-9	plg-cpx-ol adCum	-	78	80	4	38	8.0	2.9	1.2

na= not applicable

- (not present)

CHAPTER 4

PHYSICAL CHARACTERISTICS OF GRANITOID AND ASSOCIATED ROCKS

4.1 INTRODUCTION

This chapter describes the granitoid rocks exposed at and around the community of Tilting (Plate 1). As briefly discussed in Chapter 1, these granitoid rocks belong to the Fogo Island Batholith (FIB), which is a representative of widespread, voluminous Siluro-Devonian magmatism in the Appalachian-Caledonian orogen. They reveal close spatial and likely temporal relationships with the TLS, which itself represents the most primitive mafic rocks occurring together with granitoid rocks in central Newfoundland. As a result of this research, two distinct granitoid suites (FS and W-SCS) have been recognized in the study area.

The aim of this chapter is to outline field and petrographic characteristics of the granitoid rocks and to provide a basis for the interpretation of geochemical, geochronological and isotopic data. The following sections introduce the rationale for subdivision of the granitoid rocks and their field and petrographic characteristics (Table 4.1). However, emphasis is placed on the Wild-Sandy Cove Suite (W-SCS), which is texturally and compositionally more diverse and better exposed than the Fogo Suite (FS). In addition, information on the petrography and occurrence of dykes, enigmatic microgranular enclaves (fine-grained mineral assemblages within the granitoid rocks) and country rock xenoliths is presented. The relationship between the dykes and the enclaves, and the nature of the enclaves themselves is discussed in some detail. This information will be later utilized to predict the relative involvement of mantle and crustal material in the genesis of the granitoid rocks (Chapters 5-6). The data presented below do not form

a comprehensive study of the voluminous granitoid rocks of the FIB, since observations and, hence implications, are restricted to the study area. Nevertheless, it is believed that the inferences drawn from this limited data base will provide guidelines for future study.

Nomenclature and classification of granitoid and associated rocks are based on visual estimation of modal mineralogy from thin sections and are substantiated by mesonorm calculations (Figure 4.1).

4.2 SUBDIVISION OF THE GRANITOID ROCKS

The granitoid rocks of the study area display a wide range from hornblendite and quartz diorite to granodiorite and monzogranite. However, two distinct lithologies: monzogranite and quartz diorite, dominate the area. Most of the rocks examined here cluster around the quartz diorite compositional field on the QAP diagram of LeMaitre (1989; Figure 4.1), while a few fall within the monzogranite-granodiorite range. These two distinct groups of rocks display intrusive contact relations with each other and/or with the TLS. Furthermore, as summarized in Table 4.1, they each exhibit different field features including type and abundances of enclaves and relationships to cross-cutting dykes, etc. The recognition of the monzogranitic FS as distinct from the quartz dioritic W-SCS has been substantiated by geochemistry and geochronology. Indeed, in the case of poor field exposure, only geochemical criteria can be utilized to assign rocks to the appropriate suite.

Although the granitoid suites display primary igneous features, uralitization, saussuritization and chloritization are common.

4.3 FOGO SUITE (FS)

The internal structure of the FS is obscured due to poor exposure. However, the suite is typically free of enclaves and is cut by numerous mafic and intermediate dykes (Table 4.1). The suite is intruded by the W-SCS on the west side of Wild Cove (Plate 1), where the contact is sharp and discordant. On the other hand, the nature of the contact between the FS and TLS is not clear, although there are a few places where the FS appears to be intruding the TLS.

Modal Analysis

The monzogranite is a medium-grained, allotriomorphic granular rock composed of 30-45% perthite, 25-40% quartz, 20-30% plagioclase, plus minor biotite (1-3%) and opaque phases (1-2 %). This rock type was referred to as "alaskite-type granite" by Williams (1957). The granodiorites are granular, medium- to coarse-grained, and composed of 30-40% plagioclase, 15-20% alkali feldspar, 25-30% quartz, 5-10% hornblende, 3-7% biotite, and minor opaque phases (1-3%). Biotite is minor, but the only mafic mineral in the monzogranite, whereas both hornblende and biotite (up to 20 %) are found in the granodiorite.

Mineralogy

Alkali feldspars are subhedral to anhedral (2-4 mm long axes) and exhibit Carlsbad and Microcline twinning, perthitic texture and/or inclusions of small laths of plagioclase. Quartz crystals are anhedral (2-3 mm diameter) and display undulatory extinction, consertal texture and granophyric intergrowths with alkali feldspar. Most of the plagioclase grains are subhedral (3-10 mm long axes) and strongly zoned. Their cores are preferentially altered by saussuritization. Biotite is anhedral (1-3 mm long axes) and displays a pleochroic scheme of α=yellow-brown; $\beta=\gamma$= brown-dark reddish. It usually encloses opaque minerals (ilmenite and/or pyrite). Biotite grains with metamict haloes

around zircon inclusions are common. Hornblende grains are moderately chloritized, 1-5 mm in diameter, subhedral to anhedral and show a pleochroic scheme of α= yellowish green, ß= brown-green and γ= dark green. Euhedral zircon and apatite are common accessory phases, whereas subhedral, embayed titanite is rare. The absence of riebeckite, fluorite, garnet, muscovite, cordierite or sillimanite suggests that the FS is neither peralkaline nor peraluminous (Clarke, 1991). The massive and microgranophyric nature of the rocks suggest shallow level emplacement (*e.g.* Clarke, 1991).

4.4 WILD-SANDY COVE SUITE (W-SCS)

There is a wide range of rock types in the W-SCS, ranging from hornblendite to granodiorite with a variety of textures from medium- to coarse-grained to pegmatitic (Table 4.1). However, the predominant lithology is coarse-grained quartz diorite. The W-SCS typically contains numerous inclusions either as identifiable country rock xenoliths or as enigmatic microgranular enclaves. It is also locally cut by mafic and/or felsic dykes. The suite shows sharp cross-cutting intrusive features along its contact with the TLS and the FS. Field observations including sharp and discordant contact relations of the W-SCS with the other suites, together with the presence of abundant country rock xenoliths, suggest that the W-SCS is a shallow level intrusion.

The W-SCS has been divided into three petrographically distinct units (Plate 1; Table 4.2). These are informally named as: a) **the Pigeon Island Unit** (new term)- composed of hornblendite; b) **the Sandy Unit** (new term) - containing leucocratic gabbronorite; and c) **the Wild Unit** (new term) - consisting of quartz diorite, tonalite and minor granodiorite. In general, the absence of garnet, muscovite, riebeckite and sillimanite suggest that the W-SCS is neither peralkaline nor peraluminous (Clarke, 1991).

The boundary between the Pigeon Island Unit and the Sandy Unit is sharp and intrusive, where the former is cut by the latter. The contact between the Wild Unit and the Sandy Unit is delineated by faults, although there are a few places where the Wild Unit intrudes the Sandy Unit. The Pigeon Island Unit and the Wild Unit never come into contact with each other.

4.4.1 Pigeon Island Unit

The Pigeon Island Unit accounts for approximately 10% of the W-SCS and is mainly exposed at the south end of Pigeon Island (Plate 1). It is composed of coarse-grained melanocratic hornblendite and typically contains abundant (up to 50-70%) leucocratic xenoliths (Table 4.3). The xenoliths are generally subangular, 0.5-1 m in diameter and appear to be derived from the TLS (Figure 4.2).

Modal analysis

Hornblendite contains amphibole (60-75%), pyroxene (10-20%), quartz (5-10%), biotite (5-7%), plagioclase (3-5%) and pyrite (1-2%). The unit is characterized by early crystallization of pyroxene and hornblende and the late appearance of plagioclase and biotite. This is consistent with high water pressure during crystallization (Green, 1982).

Mineralogy and diagnostic textures

Hornblende crystals are subhedral to euhedral (5-20 mm length) and display brown cores and pale green rims (likely associated with Ti and Al content; Pitcher and Berger, 1972). Euhedral to subhedral orthopyroxene grains (3-10 mm length) are totally or partly replaced by light green amphiboles. Complex mineralogical zoning is common where the orthopyroxene is surrounded by an inner shell of light-green amphibole which itself is rimmed by biotite and/or chlorite. Biotites, which are anhedral to subhedral (2-7 mm length), show a pleochroic scheme of α= yellow-brown, $\beta=\gamma$= dark brown-dark

reddish brown, and a close association with amphiboles. Pyrite crystals are anhedral, up to 1-2 mm in diameter and locally associated with the biotites.

A distinct texture of this unit, "skeletal hornblende growth", is illustrated in Figure 4.3. Here, coarse-grained (>10 mm length) hornblende has an incomplete, corroded internal shell which is partly or totally rimmed by irregular light-green amphibole. In addition, the internal structure of the grain includes several quartz patches which are locally limited by the hornblende cleavage plane(s). These features suggest growth of skeletal hornblende with original hollows infilled by interstitial quartz. The corroded inner shell might reflect unstable mineral growth due to sudden pressure or temperature variation (Bard, 1986).

4.4.2 Sandy Unit

The Sandy Unit is composed of leucocratic gabbronorite and comprises approximately 20% of the W-SCS (Plate 1). The unit is predominately exposed on the west side of Sandy Cove where it includes a few xenolithic blocks near the contact with the TLS (Table 4.2). These TLS xenoliths are angular to subrounded, and 30-50 cm in diameter.

Modal analysis

The gabbronorite is medium- to coarse-grained and slightly pyroxene-phyric. It contains 50-65% plagioclase, 20-25% orthopyroxene, 10-20% clinopyroxene, 3-5% biotite, 1-3% opaque. Quartz and alkali feldspar are accessory minerals. Plagioclase, orthopyroxene and clinopyroxene exhibit a continuous range of sizes (seriate texture) suggesting variation in cooling rate. The early appearance of pyroxene and plagioclase is a diagnostic feature of the Sandy Unit and suggests crystallization under relatively low water pressure conditions (Green, 1982).

Mineralogy and diagnostic textures

Plagioclases usually with preferentially altered cores, display strong zoning, combined Carlsbad-albite twinning and/or myrmekitic texture at grain boundaries. Coarse- to medium-grained orthopyroxenes are subhedral to euhedral, 5-7 mm in length and locally show exsolution lamellae of clinopyroxene parallel to (100). Colourless clinopyroxenes are subhedral, 3-10 mm in size and usually exhibit twinning features. Biotite crystals (1-3 mm long axes) are subhedral to anhedral and display a pleochroic scheme of $\alpha =$ yellow, $ß = \gamma =$ reddish brown. They are associated with chlorite and opaque oxides. The oxide minerals, including ilmenite and magnetite, commonly occur as composite grains. Minor amounts of light green amphibole form reaction rims around pyroxene grains. It is important to note that this unit contains only minor amounts of hydrous minerals indicating crystallization from a liquid with a low water content, consistent with the early appearance of pyroxene and plagioclase.

A characteristic texture of the Sandy Unit is defined as an "orthopyroxene cluster" texture (Figure 4.4). This texture forms numerous small, randomly distributed, embayed orthopyroxene grains cemented by interstitial amphibole and/or biotite. The sizes of the clusters are similar to those of the coarse-grained orthopyroxene (up to 10-20 mm in diameter). The nature of the development of this texture is not clearly understood and might be attributed to the process of synneusis, *i.e.* partly grown crystals drift together, attach to each other and grow as one unit (Pitcher and Berger, 1972). There is no apparent evidence for continuous crystallization on the margins of the orthopyroxene grains suggesting that the aggregates were formed by an another process. In addition, the abundance of embayed orthopyroxene in such clusters implies that a process that causes mineral absorption must have formed this texture (*e.g.* Hogan, 1993). Hence, the "orthopyroxene cluster" texture is more likely attributed to the disintegration and

subsequent resorption of large, single orthopyroxene grains. This process is assumed to have taken place as a result of variation in cooling rate which resulted in chemical and physical adjustment of the crystallization conditions. This hypothesis appears to be consistent with the strong plagioclase zoning and seriate texture observed throughout the unit.

4.4.3 Wild Unit

The Wild Unit dominates the W-SCS (Plate 1) and is texturally and mineralogically more diverse than the others. It has been recognized throughout the study area, mainly along the coast-line and up to 50-200 m inland. The unit characteristically contains country rock xenoliths and microgranular enclaves which suggest that the W-SCS is a high-level intrusion. Occasionally, it is cut by mafic-intermediate and felsic dykes (Table 4.2). The unit shows sharp, discordant intrusive contacts with the FS and TLS.

The Wild Unit comprises quartz diorite and diorite, with minor amounts of tonalite and granodiorite. The unit is leucocratic and coarse-grained to pegmatitic. Pegmatitic phases occur either as irregular isolated patches (5 cm - 5 m in diameter) or as discontinuous dykes up to 1-2 m wide. The presence and abundance of pegmatitic phases suggest the liquid from which the Wild Unit crystallized was eventually water-saturated (*e.g.* Phillipots, 1990).

Modal analysis

Plagioclase and hornblende are the dominant (up to 60-90%) minerals of the Wild Unit, while quartz, biotite, pyroxene, opaque phases and alkali feldspar occur in variable abundances (0-20%). Other common accessory minerals are apatite and zircon. The proportion of hornblende and/or biotite increases with increasing quartz and alkali

feldspar content. In this unit, both plagioclase and hornblende are early crystallizing phases suggesting high water pressures during crystallization.

Mineralogy

Plagioclase grains (up to 10 mm long axes) are subhedral to euhedral, extensively zoned and slightly to strongly saussuritized. Hornblende crystals (5-10 mm diameter) are anhedral to subhedral and may contain relict pyroxene. Most rocks of the Wild Unit contain up to 5-10% pyroxene grains (3-5 mm length), mainly clinopyroxene and occasionally orthopyroxene, which are partly or totally replaced by light green to colourless amphibole. Subhedral biotite grains (2-4 mm long axes) exhibit a pleochroic scheme of α=yellow to light-brown, ß=γ= dark-brown. Magnetite and ilmenite occur as composite grains with or without pyrite inclusions. Ilmenite exsolution within the magnetite grains is quite common. Alkali feldspar has been observed within the granodioritic rocks as a subordinate phase in amounts up to 5-10%. It occurs as anhedral perthite with Carlsbad and/or microcline twinning. Euhedral zircon and apatite are ubiquitous.

4.5 DYKES

The plutonic rocks of the study area are cut by several dykes ranging in composition from mafic-intermediate to felsic. In general, the dykes are thin, 10-50 cm wide, up to 100 m long Most are mafic-intermediate in composition and run roughly in an E-W direction. A few felsic dykes cut almost all other units in a N-S direction, excluding the Pigeon Island Unit which is exposed in only a relatively small area. In the following sections, the emphasis is on the mafic-intermediate dykes and their relationship with the associated granitoid rocks.

4.5.1 Mafic-intermediate dykes

Mafic-intermediate dykes are melanocratic and slightly to strongly pyroxene- and/or plagioclase-phyric. They display a wide range of form and contact features against their granitoid host rocks. These features are mainly controlled by the crystallinity and rheology of the host rocks at the time of dyke injection (Pitcher and Berger, 1972). Three distinct dyke types have been recognized in the study area. These are: a) *cross-cutting*, b) *synplutonic*, and c) *transitional* dykes.

The *cross-cutting dykes* are intact, continuous (can be traced at least several meters) and show sharp contact features (Figure 4.5). They display characteristics which imply injection of the dykes into a completely crystalline and relatively cooler host rock, which failed in a brittle fashion (Pitcher and Berger, 1972; Pitcher 1991).

The *synplutonic dykes* are discontinuous, fragmented and display minor dislocations and/or host rock back veining (Figure 4.6). They are not as well-defined as the *cross-cutting* types. Here, the term, "*synplutonic*" refers to the emplacement of dykes into partly crystallized host rocks in which the proportion of crystals was large enough to sustain a fracture. On the basis of the experimental studies and mathematical models, brittle fracture can occur in magmas which are approximately 60 % crystallized (McBirney and Murase, 1984).

The *transitional dykes* have some characteristics of both *cross-cutting* and *synplutonic* dykes. They are relatively continuous and free of dislocation and fragmentation, but they display irregular and sigmoidal contact features (Figure 4.7). These dykes are interpreted as emplaced into almost solid, slightly cooled host rocks.

All three types of dykes are found cutting the Wild Unit of the W-SCS. The petrography of these dykes in the order of intrusion is:

a) *Synplutonic dykes*. They contain up to 3-5 % plagioclase phenocyrsts (5-10 mm

long axes) which are extensively zoned with sericitized cores. Their allotriomorphic granular groundmass is composed of 40-45% plagioclase, 10% quartz, 30% amphibole, 10-15% reddish-brown biotite, 5% magnetite and accessory apatite.

b) *Transitional types*. Although only recognized rarely, these dykes are pyroxene-phyric (up to 2-5 %) containing abundant orthopyroxene and minor clinopyroxene phenocrysts. Plagioclase (45 %), amphibole (40-45 %), pyroxene (5-10 %), quartz (1-3%) and opaque phases (2-3) form a granular groundmass.

c) *Cross-cutting dykes*. They are plagioclase-pyroxene-phyric. Pyroxene phenocrysts (7-10%) including orthopyroxene and/or clinopyroxene (10-20 mm diameter) are totally or partly replaced by amphibole and exhibit complex reaction coronas. Plagioclase phenocrysts (3-5 %) are subhedral to euhedral (10-15 mm long axes) and strongly zoned. The groundmass contains 45% plagioclase, 5% pyroxene, 30-35% green amphibole and 10% opaque phases (magnetite and pyrite).

It is important to realize that dyke injection is, in reality, continuous into a progressively cooling host. The fact that these relationships are confined to a small area (c. 1 km^2) largely precludes the possibility of significantly different host rock rheologies existing simultaneously.

In contrast to the W-SCS, the FS and TLS are always cut by *cross-cutting* dykes. Furthermore, *transional* dykes cutting the W-SCS become *cross-cutting* dykes when they intrude the FS and/or TLS. These observations are consistent with the other observations that the W-SCS cuts the TLS and FS, and the U-Pb (zircon) ages (Chapter 5).

4.5.2 Felsic dykes

There are a number of felsic dykes which cut the granitoid rocks of the study area. Most of them occur as tiny veinlets up to 1-5 cm wide, whereas others occur as cross cutting aplitic dykes up to 10-30 cm wide.

The aplitic dykes contain 30-40% quartz, 30-40% plagioclase and 20-25% alkali feldspar. Anhedral quartz grains display undulatory extinction and seriate texture (1-5 mm). Strongly perthitic, turbid alkali feldspars usually enclose coarse, complexly zoned plagioclase grains (5-10 mm). Opaque phases and biotite are the main anhedral accessory minerals.

The felsic dykes have been traditionally accepted as the youngest intrusive activity in the study area (Williams, 1957). However, during this study the relative chronology of the mafic-intermediate and felsic dykes has not been ascertained because of a lack of observed cross cutting features between them.

4.6 MICROGRANULAR ENCLAVES IN THE W-SCS

Microgranular enclaves consisting of mineral assemblages that are finer and commonly more mafic than their host rocks are diagnostic features of the W-SCS (Table 4.3). Two distinct types of microgranular enclaves have been recognized: a dominant "common-type" and a rare "apatite-rich" variety.

General characteristics of the "common-type" microgranular enclaves are as follows. They:

a) are similar in texture and modal mineralogy to the mafic-intermediate dykes;

b) are usually angular to ovoid, 30-50 cm in diameter and display sharp contact relation with their host rocks;

c) occur either as enclave swarms - *i.e.* a random concentration of enclaves up

to 60-80% in a relatively small area (Figure 4.8), or as fragmented dykes- an aligned distribution of enclaves (Figure 4.9).

The "apatite-rich" microgranular enclaves have a roughly circular outline and display rather diffuse contact relations with their host rocks. They are characterized by numerous needle-like apatite grains (Figure 4.10).

4.7 ORIGIN OF MICROGRANULAR ENCLAVES IN THE W-SCS

Microgranular enclaves are very common in high-level granitoid plutons and have been extensively studied throughout the world. They can provide invaluable information on the origin and evolution of their host rocks (Didier, 1987; Pin et al., 1990; Barbarin and Didier, 1991). Nevertheless, their origin is still a subject of debate. There are, however, four widely accepted genetic models:

a) the autholith model, which considers that microgranular enclaves are genetically related to the host pluton (Fershtater and Borodina, 1991; Barbarin and Didier, 1991);

b) the magma mingling/mixing model-which envisages coexisting immiscible magmas of different composition in the same intrusion (*e.g.* Didier, 1973; Vernon, 1990; Weibe, 1991). However, the interaction between the contrasting melts is itself a subject of debate. Herein, the term "mingling" refers to mechanical interaction in which the original liquids partially retain their identities and produce heterogenous banded or enclave-bearing rocks, while "mixing" indicates mechanical and chemical interaction producing a homogeneous hybrid magma of intermediate composition (Frost and Mahood, 1987; Barbarin and Didier, 1992).

c) the disrupted-dyke model which considers the enclaves as fragmented,

reworked *synplutonic* dykes.

d) the restite model- or a refractory residuum from the region of partial melting (Chappell and White, 1974; 1991; White and Chappell, 1977; Chen et al., 1990). In this model, microgranular enclaves are restricted to "I-type" granitic rocks, again a subject of controversy (Chappell and White, 1991).

A model to explain the origin of the microgranular enclaves in the W-SCS must take into account the following:

a) the lack of recrystallization and deformation features;

b) the presence of two distinct types, *i.e.* "common- and apatite-rich" microgranular enclaves;

c) the occurrences of enclave swarms and fragmented dykes; and

d) the close mineralogical and textural similarity between the mafic-intermediate dykes and the "common-type" microgranular enclaves.

Items a and d clearly suggest a magmatic origin and argue against the restite or refractory residuum model. Furthermore, the presence of "apatite-rich" enclaves has been used as classic evidence for a magmatic origin (*e.g.* Didier, 1987; Frost and Mahood, 1987). If it is assumed that "apatite-rich" enclaves represent rapidly crystallized blobs of mafic magma formed as an emulsion in the felsic magma (Vernon, 1980; Weibe, 1991; Barbarin and Didier, 1992), the occasional "apatite-rich" enclaves in the W-SCS favour the magma mingling/mixing model as an important, but local enclave-forming process.

On the other hand, items c and d clearly favour the "disrupted-dyke model". Supporting this, a significant field observation from the Wild Cove area is that where several *cross-cutting* type mafic dykes cut the FS, and then intrude into the Wild Unit, they form microgranular enclaves (Figure 4.11).

Assuming the fragmented, *synplutonic* dykes are indicative of coeval mafic-felsic

magmas (Pitcher, 1991; Barbarin and Didier, 1992), the "disrupted dyke model" can be regarded as a late stage, or a consequence of the "magma mingling/mixing model" (Barbarin and Didier, 1991). It is important to realize that these models fundamentally differ only in the timing of the mafic intrusion into the felsic host (Barbarin and Didier, 1991), and furthermore suggest that injection of mafic magma may be continuous into a progressively cooling felsic host. Different types of microgranular enclaves and the relationship between the mafic dykes and enclaves can thus be attributed to a sequence of interactions between coexisting mafic and felsic magmas with constantly changing rheologies. The "apatite-rich" and "common-type" enclaves represent relatively early stages of interaction between coexisting contrasting magmas and the late stage interactions are characterized by the *synplutonic*, *transitional* and *cross-cutting* dykes. These suggest that magma mingling/mixing processes play an important role in the evolution of the suite and that there is a significant contribution of a mafic magma in the form of mafic dykes.

4.8 COUNTRY ROCK XENOLITHS IN THE W-SCS

Country rock xenoliths are characteristic features of the W-SCS and range from layered olivine-gabbro to siliceous hornfelsic, supracrustal rocks.

The xenoliths derived from the TLS are typically angular to subrounded, and range in size from 5-10 cm to 0.5-2 m in diameter. They are found only within 10-50 m of the contact with the TLS, and the xenolith lithology is similar to immediately adjacent lithologies of the TLS. The xenoliths usually display sharp contact with their host rocks, although in some places, limited <u>in situ</u> chemical exchange between the xenoliths and the Pigeon Island Unit is evident from leucocratic haloes around the blocks (*cf.* Didier, 1987) (Figure 4.2)

The W-SCS also encloses supracrustal rocks which can be easily recognized in the field by their light to buff green colour and recessed weathering surface with respect to the enclosing host rocks (Figure 4.12). These hornfelsic rocks are siliceous, fine-grained, equigranular and allotriomorphic, with ubiquitous granoblastic texture. They contain 40-45% quartz, 30-35% plagioclase, 20% amphibole, and minor pyroxene, opaque oxide, chlorite and biotite. Extensive recrystallization and minor deformation prevents the determination of the original rock type. However, hornfelsic volcano-sedimentary inclusions of similar appearance have been reported by: a) Williams (1957) on the northern side of Fogo Island where the granitoid rocks intrude the Silurian volcano-sedimentary Botwood Group; and b) Kerr et al. (1995) in northeastern Newfoundland, where the Cambro-Ordovician metasedimentary rocks (*e.g.* Gander Group) have been intruded by granitoid rocks. It appears that the Silurian Botwood Group and/or Cambro-Ordovician Gander Group metasedimentary rocks are a potential source of supracrustal xenoliths throughout the W-SCS.

4.9 SUMMARY

Two distinct granitoid suites have been recognized in the study area: the monzogranitic FS and the quartz dioritic W-SCS. The FS is typically free of inclusions, whereas the W-SCS contains numerous microgranular enclaves and country rock xenoliths. Both suites display some characteristic features of high-level intrusions.

The W-SCS is the youngest granitoid in the area and comprises three distinct lithologies: the Sandy Unit, the Pigeon Island Unit and the Wild Unit. The Sandy Unit is distinguished by a lack of amphibole and the early appearance of plagioclase relative to pyroxene suggesting crystallization under low water pressures, while the other units are characterized by the early appearance of hornblende and pyroxene relative to

plagioclase, suggesting crystallization under high water pressure conditions.

Three different mafic-intermediate dyke types have been recognized and reflect the crystallinity and rheology of the host rock at the time of injection. These are *synplutonic*, *transitional* and *cross-cutting* dykes, and represent (continuous) injections into a progressively cooling host.

The W-SCS offers an exceptional opportunity to develop constraints on its genesis using field and petrographic data. A linkage between mafic-intermediate dykes and microgranular enclaves can be explained in terms of sequential occurrence of mixing and mingling between coexisting contrasting magmas. This hypothesis will be tested by geochemical and isotopic data in the following chapter (Chapter 5).

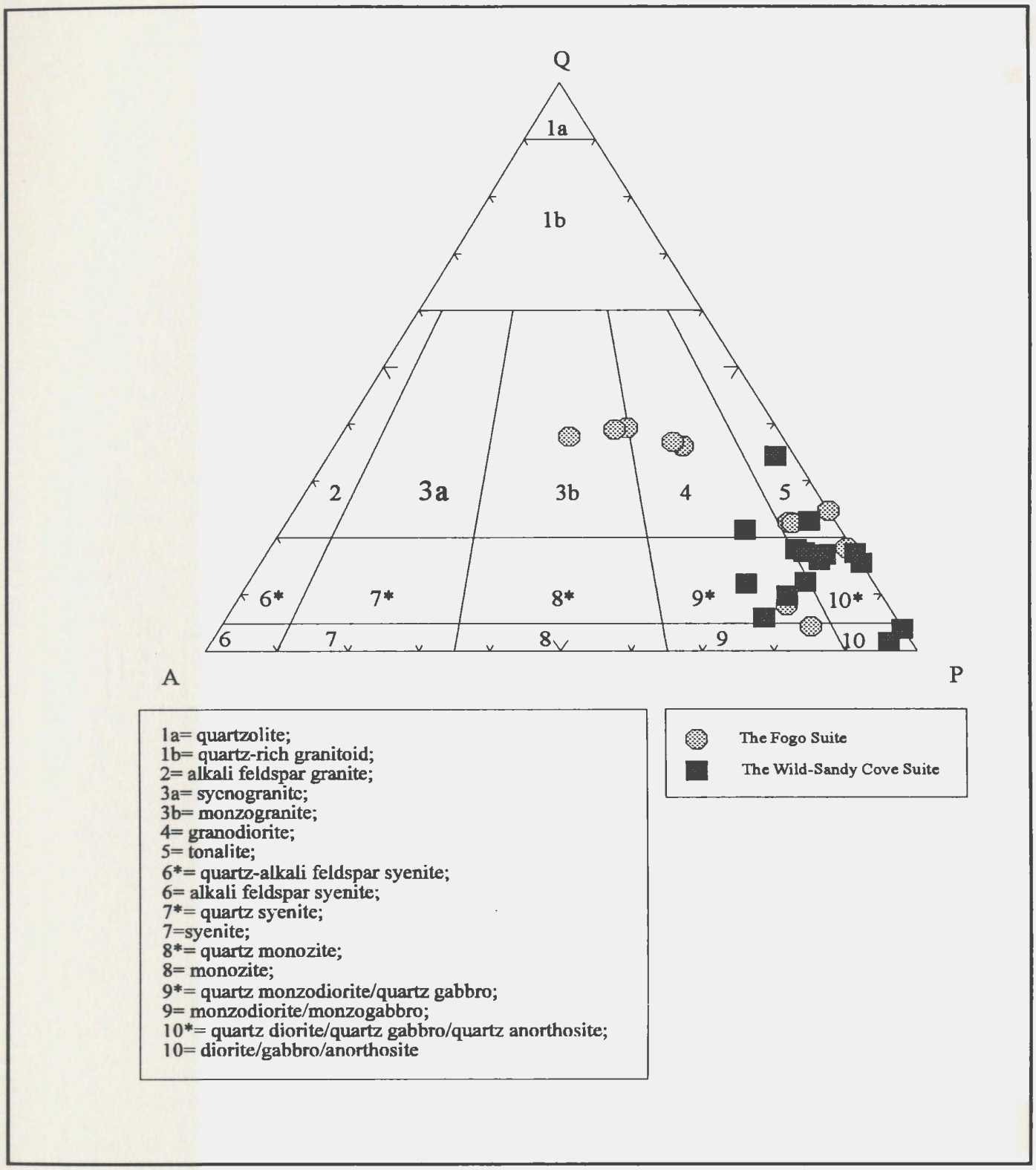

Figure 4.1 Quartz-alkali feldspar-plagioclase (Q-A-P) mesonorm diagram for granitoid rocks. Rocks names following LeMaitre (1989) are shown in inset.

Figure 4.2 Melanocratic hornblendite (PIU) contains numerous subrounded xenoliths derived from the TLS. Note the leucocratic haloes around the blocks suggesting in-situ chemical exchange. Field of view: 2 m.

Figure 4.3 Photomicrograph of skeletal amphibole crystallization (F-91-438, PIU). Coarse-grained hornblende has an incomplete corroded internal shell which is partly or totally rimmed by irregular light-green amphibole. The internal structure of the grain includes several quartz patches which are locally limited by the hornblende cleavage plane(s). Crossed nicols; field of view: 28 mm.

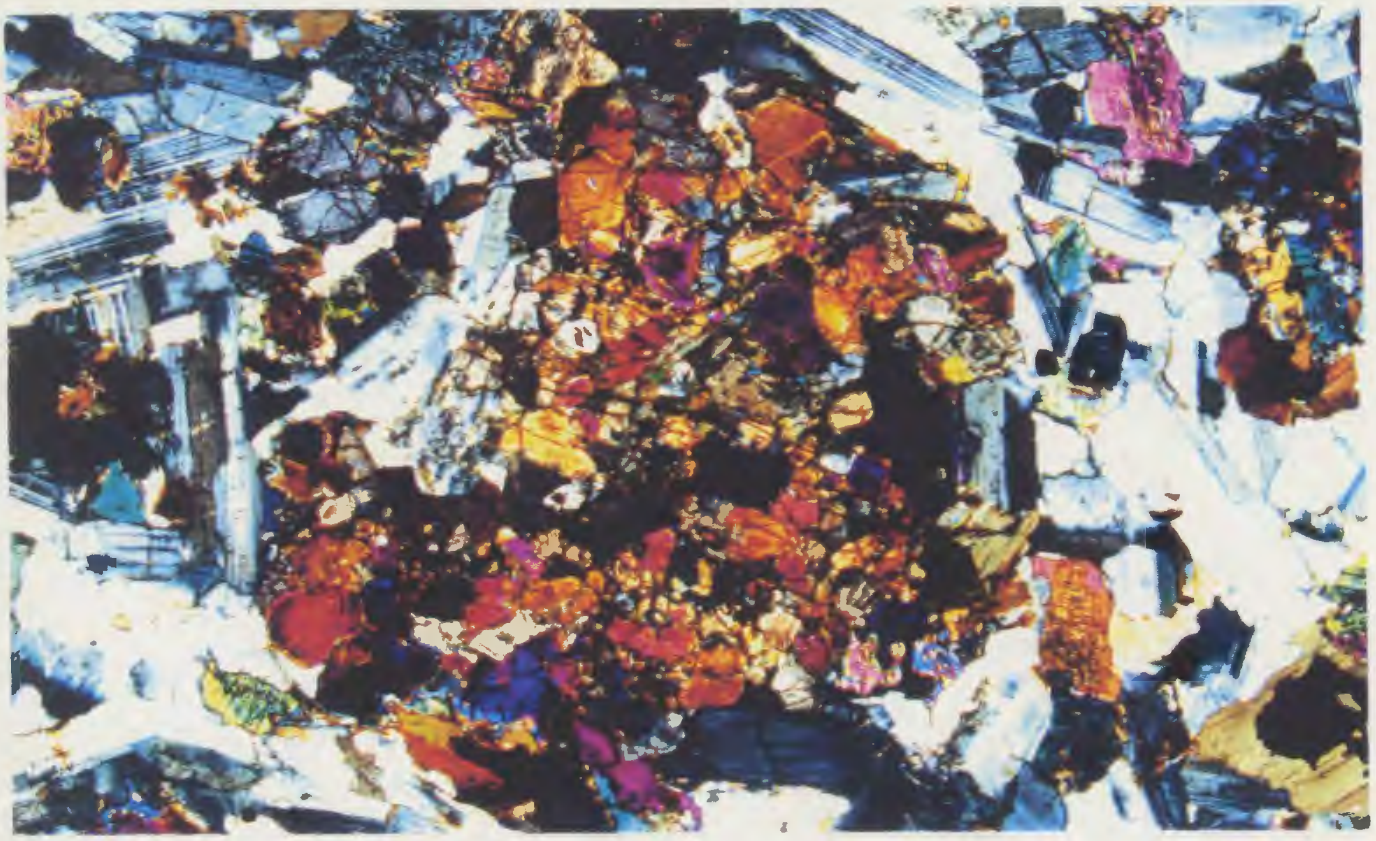

Figure 4.4 Photomicrograph of "orthopyroxene cluster" texture (F-91-54, SU) including numerous small, randomly distributed, embayed orthopyroxene grains cemented by interstitial amphibole and/or biotite. Crossed nicols; field of view: 14 mm.

Figure 4.5 Cross-cutting dyke (F-92-19D) with sharp and continuous contact relations against WU. Scale: 15 cm.

Figure 4.6 Discontinuous, fragmented synplutonic dyke with minor dislocations, and host rock back veining. Field of view: 2 m.

Figure 4.7 Continuous transitional dyke (F-91-23) with irregular contacts. Scale: 30 cm.

Figure 4.8 Common types of microgranular enclaves form enclave swarm within WU. Field of view: 100 m.

Figure 4.9 Common types of microgranular enclaves occur as fragmented dykes. Scale: 30 cm.

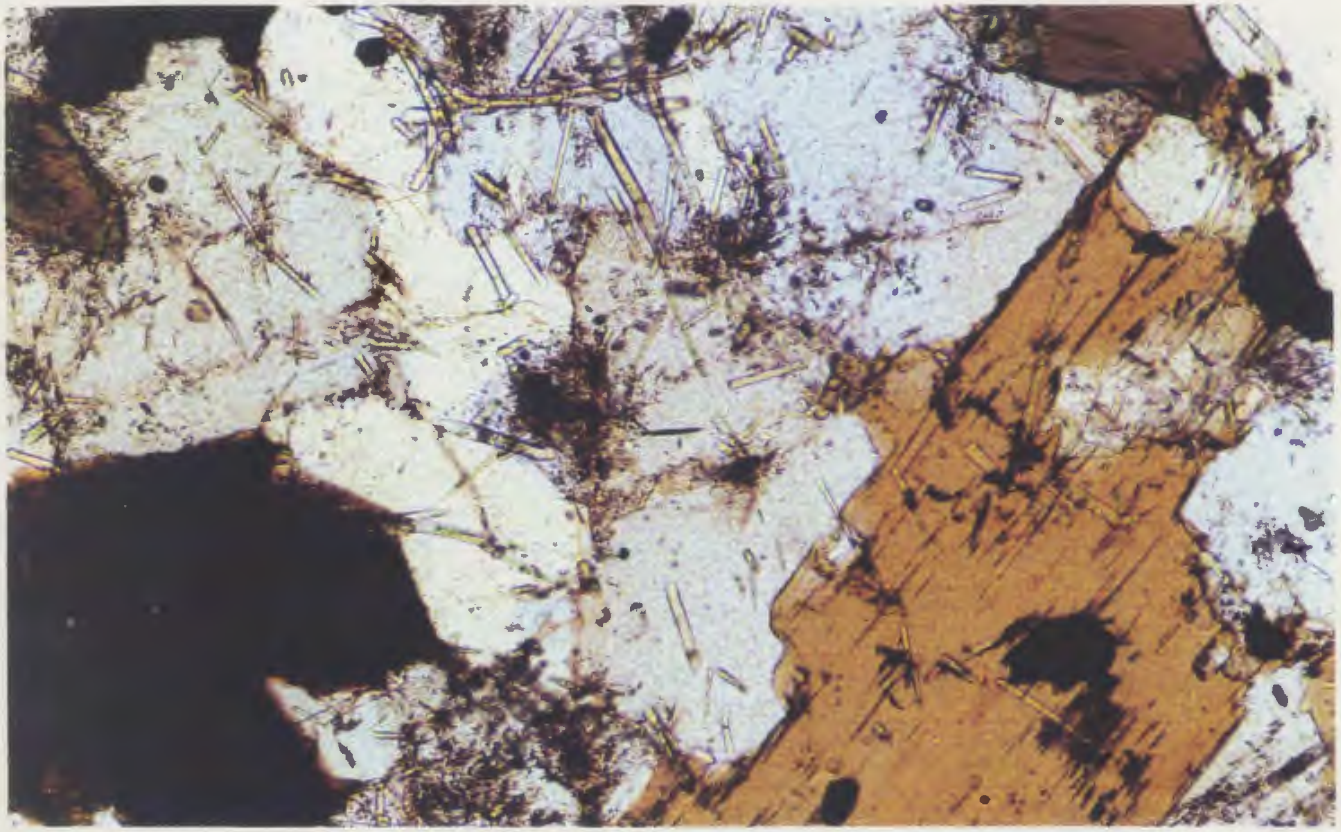

Figure 4.10 Photomicrograph of an apatite-rich microgranular enclave (F-92-14c) with numerous needle-like apatite grains. Crossed nicols; field of view: 14 mm.

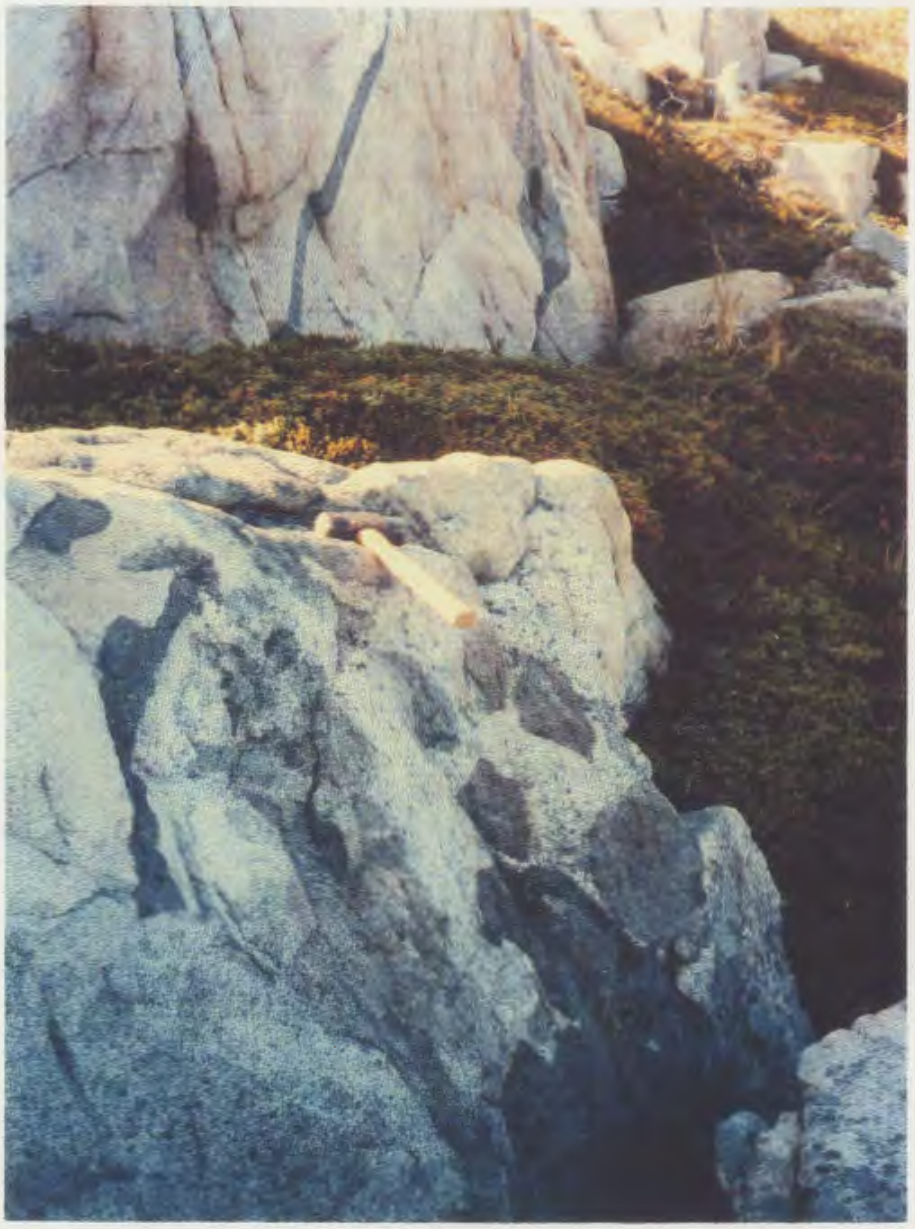

Figure 4.11 Cross-cutting type mafic dykes cut the FS (top), and then intrude into the W-SCS (bottom), thus forming microgranular enclaves illustrating "disrupted-dyke model" for the origin of microgranular enclaves in the study area. Scale: 30 cm.

Figure 4.12 Supracrustal, hornfelsic xenolith within the W-SCS. Scale: 10 cm.

Table 4.1 Field and petrographic characteristics of the granitoid rocks in the Tilting area.

GRANITOID ROCKS (Part of the Fogo Island Batholith)		
FEATURES	FOGO SUITE	WILD-SANDY COVE SUITE
Rock type	Monzogranite>>Granodiorite	Quartz-Diorite>Diorite>Gabbronorite> Hornblendite>Granodiorite
Colour	Pinkish-buff white	White to grey
Texture	Equigranular and massive	Equigranular, massive +/- porphyritic
Grain size	Medium	Coarse>medium>pegmatitic
Mafic minerals	Biotite +/- hornblende	Hornblende, pyroxene, biotite
Inclusion type	Almost free of country rock xenoliths and microgranular enclaves	Many country rock xenoliths Locally present several microgranular enclaves
Contact features	Cut by the W-SCS; ambiguous contact relation with the TLS	Sharp and intrusive contact relations with the TLS and the FS
Dykes	Cut by numerous basic dykes and few felsic dykes	Locally cut by basic +/- felsic dykes
Dyke types	Cross-cutting	Synplutonic>cross-cutting>transitional
Internal variation	Ambiguous internal structure and lithological variation	Three petrographically distinct units

Table 4.2 Petrographic subdivision of the Wild-Sandy Cove Suite.

WILD-SANDY COVE SUITE			
FEATURES	PIGEON ISLAND UNIT	SANDY UNIT	WILD UNIT
Type location	Pigeon Island	West of Sandy Cove	Wild Cove
Total % within the suite	~ 10 %	~ 20 %	~ 70 %
Rock type	Melanocratic Hornblendite	Leucocratic Gabbronorite	Qtz-Diorite>Diorite> Granodiorite
Grain size	coarse-medium	medium	coarse-pegmatitic
Inclusion type	many country rock xenoliths derived from the TLS	few country rock xenoliths derived from the TLS	microgranular enclaves and several country rock xenoliths derived both from the TLS and supracrustal rocks.
Diagnostic texture	skeletal hornblende growth	Seriate and opx-cluster texture	pegmatitic dykes
Crystallization order	early crystallization of pyroxene and hornblende	early crystallization of pyroxene and plagioclase	early crystallization of plagioclase and hornblende
Crystallization condition	high water pressure	low water presure	high water pressure/ near water saturation

Table 4.3 Inclusion types within the Wild Unit of the Wild-Sandy Cove Suite

	INCLUSIONS			
FEATURES	MICROGRANULAR ENCLAVES		XENOLITHS	
Type or derived from	Common type	Apatite-rich type	Tilting Layered Suite (TLS)	Volcano-sedimentary rocks
Texture	allotrimorphic granular	allotriomorphic granular	igneous cumulus texture	hornfelsic
Grain size	fine	fine	coarse-medium	fine
Distribution	many, near the contact areas with the Fogo Suite	few, scattered	several, near the contact with the TLS	few, scattered
Contact relations	sharp	ambiguous	sharp +/- in-situ chemical reaction	sharp
Shape	angular to subrounded	rounded	angular to subrounded	angular
Rock type	Diorite	Diorite	Pyroxenite, Gabbronorite, Gabbro, Diorite, etc	siliceous, ? volcano-sedimentary
Apatite-type	few, somewhat thick apatite	numerous, needle-like apatite	few, somewhat thick apatite	not present
Similarity	similar texture and petrography to the synplutonic dykes	similar mineralogy to the host rocks	similar texture and petrography to the TLS	? similar field features to the Botwood Group +/- the Gander Group

CHAPTER 5

GEOCHEMICAL AND ISOTOPIC CHARACTERISTICS OF THE GRANITOID AND ASSOCIATED ROCKS

5.1 INTRODUCTION

The first sections of this chapter present geochronologic data, and geochemical and isotopic characteristics of the granitoid and associated rocks. Subsequent sections develop petrogenetic constraints, and integrate these with field and petrographic characteristics of the granitoid rocks (Chapter 4), leading to a discussion of the geochemical evolution of the FS and W-SCS. Also presented in this chapter are the geochemical and isotopic characteristics of hornfelsic rocks found as supracrustal xenoliths within the study area: their geochemical and isotopic signatures are necessary for comprehensive petrogenetic modelling (see Chapter 6).

5.2 DATA PRESENTATION

5.2.1 U-Pb geochronology of the granitoid rocks

In order to determine whether the FS and the W-SCS are the result of a single or temporally unrelated magmatic events and to provide an age correction for Nd isotopic calculations, a U-Pb geochronologic study was undertaken. Zircon and titanite from the FS and zircon from the W-SCS were used to date the samples. Analytical data are presented in Table 5.1, while details of the analytical technique (see Krogh, 1982; Dunning et al., 1990b) are presented in Appendix 8. Note that all fractions presented in Figure 5.1 were abraded before analysis.

5.2.1.1 Results for the W-SCS

A sample from the Wild Unit (quartz diorite, F-91-79), collected from the eastern side of Sandy Cove (Plate 2), was selected to date this intrusion. This sample contained a number of gem-quality zircon prisms. Two zircon fractions with low total common Pb (11- 15 pg) and moderate U (147-205 pg) content were analyzed (Table 5.1). Both fractions lie on concordia (Figure 5.1) and indicate a crystallization age of 408 ± 2 Ma.

5.2.1.2. Results for the FS

The FS was dated using a monzogranite (F-91-580) collected from the east side of Wild Cove (Plate 2). This sample yielded several fractions of colourless to yellow, euhedral zircon and a few brown to yellow, slightly to strongly corroded titanite grains. Five zircon fractions were analyzed (Figure 5.1 and Table 5.1). These zircon fractions are low in total common Pb (8-20 pg) and high in U (423-591 pg), but show considerable scatter suggesting that they have a significant inherited component. However, a single grain analysis (Z1) plots on concordia at 420 ±2 Ma, and is interpreted to give the crystallization age for this suite. Two fractions (Z2 and Z3) define a discordia line, which yields a lower intercept age of 420 ±2 Ma (probability of fit 89 %). However the upper intercept age, calculated to be 2090 ±100 Ma, represents only an average age for the inherited components in the fractions analyzed and is not the age of any particular rock in the source region (*e.g.* Dunning, 1986). Two other fractions, Z4 and Z5, lie below the discordia line suggesting secondary Pb loss, and were not included in the discordia line regression.

Two titanite fractions were also analyzed, they have moderate U (77-101 pg) and high total common Pb (157-442 pg). One fraction, T1, is nearly concordant at 410 ±2 Ma, while the other, T2, displays discordance suggesting significant Pb loss.

5.2.2 Presentation of whole-rock geochemical and isotopic data

This section describes the whole rock geochemical and Nd isotopic characteristics of the granitoid and associated rocks. A wide range of samples from monzogranite to hornblendite have been analyzed for their whole rock major and trace element chemistry, while a selected subset of samples have been analyzed for their REE and Nd isotopic signatures. The complete data sets are given in Appendix 5.

Petrographic observations indicate that the granitoid and associated rocks are little affected by alteration, and that the primary mineralogy is preserved well in most samples. In some of the dykes, alteration of phenocryst phases has occurred, that is sericitization of plagioclase and uralitization of pyroxenes. In general, it is accepted that the high field strength elements (HFSE) (P, Ti, Y, Zr, Nb, Hf, Ta $\pm$ Th), transition elements (Sc, V, Cr, Ni) and REE are essentially immobile during alteration where water/rock ratios are moderate to low. However, the low field strength elements (LFSE) (Rb, Ba, K, Sr) plus Na, Si and Ca are considered susceptible to alteration. For more detailed discussions see Jenner and Swinden (1993) for mafic and intermediate rocks, and Ward et al. (1992) and Whalen et al. (1994a) for granitoid rocks. Although in general, the samples analyzed do not exhibit much evidence for alteration, only a restricted set of elements have been used on extended REE plots. This was done simply to clarify the data presentation and allow easier comparison of the mafic and felsic rocks. Following the same logic, data for the granitoid and associated rocks are presented in similar ways. Note AFM diagrams have been used to illustrate magmatic differentiation trends and some use of normative compositions is also made. Although alteration may have some impact on the use of the data in these ways, it is insignificant overall.

5.2.2.1 Data presentation for the FS

Whole rock major and trace element analyses

As noted in Chapter 4, the FS is dominated by monzogranite, with lesser granodiorite. This petrographic/mineralogic distinction is reflected in the major element trends illustrated in Figure 5.2. Rocks from the FS range in silica content from 55 to 79 wt% but there is a noticeable compositional discontinuity between 63 and 70 wt% SiO_2. The rocks having SiO_2 contents in the range of 70 to 79 wt% correspond to monzogranites, while the granodiorites correspond to the low silica group.

In the monzogranites, the ranges of compositional variation are as follows: TiO_2 (0.08 - 0.4 wt%); CaO (0.7 - 2.1 wt%); FeO (0.6 - 1.8 wt%); MgO (0.06 - 0.3 wt%); Al_2O_3 (11.8 - 13.9 wt%); Na_2O (3.2 - 4.2 wt%); K_2O (2.3 - 5.1 wt%); Ba (314 -537 ppm); Sr (57 - 199 ppm) and Rb (37 - 129 ppm). They plot in the alkali corner of the calc-alkaline field of the AFM diagram and within the trondhjemite and granite fields of the O'Connor diagram (Figure 5.3). The monzogranites have A/NK (molar ratio of Al_2O_3/Na_2O+K_2O) and A/CNK (molar ratio of $Al_2O_3/CaO+Na_2O+K_2O$) ratios between 1-1.4 and 1-1.1 and are slightly peraluminous. However, their peraluminous nature apparently reflects the degree of differentiation in these rocks and they are metaluminous for the purposes of petrogenetic modelling of source materials.

The granodioritic rocks (55-63 wt% SiO_2) are characterized by the following ranges in element composition: TiO_2 (0.4 - 1.4 wt%); CaO (3.4- 5.0 wt%); FeO (2.8 - 5.8 wt%); MgO (1.1 - 5.6 wt%); Al_2O_3 (15.4- 19.3 wt%); Na_2O (1.2 - 1.9 wt%); K_2O (0.11 - 0.38 wt%); Ba (198 - 286 ppm); Sr (282 - 384 ppm); Rb (34 - 73 ppm). They are slightly to strongly metaluminous (Figure 5.3c) and calc-alkalic (Figure 5.3a) (and as defined by Peacock (1931) where C= N+K at SiO_2 between 56 and 61 wt%). They plot within the tonalite field of the O'Connor diagram (Figure 5.3b).

In comparison, TiO_2, Al_2O_3, FeO, CaO, MgO and Sr contents of the granodiorites are somewhat higher than those of the monzogranites, while Na_2O, K_2O, Rb and Ba contents of the granodiorites are relatively lower. Overall within the FS, MgO, FeO, CaO, and/or P_2O_5 contents decrease with increasing SiO_2 content, whereas K_2O, Rb and Ba contents increase with increasing SiO_2 content.

Whole rock REE analyses

Three samples, one granodiorite (F-91-563) and two monzogranites (F-91-580 and F-92-20a) were analyzed for rare earth elements (REE)(Table 5.2). The REE patterns (alone and combined with other trace elements) are illustrated in Figure 5.4. The chondrite normalized abundances (REE_N) lie in the range of 10-70 X chondrite, have LREE enrichment relative to HREE [$(La/Lu)_N$= 3.2 - 6.1; $(La/Sm)_N$= 2.5- 3.6] and have flat HREE patterns (*i.e.* Gd-Lu; see Figure 5.4a). The monzogranites have overall lower concentrations than the granodiorite (although there is no simple relationship between REE abundance and patterns with silica content) and more well developed negative Eu-, Ti- and Sr- anomalies (Figure 5.4). All the samples show a negative Nb anomaly and enrichment in Th relative to La and Nb, and also have positive Zr relative to Nd and Sm.

Whole rock Nd Isotopic Data

The same three samples analyzed for REE were used in determining the Nd isotopic composition (Table 5.3). The overall variation in Nd isotopic composition expressed as ϵ_{Nd} at T=420 Ma ranges from -1.0 to +1.3. The lowest ϵ_{Nd} value belongs to the granodiorite (Figure 5.5), while the monzogranites have almost identical positive values. Note that the ϵ_{Nd} variations between the granodiorite and monzogranites within the FS ($\pm$ 1.2 ϵ_{Nd} unit) are analytically significant or real (see discussion in Chapter 3). There is no apparent interrelationship between REE element abundance and/or ratios and

isotopic composition (Figure 5.5).

5.2.2.2 Data presentation for the W-SCS

The W-SCS suite displays a continuous range in SiO_2 from 48 to 64 wt% SiO_2, with one sample (F-91-175a) plotting at ~70% silica. The suite, as a whole, is calc-alkalic as defined by Peacock (1931) and plots in the calc-alkaline field on the AFM diagram (Figure 5.6). The suite plots dominantly in the tonalite field on the O'Connor diagram and in the metaluminous field on the Shand index diagram (see Figure 5.6). Selected major and trace elements are plotted against SiO_2 in Figure 5.7. Several elements including CaO, FeO, MgO $\pm$ TiO_2 $\pm$ P_2O_5 display scattered negative trends; whereas Rb, Na_2O and K_2O show scattered positive trends. Samples with less than 16 wt% Al_2O_3 mainly belong to the Pigeon Island Unit and have 48-53 wt% SiO_2 and 8-14 wt% MgO contents. Samples from the Sandy Unit are characterized by limited chemical variations, typically in the range of 56-60 wt% SiO_2 and 16-17 wt % Al_2O_3. Rocks from the Wild Unit, except F-91-175a, show a continuous and wide range in SiO_2 from 49 to 64 wt% (Figure 5.7). The range of compositional variation seen in the Wild Unit overlaps that of the Sandy Unit, and for a given silica concentration they display comparable major and minor element (Mg, Ca, Fe and Ti) contents (Figure 5.7).

Whole rock REE analyses

Six samples from the W-SCS were analyzed for REE (Figure 5.8). They display similar, parallel REE patterns without significant discordance (note that it is the high silica sample 92-175a that shows the most difference). Chondrite normalized REE abundances fall between 10-110 X chondrite and display LREE enrichment relative to HREE [$(La/Lu)_N$= 6.9 - 16.1, $(La/Sm)_N$= 3.0 - 4.0]. Neither positive nor negative Eu anomalies are particularly well developed (see Figure 5.8). On the primitive mantle

normalized plot all samples show a well developed negative Nb anomaly, and somewhat higher normalized Th relative to La.

Variation in REE abundances and ratios versus silica are illustrated in Figure 5.9. The highest REE abundances are found in the most mafic compositions and decrease with increasing fractionation. Correlated with this decrease in abundance is an increase in LREE enrichment relative to the HREE [$(La/Lu)_N$]. However, the $(La/Sm)_N$ ratios are less variable and do not correlate with REE abundance.

Whole rock Nd isotopic data

The same suite of samples analyzed for REE were also used to determine the range of Nd isotopic composition in the W-SCS. The values obtained are given in Table 5.3. The Nd isotopic data of the suite, expressed as ϵ_{Nd} at T=408 Ma, are all positive and range from +0.3 to +3.2. Both the Wild Unit and the Sandy Unit show significant Nd isotopic heterogeneity, with ϵ_{Nd} values of samples from about +0.3 to +3. As illustrated in Figure 5.10, there are no clear interrelationship between REE element abundance and/or ratios and isotopic composition.

5.2.2.3 Data presentation for the dykes

A total of nine dykes were analyzed for major and trace elements. They show a wide variation in composition (Figure 5.11) with silica ranging from 46 to 76%. However, the majority of samples (7) have less than 56% SiO_2 (corresponding to basalts and basaltic andesites, or mafic to intermediate in composition), one sample would be a high-Si andesite (intermediate), and one sample is truly felsic (high-Si rhyolite). The mafic to intermediate samples are characterized by (in weight percent): TiO_2 = 1.0 to 3.1; Al_2O_3 = 15 to 20; FeO = 3.3 to 8.1; MgO = 2.0 to 7.4; CaO = 4.3 to 9.3; Na_2O = 3.4 to 6.3; and P_2O_5 = 0.4 to 1.1. As illustrated in Figure 5.11, CaO, MgO,

FeO, Sr $\pm$ TiO_2 $\pm$ P_2O_5 contents decrease with increasing SiO_2 content, while Al_2O_3, Na_2O and K_2O contents increase with increasing SiO_2. CIPW norms of dykes are presented in Appendix 6. All analyzed samples are hypersthene-normative (tholeiitic). Three samples (F-91-22, F-91-23 and F-91-234d) are olivine-normative while the others are quartz-normative.

Whole rock REE analyses

Five dykes were analyzed for REE. Each dyke represents a different lithological unit or dyke type (see Chapter 4): a) sample F-91-174d is the felsic dyke; b) sample F-92-31 is from an intermediate dyke which cuts the TLS (Zone I) and has not been traced within the granitoid suites; c) sample F-92-20b represents dykes which are intermediate, cut the FS and continue into the W-SCS as microgranular enclaves; d) sample F-91-23 is a mafic dyke cutting Zone II and Zone III; and e) sample F-92-19D represents an intermediate, *cross-cutting* type dyke. (Note: italics refer to a dyke type discussed in Chapter 4.)

Chondrite normalized REE and primitive mantle normalized extended REE patterns for these samples are illustrated in Figure 5.12. All of the samples are characterized by LREE enrichment, but the degree of this enrichment varies significantly. Three of the dykes (F-92-19D, F-92-20b, F-91-23) have quite similar degrees of LREE enrichment, and although another dyke (92-31) has similar LREE to these, it has less depleted HREE. The mafic to intermediate dykes display only poorly to moderately developed Eu-anomalies [$(Eu/Eu^*) = 0.9 - 1.1$], significant negative Nb- and Sr-anomalies, positive Zr-anomalies, and no significant Ti-anomalies, except for F-92-31. The felsic dyke is characterized by a significant negative Eu-anomaly ($Eu/Eu^* = 0.5$), strong LREE enrichment relative to HREE [$(La/Lu)_N$ (14.7) $(La/Sm)_N$ (7.1)], minor depletion in Tb, Dy, and Ho (the middle rare earth element- MREE) relative to Tm, Yb

and Lu (HREE), and well-developed negative Nb-, Ti-, and Sr- anomalies.

Whole rock Nd isotopic composition of dykes

The same samples for which REE were determined were also used for Nd isotopic analysis (Table 5.3). The overall variation in Nd isotopic composition, expressed as ϵ_{Nd} at T= 408 Ma, ranges from +0.7 to + 4.1. The highest ϵ_{Nd} value is found in the, quartz-normative, *cross-cutting* type dyke (F-92-19D). In the remaining dykes, the isotopic variation is from ϵ_{Nd} = +0.7 (in the felsic dyke) to +1.0 to +1.3 (in the mafic-intermediate dykes). That is, excluding F-92-19D, all fall within analytical uncertainty ($\pm$ 0.3 ϵ_{Nd}). Hence, there is no correlation between ϵ_{Nd} value and SiO_2 contents or the REE_N patterns or abundances (Figure 5.13).

5.2.2.4 Microgranular Enclaves

A few microgranular enclaves were selected for analysis. The compositional variation in these samples is illustrated in Figure 5.14. The range of variation observed in these samples is as follows: SiO_2 (53 to 59 wt%), TiO_2 (0.7 to 1.8 wt%), Al_2O_3 (16 to 18 wt%), CaO (4 to 9 wt%), MgO (1 to 5 wt%), Na_2O (4.5 to 5.1 wt%), K_2O (0.9 to 1.4 wt%), P_2O_5 (0.17 to 0.61 wt %). MgO, CaO, FeO,TiO_2 $\pm$ P_2O_5 versus SiO_2 show negative trends, whereas K_2O and Na_2O versus SiO_2 display positive trends. The enclaves display parallel trends to those observed in the host rock, however, they are slightly to moderately enriched in MgO, FeO, P_2O_5, Ba, Zr, and TiO_2. The enclaves are metaluminous and plot in the calc-alkaline field of the AFM diagram and the tonalite field of the O'Connor diagram (Figure 5.15).

Whole rock REE

Three microgranular enclaves, two of the "common-type" (F-92-N-1 and F-92-N-3), and one representing the "apatite-rich type" (F-92-14b), were analyzed for REE.

(Note: "common" and "apatite-rich" microgranular enclaves refer to types discussed in Chapter 4). The results are presented in Figure 5.16. The "apatite-rich" enclave has higher REE abundances and stronger LREE enrichment relative to HREE [$(La/Lu)_N$ 8.4 versus ~4.1) than those of "common-type" enclaves; nevertheless, all samples show comparable $(La/Sm)_N$ (2.1 to 2.9). Additionally, "common-type" enclaves display minor positive Eu-anomalies (Eu/Eu^*) (1.0 to 1.1), whereas the "apatite-rich type" shows minor negative Eu-anomaly (Eu/Eu^*) = 0.9. There is a strong negative Nb- and positive Zr-anomaly in the "apatite-rich" enclave. There is no apparent interrelationship between the REE abundances and SiO_2 content, for a given SiO_2 content, REE_N abundances change from 79 ppm to 164 ppm.

Only one sample, F-92-N-1, has been analyzed for whole rock Nd isotopic composition (Table 5.3). The sample has a +1.5 ϵ_{Nd} value, at 408 Ma, which is similar to that found in most of the mafic dykes (+0.9 to +1.3).

5.2.3 Data presentation for supracrustal xenoliths

Representative samples of supracrustal xenoliths, three samples within the W-SCS and four within the TLS, were analyzed. From these, two samples, F-91-77S from within the TLS and F-91-66S within the W-SCS, were also selected for REE and Nd isotopic determinations. Data are illustrated in Figures 5.17 and 5.18. Nd isotopic data are reported in Table 5.3. The important observations are as follows:

(1) samples found within the W-SCS are significantly more siliceous than those within the TLS.

(2) within a given body the xenoliths are relatively constant in composition.

(3) both samples analyzed for REE characteristics typically display LREE enrichment relative to HREE $(La/Lu)_N$= 7.0 - 8.9. Sample F-91-77S exhibits

significant MREE depletion relative to HREE $(Gd/Lu)_N = 0.78$, and a positive Eu anomalies ($Eu/Eu^* = 2.3$) (Figure 5.18); whereas, sample F-91-66S reveals a minor negative Eu anomaly ($Eu/Eu^* = 0.74$) without MREE depletion $(Gd/Lu)_N = 1.6$.

(4) despite their notably different geochemical characteristics, both have very similar, and strongly negative low ϵ_{Nd} values of -8 to -9 (Table 5.3).

5.3 DISCUSSION AND IMPLICATIONS OF U-Pb CHRONOLOGY

The mid-Silurian (420 ±2 Ma) Fogo Suite is cut by the Devonian (408 ± 2 Ma; Tucker and Mc Kerrow, 1995) Wild-Sandy Cove Suite. The age difference between the FS and the W-SCS implies that these distinct granitoid suites are the results of separate magmatic events. Furthermore, the absolute geochronology of the granitoid suites suggests that the FS was formed during the peak period of the Salinic orogeny (Dunning et al., 1990a) while the W-SCS was formed during the latter or waning stages of this orogeny.

It is important to note that the concordant age of the titanite from the FS overlaps the concordant zircon age of the quartz diorite from the W-SCS. This observation together with petrographic features of the titanite can be best explained in terms of complete isotopic resetting of titanite grains and associated Pb loss, possibly as a result of emplacement of the W-SCS.

Significance of the U-Pb geochronology on local and regional scales

On the regional scale, there are clear age and apparent lithologic correlations between the W-SCS and the Loon Bay Batholith of northeast central Newfoundland, which has an age of 408 Ma (Elliot et al., 1991). These authors considered this age to constrain the timing of several important structural events in central Newfoundland,

including the initiation of high-angle brittle faulting in the area. This appears to be in accord with field observations from the Tilting area, since late east-west trending major faults cut across most of the plutonic rocks, particularly the TLS and the FS (Plate 1). However, current knowledge is insufficient to allow further correlations.

Additionally, the age of the FS (420 $\pm$2 Ma) overlaps an age of 420 $\pm$2 Ma for the composite mafic and felsic dykes on the Port Albert Peninsula, northeast central Newfoundland (Elliot et al., 1991). These authors also regard an age of 420 $\pm$2 Ma as an upper limit on the age of the Botwood Group in central Newfoundland. This appears to be consistent with field observations from Fogo, the FIB intrudes the Botwood Group (Williams, 1993a).

There has been a tendency to correlate lithological similarities of the granitoid rocks in central Newfoundland, including the FIB, with the "Appinite Suite" of the Scottish Caledonides (*e.g.* Dunning et al., 1990a). Certainly, the field, petrographic and/or geochemical characteristics of the Appinite Suite (Pitcher and Berger, 1972; Wright and Bowes, 1979; Hamidullah and Bowes, 1987; Weiss and Troll, 1989; Platten, 1991) can be recognized in the W-SCS (Chapter 4). Nevertheless, the U-Pb geochronology clearly indicates that the W-SCS is much younger than the Appinite Suite ($U\text{-}Pb_{zircon}$ 408 Ma vs. $U\text{-}Pb_{zircon\pm\ titanite}$ 423- 429 Ma) (Rogers and Dunning, 1991). In terms of age, the FS is more correlative with the Scottish Appinite Suite.

The first chronology of granite from the FIB was provided by Wanless et al. (1965) as a $K\text{-}Ar_{biotite}$ age of 380 $\pm$16 Ma (Devonian). Recently, the batholith was dated using the $Rb/Sr_{Whole\ rock}$ method at around 411 Ma (B. Fryer, 1992, per. com.). However, as discussed above, the present study clearly shows that there are two different granitoid suites which are not temporally related to each other and there clearly exists significant or complete isotopic resetting due to the intrusion of the W-SCS. Thus, without specific

field and petrographic descriptions of the previously dated rocks from Fogo Island, the previous dates have limited value for comparative purposes.

5.4 DISCUSSION AND IMPLICATIONS OF THE GEOCHEMICAL FEATURES OF THE GRANITOID ROCKS

This section discusses the information presented above in order to develop geochemical and isotopic constraints, and integrates this information with field and petrographic characteristics of the FS and the W-SCS. Thus, in the following paragraphs: a) general geochemical and isotopic characteristics of the FS and the W-SCS are compared; b) internal geochemical variations of each suite are discussed briefly; and c) geochemical and isotopic characteristics of dyke, microgranular enclaves and their host rock (Wild Unit) are evaluated together. At the end of each section, the main implications are summarized. A comprehensive interpretation of the Nd isotopic data is not provided in this chapter, but is provided in Chapter 6. This decision was taken in order to minimize repetition and to discuss the role of different sources and mixing mechanisms for the FS, W-SCS and TLS in conjunction with the development of a petrogenetic model.

5.4.1 The FS and the W-SCS

Both the FS and the W-SCS are metaluminous to weakly peraluminous and display some similar geochemical features, *i.e.* LREE enrichment relative to HREE and a significant negative Nb-anomaly. However, they display distinct REE_N, extended REE_N and ϵ_{Nd} characteristics (Figure 5.19 and Table 5.2). These are:

a) the LREE abundances of the FS are slightly to moderately lower than those of the W-SCS;

b) The REE_N patterns of the FS typically display moderate to strong negative Eu-anomalies with flat HREE abundances, whereas those of the W-SCS, are characterized by a lack of recognizable Eu-anomalies and negatively sloping HREE patterns;

c) the extended REE_N patterns of the FS show significant negative Sr-anomalies with minor negative Ti- anomalies, whereas those of the W-SCS, excluding the most differentiated sample, display only minor negative Sr- and Ti-anomalies; and

d) the ϵ_{Nd} values of the FS at 420 Ma change from -1.0 to +1.3, whereas the ϵ_{Nd} values for the W-SCS vary significantly from +0.3 to +3.2, at 408 Ma.

Implication: There exists significant isotopic and geochemical diversity between the FS and the W-SCS.

5.4.2 Internal geochemical variations within the FS

In general, compositional variations in granitoid suites reflect: a) the effects of source-related heterogeneities; b) melting and/or melt ascent processes; or c) the effects of magma-chamber processes including fractional crystallization, magma mixing and/or assimilation fractional crystallization (AFC) (*e.g.* White and Chappell, 1977; Pitcher, 1979; 1987; Ward et at, 1992; Atherton, 1993).

Any potential process that gave rise the lithological and geochemical diversity seen in the FS must address the following features:

(a) compositional discontinuity between granodioritic and monzogranitic rocks;

(b) similar REE_N and extended REE_N characteristics of monzogranitic and granitoid rocks;

(c) decreasing REE abundances and increasing magnitudes of negative Eu- and Sr-anomalies with increasing SiO_2 contents;

(d) relatively minor ϵ_{Nd} variation throughout the suite, (-1 to +1.3 at 420 Ma).

(e) decreasing MgO, CaO, TiO_2, FeO and Al_2O_3 with increasing SiO_2 content;

(f) increasing K and Ba content with increasing silica content;

(g) negative Nb-, Ti- and Sr- anomalies; and

(h) LREE enrichment relative to HREE with flat HREE patterns.

Although items (b) and (c) suggest a genetic relationship between the different rock types of the suite, no single mechanism can account for all the observed features. Item (c) is inconsistent with successive intrusions of melts derived during episodic melting of the same or a similar source (*e.g.* Henderson, 1984), because the less evolved compositions (granodiorite) have higher REE abundances than the more evolved monzogranites. Item (a) is inconsistent with both magma mixing and fractional crystallization processes, but it could result from sampling bias (Chapter 4) or separation of magmas with different physical properties (*i.e.* liquid fractionation; Hildreth, 1981; McBirney, 1984).

Disregarding items (a) and (d), several features of the FS, including items (b), (c), (e) and (g) can be explained by fractional crystallization processes. For example, items (c), (e) and (g) imply early calcic-plagioclase and ilmenite/magnetite fractionation (*e.g.* Hanson, 1978; 1980; Henderson, 1984). Similarly, flat HREE patterns (item h) suggest that minerals (possibly zircon $\pm$ apatite $\pm$ hornblende) which have high K_d's for the HREE were not fractionated until the latter phases of magmatic evolution. Item (f) precludes crystallization of biotite $\pm$ K-feldspar (*e.g.* Hanson, 1980). Although negative Nb- and/or Ti-anomalies are consistent with ilmenite/magnetite fractionation (Thirlwall et al., 1994), the origin of high-field-strength-element (HFSE) anomalies, particularly the Nb-anomaly, is a subject of controversy. The extent of the Nb-anomaly in the FS does not change with the composition, whereas Sr- and Ti-anomalies do. This suggests that the negative Nb-anomaly is likely source related. It is also important to note that the Ti-

depletion relative to REE can be attributed to hornblende fractionation (*e.g.* Henderson, 1984), but a lack of MREE and/or HREE depletion precludes early hornblende fractionation. Taking all this information together, geochemical variations within the FS can be best explained in terms of early fractionation of plagioclase and ilmenite/magnetite, and late crystallization of zircon ± apatite ± hornblende.

However appealing it is to suggest a major role for fractional crystallization in the evolution of the FS, this does not offer an explanation for the, albeit limited, variation in Nd isotopic composition (item (d)).

5.4.3 Internal geochemical variations within the W-SCS

There are several important features that have to be considered for a better understanding of the magmatic evolution of the suite. These are:

a) The W-SCS consists of three lithologically distinct units: the Pigeon Island Unit, the Sandy Unit and the Wild Unit (Chapter 4).

b) Each unit displays its own distinct field and petrographic features. These features suggest that the Sandy Unit crystallized from a liquid under low water pressure, while the others were crystallized under high water pressure (Chapter 4).

c) The range of compositional variation seen in the Wild Unit, which dominates the W-SCS, overlaps that of the other units.

d) Samples from the Wild and Sandy Units with similar silica content have comparable major, minor and REE element abundances, and REE_N and extended REE_N patterns.

Taking all these observations together, the overall geochemical variations seen in the W-SCS clearly suggest a petrogenetic relationship between the rocks of the Sandy and

Wild Units. Although, item (b) precludes their relationship to the same batch of magma, items (b) and (d) suggest that Wild and Sandy Units may represent the products of magmas from the same source which crystallized under different physio-chemical conditions.

Relationships between Pigeon Island Unit and the other units are not clearly understood. The Pigeon Island Unit might represent a less fractionated product of the magma that produced the other units, since it is dominated by more mafic compositions. However, for a given silica content, rocks of the Pigeon Island Unit differ by lower Al_2O_3 and higher MgO precluding a fractional crystallization relationship. Therefore, the unit is better considered a product from the same or similar source that gave rise to the W-SCS.

Implication: The W-SCS is a composite intrusion. Field, petrographic and geochemical variations between the Sandy, Wild and/or Pigeon Island Units of the W-SCS can be best explained in terms of different melts from the same or similar source for the W-SCS.

5.4.4 Discussion and implications of the geochemical and isotopic characteristics of the dykes, microgranular enclaves and their host (Wild Unit, W-SCS)

The Wild Unit dominates the W-SCS, includes various forms of dykes and microgranular enclaves and displays a wide range of major, trace and isotopic compositions. As illustrated in Figure 5.20, geochemical and/or isotopic similarity between the dykes, microgranular enclaves and Wild Unit suggest a petrogenetic link between them, as predicted in Chapter 4. Thus, it is believed that understanding the origin of the geochemical and isotopic variations observed in the Wild Unit is important in elucidating the genesis of the W-SCS.

The field and petrographic features of The Wild Unit suggest mingling/mixing processes between coexisting mafic and felsic magmas. Specifically, a model is proposed (Figure 5.21) in which the principal features are based on possible physical constraints compiled from McBirney and Murase (1984) and Frost and Mahood (1987), and a model modified from Barbarin and Didier (1992). Four distinct stages of mafic-felsic interactions are recognized. These stages include formation of: a hybrid magma→ microgranular enclaves→ "*synplutonic/transitional dykes*" to "*cross-cutting dykes*". The earliest interaction of mafic and felsic magmas produced the hybrid intermediate magma which crystallized as the quartz dioritic Wild Unit, whereas the last form of interaction gave rise to the *cross-cutting* dykes. The explanation for these stages lies in the changes that accompany the evolution of compositional and rheological contrasts between the mafic and felsic components.

When mixing and mingling is prohibited by the physical properties of the mafic and felsic components (Stage IV), then the mafic component can be expected to preserve its original geochemical and isotopic identity. This stage (Stage IV) is realized by *cross-cutting* type dyke (F-91-19D), which preserves the second highest ϵ_{Nd} value (+4.1, at 408 Ma) in the Tilting area.

In stages (II) and (III), the model predicts partial chemical/temperature and isotopic equilibrium between mafic and felsic components (*cf.* Lesher, 1990; Barbarin and Didier, 1992; van der Laan and Wyllie, 1993)- *i.e.* geochemical and isotopic heterogeneity within the Wild Unit. This is consistent with the following observations:

a) presence of distinct types and forms of microgranular enclaves which display somewhat different trace elements, particularly REE characteristics;

b) overall physical, chemical and/or isotopic similarities between microgranular enclaves and mafic-intermediate dykes; and

c) different forms of mafic-intermediate dykes (*synplutonic* → *transitional* → *cross-cutting* types) which reflect increasing rheological contrast between coexisting mafic and felsic magmas.

In stage (I), hybrid "intermediate" magma giving to rise to the Wild Unit is expected. This appears to be consistent with overall continuous geochemical variations within the unit and significant variation in Nd isotopic composition (ϵ_{Nd} varies from +0.3 to +3.1, at 408 Ma). However, there is no apparent correlation between ϵ_{Nd} and SiO_2 content. In fact, it is possible to find the greatest range of isotopic variation in samples of approximately the same SiO_2 content. This may suggest that magma mixing is not evident from the chemical features- *i.e.* processes regulating the bulk chemistry of the unit may not be responsible for the variation in isotopic data. Similarly, the Wild Unit displays scattered, rather ambiguous (neither linear nor curvilinear) trends on Harker variation diagrams. From these observations, if magma mixing played a major role in the formation of the Wild Unit, it must have been very complicated. On the other hand, some geochemical features of the Wild Unit can be explained in terms of fractional crystallization processes. These are: a) REE abundances increase with decreasing SiO_2 content; and b) sample F-91-175a appears to represent a final stage of magmatic evolution during which bulk distribution coefficients of several elements changed significantly. Thus the sudden and significant decrease in Rb, Na_2O, and K_2O contents and the somewhat different extended REE_N characteristics of the sample can be explained in terms of late fractionation of biotite and K-feldspar. Taking all this information together, the chemical evolution of the Wild Unit can be best explained in terms of fractional crystallization of a magma which itself was a product of hybridization of coexisting magmas (*cf.* Frost and Mahood, 1987; Hogan and Sinha, 1989; Wiebe, 1994). This is consistent with the petrogenetic classification given below.

5.5 PETROGENETIC CLASSIFICATION OF THE GRANITOID ROCKS

Different granitoid types have been recognized on the basis a variety of characteristics, *e.g.* composition, mineralogy, tectonic setting, associated mineralization (Chappell and White, 1974; Pitcher, 1983; 1987; Pearce et al., 1984; Maniar and Piccoli, 1989; Barbarin, 1990; Castro et al., 1991; Clarke, 1991). The variety of types reflects the diversity of the origins, magma sources and subsequent crystallization processes that effect granitoids. In the present study, two main granitoid classification schemes are utilized; Barbarin (1990) and Chappell and White (1974). Barbarin (1990) classifies granitoid rocks on the basis of their source region and defines three main groups corresponding to a crustal (C-type), a mantle (T- or A-type) or a mixed (H-type, crustal and mantle) origin. On the other hand, Chappell and White's (1974) classification scheme considers granitoid rocks to dominantly be of crustal origin and defines I- and S-type granites which were extracted from igneous and sedimentary protoliths, respectively. This classification has been extended by adding an M-type for the most calc-alkaline plagiogranites and an A-type for anorogenic granites (*e.g.* Pitcher, 1983; Whalen et al., 1987). The M-type is considered to arise from a parental magma derived directly from melting of subducted oceanic crust or overlying mantle, whereas A-type granites are thought to result from partial melting of granulitic residue after extraction of an orogenic granite (Whalen et al., 1987).

5.5.1 Petrogenetic classification of the FS

Petrogenetic classification of the FS must take into account the following:

(a) the presence of inherited zircons;

(b) a lack of microgranular enclaves and country-rock xenoliths;

(c) dominantly monzogranitic with minor granodioritic rocks;

(d) a metaluminous to slightly peraluminous nature;

(e) the presence of biotite ± hornblende as the dominant ferromagnesian minerals;

f) somewhat high ϵ_{Nd} values (-1.0 to +1.3, at 420 Ma); and

(g) relatively insignificant ϵ_{Nd} variation throughout the suite.

From these observations, no unique classification can be arrived at. However, items (a), (b) and (c) argue against a significant mantle (or mantle-derived component) contribution in the origin of the FS and suggest a C-type, crustal origin, (Barbarin, 1990). As briefly mentioned above, Chappell and White's (1974) classification scheme considers dominantly crustal sources. However, application of I-, A- M- or S-type classification to the FS does not give a unique solution, either. This is partly because of: a) the high SiO_2 content of the suite, where the chemical and mineralogical composition of these different types converge; b) complexity of the FS; and c) selection of discrimination criteria. Nevertheless, several items, particularly (c), (d) and (e) clearly oppose an S-type classification. Similarly, several geochemical characteristics of the FS including relatively low Ga, Nb and Y contents (Appendix 5) preclude an A-type classification. Supporting this, rocks of the FS consistently plot in the I-type (± S-type) granite field on the discrimination diagrams of Whalen et al. (1987). Additionally, extensive studies in central Newfoundland indicate that subduction of oceanic crust was not directly involved in the genesis of those granitoid rocks younger than 440 Ma (*e.g.* Kerr et al., 1992, 1995). This argues against M-type classification. As a result, the FS is best classified as an I-type granite.

5.5.2 Petrogenetic classification of the W-SCS

A petrogenetic classification of the W-SCS has to account for the following:

a) the predominant lithology is quartz diorite;

b) the presence of numerous inclusions either as country-rock xenoliths or as microgranular enclaves;

c) the metaluminous to slightly peraluminous nature of the suite;

d) the presence of hornblende and pyroxene as the dominant ferromagnesian minerals;

e) a lack of inherited zircons;

f) the high (positive) ϵ_{Nd} values; and

g) a wide range of ϵ_{Nd} variation (+0.3 to +3.2).

These features of the W-SCS most closely resemble the field, petrographic and geochemical characteristics of H-type granites of Barbarin (1990). This suggests a mixed (crustal and mantle) origin for the magma that gave rise to the W-SCS, and is consistent with the petrogenetic model described in the previous section. Because of the mixed nature of the suite, the classification scheme of White and Chappell (1974) which considers dominantly crustal sources, has not been applied.

5.6 SUMMARY

The FS and the W-SCS represent geochemically and isotopically distinct, temporally unrelated Silurian magmatic events. The FS is a 420 $\pm$2 Ma, C-type granitoid body. Lithological and geochemical variation within the FS can be best explained in terms of fractional crystallization of early calcic-plagioclase, ilmenite and/or late crystallization of zircon $\pm$ apatite $\pm$ hornblende with or without minor magma mixing.

The W-SCS is a 408 $\pm$2 Ma, H-type, composite granitoid intrusion. The

lithological and geochemical variations within the W-SCS apparently reflect different melts from the same or similar sources. The lithological and chemical variations within the Wild Unit can be attributed to fractional crystallization of a magma which itself was a product of hybridization of coexisting contrasting magmas. Evolution of the Wild Unit is envisaged as four distinct stages of mafic-felsic magmas interaction, where each stage has its unique characteristics. In Stages I to IV, these characteristics vary from hybrid magma (Wild Unit)→ microgranular enclaves→ "*synplutonic/transitional* dykes" to "*cross-cutting* dykes". The hydrid magma which produced the Wild Unit, underwent fractional crystallization.

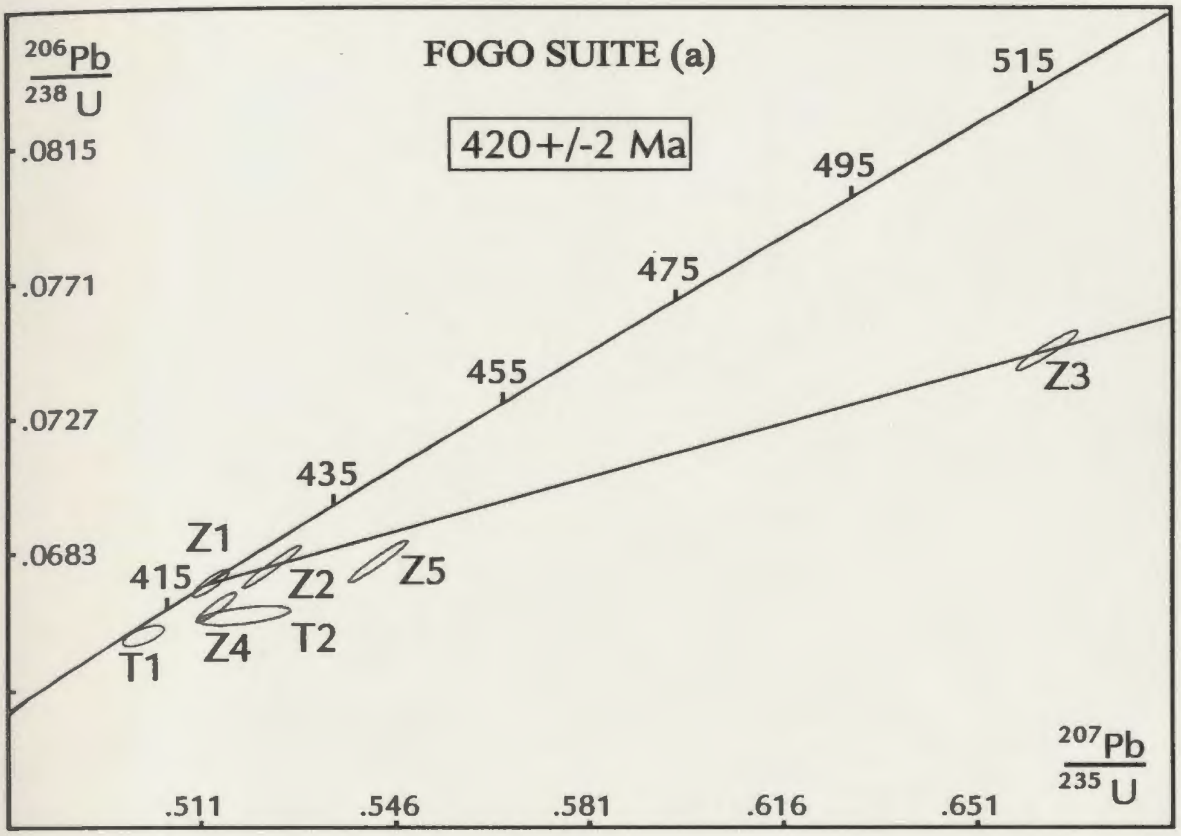

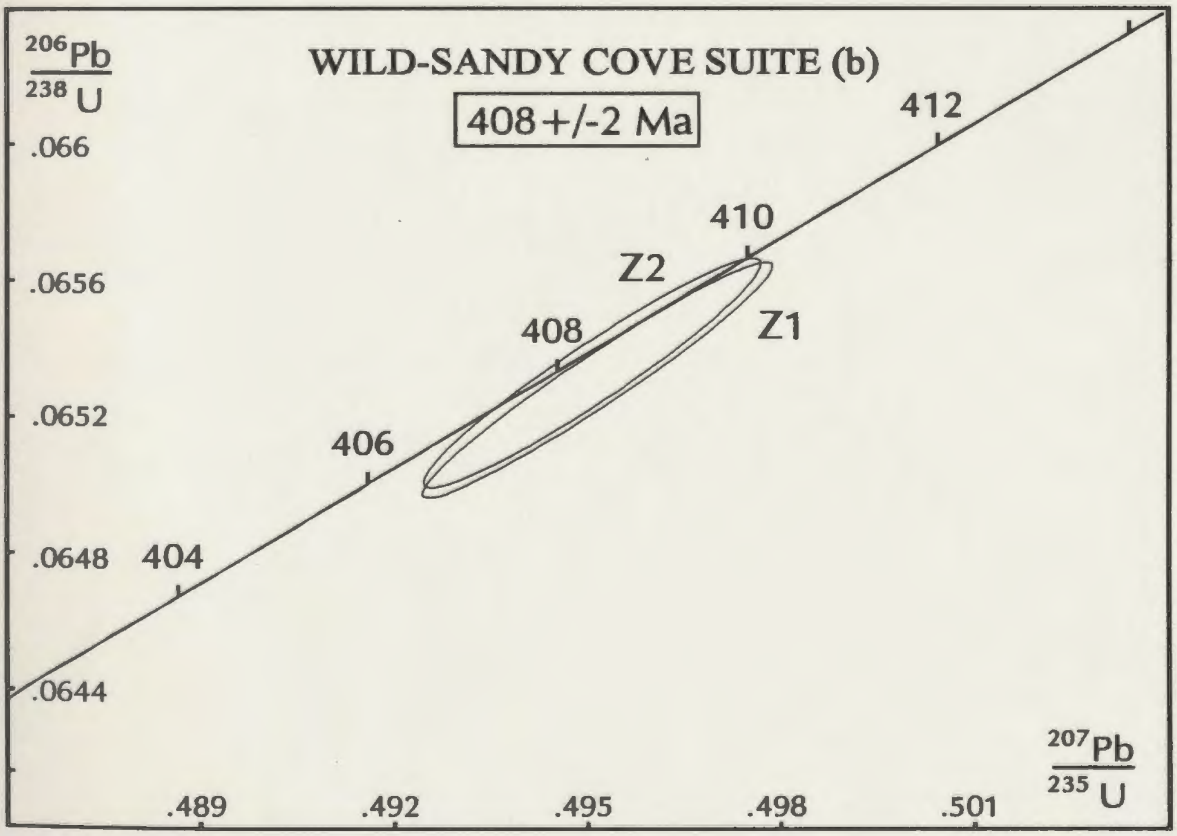

Figure 5.1 U-Pb concordia plot of zircon and/or titanite from: a) the FS (F-91-580); and b) the W-SCS (F-91-79). Z1-Z5 and T1-T2 are different zircon and titanite fractions, respectively (see Table 5.1 for detail description).

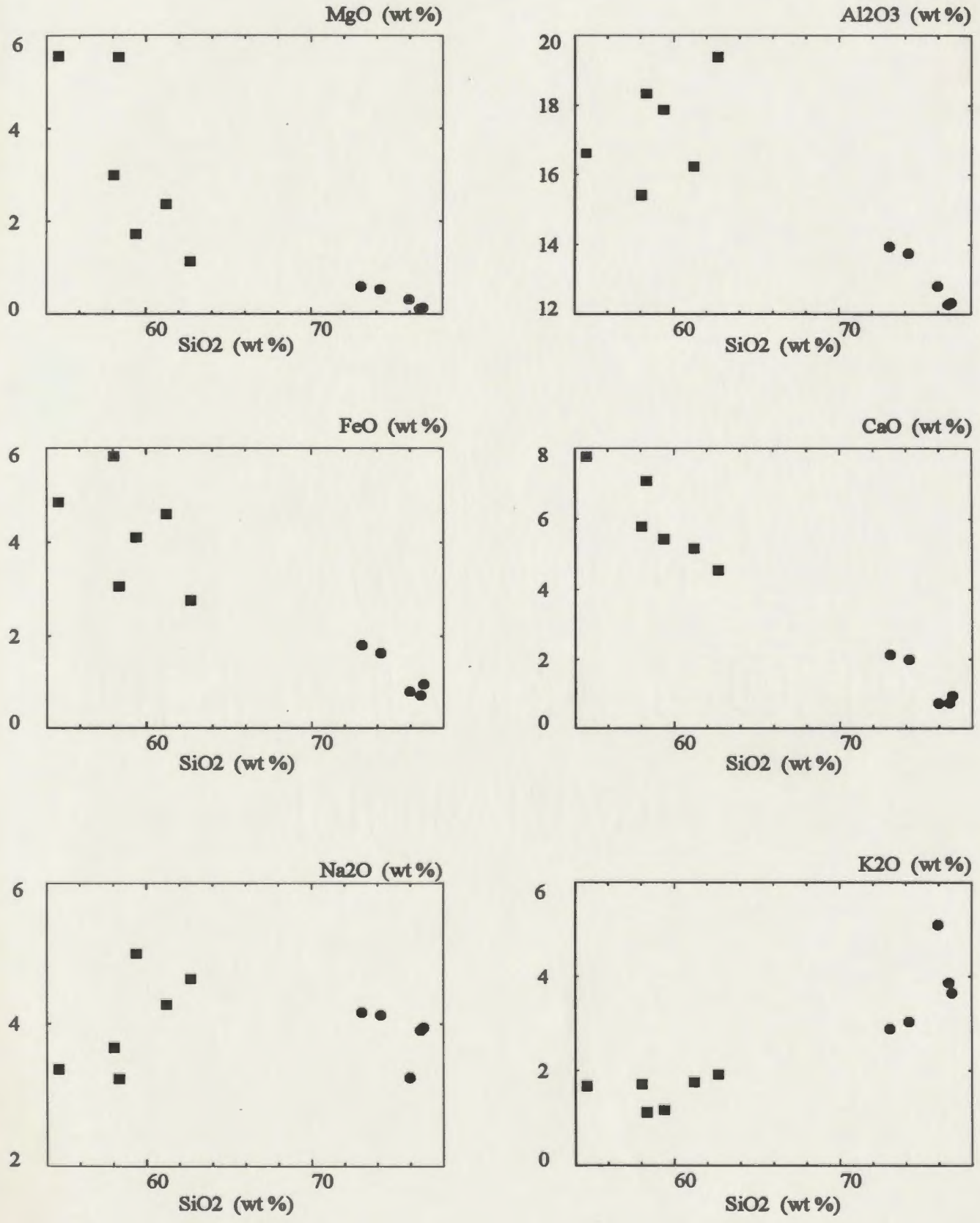

Figure 5.2a Major element Harker variation diagrams, for the FS.

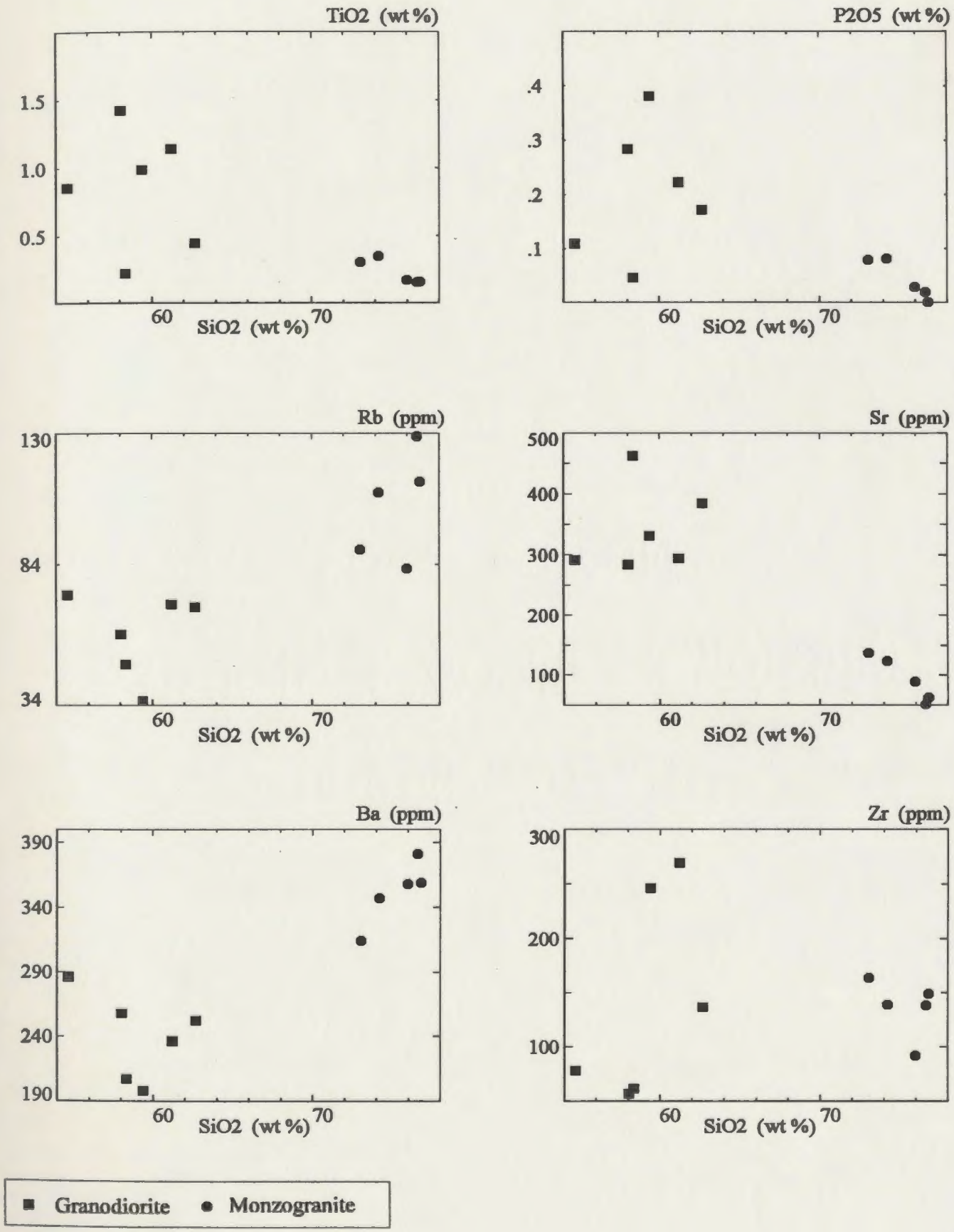

Figure 5.2b Selected minor and trace element Harker variation diagrams, for the FS.

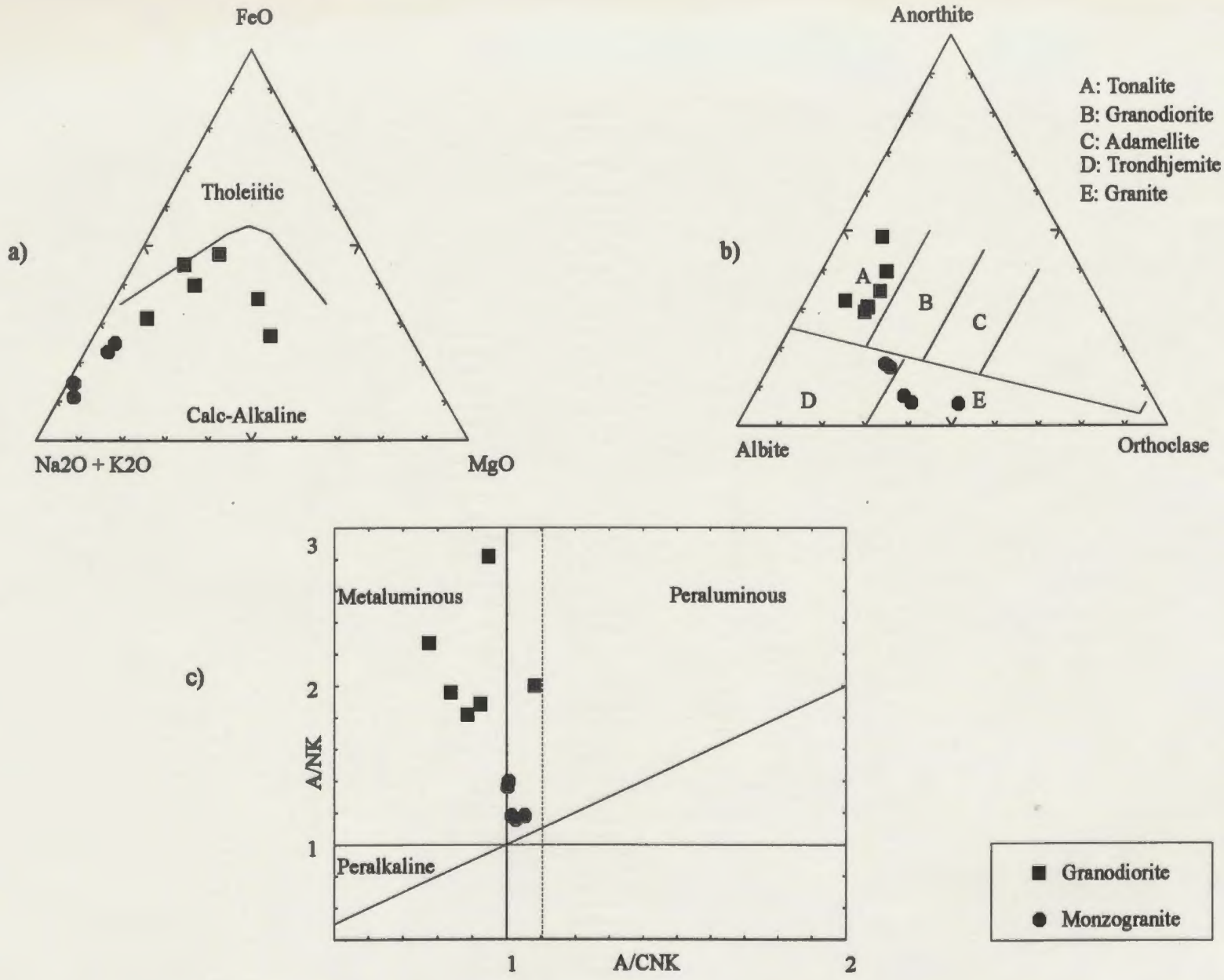

Figure 5.3 AFM diagram (a), tholeiitic and calc-alkaline fields from Irvine and Baragar (1971); plots of CIPW normative Ab-An-Or (b), fields from Barker (1979) after O'Connor (1965); and Shand index (c), molar A/NK vs A/CNK, after Maniar and Piccoli (1989), for the FS.

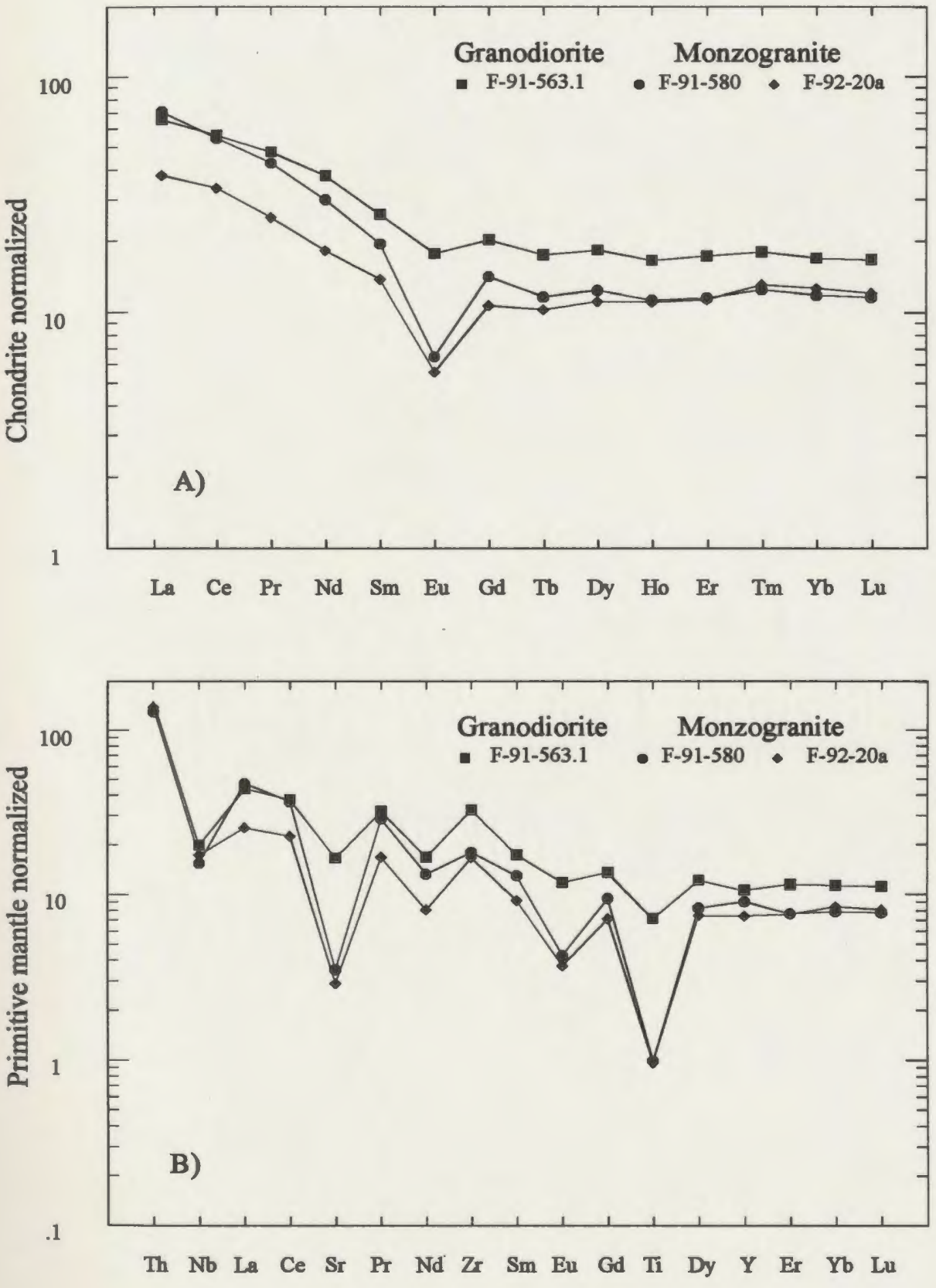

Figure 5.4 Chondrite normalized REE (A) and primitive mantle normalized extended REE (B) diagrams, for the FS.

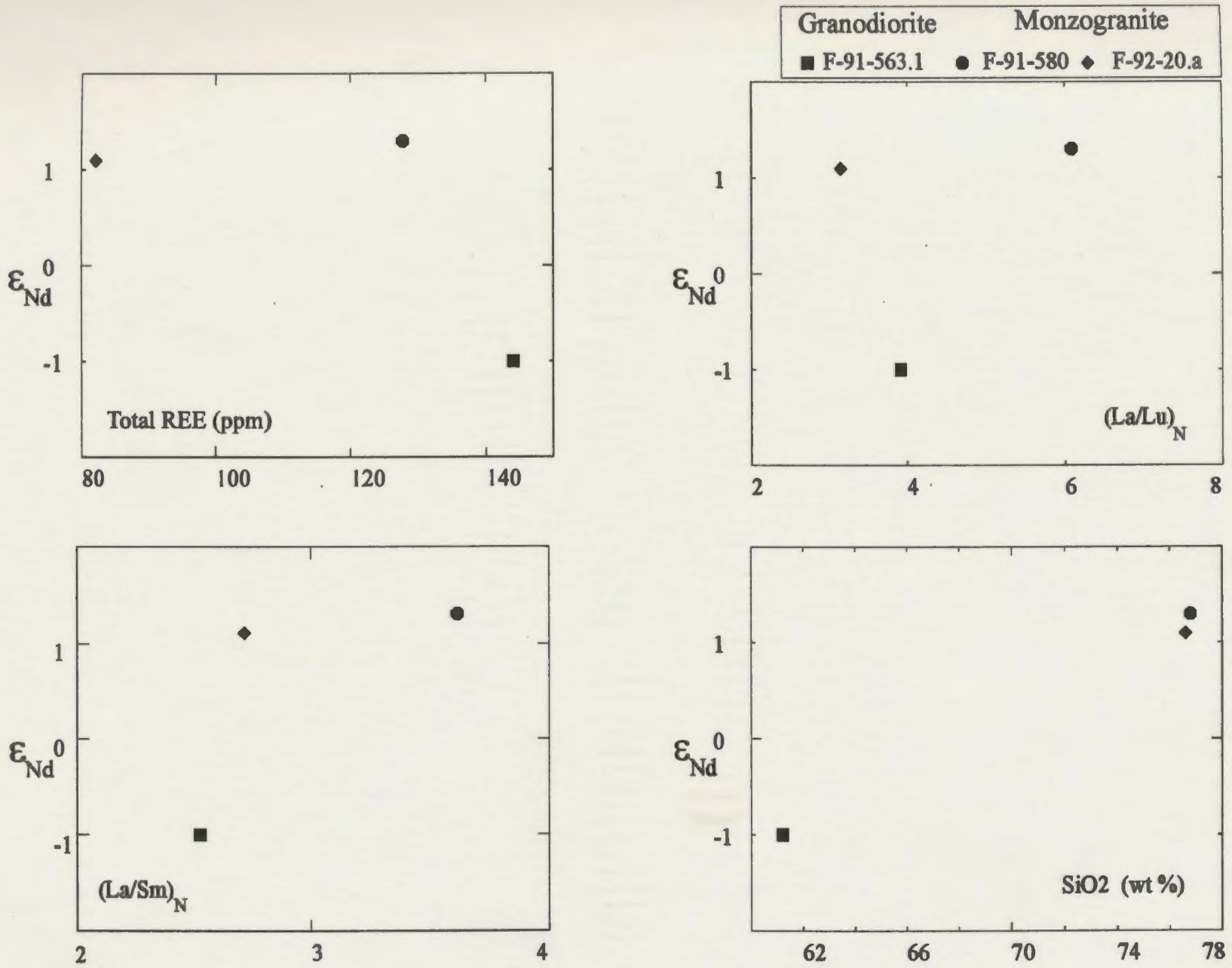

Figure 5.5 Interrelationship between Nd isotopic composition and the SiO_2, total REE abundances, $(La/Lu)_N$ and $(La/Sm)_N$, for the FS.

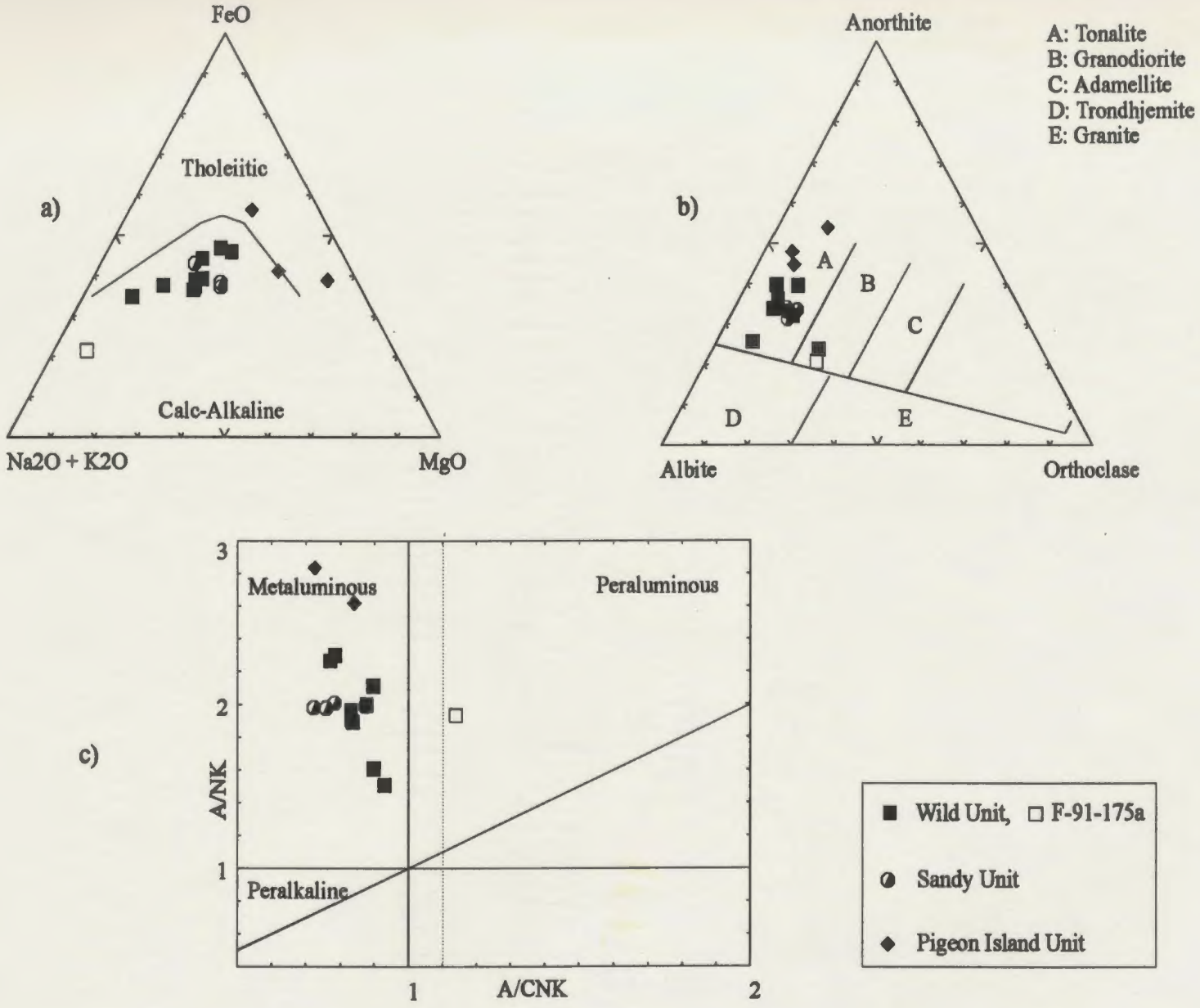

Figure 5.6 AFM diagram (a), tholeiitic and calc-alkaline fields from Irvine and Baragar (1971); plots of CIPW normative Ab-An-Or (b), fields from Barker (1979) after O'Connor (1965); and Shand index (c), molar A/NK vs A/CNK, after Maniar and Piccoli (1989), for the W-SCS.

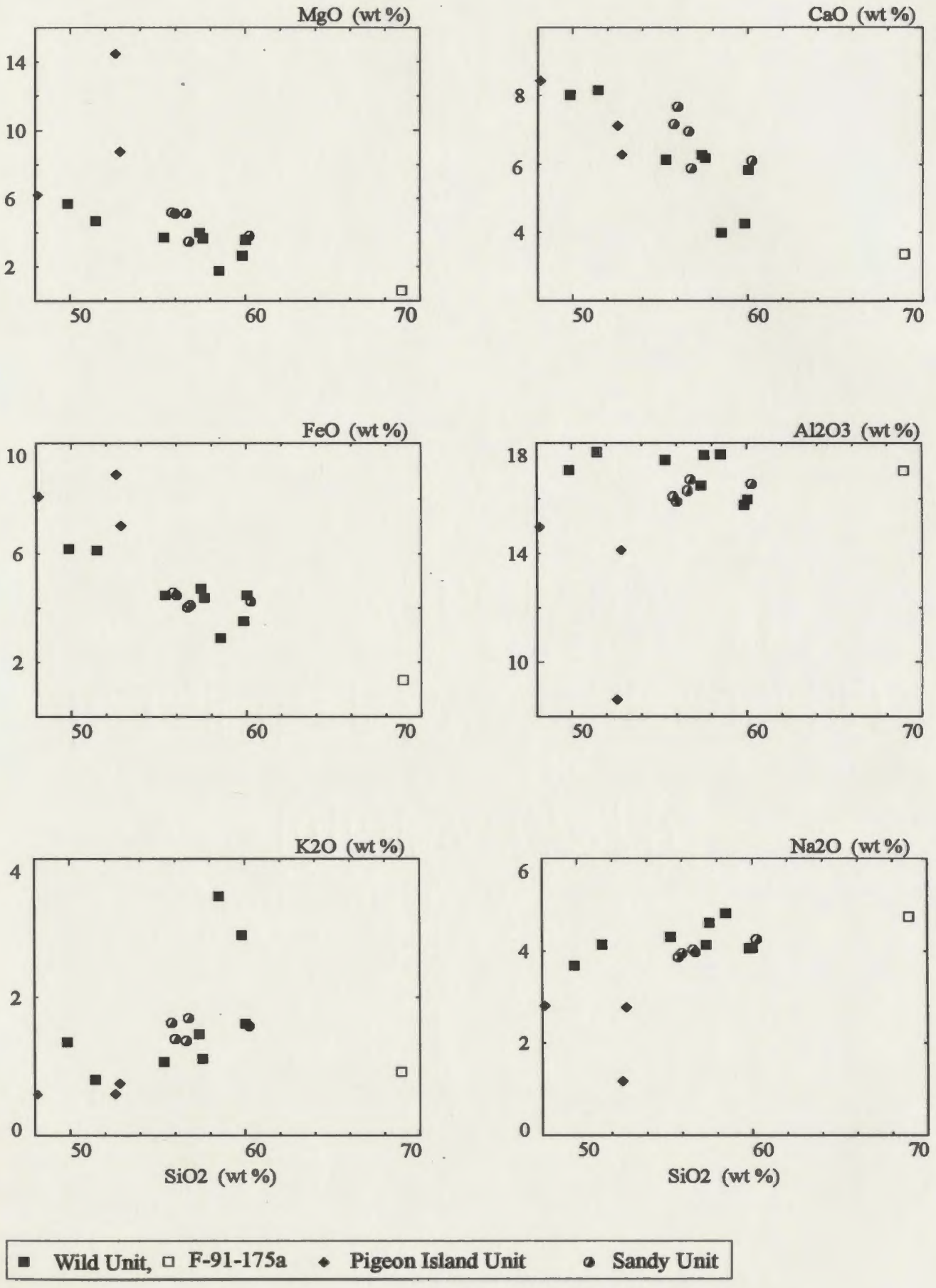

Figure 5.7a Major element Harker variation diagrams, for the W-SCS.

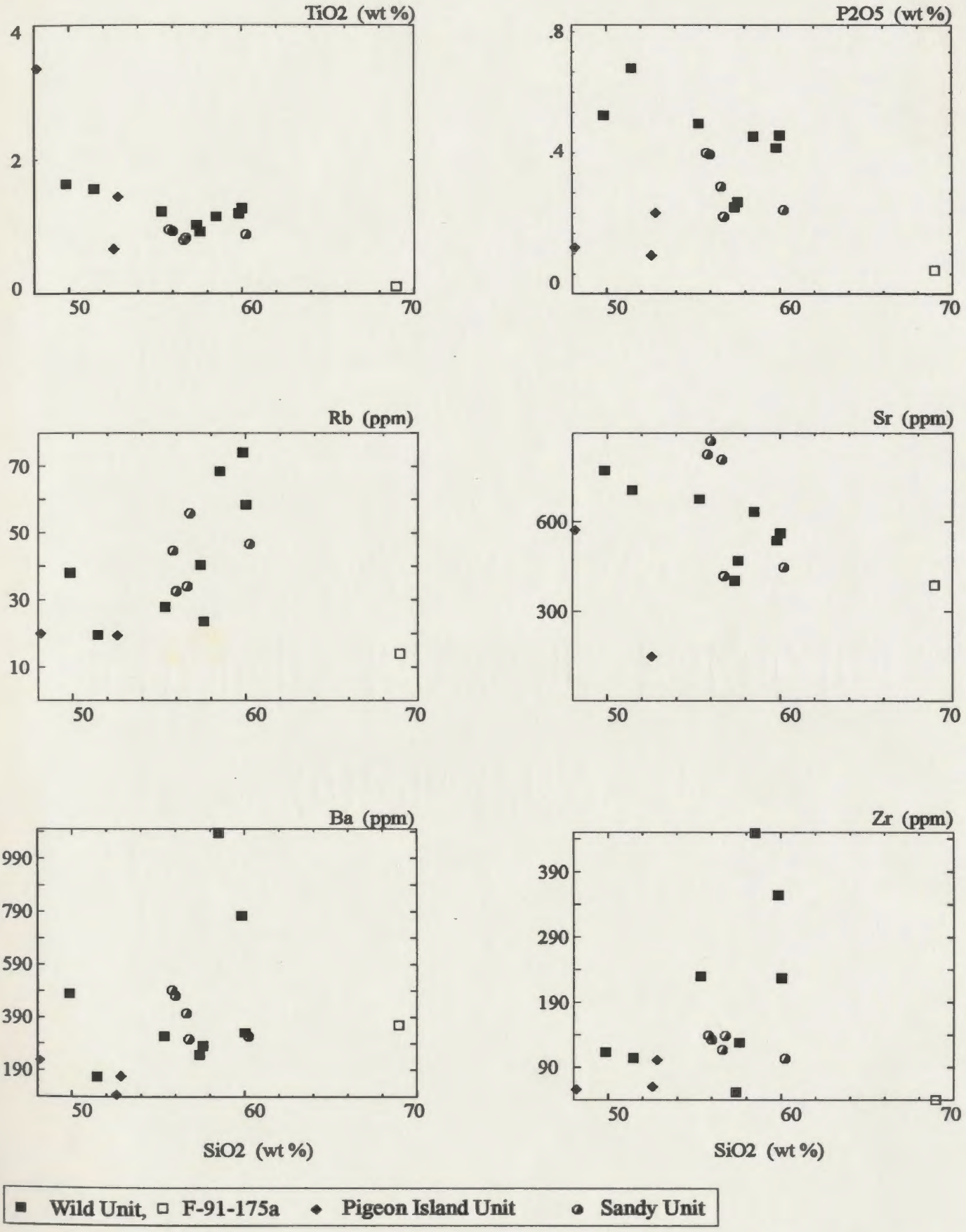

Figure 5.7b Selected minor and trace element Harker variation diagrams, for the W-SCS.

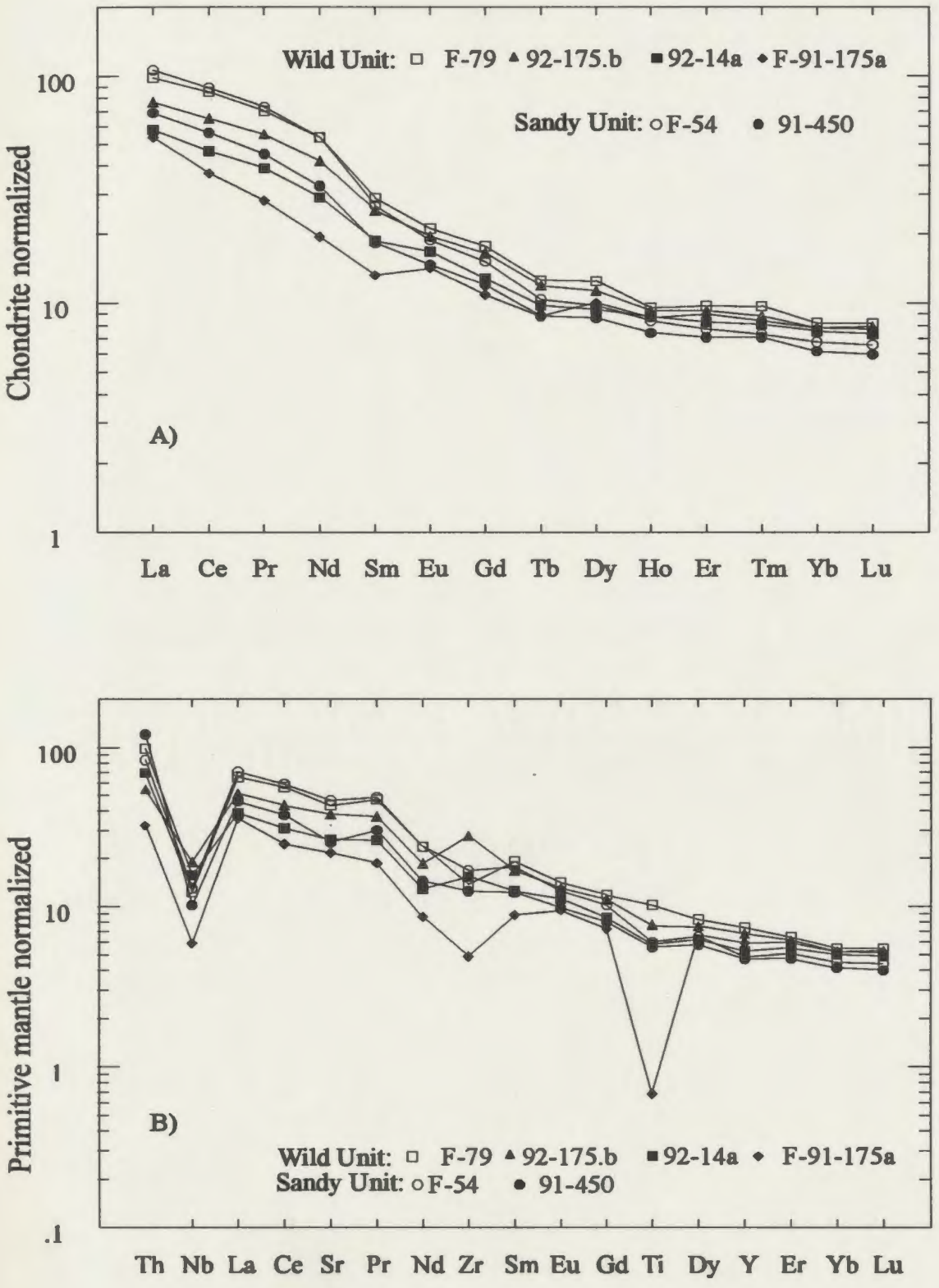

Figure 5.8 Chondrite normalized and REE (A) and primitive mantle normalized extended REE diagrams (B), for the W-SCS.

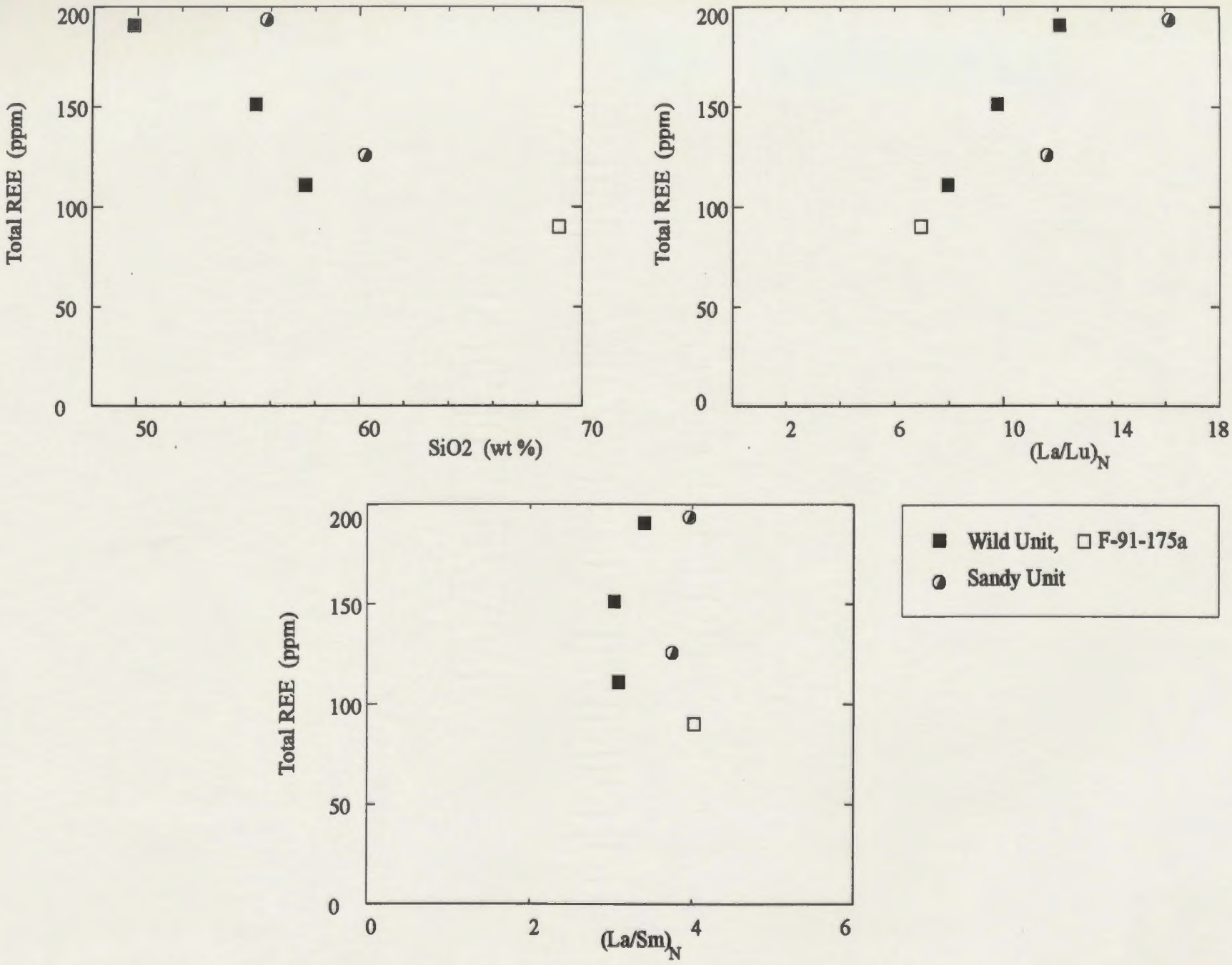

Figure 5.9 Total REE abundances versus the SiO2, $(La/Lu)_N$ and $(La/Sm)_N$, for the W-SCS.

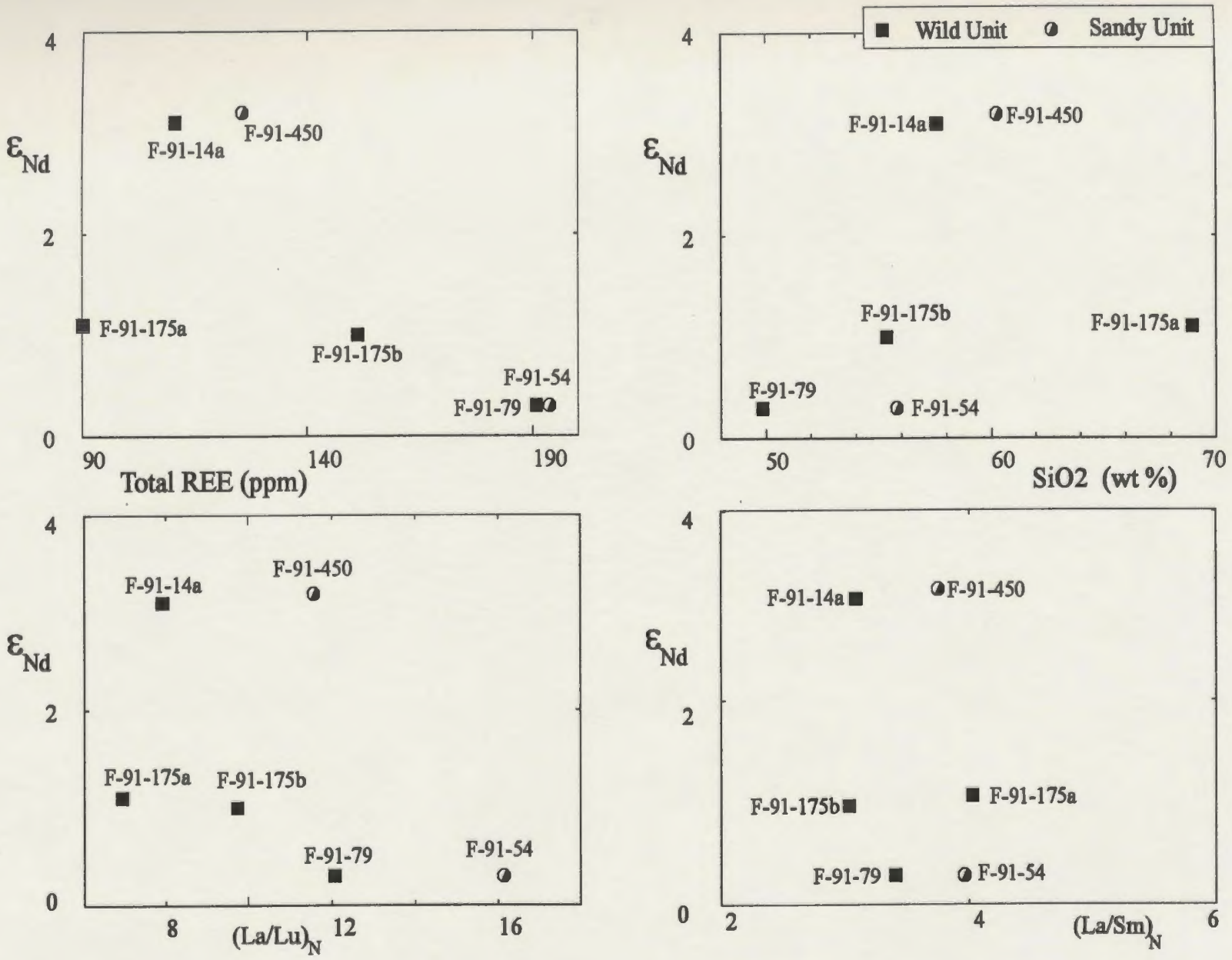

Figure 5.10 Interrelationship between Nd isotopic composition and the SiO_2, total REE abundances, $(la/Lu)_N$, and $(La/Sm)_N$, for the W-SCS.

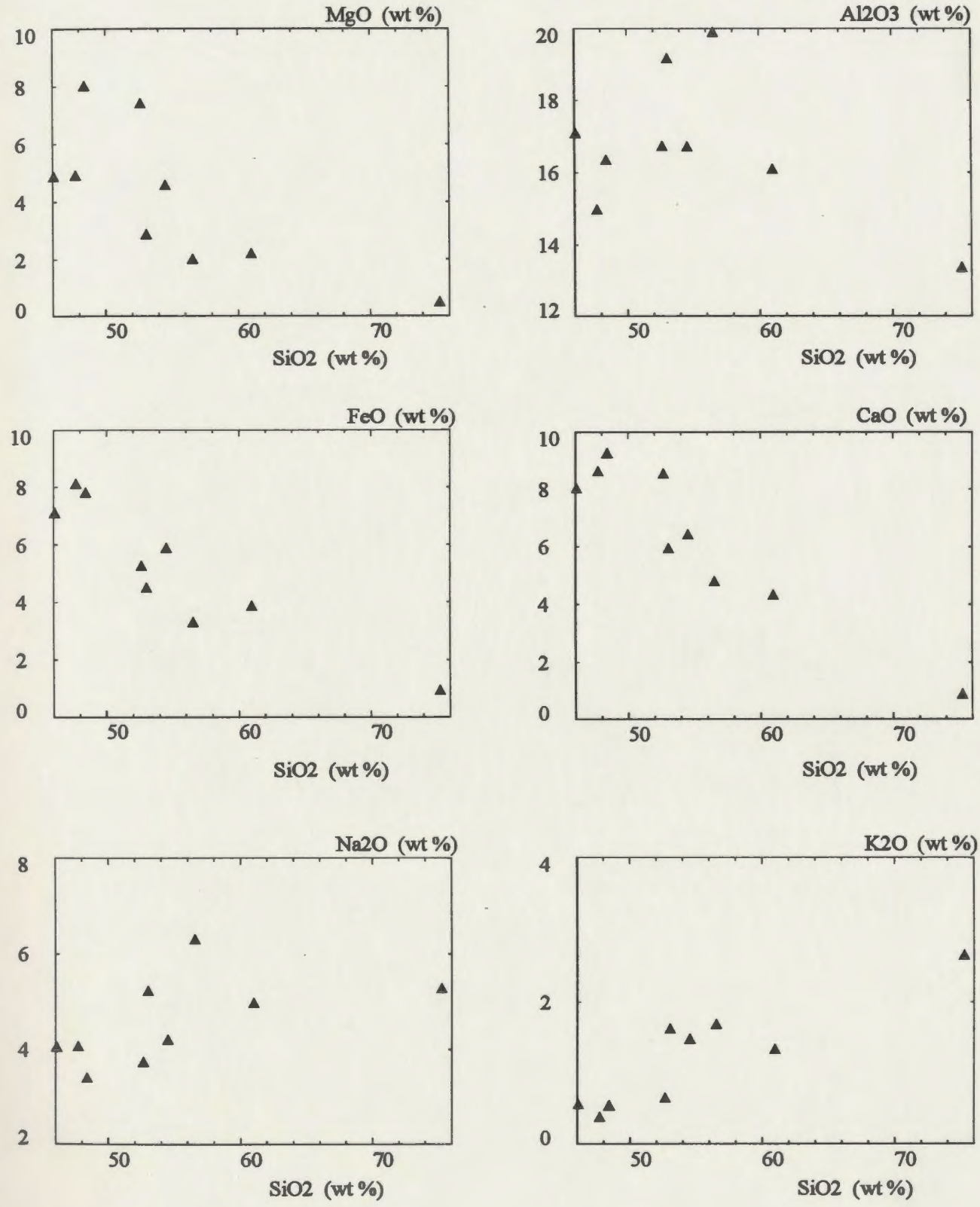

Figure 5.11a Major element Harker variation diagrams, for the dykes.

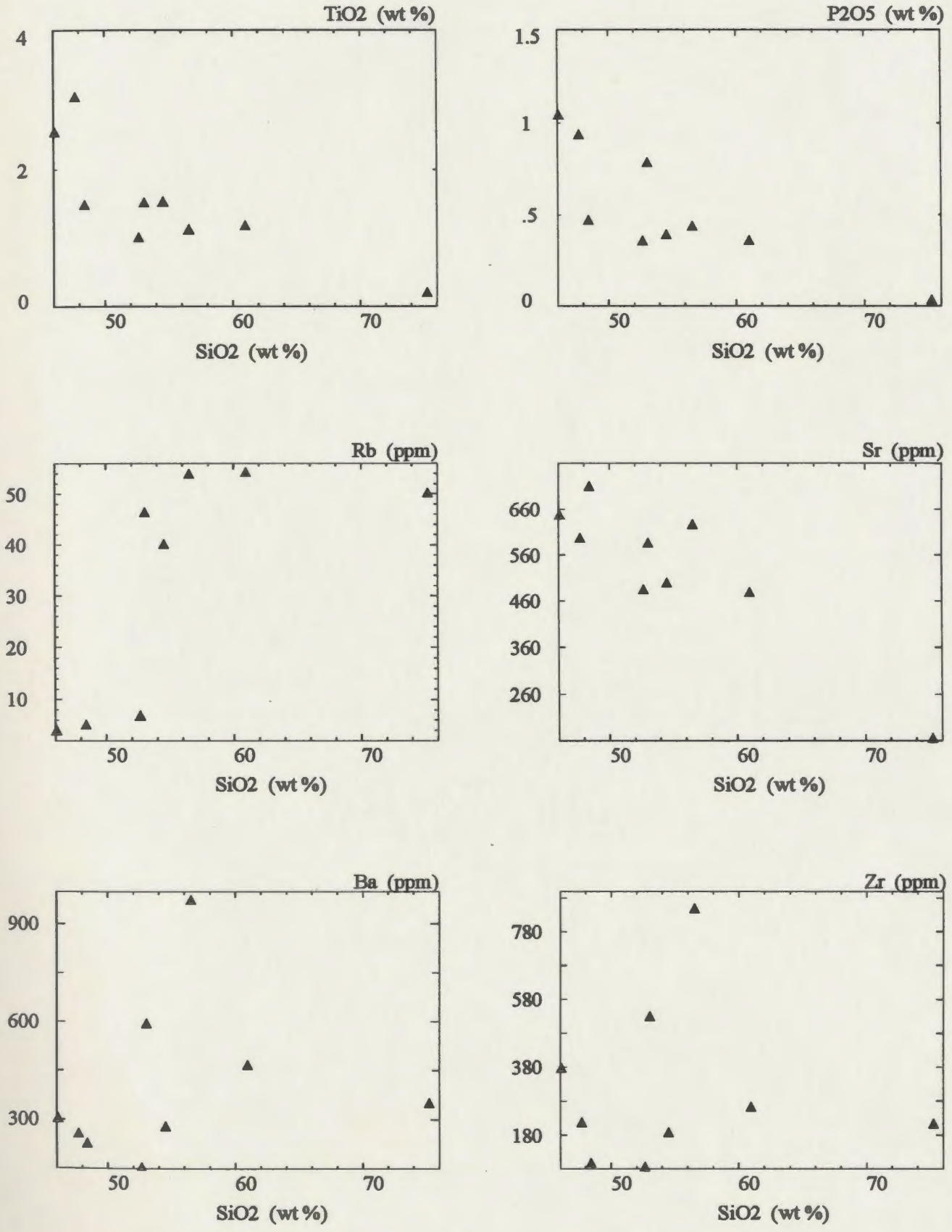

Figure 5.11b Selected minor and trace element Harker variation diagrams, for the dykes.

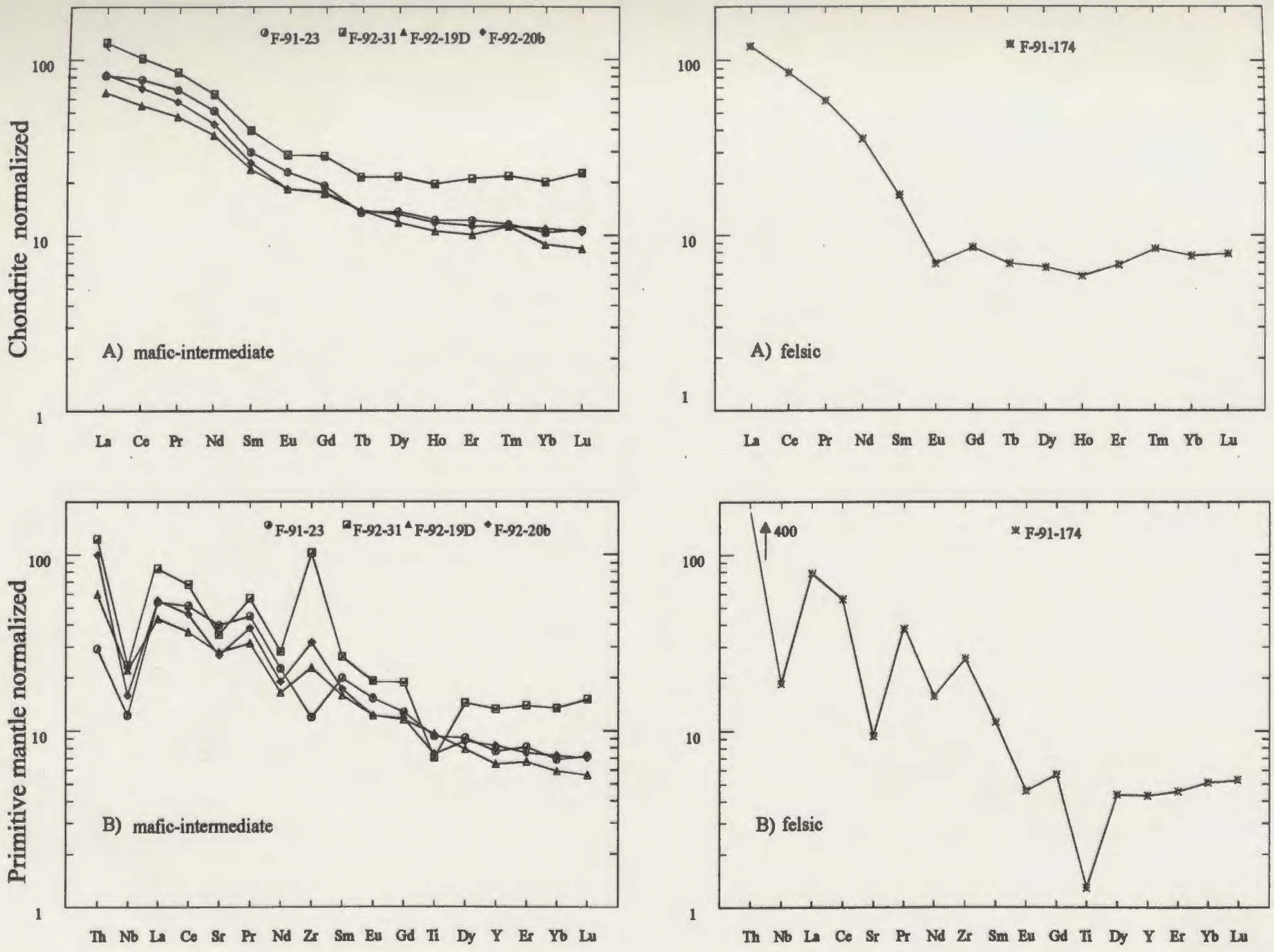

Figure 5.12 Chondrite normalized REE (A) and primitive mantle normalized extended REE (B) diagrams, for the dykes.

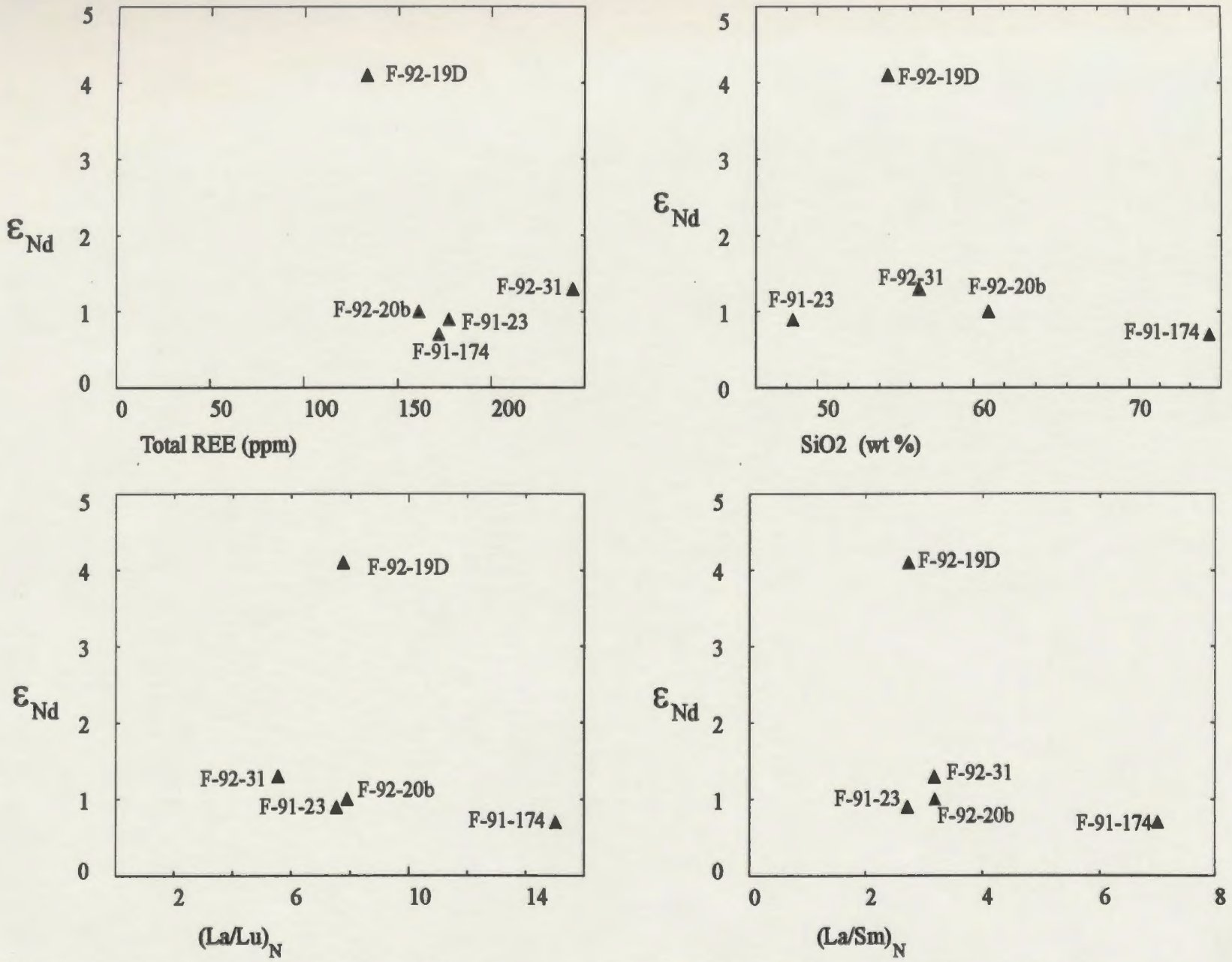

Figure 5.13 Interrelationship between Nd isotopic composition and the SiO_2, total REE abundances, $(La/Sm)_N$ and $(La/Lu)_N$, for the dykes.

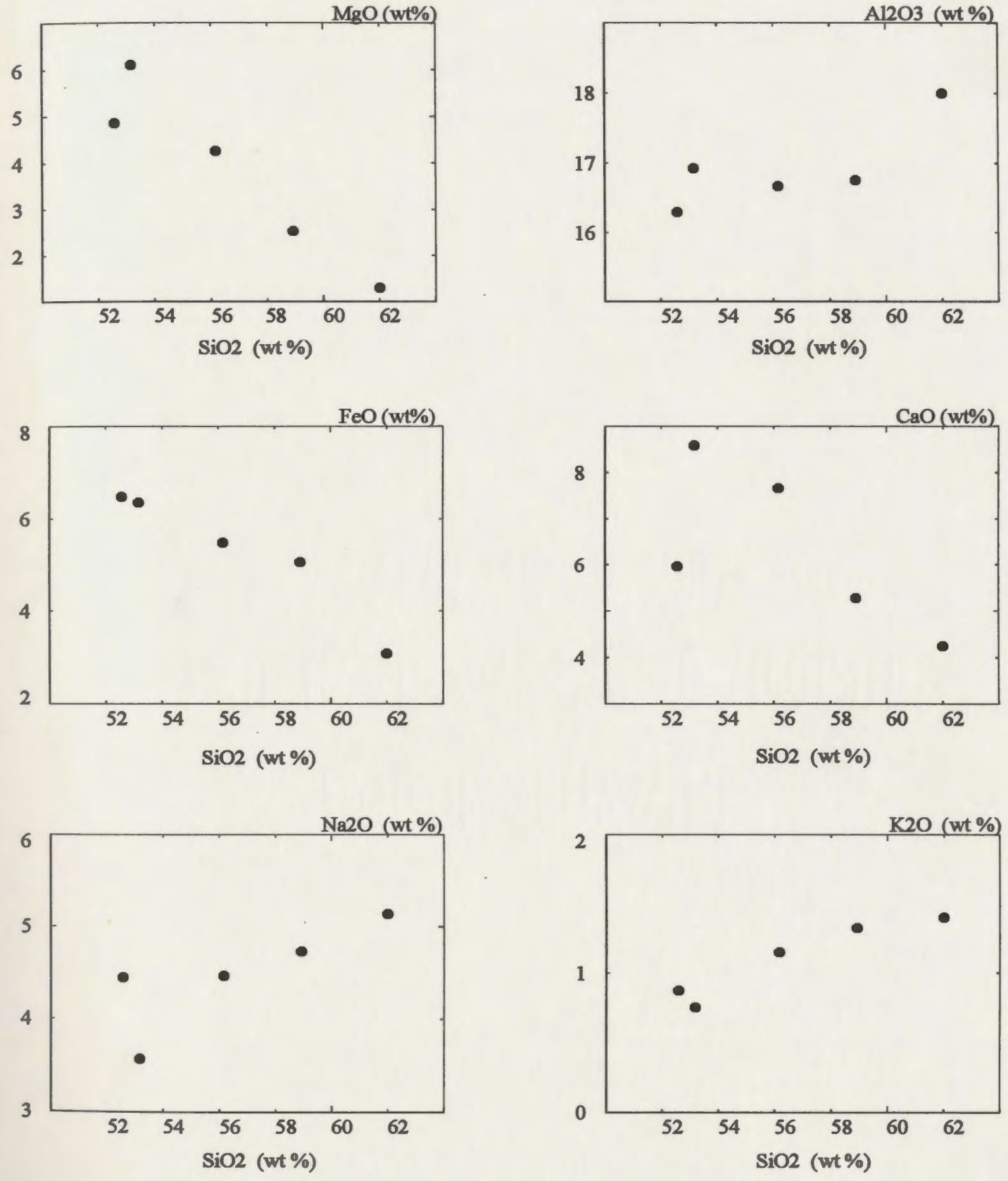

Figure 5.14a Major element Harker variation diagrams, for the microgranular enclaves.

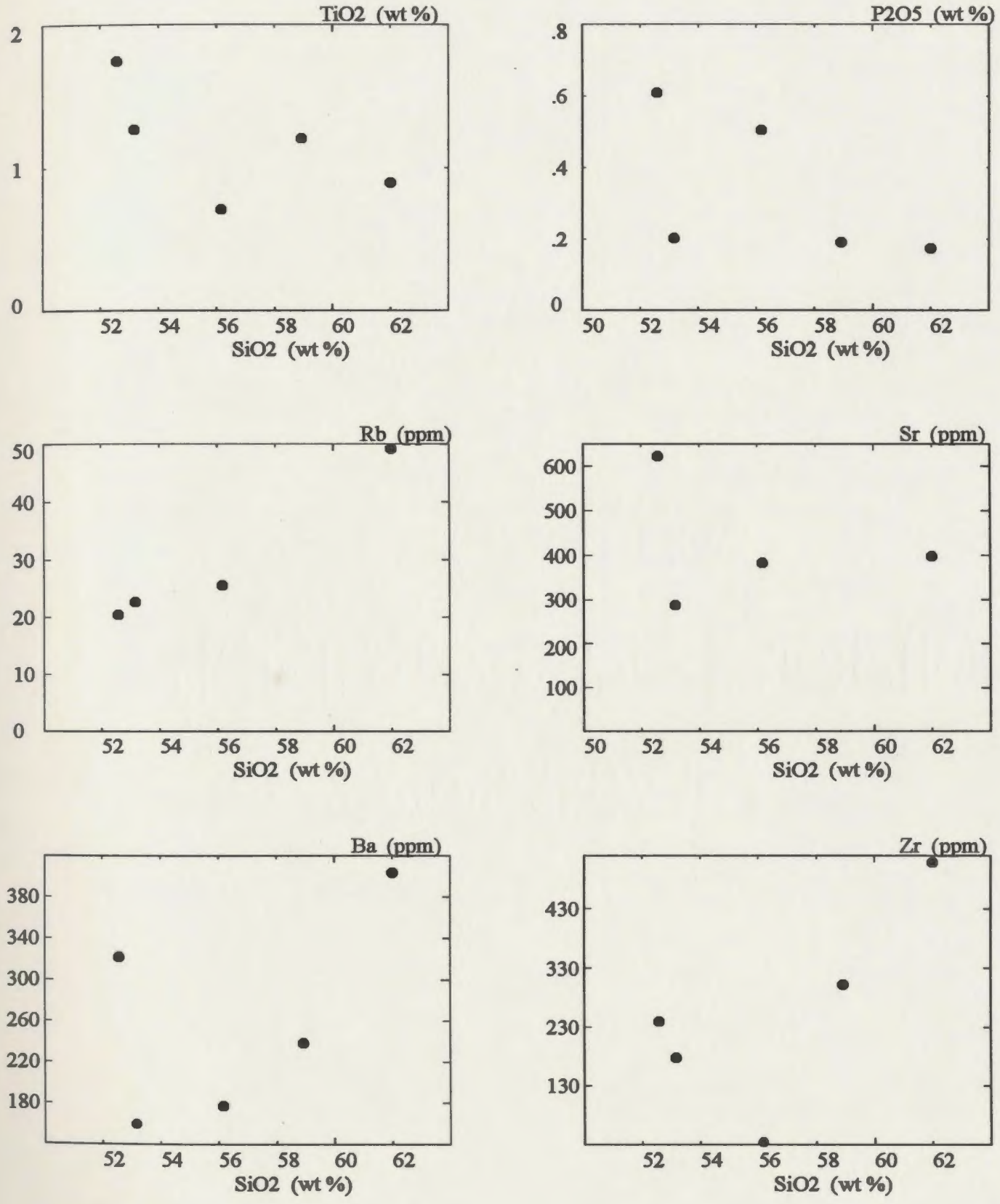

Figure5. 14b Selected minor and trace element Harker variation diagrams, for the microgranular enclaves.

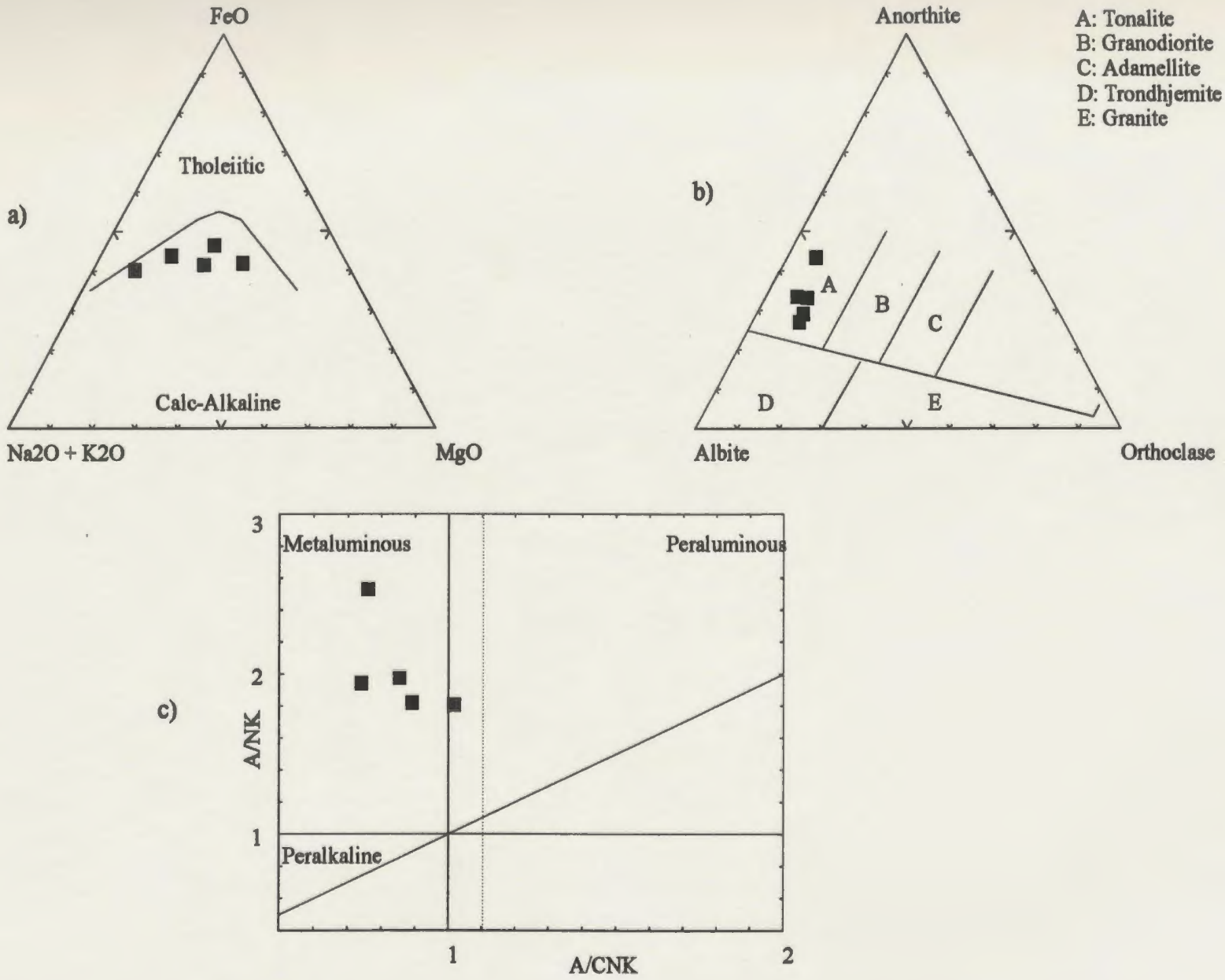

Figure 5.15 AFM diagram (a), tholeiitic and calc-alkaline fields from Irvine and Baragar (191); plot of CIPW normative Ab-An-Or (b), fileds from Barker (1979) after O'Connor (1965); and Shand Index (c), molar A/NK vs A/CNK, after Maniar and Piccoli (1989), for the microgranular enclaves.

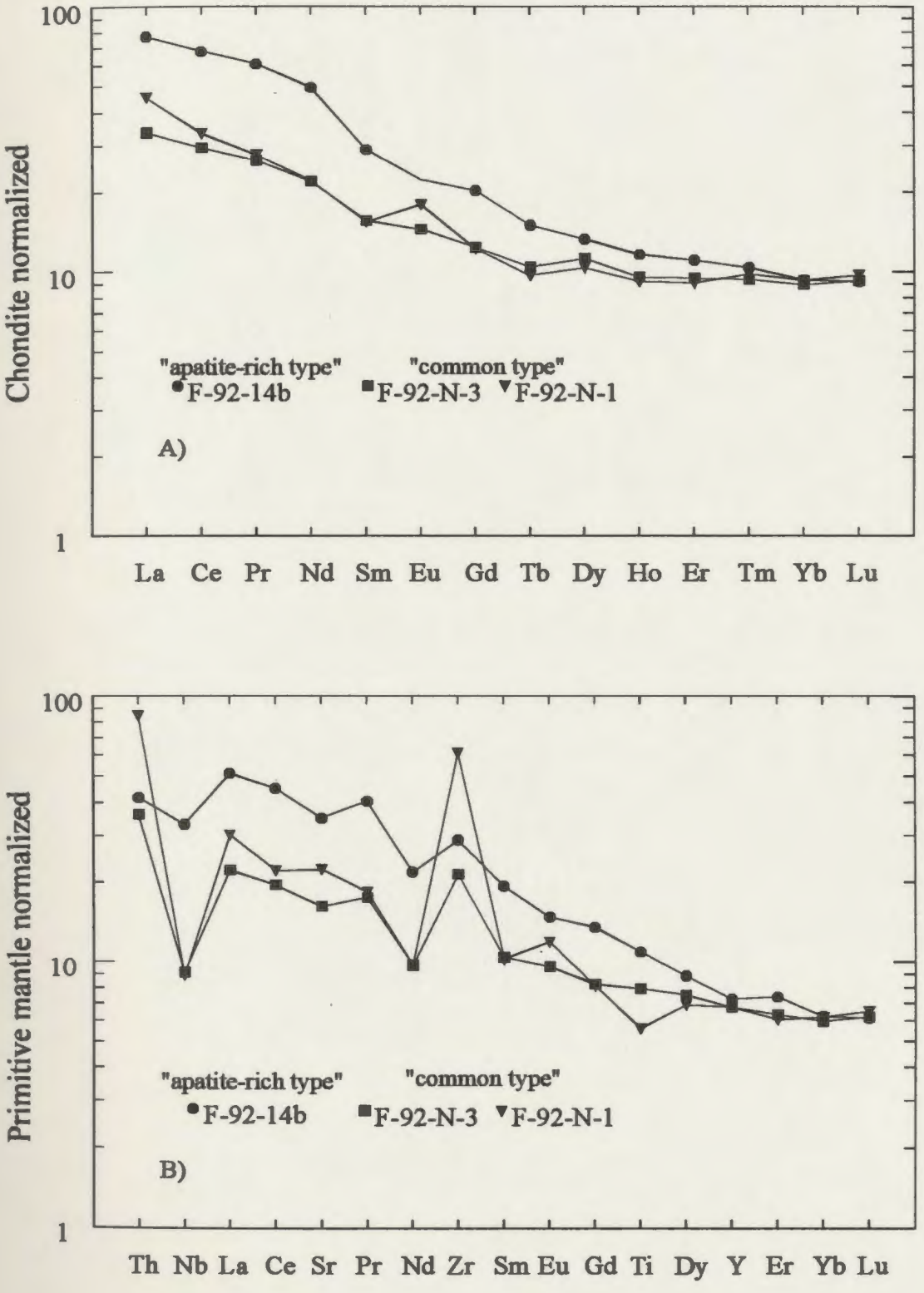

Figure 5.16 Chondrite normalized REE (A) and primitive mantle normalized extended REE (B) diagrams, for the microgranular enclaves.

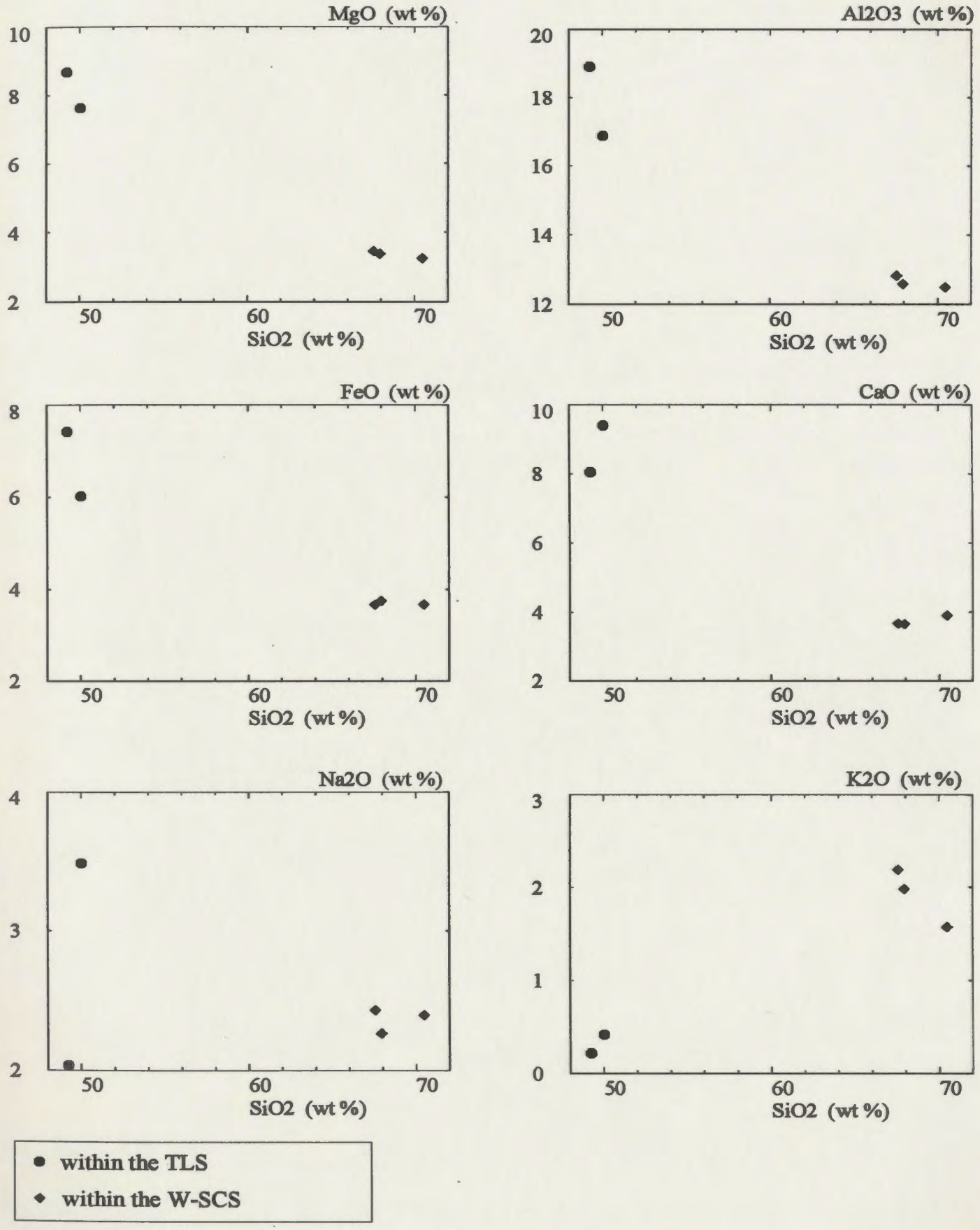

Figure 5.17a Major element Harker variation diagrams, for supracrustal rocks found as xenoliths in the Tilting area.

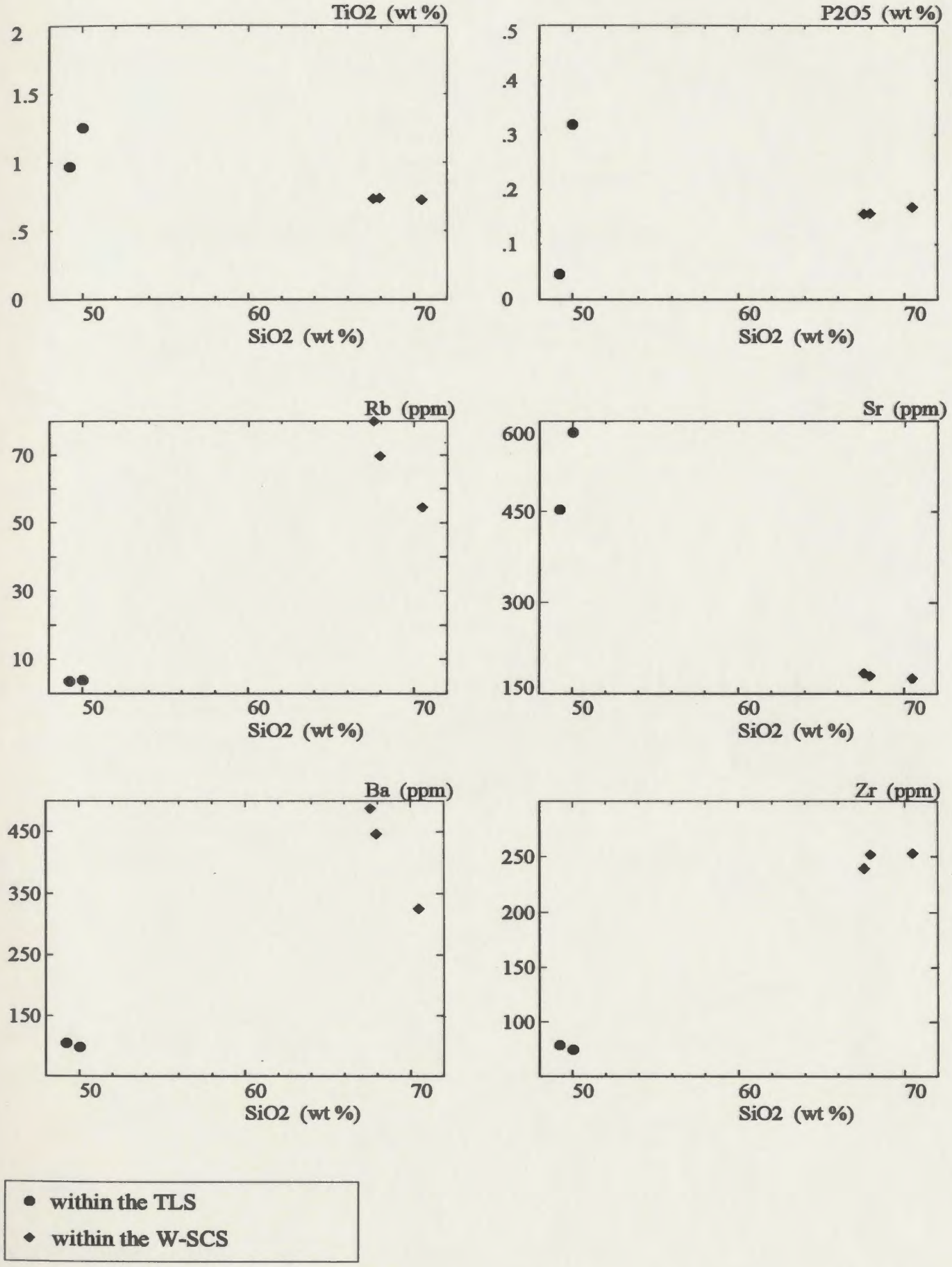

Figure 5.17b Selected minor and trace element Harker variation diagrams, for supracrustal rocks found as xenoliths within in the Tilting area.

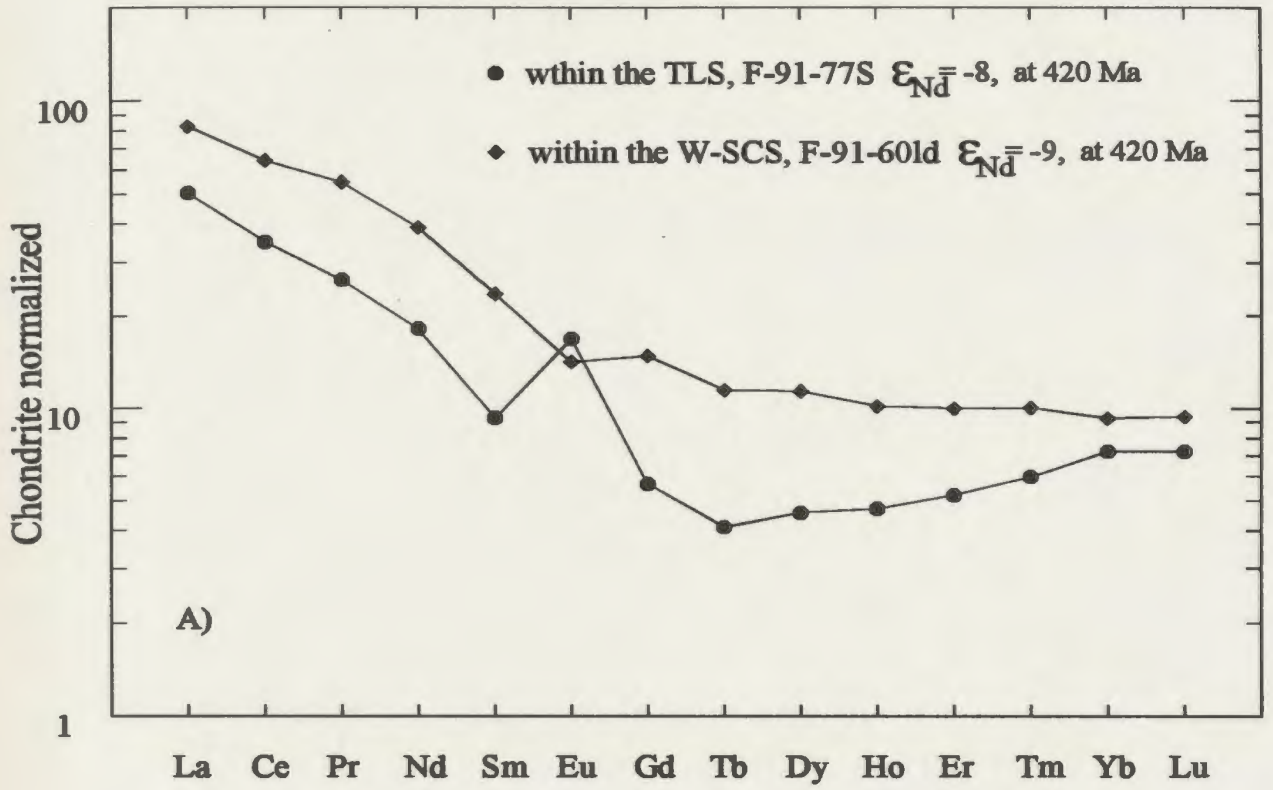

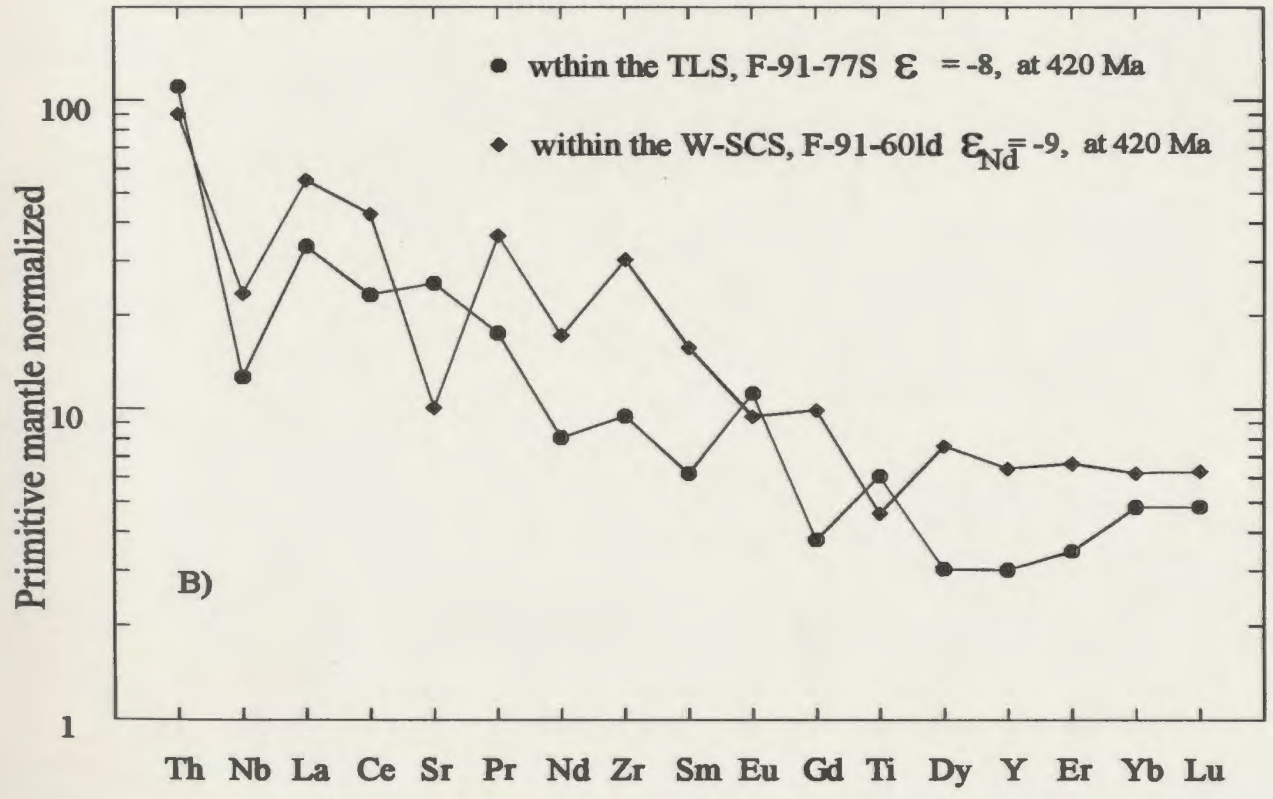

Figure 5.18 Chondrite normalized REE (A) and primitive mantle normalized extended REE (B) diagrams, for the supracrustal rocks found as xenoliths within the Tilting area.

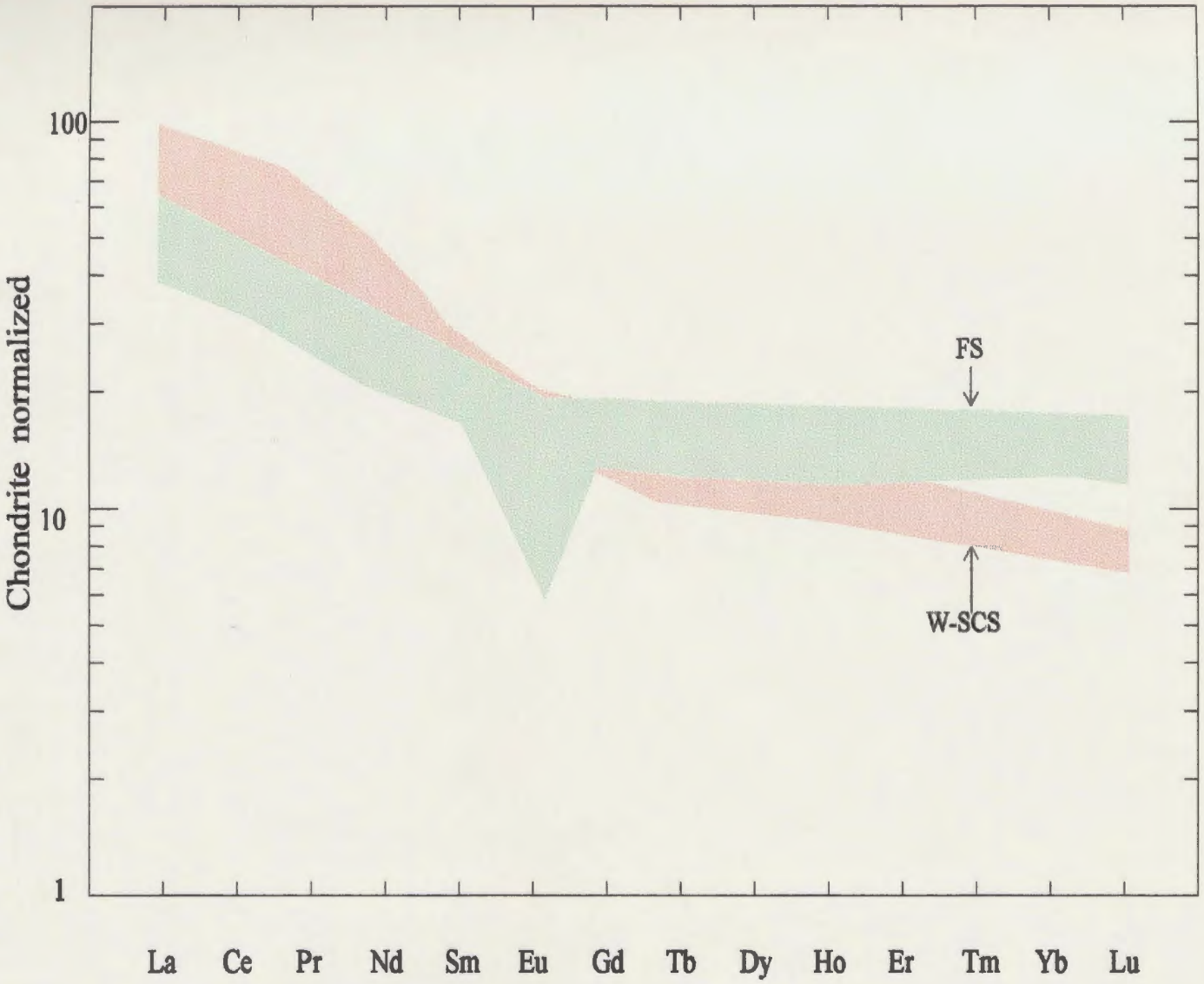

Figure 5.19 Simplified chondrite normalized REE variations for the FS and the W-SCS.

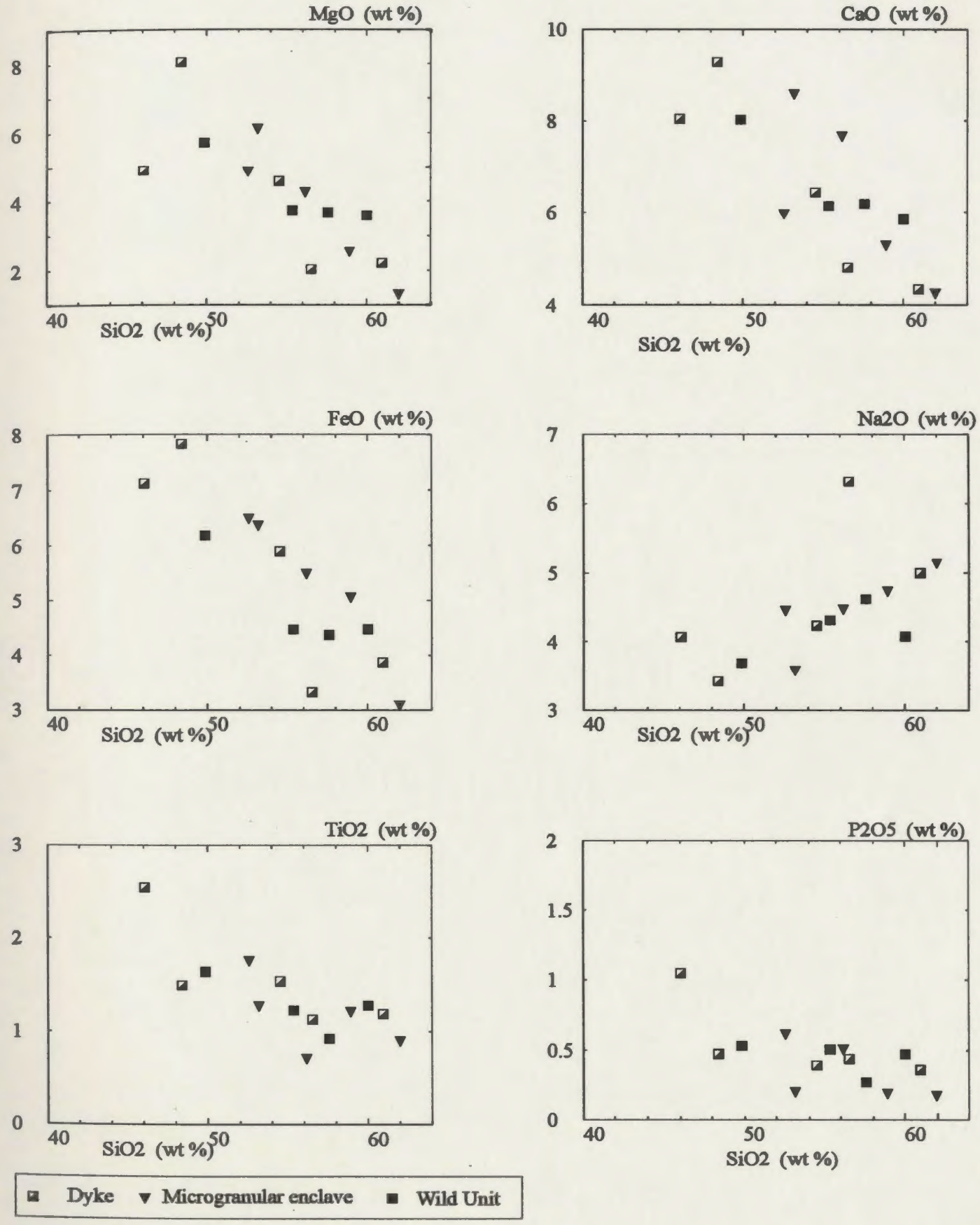

Figure 5.20 Geochemical variations of dyke, microgranular enclaves and their host rock (Wild Unit of the W-SCS).

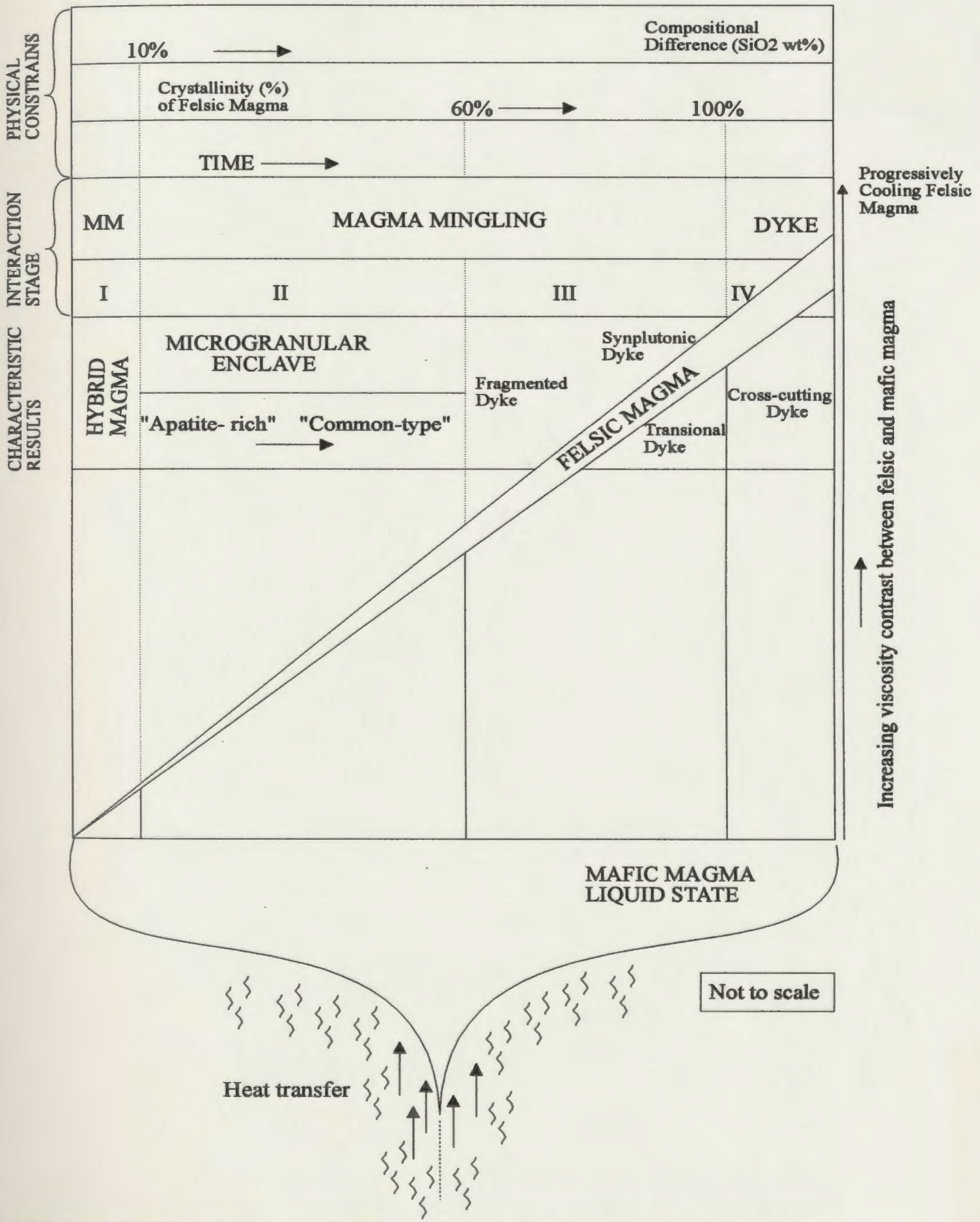

Figure 5.21 A model for co-existing contrasting magmas and their intractions. MM: magma mixing.

Table 5.1 U–Pd data.

Fraction description	Concentration weight (mg)	U (ppm)	Measured Pb rad	Pb tot. com. Pb (pg)	* Corrected Atomic ratios $^{206}Pb/^{204}Pb$	$^{208}Pb/^{206}Pb$	$^{206}Pb/^{238}Pb$	±	$^{207}Pb/^{235}Pb$	±	$^{207}Pb/^{206}Pb$	±	Age (Ma) $^{206}Pb/^{238}Pb$	$^{207}Pb/^{235}Pb$	$^{207}Pb/^{206}Pb$
Fogo Suite (F–91–580)															
Z1 1 large euh grain abr	0.009	423	30.6	9	1851	0.1928	0.06733	36	0.5127	28	0.05523	14	420	420	421
Z2 –200 abr	0.022	579	40.4	6	8542	0.1400	0.06785	56	0.5237	42	0.05598	10	423	428	452
Z3 +200 clear abr	0.063	553	42.7	20	8193	0.1346	0.07484	52	0.6634	46	0.06429	14	465	517	751
Z4 +200 abr	0.039	591	40.7	8	12022	0.1466	0.06656	38	0.5137	30	0.05598	12	415	421	451
Z5 +200 clr prisms abr	0.029	577	40.6	15	4881	0.1450	0.06802	54	0.5429	44	0.05788	12	424	440	525
T1 abr	0.115	101	7.8	157	321	0.3148	0.65650	28	0.5006	30	0.05530	26	410	412	424
T2 abr	0.128	77	5.9	442	110	0.3024	0.06630	26	0.5187	68	0.05675	64	414	424	482
Wild Sandy Cove Suite (F–91–79)															
Z1 +70 clr prisms abr	0.596	147	11.5	15	24398	0.3420	0.06531	28	0.4951	22	0.05499	6	408	408	412
Z2 –100 clr prisms abr	0.435	205	15.7	11	33302	0.3060	0.06533	28	0.4951	22	0.05496	8	408	408	411

* Ratios corrected for fractionation, spike, 5–10 pg laboratory blank and initial Pb, calculated by model of Stacey and Kramers (1975) for the age of the sample and 2 pg U blank.
2 sigma uncertainties on the isotopic ratios are presented after the ratios and refer to final digits.
Note: abr= abraded; clr= clear; tot.= total; com= common; euh= euhedral.

Table 5.2 Whole rock SiO2 contents and REE characteristics of samples from the granitoid and associated rocks.

Sample #	Description	SiO2 (wt%)	Total REE (ppm)	(La/Lu)N	(La/Sm)N	(Eu/Eu*)N
The FS						
F-91-580	Monzogranite	76.8	127.8	6.1	3.6	0.4
F-92-20a	Monzogranite	76.6	82.1	3.2	2.8	0.5
F-91-563.1	Granodiorite	61.2	144.0	3.9	2.5	0.8
The W-SCS						
F-91-54	Sandy Unit	55.8	193.7	16.1	4.0	0.9
F-91-450	Sandy Unit	60.2	125.9	11.6	3.8	1.0
F-91-79	Wild Unit	49.9	190.7	12.1	3.4	0.9
F-91-175b	Wild Unit	55.4	151.2	9.7	3.0	1.0
F-91-14a	Wild Unit	57.6	110.9	7.9	3.1	1.1
F-91-175a	Wild Unit	69.0	90.2	6.9	4.0	1.2
Dykes						
F-91-19d	"cross-cutting"	54.5	133.3	7.8	2.7	0.9
F-92-31	cut the TLS	56.5	243.3	5.6	3.2	0.9
F-91-23	"transtional"	48.4	177.4	7.5	2.7	1.0
F-92-20b	synpl/encalves	61.0	161.0	7.9	3.2	0.9
F-91-174	cut Wild Unit	75.2	171.9	15.0	7.0	0.6
Microgranular Enclaves						
F-91-14b	"apatite-rich"	52.6	164.2	8.4	2.7	0.9
F-91-N-1	"common"	62.0	87.4	4.7	2.9	1.3
F-91-N-3	"common"	53.2	79.3	3.6	2.1	1.0
Supracrustal rocks						
F-91-77s	within the TLS	49.2	79.9	7.0	5.4	2.3
F-91-60ld	within the Wild Unit	67.8	149.6	8.8	3.6	0.8

Note: see text for description of the dyke and microgranular enclaves

synpl= synplutonic

Table 5.3 The Nd isotopic data for the granitoid and associated rocks.

Map Unit	Rock Type	$^{143}Nd/^{144}Nd$	2 sem	$^{147}Sm/^{144}Nd$	Nd (ppm)	Sm (ppm)	Epsilon Nd
FS, T= 420 Ma							
F-91-580	Monzogranite	0.512520	5	0.129190	20.883	4.511	+ 1.3
F-92-20A	Monzogranite	0.512540	7	0.140770	11.942	2.818	+ 1.1
F-91-563.1	Granodiorite	0.512430	8	0.139310	19.635	4.586	- 1.0
W-SCS, T=408 Ma							
Sandy Unit							
F-91-450	Gabbronorite	0.512573	7	0.110510	18.468	3.422	+ 3.2
F-91-54	Gabbronorite	0.512414	7	0.105990	20.789	3.694	+ 0.3
Wild Unit							
F-91-79	Diorite	0.512413	6	0.106650	25.174	4.501	+ 0.3
F-92-175A	Granite	0.512516	2	0.129780	12.362	2.690	+ 1.1
F-92-175B	Diorite	0.512478	7	0.116500	29.245	5.713	+ 1.0
F-92-14A	Qtz-Diorite	0.512609	8	0.125390	15.610	3.281	+ 3.1
Dyke, T= 408 Ma							
F-92-20b	Intermediate	0.512480	12	0.117920	28.827	5.699	+ 1.0
F-92-174	Felsic	0.152389	6	0.090030	24.383	3.680	+ 0.7
F-91-23	Mafic	0.512460	4	0.112770	20.238	3.826	+ 0.9
F-92-31	Intermedaite	0.512498	5	0.119240	25.887	5.175	+ 1.3
F-92-19Dy	Mafic	0.512659	25	0.124350	12.357	2.576	+ 4.1
Microgranular Enclave, T= 408 Ma							
92-N-1	Quartz-diorite	0.512561	8	0.137740	11.891	2.746	+ 1.5
Supracrustal rocks, T= 420 Ma							
F-91-77S	Xenolith	0.511950	21	0.098640	11.689	1.933	-8.2
F-91-60S	Xenolith	0.511951	6	0.117710	26.330	5.196	-9.2

sem= standard error of the mean

Normalized to $^{146}Nd/^{144}Nd$= 0.7219

35 LaJolla determination during course of this study gave $^{143}Nd/^{144}Nd$= 0.511854 ± 6.

analytical error is less or equal to ±0.3 Epsilon unit (for detail see Chapter 3)

Sm-Nd technique described in Appendix 7

CHAPTER 6

PETROGENETIC MODELLING

6.1 INTRODUCTION

This chapter integrates the physical, geochemical and isotopic data for the plutonic rocks of the study area (the TLS, the FS and the W-SCS, Chapters 2-5) and proposes a petrogenetic model. Considering sampling and analytical restrictions together with the diversity and complexities of each suite, it would be difficult to expect a unique and completely satisfactory model. However, the main goal of this chapter, and to a large extent of this research, is to propose an internally consistent petrogenetic model that is in accord with as much information presented in the previous chapters as possible.

Several physical, geochemical and isotopic observations described in the previous chapters including: a) the occurrence of the TLS (mafic-intermediate layered intrusion) together with the granitoid suites; b) the presence of temporally and geochemically unrelated C- and H- type granitoid suites (the FS and the W-SCS, respectively); c) a wide range of positive Nd isotopic compositions (up to 6 ϵ_{Nd} units); and d) the close spatial, temporal and geochemical association of mafic-intermediate dykes, microgranular enclaves and their hybrid granitoid host-rock (the Wild Unit of the W-SCS), suggest that petrogenesis of the plutonic rocks of the Tilting area involved complex interactions between mantle-derived mafic magma and crustal-derived felsic magma. To define and evaluate the processes responsible for the evolution of the plutonic rocks of the Tilting area, it is important to identify the nature and composition of potential source materials that were available at 420 to 408 Ma.

The main tool utilized to identify the nature of potential source materials is the Nd isotopic composition of the plutonic rocks. This is because: a) the Nd isotopic

composition does not change at magmatic temperatures during partial melting or subsequent fractional crystallization; and b) the Nd isotopic signature of a magma is characteristic of the source region from which the magma was produced. Additionally, crust which has low Sm/Nd generally develops a low Nd isotopic value, whereas mantle or mantle-derived mafic magma which has high Sm/Nd develops a high Nd isotopic value. These features make the Nd isotopic system sensitive to crust-mantle interactions.

To introduce a model, potential source reservoirs and possible processes and their geochemical and isotopic consequences are discussed briefly in the following sections.

6.2 POTENTIAL SOURCE RESERVOIRS

Global reservoirs

In general, potential source materials for magmatism can be subdivided into three main reservoirs: upper crust, lower crust and mantle. The average upper crust is characterized by low Sm/Nd and low $^{143}Nd/^{144}Nd$ (negative ϵ_{Nd}, Figure 6.1; Rollison, 1993) and displays strong LREE enrichment relative to HREE, and negative Eu- and Nb-anomalies (Taylor and McLennan, 1985). The nature of the average lower crust is more ambiguous but can be characterized by: a) retarded Nd evolution relative to a chondritic source (Rollinson, 1993); b) moderate LREE enrichment relative to HREE; c) notable positive Eu anomalies (Taylor and McLennan, 1985); and d) negative Nb- anomalies (Rollinson, 1993).

As discussed by Hart (1988), there are several isotopically distinct mantle reservoirs including depleted mid-ocean ridge mantle (DMM) that gives rise to mid ocean ridge basalt (MORB) and enriched mantle (MIOB) that gives rise to ocean island basalt (OIB). The DMM is expected to show smooth REE_N and extended REE_N patterns, without any significant anomalies (*e.g.* Saunders et al., 1988; Sun and McDonough,

1989). It is characterized by high Sm/Nd; high $^{143}Nd/^{144}Nd$ (positive epsilon). For example, the estimated ϵ_{Nd} value for the Ordovician to Siluro-Devonian DMM can vary from +5 to +9 with an average +7, assuming that isotopic signatures of present day MORB represent the isotopic signatures of DMM (*cf.* Whalen et al., 1994a).

The MOIB displays significant geochemical and isotopic diversity. There are at least three isotopically distinct reservoirs that can give rise to OIB. These are: a) a source with high U/Pb (HIMU); b) enriched mantle I (EMI); and c) enriched mantle II (EMII) (Hart, 1988; Weaver, 1991). However, OIB is usually characterized by LREE enrichment relative to HREE without negative Nb- and Ti- anomalies (Weaver, 1991). From the present ϵ_{Nd} values of OIB which vary from +4 to +8 (DePaolo, 1988), the estimated ϵ_{Nd} value of Siluro-Devonian MOIB can range from +2 to +6 (Figure 6.1).

Regional and local potential reservoirs

On regional and local scales, Cambro-Ordovician supracrustal rocks of the Gander Group (*cf.* Kerr et al., 1995) and hornfelsic xenoliths found in the study area might represent upper crustal source materials. They typically have low ϵ_{Nd} values (at 420 Ma) ranging from -7 to -9 (Figure 6.1). As presented in Chapter 5, geochemical characteristics of supracrustal rocks found in the Tilting area display somewhat variable geochemical features, although they typically exhibit LREE enrichment relative to HREE with significant negative Nb anomalies.

The oldest lithologies exposed in central Newfoundland are Late Precambrian orthogneisses, deformed granitoid rocks and felsic metavolcanic rocks (Dunning and O'Brien, 1989). These Late Precambrian rocks may represent a possible basement, *i.e.* lower crustal source reservoir (*cf.* Kerr et al., 1995). They exhibit a relatively wide range of ϵ_{Nd} values from -4 to +0.5 at 420 Ma (Figure 6.1).

Samples displaying high positive ϵ_{Nd} values from the TLS and from the

intermediate-mafic dykes can be used to constrain the isotopic signature of the mafic component in the study area. The samples from the TLS (F-91-19 [ϵ_{Nd} = +5.1] and F-92-N-10 [ϵ_{Nd} = +4.9]) reveal slight to moderate LREE enrichment relative to HREE [$(La/Lu)_N$ = 3.0 and 5.4 for F-91-19 and F-92-N-10, respectively], whereas the sample (F-92-19D, ϵ_{Nd} = +4.2) from the dykes exhibits strong LREE enrichment relative to HREE [$(La/Lu)_N$ = 7.7]. It is important to remember that: a) almost all analyzed samples from the TLS and mafic-intermediate dykes exhibit significant negative Nb-anomalies, with or without Ti-anomalies, and notable LREE enrichment relative to HREE [$(La/Lu)_N$ = 2.4 to 11.9] disregarding the level of fractionation of the sample; and b) most samples are quartz-normative, including the samples having positive ϵ_{Nd} values (F-91-19; F-92-N-10 and F-92-19D).

6.3 PETROGENETIC CONSTRAINTS

Parental magma composition

The parental magma composition of Zone I-IV can be estimated from the composition of the most primitive olivine and/or orthopyroxene by assuming a K_D(olivine/liquid)(Fe/Mg) = 0.3 (Roeder and Emslie, 1970; and K_D(orthopyroxene/liquid) (Fe/Mg) = 0.28 (Neilsen and Drake, 1979). The parental liquid compositions are expected to have $X_{Mg} = 0.65_{\text{from orthopyroxene}}$ for Zone I; $X_{Mg} = 0.58_{\text{from olivine}}$ for Zone II; $X_{Mg} = 0.41_{\text{from orthopyroxene}}$ for Zone III; and $X_{Mg} = 0.56_{\text{from olivine}}$ for Zone I.

The X_{Mg} of mafic dykes varies from 0.51 to 0.66. This is in accord with the range of estimated liquid compositions based on mineral-melt partitioning data. However, considering that a liquid derived from the mantle should have a minimum $X_{Mg} \approx 0.70$ (Wyllie, 1984), none of these estimated parental liquid compositions (both from mineral-partitioning data for the TLS and from the dykes) are in equilibrium with primitive

mantle. This implies that neither the mafic-intermediate dykes nor the TLS represent primary melt from the mantle- *i.e.* magmas giving rise to the TLS and dykes must have undergone fractionation prior to intrusion. This makes it more difficult to define the geochemical consequences of potential mechanisms that might account for the range of Nd isotopes from the Tilting area. For the purpose of the following discussions, it is assumed that no fractionation process is capable of enhancing the level of: a) negative Nb-anomalies, b) LREE enrichment relative to HREE; and c) silica-saturation, high enough to account for the level observed in the area.

Potential mechanisms and their geochemical consequences

Highly positive ϵ_{Nd} values obtained from the Tilting area suggest that mafic magmas giving rise to the TLS and the dykes are likely derived from mantle sources. There are two main mechanisms by which to obtain the range of isotopic variation seen within the study area: a) assimilation of crustal material by mantle-derived mafic magma; and/or b) mantle or source heterogeneity.

Assimilation of crustal material by mantle-derived mafic magma has been the subject of debate for the last three decades (*e.g.* Dickin, 1981, Carlson et al., 1981; Thirlwall and Jones, 1983, Huppert and Sparks, 1985; 1988). There are several distinct mechanisms of crustal assimilation including: a) bulk assimilation - addition of bulk crust into the magma chamber (Thirlwall and Jones, 1983); b) assimilation fractional crystallization (AFC)- occurs in a magma chamber where the necessary heat for assimilation is released by accompanying fractional crystallization (DePaolo, 1981; 1985); and c) selective assimilation- may occur due to the different chemical diffusivities of different elements (Watson, 1982), where isotopic equilibrium between mafic magma and hydrous fluid derived from dehydration reactions of the crustal rocks surrounding the mafic magma is maintained (Dickin, 1981).

Geochemical (major and trace element) and isotopic consequences of assimilation vary with the style of the assimilation mechanism. Recent studies, particularly on continental basalt, emphasize two main modes of interrelationship between geochemical and isotopic variations (*e.g.* Hawkesworth and Norry, 1983; Huppert and Sparks, 1985). In one, the most fractionated rocks are the most contaminated ones and this is attributed to AFC mechanisms (DePaolo, 1981; Gray et al., 1981; Palacz, 1985; Stewart and DePaolo, 1990). However in the other, the most primitive samples are the most contaminated ones (Huppert and Sparks, 1985) and this is assumed to occur where mantle-derived mafic magma ascending turbulently through continental crust. However, this mechanism *"is specifically related to the situation where magma is variably fractionated in deep magma chambers and then periodically ascends to the surface"* (Huppert and Sparks, 1985). It is also important to note that assimilation may not be evident from chemical features (*i.e.* there may be no systematic interrelationship between isotopic ratios and chemical features; *cf.* Dickin, 1981; Pickett and Saleeby, 1994). This may imply that the processes regulating the bulk of the chemical variation are not responsible for the variation in isotopic data.

As briefly indicated above, there are several isotopically distinct mantle reservoirs. Although, it has been demonstrated that mantle heterogeneity exists on a km- as well as a cm-scale (Dupre and Allegre, 1980 and Dawson et al., 1980), it is very unrealistic to assume that each isotopically distinct magma batch, giving rise to the plutonic rocks in a $\sim$ 6 km^2 area, was derived from a small volume of distinct mantle which maintained its identity for a long period of time (*cf.* Dickin, 1981). Nevertheless, mantle heterogeneity may exist due to previous trace element enrichment processes in the upper mantle either as a result of migration of H_2O-rich and/or CO_2-rich fluids (mantle metasomatism) or migration of magma derived from small volumes of partial melting,

perhaps related to subduction processes (*e.g.* Hawkesworth and Norry, 1983; Pearce, 1983).

To obtain the range of isotopic variation seen in the Tilting area, two potential cases are presented (Table 6.1): **Case 1**- bulk assimilation of lower and upper crust by MORB; and **Case 2**- bulk assimilation of lower and upper crust by OIB. The significant findings are as follows:

a) the range of ϵ_{Nd} variations observed in the study area can be obtained by: i) up to 50% assimilation of lower crust by MORB and OIB; or ii) up to 20% assimilation of upper crust by MORB; or iii) up to 40% assimilation of upper crust by OIB.

b) neither bulk assimilation of lower crust nor upper crust by MORB and OIB produces notable negative Nb-anomalies; and

c) even after 50% lower- and 30% upper- crustal assimilation, MORB and OIB are still olivine-normative or only slightly quartz-normative.

Disregarding as unlikely, 50% crustal assimilation, items (b) and (c), suggest that the mafic components of the Tilting area were not derived solely from suboceanic mantle reservoirs (*i.e.* DMM and MOIB), but were likely derived from a mantle which had been modified by some kind of trace-element enrichment process. Although the nature of such an enrichment process is not clear and still subject to debate (*e.g.* Hawkesworth and Norry, 1983), in this study it is attributed to subduction-related processes in order to account for significant negative Nb-anomalies and an overall LREE enrichment relative to HREE. Dehydration processes in a subducting slab fractionate the HFSE, particularly Nb, from the LREE, leading to a prefential enrichment of LREE relative to HFSE in the overlying mantle wedge. Thus, a mantle modified by subduction-related processes (whether or not it was melted at the time of arc activity) will display a negative Nb-

anomaly (*cf.* Pearce, 1983; Pegman, 1990). Despite overall LREE enrichment relative to HREE, highly positive ϵ_{Nd} values obtained from the Tilting area suggest that the mantle giving rise to mafic components of the area, must have been modified recently.

In the following sections, petrogenetic constraints developed in the previous chapters are summarized and discussed in a single framework to define the petrogenesis of the TLS, the FS and the W-SCS. Each suite is discussed separately.

6.3.1 Petrogenesis of the TLS

The TLS is a composite intrusion and each zone is apparently crystallized from isotopically distinct magma batches under different conditions of water pressure and/or silica activity. Inter-zone isotopic heterogeneities (up to 5 ϵ_{Nd} unit) existed prior to intrusion. These isotopically and/or geochemically different magma batches are not associated with each other by means of fractionation (*e.g.* neither Zone I, Zone II nor Zone III are differentiation products of the magma that give rise to Zone IV). However, the overall correlation between ϵ_{Nd} values and the $(La/Sm)_N$ (decreasing ϵ_{Nd} value with increasing $(La/Sm)_N$) may suggest a petrogenetic link between them.

If this is the case, the next question is to explain the presence of two distinct magma types (olivine - and quartz - tholeiitic) within the TLS. Cawthorn (1978) discussed the potential genetic link between silica-saturated and silica-oversaturated magma types in the study area by means of fractionation. He pointed out that there is no fractionation process that can reduce the silica saturation level from quartz-normative to olivine-normative. Although, the reverse is possible by means of magnetite fractionation, the presence of hydrous phases indicating crystallization under water pressures at which the magnetite is not stable, lead Cawthorn (1978) to suggest that the magma types are not genetically related. Alternatively, coexisting olivine- and quartz-tholeiitic magmas

might be attributed to crustal assimilation by olivine-normative magma (*cf.* Irvine, 1970; Campbell, 1985). In this case, the olivine-normative Zone IV is considered to represent the product of the "uncontaminated" or less contaminated magma, whereas the quartz-normative Zones I-III would represent the product of the contaminated magmas. However, since Zone IV has a comparable Nd isotopic composition to that of Zone I, the two distinct magma types cannot be attributed simply to crustal contamination.

Based on experimental studies of Takashaski and Kushiro (1983) and Walter and Presnall (1994), olivine-tholeiitic magmas are likely derived from a greater depth (8-10 kbar) than quartz-tholeiitic magmas (<5 kbar). Both can be derived from the same or similar source material (such as plagioclase lherzolite) without notable variations in the degree of melting. This implies that the inter-relationship between silica-saturated and silica-oversaturated magma types can be explained in terms of differences in the pressure of partial melting. This appears to be consistent with the fact that the olivine-tholeiitic Zone IV has a lower silica activity than the quartz-normative zones (Zones I-III) .

As described in Chapter 2, the presence and abundance of amphiboles in Zones I-III suggest that these zones crystallized from hydrous magma batches. Variation in water contents of these magmas controlled the order of appearance of plagioclase relative to pyroxene and amphibole. The source of the water is ambiguous, but may be from : a) subduction-related processes (Tepper et al., 1993); and/or b) thermal breakdown of hydrous crustal phases during crustal rock assimilation (Dickin, 1981).

Inter-zone isotopic heterogeneity must have existed prior to intrusion (Chapter 3). For the purpose of simplicity, the correlation between Nd isotopic composition and $(La/Sm)_N$ within the TLS can be attributed to variable degrees of crustal contamination by parental magmas that may have been derived from the same or similar source materials. These contaminated parental magmas then gave rise to the mafic magmas that

formed Zones I-IV.

Taking all this information together, the complex physical, geochemical and isotopic nature of the TLS can be explained in terms of two main stages:

a) *processes prior to intrusion* which include:

i) variable depths of partial melting of the same or similar mantle material(s) to account for different parent magma types (quartz-tholeiitic and olivine-tholeiitic). The potential mantle source must have ϵ_{Nd} value higher than +5.1 at 420 Ma to account for the positive Nd isotopic composition of the suite, and must have been recently (likely in Ordovician) modified by subduction-related processes to provide negative Nb-anomalies, overall LREE enrichment relative to HREE, and/or variation in water contents;

ii) variable degrees of crustal contamination to account for inter-zone isotopic heterogeneity, and the apparently systematic correlation between ϵ_{Nd} and REE, and variation in water contents.

b) *processes after emplacement into the chamber*- including magma replenishment with or without subsequent mixing and/or fractionation, current deposition and postcumulus modifications. These processes regulate the layering features (physical and chemical) of the TLS.

6.3.2 Petrogenesis of the FS

The voluminous FS is a 420 ±2 Ma, metaluminous granitoid body dominated by monzogranite with minor granodiorites. It displays generally positive ϵ_{Nd} values from -1 to +1.3 at 420 Ma. The suite is a C-type granitoid body- *i.e.* it is a product of crustal anatexis. Obviously, lower and upper crust are the potential source materials. However,

the negative ϵ_{Nd} isotopic composition (-7 to -9 at 420 Ma) of regional and local supracrustal rocks preclude upper crustal rocks as the dominant source material. Similarly, the metaluminous to slightly peraluminous nature of the FS opposes a peraluminous sedimentary protolith. These observations suggest that the FS is mainly derived from lower crustal material. The nature and composition of the lower crust is not clear. However, any potential source of the FS must be able to produce large amounts of monzogranitic rocks with minor granodiorite and must have old crustal components to explain the inherited zircons of the suite. These requirements largely preclude basaltic precursors (*e.g.* Wyllie, 1984).

As discussed above, "Precambrian basement"- the oldest lithologies in central Newfoundland- may represent lower crustal material. However, the ϵ_{Nd} values obtained from these basement rocks vary from -4 to +0.5 at 420 Ma and only partly cover the isotopic spectrum from the FS (see Figure 6.1). This may imply that: a) the potential lower crust is more radiogenic than "Precambrian basement;" or b) felsic magma derived from a crust which has comparable Nd isotopic values to "Precambrian basement" has been modified by mantle-derived mafic magma(s).

The generation of the FS obviously requires significant thermal energy to melt the pre-existing lower crust and to generate crustal-derived felsic magma. This can be best explained in terms of mafic magma emplacement into the lower crust (Huppert and Sparks, 1985; 1988; Chappell and Stephens, 1988, Tepper et al., 1993; Whalen et al., 1994b).

6.3.3 Petrogenesis of the W-SCS

The W-SCS is a 408 $\pm$2 Ma, H-type, composite granitoid intrusion. It typically reveals positive ϵ_{Nd} values which vary from +0.3 to +3.2 at 408 Ma. As described in

Chapter 5, both magma mixing and mingling processes between mafic and felsic magmas play important roles in the evolution of the W-SCS. The interrelationship between the Wild Unit, microgranular enclaves and mafic-intermediate dykes reflects distinct stages of this mafic-felsic interaction.

The range of variation of Nd isotopic compositions from the W-SCS is comparable to that of the TLS and that of mafic-intermediate dykes (see Figure 6.1). Furthermore, the TLS and the mafic-intermediate dykes reveal some common geochemical features including: a) significant source-related negative Nb-anomalies; b) overall LREE enrichment relative to HREE; c) the presence of quartz- and olivine-tholeiitic magma types; and d) comparable parental liquid compositions. Taking these observations together, it is suggested that the mafic magmas giving rise to mafic-intermediate dykes within the W-SCS (*i.e.* mafic component of the W-SCS) are likely derived from the same or similar source material that gave rise to the TLS magma (*i.e.* a relatively radiogenic mantle source that is affected by subduction-related processes).

Because of the hydrid nature of the W-SCS, the potential source of the felsic component of the suite can not be fully constrained. However, the ϵ_{Nd} values of local and regional supracrustal rocks are too low to account for the isotopic spectrum of the suite (see Figure 6.1). This implies that there is no significant contribution from upper crust in the genesis of the W-SCS and the felsic component of the suite must have been mainly derived from lower crustal material. The nature and composition of the lower crust is not clear and it is possible that the felsic component of the W-SCS may be derived from the same or similar lower crustal material to that which gave rise to the FS.

From the observations presented above, the genesis of the W-SCS requires significant and fairly continuous heat and mass transfer from mantle-derived mafic magma to the lower crust. This again, can be best explained by mafic magma

underplating the lower crust (DePaolo, 1981; 1988; Huppert and Sparks, 1985; 1988; Chappell and Stephens, 1988). It is important to note that the generation of both of the granitoid suites requires a similar mechanism (emplacement of mafic magmas into the lower crust). However, the mode of interaction between mafic and felsic magmas in the W-SCS which occurs in the form of mass and heat transfer, is drastically different for that of the FS which is in the form of heat transfer with little, if any, minor mass transfer.

6.4 A PETROGENETIC MODEL

A satisfactory petrogenetic model has to account for the following three main observations; a) the presence of the TLS, together with granitoid rocks; b) the presence of two geochemically and isotopically distinct, temporally unrelated granitoid suites (the FS and the W-SCS); and c) the geochemical and isotopic similarity between the TLS and the mafic-intermediate dykes in the W-SCS.

The proposed petrogenetic model is dependent on: a) the availability of a mafic magma to interact with lower crustal rocks; and b) the mode of interaction between these components which may occur in the form of either mass or heat or both mass and heat transfer. As illustrated in Figures 6.2 and 6.3, the proposed model has three main components, Stages A to C, between $\geq$420 Ma and $\leq$408 Ma.

Stage A: Crustal thinning and extension take place as a result of lithospheric delamination (*e.g.* Sacks and Secor, 1990; Nelson, 1992; Davies et al., 1995) and/or transcurrent faulting (*e.g.* Rogers and Dunning, 1991). This results in asthenospheric ascent, partial melting of a mantle which has been recently modified by subduction-related processes (at variable depths), and extensive mafic magma emplacement into relatively cold lower crust. The earliest interactions between mantle-derived (parental)

mafic magmas and the lower crust may cause significant crustal contamination which leads to inter-zone isotopic heterogeneity and/or variation in water content. These isotopically and/or geochemically distinct magma batches ultimately give rise to the composite TLS at $\geq$420 Ma.

Stage B: Mafic magma underplating of the lower crust together with latent heat of crystallization (likely contemporaneous with the crystallization of the TLS) induces melting of overlying lower crustal rocks and generates crustal-derived felsic magmas. A crustal-derived felsic magma having an old crustal component with or without a minor mass contribution from the underlying mantle-derived mafic magma gives rise to the monzogranitic FS, at 420 Ma.

Stage C: Significant interactions between the mantle-derived mafic magmas and felsic magmas in the form of heat and mass transfer produce the composite W-SCS at 408 Ma. Continuous interactions between relatively hot mafic magma and progressively cooling hybrid magma (quartz dioritic, the Wild Unit) produce the unique field characteristics of the W-SCS. These features typically include microgranular enclaves, "synplutonic" dykes, "transitional" dykes and "cross-cutting" dykes, and represent gradually diminishing mafic-felsic magma mingling.

The mafic magmas that become an integral part of the compositional spectrum of the W-SCS are likely derived from the same or similar parental material that gives rise to the mafic-intermediate dykes as well as the TLS. Similarly, the felsic component of the W-SCS may be derived from the same or similar lower crustal material that gives rise to the FS.

On the basis of this model, the TLS, the FS and the W-SCS are the product of the same mechanism- mafic magma underplating of the lower crust. However, each suite represents a significantly different mode of interaction that took place at a different time

and/or place between the mafic magmas and the lower crust. The mode of such interactions varies from mass transfer, *i.e.* crustal contamination (the TLS), heat transfer ± minor mass transfer (the FS) to both mass and heat transfer (magma mixing and mingling, the W-SCS).

6.5 REGIONAL IMPLICATIONS

The proposed model, which is based on significant mafic underplating of the lower crust during the Silurian as a result of crustal thinning and extension, is consistent with other general models proposed to explain the composite mafic-felsic plutonism in central Newfoundland (*e.g.* Dunning et al., 1990a; Kerr et al., 1995). Nevertheless, detailed field, geochemical and isotopic studies obtained from this research necessitate caution in correlating the FIB either with other granitoid intrusions in central Newfoundland (Williams et al., 1988; 1989; Fryer et al., 1992; Kerr et al., 1992) or with the "Appinite Suites" of the Scottish Caledonides. This is because there are geochemically and isotopically distinct granitoid suites within the FIB-(*"granites and yet more granites"*; Pitcher, 1987). Similarly, this study clearly emphasizes the necessity of using caution when dealing with any previous interpretation based on geochronology obtained from K-Ar and Ar-Ar techniques. This is because of significant or complete isotopic resetting as a result of apparently continuous magmatism in the region.

Nd-isotopic compositions of the study area are consistent with an "inverted" crustal residence structure (*i.e.* lower crustal rocks have more positive ϵ_{Nd} values than those of the overlying supracrustal rocks) of central Newfoundland as suggested by Kerr et al. (1995).

Disregarding the fact that the study area occupies only a very minor part of the FIB, this research is the first comprehensive attempt to elucidate the relative roles of

crust and mantle in the genesis of Siluro-Devonian magmatism in central Newfoundland. The present observations, descriptions and discussions can serve as a framework upon which future studies can be based.

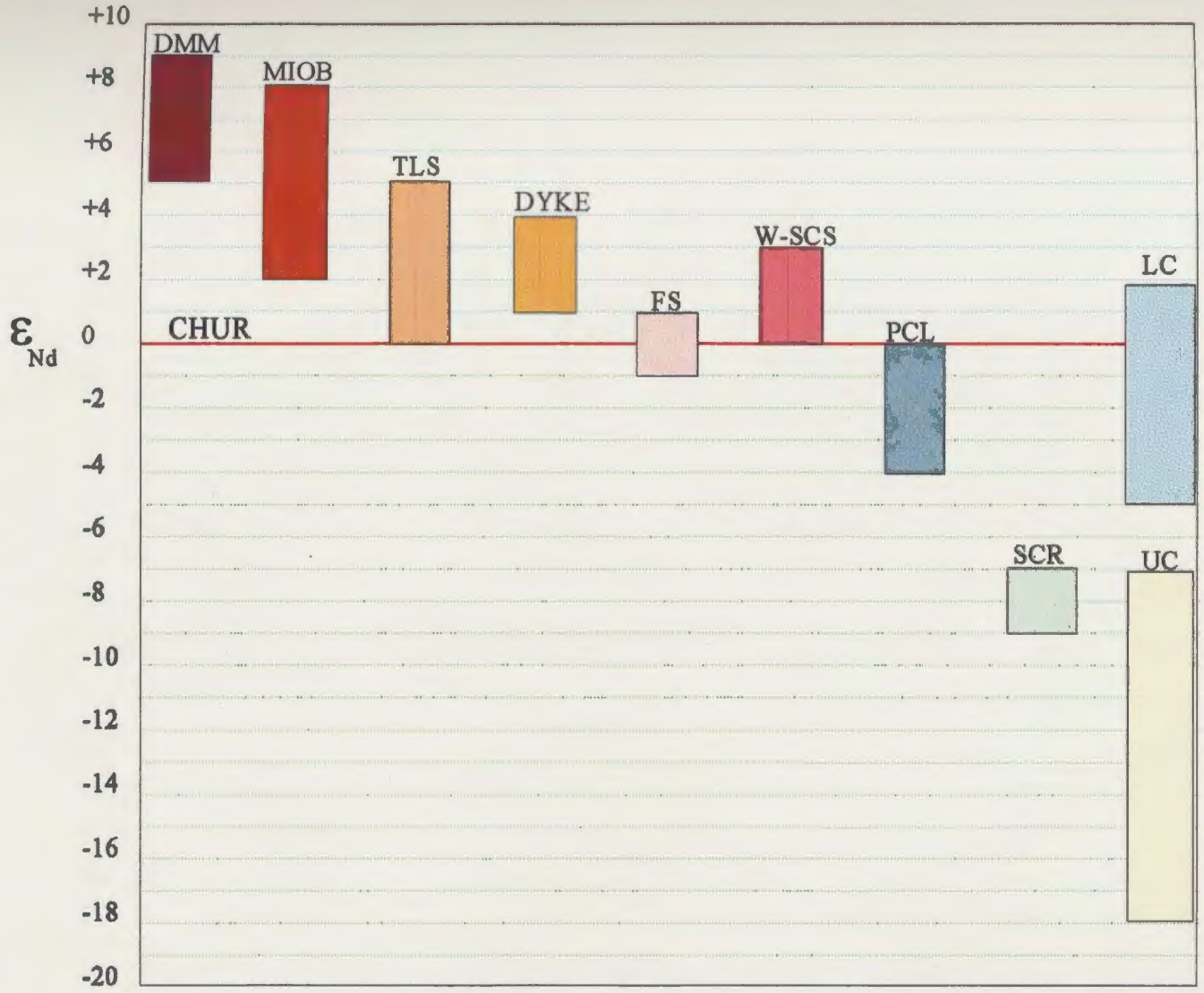

Figure 6.1 The ε_{Nd} values of potential global, regional and local source materials available at 420 Ma. DMM= Depleted MORB Mantle; MIOB= Mantle giving rise to IOB; PLC= Pre-Cambrian Lower Crust in central Nfld; SCR= Supracrustal rocks found in the Tilting area and in central Nfld; UC= Upper Crust; LC= Lower crust; and CHUR= Chondritic Uniform Reservoir

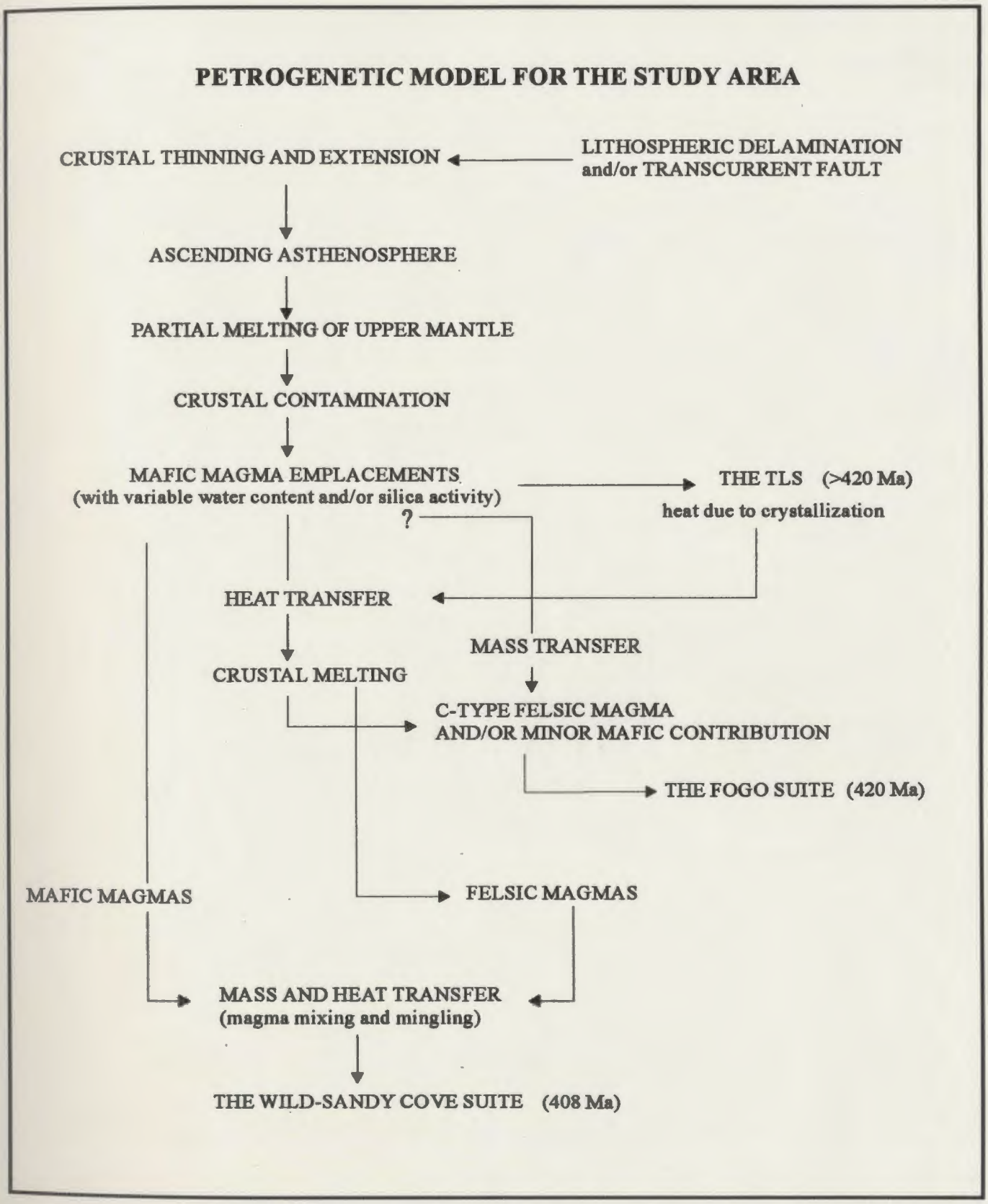

Figure 6.2 Potential interrelationships between the TLS, the FS, and the W-SCS. Flow chart of the conceptualized petrogenetic model.

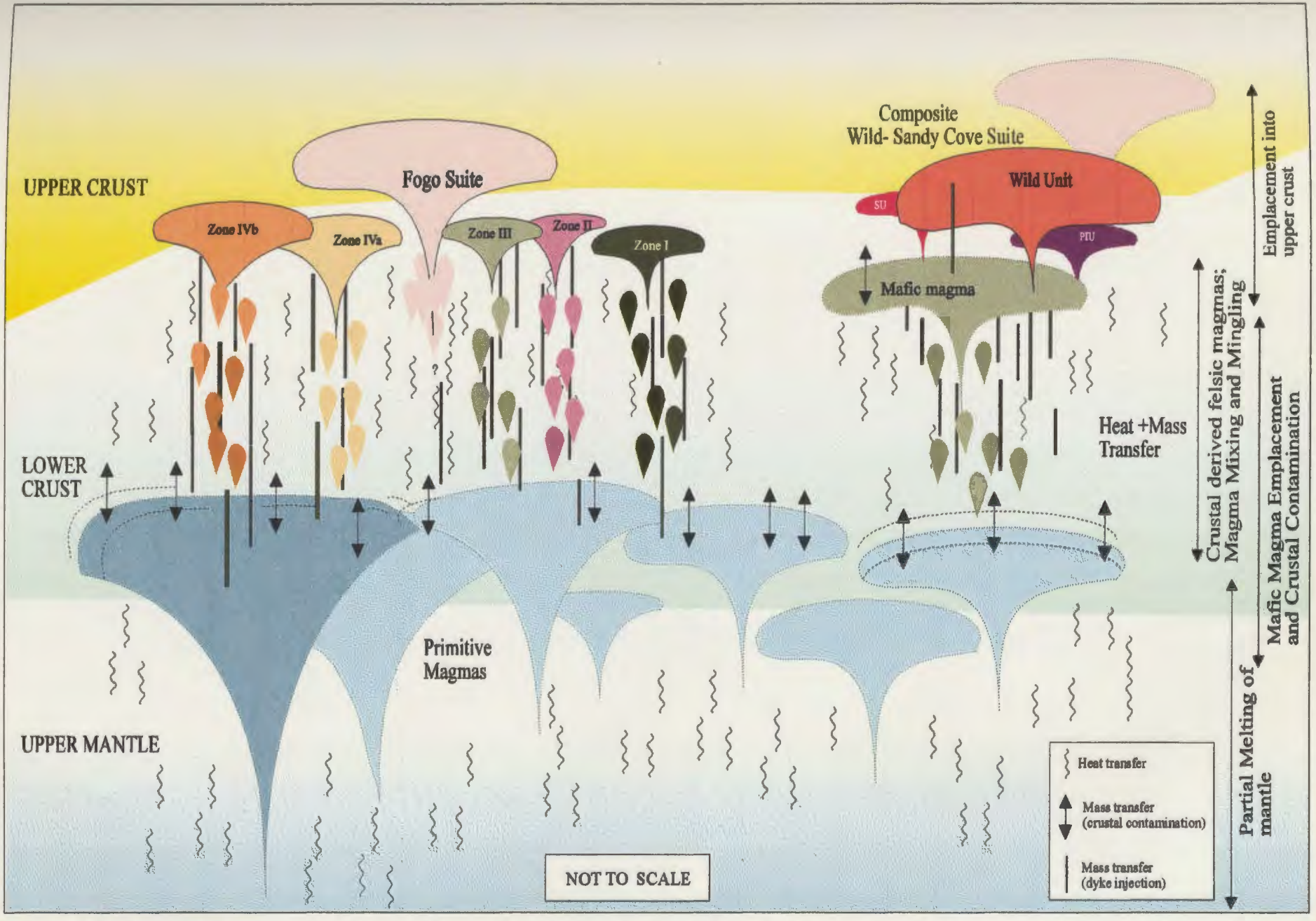

Figure 6.3 Simplified petrogenetic model for the Tilting area (see Figure 6.2 for potential interrelationships between the TLS, the FS and the W-SCS). SU: Sandy Unit; PIU: Pigeon Island Unit.

Table 6.1 Isotopic and geochemical consequences of bulk assimilation of mantle-derived mafic magma by crustal material.

Case 1: **Bulk assimilation by MORB of upper and lower crust**

% assimilation	10% LC	20% LC	30% LC	40% LC	50% LC	10% UC	20% UC	30% UC	40% UC	50% UC
SiO2 wt%	49.99	50.48	50.97	51.46	51.95	51.15	52.80	54.45	56.10	57.75
MgO wt%	7.56	7.42	7.28	7.14	7.00	7.15	6.60	6.05	5.50	4.95
Hy CIPW	9.53	13.13	16.74	20.37	24.01	12.36	18.80	20.93	19.35	17.78
Ol CPIW	12.05	9.62	7.18	4.73	2.27	8.60	2.72	0.00	0.00	0.00
Q CIPW	0.00	0.00	0.00	0.00	0.00	0.00	0.00	1.15	3.27	5.40
(La/Lu)CH	0.86	1.06	1.28	1.52	1.80	1.23	1.82	2.47	3.18	3.98
(La/Sm)CH	0.85	0.99	1.14	1.28	1.43	1.16	1.59	1.99	2.37	2.72
(La/Nb)PM	1.75	1.77	1.79	1.81	1.82	1.44	1.35	1.30	1.28	1.26
Epsilon Nd at 420 Ma	5.16	3.53	2.07	0.76	-0.42	2.48	-0.62	-2.89	-4.63	-6.00

Case 2: **Bulk assimilation by OIB of upper and lower crust**

% assimilation	10% LC	20% LC	30% LC	40% LC	50% LC	10% UC	20% UC	30% UC	40% UC	50% UC
SiO2 wt%	49.99	50.48	50.97	51.46	51.95	51.59	53.19	54.79	56.39	57.99
MgO wt%	7.56	7.42	7.28	7.14	7.00	7.02	6.49	5.95	5.42	4.88
Hy CIPW	9.21	12.85	16.50	20.16	23.83	15.32	21.44	21.06	19.47	17.88
Ol CPIW	12.21	9.77	7.31	4.84	2.36	6.56	0.89	0.00	0.00	0.00
Q CIPW	0.00	0.00	0.00	0.00	0.00	0.00	0.00	1.73	3.77	5.81
(La/Lu)CH	11.94	11.08	10.21	9.33	8.45	11.71	11.48	11.25	11.02	10.80
(La/Sm)CH	2.32	2.32	2.31	2.30	2.29	2.42	2.53	2.65	2.78	2.93
(La/Nb)PM	0.80	0.82	0.84	0.87	0.90	0.82	0.85	0.88	0.91	0.95
Epsilon Nd at 420 Ma	3.25	2.18	1.67	0.83	-0.03	2.84	1.63	0.38	-0.92	-2.28

Assumptions

	LC	UC	MORB	OIB
SiO2 wt%	54.40	66.00	49.50	49.99
MgO wt%	6.30	2.20	7.70	7.56
Nd	13.00	26.00	8.00	32.00
Hy CIPW	28.59	9.93	5.97	9.21
Ol CPIW	0.00	0.00	14.45	12.21
Q CIPW	3.61	16.04	0.00	0.00
(La/Lu)CH	3.94	9.73	0.57	11.94
(La/Sm)CH	2.18	4.20	0.60	2.32
(La/Nb)PM	1.86	1.22	1.09	0.80
Epsilon Nd at 420 Ma	-5	-10	7	4

MORB and OIB data are from Sun and McDonough (1989)

LC: average lower crust; UC: average upper crust (data are from Taylor and Mclennan, 1985)

CH: normalized to chondrite (Taylor and McLennan, 1985)

PM: normalized to primitive mantle (Taylor and McLennan, 1985)

CHAPTER 7

SUMMARY OF THE THESIS

Integrated field, petrographic, geochemical and isotopic studies of the mafic, intermediate and felsic plutonic and associated rocks of the Fogo Island Batholith in the Tilting area elucidate the relative roles of crust and mantle in the origin of Siluro-Devonian magmatism in the Appalachian-Caledonide orogen. Significant observations and conclusions are as follows:

1) A wide range of plutonic rock types from plagioclase lherzolite to monzogranite are recognized in the study area. They display a range of fabrics, textures, mineralogy and composition, but can be divided into three main suites: the mafic-intermediate Tilting Layered Suite (TLS); two granitoid suites - the Fogo Suite (FS) and the Wild-Sandy Cove Suite (W-SCS).

2) The TLS is a composite intrusion and comprises four main zones (Zones I-IV). Zone IV is further subdivided into two distinct subzones (Zone IVa and IVb).

3) Each zone (Zone I-IV) typically exhibits its own characteristic layering features including type, mode, scale, form, and attitude. However, in general, layers are planar, uniform and steeply inclined (60-70° NNW). Layer contacts are sharp and concordant and layers vary in thickness from 1-2 cm to 1-20 m. Modal, textural, phase, grain-size and cryptic variations are present, although only the first two are common. Features observed locally are: variation in thickness along strike; slump folds; deformed, wispy and modally graded layers; gradational and truncated layer contacts; finger and channel structures and cognate xenoliths.

4) Two distinct magma compositions have been recognized in the TLS: (quartz

-tholeiitic, Zones I-III and olivine-tholeiitic, Zone IV). The interrelationship between silica-saturated and silica-oversaturated magma types is attributed to differences in pressure of partial melting of the same or similar source material(s).

5) There are two main crystallization sequences in the TLS: the early crystallization of cumulus orthopyroxene occurs in Zones I-III and the late crystallization of cumulus orthopyroxene occurs in Zone IV. Variations in water pressure and silica activity appear to be significant parameters controlling the sequence of crystallization within the suite. Variations in water content induce differences in the order of appearance of cumulus plagioclase relative to cumulus pyroxene and amphibole. Variations in silica activity which appear to be due to differences in depth of partial melting, control the order of appearance of cumulus orthopyroxene relative to cumulus clinopyroxene.

6) There are changes in the composition of the cumulus phases throughout the TLS, but the correlation of these changes with stratigraphic height is not regular. Each zone has its own unique cryptic variation pattern. Zone I has the most primitive mineral compositions analyzed in the TLS. Zone II is characterized by a limited range of compositional variations and apparently systematic and sudden compositional changes between alternating cumulates. Similarly, the cryptic variation pattern of Zone III mimics the modal layering. Typically, in Zone III, different postcumulus processes appear to be operative at different stratigraphic levels. The overall cryptic variation pattern of Zone IV records a reversal in magma composition corresponding to the boundary between Zone IVa and Zone IVb. The only zone that displays weakly developed cryptic layering is Zone IVb.

7) Layering features (physical and chemical) of the TLS reflect complex

interactions of several magma chamber processes including: i) introduction of new magma batches (magma replenishment) with or without subsequent mixing of newly introduced and residual magmas into the region of crystallization (Zone II); ii) fractional crystallization (Zone IVb); iii) sedimentation in convecting magma (Zone II $\pm$ Zone III); and iv) postcumulus and/or subsolidus modifications (Zone I and/or Zone IV). The effects and consequences of processes involved in the formation of the TLS vary from zone to zone.

8) Crystallization of the TLS took place at $\sim$950°C and at low pressures ($<$ 5 kbar).

9) The TLS shows slight to strong LREE enrichment relative to HREE [$(La/Lu)_N$= (2.4 to 11.9); $(La/Sm)_N$= (1.4 to 3.0)] and significant negative Nb-anomalies with or without notable Ti-anomalies.

10) There is significant ϵ_{Nd} variation within the TLS from -0.1 to +5.1 at 420 Ma and there are three different levels of isotopic heterogeneity; i) intra-sample (0.6 to 0.8 ϵ_{Nd} unit); ii) intra-zone ($\leq$ 1 ϵ_{Nd} unit); and iii) inter-zone (1 to 5 ϵ_{Nd} unit).

11) Inter-zone isotopic heterogeneity appears to exist before the emplacement of magma batches into the chamber. The overall correlation between ϵ_{Nd} values and the $(La/Sm)_N$ may be attributed to crustal assimilation prior to intrusion.

12) Mafic magmas giving rise to the TLS may be derived from the same or similar mantle reservoir(s) which must have had ϵ_{Nd} higher than +5 at 420 Ma, and appears to have been modified by subduction-related processes leading to a selective LREE enrichment relative to HFSE, particularly Nb, and/or variation in water content.

13) The FS and W-SCS are geochemically and isotopically distinct, temporally unrelated, high-level granitoid intrusions.

14) The voluminous FS is a 420 ±2 Ma, C-type, metaluminous granitoid body dominated by monzogranite with minor granodiorites. It typically exhibits: i) LREE enrichment relative to HREE [$(La/Lu)_N$= (3.2 to 6.1) and $(La/Sm)_N$ = (0.3 to 0.4)] with flat $HREE_N$ patterns; ii) negative Eu-, Nb- and Ti-anomalies; and iii) generally positive ϵ_{Nd} values which vary from -1.0 to +1.3 at 420 Ma.

15) Lithological and geochemical variations within the FS can be best explained in terms of early fractionation of plagioclase and ilmenite/magnetite, and late crystallization of zircon ± apatite ± hornblende.

16) The FS is mainly derived from lower crustal material with or without a minor contribution from the mantle-derived mafic component. The source material apparently contained older crustal components and may have had a comparable Nd isotopic composition to "Precambrian basement" rocks- the oldest lithologies recognized in central Newfoundland.

16) The W-SCS is a 408 Ma, H-type, metaluminous composite intrusion. It contains three distinct units: **the Pigeon Island Unit**- composed of hornblendite; b) **the Sandy Unit** - containing leucocratic gabbronorite; and c) **the Wild Unit** - consisting of quartz diorite, tonalite and minor granodiorite. The observed mineralogical and/or geochemical dissimilarities between the units can be attributed to differences in crystallization conditions, such as water pressure, of magma batches which are likely derived from the same or similar source materials.

17) The W-SCS is characterized by: i) LREE enrichment relative to HREE with steeply sloping REE_N patterns [$(La/Lu)_N$= (6.9 to 16.1) $(La/Sm)_N$ =(3.0 to 4.0)]; ii) no notable Eu-anomalies; iii) significant negative Nb- anomalies with or without minor Ti-anomalies; and iv) a wide range of Nd isotopic compositions

from +0.3 to +3.2 at 408 Ma.

18) The Wild Unit dominates the W-SCS and typically contains various types of mafic-intermediate dykes, microgranular enclaves and country-rock xenoliths.

19) Three different mafic-intermediate dyke types have been recognized in the Wild Unit. These are *synplutonic*, *transitional* and *cross-cutting* dykes and they reflect the crystallinity and rheology of the host rock at the time of dyke injection.

19) The mafic-intermediate dykes reveal: i) LREE enrichment relative to HREE [$(La/Lu)_N$= 5.56- 7.89]; ii) poorly developed Eu-anomalies; iii) significant negative Nb-anomalies without significant Ti-anomalies; and iv) relatively positive ϵ_{Nd} values from +0.9 to +4.1 at 408 Ma.

20) Mafic magmas producing the mafic-intermediate dykes in the W-SCS are likely derived from the same or similar source material(s) that gave rise to the TLS.

21) Microgranular enclaves occur in two distinct types: "common-type" and "apatite-rich type". In general they display comparable texture, composition and/or isotopic features to the mafic-intermediate dykes and/or their host rocks.

22) Magma mixing and mingling processes between mantle-derived mafic and lower crust-derived felsic magmas play important roles in the evolution of the W-SCS.

23) Four distinct stages of mafic-felsic interaction are recognized in the Wild Unit. In stages I to IV, the products of these interactions vary from a hybrid magma (the Wild Unit), to microgranular enclaves, to "*synplutonic/transitional dykes*" and finally to "*cross-cutting dykes*".

24) Supracrustal xenoliths are the oldest lithologies in the study area and represent

upper crustal material. They display variable geochemical features but they are characterized by significantly negative ϵ_{Nd} values (-8 to -9 at 420 Ma).

25) A proposed model which is based on significant mafic magma underplating of the lower crust ($\geq$ 420 Ma) as a result of crustal thinning and extension due to lithospheric delamination and/or transcurrent faulting, envisages that the TLS, the FS and the W-SCS are the products of similar mechanisms. However, each suite represents a significantly different mode of interaction that took place at a different time and/or place between mafic magmas and the lower crust. The mode of such interaction varies from mass transfer (*i.e.* crustal contamination- the TLS), heat transfer $\pm$ minor mass transfer (crustal anatexis with or without minor contribution from mantle-derived mafic magma- the FS) to both mass and heat transfer (magma mixing and mingling- the W-SCS).

REFERENCES

Atherton, M.P., 1993, Granite magmatism. Journal of Geological Society, London, 150, 1009-1023.

Baird, D.M., 1958, Fogo Island map-area Newfoundland. Geological Survey of Canada Memoir 301, 43 pp.

Bard, J.P., 1986, Microtextures and Igneous and Metamorphic Rocks (Petrology and Structural Geology). D. Reidel Pub., Holland, 264 pp.

Barbarin, B., 1990, Granitoids: main petrogenetic classifications in relation to origin and tectonic setting. Geological Journal, 25, 227-238.

Barbarin, B. and Didier, J., 1991, Review of the main hypotheses proposed for the genesis and evolution of mafic microgranular enclaves. *In*: J.Didier and B. Barbarin, (Eds.) Enclaves and Granite Petrology, Elsevier, Amsterdam, 367-373.

Barbarin, B. and Didier, J., 1992, Genesis and evolution of mafic microgranular enclaves through various types of interaction between coexisting felsic and mafic magmas. Transactions of the Royal Society of Edinburgh, 83, 145-153.

Barnes, S.J., 1986, The effect of trapped liquid crystallization on cumulus mineral compositions in layered intrusions. Contrib. Mineral. Petrol., 93, 524-531.

Bedard, J.H., Sparks, R.S.J., Renner, R., Cheadle, M.J. and Hallworth, M.A., 1988, Peridotite sills and metasomatic gabbros in the Eastern Layered Series of the Rhum complex. Journal of Geological Society, London, 145, 207-224.

Best, M.G., and Mercy, E.L.P., 1967, Composition and crystallization of mafic minerals in the Guadalupe Igneous Complex, California. The American Mineralogist, 52, 436-474.

Bevier, M.L. & Whalen, J.B., 1990, Tectonic significance of Silurian magmatism in the Canadian Appalachians. Geology, 18, 411-414.

Boudreau, A.E., 1987, Pattern formation during crystallization and the formation of fine-scale layering. *In*: I. Parsons (Ed.), Origins of Igneous Layering, D.Reidel Publishing Company, Dordrecht, 453-471.

Brandies, G. Jaupart, C., & Allègre, C.J., 1984, Nucleation, crystal growth and the thermal regime of cooling magmas. Journal of Geophysical Research, 89, 10161-10177.

Brown, G.M., 1956, The layered ultrabasic rocks of Rhum, Inner Hebrides. Transactions of the Royal Society of Edinburgh, 240, 1-53.

Brown, P.E., Chambers, A.D., & Becker, S.M., 1987, A large soft-sediment fold in the Lilloise intrusion, East Greenland. *In*: I. Parsons (Ed.), Origins of Igneous Layering, D.Reidel Publishing Company, Dordrecht, 125-143.

Butcher, A.R., Young,I.M., & Faithfull, J.W., 1985, Channelled metasomatism in Rhum layered cumulates-evidence from late-stage veins. Geological Magazine, 122, 503-518.

Campbell, I.H., 1978, Some problems with the cumulus theory. Lithos, 11, 311-323.

Campbell, I.H., 1985, The difference between oceanic and continental tholeiites: a fluid dynamic explanation. Contrib. Mineral. Petrol., 91, 37-43.

Carlson, R.W., Lungmair, G,W., and MacDougall, J.D., 1991, Columbia River volcanism: the question of mantle heterogeneity or crustal contamination. Geochimica et Cosmochimica Acta, 45, 2483-2499.

Castro, A., Moreno-Ventas, I. and de La Rosa, J.D., 1991, H-type (hybrid) granitoids: a proposed revision of the granite-type classification and nomenclature. Earth-Science Reviews, 31, 237-253.

Cawthorn, R.G., 1978, The petrology of the Tilting Harbour igneous complex, Fogo Island, Newfoundland. Can. J. Earth Sci., 15, 526-539.

Cawthorn, R.G., 1982, An origin of small-scale fluctuation in orthopyroxene composition in the lower and critical zones of the Bushveld complex, South Africa. Chemical Geology, 26, 227-236.

Cawthorn, R.G., 1993, Growth nodes at the base of magnetite layers in the Upper Zone of the Bushveld Complex. (Abstract) *In*: Symposium on Layering in Igneous Complexes.

Cawthorn, G.R., Meyer,P,S., and Kruger, J., 1991, Major addition of magma at pyroxenite marker in the Western Bushveld Complex, South Africa. Journal of Petrology, 32, 739-763.

Cawthorn, G.R., Sander, B. and Jones, I.M., 1992, Evidence for the trapped liquid shift effect in the Mount Ayliff Intrusion, South Africa. Contrib. Mineral. Petrol., 111, 194-202.

Chappell, B.W. and Stephens, W.E., 1988, The origin of infracrustal (I-type) granite magmas. Transaction of the Royal Society of Edinburgh, 79, 71-86.

Chappell, B.W. and White, A.J.R., 1974, Two contrasting granite types. Pacific Geology, 1974, 8, 173-174.

Chappell, B.W. and White, A.J.R., 1991, Restite enclaves and the restite model. *In:* J.Didier and B. Barbarin (Eds.), Enclaves and Granite Petrology, Elsevier, Amsterdam, 375-382.

Chen, Y.D., Price, R.C., White, A.J.R., and Chappell, B.W., 1990, Mafic inclusions from the Glenbog and Blue Gum Granite Suites, Southeastern Australia. Journal of Geophysical Research, 95, 17757-17785.

Clarke, D.B., 1991, Granitoid Rocks. Chapman and Hall, London, UK, 283 pp.

Cocherie, A., Rossi, P., Fouillac, A.M. and Vidal, P., 1994, Crust and mantle contributions to granite genesis-An example from the Variscan batholith of Corsica, France, studied by trace element and Nd-Sr-O- isotope systematics. Chemical Geology, 115, 173-211.

Colman-Sadd, S.P., and Swinden, H.S., 1984, A tectonic window in central Newfoundland?. Geological evidence that the Appalachian Dunnage Zone may be allochthonous. Can. J. Earth Sci., 21, 1349-1367.

Davies, H.J., and von Blanckenburg, F., 1995, Slab breakoff: A model of lithosphere detachment and its test in the magmatism and deformation of collisional orogens. Earth and Planetary Science Letters, 129, 85-102.

Davis, D.W., 1982, Optimum linear regression and error estimation applied to U-Pb data. Can. J. Earth Sci., 19, 2141-2149.

Dawson, J.B., Smith, J.V., and Herving, R.L., 1980, Heterogeneity in upper-mantle

lherzolite and harzburgites. Transaction of the Royal Society of Edinburgh, 297, 323-331.

Deer, W.A., Howie, R.A. and Zussman, J., 1966, An introduction to the rock-forming minerals. Longman Group Ltd., 528 pp.

DePaolo, D., 1981, Trace element and isotopic effects of combined wallrock assimilation and fractional crystallization. Earth and Planetary Science Letters, 53, 189-202.

DePaolo, D.J., 1985, Isotopic studies of processes in mafic magma chambers: I. The Kiglapait Intrusion, Labrador. Journal of Petrology, 26, 925-951.

DePaolo, D.J., 1988, Neodymium Isotope Geochemistry. New York, Springer-Verlag: 187 pp.

DePaolo, D.J., and Wasserburg, G.J., 1976, Nd isotopic varaitions and petrogenetic models, Geophysical Research Letters, 3, 249-252.

Dickin, A.P., 1981, Isotope geochemistry of Tertiary igneous rocks from the Isle of Skye, N.W. Scotland. Journal of Petrology, 22, 155-189.

Didier, J., 1973, Granites and their enclaves: The bearing of enclaves on the origin of granites. Development in Petrology, Elsevier, Amsterdam, 393 pp.

Didier, J., 1987, Contribution of enclave studies to the understanding of origin and evolution of granitic magmas. Geologische Rundschau, 76, 41-50.

Dunning, G.R., 1986, U/Pb geochronology of the Coney Head Complex, Newfoundland. Can. J. Earth Sci., 86, 24, 1072-1075.

Dunning, G.R. and O'Brain,S.J., 1989, Late Proterozoic-early Paleozoic crust in the Hermitage flexture, Newfoundland Appalachians: U/Pb ages and tectonic significance. Geology, 89, 17, 548-551.

Dunning, G.R., O'Brien, S.J, Colman-Sadd, S.P., Blackwood, R.F.,Dickson, W.L., O'Neil, P.P., & Krough, T.E. ,1990a, Silurian orogeny in the Newfoundland Appalachians. Journal of Geology, 88, 895-913.

Dunning, G.R., Barr, S., Raeside, R.P., and Jameison, R.A., 1990b, U-Pb zircon, titanite and monazite ages in the Bras d'Or and Aspy terranes of Cape Breton Island, Nova Scotia: implications for magmatic and metamorphic history. Geological Society of America Bulletin, 102, 322-330.

Dupre, B. and Allègre, C.J., 1980, Pb-Sr-Nd isotopic correlation and the chemistry of the North Atlantic mantle. Nature, 286, 17-22.

Eastler, T.E., 1969, Silurian geology of Change Islands and eastern Notre Dame Bay, Newfoundland. Edited by M.Kay. American Association of Petroleum Geologist, Memoir 12, 425-432.

Eggler, D. and Burnham, C.W., 1973, Crystallization and fractionation trends in the system andesite-H2O-CO2-O2 at pressure to 10 Kb. Geological Society of America Bulletin, 84, 2517-2532.

Elliot, C., Dunning, G.R., and Williams, P.F., 1991, New U/Pb zircon age constrains on the timing of deformation in north-central Newfoundland and implications for early Paleozoic Appalachian orogenesis. Geological Society of America Bulletin, 91, 103, 125-135.

Freshtater, G.B. and Borodina, N.S., 1991, Enclaves in the Hercnian granitoids of the Ural Mountains, U.S.S.R. *In*: J.Didier and B. Barbarin (Eds.), Enclaves and Granite Petrology, Elsevier, Amsterdam, 83-94.

Frost, T.P. and Mahood, G.A., 1987, Field, chemical, and physical constraints on mafic-felsic magma interactions in the Lamarck Granodiorite, Sierra Nevada, California. Geological Society of America Bulletin, 99, 272-291.

Fryer, B.J., Jenner, G.A., Kerr, A., Longstaffe, F.J., 1992, Regional isotopic geochemistry of granitoid intrusions across insular Newfoundland: Monitors of crustal growth. Geological Association of Canada-Mineralogical Association of Canada Joint Annual Meeting, Abstract, 17, A36.

Gray, C.M., Cliff, R.A., and Goode, A.D.T., 1981, Neodymium-strontium isotopic evidence for extreme contamination in a layered basic intrusion. Earth and Planetary Science Letters, 56, 189-198.

Green, T.H., 1982, Anatexis of mafic crust and high pressure crystallization of andesite. *In*: R.S. Thorpe (Ed.), Andesites, John Wiley and Sons, New York, 465-488.

Hamidullah,S. and Bowes, D.R., 1987, Petrogenesis of the Appinite suite, Appin district, western Scotland. Acta Universitatis Carolina-Geologica, 4, 295-396.

Hanson, G.N., 1978, The application of trace elements to the petrogenesis of igneous rocks of granitic composition. Earth and Planetary Science Letters, 38, 26-43.

Hanson, G.N., 1980, Rare Earth Elements in petrogenetic studies of igneous systems. Ann. Rev. Earth Planet. Sci., 8, 371-406.

Harland, W.B., & Gayer, R.A.,1972, The Artic Caledonides and earlier oceans. Geological Magazine, 109, 289-314.

Hart, S.R., 1988, Heterogeneous mantle domains, signature, genesis and mixing chronologies. Earth and Planetary Science Letters, 90, 273-296.

Hawkesworth, C.J. and Norry, M.J., 1983, Introduction. *In*: C.J. Hawkesworth and M.J. Norry (Eds.), Continental Basalts and mantle Xenoliths, Shiva, Nantwich, 1-4.

Henderson, P., 1970, The significance of the mesostasis of basic layered igneous rocks. Journal of Petrology, 11, 463-473.

Henderson, P., 1984, Rare Earth Element Geochemistry. Elsevier Pub., 510 pp.

Hess, P.C., 1989, Origins of Igneous Rocks, Harvard Univ. Press., London, 336 pp.

Hildreth, W., 1981, Gradients in silicic magma chambers: Implications for lithospheric magmatism. Journal of Geophysical Research, 86, 10153-10192.

Hogan, J., 1993, Mononmineralic glomerocrysts: Textural evidence for mineral resorption during crystallization of igneous rocks. Journal of Geology, 101, 531-540.

Hogan, J.P. and Sinha, K.A., 1989, Compositional variation of plutonism in the coastal Maine magmatic province: Mode of origin and tectonic setting. *In:* Tucker, R.D. and Marvinney, R.G. (Eds.), Studies in maine Geology, 4, 1-33.

Hunter, R.H., 1987, Textural equilibrium in layered igneous rocks. *In*: I. Parsons (Ed.), Origins of Igneous Layering, D.Reidel Publishing Company, Dordrecht, 473-503.

Huppert, H.E., & Sparks, R.S.J., 1984, Double-diffusive convection due to crystallization in magmas. Ann. Rev. Earth Sci., **12**, 11-37

Huppert, H.E., and Sparks, R.S.J., 1985, Cooling and contamination of mafic and ultramafic magmas during ascent through continental crust. Earth and Planetary Science Letters, 74, 371-386.

Huppert, H.E., and Sparks, S.R.J., 1988, The generation of granitic magmas by

intrusion of basalt into continental crust. Journal of Petrology, 29, 559-624.

Irvine, T.N., 1970, Crystallization sequences in the Muskox intrusion and other layered intrusions. Geological Society of South Africa, Spec. Pub., 441-476

Irvine, T.N., 1980, Magmatic infiltration metasomatism, double- diffusive crystallization and adcumulus growth in the Muskox intrusion and other layered intrusions. *In*: R.B. Hargraves (Ed.), Physics of Magmatic Processes, Princeton Univ. Press, Princeton NJ, 325-383.

Irvine, T.N., 1982, Terminology for layered intrusions. Journal of Petrology, 23, 127-162.

Irvine, T.N., Keith, D.W. & Todd, S.G., 1983, The J-M platinum-palladium reef of the Stillwater Complex, Montana. Origin by double diffusive convective magma mixing and implications for the Bushveld. Econ. Geol., 78, 1287-1334

Irvine, T.N., 1987a, Appendix I. Glossary of terms for layered. *In*: I.Parsons (Ed.), Origins of Igneous Layering, D.Reidel Publishing Company, Dordrecht, 641-647.

Irvine, T.N., 1987b, Appendix II. Processes involved in the formation and development of layered igneous rocks. *In*: I. Parsons (Ed.), Origins of Igneous Layering, D.Reidel Publishing Company, Dordrecht, 649-656.

Irvine, T.N., 1987c, Layering and related structures in the Duke Island and Skaergaard Intrusions: Similarities, differences and origins. *In*: I.Parsons (Ed.), Origins of Igneous Layering, D.Reidel Publishing Company, Dordrecht, 185-245.

Jaffey, A.H., Flynn, K.F., Glendenin, L.E., Bentley, W.C. and Essling, A.M., 1971, Precission measurement of half-lives and specific activities of 235U and 238U. Physical Review, Section C, Nuclear Physics, 4, 1889-1906.

Jenner, G.A., and Swinden, H.S., 1993, The Pipestone Pond Complex, central Newfoundland: complex magmatism in an eastern Dunnage Zone ophiolite. Can. J. Earth Sci., 30, 434-448.

Jenner,G.A., Longerich, H.P., Jackson, S.E., and Fryer, B.J., 1990, ICP-MS- A powerful tool for high-precission trace -element anlysis in Earth sciences: Evidence from analysis of selected U.S.G.S. reference samples. Chemical Geology, 83, 133-148.

Jukes, J.B., 1843, General report of the Geological Survey of Newfoundland during the years 1839-1840.

Kerr, A., Dickson, W.L., Colman-Sadd, S.P., Fryer, B.J., and Jenner, G., 1992, Paleozoic granites and orogenic evolution in the Newfoundland Appalachians: A new type area for Caledonian magmatism?. Geological Association of Canada-Mineralogical Association of Canada Joint Annual Meeting, Abstract, 17, A56.

Kerr, A., Jenner, G.A., and Fryer, B., 1995, Sm-Nd isotopic geochemistry of Precambrian to Paleozoic granitoid suites and deep-crustal structure of the southeast margin of the Newfoundland Appalachians. Can. J. Earth Sci., 32, 224-235.

Krogh, T.E., 1982, Improved accuracy of U-Pb zircon ages by the creation of more concordant systems using air abrasion technique. Geochmica et Cosmochmica Acta, 37, 485-494.

Krogh, T.E. and Davis, G.L., 1975, The production and separation of ^{205}Pb for use as a tracer for isotope dilution analyses: Carnegie Institute of Washington Yearbook, 74, 416-417.

Leake, B.E., 1978, Nomenclature of amphibolites. The American Mineralogist, 63, 1023-1052.

Leeman, W.P. and Hawkesworth, C.J., 1986, Open magma systems: Trace element and isotopic constraints. Journal of Geophysical Research, 86, 91, 5901-5912.

LeMaitre, R.W., 1989, A Classification of Igneous Rocks and Glossary of Terms. Blackwell, Oxford, 193 pp.

Lesher, C.E., 1990, Decoupling of chemical and isotopic exchange during magma mixing. Nature, 344, 235-237.

Longerich, H.P., Jenner, G.A., Fryer, B.J., and Jackson, S.E., 1990, Inductively coupled plasma-mass spectrometric analysis of geological samples: A critical evaluation based on case studies. Chemical Geology, 83, 105-118.

Maaloe, S., 1978, The origin of rhythmic layering. Mineralogical Magazine, 42, 337-345.

Maniar, P.D. and Piccoli, P.M., 1989, Tectonic discrimination of granitoids. Geological Society of America Bulletin, 101, 635-643.

Mathison, C.I. & Booth, R.A. ,1990, Macrorhythmically layered gabbronorites in the Windimurra gabbroic complex, Western Australia. Lithos, 24, 171-180.

McBirney, A.R., 1984, Igneous Petrology, Oxford Press. Freeman, Cooper and Company, California, 504 pp.

McBirney, A.R. and Noyes, R.M., 1979, Crystallization and layering of the Skaergaard Intrusion. Journal of Petrology, 20, 487-554.

McBirney, A.,R., and Murase, T., 1984, Rheological properties of magmas. Ann. Rev. Earth Planet. Sci., 12, 337-357.

McBirney, A.R., White, C.M. and Boudreau, A.E. ,1990, Spontaneous development of concentric layering in a solidified siliceous dike, East Greenland. Earth-Science Reviews, 29, 321-330.

Mengel, F.C., 1987, Thermotectonic evolution of the Proterozoic Archean boundary in the Saglak area, northern Labrador. Unpublished Ph.D. Thesis, Memorial University of Newfoundland, 350 pp.

Murray, A., and Howley, J.P., 1881, Report of the Geological Survey of Newfoundland for, 1864-1880, London, Edward Stanford, 536p.

Moller, P., and Muecke, G.K., 1984, Significance of Europium anomalies in silicate melts and crystal-melt equilibria: a re-evaluation. Contrib. Mineral. Petrol., 87, 242-250.

Morse. S.A., 1979, Kiglapait geochemistry. II: Petrography, Ibid, 20, 591-624.

Morse, S.A., 1986, Convection in aid of adcumulus growth. Journal of Petrology, 27, 1183-1214.

Nelson, K.D., 1992, Are crustal thickness variations in old mountain belts like the Appalachians a consequence of lithospheric delamination? Geology, 20, 498-502.

Nielsen, R.L. and Drake, M.J., 1979, Pyroxene-melt equilibria. Geochimica et Cosmochimica Acta, 43, 1259-1272.

North American Stratigraphic Code., 1983, North American Commission on Stratigraphic Nomenclature. The American Association of Petroleum Geologists

Bulletin, 67, 841-875.

O'Brien, S.J., Wardle, R.J., and King, A.F., 1983, The Avolon Zone: a Pan_African terrane in the Appalachian Orogen of Canada. Geological Journal, 18, 195-222.

O'Connor, J.T., 1965, A classification of quartz-rich igneous rocks on feldspar ratios, U.S. Geological Survey, Prof. Paper, 525-B, 79-84.

Palacz, Z.A., 1985, Sr-Nd-Pb isotopic evidence for crustal contamination in the Rhum intrusion. Earth and Planetary Science Letters, 74, 35-44.

Parsons, I., 1979, The Klokken Gabbro-syenite complex, South Greenland: Cryptic variation and origin of inversely graded layering. Journal of Petrology, 20, 653-694.

Peacock, M.A., 1931, Classification of igneous rock series. Journal of Geology, 39, 54-67.

Pearce, J.A., 1983, Role of sub-continental lithosphere in magma genesis at active continental margins. *In*: C.J. Hawkesworth and M.J. Norry (Eds), Continental Basalts and mantle Xenoliths, Shiva, Nantwich, 230-249.

Pearce, J.A., Harris, N.B.W., and Tindle, A.G., 1984, Trace element discrimination diagrams for the tectonic interpretation of granitic rocks. Journal of Petrology, 25, 956-983.

Pegman, W.J., 1990, Development of continental lithospheric mantle as reflected in the chemistry of the Mesozoic Appalachian Tholeiites, U.S.A. Earth and Planetary Science Letters, 97, 316-331.

Philpotts,A.R., 1990, Principles of igneous annd metamorphic petrology. Prentince Hall, 498 pp.

Pickett, D.A., and Saleeby, J.B., 1994, Nd, Sr, and Pb isotopic characteristics of Cretaceous intrusive rocks from deep levels of the Sierra Nevada batholith, Techachapi Mountains, California. Contrib. Mineral. Petrol., 118, 198-215.

Pin, C., Binon, M., Belin, J.M., 1990, Origin of Microgranular enclaves in granitoids: Equivocal Sr-Nd Evidence from Hercynian rocks in the Massif Central (France).

Journal of Geophysical Research, 95, 17821-17828.

Pitcher, W.S., 1979, Comments on the geological environment of granites. *In*: M.P. Atherton and J. Tarney (Eds.), Origin of Granite Batholiths: Geochemical Evidences, 1-8.

Pitcher, W.S., 1983, Granite type and tectonic environment. *In*: K.J., Hsu, (Ed.), Mountain Building Processes, Academic Press, London, 18-40.

Pitcher, W.S., 1987, Granites and yet more granites forty years on. Geologische Rundschau, 76, 51-79.

Pitcher, W.S., 1991, Synplutonic dykes and mafic enclaves. *In*: J.Didier and B. Barbarin (Eds.), Enclaves and Granite Petrology (Eds.), Elsevier, Amsterdam, 383-392.

Pitcher, W.S. and Berger, A.R., 1972, The geology of Donegal: A study of granite emplacement and unroofing. Wiley- Interscience, 435 pp.

Platten, I.M., 1991, Zoning and layering in diorites of the Scottish Caledonian Appinite Suite. Geological Journal, 26, 329-348.

Poldervaart, A., and Hess, H.H., 1951, Pyroxenes in the crystallization of basaltic magma. Journal of Geology, 59, 472-489.

Rice, A., 1981, Convection fractionation: A mechanism to provide cryptic zoning (Macrosegregation), layering, crescumulates, banded tuffs and explosive volcanism in igneous processes. Journal of Geophysical Research, 86, B1, 405-417.

Robins, B. Haukvik, L., & Jansen, S., 1987, The organization and internal structure of cyclic units in the Honningsvag intrusive suite, north Norway: Implications for intrusive mechanisms, double-diffusive convection and pore-magma infiltration. *In*: I. Parsons (Ed.), Origins of Igneous Layering, D.Reidel Publishing Company, Dordrecht, 287-312.

Robinson, P., Higgins, N., annd Jenner, G.A., 1986, Determination of rare-earth elements, yttrium and scandium in rocks by an ion exchange X-rays fluorescence technique. Chemical Geology, 55, 121-137.

Roeder, P.L. and Emslie, R.F., 1970, Olivine-liquid Equilibrium. Contrib. Mineral. Petrol., 29, 275-289.

Rogers,G., and Dunning, G.R., 1991, Geochronology of appinitic and related granitic magmatism in the W Highlands of Scotland: constraints on the timing of transcurrent fault movement. Journal of the Geological Society, London., 148, 17-27.

Rollison, H., 1993, Using Geochemical Data: Evaluation, presentation, interpretation. Longman Group, UK. Ltd., 352 pp.

Quadling, K. and Cawthorn, R.G., 1993, The banded melagabbronorite/ leucogabbronorite secession from the Main Zone of the Bushveld Complex. (Abstract) *In*: Symposium on Layering in Igneous Complexes.

Sacks, P.E., Secor, D.T., 1990, Delamination in collisional orogens. Geology, 18, 999-1002.

Sandeman, H., 1985, Geology, petrology and petrogenesis of the Fogo Island Granites, Northeast Newfoundland. Unpublished Honours Thesis, Memorial University of Newfoundland. 148 pp.

Sandeman, H. and Malpas, J.G., 1995, The Fogo Island granites and associated volcanic rocks, Fogo Island, northeast, Newfoundland: the calc-alkaline to alkaline transition. Can. J. Earth Sci. (in press).

Saunders, J, K., 1990. Geology of the Mafic rocks of the Tilting Igneous Complex, Fogo Island. Unpublished Honours Thesis, Memorial University of Newfoundland, 119 pp.

Saunders, A.D., Norry, M.J., Tarney, J., 1988, Origin of MORN and chemically-depleted mantle reservoirs: Trace element constraints. Journal of Petrology, Special Lithosphere Issue, 415-445.

Shand, S.J., 1951, Eruptive rocks, John Wiley, New York.

Sinigoi, S., Antonini, P., Demarchi,G., Longinelli,A., Mazzucchelli, M., Negrini,L., and Rivalenti, G., 1991, Interactions of mantle and crustal magmas in the southern part of Ivrea Zone (Italy). Contrib. Mineral Petrol., 108, 385-395.

Sparks, R.S., Huppert, H.E., Koyaguchi, T., and Hallworth, M.A., 1993, Origin of modal and rhythmic igneous layering by sedimentation in a convecting magma chamber. Nature, 361, 246-249.

Stewart, B.W., and DePaolo,D.J., 1990, Isotopic studies of processes in mafic magma chambers: II. The Skaergaard Intrusion, East Greenland. Contrib. Mineral. Petrol., 104, 125-141.

Streckeisen, A., 1976, To each plutonic rock its proper name, Earth-Science Reviews, 12, 1-33.

Strong, D.F., 1979, The Mount Peyton Batholith, Central Newfoundland: A bimodal calc-alkaline suite. Journal of Petrology, 29, 119-138.

Strong,D.F. and Dickson, W.L., 1978, Geochemistry of Paleozoic granitoid plutons from contrasting tectonic zones of northeast Newfoundland. Can. J. Earth Sci., 15: 145-156.

Sun, S-s. and McDonough, W.F., 1989, Chemical and isotopic systematics of oceanic basalts: implications for mantle composition and processes. *In*: Magmatism in the Ocean Basins,Saunders, A.D., and Norry, M.J. (Eds.). Geological Society of Special Publication, 42, 89, 313-345.

Swinden, H.S., Jenner, G.A., Fryer, B.J., Hertogen, J., and Roddick, J.C., 1990, Petrogenesis and paleotectonic history of the Wild Bight Group, an Ordovician rifted island arc in central Newfoundland. Contrib. Mineral. Petrol., 105, 219-241.

Takahashi, E. and Kushiro., I., 1983, Melting of a dry peridotite at high pressures and basalt magma genesis. The American Mineralogist, 68, 859-879.

Taylor, S.R. and McLennan, S.M., 1985. The Continental Crust: its composition and evolution. Blackwell Scientific Pub., 312pp.

Tepper, H.J., 1991, Petrology of mafic plutons and their role in granitoid genesis, Chilliwack batholith, North Cascade, Washington. Unpublished Ph.D. Thesis, University of Washington.

Tepper, H.J., Nelson, B.K., Bergantz, W., and Irving, A.J., 1993, Petrology of the Chilliwack batholith, North Cascades,Washington: generation of calc-alkaline granitoids by melting of mafic lower crust with variable water fugacity. Contrib. Mineral. Petrol., 113, 333-351.

Thirlwall, M.F. and Jones, N.W., 1983, Isotope geochemistry and contamination mechanism of Tertiary lavas from Skye, northwest Scotland. *In*: C.J. Hawkesworth and M.J. Norry, (Eds.) Continental Basalts and mantle Xenoliths,

Shiva, Nantwich, 186-208.

Thirlwall, M.F., Smith, T.E., Graham, A.M., Theodorou, N., Hollings, P., Davidson, J.P., and Arculus, R.J., 1994, High field strength element anomalies in arc lavas: Source or Process? Journal of Petrology, 35, 819-838.

Twenhofel, W.H., and Shrock, R.R., 1937, Silurian strata of Notre Dame Bay and Exploits valley, Newfoundland. Geological Society of America Bulletin, 48, 1748-1772.

Tucker, R.D., and McKerrow, W.S., 1995, Early Paleozoic chronology: a review in light of new U - Pb zircon ages from Newfoundland and Britain. Can. J. Earth Sci., 32, 368-379.

Turner, S.P., Foden, J.D. and Morrison, R.S., 1992, Derivation of some A-type magmas by fractionation of basaltic magma: An example from the Padthaway Ridge, South Australia. Lithos, 28, 151-179.

Upton, B.G.J., 1987, Gabbroic, synogabbroic and syenitic cumulates of the Tugtut^oq younger giant dyke complex, south Greenland. *In*: I. Parsons (Ed.), Origins of Igneous Layering, D.Reidel Publishing Company, Dordrecht, 93-123.

van der Laan, S.R. and Wyllie, P.J., 1993, Experimental interaction of granitic and basaltic magmas and implications for mafic enclaves. Journal of Petrology, 34, 491-517.

Vernon, R.H., 1990, Crystallization and Hybridism in microgranitoid enclave magmas: microstructural evidence. Journal of Geophysical Research, 95, 17849-17859.

Wager, L.R. and Brown, G.M., 1968, Layered igneous rocks. Oliver and Boyd, London, 588 pp.

Wager, L.R., Brown, G.M., and Wadsworth, W.J., 1960, Types of igneous cumulates. Journal of Petrology, 1, 73-85.

Walter, M.J. and Presnall, D.C., 1994, Melting behaviour of simplified lherzolite in the system CaO-MgO-Al2O3-SiO2-Na2O from 7 to 35 kbar. Journal of Petrology, 35, 329-359.

Wang, Y. and Merino, E., 1993, Oscillatory magma crystallization by feedback between the concentrations of the reactant species and mineral growth rates. Journal of Petrology, 34, 369-382.

Wanless, R.K., Stevens, R.D., Lachance, G.R., and Rimsaite, R.Y.H., 1965, Age determinations and geological studies. Geological Survey of Canada, Paper 64-17 (Part 1)

Ward, C.D, McArthur, J.M. and Walsh, J.N., 1992, Rare earth element behaviour during evolution and alteration of the Dartmoor Granite, SW England. Journal of Petrology, 33, 785-815.

Watson, E.B., 1982, Basalt contamination by continental crust: Some experiments and models. Contrib. Mineral. Petrol., 82, 80, 73-87.

Watson, E.B., and Jurewicz,S.R., 1984, Behaviour of alkalies during diffusive interaction of granitic xenoliths with basaltic magma. Journal of Geology, 92: 121-131.

Weaver, B.L., 1991, Trace element evidence for the origin of ocean island basalts. Geology, 19, 123-126.

Weaver, B.L. and Tarney, J., 1983, Chemistry of sub-continental mantle: inferences from Archean and Proterozoic dykes and continental flood basalts. *In*: C.J. Hawkesworth and M.J. Norry (Eds), Continental Basalts and mantle Xenoliths, Shiva, Nantwich, 209-229.

Wells, P.A., 1977, Pyroxene thermometry in simple and complex systems. Contrib. Mineral. Petrol., 62, 129-139.

Weibe, R.A., 1991, Commingling of contrasted magmas and generation of mafic enclaves in granites rocks. *In:* J.Didier and B. Barbarin (Eds.), Enclaves and Granite Petrology, Elsevier, Amsterdam, 393-402.

Weibe, R.A., 1994, Silicic magma chambers as traps for basaltic magmas: The Cadillac Mountain intrusive complex, Mount Desert Island, Maine. Journal of Geology, 94, 102, 423-437.

Weiss, S. and Troll., G., 1989; The Ballachulish Igneous Complex, Scotland: Petrography, mineral chemistry and order of crystallization in the monzodiorite-quartz diorite suite and in the granite. Journal of Petrology, 30, 1069-1115.

Whalen, J.B., Currie, K.L., Chappell, B.W., 1987, A-type granites: geochemical characteristics discrimination and petrogenesis. Contrib. Mineral. Petrol., 95, 407-419.

Whalen, J.W., Jenner, G.A., Hegner, E., and Gariepy, C.,1994a, Geochemical and isotopic (Nd, O, and Pb) constraints on granite sources in the Humber and Dunnage zones, Gaspesie, Quebec, and New Brunswick: implications for the tectonics and crustal structure. Can. J. Earth Sci., 31, 323-340.

Whalen, J.W., Jenner, G.A., Currie, K.L., Barr, S.M., Frederick, J., Longstaffe, and Hegner, E., 1994b, Geochemical and isotopic characteristics of granitoids of the Avalon Zone, southern New Brunswick: Possible evidence for repeated delamination events. Journal of Geology, 94, 102, 269-282.

White, A.J.R. and Chappell, B.W., 1977, Ultrametamorphism and granitoid genesis. Tectonophysics, 43, 7-22.

Williams, H., 1957, The Tilting Igneous Complex, Fogo District, Newfoundland. Unpublished M.Sc. Thesis, Memorial University of Newfoundland, 63 pp.

Williams, H., 1979, Appalachian Orogen in Canada. Can. J. Earth Sci., 16, 792-807.

Williams, H. Colman-Sadd, S.P. and Swinden, H.S., 1988, Tectonic-stratigraphic subdivisions of central Newfoundland. Current Research, Part B, Geological Survey of Canada, Paper 88-1B, 91-98.

Williams, H., Dickson, L.W., Currie, K.L., Hayes, J.P., and Tuach, J., 1989, Preliminary report on a classification of Newfoundland granitic rocks and their relations to tectonostratigraphic zones and lower crustal blocks. Current Research, Part B, Geological Survey of Canada, Paper 89-1B, 47-53.

Williams, H., Currie, K.L., and Piasecki, M.A.J., 1993a, The Dog Bay Line: a major Silurian tectonic boundary in northeast Newfoundland. Can. J. Earth Sci., 30, 2481-2494.

Williams, H., 1993b, Stratigraphy and structure of the Botwood Belt and definition of the Dog Bay Line in northeastern Newfoundland. Current Research, Part D, Geological Survey of Canada, Paper 93-1D, 19-27.

Wilson, J.T., 1966, Did the atlantic close and then re-open? Nature, 211, 31-36.

Wood, B.J. and Banno, S., 1973, Garnet-orthopyroxene and orthopyroxene-clinopyroxene relationships in simple and complex systems. Contrib. Mineral. Petrol., 42, 109-124.

Wright, A.E., and Bowes, D.R., 1979, Geochemistry of the appinite suite. Geological Soc. of London. The Caledonides of the British Isles, 699-704.

Wyllie, P.J., 1984, Constraints imposed by experimental petrology on possible and impossible magma sources and products. Transaction of the Royal Society of Edinburgh, 310, 439-456.

APPENDIX 1

Table A1 Longitude and latitude of petrographically and geochemically analyzed samples from the Tilting area (see Plate 2).

Sample #	Map Unit	Longitude	Latitude
Zone I			
F-91-32	The TLS, Zone I	54° 03' 11"	49° 42' 35"
F-91-582 (1-5)	The TLS, Zone I	54° 03' 15"	49° 42' 18"
F-91-125	The TLS, Zone I	54° 03' 32"	49° 42' 22"
F-91-559.1	The TLS, Zone I	54° 03' 24"	49° 42' 36"
F-91-30	The TLS, Zone I	54° 03' 12"	49° 42' 35"
F-91-121	The TLS, Zone I	54° 03' 43"	49° 42' 19"
F-91-565	The TLS, Zone I	54° 03' 13"	49° 42' 16"
Zone II			
F-92-68	The TLS, Zone II	54° 03' 19"	49° 42' 40"
F-92-70	The TLS, Zone II	54° 03' 19"	49° 42' 40"
F-92-71	The TLS, Zone II	54° 03' 19"	49° 42' 40"
F-92-69	The TLS, Zone II	54° 03' 20"	49° 42' 41"
F-91-434.2	The TLS, Zone II	54° 03' 20"	49° 42' 41"
F-91-434.1	The TLS, Zone II	54° 03' 20"	49° 42' 41"
F-92-72	The TLS, Zone II	54° 03' 22"	49° 42" 42"
F-92-73	The TLS, Zone II	54° 03' 22"	49° 42' 42"
F-91-436.1	The TLS, Zone II	54° 03' 23"	49° 42' 42"
F-92-74	The TLS, Zone II	54° 03' 25"	49° 42' 44"
F-91-429	The TLS, Zone II	54° 03' 26"	49° 42' 42"
F-91-427	The TLS, Zone II	54° 03' 27"	49° 42' 44"
F-91-95P.1	The TLS, Zone II	54° 03' 31"	49° 42' 43"
F-91-95P.2	The TLS, Zone II	54° 03' 31"	49° 42' 43"
F-91-532	The TLS, Zone II	54° 03' 50"	49° 42' 30"
F-91-530	The TLS, Zone II	54° 03' 50"	49° 42' 30"
F-91-95(3 to 5)	The TLS, Zone II	54° 03' 57"	49° 42' 29"
Zone III			
F-92-N-10	The TLS, Zone III	54° 03' 46"	49° 42' 32"
F-92-N-11	The TLS, Zone III	54° 03' 46"	49° 42' 32"
F-92-N-12	The TLS, Zone III	54° 03' 46"	49° 42' 32"
F-92-N-19	The TLS, Zone III	54° 03' 47"	49° 42' 33"
F-92-N-20	The TLS, Zone III	54° 03' 47"	49° 42' 33"
F-92-N-13	The TLS, Zone III	54° 03' 48"	49° 42' 34"
F-92-N-14	The TLS, Zone III	54° 03' 48"	49° 42' 34"
F-92-N-15	The TLS, Zone III	54° 03' 48"	49° 42' 35"
F-92-N-16	The TLS, Zone III	54° 03' 48"	49° 42' 35"
F-91-15	The TLS, Zone III	54° 03' 49"	49° 42' 35"
F-92-N-17	The TLS, Zone III	54° 03' 49"	49° 42' 35"
F-92-N-18	The TLS, Zone III	54° 03' 50"	49° 42' 36"
F-91-18	The TLS, Zone III	54° 03' 50"	49° 42' 36"
F-91-19	The TLS, Zone III	54° 03' 51"	49° 42' 37"
F-91-20	The TLS, Zone III	54° 03' 51"	49° 42' 37"
F-91-21	The TLS, Zone III	54° 03' 51"	49° 42' 37"
F-91-25	The TLS, Zone III	54° 03' 53"	49° 42' 34"
F-91-26	The TLS, Zone III	54° 03' 53"	49° 42' 34"
F-91-103.2	The TLS, Zone III	54° 03' 48"	49° 42' 34"

Table A1 (Con't)

Sample #	Map Unit	Longitude	Latitude
Zone IVa			
F-91-321	The TLS, Zone IVa	54° 04' 03"	49° 42' 34"
F-91-305	The TLS, Zone IVa	54° 04' 06"	49° 42' 34"
F-91-296.1	The TLS, Zone IVa	54° 04' 09"	49° 42' 37"
F-91-296.2	The TLS, Zone IVa	54° 04' 09"	49° 42' 37"
F-91-279	The TLS, Zone IVa	54° 04' 21"	49° 42' 32"
F-91-280	The TLS, Zone IVa	54° 04' 20"	49° 42' 33"
F-91-281	The TLS, Zone IVa	54° 04' 19"	49° 42' 34"
F-91-79.2	The TLS, Zone IVa	54° 04' 34"	49° 42' 31"
F-91-82.1	The TLS, Zone IVa	54° 04' 29"	49° 42' 37"
F-91-228	The TLS, Zone IVa	54° 04' 04"	49° 42' 29"
F-91-233	The TLS, Zone IVa	54° 04' 43"	49° 42' 27"
F-91-87	The TLS, Zone IVa	54° 04' 26"	49° 42' 38"
F-91-296	The TLS, Zone IVa	54° 04' 12"	49° 42' 34"
F-91-299	The TLS, Zone IVa	54° 04' 11"	49° 42' 33"
F-91-305	The TLS, Zone IVa	54° 04' 07"	49° 42' 27"
F-91-307	The TLS, Zone IVa	54° 04' 05"	49° 42' 29"
F-91-321	The TLS, Zone IVa	54° 04' 08"	49° 42' 31"
Zone IVb			
F-91-9	The TLS, Zone IVb	54° 04' 47"	49° 42' 44"
F-91-10	The TLS, Zone IVb	54° 04' 47"	49° 42' 44"
F-91-11	The TLS, Zone IVb	54° 04' 47"	49° 42' 44"
F-91-174	The TLS, Zone IVb	54° 04' 47"	49° 42' 45"
F-91-177	The TLS, Zone IVb	54° 04' 48"	49° 42' 46"
F-91-50 (1-6)	The TLS, Zone IVb	54° 04' 44"	49° 42' 44"
F-91-152	The TLS, Zone IVb	54° 04' 50"	49° 42' 42"
F-91-154	The TLS, Zone IVb	54° 05' 00"	49° 42' 43"
F-91-155	The TLS, Zone IVb	54° 05' 02"	49° 42' 44"
F-91-156	The TLS, Zone IVb	54° 05' 06"	49° 42' 46"
F-92-10	The TLS, Zone IVb	54° 05' 12"	49° 42' 46"
F-92-12	The TLS, Zone IVb	54° 05' 13"	49° 42' 47"
F-91-176	The TLS, Zone IVb	54° 04' 51"	49° 42' 44"
F-91-202	The TLS, Zone IVb	54° 04' 52"	49° 43' 08"
F-91-203	The TLS, Zone IVb	54° 04' 54"	49° 43' 09"
F-91-166	The TLS, Zone IVb	54° 05' 02"	49° 42' 59"
F-91-168	The TLS, Zone IVb	54° 05' 02"	49° 43' 00"
F-91-169	The TLS, Zone IVb	54° 05' 04"	49° 43' 00"

Table A1 (Con't)

Sample #	Map Unit	Longitude	Latitude
FS			
F-91-580	The Fogo Suite	54° 05' 52"	49° 42' 42"
F-92-20a	The Fogo Suite	54° 05' 34"	49° 43' 19"
F-92-30	The Fogo Suite	54° 03' 10"	49° 42' 13"
F-91-563.1	The Fogo Suite	54° 03' 20"	49° 42' 19"
F-91-118	The Fogo Suite	54° 03' 43"	49° 42' 09"
F-91-595.1	The Fogo Suite	54° 03' 21"	49° 42' 03"
F-91-595.2	The Fogo Suite	54° 03' 21"	49° 42' 03"
F-91-120	The Fogo Suite	54° 03' 25"	49° 42' 12"
F-91-583	The Fogo Suite	54° 03' 09"	49° 42' 17"
F-91-596.1	The Fogo Suite	54° 03' 20"	49° 42' 00"
F-91-596.2	The Fogo Suite	54° 03' 20"	49° 42' 00"
W-SCS			
F-91-180	The Sandy Unit	54° 04' 38"	49° 42' 52"
F-91-54	The Sandy Unit	54° 04' 34"	49° 42' 52"
F-91-3	The Sandy Unit	54° 04' 29"	49° 42' 57"
F-91-188	The Sandy Unit	54° 04' 35"	49° 42' 59"
F-91-450	The Sandy Unit	54° 03' 28"	49° 42' 37"
F-92-60	The Sandy Unit	54° 03' 27"	49° 42' 35"
F-92-32	The Pigeon I. Unit	54° 03' 29"	49° 42' 32"
F-91-478(a&b)	The Pigeon I. Unit	54° 03' 20"	49° 42' 35"
F-91-24	The Wild Unit	54° 03' 50"	49° 42' 32"
F-91-79	The Wild Unit	54° 04' 35"	49° 42' 30"
F-92-176	The Wild Unit	54° 04' 02"	49° 42' 35"
F-92-175 (a&b)	The Wild Unit	54° 04' 00"	49° 42' 34"
F-91-590	The Wild Unit	54° 04' 45"	49° 43' 08"
F-91-75 (a&b)	The Wild Unit	54° 03' 42"	49° 42' 41"
F-92-14(a&b)	The Wild Unit	54° 05' 18"	49° 43' 10"
F-91-223	The Wild Unit	54° 04' 04"	49° 42' 12"
F-91-530	The Wild Unit	54° 03' 47"	49° 42' 30"
F-92-N-1(1 to 5)	The Wild Unit	54° 03' 24"	49° 42' 24"
F-91-587	The Wild Unit	54° 02' 59"	49° 42' 15'
Xenolith			
F-91-227	Xenoith	54° 05' 00"	49° 42' 30"
F-91-77S	Xenoith	54° 04' 35"	49° 42' 30"
F-91-60 (L,D,LD)	Xenoith	54° 04' 43"	49° 43' 07"
F-91-287S	Xenoith	54° 04' 17"	49° 42' 26"
F-91-88S	Xenolith	54° 04' 24"	49° 42' 37"
Dyke			
F-91-22	Dyke	54° 03' 47"	49° 42' 35"
F-91-23	Dyke	54° 03' 47"	49° 42' 35"
F-91-31	Dyke	54° 03' 25"	49° 42' 28"
F-91-234d	Dyke	54° 03' 37"	49° 42' 42"
F-92-19D	Dyke	54° 05' 26"	49° 43' 13"
F-92-174	Dyke	54° 04' 04"	49° 42' 32"
F-92-20b	Dyke	54° 05' 34"	49° 43' 19"
F-92-26	Dyke	54° 04' 54"	49° 43' 12"
F-92-34	Dyke	54° 03' 36"	49° 42' 33"

APPENDIX 2

Table A2 Petroraphically and geochemically analyzed samples from the TLS (cumulate type, field number and corresponding stratigraphic number).

Map Unit	Field #	Cumulate Type
Zone I		
Z1-1	F-91-582.1	Plg-cpx-opx
Z1-2	F-91-582.2	Opx-cpx-plg
Z1-3	F-91-582.3	Opx-cpx-plg
Z1-4	F-91-582.4	Opx-cpx-plg
Z1-5	F-91-582.5h	Opx-cpx-plg
Z1-6	F-91-582.5p	Plg-cpx-opx
Z1-7	F-91-559.1	Opx-cpx-hbl
Z1-8	F-91-125	Opx-cpx-hbl
Z1-9	F-91-32	Opx-cpx-ol
Zone II		
Z2-1	F-92-68	Ol
Z2-2	F-92-71	Plg-opx-cpx
Z2-3	F-92-70	Plg-ap
Z2-4	F-92-69	Plg-opx
Z2-5	F-91-434.2	Opx-cpx
Z2-6	F-91-434.1	Plg-ap
Z2-7	F-92-72	Plg-ap
Z2-8	F-92-73	Plg-opx-cpx
Z2-9	F-91-436.1	Plg-opx-cpx-ap
Z2-10	F-92-74	Plg-ap
Z2-11	F-91-429	Plg-opx-ap
Z2-12	F-91-427	Plg-opx-cpx-ap
Z2-13	F-91-95.1	Plg-opx-ap
Z2-14	F-91-95.3	Plg-opx-ap
Z2-15	F-91-532	Plg-ap

Map Unit	Field #	Cumulate Type
Zone III		
Z3-1	F-92-N-10	Plg-cpx-opx
Z3-2	F-92-N-11	Plg-cpx-opx
Z3-3	F-92-N-12	Opx-cpx
Z3-4	F-92-N-19	Plg-cpx-opx
Z3-5	F-92-N-20	Plg-cpx-opx
Z3-6	F-92-N-13	Plg-cpx-opx
Z3-7	F-92-N-14	Plg-opx-cpx
Z3-8	F-92-N-15	Plg-cpx-opx
Z3-9	F-92-N-16	Plg-cpx-opx
Z3-10	F-91-15	Opx-cpx
Z3-11	F-92-N-17	Opx-cpx
Z3-12	F-92-N-18	Plg-cpx-opx
Z3-13	F-91-18	Plg-cpx-opx
Z3-14	F-91-19	Opx-cpx
Z3-15	F-91-20	Opx-plg-cpx
Z3-16	F-91-21	Opx/plg-cpx
Z3-17	F-91-13	Plg-cpx-opx
Z3-18	F-91-14	Plg-opx-cpx
Z3-19	F-91-16	Plg-opx-cpx
Z3-20	F-91-17	Plg-opx-cpx
Z3-21	F-91-25	Opx-cpx
Z3-22	F-91-26	Opx-cpx
Z3-23	F-91-103.2	Opx-plg-cpx
Z3-24	F-91-15	Plg-cpx-opx

Map Unit	Field #	Cumulate Type
Zone IVa		
Z4a-1	F-91-321	Plg-cpx-opx
Z4a-2	F-91-305	Plg-cpx-opx
Z4a-3	F-91-307	Plg-cpx-opx
Z4a-4	F-91-296.1	Plg-cpx-opx
Z4a-5	F-91-296.2	Plg-cpx
Z4a-6	F-91-279..2	Ol-cpx
Z4a-7	F-91-280	Ol-plg
Z4a-8	F-91-281	Ol-plg
Z4a-9	F-91-279.1	Ol-cpx-plg
Zone IVb		
Zone 4b-1	F-91-9	Ol
Zone 4b-2	F-91-10	Ol-cpx-plg
Zone 4b-3	F-91-11	Ol-cpx-ol
Zone 4b-4	F-91-50.1	Ol-cpx-ol
Zone 4b-5	F-91-50.2b	Cpx-ol-plg
Zone 4b-6	F-91-50.2t	Plg-cpx-ol
Zone 4b-7	F-91-50.4	Cpx-ol-plg
Zone 4b-8	F-91-50.6	Plg-cpx-ol
Zone 4b-9	F-91-174	Plg-cpx-ol
Zone 4b-10	F-91-177	Plg-cpx-ol
Zone 4b-11	F-91-152	Plg-cpx-ol
Zone 4b-12	F-91-154	Plg-cpx-ol
Zone 4b-13	F-91-155	Plg-cpx-ol
Zone 4b-14	F-91-156	Plg-cpx-ol
Zone 4b-15	F-92-10	Ol
Zone 4b-16	F-92-12	Plg-cpx-ol
Zone 4b-17	F-91-176	Plg-cpx-ol

APPENDIX 3

MODAL ANALYSES

Modal analyses of selected samples from the TLS (Zone I-IV) are given in the following tables (A3.1- A3.5). Modal analyses are based on visual estimation from thin sections. For each sample, two systems of nomenclature are provided:

a) Irvine (1982) - the name of the cumulates are based upon decreasing order of abundance of cumulus minerals;

b) Streckeisen (1976)- based on total modal mineralogy from thin section.

Adcumulates, mesocumulates and orthocumulates are terms that indicate the present proportion of intercumulus material 0-7, 7-25 and 25-50% respectively (Irvine, 1980; Irvine, 1982). Postcumulus phases are indicated by *italics*.

Table A3.1 Modal analyses and nomenclature of selected samples from Zone I.

MODAL %													NOMENCLATURE	
Sample #	Ol	Opx	Cpx	Plg	Hbl	Bt	Qtz	S	Srp	K-fd	Url	Stz	IRVINE, 1982	STRECKEISEN, 1976
91-30	rlt	48	25	15	trc	3	1	3	trc	-	5	trc	Opx-Cpx Orthocumulate	Ol-Gabronorite
91-32	7	45	25	10	6	2	-	1	trc	-	3	1	Opx-Cpx-Ol Mesocumulate	Ol-Gabbronorite
91-125	-	22	14	20	20	1	2	2	-	5	14	-	Opx-Cpx-Hbl Orthocumulate	Hbl-Gabbronorite
F-91-121	-	25	35	25	10	trc	5	trc	-	trc	trc	-	Opx-Cpx Orthocumulate	Hbl-Gabbronorite
91-559.1	trc	25	20	15	20	-	5	1	-	5	4	5	Opx-Cpx-Hbl Mesocumulate	Hbl-Gabbronorite
91-582.1	-	20	24	26	20	2	2	trc	2	trc	4	trc	Plag-Opx-Cpx Orthocumulate	Hbl-Gabbronorite
91-582.2	-	25	20	17	25	-	2	1	-	trc	5	5	Opx-Cpx-Plag Orthocumulate	Hbl-Gabbronorite
91-582.3	-	26	25	17	22	-	2	trc	-	trc	5	3	Opx-Cpx-Plag Orthocumulate	Hbl-Gabbronorite
91-582.4	-	25	23	17	20	-	3	5	-	-	7	trc	Opx-Cpx-Plg Orthocumulate	Hbl-Gabbronorite
91-582.5h	-	27	20	13	24	-	-	1	-	-	15	trc	Opx-Cpx-Plg Orthocumulate	Hbl-Gabbronorite
91-582.5p	-	17	25	26	20	-	2	-	-	-	10	trc	Plg-Opx-Cpx Orthocumulate	Hbl-Gabbronorite

Table A3.2 Modal analyses and nomenclature of selected samples from Zone II

MODAL %												NOMENCLATURE	
Sample #	Ol	Opx	Cpx	Plg	Hbl	Bt	Qtz	Mg/Il	Ap	Url	Stz	IRVINE, 1982	STRECKEISEN, 1976
92-68	35	20	8	10	10	3	-	2	-	10	2	Ol Orthocumulate	Plg-Hbl-Lherzolite
92-70	-	trc	trc	45	10	5	3	2	2	23	5	Plg-Ap Orthocumulate	Hbl-Gabbro/Diorite
92-69	trc	24	trc	26	20	4	2	5	-	15	4	Plg-Opx Orthocumulate	Hbl-Cpx-Norite
91-434.2	-	25	10	15	21	3	2	6	-	15	3	Opx-Cpx Orthocumulate	Hbl-Gabbronorite
91-434.1	-	trc	trc	44	15	5	5	7	2	16	6	Plg-Ap Orthocumulate	Hbl-Diorite
92-72	-	trc	trc	40	10	4	4	12	3	25	2	Plg-Ap Orthocumulate	Hbl-Gabbro/Diorite
92-73	-	15	5	35	15	6	4	10	-	5	5	Plg-Opx-Cpx Orthocumulate	Hbl-Gabbronorite
91-436.1	-	15	5	40	20	3	4	5	3	3	2	Plg-Opx-Cpx-Ap Orthocumulate	Hbl-Gabbronorite
92-74	-	trc	trc	50	27	2	5	3	3	5	5	Plg-Ap Orthocumulate	Hbl-Gabbro/Diorite
91-429	-	10	trc	45	15	3	2	6	2	12	5	Plg-Opx-Ap Orthocumulate	Hbl-Gabbronorite
91-427	-	10	5	48	7	4	2	9	2	8	5	Plg-Opx-Cpx-Ap Mesocumulate	Hbl-Gabbronorite/Diorite
91-95.1	-	4	trc	45	17	5	4	3	2	15	5	Plg-Opx-Ap Orthocumulate	Hbl-Diorite
91-95.3	-	7	trc	45	10	5	4	4	2	18	5	Plg-Opx-Ap Orthocumulate	Hbl-Diorite
91-532	-	-	-	40	25	3	1	6	3	17	5	Plg-Ap Orthocumulate	Hbl-Diorite

Table A3.3 Modal analyses and nomenclature of selected samples from Zone III

MODAL %												NOMENCLATURE	
Sample #	Ol	Opx	Cpx	Plg	Hbl	Bt	Qtz	Mg/Il	Ap	Url	Stz	IRVINE, 1982	STRECKEISEN, 1976
91-13	-	7	8	40	20	4	2	7	trc	10	2	Plg-Cpx-Opx Orthocumulate	Hbl-Gabbronorite
91-14	-	10	8	30	20	5	2	5	-	15	5	Plg-Opx-Cpx Orthocumulate	Hbl-Gabbronorite
91-15	-	14	10	18	25	3	6	6	-	15	3	Opx-Cpx Orthocumulate	Hbl-Gabbronorite
91-16	-	25	20	30	10	2	4	6	-	3	trc	Plg-Opx-Cpx Mesocumulate	Hbl-Gabbronorite
91-17	-	10	12	50	5	2	3	3	-	10	5	Plg-Cpx-Opx Mesocumulate	Hbl-Gabbronorite
91-18	-	10	15	35	17	3	1	3	-	10	6	Plg-Cpx-Opx Orthocumulate	Hbl-Gabbronorite
91-19	-	15	15	25	25	2	4	4	-	5	5	Opx-Cpx Orthocumulate	Hbl-Gabbronorite
91-20	-	27	12	22	10	4	2	3	-	15	5	Opx-Plg-Cpx Mesocumulate	Hbl-Gabbronorite
91-21A	-	20	15	10	25	3	-	8	-	14	5	Opx-Cpx-Plg Orthocumulate	Hbl-Gabbronorite
91-21B	-	15	10	60	trc	1	-	7	-	3	4	Plg-Opx-Cpx Mesocumulate	Hbl-Gabbronorite
91-103.1	-	24	14	30	10	1	1	5	-	15	trc	Opx-Cpx Orthocumulate	Hbl-Gabbronorite
91-103.2	-	20	20	7	30	2	2	4	-	15	-	Opx/Cpx Orthocumulate	Hbl-Plg-Websterite
91-103.3	-	17	10	50	5	2	1	5	-	7	3	Plg-Opx-Cpx Mesocumulate	Gabbronorite
91-103.4a	-	13	22	40	2	4	trc	5	-	10	trc	Plg-Cpx-Opx Mesocumulate	Gabbronorite
91-103.4b	-	30	40	5	7	4	4	7	-	trc	trc	Cpx-Opx Mesocumulate	Plg-Websterite
91-541.1	-	10	8	45	5	5	5	5	trc	12	5	Plg-Opx-Cpx Mesocumulate	Hbl-Gabbronorite
91-541.2	-	6	4	40	20	7	5	7	-	6	5	Plg-Opx-Cpx Orthocumulate	Hbl-Gabbronorite
92-N-10	-	15	10	40	10	2	trc	10	trc	10	3	Plg-Opx-Cpx Mesocumulate	Hbl-Gabbronorite
92-N-11	-	17	13	50	-	trc	trc	8	trc	7	5	Plg-Opx-Cpx Mesocumulate	Gabbronorite
92-N-12	-	35	30	20	6	-	-	5	-	4	trc	Opx-Cpx Orthocumulate	Gabbronorite
92-N-13	-	7	8	55	15	3	3	4	-	3	2	Plg-Cpx-Opx Mesocumulate	Hbl-Gabbronorite
92-N-14	-	20	15	30	25	3	2	4	-	1	trc	Plg-Opx-Cpx Orthocumulate	Hbl-Gabbronorite
92-N-15	-	10	20	40	20	2	2	5	-	1	trc	Plg-Cpx-Opx Orthocumulate	Hbl-Gabbronorite
92-N-16	-	10	15	50	15	trc	trc	5	trc	5	trc	Plg-Cpx-Opx Orthocumulate	Hbl-Gabbronorite
92-N-17	-	25	10	20	25	3	trc	7	-	6	2	Opx-Cpx Orthocumulate	Hbl-Gabbronorite

Table A3.4 Modal analyses and nomenclature of selected samples from Zone IVa

	MODAL %									NOMENCLATURE	
Sample #	Ol	Opx	Cpx	Plg	Hbl	Bt	Mg/Il	Srp	Url	IRVINE, 1982	STRECKEISEN, 1976
91-79.2	14	22	40	10	5	3	4	2	-	Cpx-Ol Mesocumulate	Ol-Plg-Websterite
91-82.1	trc	15	35	47	-	1	2	-	-	Plg-Cpx-Opx Adcumulate	Gabbronorite
91-87	5	2	37	45	7	-	2	2	-	Plg-Cpx-Ol Mesocumulate	Ol-Gabbro
91-228	15	20	10	30	15	-	3	2	10	Ol-Cpx Orthocumulate	Ol-Gabbronorite
91-233.1	rit	5	25	30	15	5	2	3	15	Plg-Cpx-Opx Orthocumulate	Hbl-Gabbronorite
91-233.2	-	5	20	50	15	-	4	-	6	Plg-Cpx Orthocumulate	Gabbronorite
91-279.1	15	10	15	45	trc	trc	3	2	10	Plg-Ol-Cpx Mesocumulate	Ol-Gabbronorite
91-280	35	20	trc	25	2	3	2	5	8	Ol-Plg Orthocumulate	Ol-Hbl-Gabbronorite
91-299.1	-	trc	35	45	-	2	10	-	3	Plg-Cpx Mesocumulate	Gabbro
91-296.1a	-	15	25	45	5	-	5	-	5	Plg-Cpx-Opx Mesocumulate	Gabbronorite
91-296.1b	-	30	40	5	-	3	7	-	10	Cpx-Opx-Plg Mesocumulate	Gabbronorite
91-282	10	15	10	45	5	5	2	3	10	Plg-cpx/ol Orthocumulate	Ol-Gabbronorite

Table A3.5 Modal analyses and nomenclature of selected samples Zone IVb

	MODAL %									NOMENCLATURE	
Sample #	Ol	Opx	Cpx	Plg	Hbl	Bt	Mg/Il	Srp	Url	IRVINE, 1982	STRECKEISEN, 1976
91-1b	4	6	30	55	trc	-	2	-	3	Plg-Cpx-Ol Adcumulate	Ol-Gabbro
91-9	55	12	12	10	trc	3	3	trc	8	Ol Orthocumulate	Plag-lherzolite
91-10	40	5	20	20	-	2	trc	3	10	Ol-Cpx Orthocumulate	Ol-Gabbro
91-11	20	5	25	40	1	1	7	1	trc	Plg-Cpx-Ol Mesocumulate	Ol-Gabbro
91-50.1	13	5	25	40	-	2	4	trc	10	Plg-Cpx-Ol Mesocumulate	Ol-Gabbro
91-50.2b	30	2	40	20	-	-	4	trc	4	Cpx-Ol-Plg Mesocumulate	Ol-Gabbro
91-50.2t	10	3	30	50	-	-	3	trc	4	Plg-Cpx-Ol Mesocumulate	Ol-Gabbro
91-50.3	25	-	30	40	3	-	2	trc	-	Plg-Cpx-Ol Adcumulate	Ol-Gabbro
91-50.4	30	-	40	25	-	-	2	trc	3	Plg-Cpx-Ol Adcumulate	Ol-Gabbro
91-50.5	45	trc	20	30	3	trc	2	trc	trc	Ol-Plg-Cpx Adcumulate	Ol-Gabbro
91-50.6	17	2	25	45	-	-	3	4	5	Plg-Cpx-Ol Mesocumulate	Ol-Gabbro
91-166	60	2	15	15	trc	1	2	2	3	Ol Orthocumulate	Plg-Lherzolite
91-168	60	3	15	10	2	-	2	3	5	Ol Orthocumulate	Plg-Wehrlite
91-169	15	-	37	45	-	-	2	1	-	Plg-Cpx-Ol Adcumulate	Ol-Gabbro
91-173	60	10	7	10	trc	5	3	2	4	Ol Orthocumulate	Plg-Lherzolite
91-176	5	-	40	45	-	-	10	-	-	Plg-Cpx-Ol Mesocumulate	Ol-Gabbro
91-177	10	-	38	50	-	-	2	trc	trc	Plg-Cpx-Ol Adcumulate	Ol-Gabbro
91-178.a	3	4	35	50	trc	3	5	trc	trc	Plg-Cpx-Ol Adcumulate	Ol-Gabbro
91-202	7	10	30	45	1	1	4	2	-	Plg-Cpx-Ol Adcumulate	Ol-Gabbronorite
91-203	-	2	25	60	-	2	1	-	10	Plg-Cpx Adcumulate	Gabbro
92-10b	30	15	20	25	5	2	3	trc	-	Ol Orthocumulate	Ol-Gabbronorite
92-12a	3	4	25	58	5	1	2	2	-	Plg- Cpx-Ol Mesocumulate	Ol-Gabbro
92-24	17	10	16	25	25	3	4	trc	-	Plg-Ol-Cpx Orthocumulate	Ol-Gabbronorite

APPENDIX 4

MINERAL ANALYSES

Quantitative microprobe mineral analyses were performed at the Department of Earth Sciences, Memorial University of Newfoundland, on CAMECA SX50, equipped with a Si-energy dispersive detector (ED) and four wavelength dispersive spectrometers (WDS), using a beam of 1-2 μm diameter, an accelerating voltage of 15 kV and a beam current of 20 nA. Natural standards of olivine, hypersthene, hornblende, diopside and anorthite were systematically measured over the period in which analytical work was carried out to determine the analytical precesion.

During this study, the ED technique was utilized in most of the mineral analyses where major element variation in MgO, FeO, CaO, Al_2O_3 and/or Na_2O are the primary interest. Occasionally, the WDS method has also been employed together with the ED technique for better trace element analyses. For example, the WDS method has been utilized for Cr_2O_3, TiO_2, and MnO contents of pyroxene analyses. Samples whose trace elements analyzed by WDS technique have been indicated by an asterix (*) in the following tables.

In the following tables, mineral analyses and their formulas are grouped for olivine, orthopyroxene, clinopyroxene, plagioclase and hornblende according to zones. Additionally for plagioclases and amphibole grain number, location point as rim, core, mid and traverse (trv) are also indicated. All mineral formula calculations were based on the assumption that $Fe^{Total}=Fe^{+2}$.

OLIVINE ANALYSES

Cations calculated on the basis of 4 oxygens. Sample with * indicates CaO, NiO and MnO analyzed by WDS.

Fo% = Mg*100/(Mg+Fe).

Table A4.1 Olivine analyses, from the TLS.

Sample #:	Z1-9*	Z1-9*	Z1-9*	Z1-9*	Z2-1*	Z2-1*	Z2-1*	Z2-1*	Z4a-6*	Z4a-6*	Z4a-6*	Z4a-6*	Z4a-6*	Z4a-6*	Z4a-6*	Z4a-6*	Z4a-6*
SiO2	38.88	38.39	38.91	39.07	39.51	39.99	39.63	39.92	38.31	38.30	38.28	38.23	38.31	38.29	38.20	38.23	38.20	38.20
FeO	18.91	19.15	17.53	17.85	18.30	17.02	17.10	18.36	25.46	25.28	24.89	24.97	24.76	24.57	24.67	25.15	24.85	24.41
MnO	0.29	0.27	0.34	0.27	0.24	0.32	0.22	0.41	0.39	0.34	0.38	0.46	0.35	0.41	0.43	0.42	0.48	0.41
MgO	41.32	40.81	42.15	42.33	42.31	43.11	42.64	41.90	35.95	35.84	36.00	35.94	35.90	35.91	35.90	36.07	35.83	35.67
CaO	0.02	0.03	0.01	0.03	0.00	0.08	0.00	0.00	0.05	0.03	0.05	0.05	0.06	0.02	0.04	0.08	0.10	0.05
NiO	0.12	0.13	0.19	0.16	0.00	0.00	0.00	0.00	0.12	0.08	0.15	0.09	0.06	0.04	0.06	0.03	0.09	0.10
Total	99.54	98.78	99.12	99.70	100.37	100.52	99.60	100.59	100.28	99.85	99.75	99.74	99.45	99.24	99.30	99.97	99.54	98.84
Si	1.000	0.997	0.999	0.998	1.000	1.003	1.007	1.009	1.009	1.012	1.011	1.010	1.014	1.014	1.013	1.009	1.011	1.016
Fe	0.407	0.416	0.377	0.382	0.388	0.357	0.363	0.388	0.561	0.558	0.550	0.552	0.548	0.544	0.547	0.555	0.550	0.543
Mn	0.006	0.006	0.007	0.006	0.005	0.007	0.005	0.009	0.009	0.008	0.008	0.010	0.008	0.009	0.010	0.009	0.011	0.009
Mg	1.584	1.580	1.613	1.612	1.597	1.613	1.615	1.579	1.411	1.411	1.417	1.416	1.416	1.418	1.418	1.419	1.413	1.414
Ca	0.001	0.001	0.000	0.001	0.000	0.002	0.000	0.000	0.002	0.001	0.002	0.001	0.002	0.001	0.001	0.002	0.003	0.002
Ni	0.003	0.003	0.004	0.003	0.000	0.000	0.000	0.000	0.003	0.002	0.003	0.002	0.001	0.001	0.001	0.001	0.002	0.002
Total	3.000	3.003	3.000	3.002	2.990	2.982	2.989	2.985	2.993	2.991	2.991	2.991	2.989	2.987	2.990	2.994	2.989	2.986
Fo%	79.57	79.17	81.08	80.87	80.47	81.87	81.64	80.27	71.56	71.65	72.05	71.96	72.10	72.26	72.17	71.88	71.99	72.26

Sample #:	Z4a-7*	Z4a-7*	Z4a-7*	Z4a-7*	Z4a-7*	Z4a-7*	Z4a-7*	Z4a-8*	Z4a-8*	Z4a-8*	Z4a-8*	Z4b-1*	Z4b-1*	Z4b-1*	Z4b-1*	Z4b-1*
SiO2	38.17	38.26	38.14	37.99	38.19	38.37	38.17	38.43	38.00	38.35	38.28	39.38	39.02	38.94	39.13	38.96	39.03
FeO	23.15	23.04	23.04	23.21	23.14	23.54	23.10	23.34	23.21	23.23	23.54	18.15	18.09	18.33	18.27	18.51	18.40
MnO	0.35	0.36	0.35	0.39	0.36	0.40	0.39	0.35	0.38	0.34	0.39	0.29	0.29	0.29	0.29	0.30	0.25
MgO	38.33	38.97	38.68	38.55	38.78	38.41	38.47	38.50	38.57	38.25	38.50	42.58	42.28	42.21	42.32	42.43	42.22
CaO	0.02	0.01	0.00	0.01	0.03	0.01	0.03	0.01	0.03	0.03	0.02	0.02	0.03	0.03	0.01	0.03	0.03
NiO	0.08	0.08	0.07	0.08	0.11	0.06	0.05	0.00	0.11	0.05	0.08	0.20	0.18	0.20	0.24	0.20	0.22
Total	100.11	100.73	100.28	100.23	100.62	100.79	100.21	100.64	100.29	100.26	100.81	100.61	99.89	99.99	100.26	100.43	100.15
Si	0.997	0.992	0.994	0.992	0.992	0.996	0.995	0.998	0.991	0.999	0.994	0.998	0.997	0.995	0.997	0.992	0.995
Fe	0.506	0.500	0.502	0.507	0.503	0.511	0.504	0.507	0.506	0.506	0.511	0.385	0.386	0.392	0.389	0.394	0.393
Mn	0.008	0.008	0.008	0.009	0.008	0.009	0.009	0.008	0.008	0.008	0.009	0.006	0.006	0.006	0.006	0.006	0.006
Mg	1.492	1.506	1.502	1.500	1.502	1.486	1.495	1.490	1.500	1.486	1.490	1.608	1.610	1.608	1.607	1.611	1.605
Ca	0.001	0.000	0.000	0.000	0.001	0.000	0.001	0.000	0.001	0.001	0.001	0.001	0.001	0.001	0.000	0.001	0.001
Ni	0.002	0.002	0.001	0.002	0.002	0.001	0.001	0.000	0.002	0.001	0.002	0.004	0.004	0.004	0.005	0.004	0.005
Total	3.004	3.008	3.007	3.009	3.008	3.004	3.005	3.003	3.009	3.001	3.006	3.002	3.003	3.005	3.004	3.008	3.004
Fo%	74.69	75.09	74.96	74.75	74.91	74.41	74.80	74.62	74.76	74.58	74.45	80.70	80.64	80.41	80.50	80.34	80.35

Sample #:	Z4b-2*	Z4b-2*	Z4b-2*	Z4b-2*	Z4b-2*	Z4b-2*	Z4b-3*	Z4b-3*	Z4b-3*	Z4b-3*	Z4b-4	Z4b-5	Z4b-5	Z4b-5	Z4b-6	Z4b-6	Z4b-6
SiO2	38.32	38.23	38.28	38.25	38.28	38.25	38.45	38.69	38.30	38.62	37.73	38.01	38.39	37.73	38.23	38.16	37.55
FeO	23.13	23.29	22.89	22.87	22.89	22.87	22.22	22.33	22.68	22.00	22.44	23.02	22.80	22.64	23.16	23.15	23.59
MnO	0.37	0.36	0.36	0.40	0.36	0.40	0.35	0.34	0.40	0.35	0.35	0.34	0.29	0.36	0.45	0.32	0.24
MgO	38.71	38.84	38.58	38.44	38.58	38.44	39.41	39.34	38.69	39.52	38.70	39.05	39.35	38.44	38.92	39.05	38.13
CaO	0.04	0.03	0.03	0.04	0.03	0.04	0.03	0.03	0.03	0.04	0.00	0.00	0.00	0.00	0.00	0.00	0.00
NiO	0.07	0.06	0.07	0.06	0.07	0.06	0.03	0.10	0.06	0.08	0.08	0.00	0.04	0.00	0.06	0.05	0.06
Total	100.64	100.80	100.20	100.05	100.20	100.05	100.50	100.83	100.15	100.61	99.30	100.41	100.87	99.18	100.82	100.72	99.58
Si	0.995	0.992	0.997	0.998	0.997	0.998	0.995	0.998	0.997	0.997	0.988	0.987	0.990	0.991	0.989	0.988	0.987
Fe	0.502	0.505	0.499	0.499	0.499	0.499	0.481	0.482	0.494	0.475	0.492	0.500	0.492	0.497	0.501	0.501	0.518
Mn	0.008	0.008	0.008	0.009	0.008	0.009	0.008	0.007	0.009	0.008	0.008	0.007	0.006	0.008	0.010	0.007	0.005
Mg	1.498	1.502	1.498	1.495	1.498	1.495	1.520	1.513	1.501	1.521	1.511	1.511	1.512	1.505	1.502	1.507	1.494
Ca	0.001	0.001	0.001	0.001	0.001	0.001	0.001	0.001	0.001	0.001	0.000	0.000	0.000	0.000	0.000	0.000	0.000
Ni	0.001	0.001	0.002	0.001	0.002	0.001	0.001	0.002	0.001	0.002	0.002	0.000	0.001	0.000	0.002	0.001	0.002
Total	3.005	3.009	3.003	3.002	3.003	3.002	3.006	3.002	3.003	3.003	3.001	3.005	3.001	3.002	3.004	3.004	3.006
Fo%	74.90	74.82	75.03	74.98	75.03	74.98	75.97	75.85	75.25	76.20	75.45	75.15	75.47	75.16	74.98	75.04	74.23

Table A4.1 (Con't)

Sample #	Z4b-8	Z4b-8	Z4b-8	Z4b-9*	Z4b-9*	Z4b-9*	Z4b-9*	Z4b-10*	Z4b-10*	Z4b-10*	Z4b-10*	Z4b-10*	Z4b-11	Z4b-11	Z4b-12	Z4b-12	Z4b-12
SiO2	37.89	38.92	38.97	38.98	38.94	39.08	38.90	38.40	38.44	38.34	38.45	37.99	38.26	38.49	38.40	38.23	38.50
FeO	23.22	22.37	22.52	18.70	17.85	18.83	18.90	20.65	20.56	20.79	20.19	21.11	21.53	21.76	19.66	19.41	19.54
MnO	0.34	0.36	0.36	0.39	0.38	0.38	0.40	0.32	0.30	0.30	0.29	0.29	0.40	0.45	0.34	0.43	0.40
MgO	38.53	38.97	36.93	41.55	42.28	41.75	41.84	40.01	40.15	40.00	40.33	40.10	39.69	40.02	41.38	41.66	41.53
CaO	0.00	0.00	0.00	0.02	0.00	0.02	0.02	0.01	0.03	0.03	0.02	0.04	0.03	0.00	0.04	0.05	0.00
NiO	0.00	0.05	0.10	0.03	0.05	0.07	0.01	0.07	0.11	0.10	0.11	0.06	0.00	0.00	0.12	0.01	0.01
Total	99.97	100.67	98.88	99.67	99.50	100.13	100.08	99.46	99.58	99.56	99.38	99.61	99.92	100.73	99.95	99.79	99.98
Si	0.990	1.003	1.016	1.000	0.997	0.999	0.995	0.997	0.996	0.995	0.997	0.988	0.994	0.990	0.990	0.986	0.990
Fe	0.507	0.482	0.491	0.401	0.382	0.403	0.404	0.448	0.446	0.452	0.438	0.459	0.468	0.468	0.424	0.419	0.420
Mn	0.007	0.008	0.008	0.008	0.008	0.008	0.009	0.007	0.007	0.007	0.006	0.006	0.009	0.010	0.007	0.010	0.009
Mg	1.501	1.497	1.436	1.590	1.614	1.590	1.596	1.549	1.551	1.548	1.559	1.555	1.536	1.534	1.590	1.601	1.592
Ca	0.000	0.000	0.000	0.001	0.000	0.001	0.001	0.000	0.001	0.001	0.001	0.001	0.001	0.000	0.001	0.001	0.000
Ni	0.000	0.001	0.003	0.001	0.001	0.001	0.000	0.002	0.002	0.002	0.002	0.001	0.000	0.000	0.003	0.000	0.000
Total	3.006	2.991	2.954	3.001	3.003	3.002	3.005	3.003	3.003	3.005	3.003	3.012	3.007	3.001	3.014	3.016	3.010
Fo%	74.73	75.65	74.51	79.84	80.85	79.80	79.78	77.55	77.68	77.42	78.07	77.19	76.66	76.63	78.95	79.28	79.11

Sample #:	Z4b-12	Z4b-12	Z4b-14	Z4b-14	Z4b-14	Z4b-14	Z4b-15	Z4b-15	Z4b-15	Z4b-15	Z4b-15	Z4b-15
SiO2	38.49	38.48	37.97	37.91	38.15	38.42	37.99	38.14	37.80	37.95	37.56	37.68
FeO	19.64	19.61	23.37	23.38	23.33	22.56	24.63	23.64	24.81	24.73	25.14	25.00
MnO	0.46	0.25	0.24	0.31	0.30	0.29	0.34	0.36	0.41	0.41	0.37	0.38
MgO	41.75	41.78	38.72	39.06	39.07	39.56	37.37	37.96	37.11	37.34	36.59	36.59
CaO	0.01	0.03	0.03	0.02	0.03	0.03	0.01	0.04	0.03	0.02	0.03	0.02
NiO	0.05	0.14	0.00	0.00	0.09	0.02	0.07	0.11	0.12	0.10	0.10	0.08
Total	100.40	100.29	100.33	100.68	100.96	100.87	100.41	100.24	100.27	100.56	99.79	99.75
Si	0.987	0.988	0.990	0.984	0.989	0.992	0.996	0.997	0.994	0.994	0.994	0.997
Fe	0.421	0.421	0.510	0.508	0.506	0.487	0.540	0.517	0.546	0.542	0.557	0.553
Mn	0.010	0.006	0.005	0.007	0.007	0.006	0.008	0.008	0.009	0.009	0.008	0.009
Mg	1.596	1.599	1.505	1.511	1.510	1.523	1.460	1.479	1.454	1.458	1.444	1.443
Ca	0.000	0.001	0.001	0.001	0.001	0.001	0.000	0.001	0.001	0.001	0.001	0.001
Ni	0.001	0.003	0.000	0.000	0.002	0.000	0.002	0.002	0.003	0.002	0.002	0.002
Total	3.015	3.016	3.011	3.011	3.014	3.009	3.005	3.003	3.006	3.006	3.006	3.004
Fo%	79.12	79.15	74.70	74.86	74.90	75.76	73.00	74.11	72.72	72.91	72.17	72.29

PYROXENE ANALYSES

Cations calculated on the basis of 6 oxygens. Sample with * indicates Cr_2O_3, TiO_2, and MnO contents analyzed by WDS.

Wo% =Ca*100/(Ca+Fe+Mg);

En% = Mg*100/(Ca+Fe+Mg);

Fs% = Fe*100/(Ca+Fe+Mg); Mg# = Mg*100/(Mg+Fe).

Table A4.2 Orthopyroxene analyses, from Zone I

Sample #	Z1-1	Z1-1	Z1-2	Z1-2	Z1-2	Z1-2	Z1-2	Z1-3	Z1-3	Z1-3	Z1-3	Z1-4	Z1-4	Z1-4	Z1-5	Z1-5	Z1-5
SiO	54.92	54.29	56.06	55.67	56.10	56.15	55.82	56.08	56.24	57.74	57.30	56.02	56.42	56.08	56.18	55.26	55.32
TiO	0.27	0.12	0.15	0.14	0.18	0.15	0.06	0.13	0.11	0.18	0.00	0.16	0.23	0.20	0.11	0.13	0.12
Al2O3	1.39	1.17	1.11	1.04	1.20	1.31	1.07	1.22	0.94	1.05	0.94	1.41	1.19	0.95	0.91	1.40	1.54
Cr2O3	0.00	0.00	0.57	0.35	0.15	0.39	0.27	0.15	0.00	0.14	0.37	0.39	0.21	0.18	0.38	0.30	0.23
FeO	11.97	12.01	9.19	9.86	9.66	8.12	10.21	9.90	10.35	8.46	9.52	8.82	8.88	8.66	8.85	8.59	9.83
MnO	0.32	0.28	0.17	0.23	0.26	0.11	0.24	0.33	0.21	0.19	0.24	0.24	0.23	0.19	0.21	0.30	0.14
MgO	30.42	30.01	30.55	29.86	29.76	30.89	29.63	29.68	29.81	31.29	30.50	30.63	30.41	30.75	32.22	32.08	31.38
CaO	1.00	1.42	1.49	1.54	1.52	1.50	1.65	1.35	1.32	1.44	1.45	1.48	1.55	1.52	1.53	1.15	1.41
Na2O	0.27	0.26	0.08	0.09	0.10	0.10	0.18	0.22	0.24	0.28	0.16	0.26	0.07	0.14	0.16	0.15	0.27
Total	100.56	99.56	99.36	98.79	98.96	98.71	99.12	99.06	99.22	100.74	100.49	99.40	99.19	98.65	100.56	99.37	100.24
Si	1.942	1.943	1.979	1.983	1.991	1.985	1.988	1.989	1.994	1.997	1.997	1.974	1.990	1.989	1.964	1.950	1.948
Ti	0.007	0.003	0.004	0.004	0.005	0.004	0.002	0.004	0.003	0.005	0.000	0.004	0.006	0.005	0.003	0.004	0.003
Al	0.058	0.049	0.046	0.044	0.050	0.055	0.045	0.051	0.039	0.043	0.039	0.059	0.049	0.040	0.038	0.058	0.064
Cr	0.000	0.000	0.016	0.010	0.004	0.011	0.008	0.004	0.000	0.004	0.010	0.011	0.006	0.005	0.011	0.008	0.007
Fe	0.354	0.360	0.271	0.294	0.287	0.240	0.304	0.294	0.307	0.245	0.277	0.260	0.262	0.257	0.259	0.254	0.290
Mn	0.010	0.008	0.005	0.007	0.008	0.003	0.007	0.010	0.006	0.005	0.007	0.007	0.007	0.006	0.006	0.009	0.004
Mg	1.604	1.601	1.608	1.586	1.574	1.628	1.573	1.570	1.576	1.613	1.585	1.609	1.599	1.625	1.679	1.687	1.647
Ca	0.038	0.054	0.056	0.059	0.058	0.057	0.063	0.051	0.050	0.053	0.054	0.056	0.059	0.058	0.057	0.043	0.053
Na	0.018	0.018	0.005	0.006	0.007	0.007	0.012	0.015	0.017	0.019	0.011	0.018	0.005	0.009	0.011	0.010	0.018
Total	4.031	4.038	3.991	3.992	3.984	3.988	4.000	3.987	3.992	3.984	3.980	3.997	3.982	3.993	4.026	4.023	4.034
Wo%	1.90	2.69	2.91	3.04	3.02	2.95	3.24	2.68	2.59	2.79	2.82	2.91	3.05	2.98	2.87	2.18	2.68
En%	80.35	79.46	83.07	81.80	82.03	84.58	81.09	81.98	81.53	84.41	82.70	83.59	83.31	83.78	84.16	85.04	82.77
Fs%	17.75	17.85	14.02	15.16	14.95	12.47	15.67	15.34	15.88	12.80	14.48	13.50	13.64	13.23	12.97	12.78	14.55
Mg#	81.91	81.66	85.56	84.37	84.59	87.15	83.81	84.24	83.70	86.83	85.10	86.09	85.93	86.36	86.65	86.94	85.05

Sample #	Z1-6	Z1-6	Z1-6	Z1-6	Z1-7	Z1-8	Z1-8	Z1-8	Z1-8	Z1-9	Z1-9	Z1-9	Z1-9	Z1-9
SiO	54.04	54.04	53.83	53.76	54.75	54.61	54.13	54.61	53.95	54.02	52.89	53.06	54.58	53.31
TiO	0.17	0.29	0.16	0.16	0.25	0.20	0.27	0.21	0.28	0.13	0.16	0.13	0.14	0.20
Al2O3	1.39	1.50	1.39	1.17	1.66	1.24	1.46	0.00	1.49	0.75	1.44	0.95	0.83	1.35
Cr2O3	0.00	0.07	0.05	0.11	0.26	0.00	0.00	1.62	0.13	0.10	0.31	0.17	0.24	0.28
FeO	13.17	13.19	13.87	13.56	13.36	11.45	13.39	10.79	12.56	17.31	16.77	16.91	12.53	14.46
MnO	0.29	0.36	0.24	0.26	0.32	0.20	0.23	0.23	0.30	0.46	0.36	0.36	0.29	0.24
MgO	28.48	28.51	28.46	28.27	27.52	29.86	28.62	30.44	28.64	26.25	25.84	25.29	28.62	26.66
CaO	1.88	1.42	1.41	1.48	1.33	1.91	1.74	1.72	1.74	0.53	0.94	1.35	1.54	1.92
Na2O	0.17	0.05	0.13	0.09	0.19	0.28	0.20	0.22	0.30	0.17	0.08	0.05	0.05	0.13
Total	99.60	99.43	99.55	98.86	99.63	99.73	100.04	99.84	99.40	99.72	98.79	98.27	98.83	98.54
Si	1.947	1.947	1.945	1.954	1.965	1.947	1.941	1.948	1.941	1.973	1.949	1.968	1.971	1.954
Ti	0.005	0.008	0.004	0.004	0.007	0.005	0.007	0.006	0.008	0.004	0.005	0.004	0.004	0.005
Al	0.059	0.064	0.059	0.050	0.070	0.052	0.062	0.000	0.063	0.032	0.063	0.041	0.035	0.058
Cr	0.000	0.002	0.002	0.003	0.007	0.000	0.000	0.046	0.004	0.003	0.009	0.005	0.007	0.008
Fe	0.397	0.398	0.419	0.412	0.401	0.341	0.402	0.322	0.378	0.529	0.517	0.525	0.379	0.443
Mn	0.009	0.011	0.008	0.008	0.010	0.006	0.007	0.007	0.009	0.014	0.011	0.011	0.009	0.008
Mg	1.530	1.531	1.533	1.531	1.472	1.587	1.529	1.619	1.536	1.429	1.420	1.398	1.540	1.456
Ca	0.073	0.055	0.055	0.058	0.051	0.073	0.067	0.066	0.067	0.021	0.037	0.054	0.060	0.075
Na	0.012	0.003	0.009	0.007	0.013	0.019	0.014	0.015	0.021	0.012	0.006	0.004	0.004	0.009
Total	4.031	4.018	4.032	4.027	3.996	4.031	4.028	4.028	4.028	4.018	4.016	4.009	4.008	4.017
Wo%	3.63	2.76	2.72	2.88	2.65	3.64	3.34	3.27	3.39	1.05	1.86	2.70	2.99	3.80
En%	76.52	77.20	76.39	76.53	76.51	79.30	76.56	80.68	77.53	71.71	71.53	70.34	77.51	73.46
Fs%	19.85	20.04	20.89	20.59	20.83	17.06	20.10	16.05	19.07	26.53	26.05	26.39	19.04	22.36
Mg#	79.40	79.39	78.53	78.80	78.60	82.30	79.20	83.41	80.26	73.00	73.31	72.72	80.28	76.66

Table A4.3 Clinopyroxene analyses, from Zone I

Sample #	Z1-1	Z1-1	Z1-2	Z1-3	Z1-4	Z1-4	Z1-5	Z1-6	Z1-7	Z1-7	Z1-8	Z1-8	Z1-9	Z1-9	Z1-9
SiO	52.98	54.55	53.44	53.90	53.54	53.14	52.22	52.47	52.99	53.24	52.49	52.05	51.85	51.86	52.01
TiO	0.42	0.40	0.35	0.42	0.33	0.26	0.33	0.71	0.58	0.54	0.42	0.53	0.31	0.54	0.50
Al2O3	1.52	2.49	1.78	1.58	1.89	1.78	1.61	2.97	2.59	2.51	2.52	2.21	1.72	2.07	2.09
Cr2O3	0.24	0.09	0.11	0.17	0.28	0.46	0.11	0.28	0.42	0.33	0.59	0.28	0.34	0.32	0.30
FeO	5.54	5.34	4.68	4.31	4.17	5.18	5.21	5.61	4.59	4.88	5.37	5.73	5.06	5.92	6.04
MnO	0.11	0.22	0.21	0.20	0.04	0.18	0.27	0.08	0.00	0.25	0.09	0.22	0.16	0.19	0.21
MgO	17.49	16.46	15.78	16.30	16.83	16.19	16.65	14.83	15.85	15.50	16.28	16.06	15.33	15.32	15.35
CaO	21.53	20.22	22.94	22.57	21.65	21.97	22.61	21.28	22.02	20.70	21.80	21.66	23.11	21.94	21.98
Na2O	0.39	0.54	0.49	0.48	0.47	0.48	0.48	0.84	0.66	0.64	0.64	0.64	0.35	0.45	0.47
Total	100.23	100.31	99.76	99.93	99.19	99.63	99.50	99.08	99.70	98.56	100.19	99.38	98.23	98.60	98.95
Si	1.940	1.976	1.965	1.970	1.965	1.956	1.936	1.941	1.943	1.967	1.925	1.929	1.945	1.939	1.939
Ti	0.012	0.011	0.010	0.012	0.009	0.007	0.009	0.020	0.016	0.015	0.012	0.015	0.009	0.015	0.014
Al	0.066	0.106	0.077	0.068	0.082	0.077	0.070	0.130	0.112	0.109	0.109	0.096	0.076	0.091	0.092
Cr	0.007	0.003	0.003	0.005	0.008	0.013	0.003	0.008	0.012	0.010	0.017	0.008	0.010	0.010	0.009
Fe	0.170	0.162	0.144	0.132	0.128	0.160	0.162	0.173	0.141	0.151	0.165	0.178	0.159	0.185	0.188
Mn	0.004	0.007	0.006	0.006	0.001	0.006	0.009	0.003	0.000	0.008	0.003	0.007	0.005	0.006	0.007
Mg	0.955	0.889	0.865	0.888	0.921	0.888	0.920	0.818	0.866	0.853	0.890	0.888	0.858	0.854	0.853
Ca	0.845	0.785	0.904	0.884	0.852	0.867	0.898	0.843	0.865	0.819	0.857	0.860	0.929	0.879	0.878
Na	0.028	0.038	0.035	0.034	0.033	0.035	0.034	0.060	0.047	0.046	0.045	0.046	0.025	0.033	0.034
Total	4.026	3.976	4.008	3.999	3.999	4.009	4.041	3.996	4.002	3.977	4.023	4.027	4.016	4.012	4.014
Wo%	42.90	42.76	47.25	46.43	44.81	45.26	45.36	45.96	46.22	44.93	44.82	44.67	47.62	45.68	45.60
En%	48.49	48.43	45.22	46.65	48.46	46.40	46.48	44.59	46.27	46.81	46.56	46.10	43.97	44.37	44.28
Fs%	8.61	8.81	7.53	6.92	6.73	8.33	8.16	9.45	7.52	8.26	8.62	9.23	8.15	9.63	9.77
Mg#	84.92	84.61	85.73	87.08	87.80	84.78	85.06	82.51	86.03	85.00	84.37	83.32	84.37	82.17	81.92

Table A4.4 Orthopyroxene analyses, from Zone II

Sample #	Z2-2	Z2-2	Z2-4*	Z2-4*	Z2-4*	Z2-4*	Z2-4*	Z2-4*	Z2-4*	Z2-5*	Z2-5*	Z2-8*	Z2-8*	Z2-9	Z2-9	Z2-9	Z2-11*	Z2-11*
Si2O	53.76	53.97	52.96	52.81	52.66	53.25	52.60	52.99	52.64	52.84	53.07	53.47	53.73	51.66	52.37	51.92	53.35	52.90
Ti2O	0.11	0.18	0.14	0.13	0.28	0.15	0.22	0.10	0.22	0.11	0.13	0.17	0.07	0.48	0.12	0.21	0.13	0.17
Al2O3	0.54	0.72	0.88	0.99	1.53	0.60	0.92	0.39	1.82	1.59	1.74	1.18	0.59	0.91	0.96	0.92	0.93	1.08
Cr2O3	0.09	0.00	0.03	0.07	0.19	0.08	0.13	0.06	0.48	0.22	0.00	0.00	0.00	0.14	0.00	0.07	0.00	0.00
FeO	22.74	22.00	20.88	21.12	20.07	21.49	21.71	21.96	17.89	18.77	20.40	17.87	17.70	23.48	24.21	23.97	22.00	22.11
MnO	1.04	0.87	0.56	0.59	0.65	0.63	0.61	0.66	0.36	0.47	0.52	0.66	0.56	0.96	1.10	0.99	0.98	0.89
MgO	21.53	22.11	24.22	23.69	22.73	23.50	22.79	23.01	24.04	24.85	24.73	26.44	26.32	19.11	19.76	19.30	21.96	21.64
CaO	0.63	0.66	0.51	0.87	1.73	0.62	1.02	0.59	1.88	1.30	0.55	0.24	0.45	1.88	0.97	1.32	0.69	0.53
Na2O	0.11	0.11	0.15	0.22	0.27	0.06	0.00	0.08	0.18	0.09	0.15	0.25	0.09	0.13	0.22	0.00	0.19	0.05
Total	100.56	100.62	100.32	100.48	100.16	100.38	100.00	99.84	99.50	100.25	101.29	100.27	99.50	98.75	99.72	98.69	100.24	99.38
Si	2.002	1.995	1.958	1.953	1.950	1.971	1.960	1.978	1.943	1.942	1.937	1.948	1.972	1.977	1.985	1.986	1.985	1.983
Ti	0.003	0.005	0.004	0.004	0.008	0.004	0.006	0.003	0.006	0.003	0.004	0.005	0.002	0.014	0.003	0.006	0.004	0.005
Al	0.024	0.031	0.038	0.043	0.067	0.026	0.040	0.017	0.079	0.069	0.075	0.051	0.026	0.041	0.043	0.041	0.041	0.048
Cr	0.003	0.000	0.001	0.002	0.006	0.002	0.004	0.002	0.014	0.007	0.000	0.000	0.000	0.004	0.000	0.002	0.000	0.000
Fe	0.708	0.680	0.646	0.653	0.622	0.665	0.676	0.685	0.553	0.577	0.623	0.544	0.543	0.752	0.767	0.767	0.685	0.693
Mn	0.033	0.027	0.017	0.018	0.020	0.020	0.019	0.021	0.011	0.015	0.016	0.020	0.017	0.031	0.035	0.032	0.031	0.028
Mg	1.195	1.219	1.335	1.306	1.255	1.297	1.266	1.280	1.323	1.361	1.346	1.436	1.440	1.090	1.116	1.101	1.218	1.209
Ca	0.025	0.026	0.020	0.035	0.069	0.025	0.041	0.024	0.074	0.051	0.022	0.009	0.018	0.077	0.039	0.054	0.028	0.021
Na	0.008	0.008	0.010	0.016	0.020	0.005	0.000	0.006	0.013	0.006	0.011	0.018	0.006	0.010	0.017	0.000	0.014	0.004
Total	4.001	3.992	4.030	4.029	4.016	4.015	4.012	4.016	4.017	4.030	4.032	4.031	4.023	3.996	4.006	3.989	4.005	3.992
Wo%	1.30	1.36	1.01	1.72	3.49	1.22	2.04	1.17	3.78	2.57	1.08	0.46	0.87	4.01	2.05	2.81	1.42	1.11
En%	61.98	63.30	66.14	64.90	63.85	64.64	63.23	63.69	67.47	68.42	67.62	72.17	71.97	56.81	58.05	57.28	63.11	62.85
Fs%	36.72	35.34	31.99	32.46	31.63	33.15	33.78	34.09	28.17	29.00	31.30	27.36	27.16	39.17	39.90	39.91	35.47	36.04
Mg#	62.80	64.18	67.40	66.66	66.88	66.10	65.18	65.13	70.55	70.23	68.36	72.51	72.60	59.19	59.26	58.94	64.02	63.56

Sample #	Z2-11*	Z2-11*	Z2-11*	Z2-11*	Z2-11*	Z2-11*	Z2-11*	Z2-12*	Z2-12*	Z2-12*	Z2-12*	Z2-12*	Z2-13	Z2-13	Z2-13	Z2-14	Z2-14	Z2-14
Si2O	53.51	52.93	53.60	53.25	52.90	53.54	53.30	53.07	52.69	52.00	52.73	52.57	51.99	52.00	51.60	52.17	52.23	52.35
Ti2O	0.27	0.24	0.16	0.08	0.07	0.12	0.19	0.21	0.30	0.13	0.15	0.18	0.22	0.11	0.21	0.26	0.20	0.15
Al2O3	0.80	0.87	0.80	0.74	0.96	0.76	0.89	1.10	1.26	1.85	1.16	0.77	0.60	0.74	0.95	0.87	0.80	1.27
Cr2O3	0.00	0.08	0.00	0.09	0.00	0.00	0.00	0.02	0.00	0.02	0.00	0.00	0.00	0.00	0.00	0.00	0.00	0.00
FeO	21.60	21.66	22.20	22.03	22.01	22.03	21.82	19.97	21.05	21.79	21.67	21.90	23.08	22.97	23.36	22.91	22.98	22.41
MnO	0.84	0.87	0.84	0.87	0.75	0.85	0.98	0.58	0.65	0.74	0.80	0.85	1.03	1.16	0.76	0.89	0.85	0.99
MgO	21.45	21.64	21.96	21.80	21.49	21.80	21.40	23.82	23.43	22.28	22.60	22.67	22.37	21.77	22.17	21.90	21.82	22.16
CaO	1.70	0.93	0.77	0.69	0.55	0.65	0.67	1.82	1.36	1.39	0.92	0.65	1.10	1.45	0.93	1.28	1.01	1.06
Na2O	0.10	0.07	0.16	0.00	0.19	0.38	0.00	0.34	0.21	0.19	0.24	0.15	0.27	0.42	0.25	0.25	0.32	0.28
Total	100.26	99.29	100.49	99.56	98.92	100.14	99.25	100.93	100.95	100.39	100.27	99.74	100.67	100.62	100.22	100.53	100.21	100.67
Si	1.989	1.987	1.989	1.994	1.994	1.994	1.997	1.949	1.942	1.935	1.960	1.966	1.945	1.949	1.939	1.951	1.958	1.949
Ti	0.007	0.007	0.004	0.002	0.002	0.004	0.005	0.006	0.008	0.004	0.004	0.005	0.006	0.003	0.006	0.007	0.006	0.004
Al	0.035	0.038	0.035	0.033	0.043	0.033	0.039	0.048	0.055	0.081	0.051	0.034	0.027	0.032	0.042	0.038	0.035	0.056
Cr	0.000	0.002	0.000	0.003	0.000	0.000	0.000	0.000	0.000	0.000	0.000	0.000	0.000	0.000	0.000	0.000	0.000	0.000
Fe	0.672	0.680	0.689	0.690	0.694	0.686	0.684	0.613	0.649	0.678	0.673	0.685	0.722	0.720	0.734	0.716	0.720	0.698
Mn	0.027	0.028	0.027	0.028	0.024	0.027	0.031	0.018	0.020	0.023	0.025	0.027	0.033	0.037	0.024	0.028	0.027	0.031
Mg	1.188	1.211	1.215	1.217	1.208	1.210	1.195	1.304	1.287	1.236	1.252	1.264	1.248	1.216	1.242	1.221	1.220	1.230
Ca	0.068	0.037	0.031	0.028	0.022	0.026	0.027	0.072	0.054	0.056	0.037	0.026	0.044	0.058	0.037	0.051	0.041	0.042
Na	0.007	0.005	0.012	0.000	0.014	0.027	0.000	0.024	0.015	0.014	0.017	0.011	0.019	0.031	0.018	0.018	0.023	0.021
Total	3.993	3.995	4.001	3.994	4.001	4.007	3.978	4.034	4.030	4.027	4.019	4.017	4.045	4.047	4.043	4.031	4.030	4.030
Wo%	3.51	1.94	1.58	1.44	1.15	1.36	1.40	3.60	2.71	2.82	1.87	1.32	2.19	2.93	1.85	2.58	2.06	2.16
En%	61.65	62.79	62.80	62.89	62.78	62.96	62.73	65.56	64.70	62.75	63.81	63.99	61.95	60.98	61.68	61.39	61.57	62.43
Fs%	34.84	35.27	35.62	35.67	36.07	35.68	35.87	30.84	32.60	34.43	34.32	34.68	35.86	36.09	36.46	36.02	36.37	35.41
Mg#	63.89	64.04	63.81	63.81	63.51	63.82	63.62	68.01	66.50	64.57	65.03	64.85	63.34	62.82	62.85	63.02	62.87	63.81

Table A4.5 Clinopyroxene analyses, from Zone II

Sample #	Z2-1	Z2-1	Z2-7	Z2-7	Z2-8*	Z2-8*	Z2-8*	Z2-9	Z2-9	Z2-9	Z2-9	Z2-9	Z2-9	Z2-9	Z2-12*	Z2-12*	Z2-12*
SiO2	50.67	50.52	53.83	53.51	52.73	51.82	50.87	52.92	53.45	53.17	52.22	52.65	52.46	52.92	52.78	52.55	52.72
TiO2	1.16	1.01	0.12	0.16	0.39	0.52	2.08	0.23	0.15	0.18	0.12	0.12	0.13	0.13	0.26	0.23	0.19
Al2O3	5.08	4.01	0.97	0.94	1.57	1.97	2.49	1.01	0.85	0.76	0.97	0.83	0.77	0.79	1.38	1.01	0.97
Cr2O3	1.10	0.97	0.03	0.11	0.13	0.15	0.09	0.11	0.03	0.04	0.03	0.04	0.02	0.12	0.00	0.01	0.00
FeO	4.59	4.41	8.00	7.98	6.33	7.25	6.77	8.79	8.87	8.88	9.23	9.21	9.17	9.29	8.23	8.17	8.35
MnO	0.11	0.13	0.47	0.38	0.27	0.30	0.24	0.34	0.36	0.53	0.55	0.42	0.53	0.47	0.34	0.35	0.38
MgO	15.24	15.49	13.75	13.66	16.17	14.59	14.19	13.48	13.19	13.38	13.38	13.22	13.04	13.20	14.76	15.02	14.93
CaO	21.74	21.57	23.21	22.97	22.20	22.72	22.15	22.49	22.67	22.21	22.04	22.09	21.90	22.38	22.42	22.27	22.20
Na2O	0.89	0.92	0.43	0.48	0.54	0.54	0.58	0.33	0.29	0.21	0.39	0.44	0.42	0.46	0.56	0.44	0.51
Total	100.57	99.04	100.80	100.19	100.33	99.86	99.46	99.70	99.86	99.36	98.94	99.01	98.45	99.76	100.74	100.05	100.25
Si	1.851	1.874	1.990	1.990	1.944	1.931	1.900	1.983	1.997	1.997	1.980	1.992	1.996	1.991	1.953	1.958	1.961
Ti	0.032	0.028	0.003	0.005	0.011	0.015	0.059	0.007	0.004	0.005	0.004	0.003	0.004	0.004	0.007	0.007	0.005
Al	0.219	0.175	0.042	0.041	0.068	0.086	0.110	0.045	0.038	0.034	0.043	0.037	0.035	0.035	0.060	0.044	0.043
Cr	0.032	0.028	0.001	0.003	0.004	0.004	0.003	0.003	0.001	0.001	0.001	0.001	0.001	0.004	0.000	0.000	0.000
Fe	0.140	0.137	0.247	0.248	0.195	0.226	0.212	0.276	0.277	0.279	0.293	0.291	0.292	0.292	0.255	0.255	0.260
Mn	0.003	0.004	0.015	0.012	0.009	0.010	0.008	0.011	0.011	0.017	0.018	0.013	0.017	0.015	0.011	0.011	0.012
Mg	0.830	0.856	0.758	0.757	0.889	0.810	0.790	0.753	0.735	0.749	0.756	0.745	0.740	0.740	0.814	0.834	0.828
Ca	0.851	0.857	0.919	0.915	0.877	0.907	0.887	0.903	0.907	0.894	0.895	0.896	0.893	0.902	0.889	0.889	0.885
Na	0.063	0.066	0.031	0.035	0.039	0.039	0.042	0.024	0.021	0.015	0.029	0.032	0.031	0.033	0.040	0.032	0.036
Total	4.021	4.027	4.007	4.006	4.035	4.028	4.009	4.004	3.991	3.990	4.018	4.011	4.007	4.016	4.029	4.029	4.030
Wo%	46.72	46.33	47.77	47.64	44.73	46.67	46.95	46.75	47.29	46.51	46.06	46.35	46.39	46.64	45.41	44.95	44.86
En5	45.57	46.28	39.37	39.43	45.32	41.70	41.84	38.99	38.28	38.98	38.89	38.57	38.44	38.26	41.59	42.17	41.97
Fs%	7.71	7.39	12.86	12.93	9.95	11.63	11.20	14.26	14.43	14.51	15.05	15.08	15.17	15.10	13.01	12.88	13.17
Mg#	85.54	86.22	75.38	75.31	82.00	78.19	78.88	73.22	72.62	72.88	72.09	71.90	71.70	71.70	76.17	76.61	76.12

Table A4.6 Orthopyroxene analyses, from Zone III

Sample #:	Z3-1	Z3-1	Z3-2	Z3-2	Z3-2	Z3-2	Z3-2	Z3-3	Z3-3	Z3-3	Z3-3	Z3-4	Z3-4	Z3-4	Z3-5	Z3-5	Z3-5	Z3-5
Si2O	52.53	52.61	52.10	52.79	50.81	52.60	52.23	52.24	53.28	53.07	53.15	53.58	52.91	52.94	51.64	52.57	52.75	52.41
Ti2O	0.39	0.38	0.28	0.29	0.29	0.29	0.35	0.31	0.14	0.26	0.32	0.14	0.22	0.17	0.20	0.22	0.32	0.19
Al2O3	1.27	1.35	0.89	0.82	4.53	1.11	1.36	1.15	0.66	1.32	1.16	0.67	1.32	1.37	1.49	1.43	1.31	0.79
Cr2O3	0.04	0.00	0.01	0.00	0.01	0.04	0.00	0.16	0.12	0.00	0.04	0.00	0.04	0.00	0.09	0.02	0.00	0.02
FeO	20.67	20.43	22.68	22.83	20.34	22.59	21.61	21.28	21.52	18.76	18.97	19.56	19.40	19.79	21.76	21.07	20.00	22.94
MnO	0.60	0.63	0.59	0.60	0.55	0.59	0.55	0.56	0.57	0.43	0.53	0.58	0.46	0.49	0.60	0.53	0.48	0.66
MgO	23.47	23.16	22.06	22.33	22.17	22.74	22.78	23.09	23.71	25.31	25.01	25.38	23.94	24.17	22.20	24.02	24.10	22.53
CaO	1.44	1.78	1.46	1.16	1.27	0.86	1.05	1.01	0.52	0.72	0.86	0.60	1.82	1.68	1.67	0.59	1.29	0.58
Na2O	0.21	0.16	0.19	0.16	0.25	0.18	0.26	0.23	0.23	0.13	0.22	0.13	0.12	0.17	0.29	0.07	0.03	0.02
Total	100.61	100.49	100.26	100.97	100.21	100.99	100.20	100.03	100.75	100.01	100.25	100.66	100.23	100.79	99.92	100.52	100.28	100.14
Si	1.940	1.944	1.950	1.958	1.880	1.948	1.943	1.945	1.965	1.947	1.949	1.962	1.951	1.944	1.936	1.941	1.945	1.960
Ti	0.011	0.010	0.008	0.008	0.008	0.008	0.010	0.009	0.004	0.007	0.009	0.004	0.006	0.005	0.006	0.006	0.009	0.005
Al	0.055	0.059	0.039	0.036	0.198	0.048	0.060	0.050	0.029	0.057	0.050	0.029	0.057	0.059	0.066	0.062	0.057	0.035
Cr	0.001	0.000	0.000	0.000	0.000	0.001	0.000	0.005	0.004	0.000	0.001	0.000	0.001	0.000	0.003	0.001	0.000	0.001
Fe	0.638	0.631	0.710	0.708	0.629	0.700	0.672	0.663	0.664	0.575	0.582	0.599	0.598	0.608	0.682	0.651	0.617	0.718
Mn	0.019	0.020	0.019	0.019	0.017	0.018	0.017	0.018	0.018	0.013	0.016	0.018	0.014	0.015	0.019	0.017	0.015	0.021
Mg	1.292	1.276	1.231	1.235	1.222	1.255	1.264	1.282	1.304	1.384	1.367	1.385	1.316	1.323	1.241	1.322	1.325	1.256
Ca	0.057	0.070	0.059	0.046	0.050	0.034	0.042	0.040	0.020	0.028	0.034	0.024	0.072	0.066	0.067	0.023	0.051	0.023
Na	0.015	0.012	0.014	0.011	0.018	0.013	0.019	0.017	0.016	0.009	0.015	0.009	0.009	0.012	0.021	0.005	0.003	0.001
Total	4.029	4.022	4.029	4.021	4.022	4.026	4.027	4.028	4.023	4.022	4.024	4.029	4.024	4.030	4.039	4.028	4.020	4.019
Wo%	2.87	3.56	2.93	2.32	2.65	1.71	2.12	2.04	1.03	1.43	1.71	1.18	3.62	3.30	3.37	1.17	2.56	1.17
Ens%	65.00	64.52	61.56	62.07	64.27	63.11	63.89	64.58	65.58	69.63	68.95	68.99	66.25	66.25	62.35	66.24	66.49	62.90
Fs%	32.12	31.92	35.51	35.61	33.08	35.18	33.99	33.39	33.39	28.94	29.34	29.83	30.13	30.45	34.28	32.60	30.96	35.93
Mg#	66.93	66.90	63.42	63.55	66.02	64.21	65.27	65.92	66.27	70.64	70.15	69.81	68.74	68.51	64.52	67.02	68.23	63.64

Sample #:	Z3-5	Z3-6	Z3-6	Z3-6	Z3-6	Z3-6	Z3-7	Z3-7	Z3-7	Z3-7	Z3-7	Z3-7	Z3-8	Z3-8	Z3-8	Z3-8	Z3-8	Z3-8
Si2O	51.96	51.46	51.85	51.55	51.43	50.15	53.39	52.90	52.72	52.56	52.57	52.56	52.24	50.08	51.76	51.44	52.33	52.73
Ti2O	0.24	0.11	0.24	0.25	0.19	2.24	0.22	0.19	0.22	0.23	0.26	0.13	0.22	1.90	0.53	0.32	0.12	0.20
Al2O3	1.12	2.06	1.98	1.72	1.83	0.88	1.35	1.26	1.42	1.46	1.47	1.16	0.74	1.07	1.17	1.34	1.39	1.06
Cr2O3	0.00	0.00	0.03	0.00	0.00	0.02	0.00	0.09	0.13	0.00	0.12	0.04	0.00	0.00	0.00	0.04	0.00	0.02
FeO	22.42	21.77	21.33	23.15	21.45	22.73	19.62	19.41	20.38	20.34	20.31	20.55	22.90	23.34	22.89	15.10	22.25	22.64
MnO	0.63	0.47	0.46	0.51	0.56	0.44	0.51	0.55	0.61	0.49	0.52	0.54	0.67	0.74	0.74	0.32	0.53	0.66
MgO	22.33	22.78	23.76	22.32	22.24	22.29	24.79	24.53	23.82	23.55	23.17	22.43	22.13	21.01	21.55	16.49	22.33	22.35
CaO	1.78	0.51	0.55	0.75	1.60	1.12	0.71	0.99	0.64	1.01	1.67	2.06	1.44	1.90	1.27	14.12	1.86	1.54
Na2O	0.11	0.17	0.23	0.15	0.28	0.00	0.15	0.30	0.08	0.03	0.14	0.15	0.30	0.13	0.18	0.23	0.21	0.21
Total	100.57	99.32	100.42	100.39	99.58	99.86	100.76	100.20	100.00	99.68	100.25	99.62	100.64	100.17	100.10	99.41	101.04	101.42
Si	1.940	1.934	1.920	1.929	1.930	1.892	1.953	1.948	1.953	1.951	1.948	1.966	1.951	1.897	1.945	1.946	1.945	1.952
Ti	0.007	0.003	0.007	0.007	0.005	0.064	0.006	0.005	0.006	0.006	0.007	0.004	0.006	0.054	0.015	0.009	0.003	0.006
Al	0.049	0.091	0.086	0.076	0.081	0.039	0.058	0.055	0.062	0.064	0.064	0.051	0.033	0.048	0.052	0.060	0.061	0.046
Cr	0.000	0.000	0.001	0.000	0.000	0.001	0.000	0.003	0.004	0.000	0.004	0.001	0.000	0.000	0.000	0.001	0.000	0.001
Fe	0.700	0.684	0.661	0.724	0.673	0.717	0.600	0.598	0.631	0.631	0.630	0.643	0.715	0.739	0.720	0.478	0.692	0.701
Mn	0.020	0.015	0.014	0.016	0.018	0.014	0.016	0.017	0.019	0.015	0.016	0.017	0.021	0.024	0.024	0.010	0.017	0.021
Mg	1.243	1.276	1.312	1.245	1.244	1.254	1.351	1.347	1.315	1.303	1.280	1.250	1.232	1.186	1.208	0.930	1.237	1.233
Ca	0.071	0.021	0.022	0.030	0.065	0.045	0.028	0.039	0.025	0.040	0.066	0.083	0.058	0.077	0.051	0.573	0.074	0.061
Na	0.008	0.012	0.016	0.011	0.021	0.000	0.011	0.021	0.006	0.002	0.010	0.011	0.022	0.010	0.013	0.017	0.015	0.015
Total	4.037	4.036	4.039	4.038	4.035	4.026	4.023	4.033	4.020	4.013	4.026	4.025	4.038	4.035	4.027	4.024	4.044	4.035
Wo%	3.54	1.03	1.09	1.51	3.26	2.25	1.40	1.96	1.28	2.04	3.36	4.19	2.87	3.85	2.59	28.91	3.70	3.07
Ens%	61.71	64.42	65.78	62.26	62.78	62.18	68.27	67.90	66.70	65.99	64.79	63.28	61.45	59.23	61.03	46.97	61.77	61.81
Fs%	34.76	34.54	33.13	36.23	33.97	35.57	30.32	30.14	32.02	31.97	31.86	32.53	35.68	36.91	36.37	24.13	34.53	35.12
Mg#	63.97	65.10	66.51	63.21	64.89	63.61	69.24	69.26	67.57	67.36	67.04	66.05	63.27	61.61	62.66	66.06	64.14	63.77

Table A4.6(Con't)

Sample #:	Z3-10	Z3-10	Z3-10	Z3-10	Z3-10	Z3-10	Z3-10	Z3-10	Z3-10	Z3-10	Z3-10	Z3-10	Z3-10	Z3-11	Z3-11	Z3-11	Z3-12	Z3-12
Si2O	52.47	51.93	52.42	52.18	51.99	52.12	52.00	51.96	52.28	51.55	51.81	51.91	51.57	52.30	52.47	53.21	52.69	52.56
Ti2O	0.22	0.27	0.20	0.33	0.23	0.22	0.23	0.18	0.13	0.85	0.28	0.25	0.33	0.15	0.19	0.29	0.14	0.12
Al2O3	0.55	1.07	0.54	1.14	1.08	0.85	1.06	1.09	1.11	1.12	1.05	1.19	1.13	0.82	0.88	1.39	0.97	1.15
Cr2O3	0.01	0.14	0.13	0.07	0.07	0.06	0.01	0.00	0.11	0.12	0.06	0.13	0.07	0.00	0.00	0.00	0.00	0.03
FeO	21.83	21.41	21.53	21.18	20.45	21.33	20.69	20.57	19.63	21.38	21.11	21.24	21.45	23.18	23.08	19.06	22.49	22.25
MnO	0.71	0.52	0.57	0.55	0.50	0.68	0.53	0.56	0.56	0.68	0.58	0.57	0.62	0.80	0.74	0.57	0.79	0.62
MgO	22.96	23.57	22.83	23.47	22.59	23.14	22.97	22.78	22.67	23.45	22.60	23.72	23.45	22.65	22.36	24.45	22.76	23.10
CaO	0.56	0.84	0.74	0.66	1.96	0.66	1.83	1.99	2.82	0.59	1.29	0.69	0.54	0.80	1.16	1.62	0.97	1.20
Na2O	0.08	0.20	0.16	0.19	0.23	0.06	0.23	0.30	0.30	0.16	0.25	0.31	0.19	0.18	0.16	0.30	0.11	0.12
Total	99.39	99.95	99.12	99.77	99.11	99.13	99.55	99.43	99.62	99.90	99.02	100.01	99.35	100.88	101.04	100.89	100.93	101.15
Si	1.969	1.939	1.973	1.948	1.952	1.958	1.945	1.946	1.952	1.928	1.951	1.935	1.938	1.950	1.952	1.944	1.955	1.946
Ti	0.006	0.008	0.006	0.009	0.007	0.006	0.007	0.005	0.004	0.024	0.008	0.007	0.009	0.004	0.005	0.008	0.004	0.003
Al	0.024	0.047	0.024	0.050	0.048	0.038	0.047	0.048	0.049	0.050	0.047	0.052	0.050	0.036	0.039	0.060	0.043	0.050
Cr	0.000	0.004	0.004	0.002	0.002	0.002	0.000	0.000	0.003	0.004	0.002	0.004	0.002	0.000	0.000	0.000	0.000	0.001
Fe	0.685	0.669	0.678	0.661	0.642	0.670	0.647	0.644	0.613	0.669	0.665	0.662	0.674	0.723	0.718	0.582	0.698	0.689
Mn	0.022	0.016	0.018	0.017	0.016	0.022	0.017	0.018	0.018	0.022	0.018	0.018	0.020	0.025	0.023	0.018	0.025	0.020
Mg	1.284	1.312	1.281	1.306	1.265	1.296	1.281	1.271	1.262	1.308	1.269	1.318	1.314	1.259	1.240	1.332	1.259	1.275
Ca	0.023	0.033	0.030	0.026	0.079	0.027	0.074	0.080	0.113	0.024	0.052	0.028	0.022	0.032	0.046	0.063	0.039	0.048
Na	0.006	0.015	0.012	0.014	0.017	0.005	0.017	0.022	0.022	0.012	0.018	0.022	0.014	0.013	0.012	0.021	0.008	0.009
Total	4.019	4.043	4.025	4.034	4.028	4.023	4.034	4.034	4.034	4.038	4.029	4.047	4.043	4.041	4.036	4.029	4.029	4.041
Wo%	1.13	1.66	1.50	1.32	3.98	1.33	3.67	4.01	5.68	1.18	2.62	1.37	1.07	1.58	2.30	3.20	1.93	2.38
Ens%	64.47	65.14	64.42	65.50	63.68	65.04	63.99	63.71	63.49	65.38	63.90	65.65	65.37	62.52	61.87	67.35	63.09	63.37
Fs%	34.40	33.20	34.08	33.17	32.35	33.63	32.34	32.28	30.84	33.44	33.48	32.98	33.56	35.90	35.83	29.45	34.98	34.25
Mg#	65.21	66.24	65.40	66.38	66.31	65.91	66.43	66.37	67.31	66.16	65.62	66.56	66.08	63.53	63.32	69.58	64.33	64.92

Sample #:	Z3-12	Z3-13	Z3-13	Z3-13	Z3-13	Z3-13	Z3-14	Z3-14	Z3-14	Z3-14	Z3-14	Z3-14	Z3-14	Z3-15	Z3-15	Z3-15	Z3-15	Z3-15
Si2O	52.64	51.40	51.59	51.56	51.86	51.81	52.50	51.99	51.92	52.08	52.31	52.09	52.28	52.54	52.28	52.49	52.15	52.10
Ti2O	0.16	0.26	0.16	0.18	0.14	0.19	0.17	0.28	0.21	0.21	0.13	0.24	0.12	0.13	0.23	0.18	0.31	0.19
Al2O3	1.14	1.12	1.14	0.92	0.69	0.56	1.12	1.23	1.37	1.16	1.30	0.99	0.39	1.38	0.72	1.06	1.29	1.58
Cr2O3	0.00	0.00	0.00	0.04	0.07	0.00	0.09	0.08	0.03	0.02	0.05	0.00	0.08	0.05	0.08	0.05	0.00	0.22
FeO	21.92	22.93	23.01	22.26	23.17	22.77	20.54	21.64	21.30	21.21	20.69	21.27	21.61	19.40	19.25	19.73	19.71	19.86
MnO	0.57	0.71	0.81	0.89	0.66	0.75	0.64	0.72	0.56	0.59	0.53	0.55	0.61	0.62	0.55	0.44	0.52	0.44
MgO	22.78	21.79	21.62	21.82	21.95	22.06	23.95	22.89	23.41	23.20	23.41	23.41	22.96	24.24	23.24	24.36	23.70	24.39
CaO	1.52	1.40	1.15	1.75	0.86	0.83	1.04	0.85	1.00	1.20	1.00	0.51	0.69	1.36	2.60	0.63	1.49	0.93
Na2O	0.16	0.07	0.17	0.27	0.13	0.11	0.27	0.14	0.33	0.19	0.23	0.09	0.24	0.21	0.19	0.05	0.13	0.11
Total	100.89	99.69	99.65	99.69	99.54	99.08	100.32	99.82	100.13	99.86	99.65	99.15	98.97	99.91	99.15	99.00	99.30	99.81
Si	1.950	1.940	1.949	1.945	1.960	1.963	1.944	1.946	1.933	1.945	1.951	1.954	1.972	1.948	1.958	1.956	1.945	1.931
Ti	0.005	0.008	0.004	0.005	0.004	0.005	0.005	0.008	0.006	0.006	0.004	0.007	0.003	0.004	0.006	0.005	0.009	0.005
Al	0.050	0.050	0.051	0.041	0.031	0.025	0.049	0.054	0.060	0.051	0.057	0.044	0.017	0.060	0.032	0.047	0.057	0.069
Cr	0.000	0.000	0.000	0.001	0.002	0.000	0.003	0.002	0.001	0.000	0.001	0.000	0.002	0.001	0.002	0.002	0.000	0.007
Fe	0.679	0.724	0.727	0.702	0.732	0.722	0.636	0.678	0.663	0.663	0.646	0.667	0.682	0.601	0.603	0.615	0.615	0.616
Mn	0.018	0.023	0.026	0.029	0.021	0.024	0.020	0.023	0.018	0.019	0.017	0.017	0.020	0.019	0.018	0.014	0.016	0.014
Mg	1.258	1.226	1.218	1.227	1.237	1.246	1.322	1.277	1.299	1.292	1.302	1.309	1.291	1.340	1.298	1.354	1.318	1.348
Ca	0.060	0.057	0.047	0.071	0.035	0.034	0.041	0.034	0.040	0.048	0.040	0.021	0.028	0.054	0.104	0.025	0.060	0.037
Na	0.012	0.005	0.013	0.020	0.010	0.008	0.019	0.010	0.024	0.014	0.017	0.007	0.017	0.015	0.014	0.004	0.010	0.008
Total	4.032	4.032	4.034	4.040	4.032	4.027	4.039	4.032	4.044	4.037	4.034	4.025	4.033	4.042	4.036	4.021	4.028	4.033
Wo%	3.02	2.82	2.34	3.53	1.75	1.68	2.07	1.72	1.98	2.40	2.00	1.04	1.39	2.71	5.21	1.26	2.99	1.84
Ens%	62.98	61.10	61.15	61.35	61.71	62.26	66.12	64.21	64.89	64.51	65.51	65.55	64.53	67.15	64.72	67.90	66.15	67.37
Fs%	34.00	36.08	36.51	35.12	36.54	36.06	31.81	34.07	33.13	33.09	32.49	33.41	34.07	30.15	30.08	30.84	30.85	30.79
Mg#	64.94	62.87	62.62	63.59	62.81	63.32	67.51	65.34	66.20	66.10	66.85	66.24	65.44	69.02	68.27	68.77	68.19	68.63

Table A4.6 (Con't)

Sample #:	Z3-15	Z3-15	Z3-15	Z3-15	Z3-16	Z3-16	Z3-16	Z3-16	Z3-16	Z3-16	Z3-16	Z3-16	Z3-16	Z3-16	Z3-16	Z3-16	Z3-16	Z3-16
Si2O	52.12	51.97	51.73	52.68	52.82	52.61	52.38	51.74	51.95	51.42	52.01	52.29	52.28	52.09	51.67	51.55	52.61	51.86
Ti2O	0.68	0.61	0.67	0.17	0.12	0.08	0.17	0.26	0.26	0.25	0.28	0.15	0.27	0.18	0.34	0.24	0.16	0.27
Al2O3	0.73	1.65	1.35	0.95	1.25	1.01	1.67	1.13	1.66	1.46	1.01	1.36	1.06	1.05	0.94	1.47	1.21	0.97
Cr2O3	0.11	0.12	0.16	0.16	0.00	0.08	0.03	0.00	0.08	0.06	0.04	0.02	0.08	0.04	0.05	0.09	0.07	0.00
FeO	20.99	19.54	19.94	7.31	19.58	21.47	20.37	20.73	20.18	20.05	22.04	19.40	19.92	21.73	21.00	20.00	19.96	21.07
MnO	0.58	0.40	0.36	0.20	0.47	0.55	0.61	0.50	0.48	0.48	0.64	0.51	0.50	0.60	0.66	0.57	0.35	0.57
MgO	23.64	23.34	23.31	15.07	23.73	23.80	24.23	23.83	23.91	23.27	22.43	23.73	23.80	23.04	22.79	23.57	24.53	23.04
CaO	0.55	2.29	2.12	21.99	1.49	0.53	0.58	0.62	1.16	1.08	1.12	1.91	1.04	0.81	1.21	1.14	0.60	0.90
Na2O	0.19	0.12	0.26	0.47	0.09	0.18	0.11	0.10	0.19	0.21	0.12	0.37	0.14	0.07	0.21	0.32	0.08	0.13
Total	99.59	100.04	99.89	99.01	99.55	100.33	100.14	98.91	99.86	98.29	99.69	99.74	99.07	99.60	98.88	98.95	99.59	98.80
Si	1.949	1.928	1.924	1.972	1.961	1.955	1.937	1.943	1.932	1.943	1.952	1.941	1.954	1.951	1.951	1.934	1.951	1.954
Ti	0.019	0.017	0.019	0.005	0.003	0.002	0.005	0.007	0.007	0.007	0.008	0.004	0.008	0.005	0.010	0.007	0.005	0.008
Al	0.032	0.072	0.059	0.042	0.055	0.044	0.073	0.050	0.073	0.065	0.045	0.060	0.047	0.046	0.042	0.065	0.053	0.043
Cr	0.003	0.004	0.005	0.005	0.000	0.002	0.001	0.000	0.002	0.002	0.001	0.001	0.002	0.001	0.002	0.003	0.002	0.000
Fe	0.656	0.606	0.620	0.229	0.608	0.667	0.630	0.651	0.627	0.634	0.692	0.602	0.623	0.681	0.663	0.627	0.619	0.664
Mn	0.018	0.013	0.011	0.007	0.015	0.017	0.019	0.016	0.015	0.015	0.020	0.016	0.016	0.019	0.021	0.018	0.011	0.018
Mg	1.318	1.291	1.293	0.841	1.314	1.318	1.336	1.334	1.325	1.311	1.255	1.313	1.326	1.287	1.283	1.318	1.356	1.294
Ca	0.022	0.091	0.084	0.882	0.059	0.021	0.023	0.025	0.046	0.044	0.045	0.076	0.042	0.033	0.049	0.046	0.024	0.036
Na	0.014	0.009	0.019	0.034	0.006	0.013	0.008	0.007	0.014	0.016	0.008	0.026	0.011	0.005	0.015	0.024	0.006	0.009
Total	4.033	4.031	4.035	4.017	4.021	4.041	4.031	4.032	4.041	4.035	4.027	4.039	4.028	4.027	4.035	4.041	4.027	4.026
Wo%	1.10	4.58	4.23	45.18	2.99	1.06	1.16	1.24	2.31	2.21	2.27	3.82	2.09	1.64	2.46	2.30	1.20	1.82
En%	66.03	64.92	64.71	43.09	66.31	65.70	67.16	66.37	66.30	65.92	63.00	65.94	66.62	64.33	64.30	66.19	67.83	64.90
Fs%	32.88	30.49	31.06	11.73	30.70	33.25	31.68	32.39	31.39	31.87	34.74	30.24	31.29	34.04	33.24	31.51	30.97	33.29
Mg#	66.76	68.04	67.57	78.60	68.35	66.40	67.95	67.21	67.87	67.41	64.46	68.56	68.05	65.40	65.92	67.75	68.65	66.10

Table A4.7 Clinopyroxene analyses, from Zone III

Sample #:	Z3-1	Z3-1	Z3-1	Z3-1	Z3-2	Z3-2	Z3-2	Z3-2	Z3-3	Z3-3	Z3-3	Z3-4	Z3-4	Z3-4	Z3-4	Z3-4	Z3-4
SiO2	51.60	51.54	51.89	52.09	52.80	51.73	51.98	52.83	53.11	52.79	52.66	52.72	52.19	52.66	53.12	52.97	53.09
Ti2O	0.79	0.67	0.68	0.45	0.30	0.58	0.38	0.37	0.33	0.39	0.44	0.29	0.29	0.33	0.19	0.36	0.17
Al2O3	2.51	2.25	2.44	1.67	1.30	2.16	1.59	1.24	1.16	1.26	1.54	1.21	1.88	1.39	0.95	1.12	1.19
Cr2O3	0.02	0.05	0.00	0.00	0.04	0.04	0.02	0.04	0.08	0.10	0.13	0.06	0.05	0.11	0.00	0.07	0.02
FeO	8.24	10.27	8.62	10.16	9.81	11.40	13.44	8.16	8.96	8.55	7.94	8.13	9.31	9.27	7.83	7.40	7.90
MnO	0.32	0.32	0.30	0.38	0.28	0.33	0.40	0.24	0.24	0.29	0.26	0.22	0.21	0.25	0.27	0.19	0.24
MgO	14.16	15.02	14.36	14.93	14.45	14.67	15.50	15.00	15.43	15.29	14.65	15.10	15.22	15.59	15.52	15.00	15.04
CaO	22.55	19.92	22.21	20.06	21.38	19.57	17.07	21.92	20.91	21.65	22.43	22.47	20.93	20.62	22.26	22.86	22.87
NaO	0.44	0.52	0.49	0.54	0.52	0.58	0.53	0.57	0.57	0.64	0.75	0.43	0.66	0.45	0.29	0.40	0.51
Total	100.63	100.57	101.00	100.29	100.88	101.07	100.91	100.37	100.81	100.94	100.80	100.64	100.73	100.65	100.42	100.38	101.01
Si	1.915	1.918	1.919	1.942	1.958	1.923	1.939	1.958	1.961	1.949	1.947	1.952	1.935	1.950	1.965	1.961	1.957
Ti	0.022	0.019	0.019	0.013	0.008	0.016	0.011	0.010	0.009	0.011	0.012	0.008	0.008	0.009	0.005	0.010	0.005
Al	0.110	0.099	0.106	0.074	0.057	0.095	0.070	0.054	0.051	0.055	0.067	0.053	0.082	0.061	0.041	0.049	0.052
Cr	0.001	0.001	0.000	0.000	0.001	0.001	0.001	0.001	0.002	0.003	0.004	0.002	0.001	0.003	0.000	0.002	0.000
Fe	0.256	0.320	0.267	0.317	0.304	0.354	0.419	0.253	0.277	0.264	0.245	0.252	0.289	0.287	0.242	0.229	0.244
Mn	0.010	0.010	0.010	0.012	0.009	0.010	0.013	0.007	0.008	0.009	0.008	0.007	0.007	0.008	0.008	0.006	0.007
Mg	0.783	0.833	0.791	0.830	0.799	0.813	0.862	0.829	0.849	0.842	0.807	0.834	0.841	0.861	0.856	0.828	0.827
Ca	0.896	0.794	0.880	0.802	0.850	0.780	0.682	0.871	0.827	0.856	0.888	0.892	0.831	0.818	0.882	0.907	0.903
Na	0.032	0.038	0.035	0.039	0.037	0.042	0.039	0.041	0.041	0.046	0.054	0.031	0.047	0.032	0.021	0.029	0.037
Total	4.024	4.032	4.027	4.028	4.023	4.034	4.035	4.025	4.024	4.034	4.033	4.03	4.04	4.03	4.02	4.02	4.03
Wo%	46.32	40.79	45.41	41.13	43.51	40.04	34.74	44.60	42.35	43.65	45.77	45.10	42.39	41.62	44.55	46.17	45.78
En%	40.47	42.80	40.84	42.60	40.91	41.76	43.91	42.44	43.49	42.91	41.59	42.16	42.88	43.78	43.22	42.16	41.88
Fs%	13.21	16.41	13.75	16.27	15.58	18.20	21.35	12.96	14.17	13.45	12.65	12.74	14.72	14.60	12.23	11.67	12.34
Mg#	75.39	72.28	74.81	72.37	72.42	69.64	67.28	76.61	75.43	76.13	76.68	76.80	74.44	75.00	77.94	78.32	77.24

Sample #:	Z3-5	Z3-5	Z3-5	Z3-6	Z3-6	Z3-7	Z3-7	Z3-7	Z3-7	Z3-8	Z3-9	Z3-9	Z3-9	Z3-9	Z3-9	Z3-10	Z3-11
SiO2	53.16	52.23	52.47	52.28	51.78	52.56	51.46	50.38	52.53	52.96	52.63	51.79	52.20	51.58	52.07	51.77	52.35
Ti2O	0.14	0.47	0.32	0.12	0.35	0.37	0.53	0.21	0.34	0.07	0.28	0.23	0.52	0.51	0.41	0.41	0.24
Al2O3	0.73	1.89	1.38	0.79	1.45	1.37	2.42	6.72	1.45	0.77	1.35	1.25	1.95	2.11	1.79	1.10	1.34
Cr2O3	0.00	0.06	0.06	0.02	0.03	0.15	0.22	0.09	0.10	0.07	0.00	0.07	0.00	0.04	0.03	0.10	0.09
FeO	8.95	9.34	8.65	8.45	8.81	7.94	8.13	7.30	7.90	8.87	10.94	9.51	9.56	9.02	12.08	8.60	8.65
MnO	0.31	0.29	0.26	0.20	0.12	0.26	0.30	0.24	0.27	0.25	0.35	0.27	0.26	0.32	0.34	0.27	0.30
MgO	14.88	14.48	14.48	14.56	14.12	14.84	13.94	14.06	14.91	14.51	14.92	14.61	13.91	14.24	15.32	14.66	14.47
CaO	22.26	21.34	22.21	21.87	22.06	22.17	21.96	21.53	22.12	22.15	20.06	21.54	22.10	21.81	18.72	21.52	22.34
NaO	0.45	0.54	0.49	0.47	0.57	0.54	0.67	0.49	0.40	0.45	0.54	0.41	0.35	0.55	0.39	0.63	0.52
Total	100.88	100.63	100.33	98.76	99.30	100.20	99.63	101.02	100.03	100.10	101.07	99.68	100.84	100.18	101.16	99.04	100.30
Si	1.969	1.940	1.953	1.975	1.951	1.952	1.926	1.846	1.954	1.98	1.95	1.95	1.94	1.93	1.93	1.95	1.95
Ti	0.004	0.013	0.009	0.003	0.010	0.010	0.015	0.006	0.009	0.00	0.01	0.01	0.01	0.01	0.01	0.01	0.01
Al	0.032	0.083	0.061	0.035	0.064	0.060	0.107	0.290	0.064	0.03	0.06	0.06	0.09	0.09	0.08	0.05	0.06
Cr	0.000	0.002	0.002	0.001	0.001	0.004	0.007	0.003	0.003	0.00	0.00	0.00	0.00	0.00	0.00	0.00	0.00
Fe	0.277	0.290	0.269	0.267	0.278	0.247	0.255	0.224	0.246	0.28	0.34	0.30	0.30	0.28	0.38	0.27	0.27
Mn	0.010	0.009	0.008	0.006	0.004	0.008	0.010	0.008	0.009	0.01	0.01	0.01	0.01	0.01	0.01	0.01	0.01
Mg	0.821	0.802	0.804	0.820	0.793	0.822	0.778	0.768	0.827	0.81	0.83	0.82	0.77	0.79	0.85	0.82	0.80
Ca	0.883	0.849	0.886	0.886	0.891	0.882	0.881	0.845	0.882	0.89	0.80	0.87	0.88	0.87	0.74	0.87	0.89
Na	0.032	0.039	0.036	0.034	0.041	0.039	0.049	0.035	0.029	0.03	0.04	0.03	0.03	0.04	0.03	0.05	0.04
Total	4.03	4.03	4.03	4.028	4.033	4.02	4.03	4.02	4.02	4.03	4.03	4.04	4.02	4.03	4.03	4.04	4.03
Wo%	44.56	43.76	45.23	44.89	45.40	45.23	46.04	46.02	45.11	44.97	40.64	43.70	45.17	44.82	37.85	44.26	45.38
En%	41.45	41.29	41.03	41.58	40.44	42.13	40.66	41.80	42.32	40.98	42.06	41.24	39.57	40.71	43.09	41.94	40.90
Fs%	13.99	14.95	13.74	13.53	14.16	12.64	13.30	12.18	12.57	14.05	17.30	15.06	15.26	14.46	19.07	13.80	13.72
Mg#	74.77	73.42	74.91	75.44	74.07	76.92	75.34	77.44	77.10	74.47	70.86	73.25	72.17	73.79	69.32	75.24	74.88

Table A4.7 (Con't)

Sample #:	Z3-11	Z3-12	Z3-12	Z3-14	Z3-14	Z3-14	Z3-16	Z3-16	Z3-16	Z3-16	Z3-16	Z3-16	Z3-16	Z3-16
SiO2	52.40	52.76	51.76	51.98	51.76	52.44	51.66	51.78	51.95	51.50	51.79	51.97	51.76	51.20
Ti2O	0.19	0.15	0.39	0.37	0.32	0.18	0.30	0.24	0.30	0.31	0.18	0.14	0.23	0.47
Al2O3	1.40	0.84	1.86	1.21	1.35	0.78	1.16	1.26	1.29	1.32	1.03	0.88	1.22	2.12
Cr2O3	0.16	0.03	0.07	0.06	0.05	0.09	0.14	0.16	0.06	0.15	0.04	0.09	0.12	0.07
FeO	9.09	8.56	8.67	9.22	8.23	7.56	8.48	8.31	9.55	7.91	8.57	7.80	7.73	8.56
MnO	0.34	0.23	0.33	0.36	0.26	0.16	0.23	0.23	0.31	0.24	0.29	0.19	0.29	0.36
MgO	14.87	14.59	14.35	15.17	14.36	15.15	14.74	14.87	15.42	14.52	15.38	15.06	14.81	13.96
CaO	21.56	22.41	22.16	20.80	22.11	21.99	21.30	21.59	20.16	22.27	20.79	21.94	22.21	21.58
NaO	0.52	0.40	0.60	0.49	0.60	0.46	0.72	0.53	0.47	0.59	0.59	0.51	0.56	0.53
Total	100.53	99.96	100.19	99.66	99.05	98.81	98.74	98.98	99.51	98.81	98.66	98.58	98.92	98.85
Si	1.95	1.970	1.933	1.95	1.95	1.97	1.953	1.950	1.949	1.945	1.956	1.963	1.952	1.935
Ti	0.01	0.004	0.011	0.01	0.01	0.01	0.012	0.007	0.009	0.009	0.005	0.004	0.007	0.013
Al	0.06	0.037	0.082	0.05	0.06	0.03	0.049	0.056	0.057	0.059	0.046	0.039	0.054	0.095
Cr	0.00	0.001	0.002	0.00	0.00	0.00	0.003	0.005	0.002	0.005	0.001	0.003	0.004	0.002
Fe	0.28	0.267	0.271	0.29	0.26	0.24	0.271	0.262	0.300	0.250	0.271	0.246	0.244	0.271
Mn	0.01	0.007	0.011	0.01	0.01	0.01	0.009	0.007	0.010	0.008	0.009	0.006	0.009	0.012
Mg	0.82	0.812	0.799	0.85	0.81	0.85	0.824	0.835	0.862	0.818	0.866	0.848	0.832	0.787
Ca	0.86	0.896	0.887	0.84	0.89	0.89	0.87	0.871	0.811	0.901	0.842	0.888	0.897	0.874
Na	0.04	0.029	0.044	0.04	0.04	0.03	0.046	0.039	0.034	0.043	0.043	0.037	0.041	0.039
Total	4.03	4.02	4.04	4.03	4.03	4.03	4.04	4.03	4.03	4.04	4.04	4.03	4.04	4.03
Wo%	43.70	45.37	45.33	42.35	45.57	44.91	44.26	44.27	41.10	45.78	42.54	44.79	45.47	45.25
En%	41.92	41.10	40.82	42.99	41.18	43.05	41.94	42.43	43.72	41.53	43.78	42.79	42.17	40.74
Fs%	14.38	13.53	13.85	14.66	13.25	12.04	13.80	13.30	15.19	12.69	13.68	12.42	12.36	14.01
Mg#	74.46	75.23	74.67	74.58	75.66	78.14	75.24	76.13	74.22	76.60	76.19	77.50	77.34	74.41

Table A4.8 Orthopyroxene analyses, from Zone IV

Sample#	ZAa-1	ZAa-1	ZAa-1	ZAa-1	ZAa-1	ZAa-1	ZAa-1	ZAa-2	ZAa-2	ZAa-2	ZAa-3	ZAa-3	ZAa-3	ZAa-4	ZAa-4	ZAa-4
Si2O	53.88	53.02	53.42	53.44	53.08	52.68	53.19	54.53	54.07	53.98	52.43	52.98	52.79	52.95	53.06	52.88
Ti2O	0.24	0.64	0.28	0.25	0.33	0.43	0.24	0.38	0.22	0.40	1.34	0.18	0.41	0.22	0.28	0.17
Al2O3	1.32	1.36	1.35	1.46	1.71	1.64	1.88	1.55	1.61	1.62	1.74	1.80	1.25	1.82	1.95	1.20
Cr2O3	0.10	0.05	0.02	0.06	0.13	0.00	0.00	0.04	0.03	0.03	0.12	0.02	0.06	0.04	0.07	0.00
FeO	17.75	16.61	16.90	16.58	16.98	18.49	16.28	13.87	13.81	13.97	16.89	18.38	18.88	18.23	17.88	19.16
MnO	0.62	0.56	0.59	0.45	0.49	0.27	0.45	0.29	0.33	0.38	0.33	0.36	0.38	0.53	0.39	0.63
MgO	26.58	26.54	26.43	26.48	25.90	25.32	26.16	28.71	27.77	27.92	25.47	25.23	24.70	25.51	25.21	24.95
CaO	0.70	1.25	1.17	1.54	1.57	1.12	1.88	1.46	2.11	1.44	1.79	1.52	1.44	1.03	1.47	1.18
Na2O	0.28	0.11	0.17	0.18	0.07	0.16	0.25	0.03	0.14	0.09	0.19	0.10	0.16	0.00	0.36	0.25
Total	101.47	100.14	100.34	100.44	100.27	100.11	100.34	100.89	100.09	99.84	100.31	100.58	100.06	100.33	100.68	100.43
Si	1.942	1.932	1.943	1.941	1.935	1.933	1.930	1.941	1.945	1.944	1.915	1.934	1.945	1.934	1.932	1.942
Ti	0.007	0.018	0.008	0.007	0.009	0.012	0.007	0.010	0.006	0.011	0.037	0.005	0.011	0.006	0.008	0.005
Al	0.056	0.058	0.058	0.063	0.074	0.071	0.081	0.065	0.068	0.069	0.075	0.078	0.054	0.078	0.084	0.052
Cr	0.003	0.002	0.001	0.002	0.004	0.000	0.000	0.001	0.001	0.001	0.004	0.001	0.002	0.001	0.002	0.000
Fe	0.535	0.506	0.514	0.504	0.518	0.567	0.494	0.413	0.415	0.421	0.516	0.561	0.582	0.557	0.544	0.588
Mn	0.019	0.017	0.018	0.014	0.015	0.008	0.014	0.009	0.010	0.012	0.010	0.011	0.012	0.016	0.012	0.020
Mg	1.428	1.441	1.433	1.434	1.408	1.385	1.415	1.523	1.489	1.499	1.387	1.373	1.356	1.389	1.368	1.366
Ca	0.027	0.049	0.046	0.060	0.061	0.044	0.073	0.056	0.082	0.056	0.070	0.059	0.057	0.040	0.057	0.046
Na	0.020	0.008	0.012	0.012	0.005	0.011	0.018	0.002	0.010	0.006	0.014	0.007	0.011	0.000	0.025	0.018
Total	4.036	4.031	4.033	4.035	4.028	4.031	4.032	4.020	4.026	4.018	4.028	4.030	4.030	4.022	4.032	4.037
Wo%	1.37	2.45	2.29	3.00	3.09	2.21	3.69	2.80	4.10	2.82	3.55	2.98	2.84	2.02	2.91	2.32
Enst%	71.76	72.20	71.91	71.78	70.86	69.38	71.39	76.48	74.98	75.88	70.30	68.88	67.99	69.94	69.46	68.27
Fs%	26.87	25.35	25.80	25.22	26.05	28.41	24.92	20.72	20.91	21.30	26.15	28.15	29.17	28.04	27.63	29.41
Mg#	72.75	74.01	73.59	74.00	73.12	70.94	74.13	78.68	78.19	78.08	72.88	70.99	69.98	71.38	71.54	69.89

Sample #	ZAa-7	ZAa-7	ZAa-7	ZAa-8	ZAa-8	ZAa-8	ZAa-8	ZAa-8
Si2O	54.09	53.96	53.88	54.15	53.89	53.78	53.60	53.06
Ti2O	0.26	0.31	0.42	0.35	0.32	0.42	0.41	0.28
Al2O3	1.31	1.50	1.54	1.75	1.67	1.44	1.54	1.95
Cr2O3	0.06	0.10	0.04	0.24	0.28	0.12	0.15	0.07
FeO	14.06	15.44	15.67	13.95	14.58	14.73	14.33	17.88
MnO	0.38	0.36	0.34	0.37	0.34	0.40	0.35	0.39
MgO	26.32	27.83	27.40	28.54	28.18	27.93	27.00	25.21
CaO	3.23	1.07	1.06	1.02	0.79	0.83	2.14	1.47
Na2O	0.07	0.13	0.04	0.23	0.00	0.13	0.10	0.36
Total	99.79	100.69	100.38	100.61	100.05	99.78	99.61	100.68
Si	1.958	1.939	1.941	1.933	1.938	1.943	1.943	1.932
Ti	0.007	0.008	0.012	0.010	0.009	0.012	0.011	0.008
Al	0.056	0.063	0.066	0.074	0.071	0.061	0.066	0.084
Cr	0.002	0.003	0.001	0.007	0.008	0.003	0.004	0.002
Fe	0.426	0.464	0.472	0.417	0.438	0.445	0.434	0.544
Mn	0.012	0.011	0.010	0.011	0.010	0.012	0.011	0.012
Mg	1.420	1.491	1.471	1.519	1.511	1.504	1.459	1.368
Ca	0.125	0.041	0.041	0.039	0.030	0.032	0.083	0.057
Na	0.005	0.009	0.003	0.016	0.000	0.009	0.007	0.025
Total	4.011	4.029	4.017	4.025	4.015	4.022	4.018	4.032
Wo%	6.36	2.07	2.07	1.97	1.54	1.63	4.20	2.91
Enst%	72.04	74.69	74.14	76.93	76.31	75.90	73.82	69.46
Fs%	21.60	23.24	23.79	21.09	22.15	22.47	21.98	27.63
Mg#	76.93	76.27	75.71	78.48	77.51	77.16	77.06	71.54

Table A4. 9 Clinopyroxene analyses , from Zone IV

Sample #	ZAa-1	ZAa-1	ZAa-1	ZAa-2	ZAa-2	ZAa-2	ZAa-2	ZAa-3	ZAa-3	ZAa-4	ZAa-4	ZAa-4	ZAa-5	ZAa-5	ZAa-5	ZAa-5	ZAa-5
Si2O	51.03	51.35	50.65	51.91	51.96	51.49	51.97	51.30	51.53	52.30	51.36	52.38	49.39	51.35	52.13	51.28	51.74
Ti2O	0.77	0.86	1.09	0.58	0.72	0.75	0.53	0.81	0.87	0.58	0.60	0.45	2.58	0.76	0.37	0.81	0.50
Al2O3	3.26	2.83	4.09	2.91	2.73	2.70	2.19	2.94	2.89	2.00	2.96	1.71	2.46	3.02	2.96	3.38	3.05
Cr2O3	0.06	0.07	0.35	0.12	0.12	0.13	0.07	0.13	0.11	0.08	0.05	0.08	0.02	0.03	0.02	0.56	0.27
FeO	7.56	9.59	7.57	7.51	7.71	8.26	8.39	7.86	7.33	7.68	8.05	7.37	11.26	8.45	7.76	5.76	7.07
MnO	0.20	0.26	0.27	0.17	0.29	0.32	0.18	0.30	0.28	0.27	0.14	0.29	0.22	0.22	0.15	0.24	0.21
MgO	15.00	15.77	14.59	14.99	15.23	15.22	15.19	15.31	14.73	15.05	14.51	14.81	15.57	15.72	15.32	15.58	15.11
CaO	21.70	19.57	21.50	21.97	21.53	21.59	21.64	21.36	22.59	22.31	22.01	22.85	18.30	20.40	21.18	22.23	21.39
Na2O	0.61	0.52	0.57	0.52	0.32	0.40	0.41	0.61	0.55	0.52	0.60	0.50	0.44	0.57	0.50	0.50	0.62
Total	100.19	100.81	100.68	100.66	100.61	100.84	100.57	100.63	100.88	100.80	100.29	100.44	100.24	100.51	100.38	100.33	99.94
Si	1.894	1.899	1.871	1.915	1.917	1.904	1.925	1.898	1.902	1.931	1.909	1.941	1.854	1.899	1.924	1.888	1.916
Ti	0.022	0.024	0.030	0.016	0.020	0.021	0.015	0.022	0.024	0.016	0.017	0.013	0.073	0.021	0.010	0.022	0.014
Al	0.143	0.124	0.178	0.126	0.119	0.118	0.096	0.128	0.126	0.087	0.130	0.075	0.109	0.132	0.129	0.147	0.133
Cr	0.002	0.002	0.010	0.004	0.004	0.004	0.002	0.004	0.003	0.002	0.002	0.002	0.001	0.001	0.001	0.016	0.008
Fe	0.235	0.297	0.234	0.232	0.238	0.255	0.260	0.243	0.226	0.237	0.250	0.229	0.354	0.261	0.240	0.178	0.219
Mn	0.006	0.008	0.009	0.005	0.009	0.010	0.006	0.010	0.009	0.008	0.005	0.009	0.007	0.007	0.005	0.008	0.007
Mg	0.830	0.869	0.803	0.824	0.838	0.839	0.838	0.845	0.810	0.829	0.804	0.818	0.871	0.867	0.843	0.855	0.834
Ca	0.863	0.776	0.851	0.869	0.851	0.856	0.859	0.847	0.894	0.883	0.877	0.908	0.736	0.808	0.838	0.877	0.848
Na	0.044	0.037	0.041	0.037	0.023	0.029	0.030	0.043	0.039	0.037	0.043	0.036	0.032	0.041	0.036	0.035	0.044
Total	4.037	4.036	4.026	4.028	4.018	4.034	4.030	4.040	4.034	4.030	4.037	4.030	4.036	4.036	4.024	4.026	4.022
Wo%	44.77	39.96	45.08	45.13	44.18	43.88	43.89	43.78	46.30	45.30	45.39	46.44	37.53	41.75	43.63	45.93	44.63
Enst%	43.06	44.77	42.54	42.83	43.47	43.02	42.84	43.65	41.99	42.53	41.65	41.86	44.44	44.76	43.90	44.77	43.86
Fs%	12.17	15.27	12.38	12.03	12.35	13.10	13.27	12.57	11.71	12.18	12.96	11.69	18.03	13.49	12.48	9.29	11.51
Mg#	77.96	74.57	77.46	78.07	77.87	76.66	76.34	77.64	78.19	77.74	76.27	78.17	71.14	76.84	77.87	82.81	79.21

Sample #	ZAb-2*	ZAb-2*	ZAb-2*	ZAb-2*	ZAb-2*	ZAb-2*	ZAb-2*	ZAb-3*	ZAb-3*	ZAb-3*	ZAb-3*	ZAb-3*	ZAb-4	ZAb-4	ZAb-5	ZAb-5	ZAb-5	ZAb-5
Si2O	48.29	50.01	49.77	50.03	50.24	49.93	49.45	49.35	49.96	50.02	48.61	49.72	49.90	50.45	50.00	49.92	49.77	50.62
Ti2O	1.51	1.25	1.29	1.20	1.39	1.15	1.47	1.56	1.28	1.32	1.31	1.29	1.11	1.08	1.02	1.09	1.14	0.82
Al2O3	3.66	4.15	4.08	3.93	4.61	3.81	4.27	3.82	3.91	3.69	3.88	3.80	4.08	3.82	3.66	3.51	4.07	3.24
Cr2O3	0.30	0.24	0.10	0.18	0.14	0.30	0.15	0.05	0.17	0.08	0.20	0.21	0.18	0.09	0.14	0.16	0.17	0.13
FeO	10.02	6.66	6.92	6.65	6.70	6.91	6.65	7.94	7.97	8.00	9.87	6.94	6.81	7.28	7.21	8.33	6.76	7.00
MnO	0.16	0.17	0.15	0.15	0.18	0.13	0.16	0.17	0.17	0.17	0.15	0.16	0.16	0.25	0.16	0.11	0.20	0.00
MgO	14.29	14.92	14.41	14.71	14.58	14.82	14.33	14.10	14.93	14.81	14.53	14.28	14.71	15.40	14.91	15.45	14.49	14.74
CaO	21.04	21.83	21.93	22.10	22.74	22.52	22.42	22.71	21.32	21.79	21.27	22.72	22.02	21.75	21.76	20.41	22.82	22.30
Na2O	0.58	0.80	0.72	0.72	0.43	0.46	0.42	0.46	0.52	0.41	0.52	0.57	0.60	0.55	0.62	0.51	0.61	0.60
Total	99.86	100.04	99.36	99.67	101.00	100.02	99.32	100.16	100.22	100.29	100.32	99.70	99.55	100.66	99.48	99.49	100.01	99.45
Si	1.827	1.856	1.862	1.864	1.848	1.858	1.851	1.845	1.858	1.861	1.827	1.859	1.862	1.863	1.868	1.868	1.854	1.890
Ti	0.043	0.035	0.036	0.034	0.038	0.032	0.041	0.044	0.036	0.037	0.037	0.036	0.031	0.030	0.029	0.031	0.032	0.023
Al	0.163	0.182	0.180	0.173	0.200	0.167	0.188	0.168	0.171	0.162	0.172	0.168	0.179	0.166	0.161	0.155	0.179	0.143
Cr	0.009	0.007	0.003	0.005	0.004	0.009	0.005	0.001	0.005	0.002	0.006	0.006	0.005	0.003	0.004	0.005	0.005	0.004
Fe	0.317	0.207	0.216	0.207	0.206	0.215	0.208	0.248	0.248	0.249	0.310	0.217	0.212	0.225	0.225	0.261	0.211	0.219
Mn	0.005	0.005	0.005	0.005	0.006	0.004	0.005	0.006	0.006	0.005	0.005	0.005	0.005	0.008	0.005	0.004	0.006	0.000
Mg	0.806	0.826	0.804	0.817	0.799	0.822	0.799	0.786	0.827	0.821	0.814	0.796	0.818	0.848	0.830	0.862	0.805	0.821
Ca	0.853	0.868	0.879	0.883	0.896	0.898	0.899	0.910	0.849	0.869	0.857	0.910	0.880	0.860	0.871	0.819	0.910	0.892
Na	0.043	0.058	0.052	0.052	0.031	0.034	0.031	0.034	0.037	0.030	0.038	0.042	0.044	0.039	0.045	0.037	0.044	0.043
Total	4.066	4.043	4.037	4.039	4.027	4.039	4.027	4.043	4.037	4.035	4.066	4.039	4.037	4.042	4.039	4.040	4.045	4.035
Wo%	43.16	45.68	46.29	46.29	47.13	46.40	47.15	46.80	44.13	44.80	43.24	47.32	46.06	44.52	45.21	42.17	47.29	46.19
Enst%	40.79	43.45	42.31	42.85	42.03	42.49	41.93	40.43	42.99	42.37	41.10	41.39	42.82	43.85	43.10	44.41	41.78	42.49
Fs%	16.05	10.87	11.39	10.87	10.83	11.12	10.92	12.77	12.89	12.83	15.66	11.29	11.12	11.63	11.69	13.42	10.93	11.31
Mg#	71.76	79.99	78.78	79.77	79.51	79.26	79.33	75.99	76.94	76.75	72.41	78.57	79.39	79.04	78.66	76.79	79.26	78.97

Table A4.9 (Con't)

Sample #	Z4b-6	Z4b-6	Z4b-6	Z4b-6	Z4b-6	Z4b-7	Z4b-7	Z4b-8	Z4b-8	Z4b-8	Z4b-8	Z4b-8	Z4b-9*	Z4b-9*	Z4b-9*	Z4b-9*	Z4b-10*	Z4b-10*
Si2O	49.50	49.92	49.51	50.38	49.81	49.81	50.33	51.58	49.48	49.99	50.86	49.40	49.96	50.85	50.09	51.17	52.18	49.81
Ti2O	1.35	1.06	1.14	1.04	1.17	1.11	0.92	0.97	1.28	1.10	1.18	1.23	1.12	1.00	1.14	0.74	0.43	1.28
Al2O3	3.79	3.79	4.10	3.49	4.19	4.15	3.94	3.48	4.04	3.61	3.71	4.15	3.35	3.18	3.49	2.55	1.31	3.79
Cr2O3	0.08	0.18	0.12	0.10	0.18	0.33	0.20	0.00	0.27	0.12	0.09	0.09	0.03	0.03	0.17	0.02	0.08	0.11
FeO	8.22	6.76	7.25	6.99	7.11	6.66	6.79	7.29	6.95	7.02	7.45	7.17	8.66	7.28	6.86	11.40	7.39	6.94
MnO	0.14	0.14	0.21	0.19	0.00	0.16	0.16	0.17	0.13	0.18	0.21	0.19	0.23	0.24	0.23	0.34	0.18	0.18
MgO	15.00	14.54	14.35	14.85	14.64	14.16	14.07	14.99	14.28	14.51	14.71	14.72	15.57	14.47	14.21	17.20	14.86	14.13
CaO	20.78	22.56	22.13	21.92	21.81	22.11	21.53	21.24	22.12	22.48	21.85	21.29	20.30	22.59	22.66	16.09	22.26	22.38
Na2O	0.54	0.59	0.65	0.43	0.76	0.47	0.70	0.43	0.62	0.47	0.59	0.61	0.57	0.59	0.58	0.40	0.46	0.58
Total	99.39	99.53	99.45	99.39	99.65	98.96	98.63	100.17	99.16	99.47	100.65	98.85	99.78	100.22	99.41	99.91	99.15	99.19
Si	1.857	1.866	1.856	1.882	1.858	1.868	1.890	1.904	1.857	1.870	1.878	1.856	1.868	1.890	1.876	1.906	1.954	1.869
Ti	0.038	0.030	0.032	0.029	0.033	0.031	0.026	0.027	0.036	0.031	0.033	0.035	0.032	0.028	0.032	0.021	0.012	0.036
Al	0.168	0.167	0.181	0.154	0.184	0.183	0.174	0.152	0.179	0.159	0.162	0.184	0.148	0.139	0.154	0.112	0.058	0.168
Cr	0.002	0.005	0.004	0.003	0.005	0.010	0.006	0.000	0.008	0.003	0.003	0.003	0.001	0.001	0.005	0.001	0.003	0.003
Fe	0.258	0.211	0.227	0.218	0.222	0.209	0.213	0.225	0.218	0.220	0.230	0.225	0.271	0.226	0.215	0.355	0.231	0.218
Mn	0.005	0.005	0.007	0.006	0.000	0.005	0.005	0.005	0.004	0.006	0.007	0.006	0.007	0.008	0.007	0.011	0.006	0.006
Mg	0.839	0.810	0.802	0.827	0.814	0.792	0.788	0.825	0.799	0.810	0.810	0.824	0.868	0.802	0.793	0.956	0.830	0.790
Ca	0.835	0.903	0.889	0.877	0.872	0.889	0.866	0.840	0.890	0.901	0.865	0.857	0.813	0.900	0.909	0.642	0.893	0.900
Na	0.039	0.043	0.047	0.031	0.055	0.034	0.051	0.031	0.045	0.034	0.043	0.044	0.041	0.042	0.042	0.029	0.033	0.042
Total	4.040	4.040	4.044	4.027	4.042	4.021	4.019	4.009	4.036	4.034	4.028	4.034	4.048	4.035	4.033	4.032	4.020	4.031
Wo%	43.22	46.94	46.34	45.63	45.70	47.04	46.39	44.45	46.66	46.69	45.40	44.95	41.67	46.68	47.42	32.89	45.71	47.16
Enst%	43.43	42.09	41.80	43.01	42.68	41.91	42.19	43.64	41.91	41.93	42.51	43.23	44.46	41.59	41.37	48.92	42.45	41.42
Fs%	13.35	10.97	11.85	11.36	11.62	11.06	11.42	11.91	11.43	11.38	12.08	11.82	13.87	11.73	11.20	18.19	11.84	11.42
Mg#	76.49	79.32	77.91	79.10	78.60	79.13	78.71	78.56	78.57	78.65	77.87	78.53	76.22	78.00	78.69	72.90	78.19	78.39

Sample #	Z4b-10*	Z4b-10*	Z4b-11	Z4b-11	Z4b-11	Z4b-12	Z4b-12	Z4b-12	Z4b-12	Z4b-12	Z4b-12	Z4b-13	Z4b-13	Z4b-14	Z4b-14	Z4b-14	Z4b-14
SiO2	50.45	49.29	51.12	50.06	51.03	50.76	50.37	49.51	49.84	50.06	50.38	50.17	49.39	49.09	49.42	49.99	49.72
TiO2*	1.17	1.43	0.75	1.10	0.79	0.71	0.94	1.24	1.01	0.88	0.80	1.10	1.10	1.28	1.24	0.96	1.00
Al2O3	3.39	3.89	2.95	3.54	3.17	3.06	3.73	4.11	3.71	3.57	3.77	3.40	3.71	4.16	3.61	3.40	3.43
Cr2O3*	0.11	0.10	0.32	0.14	0.26	0.28	0.32	0.25	0.19	0.32	0.28	0.05	0.19	0.31	0.11	0.22	0.26
FeO	7.98	7.32	6.73	7.84	6.57	6.21	5.93	7.15	7.20	7.01	6.46	8.51	9.76	7.30	9.12	8.90	8.99
MnO*	0.15	0.14	0.15	0.23	0.22	0.06	0.03	0.13	0.16	0.21	0.14	0.25	0.14	0.19	0.14	0.12	0.11
MgO	15.70	14.28	15.53	15.24	15.52	15.63	14.85	14.62	14.55	14.66	15.61	15.79	15.54	14.01	14.84	15.11	15.44
CaO	20.42	21.98	21.25	20.33	21.26	21.81	22.65	21.82	21.76	21.41	21.54	19.66	18.41	21.61	20.13	19.85	19.56
Na2O	0.43	0.48	0.46	0.45	0.46	0.55	0.52	0.57	0.55	0.52	0.60	0.58	0.47	0.66	0.47	0.62	0.58
Total	99.80	98.91	99.27	98.94	99.28	99.07	99.34	99.39	98.96	98.65	99.59	99.51	98.71	98.61	99.10	99.16	99.09
Si	1.877	1.857	1.906	1.881	1.899	1.895	1.877	1.855	1.873	1.883	1.874	1.876	1.867	1.855	1.866	1.880	1.872
Ti	0.033	0.040	0.021	0.031	0.022	0.020	0.026	0.035	0.029	0.025	0.022	0.031	0.031	0.037	0.035	0.027	0.028
Al	0.149	0.173	0.130	0.157	0.139	0.135	0.164	0.182	0.164	0.158	0.165	0.150	0.165	0.186	0.161	0.151	0.152
Cr	0.003	0.003	0.009	0.004	0.008	0.008	0.009	0.007	0.006	0.010	0.008	0.002	0.006	0.009	0.003	0.006	0.008
Fe	0.248	0.231	0.210	0.246	0.204	0.194	0.185	0.224	0.226	0.221	0.201	0.266	0.309	0.231	0.288	0.280	0.283
Mn	0.005	0.004	0.005	0.007	0.007	0.002	0.001	0.004	0.005	0.007	0.005	0.008	0.005	0.006	0.005	0.004	0.004
Mg	0.871	0.802	0.863	0.853	0.861	0.870	0.825	0.817	0.815	0.822	0.866	0.880	0.876	0.789	0.836	0.847	0.866
Ca	0.814	0.887	0.849	0.818	0.848	0.872	0.905	0.876	0.876	0.863	0.859	0.787	0.746	0.875	0.815	0.800	0.789
Na	0.031	0.035	0.033	0.033	0.033	0.040	0.038	0.042	0.040	0.038	0.044	0.042	0.034	0.048	0.035	0.045	0.042
Total	4.030	4.033	4.03	4.03	4.02	4.04	4.03	4.04	4.03	4.03	4.04	4.041	4.038	4.035	4.043	4.040	4.045
Wo%	42.11	46.21	44.18	42.66	44.31	45.06	47.25	45.71	45.68	45.28	44.61	40.73	38.63	46.19	42.04	41.52	40.71
En%	45.05	41.77	44.90	44.49	45.01	44.92	43.09	42.61	42.51	43.14	44.96	45.52	45.38	41.65	43.11	43.95	44.69
Fs%	12.84	12.01	10.92	12.84	10.68	10.02	9.66	11.68	11.80	11.58	10.44	13.76	15.99	12.17	14.85	14.53	14.60
Mg#	77.81	77.66	80.43	77.60	80.82	81.77	81.69	78.48	78.27	78.84	81.16	76.79	73.94	77.39	74.37	75.16	75.38

Table A4.9 (Con't)

Sample #	Z4b-15*1	Z4b-15*1	Z4b-15*1	Z4b-15*1	Z4b-15*1	Z4a-8pc	Z4b-16	Z4b-16	Z4b-16	Z4b-16
SiO2	49.32	49.68	49.43	49.43	49.77	51.42	50.13	50.62	50.02	49.78
TiO2	1.39	1.31	1.39	1.42	1.13	0.00	1.24	0.87	1.17	1.20
Al2O3	4.15	3.35	3.53	4.31	4.17	0.05	3.58	3.26	3.39	4.06
Cr2O3	0.44	0.30	0.33	0.45	0.75	0.00	0.21	0.10	0.09	0.28
FeO	7.48	7.17	7.36	6.25	6.74	0.33	7.03	6.96	7.99	7.44
MnO	0.17	0.19	0.25	0.15	0.11	0.16	0.15	0.14	0.21	0.20
MgO	14.16	14.53	14.38	14.23	15.34	0.00	14.43	14.89	14.81	14.00
CaO	21.81	21.98	21.71	23.00	21.08	48.96	22.55	22.06	20.56	22.21
N2O	0.48	0.66	0.62	0.43	0.25	0.00	0.36	0.42	0.54	0.65
Total	99.40	99.16	99.01	99.67	99.34	100.93	99.69	99.31	98.79	99.81
Si	1.850	1.868	1.862	1.845	1.856	1.981	1.871	1.891	1.883	1.860
Ti	0.039	0.037	0.040	0.040	0.032	0.000	0.035	0.025	0.033	0.034
Al	0.184	0.148	0.157	0.190	0.183	0.002	0.158	0.144	0.151	0.179
Cr	0.013	0.009	0.010	0.013	0.022	0.000	0.006	0.003	0.003	0.008
Fe	0.235	0.226	0.232	0.195	0.210	0.011	0.220	0.217	0.251	0.233
Mn	0.005	0.006	0.008	0.005	0.003	0.005	0.005	0.005	0.007	0.006
Mg	0.792	0.814	0.808	0.791	0.852	0.000	0.803	0.829	0.831	0.780
Ca	0.877	0.885	0.876	0.920	0.842	2.021	0.902	0.883	0.829	0.889
Na	0.035	0.048	0.045	0.031	0.018	0.000	0.026	0.031	0.039	0.047
Total	4.030	4.041	4.038	4.030	4.019	4.021	4.025	4.027	4.027	4.036
Wo%	46.06	45.99	45.74	48.24	44.21	99.47	46.86	45.76	43.39	46.76
En%	41.61	42.30	42.16	41.52	44.76	0.00	41.73	42.97	43.46	41.01
Fs%	12.33	11.71	12.10	10.24	11.04	0.53	11.41	11.27	13.15	12.23
Mg#	77.14	78.31	77.69	80.21	80.22	0.00	78.53	79.23	76.77	77.02

PLAGIOCLASE ANALYSES

Cations calculated on the basis of 8 oxygens.

An% =Ca*100/(Ca+Na+K);

Ab% = Na*100/(Ca+Na+K);

Or% = K*100/(Ca+Na+K).

Table A4.10 Plagioclase analyses, from Zone I.

Sample #	Z1-1	Z1-1	Z1-1	Z1-1	Z1-2	Z1-2	Z1-2	Z1-2	Z1-2	Z1-2	Z1-2	Z1-2	Z1-2	Z1-2	Z1-2	Z1-3	Z1-3
Grain #	n2	n6	n6	n1	n3	n3	n3	n3	n3	n3	n3	n3	n4	n4	n4	n1	n5	n5
P.Loc.	core	core	rim	core	rim	mid	core	core	mid	mid	pth	rim	core	rim	mid	core	core	core
SiO2	47.01	47.06	54.64	47.06	47.37	47.43	47.03	47.75	47.49	47.44	46.14	47.87	48.24	46.36	47.54	47.75	48.66	48.18
Al2O3	33.69	33.84	28.64	33.84	32.85	32.94	33.40	33.30	33.15	32.49	33.68	33.16	33.08	33.55	32.93	33.30	33.18	33.00
FeO	0.19	0.16	0.00	0.16	0.29	0.13	0.25	0.27	0.35	0.33	0.26	0.19	0.26	0.32	0.08	0.27	0.28	0.17
CaO	16.68	16.64	10.80	16.64	16.28	16.43	16.80	16.51	16.55	16.21	17.06	16.43	16.19	16.82	16.04	16.51	15.88	15.84
Na2O	2.09	1.94	5.17	1.94	2.11	2.16	1.94	1.91	2.07	2.26	1.59	2.09	2.25	1.74	2.25	1.91	2.37	2.11
K2O	0.00	0.00	0.18	0.00	0.04	0.03	0.02	0.00	0.01	0.09	0.06	0.04	0.05	0.01	0.06	0.00	0.05	0.00
Total	99.65	99.64	99.43	99.64	98.93	99.11	99.45	99.73	99.60	98.82	98.79	99.77	100.07	98.80	98.89	99.73	100.42	99.30
Si	2.166	2.166	2.475	2.166	2.196	2.195	2.172	2.194	2.188	2.204	2.147	2.199	2.208	2.156	2.201	2.194	2.217	2.217
Al	1.829	1.836	1.529	1.836	1.795	1.796	1.818	1.803	1.800	1.779	1.847	1.795	1.785	1.839	1.797	1.803	1.782	1.790
Fe	0.007	0.006	0.000	0.006	0.011	0.005	0.010	0.011	0.013	0.013	0.010	0.007	0.010	0.012	0.003	0.011	0.011	0.007
Ca	0.824	0.821	0.524	0.821	0.809	0.814	0.832	0.813	0.817	0.807	0.851	0.808	0.794	0.838	0.796	0.813	0.775	0.781
Na	0.186	0.173	0.454	0.173	0.189	0.193	0.174	0.170	0.185	0.204	0.143	0.186	0.200	0.157	0.202	0.170	0.209	0.188
K	0.000	0.000	0.010	0.000	0.002	0.002	0.001	0.000	0.000	0.005	0.004	0.002	0.003	0.001	0.004	0.000	0.003	0.000
Total	5.012	5.002	4.993	5.002	5.002	5.005	5.007	4.990	5.004	5.011	5.002	4.998	5.000	5.003	5.003	4.990	4.998	4.982
An%	81.55	82.60	53.02	82.60	80.84	80.65	82.58	82.71	81.54	79.43	85.30	81.11	79.66	84.18	79.44	82.71	78.52	80.60
Ab%	18.45	17.40	45.92	17.40	18.92	19.16	17.29	17.29	18.42	20.07	14.35	18.65	20.02	15.77	20.20	17.29	21.20	19.40
Or%	0.00	0.00	1.06	0.00	0.25	0.18	0.13	0.00	0.05	0.50	0.35	0.25	0.32	0.06	0.36	0.00	0.28	0.00

Sample #	Z1-3	Z1-5	Z1-5	Z1-5	Z1-5	Z1-6	Z1-6	Z1-6	Z1-7	Z1-7	Z1-7	Z1-7	Z1-7	Z1-7
Grain #	n1	n1	n1	n1	n1	n2	n2	n4	n1	n1	n3	n6	n8	n9
P.Loc	core	core	rim	rim	core	rim	core	core	PC	PC	PC	PC	PC	PC
SiO2	48.18	46.42	52.74	52.79	46.42	54.52	46.89	48.35	46.89	48.42	50.75	48.42	49.34	51.50
Al2O3	33.00	34.64	29.61	29.72	34.64	29.00	34.01	33.33	34.01	32.26	31.88	32.26	31.85	30.32
FeO	0.17	0.22	0.27	0.16	0.22	0.22	0.21	0.21	0.21	0.27	0.16	0.27	0.29	0.14
CaO	15.84	17.14	11.32	11.69	17.14	11.25	17.10	16.24	17.10	15.65	14.47	15.65	14.98	13.44
Na2O	2.11	1.74	5.11	4.85	1.74	5.19	1.88	2.19	1.88	2.69	3.22	2.69	2.99	3.79
K2O	0.00	0.00	0.20	0.17	0.00	0.17	0.04	0.00	0.04	0.00	0.06	0.00	0.05	0.00
Total	99.30	100.16	99.26	99.38	100.16	100.35	100.12	100.32	100.12	99.29	100.54	99.29	99.50	99.19
Si	2.217	2.131	2.407	2.405	2.131	2.455	2.153	2.206	2.153	2.233	2.298	2.233	2.266	2.357
Al	1.790	1.874	1.593	1.596	1.874	1.539	1.840	1.792	1.840	1.754	1.701	1.754	1.724	1.636
Fe	0.007	0.008	0.010	0.006	0.008	0.008	0.008	0.008	0.008	0.010	0.006	0.010	0.011	0.005
Ca	0.781	0.843	0.554	0.571	0.843	0.543	0.841	0.794	0.841	0.773	0.702	0.773	0.737	0.659
Na	0.188	0.154	0.452	0.429	0.154	0.453	0.168	0.194	0.168	0.241	0.283	0.241	0.266	0.336
K	0.000	0.000	0.012	0.010	0.000	0.010	0.002	0.000	0.002	0.000	0.003	0.000	0.003	0.000
Total	4.982	5.010	5.028	5.016	5.010	5.007	5.012	4.995	5.012	5.011	4.994	5.011	5.007	4.993
An%	80.60	84.49	54.42	56.56	84.49	53.96	83.21	80.37	83.21	76.25	71.03	76.25	73.24	66.25
Ab%	19.40	15.49	44.42	42.49	15.49	45.04	16.59	19.63	16.59	23.75	28.64	23.75	26.46	33.75
Or%	0.00	0.03	1.16	0.95	0.03	0.99	0.20	0.00	0.20	0.00	0.33	0.00	0.30	0.00

Table A4.10 (Con't)

Sample #	Z1-8	Z1-8	Z1-8	Z1-9	Z1-9	Z1-9	Z1-9	Z1-9	Z1-9	Z1-9	Z1-9	Z1-9	Z1-9
Grain #	n1	n4	n11	n1	n1	n1	n1	n3	n3	n5	n5	n5	n1
P.Loc	PC	PC	PC	PC	PC	PC	PC	PC	PC	PC	PC	PC	PC
SiO2	52.26	59.42	52.26	54.50	54.60	51.70	52.10	52.30	51.40	52.70	52.40	55.70	51.40
Al2O3	29.35	24.26	29.35	28.80	29.10	30.40	30.30	30.50	30.80	30.30	29.70	28.20	30.80
FeO	1.00	0.00	1.00	0.00	0.20	0.10	0.20	0.40	0.10	0.00	0.20	0.10	0.10
CaO	11.71	6.15	11.71	11.50	11.70	13.90	13.60	13.20	14.00	13.10	12.90	10.60	14.00
Na2O	4.79	1.69	4.79	4.70	4.60	3.50	3.50	3.50	3.30	4.00	3.60	5.00	3.30
K2O	0.14	7.87	0.14	0.10	0.10	0.10	0.20	0.00	0.10	0.10	0.10	0.10	0.10
Total	99.25	99.38	99.25	99.60	100.30	99.70	99.90	99.90	99.70	100.20	98.90	99.70	99.70
Si	2.396	2.717	2.396	2.465	2.456	2.356	2.368	2.372	2.342	2.383	2.398	2.509	2.342
Al	1.586	1.307	1.586	1.535	1.543	1.632	1.623	1.630	1.654	1.615	1.602	1.497	1.654
Fe	0.038	0.000	0.038	0.000	0.008	0.004	0.008	0.015	0.004	0.000	0.008	0.004	0.004
Ca	0.575	0.301	0.575	0.557	0.564	0.679	0.662	0.641	0.683	0.635	0.632	0.512	0.683
Na	0.425	0.149	0.425	0.412	0.401	0.309	0.308	0.308	0.291	0.351	0.319	0.437	0.291
K	0.008	0.459	0.008	0.006	0.006	0.006	0.012	0.000	0.006	0.006	0.006	0.006	0.006
Total	5.028	4.934	5.028	4.976	4.976	4.986	4.981	4.967	4.980	4.988	4.964	4.964	4.980
An%	57.00	33.09	57.00	57.15	58.08	68.30	67.42	67.58	69.68	64.04	66.04	53.63	69.68
Ab%	42.17	16.43	42.17	42.26	41.32	31.12	31.40	32.42	29.72	35.38	33.35	45.77	29.72
Or%	0.83	50.48	0.83	0.59	0.59	0.59	1.18	0.00	0.59	0.58	0.61	0.60	0.59

Table A4.11 Plagioclase analyses, from Zone II.

Sample #	Z2-1	Z2-1	Z2-1	Z2-1	Z2-2	Z2-2	Z2-2	Z2-2	Z2-2	Z2-2	Z2-2	Z2-2	Z2-2	Z2-2	Z2-2	Z2-3	Z2-3	Z2-3
Grain #	n1	n2	n3	n4	n5/6	n1	n5-6	n5-6	n5-6	n1	n1	n1	n1	n1	n1	p2	p2	p2
P.Loc.	PC	PC	PC	PC	rim	rim	core	mid	rim	rim	rim	rim	core	mid	rim	rim	rim	mid
Si02	56.82	58.43	50.13	58.36	58.34	60.75	54.78	56.91	57.44	59.32	56.37	56.58	56.07	52.55	54.22	60.81	59.30	58.08
Al2O3	28.05	26.83	30.91	26.93	27.02	26.39	29.09	27.60	27.33	26.71	27.76	27.78	27.75	30.58	28.84	24.47	25.59	26.49
FeO	0.15	0.00	0.66	0.21	0.22	0.18	0.24	0.26	0.22	0.25	0.16	0.15	0.28	0.21	0.33	0.37	0.19	0.33
CaO	9.49	8.19	13.23	7.96	8.89	8.02	10.69	9.16	8.63	7.92	9.29	9.15	9.10	12.34	10.52	6.15	7.50	8.58
Na2O	5.74	6.29	3.19	5.59	6.06	4.99	4.65	5.07	4.63	4.28	5.33	5.01	6.17	4.71	5.52	7.46	7.05	6.54
K2O	0.00	0.00	0.00	0.00	0.24	0.29	0.19	0.34	0.27	0.30	0.27	0.24	0.37	0.24	0.31	0.45	0.35	0.19
Total	100.43	99.86	99.15	99.05	100.78	100.62	99.64	99.34	98.51	98.78	99.17	98.91	99.74	100.63	99.73	99.72	99.97	100.20
Si	2.538	2.609	2.322	2.616	2.590	2.672	2.472	2.561	2.592	2.653	2.544	2.554	2.529	2.371	2.457	2.713	2.649	2.597
Al	1.477	1.412	1.687	1.423	1.414	1.368	1.547	1.464	1.454	1.408	1.477	1.478	1.475	1.627	1.540	1.287	1.347	1.396
Fe	0.006	0.000	0.025	0.008	0.008	0.007	0.009	0.010	0.008	0.010	0.006	0.006	0.011	0.008	0.012	0.014	0.007	0.012
Ca	0.454	0.392	0.657	0.382	0.423	0.378	0.517	0.442	0.417	0.379	0.449	0.443	0.439	0.597	0.511	0.294	0.359	0.411
Na	0.497	0.544	0.286	0.486	0.522	0.425	0.407	0.443	0.405	0.371	0.466	0.438	0.540	0.412	0.485	0.645	0.610	0.567
K	0.000	0.000	0.000	0.000	0.014	0.017	0.011	0.019	0.015	0.017	0.015	0.014	0.021	0.014	0.018	0.026	0.020	0.011
Total	4.972	4.957	4.978	4.915	4.971	4.865	4.963	4.938	4.891	4.837	4.958	4.933	5.014	5.029	5.024	4.979	4.992	4.994
An%	47.77	41.84	69.65	44.02	44.12	46.11	55.33	48.87	49.82	49.45	48.25	49.49	43.94	58.34	50.37	30.49	36.29	41.57
Ab%	52.23	58.16	30.35	55.98	54.44	51.87	43.52	48.97	48.34	48.34	50.08	48.97	53.95	40.31	47.86	66.83	61.70	57.36
Or%	0.00	0.00	0.00	0.00	1.45	2.02	1.15	2.15	1.84	2.21	1.66	1.54	2.11	1.35	1.77	2.68	2.01	1.07

Sample #	Z2-3	Z2-3	Z2-3	Z2-3	Z2-3	Z2-3	Z2-3	Z2-3	Z2-3	Z2-3	Z2-3	Z2-3	Z2-3	Z2-3	Z2-3	Z2-3	Z2-3	Z2-3
Grain #	p2	p2	p2	n2	n2	n2	n2	n2	n2	n2	n2	n2	n2	p3	p3	p3	p3	p3
P.Loc.	mid	rim	rim	rim	mid	core	core	core	core	core	core	mid	rim	rim	mid	core	mid	rim
Si02	54.04	53.76	53.96	60.64	58.51	53.43	53.41	57.39	55.87	57.05	53.88	57.13	60.16	59.49	52.32	53.75	55.67	58.94
Al2O3	29.11	29.04	28.90	24.27	25.65	29.01	29.13	26.57	27.48	26.95	28.63	27.07	24.54	25.66	30.13	28.71	27.86	25.70
FeO	0.30	0.26	0.11	0.20	0.13	0.09	0.24	0.20	0.16	0.23	0.18	0.17	0.18	0.20	0.25	0.28	0.21	0.24
CaO	11.66	11.69	11.50	6.07	7.79	11.55	11.78	9.00	9.79	9.32	11.33	9.24	6.43	7.40	12.86	11.50	10.47	7.85
Na2O	4.89	4.73	4.77	7.24	6.66	4.78	4.69	5.95	5.75	6.07	5.02	6.09	7.35	6.69	4.27	4.78	5.68	6.78
K2O	0.22	0.18	0.16	0.60	0.46	0.20	0.23	0.40	0.33	0.38	0.23	0.32	0.48	0.40	0.13	0.20	0.28	0.45
Total	100.21	99.66	99.40	99.02	99.21	99.07	99.48	99.51	99.38	100.00	99.27	100.03	99.13	99.84	99.95	99.21	100.17	99.96
Si	2.440	2.440	2.451	2.722	2.636	2.437	2.430	2.585	2.529	2.563	2.454	2.564	2.701	2.656	2.377	2.449	2.507	2.637
Al	1.549	1.553	1.547	1.284	1.362	1.560	1.562	1.410	1.466	1.427	1.537	1.432	1.299	1.350	1.613	1.542	1.478	1.355
Fe	0.011	0.010	0.004	0.008	0.005	0.004	0.009	0.008	0.006	0.009	0.007	0.006	0.007	0.007	0.009	0.011	0.008	0.009
Ca	0.564	0.568	0.560	0.292	0.376	0.565	0.574	0.434	0.475	0.449	0.553	0.444	0.309	0.354	0.626	0.562	0.505	0.377
Na	0.428	0.416	0.420	0.630	0.582	0.422	0.414	0.520	0.504	0.529	0.443	0.530	0.640	0.579	0.376	0.422	0.496	0.588
K	0.012	0.010	0.009	0.034	0.026	0.012	0.013	0.023	0.019	0.022	0.013	0.019	0.027	0.022	0.008	0.012	0.016	0.026
Total	5.005	4.997	4.990	4.968	4.987	5.000	5.003	4.981	4.999	4.998	5.006	4.995	4.983	4.970	5.009	4.997	5.010	4.992
An%	56.17	57.13	56.59	30.54	38.23	56.53	57.33	44.43	47.57	44.91	54.78	44.76	31.68	37.03	61.99	56.42	49.67	38.02
Ab%	42.59	41.82	42.45	65.89	59.09	42.28	41.32	53.20	50.52	52.94	43.91	53.36	65.51	60.61	37.24	42.38	48.75	59.40
Or%	1.24	1.05	0.96	3.56	2.68	1.19	1.34	2.37	1.91	2.16	1.31	1.87	2.81	2.35	0.77	1.20	1.57	2.58

Table A4.11 (Con't)

Sample #	Z2-4	Z2-4	Z2-4	Z2-5	Z2-5	Z2-5	Z2-5	Z2-6	Z2-6	Z2-6	Z2-6	Z2-6	Z2-6	Z2-6	Z2-6	Z2-6	Z2-6	Z2-6
Grain #	n3	n4	n5	n2	n2	n3	n3	n4	n4	n4	n4	n4	n4	n1	n1	n2	n3	n1
P.Loc.	rim	core	rim	PC	PC	PC	PC	core	mid	rim	rim	rim	mid	core	core	core2	core	rim
Si02	60.20	57.40	57.60	58.54	54.08	53.28	56.33	54.98	56.96	56.08	55.71	55.23	55.01	51.54	55.57	55.35	55.13	56.47
Al2O3	25.70	26.90	27.20	26.35	28.29	29.54	26.94	29.31	27.46	28.00	28.58	29.05	28.72	30.78	28.88	28.40	28.59	27.79
FeO	0.40	0.20	0.30	0.19	0.17	0.20	0.07	0.15	0.25	0.23	0.15	0.21	0.30	0.29	0.30	0.30	0.23	0.00
CaO	7.60	9.00	9.50	7.51	10.14	11.40	8.52	11.39	9.91	10.39	11.03	11.09	11.35	12.53	10.13	9.59	10.27	9.67
Na2O	6.80	5.70	5.70	7.29	5.93	5.10	6.81	4.77	6.03	5.55	5.01	5.22	5.02	4.70	6.01	6.40	5.93	5.83
K2O	0.28	0.23	0.25	0.21	0.19	0.13	0.16	0.19	0.15	0.31	0.32	0.32	0.18	0.14	0.26	0.15	0.07	0.21
Total	100.98	99.43	100.55	100.09	98.81	99.64	98.83	100.65	100.52	100.32	100.65	100.90	100.58	99.99	101.15	100.19	100.23	99.97
Si	2.660	2.582	2.569	2.615	2.472	2.419	2.558	2.459	2.542	2.513	2.491	2.467	2.470	2.345	2.480	2.491	2.480	2.535
Al	1.338	1.426	1.430	1.387	1.523	1.581	1.442	1.545	1.444	1.478	1.506	1.529	1.520	1.651	1.519	1.507	1.516	1.470
Fe	0.015	0.008	0.011	0.007	0.006	0.008	0.003	0.006	0.009	0.009	0.006	0.008	0.011	0.011	0.011	0.011	0.009	0.000
Ca	0.360	0.434	0.454	0.359	0.497	0.554	0.415	0.546	0.474	0.499	0.528	0.530	0.546	0.611	0.484	0.462	0.495	0.465
Na	0.582	0.497	0.493	0.631	0.526	0.449	0.599	0.414	0.522	0.482	0.435	0.452	0.437	0.415	0.520	0.558	0.518	0.508
K	0.016	0.013	0.014	0.012	0.011	0.008	0.009	0.011	0.009	0.018	0.018	0.018	0.010	0.008	0.015	0.008	0.004	0.012
Total	4.970	4.960	4.970	5.013	5.035	5.018	5.025	4.981	5.001	4.998	4.983	5.004	4.994	5.041	5.028	5.039	5.022	4.990
An%	37.55	45.95	47.24	35.84	48.05	54.87	40.53	56.24	47.18	49.96	53.85	53.02	54.98	59.09	47.53	44.93	48.71	47.24
Ab%	60.80	52.66	51.28	62.96	50.87	44.39	58.58	42.65	51.95	48.28	44.29	45.16	44.01	40.11	51.01	54.25	50.92	51.53
Or%	1.65	1.40	1.48	1.20	1.08	0.74	0.89	1.10	0.87	1.76	1.87	1.82	1.01	0.80	1.46	0.82	0.37	1.23

Sample #	Z2-6	Z2-6	Z2-6	Z2-6	Z2-6	Z2-6	Z2-6	Z2-6	Z2-6	Z2-6	Z2-8	Z2-8	Z2-8	Z2-8	Z2-8	Z2-8	Z2-8	Z2-8
Grain #	n1	n1	n1	n2	n2	n2	n3	n3	n3	n3	n1	n1	n1	p2	p2	p3	p3	n2
P. Loc	core	mid	rim	rim	core	mid	rim	mid	mid	rim	core	mid	rim	core	rim	core	rim	p1
SiO2	56.66	57.14	57.38	56.72	56.65	57.64	54.34	55.83	53.47	53.77	51.37	51.50	54.21	52.46	51.93	54.62	54.94	54.00
Al2O3	28.07	27.84	27.42	27.95	27.89	27.12	29.49	28.34	30.10	29.88	30.74	30.89	29.48	30.71	31.31	29.11	28.91	29.43
FeO	0.27	0.15	0.13	0.17	0.10	0.15	0.24	0.36	0.22	0.20	0.06	0.11	0.22	0.11	0.28	0.21	0.06	0.02
CaO	10.22	9.92	9.55	10.01	10.00	9.39	11.87	10.48	12.58	12.49	12.91	12.98	10.98	12.34	13.08	10.42	10.37	10.94
Na2O	5.58	5.73	5.82	6.00	5.52	6.13	4.56	5.47	4.58	4.54	4.15	4.34	5.33	4.57	4.45	5.68	5.61	5.43
K2O	0.15	0.21	0.10	0.12	0.25	0.08	0.06	0.17	0.12	0.05	0.07	0.07	0.11	0.05	0.05	0.07	0.02	0.06
Total	100.95	100.85	100.26	100.80	100.31	100.28	100.25	100.66	100.84	100.69	99.30	99.89	100.34	100.23	101.09	100.11	99.92	99.88
Si	2.524	2.540	2.560	2.526	2.533	2.570	2.440	2.499	2.399	2.412	2.348	2.343	2.440	2.371	2.337	2.460	2.475	2.440
Al	1.473	1.459	1.442	1.467	1.470	1.425	1.560	1.495	1.592	1.580	1.656	1.656	1.564	1.636	1.660	1.545	1.535	1.567
Fe	0.010	0.006	0.005	0.006	0.004	0.006	0.009	0.014	0.008	0.007	0.002	0.004	0.008	0.004	0.011	0.008	0.002	0.001
Ca	0.488	0.473	0.456	0.478	0.479	0.449	0.571	0.503	0.605	0.600	0.632	0.632	0.530	0.598	0.630	0.503	0.501	0.530
Na	0.482	0.494	0.504	0.518	0.478	0.530	0.397	0.475	0.398	0.395	0.368	0.383	0.466	0.400	0.388	0.496	0.490	0.476
K	0.008	0.012	0.006	0.007	0.014	0.004	0.003	0.010	0.007	0.003	0.004	0.004	0.006	0.003	0.003	0.004	0.001	0.003
Total	4.985	4.983	4.973	5.003	4.978	4.984	4.980	4.995	5.008	4.997	5.010	5.023	5.014	5.012	5.029	5.017	5.004	5.016
An%	49.88	48.31	47.26	47.64	49.32	45.65	58.81	50.92	59.89	60.14	62.98	62.02	52.87	59.72	61.71	50.15	50.46	52.50
Ab%	49.25	50.50	52.17	51.71	49.24	53.90	40.85	48.10	39.43	39.57	36.62	37.57	46.48	40.02	38.02	49.43	49.41	47.18
Or%	0.86	1.19	0.57	0.65	1.44	0.45	0.34	0.97	0.68	0.29	0.40	0.41	0.64	0.26	0.27	0.42	0.13	0.32

Table A4. 11 (Con't)

Sample #	Z2-8	Z2-8	Z2-8	Z2-8	Z2-9	Z2-9	Z2-9	Z2-9	Z2-9	Z2-9	Z2-9	Z2-9	Z2-9	Z2-9	Z2-9	Z2-9	Z2-9
Grain #	n2	n3	n3	n3	n1	n1	n1	n1	p2	p2	n2	n2	n2	n2	n2	n2	n2
P.Loc.	p2	plc1	cr1	rim	rim	mid	core	core	core	rim	rim	mid	mid	mid	core	core	rim
SiO2	51.38	53.55	51.60	54.32	57.13	56.83	55.92	55.42	53.23	56.08	58.71	59.08	57.73	55.00	58.20	56.59	55.23
Al2O3	31.01	29.77	30.93	29.31	26.49	26.87	27.23	27.73	29.31	27.29	25.53	25.27	26.39	28.21	25.76	26.80	27.94
FeO	0.08	0.12	0.23	0.04	0.19	0.05	0.18	0.21	0.14	0.12	0.28	0.30	0.12	0.03	0.34	0.19	0.16
CaO	12.98	11.20	13.00	10.84	8.94	8.88	9.76	10.32	12.28	9.75	7.45	7.44	8.47	10.77	7.94	9.31	10.70
Na2O	4.39	5.31	4.39	5.64	6.30	6.06	5.80	5.49	4.55	5.86	6.87	6.85	6.24	5.28	6.01	5.99	5.39
K2O	0.03	0.05	0.06	0.00	0.35	0.35	0.37	0.31	0.20	0.33	0.33	0.51	0.40	0.30	0.41	0.33	0.24
Total	99.87	100.00	100.21	100.14	99.41	99.03	99.27	99.48	99.71	99.43	99.16	99.45	99.35	99.58	98.66	99.20	99.66
Si	2.338	2.420	2.342	2.447	2.580	2.571	2.535	2.510	2.418	2.537	2.644	2.655	2.600	2.490	2.633	2.562	2.499
Al	1.663	1.586	1.654	1.556	1.410	1.433	1.455	1.481	1.570	1.455	1.355	1.338	1.401	1.505	1.374	1.430	1.490
Fe	0.003	0.004	0.009	0.001	0.007	0.002	0.007	0.008	0.005	0.005	0.011	0.011	0.005	0.001	0.013	0.007	0.006
Ca	0.633	0.542	0.632	0.523	0.433	0.431	0.474	0.501	0.598	0.472	0.359	0.358	0.409	0.522	0.385	0.452	0.519
Na	0.387	0.466	0.387	0.493	0.551	0.531	0.510	0.482	0.401	0.514	0.600	0.597	0.545	0.463	0.527	0.525	0.473
K	0.002	0.003	0.003	0.000	0.020	0.020	0.021	0.018	0.012	0.019	0.019	0.029	0.023	0.017	0.024	0.019	0.014
Total	5.025	5.021	5.026	5.021	5.001	4.988	5.003	4.999	5.003	5.002	4.988	4.989	4.983	4.998	4.955	4.995	5.000
An%	61.92	53.65	61.85	51.52	43.09	43.84	47.17	50.04	59.15	47.01	36.72	36.37	41.87	52.10	41.15	45.33	51.58
Ab%	37.89	46.07	37.83	48.48	54.88	54.10	50.71	48.15	39.67	51.11	61.32	60.66	55.79	46.19	56.33	52.74	47.03
Or%	0.19	0.28	0.32	0.00	2.03	2.06	2.12	1.81	1.17	1.88	1.95	2.97	2.35	1.71	2.51	1.93	1.39

Sample #	Z2-10	Z2-10	Z2-10	Z2-10	Z2-11	Z2-11	Z2-11	Z2-11	Z2-11	Z2-11	Z2-11	Z2-11	Z2-11	Z2-11	Z2-11	Z2-11	Z2-11	Z2-11
Grain #	n3	n4	n4	n5	n4	n4	n4	n1	n1	p2	p2	n3	n2	n3	n3	n3	n3	n1
P.Loc.	core	core	rim	core	core	mid	rim	core	rim	core	rim	rim	mid	rim	mid	core	mid	rim
Si2O	54.36	53.22	55.11	56.24	54.98	54.52	57.10	57.65	55.03	54.36	55.49	56.76	55.40	57.09	55.20	55.75	56.85	57.19
Al2O3	29.09	29.91	28.38	27.35	28.50	28.71	27.24	26.62	28.17	28.92	28.31	27.49	28.27	27.40	28.84	28.20	28.03	27.17
FeO	0.21	0.18	0.31	0.12	0.16	0.18	0.31	0.21	0.16	0.17	0.24	0.19	0.25	0.16	0.29	0.26	0.22	0.33
CaO	10.62	11.84	9.82	8.92	10.29	10.54	8.52	8.14	10.06	10.56	9.80	9.72	10.71	9.58	11.24	10.38	10.33	9.31
Na2O	5.70	5.12	6.06	6.64	5.66	5.55	6.08	6.79	5.54	5.37	5.95	6.05	5.32	5.89	5.15	5.44	5.74	6.05
K2O	0.21	0.10	0.20	0.30	0.27	0.23	0.29	0.35	0.28	0.24	0.27	0.31	0.29	0.39	0.25	0.31	0.26	0.29
Total	100.18	100.38	99.89	99.56	99.86	99.73	99.53	99.77	99.25	99.60	100.07	100.33	99.99	100.35	100.96	100.33	101.21	100.34
Si	2.452	2.403	2.488	2.540	2.483	2.467	2.569	2.590	2.497	2.462	2.498	2.540	2.493	2.552	2.470	2.503	2.523	2.560
Al	1.547	1.592	1.510	1.456	1.517	1.532	1.444	1.409	1.506	1.544	1.502	1.450	1.499	1.443	1.521	1.492	1.466	1.434
Fe	0.008	0.007	0.012	0.004	0.006	0.007	0.012	0.008	0.006	0.006	0.009	0.007	0.009	0.006	0.011	0.010	0.008	0.012
Ca	0.513	0.573	0.475	0.432	0.498	0.511	0.411	0.392	0.489	0.512	0.473	0.466	0.517	0.459	0.539	0.499	0.491	0.446
Na	0.498	0.448	0.531	0.581	0.496	0.487	0.530	0.592	0.488	0.471	0.520	0.525	0.464	0.510	0.446	0.473	0.494	0.525
K	0.012	0.006	0.012	0.017	0.015	0.013	0.017	0.020	0.016	0.014	0.016	0.018	0.016	0.022	0.014	0.018	0.014	0.017
Total	5.030	5.028	5.028	5.031	5.015	5.017	4.982	5.011	5.002	5.009	5.018	5.006	4.998	4.992	5.000	4.996	4.998	4.994
An%	50.14	55.77	46.70	41.91	49.32	50.55	42.90	39.04	49.27	51.37	46.90	46.22	51.79	46.29	53.92	50.42	49.13	45.17
Ab%	48.66	43.66	52.16	56.43	49.14	48.13	55.38	58.94	49.11	47.26	51.54	52.02	46.57	51.47	44.66	47.80	49.42	53.15
Or%	1.20	0.57	1.14	1.66	1.53	1.32	1.72	2.02	1.62	1.37	1.56	1.76	1.64	2.24	1.42	1.78	1.45	1.68

Table A4.11 (Con't)

Sample #	Z2-12	Z2-12	Z2-12	Z2-12	Z2-12	Z2-12	Z2-12	Z2-12	Z2-12	Z2-12	Z2-12	Z2-12	Z2-12	Z2-12	Z2-12	Z2-12
Grain #	n1	n1	n1	n1	n1	n1	n1	n1	n1	n1	n2	n2	n2	n2	n2	n2
P.Loc.	mid	mid	core	core	core	core	mid	mid	rim	rim	rim	rim	mid	mid	core	rim
SiO2	57.01	56.27	56.34	56.76	56.64	56.50	57.13	57.73	57.92	56.88	59.27	59.38	55.34	54.67	55.81	57.41
Al2O3	27.38	27.84	28.20	28.02	27.99	28.06	27.48	27.05	27.41	27.81	26.14	26.54	28.78	29.48	28.54	27.24
FeO	0.17	0.35	0.28	0.27	0.17	0.40	0.13	0.22	0.15	0.25	0.33	0.37	0.29	0.30	0.35	0.18
CaO	9.67	10.01	10.08	10.20	9.92	10.28	9.66	9.02	9.02	9.94	8.20	8.29	11.24	11.51	10.85	9.35
Na2O	5.86	5.91	5.73	5.84	5.85	5.81	5.99	6.30	5.89	5.85	6.58	6.40	5.18	5.03	5.15	6.16
K2O	0.31	0.29	0.22	0.31	0.29	0.29	0.28	0.35	0.39	0.26	0.37	0.36	0.22	0.19	0.24	0.16
Total	100.23	100.66	100.86	101.40	100.69	101.35	100.53	100.45	100.63	100.74	100.88	101.34	101.29	101.17	100.94	100.31
Si	2.551	2.519	2.514	2.522	2.526	2.514	2.549	2.574	2.574	2.533	2.628	2.620	2.473	2.443	2.492	2.563
Al	1.444	1.469	1.483	1.467	1.471	1.472	1.445	1.421	1.435	1.460	1.366	1.380	1.516	1.552	1.502	1.433
Fe	0.006	0.013	0.011	0.010	0.006	0.015	0.005	0.008	0.006	0.009	0.012	0.014	0.011	0.011	0.013	0.007
Ca	0.464	0.480	0.482	0.485	0.474	0.490	0.462	0.431	0.430	0.475	0.389	0.392	0.538	0.551	0.519	0.447
Na	0.508	0.513	0.496	0.503	0.506	0.501	0.518	0.544	0.508	0.505	0.565	0.548	0.449	0.435	0.446	0.533
K	0.018	0.016	0.013	0.017	0.016	0.017	0.016	0.020	0.022	0.015	0.021	0.020	0.013	0.011	0.014	0.009
Total	4.990	5.011	4.998	5.005	5.000	5.009	4.995	4.998	4.974	4.997	4.982	4.974	5.000	5.004	4.986	4.992
An%	46.87	47.57	48.68	48.26	47.58	48.65	46.38	43.30	44.77	47.73	39.91	40.85	53.85	55.25	53.05	45.18
Ab%	51.36	50.81	50.05	50.01	50.78	49.70	52.03	54.69	52.92	50.78	57.93	57.06	44.89	43.66	45.54	53.91
Or%	1.77	1.61	1.27	1.73	1.64	1.65	1.58	2.01	2.31	1.49	2.16	2.09	1.27	1.09	1.41	0.90

Sample #	Z2-13	Z2-13	Z2-13	Z2-13	Z2-13	Z2-13	Z2-13	Z2-13	Z2-13	Z2-13	Z2-13	Z2-13	Z2-13	Z2-13	Z2-13	Z2-13	Z2-13	Z2-13
Grain #	n7	n7	n1	n1	n1	n1	n2	n2	n2	n2	n3	n3	n3	n3	n4	n4	n4	n5
P.Loc.	core	core	core/ch	core	core	core	core	core/ch	core	rim	rim	mid	core	rim	mid	core	core	core
SiO2	56.56	58.42	56.99	58.11	60.04	58.41	58.45	58.61	56.75	56.68	56.32	58.97	55.22	57.37	58.01	54.28	55.11	56.22
Al2O3	27.16	25.83	27.09	26.14	25.23	26.30	26.02	26.01	27.02	26.92	27.27	26.03	28.52	26.51	26.01	27.80	28.48	27.61
FeO	0.20	0.23	0.19	0.24	0.21	0.23	0.22	0.26	0.17	0.20	0.15	0.15	0.15	0.08	0.13	0.26	0.09	0.13
CaO	9.24	7.77	9.18	8.04	7.02	8.04	7.79	7.83	9.12	9.38	9.45	7.80	10.61	8.50	8.08	10.63	10.48	9.82
Na2O	6.35	7.02	6.19	6.80	7.33	6.87	7.01	7.11	6.14	6.06	6.18	7.13	5.60	6.78	6.86	5.42	5.48	6.03
K2O	0.26	0.27	0.31	0.40	0.37	0.34	0.25	0.21	0.31	0.14	0.25	0.26	0.18	0.31	0.30	0.17	0.22	0.24
Total	99.85	99.70	99.95	99.96	100.28	100.31	99.73	100.14	99.65	99.37	99.79	100.32	100.36	99.68	99.62	98.78	99.86	100.16
Si	2.549	2.626	2.560	2.610	2.673	2.611	2.621	2.622	2.560	2.560	2.542	2.628	2.483	2.585	2.613	2.486	2.486	2.528
Al	1.443	1.368	1.434	1.384	1.324	1.385	1.375	1.371	1.437	1.433	1.451	1.367	1.511	1.408	1.381	1.501	1.514	1.464
Fe	0.008	0.009	0.007	0.009	0.008	0.009	0.008	0.010	0.006	0.007	0.006	0.005	0.006	0.003	0.005	0.010	0.004	0.005
Ca	0.446	0.374	0.442	0.387	0.335	0.385	0.374	0.375	0.441	0.454	0.457	0.372	0.511	0.410	0.390	0.522	0.506	0.473
Na	0.555	0.612	0.540	0.592	0.633	0.595	0.609	0.617	0.537	0.531	0.541	0.616	0.488	0.592	0.599	0.481	0.479	0.526
K	0.015	0.016	0.018	0.023	0.021	0.019	0.014	0.012	0.018	0.008	0.014	0.015	0.010	0.018	0.017	0.010	0.013	0.014
Total	5.015	5.004	5.001	5.005	4.992	5.004	5.003	5.007	4.999	4.993	5.010	5.003	5.010	5.016	5.005	5.009	5.002	5.010
An%	43.91	37.35	44.25	38.65	33.88	38.52	37.51	37.39	44.26	45.73	45.18	37.13	50.62	40.22	38.76	51.51	50.73	46.70
Ab%	54.64	61.08	54.00	59.09	64.01	59.53	61.08	61.44	53.94	53.46	53.42	61.41	48.34	58.04	59.54	47.53	48.01	51.93
Or%	1.45	1.57	1.76	2.26	2.11	1.95	1.41	1.17	1.80	0.81	1.40	1.46	1.03	1.74	1.71	0.95	1.26	1.38

Table A4.11 (Con't)

Sample #	Z2-13	Z2-14	Z2-14	Z2-14	Z2-14	Z2-14	Z2-14	Z2-14	Z2-14	Z2-14	Z2-14	Z2-14	Z2-14	Z2-14	Z2-14	Z2-14
Grain #	n5	n1	n2	n3	n4	n1	n2	n3	n3	n3	n3	n6	n7	n7	n8	n8
P.Loc	core	core	core	rim	rim	core	core	core	core	core	core	core	core	core	core	core
SiO2	55.85	54.74	54.82	58.39	58.10	55.37	58.04	58.79	54.86	56.69	54.78	57.53	57.32	57.00	54.92	54.98
Al2O3	27.61	28.52	28.34	25.87	25.94	28.08	0.00	26.25	28.30	27.03	28.43	26.77	26.99	27.58	28.02	27.99
FeO	0.26	0.29	0.16	0.16	0.34	0.23	0.16	0.20	0.18	0.30	0.26	0.00	0.18	0.18	0.20	0.15
CaO	9.99	10.84	10.61	8.02	8.03	10.14	8.30	8.11	10.71	9.13	11.01	8.68	8.96	9.56	10.22	10.36
Na2O	5.87	5.02	5.28	6.67	6.60	5.45	6.37	6.84	5.30	5.85	4.90	6.30	6.16	5.88	5.38	5.31
K2O	0.21	0.17	0.23	0.27	0.21	0.25	0.29	0.31	0.24	0.32	0.27	0.43	0.28	0.22	0.19	0.20
Total	99.79	99.57	99.54	99.37	99.34	99.60	99.81	100.78	99.66	99.44	99.66	99.92	99.89	100.87	99.11	99.10
Si	2.521	2.478	2.485	2.626	2.619	2.504	3.532	2.618	2.484	2.561	2.479	2.585	2.572	2.548	2.499	2.500
Al	1.469	1.522	1.514	1.371	1.378	1.497	0.000	1.378	1.511	1.439	1.517	1.418	1.428	1.453	1.503	1.500
Fe	0.010	0.011	0.006	0.006	0.013	0.009	0.008	0.008	0.007	0.011	0.010	0.000	0.007	0.007	0.008	0.006
Ca	0.483	0.526	0.515	0.387	0.388	0.491	0.541	0.387	0.520	0.442	0.534	0.418	0.431	0.458	0.498	0.505
Na	0.514	0.441	0.464	0.581	0.577	0.478	0.752	0.591	0.465	0.512	0.430	0.549	0.536	0.510	0.474	0.468
K	0.012	0.010	0.013	0.015	0.012	0.014	0.022	0.017	0.014	0.018	0.016	0.024	0.016	0.012	0.011	0.011
Total	5.008	4.986	4.997	4.987	4.987	4.994	4.855	4.998	5.000	4.984	4.986	4.993	4.990	4.987	4.993	4.990
An%	47.87	53.85	51.92	39.32	39.70	49.94	41.15	38.89	52.05	45.44	54.48	42.15	43.82	46.74	50.65	51.28
Ab%	50.92	45.17	46.76	59.14	59.05	48.60	57.14	59.36	46.58	52.68	43.91	55.38	54.52	52.00	48.24	47.56
Or%	1.21	0.98	1.33	1.55	1.25	1.46	1.71	1.75	1.37	1.88	1.61	2.47	1.65	1.26	1.11	1.16

Table A4.12 Plagioclase analyses, from Zone III

Grain #	Z3-1	Z3-1	Z3-1	Z3-2	Z3-2	Z3-3	Z3-3	Z3-4	Z3-4	Z3-4	Z3-4	Z3-4	Z3-4	Z3-5	Z3-5	Z3-5	Z3-5
P. Loc.	n3	n4	n5	n1	n2	n2	n3	n1	n1	n2	n3	n3	n4	n1	n1	n2	n2
Si02	core	core	core	core	core	PC	PC	core	rim	core	core	core	rim	core	core	core	core
Al2O3	54.78	54.61	55.86	55.84	54.45	54.37	54.72	53.93	52.90	52.81	54.41	53.79	56.56	54.17	55.23	54.59	54.64
FeO	29.23	29.28	28.61	28.43	29.20	28.36	29.66	29.71	29.96	30.08	29.37	29.63	28.17	29.05	28.93	29.75	29.24
CaO	0.30	0.36	0.23	0.22	0.36	0.43	0.11	0.16	0.19	0.02	0.24	0.09	0.09	0.13	0.17	0.20	0.12
Na2O	10.57	11.20	9.58	9.77	10.98	10.40	10.82	11.34	11.89	11.88	10.84	11.27	9.32	10.78	10.38	10.92	10.67
K2O	5.78	5.46	5.99	5.84	5.23	5.44	5.42	5.39	4.86	4.68	5.21	5.18	6.15	5.23	5.84	5.30	5.62
Total	0.24	0.22	0.27	0.30	0.28	0.24	0.17	0.28	0.16	0.17	0.15	0.22	0.27	0.27	0.28	0.25	0.34
	100.89	101.14	100.53	100.40	100.50	99.25	100.89	100.80	99.95	99.63	100.23	100.18	100.56	99.63	100.82	101.01	100.63
Si																	
Al	2.454	2.444	2.500	2.503	2.449	2.474	2.447	2.423	2.398	2.398	2.449	2.427	2.526	2.454	2.472	2.441	2.453
Fe	1.543	1.545	1.509	1.502	1.548	1.521	1.563	1.573	1.601	1.610	1.558	1.576	1.483	1.551	1.526	1.568	1.547
Ca	0.011	0.013	0.008	0.008	0.014	0.017	0.004	0.006	0.007	0.001	0.009	0.004	0.003	0.005	0.006	0.007	0.004
Na	0.507	0.537	0.460	0.469	0.529	0.507	0.519	0.546	0.577	0.578	0.523	0.545	0.446	0.523	0.498	0.523	0.513
K	0.502	0.474	0.519	0.508	0.456	0.480	0.470	0.470	0.427	0.427	0.455	0.453	0.533	0.459	0.507	0.460	0.489
Total	0.014	0.013	0.016	0.017	0.016	0.014	0.010	0.016	0.009	0.009	0.009	0.013	0.015	0.015	0.016	0.014	0.020
	5.032	5.027	5.013	5.008	5.012	5.012	5.012	5.033	5.020	5.008	5.003	5.018	5.006	5.008	5.026	5.012	5.027
An%																	
Ab%	49.61	52.47	46.21	47.20	52.86	50.64	51.95	52.92	56.92	57.83	53.00	53.90	44.87	52.43	48.79	52.48	50.22
Or%	49.07	46.31	52.22	51.05	45.54	47.94	47.06	45.53	42.15	41.20	46.13	44.85	53.58	46.02	49.67	46.10	47.86
	1.32	1.23	1.57	1.75	1.60	1.41	0.99	1.55	0.93	0.93	0.08	1.26	1.55	1.55	1.54	1.42	1.92

Sample #	Z3-5	Z3-6	Z3-6	Z3-6	Z3-6	Z3-6	Z3-6	Z3-7	Z3-7	Z3-7	Z3-8	Z3-8	Z3-8	Z3-8	Z3-8	Z3-9	Z3-9
Grain #	n2	n4	n5	n5	n6	n6	n4	n2	n2	n2	n3	n3	n2	n2	n2	n1	n1
P.loc.	core	rim	core	rim	core	rim	core	core	core	core	core	core	core	rim	core	core	rim
Si02	58.30	57.52	52.50	55.88	52.67	53.32	53.37	52.99	54.78	53.36	53.55	53.92	54.80	55.81	56.58	50.15	54.70
Al2O3	26.35	26.36	29.57	27.78	29.46	29.20	29.12	29.66	28.88	30.06	29.82	28.87	29.11	28.26	27.73	33.19	29.27
FeO	0.19	0.25	0.24	0.23	0.19	0.28	0.35	0.14	0.24	0.23	0.33	0.36	0.19	0.32	0.58	0.43	0.15
CaO	7.83	8.00	11.43	9.23	11.62	11.12	11.03	11.74	10.55	11.91	11.51	10.84	10.55	9.67	9.20	10.58	10.68
Na2O	7.05	6.67	4.79	6.10	5.07	5.09	4.95	5.06	5.54	4.90	5.16	5.02	5.68	5.85	6.35	4.78	5.36
K2O	0.00	0.50	0.20	0.39	0.31	0.31	0.31	0.23	0.28	0.20	0.31	0.41	0.33	0.30	0.39	0.25	0.39
Total	99.73	99.32	98.72	99.60	99.33	99.32	99.13	99.82	100.27	100.66	100.67	99.42	100.66	100.20	100.83	99.39	100.55
Si	2.612	2.597	2.407	2.524	2.406	2.430	2.435	2.406	2.467	2.402	2.412	2.452	2.460	2.508	2.530	2.287	2.456
Al	1.391	1.402	1.598	1.479	1.586	1.568	1.566	1.587	1.533	1.595	1.583	1.547	1.540	1.496	1.461	1.783	1.549
Fe	0.007	0.010	0.009	0.009	0.007	0.011	0.013	0.005	0.009	0.009	0.012	0.014	0.007	0.012	0.022	0.016	0.006
Ca	0.376	0.387	0.561	0.447	0.569	0.543	0.539	0.571	0.509	0.574	0.555	0.528	0.507	0.465	0.441	0.517	0.514
Na	0.613	0.584	0.426	0.534	0.449	0.450	0.438	0.446	0.484	0.428	0.451	0.443	0.494	0.509	0.550	0.423	0.467
K	0.000	0.029	0.012	0.023	0.018	0.018	0.018	0.014	0.016	0.012	0.018	0.024	0.019	0.017	0.022	0.015	0.022
Total	4.999	5.009	5.013	5.015	5.035	5.020	5.010	5.030	5.017	5.020	5.031	5.008	5.027	5.007	5.026	5.040	5.014
An%	38.02	38.69	56.21	44.50	54.87	53.73	54.17	55.43	50.47	56.66	54.25	53.09	49.70	46.94	43.50	54.17	51.22
Ab%	61.98	58.41	42.61	53.24	43.37	44.49	44.04	43.25	47.95	42.19	44.03	44.50	48.43	51.35	54.32	44.31	46.55
Or%	0.00	2.91	1.18	2.26	1.76	1.79	1.78	1.32	1.58	1.15	1.72	2.42	1.87	1.71	2.18	1.52	2.22

Table A4. 12 (Con't)

Sample #	Z3-9	Z3-9	Z3-9	Z3-9	Z3-10	Z3-10	Z3-10	Z3-11	Z3-11	Z3-11	Z3-11	Z3-11	Z3-11	Z3-12	Z3-12	Z3-12	Z3-12
Grain #	n1	n2	n3	n4	n1	n1	n2	n1	n2	n4	n3	n3	n3	n3	n3	n3	n3
P.Loc.	mid	core	core	core	PC	PC	PC	PC	PC	PC	PC	PC	PC	core	rim	core	mid
SiO2	54.30	56.10	55.90	53.77	53.53	54.10	54.19	61.12	58.71	53.87	61.18	54.47	52.85	54.53	55.37	55.06	55.51
Al2O3	29.26	27.97	27.93	29.86	29.25	29.22	28.90	24.94	26.25	29.78	24.74	28.96	29.00	28.15	28.40	28.98	28.42
FeO	0.03	0.29	0.27	0.05	0.23	0.13	0.08	0.23	0.22	0.23	0.15	0.16	0.13	0.24	0.26	0.31	0.12
CaO	10.55	9.52	9.43	11.42	10.84	10.70	10.23	5.66	7.55	11.47	5.49	10.39	10.73	10.03	10.10	10.49	10.13
Na2O	5.41	6.03	5.67	5.11	5.09	5.14	5.08	7.20	5.92	5.39	8.13	5.78	5.31	5.79	5.53	5.61	6.07
K2O	0.32	0.44	0.35	0.27	0.13	0.16	0.17	0.42	0.30	0.24	0.23	0.19	0.17	0.26	0.26	0.23	0.25
Total	99.88	100.37	99.56	100.47	99.06	99.45	98.66	99.57	98.95	100.99	99.92	99.95	98.18	99.01	99.92	100.69	100.50
Si	2.453	2.518	2.523	2.420	2.439	2.452	2.470	2.719	2.638	2.418	2.717	2.460	2.432	2.485	2.495	2.468	2.491
Al	1.557	1.480	1.486	1.584	1.571	1.561	1.552	1.308	1.390	1.575	1.295	1.542	1.573	1.512	1.508	1.531	1.503
Fe	0.001	0.011	0.010	0.002	0.009	0.005	0.003	0.008	0.008	0.009	0.006	0.006	0.005	0.009	0.010	0.012	0.004
Ca	0.511	0.458	0.456	0.551	0.529	0.519	0.500	0.270	0.363	0.552	0.261	0.503	0.529	0.490	0.488	0.504	0.487
Na	0.474	0.525	0.497	0.446	0.449	0.451	0.449	0.621	0.516	0.469	0.700	0.506	0.473	0.511	0.484	0.488	0.528
K	0.019	0.025	0.020	0.015	0.007	0.009	0.010	0.024	0.017	0.014	0.013	0.011	0.010	0.015	0.015	0.013	0.015
Total	5.015	5.017	4.992	5.018	5.004	4.998	4.984	4.950	4.933	5.036	4.992	5.028	5.023	5.023	4.999	5.016	5.029
An%	50.90	45.44	46.88	54.44	53.67	52.99	52.14	29.51	40.53	53.32	26.82	49.32	52.27	48.19	49.46	50.14	47.31
Ab%	47.24	52.07	51.02	44.06	45.57	46.06	46.86	67.91	57.57	45.35	71.84	49.63	46.76	50.31	49.05	48.53	51.28
Or%	1.86	2.50	2.10	1.50	0.76	0.95	1.00	2.59	1.91	1.32	1.33	1.06	0.97	1.50	1.49	1.34	1.41

Sample #	Z3-12	Z3-13	Z3-13	Z3-13	Z3-13	Z3-13	Z3-13	Z3-13	Z3-13	Z3-14	Z3-14	Z3-14	Z3-14	Z3-14	Z3-14	Z3-15	Z3-15
Grain #	n3	1	1	2	2	2	3	3	3	1	2	2	3	4	4	n1	n1
P.Loc	rim	core	rim	core	mid	rim	core	mid	rim	PC	PC	PC	PC	PC	PC	core	mid
Si2O	55.43	54.78	52.97	53.59	54.97	56.82	53.70	53.56	52.99	56.52	56.28	57.17	53.32	58.31	53.57	52.56	56.47
Al2O3	29.33	28.46	29.04	29.25	28.19	26.66	29.20	28.98	29.19	27.57	27.55	26.66	29.81	26.66	29.05	29.70	27.25
FeO	0.28	0.25	0.28	0.15	0.26	0.23	0.19	0.28	0.26	0.22	0.10	0.21	0.35	0.25	0.25	0.13	0.20
CaO	10.69	10.25	11.18	10.90	9.96	8.30	10.88	10.81	11.26	9.04	8.86	8.21	11.39	7.67	11.12	11.58	8.69
Na2O	5.60	5.47	5.04	5.34	5.66	6.17	5.24	5.26	4.96	6.06	6.09	6.23	4.96	6.46	4.59	4.97	6.42
K2O	0.25	0.30	0.19	0.25	0.33	0.32	0.29	0.26	0.23	0.37	0.30	0.40	0.25	0.33	0.25	0.23	0.27
Total	101.58	99.51	98.70	99.48	99.37	98.49	99.50	99.15	98.90	99.78	99.18	98.88	100.07	99.68	98.83	99.17	99.30
Si	2.464	2.482	2.429	2.436	2.493	2.582	2.439	2.442	2.425	2.544	2.545	2.588	2.413	2.611	2.446	2.401	2.552
Al	1.536	1.520	1.569	1.567	1.507	1.428	1.563	1.557	1.574	1.462	1.468	1.422	1.590	1.407	1.563	1.599	1.452
Fe	0.010	0.009	0.011	0.006	0.010	0.009	0.007	0.011	0.010	0.008	0.004	0.008	0.013	0.009	0.010	0.005	0.008
Ca	0.509	0.498	0.549	0.531	0.484	0.404	0.530	0.528	0.552	0.436	0.429	0.398	0.552	0.368	0.544	0.567	0.421
Na	0.483	0.480	0.448	0.471	0.498	0.543	0.461	0.465	0.440	0.529	0.534	0.546	0.435	0.560	0.406	0.440	0.563
K	0.014	0.017	0.011	0.015	0.019	0.018	0.017	0.015	0.013	0.021	0.018	0.023	0.014	0.019	0.015	0.014	0.016
Total	5.017	5.007	5.016	5.024	5.011	4.985	5.018	5.019	5.015	5.000	4.997	4.986	5.017	4.975	4.983	5.026	5.011
An%	50.58	50.02	54.48	52.22	48.36	41.85	52.58	52.37	54.88	44.23	43.78	41.13	55.11	38.86	56.37	55.53	42.12
Ab%	47.98	48.26	44.43	46.34	49.76	56.26	45.78	46.12	43.78	53.64	54.43	56.47	43.46	59.15	42.11	43.13	56.30
Or%	1.43	1.72	1.09	1.43	1.89	1.89	1.64	1.51	1.34	2.13	1.79	2.39	1.43	1.98	1.52	1.34	1.58

Table A4.12 (Con't)

Sample #	Z3-15	Z3-15	Z3-15	Z3-16	Z3-16	Z3-16	Z3-16	Z3-16	Z3-16	Z3-16	Z3-16	Z3-16	Z3-16	Z3-16	Z3-16	Z3-16	Z3-16
Grain #	n1	n2	n2	1	2	3	3	4	5	6	7	7	7	8	8	9	10
P.Loc	rim	core	core	core	core	core	core	rim	core	core	core	mid	rim	core	mid	core	core
Si2O	60.08	53.47	53.06	56.19	52.92	53.15	54.65	53.28	52.62	53.51	53.63	53.99	55.44	53.39	56.18	52.00	56.79
Al2O3	25.09	28.84	29.24	27.69	29.68	29.64	28.39	29.37	29.74	28.93	29.14	29.08	27.77	29.48	27.74	30.55	26.69
FeO	0.30	0.16	0.21	0.18	0.27	0.19	0.22	0.16	0.25	0.23	0.28	0.06	0.37	0.18	0.08	0.21	0.19
CaO	6.02	10.85	11.09	9.02	11.52	11.23	9.86	10.93	11.56	10.80	10.85	10.77	9.15	10.99	9.03	12.45	8.26
Na2O	7.40	5.19	5.05	6.03	4.92	5.02	5.41	5.26	4.83	5.26	5.08	5.31	5.90	5.11	5.80	4.35	6.24
K2O	0.50	0.19	0.20	0.21	0.23	0.20	0.29	0.25	0.17	0.20	0.26	0.20	0.23	0.23	0.32	0.14	0.37
Total	99.40	98.71	98.84	99.33	99.55	99.42	98.83	99.24	99.17	98.92	99.25	99.41	98.85	99.37	99.15	99.70	98.55
Si	2.689	2.447	2.427	2.538	2.408	2.417	2.489	2.428	2.403	2.444	2.441	2.451	2.521	2.428	2.540	2.366	2.580
Al	1.324	1.555	1.576	1.474	1.592	1.589	1.524	1.577	1.601	1.557	1.564	1.556	1.488	1.580	1.478	1.638	1.429
Fe	0.011	0.006	0.008	0.007	0.010	0.007	0.008	0.006	0.009	0.009	0.011	0.002	0.014	0.007	0.003	0.008	0.007
Ca	0.289	0.532	0.543	0.437	0.562	0.547	0.481	0.534	0.566	0.528	0.529	0.524	0.446	0.535	0.437	0.607	0.402
Na	0.642	0.460	0.448	0.528	0.434	0.443	0.478	0.464	0.428	0.465	0.448	0.467	0.520	0.451	0.509	0.384	0.549
K	0.029	0.011	0.012	0.012	0.013	0.012	0.017	0.014	0.010	0.011	0.015	0.012	0.013	0.013	0.018	0.008	0.021
Total	4.984	5.012	5.014	4.995	5.020	5.015	4.997	5.023	5.016	5.016	5.008	5.011	5.002	5.014	4.985	5.011	4.990
An%	30.09	53.01	54.21	44.71	55.67	54.62	49.31	52.70	56.40	52.57	53.31	52.25	45.55	53.59	45.35	60.75	41.33
Ab%	66.93	45.89	44.64	54.06	43.01	44.22	48.96	45.88	42.64	46.30	45.14	46.57	53.11	45.11	52.76	38.41	56.46
Or%	2.99	1.10	1.15	1.23	1.32	1.16	1.72	1.41	0.96	1.13	1.55	1.18	1.34	1.31	1.89	0.84	2.21

Sample #	Z3-16	Z3-16
Grain #	11	12
P.Loc.	core	core
Si2O	53.47	53.27
Al2O3	29.31	29.71
FeO	0.23	0.23
CaO	10.83	10.99
Na2O	5.40	4.89
K2O	0.26	0.18
Total	99.49	99.28
Si	2.431	2.423
Al	1.570	1.592
Fe	0.009	0.009
Ca	0.528	0.536
Na	0.476	0.432
K	0.015	0.010
Total	5.029	5.002
An%	51.78	54.79
Ab%	46.73	44.14
Or%	1.49	1.07

Table A4.13 Plagioclase analyses, from Zone IV

Sample #	ZAa-1	ZAa-1	ZAa-1	ZAa-1	ZAa-1	ZAa-2	ZAa-2	ZAa-2	ZAa-2	ZAa-3	ZAa-3	ZAa-3	ZAa-3	ZAa-3	ZAa-4	ZAa-4	ZAa-4	ZAa-4
Grian #	n1	n1	n2	n2	n2	n2	n2	n3	n3	n2	n2	n3	n3	n4	n1	n1	n1	n2
P.Loc	core	mid	core	mid	rim	core	core	core	rim	core	core	core	rim	core	core	core	core	core
SiO2	51.94	55.35	55.31	53.42	53.04	53.54	51.91	48.99	51.78	52.32	51.94	52.24	55.60	51.47	52.70	52.69	53.36	54.34
Al2O3	31.07	28.56	28.26	29.63	29.89	29.50	30.61	32.94	30.18	30.03	30.29	30.41	28.86	30.89	30.43	29.70	30.12	29.28
FeO	0.30	0.39	0.26	0.30	0.27	0.14	0.28	0.32	0.51	0.25	0.23	0.19	0.26	0.36	0.09	0.33	0.20	0.20
CaO	12.81	10.23	9.94	11.24	11.76	11.37	12.69	14.89	12.82	12.44	12.35	12.44	10.04	12.90	12.23	11.68	12.02	10.89
Na2O	4.34	5.82	5.90	5.01	4.89	4.92	4.24	2.98	4.35	4.39	4.58	4.50	5.49	4.15	4.47	4.64	4.90	5.29
K2O	0.14	0.31	0.36	0.28	0.32	0.29	0.32	0.12	0.21	0.34	0.27	0.22	0.25	0.24	0.27	0.28	0.19	0.25
Total	100.60	100.67	100.03	99.89	100.16	99.77	100.06	100.24	99.84	99.78	99.66	99.99	100.50	100.02	100.19	99.32	100.79	100.27
Si	2.346	2.483	2.494	2.420	2.402	2.427	2.358	2.235	2.361	2.382	2.368	2.372	2.490	2.342	2.384	2.404	2.400	2.448
Al	1.654	1.510	1.502	1.582	1.595	1.576	1.639	1.771	1.622	1.611	1.628	1.627	1.523	1.656	1.622	1.597	1.597	1.555
Fe	0.011	0.015	0.010	0.011	0.010	0.005	0.011	0.012	0.019	0.010	0.009	0.007	0.010	0.014	0.003	0.012	0.008	0.008
Ca	0.620	0.492	0.480	0.546	0.570	0.552	0.618	0.728	0.627	0.607	0.603	0.605	0.482	0.629	0.593	0.571	0.579	0.526
Na	0.380	0.506	0.516	0.440	0.429	0.433	0.374	0.264	0.384	0.388	0.405	0.396	0.477	0.366	0.392	0.410	0.427	0.462
K	0.008	0.018	0.021	0.016	0.018	0.017	0.019	0.007	0.012	0.020	0.015	0.013	0.014	0.014	0.016	0.016	0.011	0.014
Total	5.020	5.024	5.023	5.017	5.025	5.010	5.018	5.016	5.026	5.017	5.028	5.019	4.995	5.020	5.009	5.011	5.021	5.013
An%	61.50	48.43	47.24	54.45	56.04	55.13	61.16	72.90	61.26	59.81	58.94	59.70	49.50	62.33	59.24	57.25	56.93	52.43
Ab%	37.70	49.81	50.72	43.91	42.15	43.17	36.97	26.43	37.57	38.21	39.54	39.05	49.01	36.27	39.20	41.11	42.01	46.12
Or%	0.80	1.76	2.03	1.64	1.82	1.70	1.86	0.68	1.18	1.97	1.51	1.25	1.49	1.40	1.56	1.64	1.06	1.45

Sample #	ZAa-4	ZAa-5	ZAa-5	ZAa-5	ZAa-5	ZAa-6	ZAa-6	ZAa-6	ZAa-6	ZAa-6	ZAa-6	ZAa-6	ZAa-6	ZAa-6	ZAa-6	ZAa-6	ZAa-6	ZAa-6
Grain #	n2	n1	n1	n1	n2	n1	n2	n3	n4	n5	n6	n7	n6	n6	n7	n7	n7	n8
P.Loc.	core	core	core	rim	core	PC	PC	PC	PC	PC	PC	PC	PC	PC	PC	PC	PC	PC
Si2O	52.09	50.69	52.96	57.58	53.08	52.99	52.90	53.17	53.38	53.63	53.65	53.37	53.60	53.46	53.28	53.75	53.35	52.63
Al2O3	28.87	31.91	29.76	27.05	30.19	29.62	30.09	29.60	29.80	29.30	29.58	28.70	29.25	29.23	29.32	28.84	29.07	28.93
FeO	2.20	0.26	0.04	0.09	0.19	0.14	0.16	0.50	0.26	0.31	0.14	0.25	0.25	0.20	0.42	0.21	0.23	1.70
CaO	11.04	13.66	11.52	8.64	11.77	12.32	12.53	12.16	12.30	11.77	12.08	11.76	12.05	11.95	11.91	11.35	11.44	11.36
Na2O	5.13	3.86	5.01	6.79	4.79	4.64	4.43	4.68	4.67	4.93	4.74	4.83	4.87	4.63	4.67	4.94	5.05	4.99
K2O	0.23	0.15	0.13	0.36	0.18	0.13	0.13	0.10	0.11	0.16	0.20	0.17	0.20	0.15	0.13	0.18	0.12	0.12
Total	99.56	100.53	99.43	100.50	100.20	99.70	100.09	100.20	100.53	100.08	100.25	98.83	99.96	99.42	99.73	99.06	99.04	99.73
Si	2.395	2.298	2.409	2.572	2.398	2.405	2.392	2.407	2.407	2.427	2.420	2.439	2.424	2.428	2.420	2.447	2.432	2.407
Al	1.564	1.705	1.596	1.424	1.607	1.585	1.604	1.579	1.583	1.562	1.572	1.545	1.559	1.564	1.569	1.547	1.562	1.560
Fe	0.084	0.010	0.002	0.003	0.007	0.005	0.006	0.019	0.010	0.012	0.005	0.010	0.009	0.008	0.016	0.008	0.009	0.065
Ca	0.544	0.664	0.562	0.413	0.570	0.599	0.607	0.590	0.594	0.571	0.584	0.576	0.584	0.581	0.579	0.553	0.559	0.556
Na	0.458	0.339	0.442	0.588	0.420	0.408	0.388	0.410	0.409	0.433	0.414	0.428	0.427	0.408	0.411	0.436	0.446	0.442
K	0.014	0.008	0.008	0.020	0.010	0.008	0.008	0.006	0.007	0.009	0.011	0.010	0.011	0.009	0.008	0.010	0.007	0.007
Total	5.059	5.023	5.018	5.020	5.013	5.010	5.004	5.011	5.009	5.013	5.007	5.007	5.015	4.998	5.004	5.003	5.014	5.038
An%	53.56	65.63	55.55	41.47	57.00	59.02	60.52	58.63	58.87	56.36	57.85	56.81	57.13	58.26	58.05	55.34	55.23	55.33
Ab%	45.09	33.53	43.69	57.55	41.99	40.22	38.72	40.81	40.48	42.74	41.04	42.20	41.76	40.88	41.19	43.62	44.11	43.99
Or%	1.35	0.84	0.76	1.98	1.01	0.76	0.76	0.56	0.65	0.90	1.11	0.99	1.10	0.86	0.76	1.04	0.66	0.69

Table A4. 13 (Con't)

Sample #	Z4a-6	Z4a-6	Z4a-6	Z4a-6	Z4a-7	Z4a-7	Z4a-7	Z4a-7	Z4a-7	Z4a-7	Z4a-8	Z4a-8	Z4a-8	Z4a-8	Z4b-2	Z4b-2	Z4b-2	Z4b-2
Grain #	n8	n8	n8	n8	n1	n1	n1	n2	n2	n2	n2	n2	n3	n3	n2	n2	n3	n3
P.Loc	PC	PC	PC	PC	core	core	rim	rim	core	rim	core	rim	core	rim	core	rim	ere	rim
SiO2	53.48	53.58	53.53	53.34	50.90	50.30	52.80	52.00	51.00	55.30	53.40	54.00	52.00	52.70	51.10	51.80	53.70	51.90
Al2O3	29.12	29.48	29.18	29.08	31.90	32.20	30.10	29.20	31.20	29.10	30.10	29.90	31.00	30.70	31.20	31.50	30.60	30.90
FeO	0.67	0.27	0.00	0.46	0.10	0.10	0.20	0.80	0.30	0.10	0.20	0.10	0.20	0.10	0.30	0.30	0.10	0.30
CaO	11.95	11.97	11.80	11.79	14.80	15.50	13.10	12.40	14.70	11.20	12.80	12.50	13.90	13.30	14.50	13.80	12.80	13.90
Na2O	4.90	4.86	4.89	4.72	2.90	2.70	4.00	3.50	2.80	4.80	4.10	4.40	3.50	4.00	3.20	3.20	4.00	3.60
K2O	0.22	0.14	0.10	0.12	0.02	0.06	0.05	0.38	0.02	0.03	0.04	0.00	0.07	0.05	0.04	0.03	0.00	0.03
Total	100.35	100.29	99.50	99.51	100.62	100.86	100.25	98.28	100.02	100.53	100.64	100.90	100.67	100.85	100.34	100.63	101.20	100.63
Si	2.421	2.420	2.432	2.428	2.301	2.275	2.387	2.402	2.320	2.474	2.401	2.419	2.346	2.370	2.319	2.335	2.398	2.345
Al	1.554	1.569	1.563	1.560	1.700	1.716	1.604	1.589	1.673	1.535	1.595	1.578	1.649	1.627	1.669	1.674	1.610	1.645
Fe	0.025	0.010	0.000	0.017	0.006	0.006	0.010	0.021	0.014	0.006	0.008	0.004	0.008	0.004	0.011	0.011	0.004	0.011
Ca	0.580	0.579	0.574	0.575	0.004	0.004	0.008	0.031	0.011	0.004	0.617	0.600	0.672	0.641	0.705	0.667	0.612	0.673
Na	0.430	0.426	0.431	0.416	0.717	0.751	0.635	0.614	0.716	0.537	0.357	0.382	0.306	0.349	0.282	0.280	0.346	0.315
K	0.013	0.008	0.006	0.007	0.254	0.237	0.351	0.313	0.247	0.416	0.002	0.000	0.004	0.003	0.002	0.002	0.000	0.002
Total	5.023	5.012	5.005	5.004	4.977	4.987	4.987	4.971	4.968	4.968	4.981	4.983	4.985	4.993	4.988	4.968	4.970	4.991
An%	56.67	57.20	56.84	57.60	73.74	75.77	64.22	64.63	74.28	56.22	63.16	61.09	68.42	64.57	71.29	70.31	63.88	67.97
Ab%	42.06	42.02	42.61	41.72	26.15	23.88	35.49	33.01	25.60	43.60	36.61	38.91	31.17	35.14	28.47	29.50	36.12	31.86
Or%	1.26	0.78	0.55	0.69	0.12	0.35	0.29	2.36	0.12	0.18	0.23	0.00	0.41	0.29	0.23	0.18	0.00	0.17

Sample #	Z4b-2	Z4b-2	Z4b-2	Z4b-3	Z4b-3	Z4b-3	Z4b-5	Z4b-5	Z4b-5	Z4b-6	Z4b-6	Z4b-6	Z4b-6	Z4b-8	Z4b-8	Z4b-8	Z4b-8	Z4b-9
Grain #	n6	n7	n7	n2	n2	n3	n2	n2	n2	n1	n2	n3	n3	n1	n2	n2	n3	n1
P.Loc	core	core	rim	core	core	core	core	core	rim	core	core	core	rim	core	core	core	core	core
SiO2	51.90	52.60	52.90	51.80	53.20	52.50	49.18	50.26	49.11	50.05	50.02	51.13	61.23	49.43	51.60	52.09	51.56	53.50
Al2O3	31.10	30.10	30.70	31.30	29.90	30.00	32.37	31.30	31.88	31.39	32.00	31.00	24.53	31.98	30.68	31.22	31.08	29.70
FeO	0.10	0.30	0.30	0.30	0.40	0.50	0.26	0.20	0.39	0.40	0.32	0.17	0.34	0.40	0.46	0.21	0.25	0.20
CaO	13.70	13.20	13.40	14.40	13.20	12.80	15.18	13.53	14.43	13.97	14.39	13.32	5.95	14.23	12.85	13.40	13.41	12.70
Na2O	3.50	4.00	4.10	3.30	3.90	3.70	2.66	3.60	3.10	3.40	3.15	3.67	6.52	3.21	3.74	3.70	3.67	4.10
K2O	0.03	0.00	0.05	0.04	0.11	0.13	0.10	0.08	0.10	0.15	0.12	0.08	0.67	0.00	0.09	0.08	0.07	0.30
Total	100.33	100.20	101.45	101.14	100.71	99.63	99.83	99.19	99.15	99.70	100.07	99.44	99.45	99.36	100.08	100.82	100.39	100.50
Si	2.346	2.382	2.368	2.330	2.397	2.389	2.252	2.310	2.265	2.297	2.281	2.336	2.733	2.271	2.355	2.347	2.340	2.412
Al	1.657	1.606	1.620	1.659	1.587	1.609	1.747	1.696	1.733	1.698	1.720	1.669	1.290	1.732	1.650	1.658	1.663	1.578
Fe	0.004	0.011	0.011	0.011	0.015	0.019	0.010	0.008	0.015	0.015	0.012	0.006	0.013	0.015	0.018	0.008	0.010	0.008
Ca	0.664	0.640	0.643	0.694	0.637	0.624	0.745	0.666	0.713	0.687	0.703	0.652	0.284	0.701	0.628	0.647	0.652	0.613
Na	0.307	0.351	0.356	0.288	0.341	0.326	0.236	0.321	0.277	0.303	0.278	0.325	0.564	0.286	0.331	0.323	0.323	0.358
K	0.002	0.000	0.003	0.002	0.006	0.008	0.006	0.005	0.006	0.009	0.007	0.005	0.038	0.000	0.005	0.004	0.004	0.017
Total	4.979	4.991	5.001	4.985	4.983	4.974	4.995	5.005	5.010	5.009	5.002	4.994	4.923	5.005	4.987	4.988	4.992	4.987
An%	68.26	64.58	64.18	70.52	64.74	65.14	75.52	67.19	71.59	68.80	71.13	66.44	32.06	71.02	65.16	66.39	66.62	62.02
Ab%	31.56	35.42	35.53	29.24	34.61	34.07	23.90	32.35	27.82	30.33	28.14	33.08	63.62	28.98	34.28	33.16	32.95	36.23
Or%	0.18	0.00	0.29	0.23	0.64	0.79	0.58	0.46	0.59	0.87	0.73	0.48	4.33	0.00	0.56	0.45	0.43	1.74

Table A4.13 (Con't)

Sample #	Z4b-9	Z4b-9	Z4b-9	Z4b-10	Z4b-10	Z4b-10	Z4b-10	Z4b-10	Z4b-10	Z4b-10	Z4b-11	Z4b-11	Z4b-12	Z4b-12	Z4b-12	Z4b-12	Z4b-12	Z4b-12
Grain #	n1	n2	n4	n2	n2	n3	n3	n4	n4	n4	n-3	n-3	n1	n1	n1	n1	n3	n3
P.Loc	rim	core	core	core	core	rim	core	rim	core	rim	core	core	core	core	rim	core	core	core
SiO2	53.20	55.10	53.30	51.00	52.60	52.30	52.20	51.60	55.10	52.00	51.66	53.30	47.98	47.79	49.42	47.18	47.34	47.50
Al2O3	30.00	28.30	30.10	31.40	30.60	30.60	30.60	31.00	28.90	30.70	29.41	29.85	32.84	32.89	31.44	33.40	33.05	32.78
FeO	0.20	0.40	0.40	0.10	0.20	0.30	0.30	0.40	0.40	0.20	2.44	0.14	0.35	0.30	0.40	0.38	0.33	0.24
CaO	12.90	11.40	13.00	14.30	13.60	13.50	13.50	14.00	11.60	13.60	11.37	11.29	15.08	15.22	13.87	15.69	15.34	15.46
Na2O	4.00	4.80	3.90	2.80	3.50	3.70	3.60	3.30	4.60	3.50	4.76	5.02	2.92	2.90	3.46	2.34	2.73	2.52
K2O	0.30	0.40	0.20	0.10	0.20	0.10	0.20	0.10	0.20	0.10	0.30	0.29	0.07	0.02	0.09	0.06	0.03	0.07
Total	100.60	100.40	100.90	99.70	100.70	100.50	100.40	100.40	100.80	100.10	99.94	99.89	99.25	99.13	98.68	99.05	98.82	98.57
Si	2.398	2.481	2.396	2.322	2.370	2.363	2.362	2.337	2.468	2.357	2.371	2.414	2.214	2.209	2.285	2.184	2.196	2.207
Al	1.594	1.502	1.595	1.685	1.625	1.629	1.632	1.655	1.525	1.640	1.591	1.593	1.786	1.791	1.713	1.822	1.807	1.795
Fe	0.008	0.015	0.015	0.004	0.008	0.011	0.011	0.015	0.015	0.008	0.093	0.005	0.013	0.012	0.016	0.015	0.013	0.009
Ca	0.623	0.550	0.626	0.698	0.657	0.654	0.654	0.680	0.557	0.661	0.559	0.548	0.746	0.753	0.687	0.778	0.762	0.770
Na	0.350	0.419	0.340	0.247	0.306	0.324	0.316	0.290	0.399	0.308	0.424	0.441	0.262	0.260	0.310	0.210	0.246	0.227
K	0.017	0.023	0.011	0.006	0.011	0.006	0.012	0.006	0.011	0.006	0.017	0.017	0.004	0.001	0.005	0.004	0.001	0.004
Total	4.989	4.989	4.983	4.962	4.976	4.987	4.986	4.983	4.975	4.979	5.055	5.018	5.026	5.027	5.016	5.012	5.025	5.011
An%	62.94	55.44	64.05	73.39	67.42	66.46	66.66	69.68	57.53	67.82	55.89	54.47	73.72	74.23	68.54	78.45	75.50	76.92
Ab%	35.32	42.24	34.77	26.00	31.40	32.96	32.17	29.72	41.29	31.58	42.37	43.86	25.85	25.64	30.92	21.17	24.35	22.64
Or%	1.74	2.32	1.17	0.61	1.18	0.59	1.18	0.59	1.18	0.59	1.74	1.67	0.44	0.13	0.54	0.38	0.15	0.44

Sample #	Z4b-13	Z4b-13	Z4b-13	Z4b-13	Z4b-13	Z4b-14	Z4b-14	Z4b-14	Z4b-14	Z4b-14	Z4b-14	Z4b-14	Z4b-15	Z4b-15	Z4b-15	Z4b-16
Grain #	n1	n1	n1	n2	n4	n1	n1	n3	n3	n3	n3	n3	n2	n4	n5	n4
P.Loc	rim	core	core	core	core	core	core	core	core	mid	rim	core	PC	PC	PC	core
SiO2	51.76	50.77	51.10	50.70	51.35	51.99	51.34	52.24	51.11	49.09	51.16	51.17	54.70	54.70	55.20	54.70
Al2O3	30.54	30.34	30.46	30.96	30.04	30.47	30.47	30.11	30.54	31.55	30.26	30.95	29.20	29.20	29.20	29.00
FeO	0.15	0.28	0.29	0.27	0.83	0.26	1.10	0.25	0.15	0.00	0.37	0.23	0.10	0.20	0.10	0.30
CaO	12.42	12.52	12.75	12.93	12.02	12.24	12.47	11.96	12.76	14.05	12.63	12.88	11.90	11.80	11.50	11.80
Na2O	4.36	4.20	4.24	3.87	4.25	4.52	4.61	4.62	4.13	3.41	4.24	4.10	4.60	4.70	4.80	4.70
K2O	0.18	0.16	0.22	0.18	0.25	0.16	0.12	0.13	0.11	0.08	0.14	0.10	0.10	0.00	0.10	0.30
Total	99.42	98.27	99.07	98.91	98.74	99.63	100.13	99.31	98.80	98.18	98.79	99.43	100.60	100.60	100.90	100.80
Si	2.362	2.348	2.347	2.330	2.365	2.368	2.342	2.384	2.349	2.278	2.354	2.338	2.453	2.453	2.465	2.454
Al	1.643	1.653	1.649	1.677	1.631	1.636	1.638	1.620	1.654	1.726	1.641	1.667	1.543	1.543	1.537	1.533
Fe	0.006	0.011	0.011	0.010	0.032	0.012	0.042	0.010	0.006	0.000	0.014	0.009	0.004	0.008	0.004	0.011
Ca	0.608	0.620	0.627	0.637	0.593	0.597	0.610	0.585	0.628	0.699	0.622	0.631	0.572	0.567	0.550	0.567
Na	0.386	0.377	0.378	0.344	0.380	0.399	0.408	0.409	0.368	0.307	0.378	0.364	0.400	0.409	0.416	0.409
K	0.011	0.010	0.013	0.010	0.015	0.009	0.007	0.007	0.007	0.005	0.008	0.006	0.006	0.000	0.006	0.017
Total	5.015	5.019	5.024	5.009	5.016	5.019	5.047	5.014	5.012	5.015	5.018	5.014	4.98	4.98	4.98	4.99
An%	60.52	61.64	61.61	64.21	60.08	59.38	59.50	58.41	62.63	69.14	61.72	63.06	58.50	58.11	56.64	57.11
Ab%	38.41	37.41	37.12	34.73	38.43	39.68	39.80	40.85	36.71	30.39	37.47	36.35	40.92	41.89	42.78	41.16
Or%	1.07	0.95	1.27	1.05	1.50	0.94	0.70	0.74	0.66	0.47	0.81	0.59	0.59	0.00	0.59	1.73

AMPHIBOLE ANALYSES

Cations calculated on the basis of 13 cations.

Mg# = Mg*100/(Mg+Fe)

Table A4.14Amphibole analyses, from Zone I.

Sample #	Z1-1	Z1-1	Z2-2	Z1-2	Z1-2	Z1-2	Z1-2	Z1-3	Z1-3	Z1-3	Z1-3	Z1-3	Z1-3	Z1-3	Z1-4	Z1-4	Z1-4
Grain #	n1	n1	n1	n2	n3	n3	n1	n2	n1	n1	n1	n2	n2	n3	n1	n1	n1
PLoc	core	rim	euhed	euhed	pk	pk	core	core	rim	core	rim	core	rim	core	core	core	rim
SiO2	45.34	48.16	53.80	54.20	54.40	52.20	44.60	45.60	54.45	45.97	50.64	45.57	48.81	46.08	49.80	49.90	45.40
TiO2	2.65	1.69	0.18	0.33	0.19	0.44	3.17	2.51	0.31	3.00	0.85	3.25	1.63	2.81	1.04	1.03	2.49
Al2O3	9.80	8.35	3.36	3.08	3.23	5.02	10.20	9.66	3.45	10.16	6.71	10.29	8.29	9.94	6.41	6.42	9.99
Cr2O3	0.14	0.15	0.02	0.05	0.05	0.14	0.11	0.22	0.08	0.13	0.16	0.18	0.17	0.26	0.12	0.15	0.25
FeO	8.49	7.36	6.77	6.27	6.33	6.22	7.94	7.94	6.49	8.03	6.81	7.69	7.21	7.25	7.96	7.08	8.16
MnO	0.09	0.08	0.18	0.27	0.21	0.10	0.06	0.05	0.13	0.12	0.11	0.00	0.00	0.13	0.20	0.09	0.02
MgO	16.87	18.53	18.90	19.30	19.60	18.90	15.50	15.80	19.50	15.79	18.45	15.97	17.45	16.29	17.50	17.80	15.90
CaO	11.74	11.69	11.80	11.90	12.10	11.90	11.80	12.00	11.73	11.70	11.81	11.39	11.55	11.56	11.70	11.70	11.70
Na2O	2.22	1.87	0.52	0.54	0.62	0.92	2.04	2.02	0.77	2.03	1.49	2.24	1.84	2.09	1.40	1.37	1.96
K2O	0.49	0.34	0.13	0.15	0.13	0.22	0.50	0.54	0.13	0.47	0.28	0.43	0.38	0.51	0.30	0.24	0.44
Total	97.83	98.22	95.66	96.09	96.86	96.06	95.92	96.34	97.04	97.40	97.31	97.01	97.33	96.92	96.43	95.78	96.31
Si	6.454	6.715	7.611	7.629	7.598	7.375	6.522	6.639	7.577	6.592	7.109	6.544	6.898	6.614	7.103	7.137	6.573
Al	1.646	1.373	0.560	0.512	0.532	0.836	1.760	1.659	0.567	1.718	1.111	1.743	1.382	1.683	1.078	1.083	1.706
Cr	0.016	0.017	0.002	0.006	0.006	0.016	0.013	0.025	0.009	0.015	0.018	0.020	0.019	0.030	0.014	0.017	0.029
Fe#3	0.579	0.767	0.434	0.391	0.413	0.410	0.116	0.072	0.476	0.191	0.465	0.239	0.385	0.223	0.461	0.394	0.315
Ti	0.284	0.177	0.019	0.035	0.020	0.047	0.349	0.275	0.032	0.324	0.090	0.351	0.173	0.303	0.112	0.111	0.271
Mg	3.579	3.850	3.985	4.049	4.080	3.979	3.378	3.428	4.044	3.374	3.860	3.418	3.675	3.485	3.720	3.794	3.431
Fe#2	0.431	0.091	0.367	0.347	0.326	0.325	0.855	0.894	0.279	0.772	0.334	0.685	0.467	0.648	0.488	0.453	0.673
Mn	0.011	0.009	0.022	0.032	0.025	0.012	0.007	0.006	0.015	0.015	0.013	0.000	0.000	0.016	0.024	0.011	0.002
Ca	1.791	1.746	1.789	1.795	1.811	1.801	1.849	1.872	1.749	1.798	1.776	1.753	1.749	1.778	1.788	1.793	1.815
Na	0.613	0.506	0.143	0.147	0.168	0.252	0.579	0.570	0.208	0.564	0.406	0.623	0.504	0.581	0.387	0.380	0.550
K	0.089	0.060	0.023	0.027	0.023	0.040	0.093	0.100	0.023	0.086	0.050	0.079	0.069	0.093	0.055	0.044	0.081
Sum Cat	15.493	15.313	14.955	14.969	15.002	15.093	15.521	15.543	14.980	15.448	15.232	15.455	15.322	15.453	15.230	15.217	15.447

Sample #	Z1-5	Z1-5	Z1-5	Z1-5	Z1-6	Z1-6	Z1-7	Z1-8	Z1-8	Z1-8	Z1-8	Z1-9	Z1-9	Z1-9
Grain #	n1	n1	n2	n2	n1	n1	n1	n1	n1	n2	n3	n1	n2	n3
P.LOc	core	core	core	core	core	rim	core	core	rim	core	core	core	core	core
SiO2	48.70	50.60	53.50	54.00	43.70	46.00	42.35	41.60	43.11	42.05	51.72	42.60	41.90	42.10
TiO2	1.14	0.68	0.21	0.24	3.43	2.19	3.60	4.12	3.63	3.42	0.60	3.33	4.02	3.97
Al2O3	7.19	5.72	2.80	3.17	10.60	9.08	10.87	11.16	9.81	11.00	3.86	11.70	11.70	11.80
Cr2O3	0.07	0.06	0.12	0.15	0.16	0.21	0.43	0.62	0.39	0.49	0.00	1.09	1.21	1.10
FeO	7.49	7.04	6.97	7.56	8.46	8.28	10.30	10.87	11.36	10.41	9.99	8.05	7.98	8.33
MnO	0.10	0.10	0.12	0.14	0.13	0.07	0.15	0.17	0.18	0.10	0.11	0.06	0.12	0.09
MgO	18.20	19.00	19.90	19.70	16.10	17.10	12.88	13.69	14.01	13.84	17.82	15.70	15.20	15.30
CaO	11.70	11.80	12.00	11.90	11.60	11.60	11.69	11.10	11.08	11.49	11.29	11.80	11.80	11.90
Na2O	1.41	1.14	0.54	0.72	2.37	2.14	2.38	2.71	2.35	2.26	0.93	2.39	2.55	2.50
K2O	0.29	0.22	0.11	0.15	0.52	0.40	0.67	0.47	0.63	0.64	0.22	0.00	0.00	0.00
Total	96.29	96.36	96.27	97.73	97.07	97.07	95.32	96.51	96.55	95.70	96.54	96.72	96.48	97.09
Si	6.914	7.135	7.507	7.481	6.306	6.572	6.390	6.146	6.350	6.254	7.330	6.157	6.113	6.100
Al	1.204	0.951	0.463	0.518	1.804	1.530	1.935	1.945	1.705	1.930	0.645	1.994	2.013	2.017
Cr	0.008	0.007	0.013	0.016	0.018	0.024	0.051	0.072	0.045	0.058	0.000	0.125	0.140	0.126
Fe#3	0.716	0.711	0.660	0.700	0.475	0.614	0.000	0.395	0.458	0.303	0.818	0.519	0.329	0.394
Ti	0.122	0.072	0.022	0.025	0.372	0.235	0.409	0.458	0.402	0.383	0.064	0.362	0.441	0.433
Mg	3.851	3.993	4.162	4.067	3.462	3.641	2.896	3.014	3.076	3.068	3.764	3.382	3.305	3.304
Fe#2	0.173	0.119	0.129	0.175	0.546	0.375	1.300	0.948	0.942	0.992	0.341	0.454	0.645	0.615
Mn	0.012	0.012	0.014	0.016	0.016	0.008	0.019	0.021	0.022	0.013	0.013	0.007	0.015	0.011
Ca	1.780	1.783	1.804	1.766	1.794	1.776	1.890	1.757	1.749	1.831	1.714	1.827	1.845	1.848
Na	0.388	0.312	0.147	0.193	0.663	0.593	0.696	0.777	0.671	0.652	0.256	0.670	0.721	0.702
K	0.053	0.040	0.020	0.027	0.096	0.073	0.129	0.089	0.118	0.121	0.040	0.000	0.000	0.000
Sum Cat	15.221	15.134	14.971	14.986	15.552	15.442	15.715	15.622	15.538	15.604	15.010	15.497	15.566	15.550

Table A4.15 Amphibole analyses, from Zone II

Sample #	Z2-2	Z2-2	Z2-2	Z2-2	Z2-2	Z2-2	Z2-2	Z2-2	Z2-2	Z2-2	Z2-5	Z2-5	Z2-5	Z2-5	Z2-5	Z2-6	Z2-6	Z2-6
Grain #	n1	n1	n2	n2	n2	n2	n1	n2	n2	n3	n1	n1	n1	n1	n1	n1	n1	n1
P.Loc	core	core	core	rim	rim	rim	pk	pk	pk	pk	core	core	rim	rim	rim	trv	trv	trv
SiO2	48.90	48.90	48.90	49.40	49.20	51.70	42.88	42.81	42.94	42.75	43.30	43.80	48.00	49.10	44.90	48.10	48.60	48.60
TiO2	1.56	1.56	1.50	1.41	1.41	0.96	3.79	3.50	3.46	3.45	3.36	3.47	1.96	1.64	2.93	1.81	1.72	1.48
Al2O3	6.40	6.40	6.56	6.24	6.55	4.51	10.64	10.86	10.69	10.69	10.90	10.50	7.53	6.67	9.71	7.46	7.34	7.13
Cr2O3	0.00	0.00	0.00	0.01	0.01	0.05	0.08	0.00	0.00	0.00	0.38	0.33	0.21	0.25	0.42	0.08	0.05	0.00
FeO	12.70	12.70	12.70	12.80	12.80	11.60	14.43	14.95	14.60	14.13	12.70	12.30	11.20	11.10	12.20	12.30	12.60	12.80
MnO	0.26	0.26	0.23	0.28	0.20	0.26	0.12	0.19	0.16	0.17	0.12	0.26	0.14	0.15	0.14	0.22	0.23	0.23
MgO	14.20	14.20	14.30	14.70	14.30	15.80	12.51	12.47	12.57	13.09	13.20	13.80	15.70	16.30	14.30	15.20	14.90	15.00
CaO	11.70	11.70	11.70	11.80	12.10	11.80	10.84	10.98	11.24	11.35	11.70	11.60	11.60	11.50	11.50	11.70	11.80	11.90
Na2O	1.00	1.00	1.00	1.06	0.94	0.91	2.16	2.14	1.89	1.96	2.10	2.14	1.57	1.38	2.02	1.07	1.13	1.12
K2O	0.50	0.50	0.59	0.53	0.61	0.35	0.61	0.63	0.78	0.73	0.54	0.53	0.45	0.42	0.58	0.49	0.51	0.52
total	97.22	97.22	97.48	98.23	98.12	97.94	98.06	98.53	98.33	98.32	98.30	98.73	98.36	98.51	98.70	98.43	98.88	98.78
Si	7.093	7.093	7.072	7.082	7.092	7.365	6.252	6.218	6.256	6.215	6.298	6.318	6.827	6.930	6.448	6.838	6.903	6.914
Al	1.095	1.095	1.119	1.055	1.114	0.758	1.830	1.861	1.837	1.833	1.870	1.786	1.263	1.111	1.645	1.250	1.229	1.197
Cr	0.000	0.000	0.000	0.001	0.001	0.006	0.009	0.000	0.000	0.000	0.044	0.038	0.024	0.028	0.048	0.009	0.006	0.000
Fe#3	0.369	0.369	0.396	0.458	0.282	0.382	0.714	0.801	0.705	0.759	0.416	0.506	0.590	0.721	0.570	0.730	0.597	0.627
Ti	0.170	0.170	0.163	0.152	0.153	0.103	0.416	0.382	0.379	0.377	0.368	0.376	0.210	0.174	0.316	0.194	0.184	0.158
Mg	3.070	3.070	3.082	3.141	3.072	3.355	2.718	2.699	2.729	2.836	2.861	2.966	3.328	3.429	3.061	3.220	3.154	3.180
Fe#2	1.172	1.172	1.140	1.076	1.262	1.000	1.046	1.015	1.074	0.959	1.129	0.977	0.742	0.590	0.895	0.732	0.900	0.896
Mn	0.032	0.032	0.028	0.034	0.024	0.031	0.015	0.023	0.020	0.021	0.015	0.032	0.017	0.018	0.017	0.026	0.028	0.028
Ca	1.818	1.818	1.813	1.813	1.869	1.801	1.694	1.709	1.755	1.768	1.823	1.793	1.768	1.739	1.770	1.782	1.796	1.814
Na	0.282	0.282	0.280	0.294	0.263	0.252	0.610	0.603	0.534	0.552	0.593	0.598	0.433	0.378	0.562	0.295	0.311	0.309
K	0.093	0.093	0.109	0.097	0.112	0.064	0.113	0.117	0.145	0.135	0.100	0.098	0.082	0.076	0.106	0.089	0.092	0.094
Sum Cat	15.192	15.192	15.202	15.204	15.244	15.116	15.418	15.428	15.434	15.456	15.516	15.489	15.282	15.193	15.438	15.166	15.199	15.217

Sample #	Z2-6	Z2-6	Z2-6	Z2-7	Z2-7	Z2-7	Z2-7	Z2-8	Z2-8	Z2-8	Z2-9	Z2-9	Z2-9	Z2-10	Z2-10	Z2-10	Z2-10	Z-2-11
Grain #	n1	n1	n1	n1	n1	n2	n2	n1	n2	n3	n1	n1	n1	n1	n1	n2	n3	n1
P.Loc	trv	trv	trv	core	rim	core	rim	core	pdeopx	core	rim	core	rim	core	rim	core	core	core
SiO2	47.20	47.20	47.20	47.60	47.40	43.90	47.30	42.00	41.60	42.20	49.00	46.50	50.40	45.50	46.00	43.40	43.90	46.20
TiO2	1.38	1.55	1.51	1.48	1.61	2.73	1.65	2.74	2.81	1.38	1.03	1.91	0.75	2.08	1.82	2.64	2.50	1.82
Al2O3	6.83	6.85	6.97	6.32	7.13	9.20	6.78	11.90	12.40	12.40	6.32	7.92	4.87	8.45	8.04	10.10	9.54	8.07
Cr2O3	0.06	0.16	0.12	0.03	0.00	0.07	0.02	0.11	0.05	0.03	0.11	0.03	0.07	0.05	0.06	0.00	0.02	0.08
FeO	12.30	12.80	12.50	13.60	13.90	14.50	13.50	12.70	13.10	12.50	14.60	14.60	13.30	15.00	15.20	15.80	15.20	13.40
MnO	0.24	0.20	0.11	0.31	0.30	0.23	0.26	0.16	0.15	0.26	0.27	0.40	0.46	0.32	0.32	0.40	0.31	0.22
MgO	14.40	14.50	14.50	14.40	14.40	12.70	14.40	13.00	13.20	13.90	13.80	12.50	14.50	13.20	13.30	12.10	12.50	14.40
CaO	11.80	11.50	11.60	11.80	11.50	11.40	11.70	11.30	11.30	11.20	11.60	11.50	11.40	11.20	11.30	11.30	11.40	11.20
Na2O	0.99	1.10	1.26	1.07	1.24	1.58	1.01	2.23	2.47	2.27	0.89	1.34	0.72	1.36	1.29	1.74	1.57	1.18
K2O	0.55	0.47	0.49	0.50	0.58	0.74	0.61	0.67	0.75	0.48	0.50	0.84	0.31	0.51	0.49	0.72	0.67	0.57
total	95.75	96.33	96.26	97.11	98.06	97.05	97.23	96.81	97.83	96.62	98.12	97.54	96.78	97.67	97.82	98.20	97.61	97.14
Si	6.950	6.890	6.909	6.930	6.819	6.477	6.868	6.182	6.067	6.145	7.053	6.832	7.289	6.605	6.666	6.348	6.438	6.673
Al	1.186	1.179	1.204	1.086	1.210	1.601	1.162	2.067	2.133	2.130	1.072	1.373	0.831	1.446	1.375	1.742	1.650	1.375
Cr	0.007	0.018	0.014	0.003	0.000	0.008	0.002	0.013	0.006	0.003	0.013	0.003	0.008	0.006	0.007	0.000	0.002	0.009
Fe#3	0.493	0.685	0.544	0.650	0.805	0.635	0.701	0.623	0.740	1.050	0.668	0.378	0.627	0.923	0.927	0.812	0.767	0.972
Ti	0.153	0.170	0.166	0.162	0.174	0.303	0.180	0.303	0.308	0.151	0.111	0.211	0.082	0.227	0.198	0.290	0.276	0.198
Mg	3.160	3.154	3.163	3.125	3.088	2.793	3.116	2.852	2.869	3.016	2.960	2.737	3.125	2.856	2.873	2.637	2.732	3.100
Fe#2	1.022	0.877	0.987	1.006	0.867	1.155	0.939	0.941	0.858	0.473	1.089	1.416	0.981	0.898	0.915	1.121	1.097	0.646
Mn	0.030	0.025	0.014	0.038	0.037	0.029	0.032	0.020	0.019	0.032	0.033	0.050	0.056	0.039	0.039	0.050	0.039	0.027
Ca	1.862	1.799	1.819	1.841	1.773	1.802	1.820	1.782	1.766	1.747	1.789	1.810	1.767	1.742	1.755	1.771	1.791	1.733
Na	0.282	0.311	0.358	0.302	0.346	0.452	0.285	0.637	0.698	0.641	0.248	0.382	0.202	0.383	0.362	0.493	0.447	0.331
K	0.103	0.088	0.092	0.093	0.106	0.139	0.113	0.126	0.140	0.089	0.092	0.157	0.057	0.094	0.091	0.134	0.125	0.105
Sum Cat	15.248	15.198	15.269	15.236	15.225	15.394	15.218	15.545	15.604	15.478	15.129	15.350	15.026	15.219	15.208	15.399	15.363	15.169

Table A4.15 (Con't)

Sample #	Z-2-11	Z2-14	Z2-14	Z2-14	Z2-14	Z2-14	Z2-14	Z2-14	Z2-14
Grain #	n1	n1	n1	n2	n2	n3	n3	n4	n4
P.Loc	rim	pk	pk	pk	pk	pk	pk	pk	pk
SiO2	44.60	43.73	43.52	42.70	42.93	49.51	44.90	48.24	49.29
TiO2	1.96	2.99	3.27	3.54	3.59	1.21	2.63	1.25	1.14
Al2O3	9.18	9.99	10.27	10.74	10.20	6.12	8.89	6.66	6.39
Cr2O3	0.00	0.14	0.00	0.08	0.00	0.00	0.00	0.00	0.00
FeO	13.70	14.91	14.40	14.63	14.90	12.95	14.46	12.76	12.78
MnO	0.20	0.20	0.23	0.22	0.17	0.39	0.30	0.37	0.39
MgO	13.50	12.68	12.72	12.53	12.60	15.79	13.40	15.39	16.35
CaO	11.30	10.93	10.87	11.16	11.00	11.02	11.01	11.00	11.35
Na2O	1.26	2.00	2.08	2.15	2.00	1.15	1.54	1.60	1.07
K2O	0.71	0.70	0.69	0.62	0.64	0.41	0.82	0.42	0.33
total	96.41	98.27	98.05	98.37	98.03	98.55	97.95	97.69	99.09
Si	6.540	6.358	6.336	6.224	6.268	6.971	6.509	6.895	6.885
Al	1.588	1.714	1.764	1.846	1.756	1.016	1.520	1.122	1.053
Cr	0.000	0.016	0.000	0.009	0.000	0.000	0.000	0.000	0.000
Fe#3	0.857	0.801	0.740	0.712	0.793	1.060	0.885	0.930	1.130
Ti	0.216	0.327	0.358	0.388	0.394	0.128	0.287	0.134	0.120
Mg	2.950	2.748	2.760	2.722	2.742	3.313	2.895	3.278	3.404
Fe#2	0.824	1.012	1.013	1.072	1.026	0.452	0.868	0.595	0.301
Mn	0.025	0.025	0.028	0.027	0.021	0.047	0.037	0.045	0.046
Ca	1.776	1.703	1.696	1.743	1.721	1.663	1.710	1.685	1.699
Na	0.358	0.564	0.587	0.608	0.566	0.314	0.433	0.443	0.290
K	0.133	0.130	0.128	0.115	0.119	0.074	0.152	0.077	0.059
Sum Cat	15.267	15.397	15.411	15.466	15.406	15.050	15.295	15.205	15.047

Table A4.16 Amphibole analyses , from Zone III and Zone IV

Sample #	Z3-13	Z3-14	Z3-14	Z3-18	Z3-23	Z3-23	Z3-23	Z4b-1	Z4b-1	Z4b-1	Z4b-1	Z4a-10	Z4b-10
SiO2	47.70	47.40	42.30	46.20	48.11	47.51	49.74	42.62	41.90	41.52	42.12	42.19	42.11
TiO2	1.39	1.90	4.19	1.96	1.87	2.30	1.59	3.33	4.02	4.76	3.97	3.64	3.54
Al2O3	6.43	6.69	10.90	7.30	6.60	7.38	5.63	11.69	11.70	11.44	11.79	11.52	10.59
Cr2O3	0.00	0.13	0.10	0.00	0.17	0.00	0.00	1.09	1.21	1.20	1.10	0.00	0.00
FeO	12.50	11.60	13.00	13.40	11.55	11.31	10.41	8.05	7.98	7.85	8.33	11.69	13.45
MnO	0.08	0.13	0.18	0.08	0.15	0.14	0.25	0.06	0.12	0.09	0.09	0.22	0.14
MgO	14.70	15.30	12.70	14.40	15.90	15.68	16.99	15.70	15.20	15.08	15.29	12.98	12.13
CaO	11.40	11.40	11.10	11.30	10.91	11.21	11.46	11.79	11.79	11.82	11.94	11.34	11.55
Na2O	1.07	1.23	2.37	1.31	1.74	1.71	1.07	2.39	2.55	2.55	2.51	1.98	1.73
K2O	0.54	0.58	0.66	0.72	0.61	0.76	0.47	1.20	1.26	1.33	1.25	0.69	0.90
Total	95.81	96.36	97.50	96.67	97.61	98.00	97.61	97.92	97.73	97.64	98.39	96.25	96.14
Si	6.986	6.890	6.225	6.747	6.879	6.795	7.043	6.159	6.113	6.088	6.104	6.245	6.314
Al	1.111	1.147	1.892	1.257	1.121	1.245	0.957	1.841	1.887	1.912	1.896	1.755	1.686
Cr	0.000	0.015	0.012	0.000	0.019	0.000	0.000	0.152	0.126	0.067	0.119	0.257	0.186
Fe#3	0.627	0.638	0.418	0.777	0.763	0.621	0.763	0.125	0.140	0.139	0.126	0.000	0.000
Ti	0.153	0.208	0.464	0.215	0.201	0.247	0.169	0.298	0.098	0.000	0.142	0.392	0.316
Mg	3.209	3.314	2.785	3.134	3.388	3.342	3.585	0.362	0.441	0.525	0.433	0.405	0.399
Fe#2	0.904	0.772	1.182	0.860	0.610	0.732	0.453	3.381	3.305	3.295	3.302	2.863	2.710
Mn	0.010	0.016	0.022	0.010	0.018	0.017	0.030	0.675	0.876	0.963	0.867	1.055	1.371
Ca	1.789	1.776	1.750	1.768	1.672	1.718	1.739	0.007	0.015	0.011	0.011	0.028	0.018
Na	0.304	0.346	0.677	0.371	0.482	0.474	0.293	1.826	1.843	1.857	1.854	1.799	1.855
K	0.101	0.108	0.124	0.134	0.111	0.139	0.085	0.669	0.721	0.725	0.705	0.568	0.503
Sum Cat	15.194	15.230	15.550	15.273	15.265	15.331	15.117	15.717	15.799	15.831	15.790	15.497	15.531

APPENDIX 5

GEOCHEMICAL ANALYTICAL TECHNIQUES

Before crushing, samples were cleaned in distilled water and cut into small 1-2 cm^3 pieces, and cleaned in distilled water and dried. Then they were ground to a fine powder in a tungsten-carbide puck mill.

Major element oxides were determined by Inductively Coupled Plasma (ICP) at the Department of Mines and Energy, Newfoundland. The following elements- Ti, Mn, P, Y, Nb and Zr - were determined by XRF at Memorial University of Newfoundland. The rare earth elements (REE), Hf, Ta and Th were determined by Inductively Coupled Plasma-Mass Spectrometry (ICP-MS) at Memorial University of Newfoundland (for detail see Longerich et al., 1990; Jenner et al., 1990). A Na_2O_2 sinter dissolution (Robinson et al., 1986) technique was used.

Table A5.1 Whole rock geochemical analyses , from the TLS.

Sample#	F-91-582.1	F-91-582.2	F-92-69	F-92-70	F-92-68	F-19	F-20	N-10	F-91-50.2b	F-91-174
Map Unit	Zone I	Zone I	Zone II	Zone II	Zone II	Zone III	Zone III	Zone III	Zone IVb	Zone IVb
SiO2	52.4	52.4	52.7	53.6	44.6	49.8	52.6	44.8	41.6	50.1
Al2O3	11.2	8.5	11.8	17.1	8.6	6.8	8.7	16.1	9.4	23.6
Fe2O3	1.1	1.4	2.0	1.9	2.9	2.8	2.6	4.7	2.9	1.6
FeO	4.5	5.0	7.9	5.1	11.6	9.7	9.1	7.8	10.4	2.6
MgO	14.0	16.1	11.2	5.9	22.7	13.2	12.3	5.5	22.1	4.4
CaO	11.8	11.2	6.4	8.3	5.8	9.6	8.1	10.6	6.6	12.1
Na2O	1.4	1.2	2.5	3.5	1.1	1.5	1.8	3.1	0.9	3.2
K2O	0.5	0.5	0.8	0.7	0.4	0.7	0.7	0.3	0.1	0.3
TiO2	0.35	0.40	0.89	1.02	0.80	2.27	2.13	2.96	0.69	0.46
MnO	0.13	0.15	0.21	0.12	0.24	0.25	0.21	0.15	0.22	0.05
P2O5	0.06	0.07	0.22	0.22	0.07	0.42	0.19	1.45	0.10	0.08
L.O.I.	1.24	1.70	1.67	1.56	0.80	1.60	1.24	1.12	3.84	1.01
Total	98.63	98.57	98.30	99.17	99.71	98.69	99.62	98.65	99.06	99.60
Mg#	84.80	85.05	71.46	67.12	77.69	70.83	70.74	55.87	79.14	74.86
Cu	65	62	40	28	34	85	83	54	22	12
Zn	44	48	94	54	110	86	74	91	83	20
Cr	456	617	744	93	1726	549	382	74	141	71
Ni	187	211	299	69	479	253	214	34	360	34
V	102	120	159	138	195	248	177	278	106	18
Sc	36	32	30	27	23	48	32	28	18	82
Ba	141	113	144	139	95	86	104	100	94	224
Rb	17	16	24	19	12	17	25	7	3	3
Sr	453	294	321	525	348	161	280	748	504	1389
Zr	25	36	56	52	51	89	55	51	15	9
Nb	1.7	1.9	4.1	4.0	2.2	6.1	5.1	9.0	1.2	0.5
Y	7.0	8.4	17.9	12.7	9.0	19.3	35.2	32.0	4.0	5.0
Hf	0.9	1.2	1.9	1.8	1.5	2.2	2.7	1.5	0.6	0.6
Ta	0.5	0.5	0.7	0.7	0.6	1.0	0.9	0.9	0.2	0.5
Th	1.3	1.7	1.9	3.3	1.2	1.9	2.4	0.5	0.5	0.3
La	6.08	6.80	12.0	10.2	6.68	12.6	6.2	16.4	4.18	7.70
Ce	14.0	16.2	28.6	22.7	16.1	33.7	15.6	45.5	9.96	16.9
Pr	1.79	2.12	3.54	2.74	2.04	4.75	2.19	6.52	1.27	2.09
Nd	7.54	9.06	14.4	11.08	8.80	21.8	10.5	30.6	5.23	9.37
Sm	1.55	1.96	3.16	2.61	1.97	5.81	2.85	7.12	1.11	1.69
Eu	0.48	0.53	0.91	0.97	0.73	1.42	0.93	2.36	0.39	0.77
Gd	1.45	1.80	3.23	2.50	1.31	6.17	3.12	7.43	1.03	1.35
Tb	0.23	0.24	0.47	0.39	0.29	0.95	0.55	0.99	0.13	0.21
Dy	1.43	1.70	3.06	2.40	2.05	6.44	3.70	6.40	0.79	1.23
Ho	0.26	0.31	0.62	0.46	0.40	1.16	0.68	1.10	0.13	0.22
Er	0.68	0.81	1.72	1.24	1.13	3.35	2.06	2.90	0.37	0.56
Tm	0.09	0.12	0.26	0.18	0.16	0.48	0.27	0.38	0.05	0.07
Yb	0.68	0.78	1.74	1.16	1.31	3.15	1.65	2.19	0.33	0.44
Lu	0.09	0.11	0.25	0.18	0.20	0.44	0.27	0.31	0.05	0.08
(Eu/Eu*)CHUR	0.96	0.85	0.86	1.15	1.15	0.95	0.72	0.98	1.10	1.21
(La/Lu)CHUR	6.93	6.38	4.98	6.02	3.45	3.01	2.39	5.41	7.99	10.51
(La/Sm)CHUR	2.40	2.10	2.40	2.50	2.10	1.39	1.37	1.45	2.40	2.90
(Gd/Lu)CHUR	1.70	2.24	1.99	1.56	0.82	1.93	1.29	3.07	1.20	1.60
(Nb/La)PRIM	0.28	0.27	0.34	0.39	0.32	0.48	0.81	0.54	0.27	0.06

Table A5.1 (Con't)

Sample#	F-91-176	F-91-279.1	F-91-280	F-91-9	F-91-10	F-91-11*	F-91-582.3	F-91-582.4	F-91-582.5	F-91-32
Map Unit	Zone IVb	Zone IVa	Zone IVa	Zone IVb	Zone IVb	Zone IVb	Zone I	Zone I	Zone I	Zone I
SiO2	43.6	48.4	46.6	42.6	42.5	46.1	50.6	54.6	53.4	53.0
Al2O3	16.6	18.6	8.9	6.4	9.8	17.2	13.6	5.2	11.3	8.0
Fe2O3	6.6	2.7	2.8	3.3	2.7	NA	1.5	1.8	1.1	2.0
FeO	7.8	4.8	10.0	8.5	10.8	7.9	4.0	5.2	4.4	8.7
MgO	6.0	9.1	20.8	28.5	22.7	11.5	13.6	18.1	14.0	19.0
CaO	12.0	11.0	5.8	4.1	7.2	13.8	12.4	10.6	11.1	5.4
Na2O	2.3	2.6	1.1	0.9	1.1	1.7	1.4	1.0	1.4	1.3
K2O	0.2	0.3	0.3	0.4	0.1	0.2	0.3	0.5	0.4	0.3
TiO2	2.03	0.48	0.51	0.43	0.51	1.52	0.28	0.43	0.30	0.60
MnO	0.10	0.12	0.24	0.18	0.21	0.1	0.12	0.17	1.32	0.22
P2O5	0.04	0.06	0.06	0.27	0.09	0.12	0.04	0.07	0.04	0.14
L.O.I.	1.75	1.36	2.38	4.00	3.10	NA	1.34	1.91	1.15	1.31
Total	98.99	99.54	99.48	99.69	100.68	100.22	99.04	99.56	100.06	99.78
Mg#	57.82	77.02	78.79	85.63	78.93	NA	85.95	85.99	85.10	79.45
Cu	104	67	37	28	32	94	56	66	71	34
Zn	56	41	94	82	85	27	39	56	115	93
Cr	37	325	420	1459	129	639	460	805	485	1088
Ni	44	111	267	1071	350	179	171	269	183	236
V	583	102	99	74	81	211	81	123	94	186
Sc	35	26	24	11	16	38	39	40	39	27
Ba	114	125	94	119	88	134	78	114	189	66
Rb	2	3	5	12	3	2	10	15	14	7
Sr	997	601	298	347	569	1013	564	135	471	183
Zr	12	25	31	45	19	21	18	43	26	27
Nb	0.5	1.4	1.8	1.9	0.9	2.4	0.8	1.8	1.7	2.3
Y	8.1	7.0	7.5	8.2	4.2	7.0	5.4	9.2	6.8	9.1
Hf	0.7	0.8	0.8	0.9	0.6	1.1				
Ta	0.3	0.4	0.2	0.1	0.2	1.2				
Th	0.5	0.8	0.8	1.1	0.4	0.4				
La	5.18	6.04	5.33	8.00	5.43	7.66				
Ce	13.5	13.2	13.1	18.9	12.4	19.1				
Pr	1.88	1.58	1.69	2.33	1.60	2.64				
Nd	8.61	6.69	6.92	9.18	6.78	12.08				
Sm	2.11	1.43	1.52	1.73	1.35	2.60				
Eu	0.77	0.71	0.48	0.42	0.51	1.00				
Gd	1.88	1.41	1.45	1.31	1.02	2.45				
Tb	0.27	0.20	0.23	0.18	0.17	0.32				
Dy	1.65	1.36	1.51	1.21	0.85	1.97				
Ho	0.30	0.26	0.29	0.21	0.17	0.34				
Er	0.83	0.71	0.89	0.59	0.49	0.92				
Tm	0.10	0.09	0.13	0.08	0.07	1.12				
Yb	0.70	0.61	0.82	0.50	0.39	0.68				
Lu	0.09	0.11	0.13	0.07	0.06	0.11				
(Eu/Eu*)CHUR	1.16	1.51	0.97	0.82	1.91	1.19				
(La/Lu)CHUR	5.74	5.73	4.18	11.86	9.55	7.23				
(La/Sm)CHUR	1.60	2.70	2.20	3.00	2.40	1.90				
(Gd/Lu)CHUR	2.40	1.70	1.70	1.60	1.30	3.10				
(Nb/La)PRIM	0.10	0.22	0.34	0.24	0.17	0.31				

Table A5.1 (Con't)

Sample#	F-91-532.1	F-13	F-14	F-15	F-26	F-91-103.2	N-11	N-12	F-91-1	F-91-2
Map Unit	Zone II	Zone III	Zone III	Zone III	Zone III	Zone III	Zone III	Zone III	Zone IVb	Zone IVb
SiO2	49.4	49.5	51.7	50.0	49.2	49.6	48.7	50.8	50.0	50.0
Al2O3	16.6	15.3	10.8	7.3	12.8	4.1	16.0	7.0	17.0	17.8
Fe2O3	3.9	3.4	3.2	2.8	2.9	3.3	3.2	4.1	2.4	2.3
FeO	6.8	7.5	8.2	9.3	8.4	12.6	7.6	11.1	4.3	4.2
MgO	4.7	5.5	9.8	12.9	9.2	14.2	6.0	14.8	7.2	6.8
CaO	8.8	8.9	8.2	9.8	8.8	8.7	9.5	5.0	12.4	12.6
Na2O	3.6	3.4	2.4	1.6	2.3	0.8	3.4	1.4	2.5	2.7
K2O	1.0	0.7	1.0	0.6	0.5	0.5	0.5	0.8	0.4	0.3
TiO2	2.38	2.51	2.17	2.10	2.90	4.02	2.30	1.39	0.94	0.85
MnO	0.12	0.16	0.25	0.23	0.14	0.27	0.14	0.30	0.09	0.09
P2O5	1.76	1.28	0.27	0.39	0.13	0.15	0.99	0.54	0.29	0.14
L.O.I.	1.15	1.01	2.02	1.61	1.92	1.49	0.99	1.45	1.31	0.96
Total	100.23	99.20	99.91	98.75	99.08	99.68	99.12	98.71	98.71	98.74
MG#	55.26	56.71	68.10	71.08	66.16	66.72	58.57	70.51	74.96	74.24
Cu	53	36	58	76	53	135	50	126	68	59
Zn	86	78	165	79	68	115	72	122	25	30
Cr	26	64	354	523	227	418	179	906	300	203
Ni	20	32	126	235	151	260	107	372	107	101
V	306	218	242	238	241	352	211	233	156	161
Sc	42	27	43	43	39	59	25	33	27	26
Ba	214	151	199	83	117	53	133	138	194	225
Rb	27	19	31	16	14	16	9	26	8	7
Sr	645	593	276	196	454	78	705	211	1031	1032
Zr	107	98	103	83	47	93	45	43	54	63
Nb	12.9	12.8	11.0	8.4	5.9	13.3	10.4	5.6	2.4	2.0
Y	56.9	34.3	40.8	33.0	13.3	30.4	27.7	22.4	11.0	9.7

Sample#	F-91-281.1	F-91-281.2	F-91-50.6	F-92-71	F-92-72	F-92-73	F-92-74	N-13	N-14	N-16
Map Unit	Zone IVa	Zone IVa	Zone IVb	Zone II	Zone II	Zone II	Zone II	Zone III	Zone III	Zone III
SiO2	45.8	47.8	42.0	53.2	48.3	47.8	52.1	52.7	49.7	46.8
Al2O3	13.0	3.4	9.4	17.7	17.2	19.0	18.1	17.6	10.3	17.2
Fe2O3	1.8	0.8	3.1	3.1	5.1	2.8	2.8	1.7	2.4	4.6
FeO	8.8	8.1	10.4	5.3	6.7	6.0	5.3	5.4	9.4	7.2
MgO	18.6	16.5	21.2	4.2	4.6	8.6	5.0	5.7	9.6	5.0
CaO	6.6	9.8	7.4	7.8	8.9	8.9	8.9	9.3	8.6	9.5
Na2O	1.6	0.4	1.0	4.2	3.6	3.0	3.6	3.6	2.1	3.4
K2O	0.4	0.4	0.1	0.7	0.6	0.5	0.6	0.7	0.7	0.4
TiO2	0.31	0.48	0.72	1.649	2.361	1.190	1.597	1.04	3.86	2.92
MnO	0.17	0.22	0.20	0.099	0.128	0.145	0.123	0.12	0.21	0.17
P2O5	0.08	0.07	0.10	0.167	0.503	0.138	0.284	0.27	0.17	1.30
L.O.I.	1.69	10.24	3.38	0.92	1.24	1.42	1.19	1.31	1.76	0.68
Total	98.82	98.34	99.06	98.92	99.26	99.32	99.49	99.33	98.91	99.23
MG#	79.04	78.53	78.46	58.55	54.84	71.87	62.55	65.35	64.62	55.02

Table A5.1 (Con't)

Sample#	F-91-233.1	F-91-279.2	N-17	N-18
Map Unit	Zone IVa	Zone IVa	Zone III	Zone III
SiO2	48.15	46.32	48.32	47.87
Al2O3	16.72	12.52	6.89	14.88
Fe2O3	2.69	3.41	3.88	3.03
FeO	8.78	7.89	11.87	7.73
MgO	5.87	14.47	12.51	6.38
CaO	10.87	9.63	8.24	8.91
Na2O	2.93	1.76	1.42	3.11
K2O	0.33	0.35	0.65	0.74
TiO2	1.96	0.65	3.16	4.42
MnO	0.14	0.19	0.30	0.17
P2O5	0.28	0.08	0.35	0.27
L.O.I.	1.59	2.50	1.83	1.15
Total	100.30	99.77	99.42	98.67
MG#	54.37	76.58	65.27	59.56
S	3630	2615		
Cu	47	86		
Zn	76	67		
Cl	330	142		
Cr	142	426		
Ni	50	174		
V	478	152		
Sc	38	29		
Ba	109	91		
Rb	4	10		
Sr	596	367		
Zr	50	37		
Nb	4.3	1.5		
Y	17.2	9.8		

Table A5.2 Whole rock geochemical analyses, from the FS.

Sample	F-91-580	F-91-563.1	F-92-20a	F-91-595.1	F-91-596.1	F-91-118	F-91-583	F-91-596.2	F-92-30
Map Unit	FS	FS	FS	FS	FS	FS	FS	FS	FS
SiO2	76.8	61.2	76.6	58.0	54.7	73.0	59.4	62.7	58.4
Al2O3	12.3	16.2	12.3	15.4	16.6	13.9	17.9	19.4	18.3
Fe2O3	0.4	1.1	0.7	2.0	1.3	0.8	2.6	0.8	0.6
FeO	1.0	4.6	0.7	5.8	4.8	1.8	4.1	2.8	3.1
MgO	0.1	2.4	0.1	3.0	5.6	0.6	1.7	1.1	5.5
CaO	0.9	5.2	0.7	5.8	7.8	2.1	5.4	4.5	7.1
Na2O	4.0	4.3	3.9	3.7	3.4	4.2	5.0	4.6	3.2
K2O	3.7	1.8	3.9	1.7	1.7	2.9	1.2	1.9	1.1
TiO2	0.16	1.14	0.15	1.42	0.85	0.31	0.99	0.44	0.22
MnO	0.03	0.12	0.03	0.22	0.17	0.06	0.13	0.07	0.09
P2O5	0.00	0.22	0.02	0.28	0.11	0.08	0.38	0.17	0.05
LOI	0.39	1.13	0.37	1.42	2.61	0.64	0.97	1.66	2.10
Total	99.76	99.26	99.55	98.76	99.57	100.49	99.76	100.22	99.78
Mg#	20.80	47.78	22.78	47.70	67.16	37.17	42.75	42.21	76.35
Zn	27	72	11	116	54	23	75	26	36
Cr	25	20	0	9	193	<7	<7	<7	18
Ni	5	4	<3	5	24	<4	5	<3	42
V	1	131	5	242	193	16	85	52	35
Sc	7	20	2	32	32	7	19	5	15
Ba	359	236	381	258	286	314	198	252	207
Rb	113.2	70	129	59	73	89	36	69	49
Sr	63	294	52	283	291	137	331	384	462
Ga	15	20	15	19	16	19	24	21	17
Zr	149	269	138	57	78	164	246	136	61
Nb	8.6	11.1	9.7	12.7	4.4	11.1	10.0	4.0	5.7
Y	30.8	36.4	25.2	31.6	16.7	37.9	29.8	7.7	20.8
Hf	3.8	8.4	4.1						
Ta	0.3	1.5	0.6						
Th	8.3	9.7	8.9						
La	25.9	24.0	14.0						
Ce	52.3	53.7	32.1						
Pr	5.89	6.55	3.45						
Nd	21.3	26.9	13.0						
Sm	4.50	5.98	3.18						
Eu	0.56	1.54	0.49						
Gd	4.34	6.19	3.28						
Tb	0.67	1.01	0.60						
Dy	4.72	6.97	4.24						
Ho	0.96	1.41	0.94						
Er	2.87	4.30	2.83						
Tm	0.44	0.64	0.47						
Yb	2.93	4.21	3.14						
Lu	0.44	0.64	0.46						
(Eu/Eu*)CHUR	0.38	0.77	0.46						
(La/Lu)CHUR	6.08	3.91	3.15						
(La/Sm)CHUR	0.36	0.25	0.28						
(Gd/Lu)CHUR	1.22	1.21	0.89						
(Nb/La)PRIM	0.33	0.45	0.68						

Table A5.2 (Con't)

Sample	F-91-120	F-91-50Gr	F-92-49	F-91-180
Map Unit	FS	FS	FS	FS
SiO2	74.2	78.9	75.4	76.0
Al2O3	13.8	11.8	12.3	12.8
Fe2O3T	2.5	0.9	1.4	1.2
Fe2O3	0.7	0.1	0.8	0.3
FeO	1.6	0.7	0.6	0.8
MgO	0.5	0.1	0.1	0.3
CaO	2.0	1.4	0.8	0.7
Na2O	4.1	4.1	4.0	3.2
K2O	3.0	2.3	3.6	5.1
TiO2	0.35	0.08	0.15	0.16
MnO	0.05	0.01	0.02	0.02
P2O5	0.08	0.01	0.03	0.03
LOI	0.34	0.58	0.36	0.73
Total	100.83	100.15	98.16	100.22
Mg#	36.88	12.44	28.59	41.93
Cu	2	4	1	3
Zn	29	<2	12	<2
Cr	<7	<7	<7	<7
Ni	<3	<3	<3	<4
V	17	2	2	14
Sc	9	0	3	2
Ba	347	537	407	358
Rb	109	37	91	83
Sr	123	199	57	89
Ga	18	15	13	14
Zr	139	74	149	92
Nb	9	2	4	8
Y	33.0	6.7	12.1	14.9

Table A5.3 Whole rock geochemical analyses, from the W-SCS.

Sample	F-91-79	F-92-175.b	F-92-14a	F-91-175a	F-91-223	F-91-450	F-91-54
Map Unit	WU	WU	WU	WU	WU	SU	SU
SiO2	49.9	55.3	57.6	69.0	58.9	60.2	55.8
Al2O3	17.0	17.4	17.6	17.0	17.5	16.5	16.1
Fe2O3	3.2	3.1	1.8	0.4	1.7	1.5	2.3
FeO	6.2	4.5	4.4	1.4	4.6	4.2	4.6
MgO	5.7	3.7	3.7	0.6	2.0	3.8	5.2
CaO	8.0	6.1	6.2	3.4	5.5	6.1	7.2
Na2O	3.7	4.3	4.6	4.7	4.7	4.3	3.9
K2O	1.4	1.1	1.1	0.9	1.6	1.6	1.6
TiO2	1.64	1.22	0.93	0.11	1.03	0.89	0.96
MnO	0.15	0.12	0.11	0.05	0.09	0.10	0.09
P2O5	0.53	0.51	0.27	0.07	0.42	0.25	0.42
LOI	2.22	1.63	1.40	0.77	1.08	1.01	1.02
Total	99.57	98.97	99.58	98.35	99.07	100.52	99.12
Mg#	62.18	59.75	59.93	44.49	43.33	61.51	66.84
Zn	81	75	65	23	55	59	68
Cr	155	68	59	<7	7	75	140
Ni	62	35	35	<4	9	32	83
V	247	138	133	9	93	138	143
Sc	31	19	19	7	23	20	17
Ba	480	318	281	360	228	318	493
Rb	38	28	23	14	54	47	45
Sr	773	676	468	387	352	447	828
Ga	20	21	23	20	22	19.00	21
Zr	113	230	128	40	230	104	139
Nb	9.6	10.6	8.8	3.3	9.1	5.7	6.2
Y	24.7	22.7	18.2	20.5	26.3	16.1	16.4
Hf	3.6	4.6	4.0	1.6	7.8	3.6	6.1
Ta	0.9	1.2	1.6	1.3	1.0	0.7	0.6
Th	4.4	3.5	6.3	2.1	5.7	7.8	5.4
La	36.1	28.2	21.3	19.6	22.4	25.3	38.9
Ce	81.5	62.2	44.5	35.5	47.0	53.9	85.0
Pr	9.67	7.57	5.35	3.86	5.68	6.18	10.0
Nd	38.2	30.0	20.7	13.9	24.5	23.1	38.2
Sm	6.66	5.85	4.33	3.07	5.85	4.25	6.17
Eu	1.84	1.70	1.46	1.24	2.05	1.28	1.64
Gd	5.42	5.07	3.93	3.32	5.67	3.67	4.67
Tb	0.73	0.69	0.57	0.51	0.81	0.51	0.60
Dy	4.75	4.31	3.57	3.81	5.71	3.28	3.72
Ho	0.81	0.79	0.74	0.73	1.05	0.63	0.71
Er	2.42	2.30	2.06	2.22	3.05	1.77	1.91
Tm	0.34	0.31	0.29	0.30	0.42	0.25	0.26
Yb	2.03	1.93	1.86	1.93	2.71	1.53	1.67
Lu	0.31	0.30	0.28	0.29	0.41	0.23	0.25
(Eu/Eu*)CHUR	0.91	0.93	1.06	1.18	1.07	0.97	0.90
(La/Lu)CHUR	12.06	9.74	7.91	6.94	5.68	11.57	16.13
(La/Sm)CHUR	3.41	3.03	3.09	4.03	2.41	3.75	3.96
(Gd/Lu)CHUR	2.18	2.10	1.75	1.41	1.72	2.01	2.33
(Nb/La)PRIM	0.26	0.37	0.41	0.16	0.40	0.22	0.16

Table A5.3 (Con't)

Sample	F-91-610	F-91-518.2	F-92-176	F-24	F-3	F-91-188	F-92-60	F-91-478a	F-91-478b
Map Unit	WU	WU	WU	WU	SU	SU	SU	PIU	PIU
SiO2	58.6	49.4	60.0	51.5	56.0	56.6	56.8	52.6	48.2
Al2O3	19.7	18.3	16.0	17.7	15.9	16.3	16.7	8.6	15.0
Fe2O3	0.9	3.2	0.9	2.6	2.3	2.5	3.1	1.6	4.8
FeO	3.2	4.6	4.5	6.1	4.5	4.0	4.1	8.9	8.1
MgO	1.9	5.7	3.6	4.7	5.1	5.1	3.5	14.5	6.2
CaO	4.0	8.9	5.8	8.2	7.7	7.0	5.9	7.1	8.4
Na2O	6.5	3.4	4.1	4.1	4.0	4.0	4.0	1.2	2.8
K2O	1.5	1.4	1.6	0.8	1.4	1.4	1.7	0.6	0.6
TiO2	1.00	1.33	1.28	1.56	0.93	0.80	0.84	0.66	2.91
MnO	0.07	0.16	0.10	0.12	0.10	0.10	0.10	0.21	0.17
P2O5	0.31	0.13	0.47	0.67	0.42	0.32	0.23	0.11	0.16
LOI	1.64	2.42	1.27	1.37	0.88	1.82	1.23	3.41	1.51
Total	99.30	99.02	99.61	99.36	99.14	99.93	98.16	99.51	98.90
Mg#	50.73	69.01	58.78	57.63	67.12	69.40	60.15	74.42	57.86
Zn	27	48	65	57	62	67	57	9	79
Cr	22	80	61	49	155	125	77	1326	51
Ni	25	39	33	24	75	75	31	216	27
V	77	240	160	224	151	137	128	174	438
Sc	7	34	23	30	16	17	17	37	39
Ba	464	524	331	165	472	405	306	98	228
Rb	43	57	58	19	33	34	56	19	20
Sr	734	909	561	707	874	811	417	148	20
Ga	23	20	22	18	11	20	21	13	573
Zr	651	67	227	104	132	117	138	61	56
Nb	7.50	3.37	8.94	9.60	5.21	5.64	5.91	3.50	5.60
Y	11.20	14.20	20.02	38.44	16.64	14.76	16.93	15.70	13.40

Sample	N-5	F-91-590.1	F-92-75a	F-92-75b	F-92-32
Map Unit	WU	WU	WU	WU	PIU
SiO2	71.9	57.4	59.8	58.5	52.8
Al2O3	14.2	16.5	15.8	17.6	14.1
Fe2O3	0.9	1.6	2.5	2.7	1.8
FeO	1.7	4.7	3.5	2.9	7.0
MgO	0.6	4.0	2.6	1.8	8.8
CaO	2.2	6.3	4.3	4.0	6.3
Na2O	4.4	4.1	4.1	4.8	2.8
K2O	2.3	1.5	2.9	3.5	0.8
TiO2	0.37	1.02	1.19	1.15	1.45
MnO	0.06	0.11	0.09	0.09	0.15
P2O5	0.09	0.26	0.44	0.47	0.24
LOI	0.64	2.10	1.30	1.05	2.98
Total	99.28	99.54	98.48	98.51	99.18
Mg#	38.16	60.15	57.31	52.07	68.97
Zn	23	56	65	68	
Cr	16	59	23	<7	
Ni	<5	39	22	<4	
V	17	137	129	91	
Sc	7	20	15	14	
Ba	382	247	774	1085	
Rb	59	40	74	68	
Sr	151	401	536	633	
Ga	18	20	21	23	
Zr	172	52	354	449	
Nb	10	8	14	19	
Y	28	18	29	38	

Table A5.4 Whole rock geochemical analyses, from inclusions

Sample	N-1	N-3	F-92-14b	F-91-60ld	F-91-77s	N-5	F-91-587	F-91-287.2	F-91-88s
Rock Type	Encl	Encl	Encl	Metsd	Metsd	Encl	Encl	Metsd	Metsd
SiO2	62.0	53.2	52.6	67.9	49.2	71.9	56.2	50.0	46.0
Al2O3	18.0	16.9	16.3	12.6	18.9	14.2	16.7	16.9	18.7
Fe2O3	2.4	1.3	2.5	0.6	3.0	0.9	1.7	2.2	4.7
FeO	3.1	6.4	6.5	3.8	7.4	1.7	5.5	6.0	6.4
MgO	1.3	6.1	4.9	3.4	8.7	0.6	4.3	7.6	5.9
CaO	4.3	8.6	6.0	3.7	8.1	2.2	7.7	9.4	10.0
Na2O	5.1	3.6	4.4	2.4	2.0	4.4	4.5	3.5	3.3
K2O	1.4	0.8	0.9	2.0	0.2	2.3	1.2	0.4	0.4
TiO2	0.88	1.21	1.75	0.74	0.97	0.37	0.71	1.25	2.26
MnO	0.09	0.14	0.15	0.07	0.25	0.06	0.20	0.13	0.14
P2O5	0.20	0.24	0.61	0.16	0.05	0.09	0.51	0.32	0.45
LOI	1.42	1.65	2.71	1.14	1.59	0.64	1.14	1.68	1.07
Total	100.16	99.99	99.26	98.33	100.42	99.28	100.09	99.46	99.40
Mg#	42.84	63.13	57.20	61.58	67.60	38.16	58.04	69.32	62.19
Zn	50	63	96	58	208	23	114	83	82
Cr	7	208	47	148	392	16	51	336	77
Ni	<5	71	41	59	179	<5	32	158	51
V	37	171	146	94	210	17	78	218	286
Sc	13	39	20	14	32	7	52	27	38
Ba	404	160	322	446	105	382	178	98	64
Rb	49	27	20	70	4	59	26	4	2
Sr	398	288	623	180	453	151	383	582	552
Zr	509	178	240	252	79	172	35	74	54
Nb	12.2	9.9	18.6	13.2	7.1	9.8	9.3	5.4	4.9
Y	23.1	22.7	24.6	22.3	10.5	28.4	122.3	19.6	25.2
Hf	11.3	4.6	6.7	6.6	2.3				
Ta	1.4	1.0	0.6	1.9	0.8				
Th	5.4	2.3	2.7	5.8	0.7				
La	16.7	12.3	28.3	30.3	18.5				
Ce	31.8	28.1	64.8	61.5	33.5				
Pr	3.79	3.60	8.33	7.50	3.61				
Nd	15.7	15.6	35.2	27.7	13.0				
Sm	3.57	3.61	6.70	5.47	2.15				
Eu	1.56	1.26	1.94	1.24	1.47				
Gd	3.75	3.78	6.21	4.54	1.74				
Tb	0.56	0.61	0.87	0.67	0.24				
Dy	3.95	4.29	5.07	4.33	1.74				
Ho	0.78	0.82	0.99	0.86	0.40				
Er	2.26	2.36	2.76	2.48	1.30				
Tm	0.35	0.33	0.37	0.36	0.21				
Yb	2.30	2.22	2.32	2.30	1.79				
Lu	0.37	0.35	0.35	0.36	0.28				
(Eu/Eu*)CHUR	1.30	1.04	0.91	0.74	2.26				
(La/Lu)CHUR	4.67	3.61	8.46	8.78	6.97				
(La/Sm)CHUR	2.94	2.14	2.66	3.49	5.42				
(Gd/Lu)CHUR	1.26	1.33	2.23	1.58	0.78				
(Nb/La)PRIM	0.72	0.79	0.65	0.43	0.38				

Table A5.4 (Con't)

Sample	F-91-60sl	F-91-60sd	F-91-227.S	N-2
Rock Type	Metsd	Metsd	Metsd	Encl
SiO2	70.5	67.6	67.5	58.9
Al2O3	12.5	12.8	11.4	16.8
Fe2O3	0.6	0.7	0.5	1.8
FeO	3.7	3.7	3.2	5.1
MgO	3.2	3.5	4.5	2.5
CaO	3.9	3.7	7.4	5.3
Na2O	2.4	2.4	2.1	4.7
K2O	1.6	2.2	0.2	1.3
TiO2	0.73	0.74	0.59	1.21
MnO	0.07	0.07	0.07	0.16
P2O5	0.17	0.16	0.28	0.19
LOI	0.99	1.28	0.72	0.95
Total	100.33	98.75	98.35	98.90
Mg#	61.16	62.62	71.09	47.18
Zn	50	56	26	
Cr	139	135	411	
Ni	54	60	102	
V	95	93	100	
Sc	10	10	21	
Ba	326	488	56	
Rb	54	78	3.6	
Sr	175	184	388	
Zr	253	239	129	
Nb	12.7	12.9	3.9	
Y	22.8	21.6	16.9	

Table A5.5 Whole rock geochemical anlayses, from the dykes.

Samples	F-92-20b	F-92-174	F-22	F-23	F-92-31	F-92-19	F-230.2 dyke	F-182.2 dyke	F-313.3 dyk
Map Unit	Dyke	Dyke	Dyke	Dyke	Dyke	Dyke	Dyke	Dyke	Dyke
Rock type	Andesite	Rhylite	Andesite	Andesite	MicroGrdrt	Andesite	Dolerite	Andesite	Rhyolite
SiO2	61.0	75.2	52.7	48.4	56.5	54.5	47.2	33.3	76.5
Al2O3	16.1	13.4	16.8	16.4	19.9	16.7	15.1	11.2	12.3
Fe2O3	2.1	0.2	1.9	2.7	3.6	2.0	4.2	7.2	0.1
FeO	3.9	1.0	5.3	7.8	3.3	5.9	7.4	12.9	0.8
MgO	2.2	0.5	7.4	8.0	2.0	4.6	7.1	6.8	0.3
CaO	4.3	0.9	8.6	9.3	4.8	6.4	11.0	14.6	0.6
Na2O	5.0	5.3	3.8	3.4	6.3	4.2	2.9	1.5	3.1
K2O	1.3	2.7	0.7	0.5	1.7	1.5	0.2	0.2	5.1
TiO2	1.19	0.21	1.02	1.49	1.13	1.54	2.37	5.52	0.19
MnO	0.10	0.01	0.13	0.17	0.07	0.12	0.16	0.12	0.01
P2O5	0.36	0.03	0.36	0.47	0.44	0.39	1.14	4.36	0.01
LOI	0.99	1.02	1.41	1.43	0.90	1.37	1.03	1.86	0.64
Total	98.54	100.42	99.82	100.12	100.72	99.31	99.82	99.43	99.71
Mg#	50.48	48.61	61.00	64.67	52.21	58.09	62.94	48.58	34.66
Cu	18	15	29	29	26	34	43	58	6
Zn	81	<2	68	77	91	81	77	75	0
Cr	<7	<7	360	62	<7	78	148	20	<7
Ni	5	<4	168	53	14	56	45	40	<4
V	122	19	201	274	67	168	325	769	12
Sc	18	<8	32	36	13	22	40	46	<7
Ba	469	351	158	230	975	281	154	139	428
Rb	54	50	7	5	54	40	2	4	104
Sr	479	166	485	710	627	500	730	852	152
Ga	20	18	16	<5	28	20	20	19	12
Zr	264	214	87	99	850	189	41	23	117
Nb	8.9	10.4	4.8	6.9	11.3	11.1	4.9	2.8	7.1
Y	28.5	14.7	33.3	25.8	44.7	21.7	27.1	14.8	12.6
Hf	5.4	5.5	3.0	3.4	18.6	5.4			
Ta	1.3	1.9	0.7	0.5	0.9	0.0			
Th	6.4	25.4	1.5	1.9	7.9	3.8			
La	30.4	43.4	7.0	29.8	46.0	23.9			
Ce	66.0	80.6	16.2	73.9	97.3	52.4			
Pr	7.91	8.00	2.12	9.23	11.66	6.53			
Nd	30.6	25.2	10.0	36.3	45.3	26.5			
Sm	5.97	3.86	2.68	6.89	9.13	5.54			
Eu	1.61	0.58	0.99	2.00	2.50	1.59			
Gd	5.41	2.55	3.08	5.87	8.63	5.26			
Tb	0.77	0.39	0.48	0.78	1.24	0.76			
Dy	4.97	2.51	3.33	5.20	8.20	4.55			
Ho	0.99	0.51	0.67	1.04	1.66	0.93			
Er	2.81	1.68	1.86	3.03	5.20	2.51			
Tm	0.42	0.26	0.25	0.41	0.77	0.35			
Yb	2.73	1.91	1.72	2.56	4.99	2.21			
Lu	0.41	0.31	0.26	0.41	0.86	0.32			
(Eu/Eu*)CHUR	0.85	0.54	1.05	0.94	0.85	0.89			
(La/Lu)CHUR	7.62	14.67	2.79	7.54	5.56	7.73			
(La/Sm)CHUR	3.20	7.07	1.64	2.72	3.17	2.72			
(Gd/Lu)CHUR	1.63	1.04	1.47	1.78	1.25	2.04			
(Nb/La)PRIM	0.29	0.24	0.68	0.23	0.24	0.46			

Table A5.5 (Con't)

Samples	F-313.2 dyke	F-92-34	F-91-234d	F-92-68dy	F-92-26	F-91-563.3
Map Unit	Dyke	Dyke	Dyke	Dyke	Dyke	Dyke
Rock type	Andesite	Andesite	Andesite	Andesite	Andesite	Andesite
SiO2	48.5	53.0	46.1	52.3	47.7	57.1
Al2O3	17.0	19.2	17.1	18.0	15.0	16.5
Fe2O3	4.7	3.4	7.1	4.1	5.7	1.3
FeO	6.5	4.5	7.1	5.1	8.1	5.4
MgO	5.1	2.9	4.9	3.3	4.9	3.8
CaO	8.8	6.0	8.0	7.0	8.6	6.8
Na2O	4.0	5.3	4.1	4.5	4.1	4.1
K2O	1.1	1.6	0.6	0.9	0.4	1.3
TiO2	2.14	1.52	2.55	1.73	3.05	1.18
MnO	0.17	0.11	0.22	0.13	0.19	0.13
P2O5	0.97	0.79	1.05	0.65	0.94	0.20
LOI	1.23	1.03	1.16	1.68	0.93	1.27
Total	100.22	99.32	99.97	99.38	99.65	99.15
Mg#	58.11	53.23	55.04	53.28	51.91	56.02
Cu	35	11	36	23	34	25
Zn	113	98	160	110	115	78
Cr	38	10	27	17	20	76
Ni	28	9	24	18	6	20
V	308	119	247	184	333	162
Sc	36	19	31	31	34	29
Ba	702	596	306	238	259	174
Rb	24	46	4	19	2	43
Sr	986	587	649	525	597	312
Ga	22	27	26	26	24	20
Zr	196	531	378	344	218	261
Nb	14.4	15.4	17.5	13.1	10.5	9.1
Y	37.0	38.2	59.6	46.2	38.7	25.8

APPENDIX 6

Table A6.1 CIPW norms for the TLS.

Sample #	F-91-32	F-91-582.1	F-91-582.2	F-91-582.3	F-91-582.4	F-91-582.5	F-92-68	F-92-69	F-92-70	F-92-71
Map Unit	Zone I	Zone I	Zone I	Zone I	Zone I	Zone I	Zone II	Zone II	Zone II	Zone II
Quartz	1.80	1.08	1.13	0.00	3.32	2.58	0.00	2.56	3.95	3.75
Corundum	0.00	0.00	0.00	0.00	0.00	0.00	0.00	0.00	0.00	0.00
Zircon	0.01	0.01	0.01	0.01	0.02	0.01	0.01	0.01	0.01	0.01
Orthoclase	1.48	2.86	2.96	1.75	2.93	2.55	2.53	4.82	4.13	4.07
Albite	10.06	11.48	9.35	11.67	8.56	11.28	9.07	21.12	29.86	35.77
Anorthite	15.66	23.16	16.70	30.07	8.24	24.00	17.40	18.57	28.84	27.18
Halite	0.03	0.03	0.03	0.00	0.00	0.05	0.00	0.00	0.00	0.00
Diopside	8.06	28.05	30.60	24.69	34.74	27.19	8.58	9.31	8.83	8.26
Hypersthene	56.83	28.34	33.16	23.64	36.26	29.21	29.04	35.11	16.77	10.90
Olivine	0.00	0.00	0.00	3.16	0.00	0.00	16.55	0.00	0.00	0.00
Magnetite	2.87	1.55	1.96	2.11	2.57	1.61	1.40	2.91	2.78	4.56
Chromite	0.23	0.10	0.13	0.08	0.13	0.10	0.30	0.12	0.01	0.02
Hematite	0.00	0.00	0.00	0.00	0.00	0.00	0.04	0.00	0.00	0.00
Ilmenite	1.15	0.66	0.76	0.49	0.81	0.58	1.51	1.69	1.94	3.13
Apatite	0.34	0.13	0.16	0.09	0.16	0.10	0.16	0.52	0.52	0.40
Pyrite	0.27	0.16	0.12	0.00	0.00	0.10	0.00	0.00	0.00	0.00

Sample #	F-92-72	F-92-73	F-92-74	F-91-532.1	F-91-13	F-91-14	F-91-15	F-91-16	F-91-17	F-91-18
Map Unit	Zone II	Zone II	Zone II	Zone II	Zone III	Zone III	Zone III	Zone III	Zone III	Zone III
Quartz	1.27	0.00	3.22	2.86	2.87	3.55	1.53	2.43	1.74	2.40
Corundum	0.00	0.00	0.00	0.00	0.00	0.00	0.00	0.00	0.00	0.00
Zircon	0.02	0.02	0.02	0.02	0.02	0.02	0.02	0.01	0.01	0.02
Orthoclase	3.67	3.08	3.65	6.04	4.14	5.98	3.67	3.02	4.03	2.96
Albite	30.15	25.01	30.40	29.57	28.30	19.82	13.66	16.27	31.06	20.62
Anorthite	29.23	36.92	31.34	26.65	24.69	15.98	10.98	14.35	30.40	19.80
Halite	0.00	0.00	0.00	0.05	0.02	0.01	0.01	0.01	0.01	0.01
Diopside	9.36	5.22	8.84	4.50	9.39	18.43	28.15	16.14	10.98	17.01
Hypersthene	11.29	9.13	13.12	15.18	16.04	24.75	29.99	37.90	13.63	24.94
Olivine	0.00	11.97	0.00	0.00	0.00	0.00	0.00	0.00	0.00	0.00
Magnetite	7.41	3.99	4.05	5.60	4.99	4.57	4.13	3.04	3.03	5.80
Chromite	0.00	0.00	0.01	0.01	0.01	0.08	0.11	0.11	0.01	0.05
Hematite	0.00	0.00	0.00	0.00	0.00	0.00	0.00	0.00	0.00	0.00
Ilmenite	4.48	2.26	3.03	4.51	4.78	4.12	4.00	3.29	1.79	3.52
Apatite	1.19	0.33	0.67	4.17	3.04	0.65	0.93	0.78	0.92	0.93
Pyrite	0.00	0.00	0.00	0.12	0.11	0.12	0.20	0.22	0.02	0.30

Table A6.1 (Con't)

Sample #	F-91-19	F-91-20	F-91-21	F-91-25	F-91-26	F-91-103.2	N-10	N-11	N-12	N-13
Map Unit	Zone III	Zone III	Zone III	Zone III	Zone III	Zone III	Zone III	Zone III	Zone III	Zone III
Quartz	1.51	4.64	3.22	5.11	2.56	5.27	0.00	0.00	3.57	1.45
Corundum	0.00	0.00	0.00	0.00	0.00	0.00	0.00	0.00	0.00	0.00
Zircon	0.02	0.01	0.02	0.01	0.01	0.02	0.01	0.01	0.01	0.01
Orthoclase	4.08	4.27	2.72	2.07	2.84	2.84	2.07	2.68	4.54	3.85
Albite	12.71	15.21	20.41	8.51	18.87	6.66	25.67	28.53	12.23	30.77
Anorthite	9.78	13.55	19.21	10.01	23.52	6.32	29.33	27.10	10.38	29.71
Halite	0.01	0.02	0.01	0.02	0.01	0.02	0.02	0.00	0.00	0.00
Diopside	28.20	20.39	14.97	22.79	15.69	28.95	11.24	12.19	8.86	11.95
Hypersthene	31.25	32.00	23.47	36.98	23.63	35.19	11.75	16.58	47.75	15.29
Olivine	0.00	0.00	0.00	0.00	0.00	0.00	1.64	0.01	0.00	0.00
Magnetite	4.13	3.73	5.22	7.08	4.18	4.76	6.83	4.58	6.01	2.42
Chromite	0.12	0.08	0.06	0.13	0.05	0.09	0.02	0.03	0.14	0.00
Hematite	0.00	0.00	0.00	0.00	0.00	0.00	0.00	0.00	0.00	0.00
Ilmenite	4.31	4.04	7.46	5.91	5.52	7.63	5.63	4.64	2.63	1.97
Apatite	1.00	0.45	0.39	0.34	0.31	0.35	3.44	1.78	1.27	0.64
Pyrite	0.22	0.23	0.14	0.21	0.16	0.36	0.12	0.00	0.00	0.00
Total	97.34	98.60	97.30	99.18	97.34	98.44	97.75	98.14	97.40	98.06

Sample #	N-14	N-16	N-17	N-18	F-91-1	F-91-2	F-91-9	F-91-10	F-91-233.1	F-91-279.2
Map Unit	Zone III	Zone III	Zone III	Zone III	Zone IVb	Zone IVb	Zone IVb	Zone IVb	Zone IVa	Zone IVa
Quartz	3.65	0.62	2.01	0.86	1.21	0.11	0.00	0.00	0.00	0.00
Corundum	0.00	0.00	0.00	0.00	0.00	0.00	0.00	0.00	0.00	0.00
Zircon	0.03	0.01	0.02	0.02	0.01	0.01	0.01	0.00	0.01	0.01
Orthoclase	4.20	2.58	3.84	4.39	2.13	1.95	2.31	0.77	1.95	2.07
Albite	17.68	28.99	11.99	26.29	20.81	22.27	6.24	8.44	23.81	14.43
Anorthite	16.75	30.26	10.53	24.46	34.33	35.82	13.07	21.88	32.04	25.50
Halite	0.00	0.00	0.00	0.00	0.01	0.01	0.07	0.03	0.05	0.02
Diopside	19.88	6.92	22.64	14.36	20.64	21.02	4.66	10.62	16.63	17.48
Hypersthene	23.72	13.94	34.11	13.72	12.48	11.40	17.84	5.76	12.62	13.48
Olivine	0.00	0.00	0.00	0.00	0.00	0.00	45.22	44.98	2.96	17.64
Magnetite	3.53	6.67	5.62	4.40	3.42	3.32	4.79	3.91	3.90	4.95
Chromite	0.06	0.00	0.10	0.02	0.06	0.04	0.31	0.03	0.03	0.09
Hematite	0.00	0.00	0.00	0.00	0.00	0.00	0.00	0.00	0.00	0.00
Ilmenite	7.32	5.55	6.00	8.40	1.79	1.62	0.81	0.97	3.71	1.24
Apatite	0.40	3.09	0.84	0.65	0.68	0.34	0.64	0.22	0.66	0.20
Pyrite	0.00	0.00	0.00	0.00	0.05	0.07	0.12	0.13	0.68	0.49
Total	97.22	98.64	97.70	97.57	97.63	98.00	96.09	97.75	99.06	97.58

Table A6.1 (Con't)

Sample #	F-91-279.1	F-91-280	F-91-281.1	F-91-281.2	F-91-50.2b	F-91-50.2t	F-91-50.6	F-91-176	F-91-173	F-91-174
Map Unit	Zone IVa	Zone IVa	Zone IVa	Zone IVa	Zone IVb	Zone IVb	Zone IVb	Zone IVb	Zone IVb	Zone IVb
Quartz	0.00	0.00	0.00	1.38	0.00	0.00	0.00	0.00	0.00	0.00
Corundum	0.00	0.00	0.00	0.00	0.00	0.00	0.00	0.00	0.00	0.00
Zircon	0.00	0.01	0.01	0.01	0.00	0.00	0.00	0.00	0.01	0.00
Orthoclase	1.54	1.54	2.21	2.62	0.85	1.22	0.83	1.06	1.36	1.99
Albite	21.75	8.51	13.15	3.04	6.99	20.93	8.85	19.09	5.27	26.97
Anorthite	38.46	19.08	27.44	6.46	21.65	46.74	20.56	34.66	15.84	49.26
Halite	0.02	0.04	0.00	0.00	0.05	0.01	0.00	0.03	0.09	0.00
Diopside	12.86	7.39	3.97	33.61	8.69	18.37	12.35	20.03	9.74	8.81
Hypersthene	9.03	33.58	16.83	38.66	11.42	0.17	7.51	3.65	18.18	5.56
Olivine	9.39	21.59	30.14	0.00	39.67	8.33	39.41	5.12	38.04	2.75
Magnetite	3.89	4.12	2.62	1.20	4.26	1.86	4.55	9.51	5.23	2.35
Chromite	0.07	0.09	0.08	0.23	0.03	0.05	0.03	0.01	0.29	0.00
Hematite	0.00	0.00	0.00	0.00	0.00	0.00	0.00	0.00	0.00	0.00
Ilmenite	0.91	0.97	0.58	0.91	1.31	0.88	1.37	3.86	0.77	0.92
Apatite	0.13	0.15	0.18	0.16	0.24	0.07	0.24	0.09	0.32	0.17
Pyrite	0.41	0.23	0.00	0.00	0.20	0.10	0.00	0.41	0.17	0.02
Total	98.48	97.30	97.20	88.27	95.38	98.72	95.72	97.52	95.31	98.82

Table A6.2 CIPW norms for the dykes

Sample#	F-91-22	F-91-23	F-92-31	F-92-34	F-91-234d	F-92-68d	F-92-26	F-92-19d
Quartz	0.00	0.00	1.00	0.34	0.00	4.45	0.42	3.57
Corundum	0.00	0.00	0.04	0.00	0.00	0.00	0.00	0.00
Zircon	0.02	0.02	0.17	0.11	0.08	0.07	0.04	0.04
Orthoclase	3.84	3.19	10.01	9.65	3.30	5.18	2.25	8.82
Albite	31.41	28.75	52.48	43.78	33.65	37.55	34.07	34.92
Anorthite	27.15	27.86	21.48	24.35	27.25	26.77	21.73	22.76
Halite	0.02	0.01	0.05	0.04	0.04	0.02	0.03	0.05
Diopside	10.60	12.47	0.00	0.37	4.89	3.09	12.28	5.57
Hypersthene	19.76	4.88	6.48	10.15	9.34	9.83	11.59	15.51
Olivine	0.18	13.67	0.00	0.00	2.73	0.00	0.00	0.00
Magnetite	2.71	3.87	5.15	4.95	10.32	5.99	8.24	2.91
Chromite	0.08	0.01	0.00	0.00	0.01	0.00	0.00	0.02
Hematite	0.00	0.00	0.00	0.00	0.00	0.00	0.00	0.00
Ilmenite	1.93	2.83	2.15	2.89	4.83	3.29	5.80	2.92
Apatite	0.85	1.13	1.05	1.87	2.49	1.55	2.23	0.93
Pyrite	0.04	0.25	0.03	0.02	0.09	0.08	0.31	0.06
Total	98.59	98.94	100.10	98.51	99.02	97.88	98.99	98.07

Sample#	F-92-20b	F-91-563.3	F-92-174
Quartz	14.57	7.28	31.26
Corundum	0.00	0.00	0.26
Zircon	0.05	0.06	0.04
Orthoclase	7.90	7.68	15.70
Albite	41.02	34.68	44.46
Anorthite	18.26	22.90	4.42
Halite	0.07	0.00	0.02
Diopside	0.99	8.03	0.00
Hypersthene	8.65	12.73	2.55
Olivine	0.00	0.00	0.00
Magnetite	3.02	1.89	0.27
Chromite	0.00	0.01	0.00
Hematite	0.00	0.00	0.00
Ilmenite	2.25	2.23	0.39
Apatite	0.86	0.47	0.08
Pyrite	0.02	0.00	0.01
Total	97.65	97.96	99.47

APPENDIX 7

Sm-Nd ISOTOPIC TECHNIQUE AND NOMENCLATURE

The Sm-Nd isotopic analyses were carried out at Department of Earth Sciences, Memorial University of Newfoundland. Chemical separations were carried out in clean laboratory conditions by using reagents doubly distilled in quartz and/or two-bottle Teflon sills. Approximately 100-200 mg of samples with different compositions were dissolved in HF-HNO_3, initially in an open beaker and then 10-15 days at 220°C in high pressure Teflon bombs. Fluorides were converted to perchlorates which were then dissolved in HCL in two stages of evaporation. Samples were taken up in 6N HCL, heated to homogenization; 2/3 was taken for Nd isotope composition (IC) and 1/3 for Nd and Sm isotope dilution (ID) analyses. A mixed ^{150}Nd-^{147}Sm spike was mixed with the ID fraction of the solution which was then evaporated to dryness. Nd and Sm were separated using a three stage ion exchange procedure. The REE were initially separated in HCL, using 10 ml of Amberlite CG-120 cation exchange resin in 30 cm quartz columns. Ba was separated from the REE in a small HNO_3 column. Nd and Sm were separated in quartz columns using Teflon powder coated with di-2-ethylhexyl orthophosphoric acid. Samples were analyzed in static mode on a Finnigan Mat 262 multi-collector mass spectrometer.

The notation for Sm-Nd isotopic data used in thesis follows the notation of DePaola and Wasserburg (1976). Initial epsilon Nd ($\epsilon_{Nd(i)}$) corresponds the initial $^{143}Nd/^{144}Nd$ value of a sample over the that of the chondritic uniform reservoir (CHUR).

$$\epsilon_{Nd(i)} = [(^{143}Nd/^{144}Nd_{(i)sample}/^{143}Nd/^{144}Nd_{(i)CHUR}-1)]*10^4,$$

Where the subscript (i) takes into the account the time of formation of the sample. During this study, the following reference values for the CHUR $^{147}Sm/^{143}Nd = 0.1967$; and present day $^{143}Nd/^{144}Nd = 0.512638$.

APPENDIX 8
U/Pb GEOCHRONOLOGY
ANALYTICAL TECHINQUE

The U/Pb geochronology was performed at the Department of Earth Sciences, Memorial University of Newfoundland.

The rock samples were crushed and minerals suitable for geochronology were separated under clean conditions using a rock crusher, Wilfley panning table, Frantz magnetic separator, sieves and heavy liquids. After final magnetic separation, several high quality zircon and titanite fractions were selected for analyses. To reduce the effect of potential Pb-loss due to alteration, the outher surfaces of the fractions were removed by abrasion (Krogh, 1982).

After abrasion, the best grains were selected and washed in distilled nitric acid, water and acetone. The fractions were weighed into Teflon capsules with a mixed $^{205}Pb/^{235}U$ isotopic tracer (Krogh and Davis, 1975) and Hf and HNO_3 acid for dissolution. Zircon dissolution was carried out in an oven at 210°C over 5 days, while titanite dissolution was carried out on a hot plate. Then, U and Pb were separated on ion exchange columns, using standard procedures (Dunning et al., 1990b) and were loaded on silica gel with phosphoric acid onto a Re filament. The isotopic compositions of Pb and U were measured on a multi-collector MAT 262 thermal ionization mass spectrometer.

Ages were calculated using decay constants of Jaffey et al. (1971). Errors on the isotopic ratios were calculated by propagating uncertainties in measurement of isotopic ratios, fractionation and amount of blank with a program modified after an unpublished

error propagation program written by L.Heaman (J. Connely, 1995 per. comm.). Linear regressions were calculated using the procedure of Davis (1982). All ages reported here are the $^{206}Pb/^{238}U$ ages, which are relatively insensitive to uncertainties in the common-Pb correction (Dunning et al., 1990b).

APPENDIX 9

Table A9. Trace element normalizing values.

	Chondrite	Primitive Mantle
Rb	3.4500	0.5500
Ba	3.4100	5.1000
Th	0.0425	0.0640
Nb	0.3750	0.5600
La	0.3670	0.5510
Ce	0.9570	1.4360
Sr	11.9000	17.8000
Pr	0.1370	0.2020
Nd	0.7110	1.6070
Zr	5.5400	8.3000
Sm	0.2310	0.3470
Eu	0.0870	0.1310
Gd	0.3060	0.4590
Tb	0.0580	0.0870
Ti	654	960
Dy	0.3810	0.5720
Y	2.2500	3.4000
Ho	0.0851	0.1280
Er	0.2490	0.3740
Tm	0.0356	0.0540
Yb	0.2480	0.3720
Lu	0.0381	0.0570

Data are compiled from Taylor and McLennan (1985)

APPENDIX 10

Table A10. List of publication and presentations produced from this research

Publication:

Aydin, N.S., Malpas, J., and Jenner, G., 1995, Physical Characteristics of the Tilting Layered Suite, Fogo Island, Newfoundland. South. African Journal of Geology, Special Issue on Layered Igneous Rocks, 94, V4.

Presentations:

Aydin, N.S., 1992, Layering characteristics of the Tilting Igneous Complex, Fogo Island, Newfoundland. Geological Association of Canada-Mineralogical Association of Canada Joint Annual Meeting, Abstract, 17, A4.

Aydin, N.S., Malpas, J., Jenner, G., and Cawood, P., 1993, Petrogenesis of the layered series in the Tilting Igneous Complex, Fogo Island, Newfoundland: Evidence for complex magma chamber processes. Symposium on Layering in Igneous Complexes, South Africa (Abstract).

Aydin, N.S., Malpas, J., and Jenner, G., 1994, Mingling and mixing between contrasting coexisting magmas: Example from the Fogo Island Batholith, Newfoundland. International Volcanology Congress, IAVCEI, Ankara, Turkey (Abstract).

Aydin, N.S., Malpas, J., and Jenner, G., 1995, Geochemical and Isotopic constraints on the evolution of the Tilting Layered Suite, Newfoundland: A window to mafic magma chamber processes. Symposium on Magmatic Processes-Do the answer lie in the Rocks? Sheffield, UK, (Abstract).